Molecular and Morphogenetic Analysis of Body Axis Formation in the Spider *Parasteatoda tepidariorum*

Doctoral thesis

for

the award of the doctoral degree

of the Faculty of Mathematics and Natural Sciences

of the University of Cologne

submitted by

Ruixun Wang

2025

Tables of Contents

Abstract

Background

Research in *Parasteatoda tepidariorum* (Pt) revealed that the animal relies on cell migration to establish the dorsal–ventral (DV) axis after the formation of the blastoderm and germ disc in earlier stages. The migrating cell clusters, named as the “cumulus”, exhibited features similar to the “Organizer” in frogs and enabled the differentiation of neighbouring cells independently, resulting in changes in body patterning. Several key genes were identified in previous studies; these genes were expressed in the cumulus or primary thickening regions from which the cumulus migrated at early stages, and their knockdown lead to loss of the DV axis. Among these, *Ets4* was highlighted for its role in maintaining cumulus integrity.

Result

A series of experiments were designed and performed to compare wild-type (WT) and *Ets4* RNAi embryos. Morphological observations through videos and time-series HCR staining images confirmed that the two embryo types resembled each other until the formation of the germ disc and the invagination of primary thickening cells in the central region of the germ disc. However, differentiation between *Ets4*$^{+}$ and *Ets4*$^{-}$ cells enabled an asymmetric pattern in wild-type embryos, which was absent in *Ets4* RNAi embryos. As a result, clusters of *Ets4*$^{+}$ cells remained tightly grouped and migrated outward in later stages, whereas in *Ets4* RNAi embryos, the cumulus were dispersed.

These observations were confirmed by RNA-seq analysis, which showed that genes related to cell migration and certain differentiation directions, were expressed at higher levels in wild-type embryos than in *Ets4* RNAi embryos. Functional analysis of some downstream genes affected by *Ets4* RNAi suggested that they participate in invagination and cumulus migration processes, resulting in various phenotypes with differing degrees of disruption to normal development.

In addition, a large number of genes were tested for expression via *in situ* hybridization experiments, revealing diverse temporal and spatial expression patterns. Surprisingly, *Ets4* appeared to regulate almost all genes of certain types while being completely independent of others. Results from RNA-seq and in situ hybridization analyses statistically confirmed each other’s reliability.

Conclusion

Through morphological analysis, A clearer understanding of the invagination process is reached, and I confirmed that the primary thickening region at stage 4 consisted of at least two distinct cell types. Only the *Ets4*$^{+}$ cells were the future cumulus. A hypothesis has been proposed that the uneven arrangement of *Ets4*$^{+}$ cells lead to asymmetric expression of *fgf8* in the germ disc at later stages, thereby determining the direction of movement and the future DV axis.

A large number of genes was selected, potentially downstream of *Ets4*. Analysis of these genes indicated that the function of *Ets4* operated at least on two levels: (1) regulating genes and pathways related to cell adhesion, the cytoskeleton, and cell movement; and (2) directly or indirectly regulating the Wnt, Hedgehog (Hh), dpp, and Fgf signaling pathways, which lead to the differentiation of neighboring cells.

Based on this, some further insight are gained into axis formation during *Pt* development.

1 Introduction

Animal Body axes.

Development is the process by which a simple egg grows into a highly organized organism (Developmental Biology, 11th edition, Gilbert & Barresi). This process is accomplished gradually. For example, in animal development, body axis establishment typically precedes organogenesis.

Animal body axes include the Anterior-Posterior (AP) axis, Dorsal-Ventral (DV) axis, and Left-Right (LR) axis. The number of body axes in a particular animal is determined by its morphological symmetry. Radially symmetric animals possess only the AP axis, while bilaterally symmetric animals have all three axes, which are formed gradually during development (Genikhovich & Technau, 2017).

There is vast diversity among animals in the mechanisms of axis determination. In fly development, the future AP and DV axes originate from the regional distribution of maternal proteins and mRNAs, which form gradients in the early embryo through diffusion and degradation. As a result, a series of downstream genes are expressed in specific regions, guiding distinct differentiation potentials (Driever & Nusslein-Volhard, 1988; Roth et al., 1995).

In frog development, the fertilization process activates signaling factors that induce dorsal specification in the gray crescent region, located opposite the sperm entry site (see Figure. 1). This leads to the initiation of gastrulation and the eventual establishment of the AP and DV axes. Notably, cells and their descendants in the dorsal blastopore lip, termed the 'Organizer,' can autonomously induce dorsal mesoderm and are capable of generating additional body axes through grafting experiments (De Robertis, 2009; Asashima & Satou-Kobayashi, 2024).

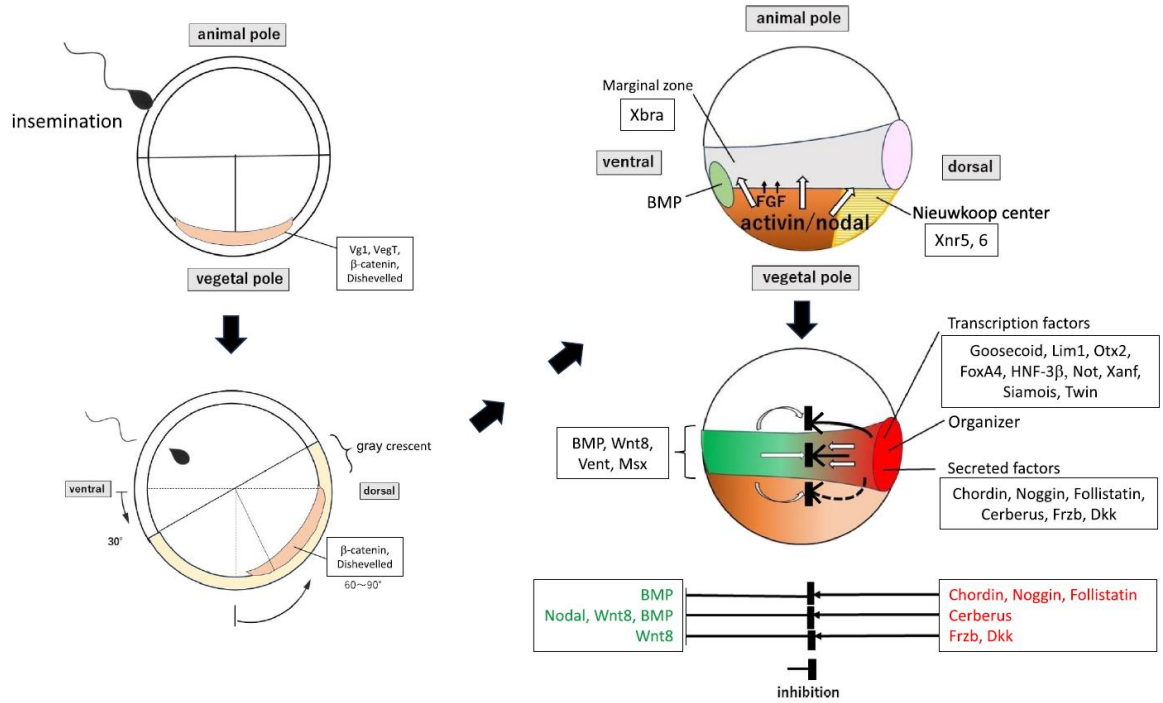

Figure 1. Schematic drawing from Asashima and Satou-Kobayashi, 2024 (Figure 9), illustrating the site of sperm entry, the 'Organizer' cells, and the animal body axes. The figure indicates the expression of secreted factors such as BMP, Wnt8, and FGF during development, as well as the gene regulatory networks active in different regions at various developmental stages.

Conserved secreted factors function in animal body axis formation.

In flies, frogs, and most other animals studied, however, the formation of body axes is consistently preceded by the establishment of specific secreted factors (morphogens), followed by the regional specification of cells in various directions and to differing extents. These secreted factors are highly conserved: Wnt family genes specify the AP axis in most bilaterally symmetrical animals, while BMP signaling is used to specify the DV axis across the entire animal kingdom (see Figure 2; Heldin et al., 1997; Saito-Diaz et al., 2013; De Robertis, 2008;Genikhovich & Technau, 2017;Panfilio, 2022), with the exception of insects, where Toll signaling functions in DV axis formation (Roth, 2025).

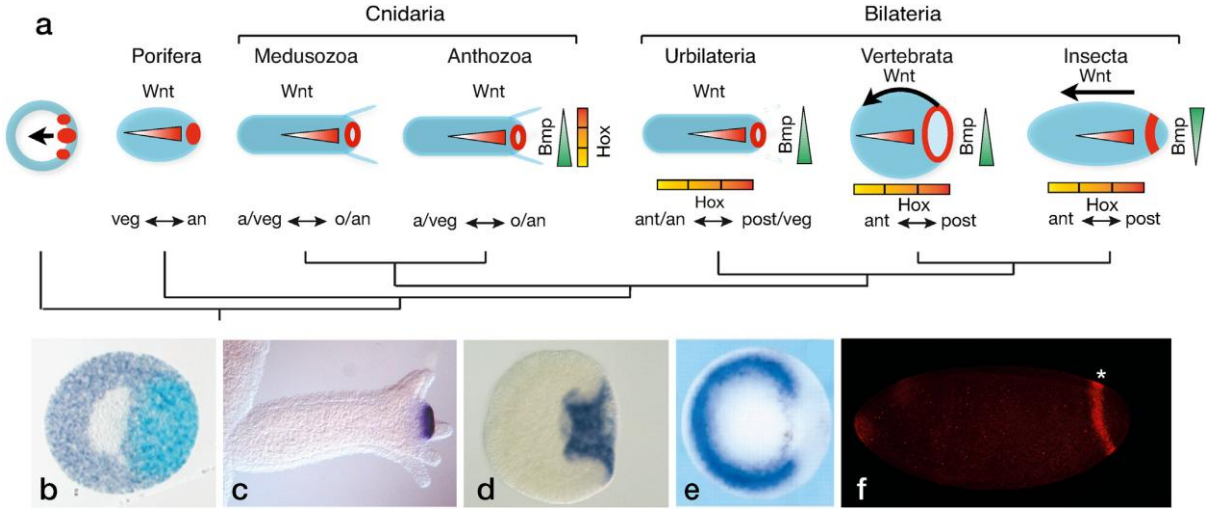

Figure 2. Adapted from Holstein, 2022, Figure 8. The AP and DV body axes in various metazoan species are associated with Wnt and BMP gradients. (b) Amphimedon. (c) Hydra. (d) Nematostella. (e) Xenopus. (f) Drosophila.

Other secreted factors, such as Fgf and Hh, are consistently found to be relevant to the formation of body axes or the axis of specific organs (Bökel & Brand, 2013;Ornitz & Itoh, 2015;Briscoe & Thérond, 2013;Ingham & McMahon, 2001).

Parasteatoda tepidariorum: early development and body axes formation

Chelicerates are a group of arthropods and sister to other arthropods like insects, crustaceans and myriapods (Schwager, Schönauer, et al., 2015). These invertebrate animals include horseshoe crabs, ticks, scorpions, spiders, and others. During the development of spiders, some horseshoe crab species, and certain tick species, a special process occurs in which a cluster of cells migrates to determine the future body axes (Hilbrant et al., 2012) .

There has been extensive research on the development of *Parasteatoda tepidariorum* (*Pt*, common house spider) (Akiyama-Oda & Oda, 2003; Hilbrant et al., 2012; Holm, 1952.; Mittmann & Wolff, 2012) (supplementary Figure 1, left half from Mittmann and Wolff, 2012 and right half from result in this thesis). The early development and formation of AP and DV axes of the animal has been well understood at the morphological level.

In Pt embryos, the first few nuclear mitoses occur at the center of the egg, which is spherical in shape and contains a large quantity of yolk. Cellularization occurs by the 16-nuclei stage. At the 16- or 32-

nuclei stage, the energids move to the surface of the egg (Kanayama et al., 2010; Mittmann & Wolff, 2012).

More cell divisions occur, and at some point, the majority of the cells condense into a smaller volume in a coordinated manner, moving away from the location of the polar body and forming the germ disc (Pechmann, 2016; Wang & Pechmann, 2024.).

The center of the germ disc shows a higher cell density and will develop into the blastopore, also known as the "primary thickening region", which will later become the posterior side of the animal (Figure 3b, pt and "P" region). The remaining minority of cells are located near the polar bodies, where they become flat and thin, giving rise to the future extraembryonic region (Figure 3a, yellow region with red dots).

The primary thickening region (Figure 3b, pt) is the first multicellular region of the animal. A group of motile cells are generated within this region, moving toward the rim of the germ disc. This group is referred to as the cumulus (Figure 3a, cu). The portion of the germ disc through which the cumulus cells pass will open up and form the future dorsal region of the animal (Figure 3a, df; Figure 3b, "D" region). Cells on the two sides of this region move in opposite directions to form the germ band (Figure 3b, stage 6 and stage 7). The rim cells on the opposite side of the cumulus migration path will become the future anterior region (Figure 3b, "A" region). The remaining cells of the germ disc are in a "default" state, developing into the ventral tissue at this stage (Figure 3b, stage 8, "V" region). Through this process, the radially symmetric germ disc converts into a bilaterally symmetric germ band (Prpic & Pechmann, 2022).

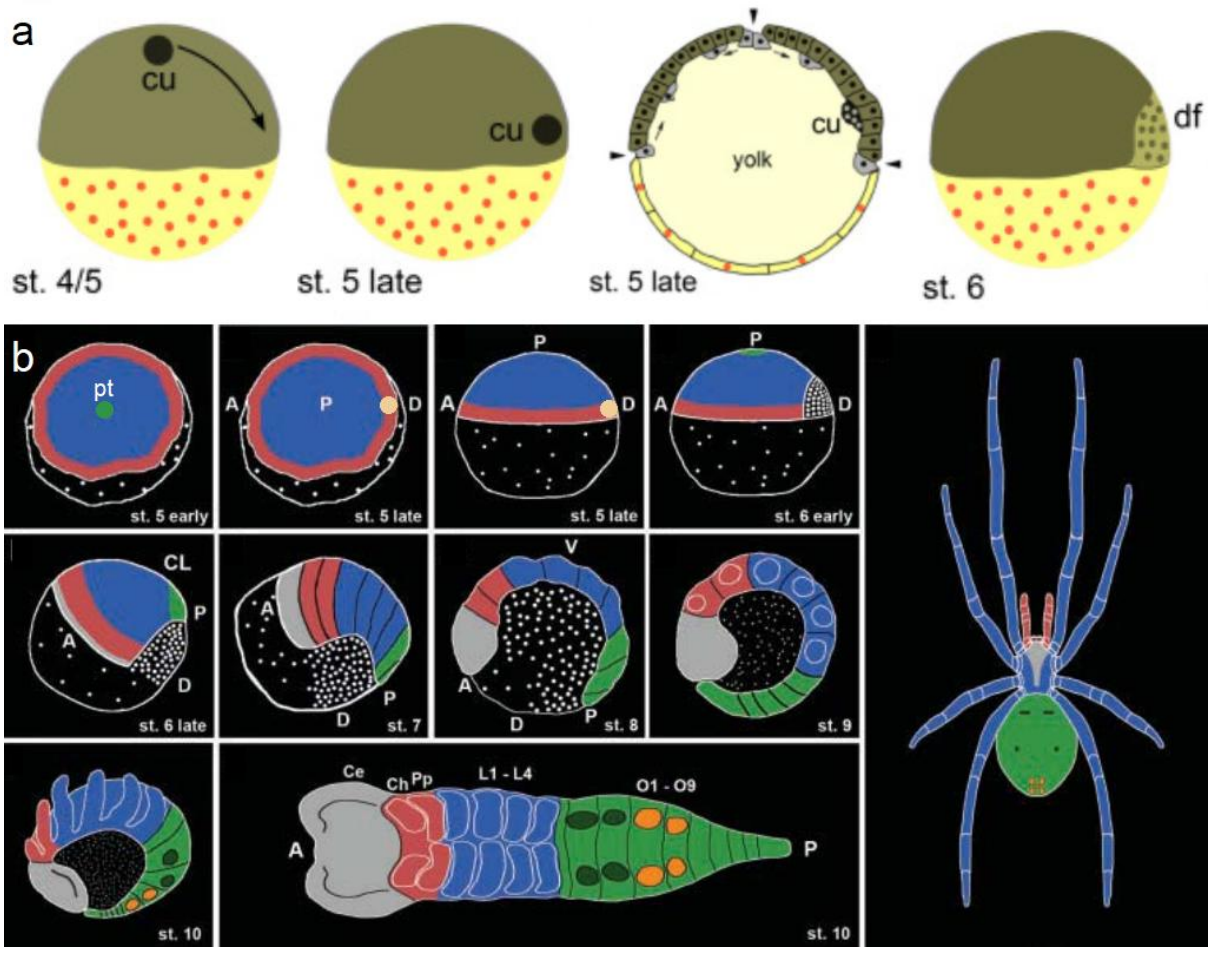

Figure 3. Schematic image to illustrate the development of the spider Parasteatoda tepidariorum. (a) Figure 1 from Prpic and Pechmann, 2022. Major developmental processes at germ disc and early germ band stage in the

spider Parasteatoda tepidariorum. Cumulus located beneath the ectoderm and migrate at stage 5 through a radius of the germ disc, and eventually promote the establishment of DV axis. The figure also illustrates the gastrulation and movement of certain germ disc cells (arrow head), which will not be mentioned in this part. Cu (black dot): cumulus. Df (Green region with green dot): dorsal field. Hl: head lobe. Region in green: Embryonic region, or germ disc at this stage. Yellow region with red dot: Extraembryonic region. Region in bright yellow: yolk. (b) Modified after Figure 4, McGregor et al., 2008. A: Anterior, P: Posterior, D: Dorsal, V: Ventral. Pt (green dot): primary thickening region. Yellow dot at late stage 5: cumulus. CL: caudal lobe. Ce: cephalic lobe. Ch: Chelicerate. Cp: pedipalpal segment. L1-L4: leg bearing segments 1 to 4. O1-O9: opisthosomal segments 1 to 9. Region in grey: head parts. Region in red: cheliceral and pedipalpal-bearing segments. Region in blue: leg-bearing segments. Light green: primary thickening region at stage 4, opisthosomal segments since stage 6. White dots: Extraembryonic cells, and dorsal field cells.

The cumulus function as an "Organizer"

Animals with a completely damaged primary thickening region will not form the DV axis; instead, they form a radially symmetric tube structure with ventral gene expression (Oda et al., 2020).

Moreover, in some transplantation experiments (Figure 4), twin spiders could be produced by adding ectopic cumuli at the proper positions (Holm, 1952; Oda et al., 2020;Pechmann, 2020). This suggests that cumulus cells can independently induce the differentiation of surrounding cells and are capable of generating the dorsal-ventral axis. Therefore, cumulus cells are considered to have characteristics similar to the 'Organizer' in frogs.

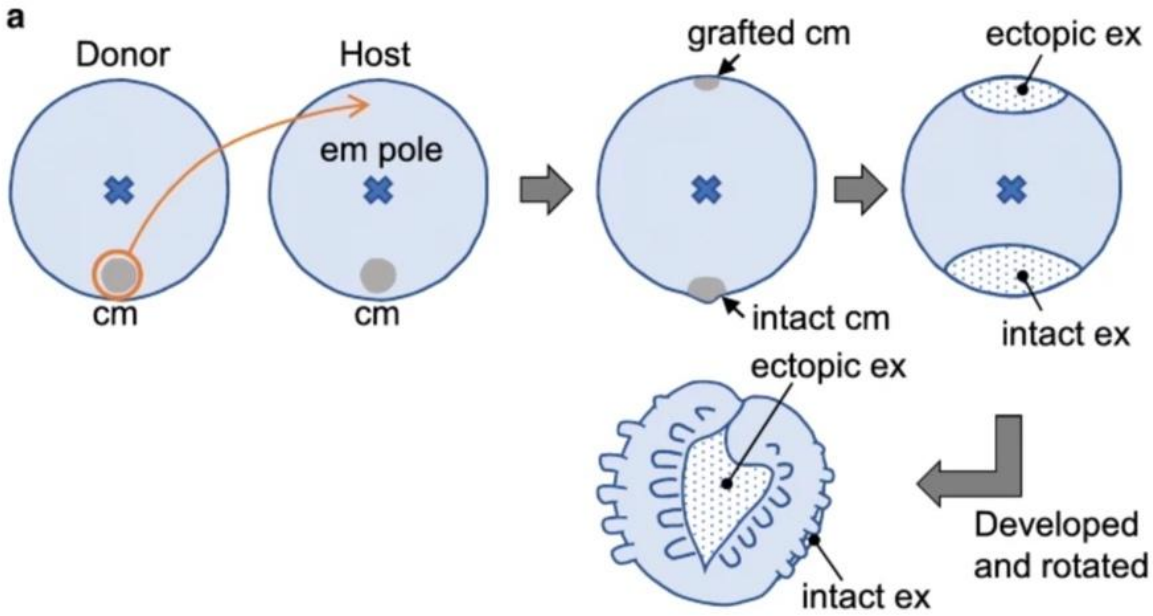

Figure 4. From (Oda et al., 2020). Transplantation experiment of cumulus cells demonstrates that cumulus cells can function as an 'organizer' to induce the differentiation of neighboring cells and establish the body axis. Cm: Cumulus cells. Em pole: Embryonic pole, previously the primary thickening region, and the future posterior region of the embryo. Ex: Extraembryonic region, also the dorsal field in this image.

Published key factors in Parasteatoda tepidariorum axes formation.

During the development of *Pt*, from stage 3 to stage 4, the genes *dpp* (*Bmp*), and *fgf8* are expressed in the primary thickening region (Akiyama-Oda & Oda, 2003; Wang et al., 2023). *hh* is expressed in the rim cells of the germ disc (Akiyama-Oda & Oda, 2010). At stage 5, *dpp* are expressed in the moving

cumulus cells. *Fgf8*, on the other hand, is expressed in an asymmetric region in a highly dynamic manner, with considerable variability between samples (Figure 6 B).

Wnt8b is the only *wnt* gene in Pt that show expression at germ disc stage (Janssen et al., 2021). However, previous publications mainly focus on its role in later developmental stages. Experiments show that the loss of the *Wnt8* gene causes defects in the posterior region after germ band formation (McGregor et al., 2008). The knockdown of *hh* shows contraction of the germ disc, a loss of anterior gene expression. Additionally, Hh signaling controls body axis segmentation through regulation of Msx1 (Akiyama-Oda & Oda, 2020). In summary, the key genes involved in axis formation in *Pt* resemble those in most other animals in general, but differ in their details (Figures 1 and 2).

The absence of the genes *dpp* (Akiyama-Oda & Oda, 2006), *ptc* (Akiyama-Oda and Oda, 2010), and *fgf* leads to defects in DV axis formation, result in tube-shaped structures in varying proportions (Figure 5, row "RNAi phenotype"). Additionally, a high proportion of *Ets4* RNAi embryos form radially symmetrical tube structures and lack a DV axis. *Ets4* (also known as *Spdef* and *Ets98B*), shows expression in the primary thickening region at stages 3 and 4, and in the migrating cumulus at stage 5 (Figure 5, column "Ets4"). It is a transcription factor, also considered to regulate the expression of *twist* and *hunchback* (Figure 5, row "Ets4 RNAi St.4";(Pechmann, 2017).

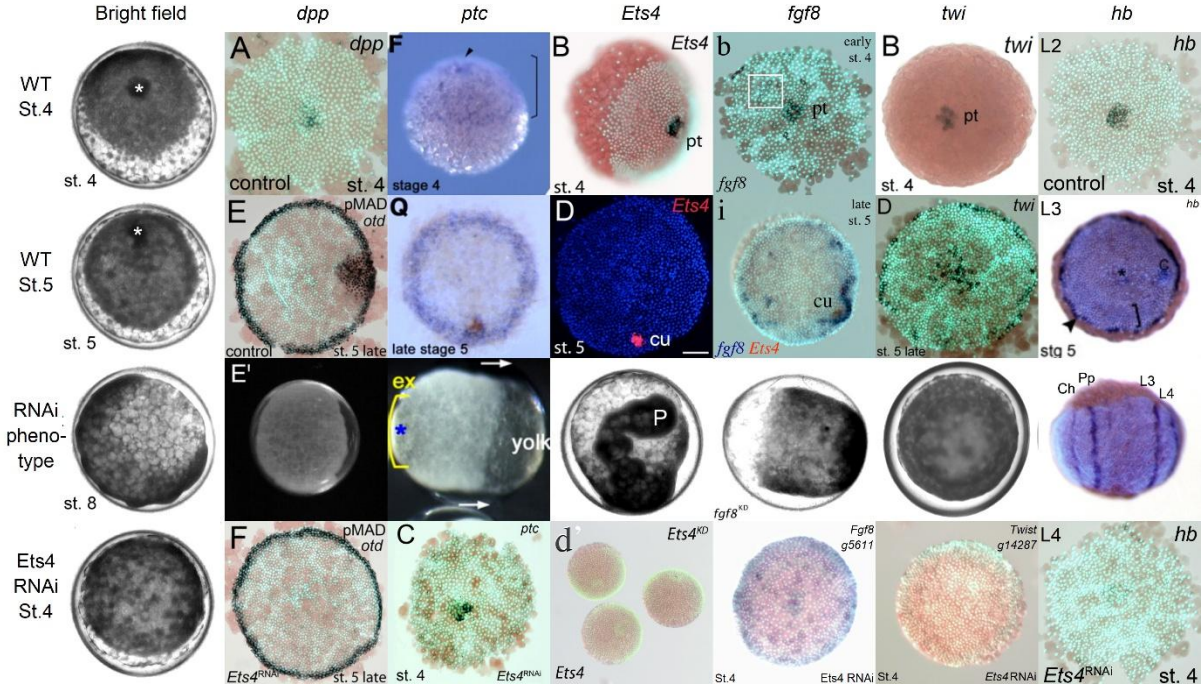

Figure 5. Expression of *dpp, ptc, Ets4, fgf8, twist, hb* at stage 4 and stage 5 in WT embryo, at stage 4 in Ets4 RNAi, and the phenotype of *dpp* RNAi, *ptc* RNAi, *Ets4* RNAi, *fgf8* RNAi, *twi* RNAi (Result Chapter IV of this thesis) as well as *hb* RNAi. Other Image were from Akiyama-Oda and Oda, 2006; Schwager et al., 2009; Pechmann, 2017).

Notably, the genes that exhibit a knockdown phenotype resulting in tube formation (*dpp*, *ptc*, *Ets4*, *fgf*, *twi*) all show expression in the primary thickening region at stage 4 in WT embryos (Figure 5, row "WT St.4"; Figure 6 A). And the tube-shaped embryos from these RNAi experiments express ventral marker gene *sog* ubiquitiously (Figure 6, C).

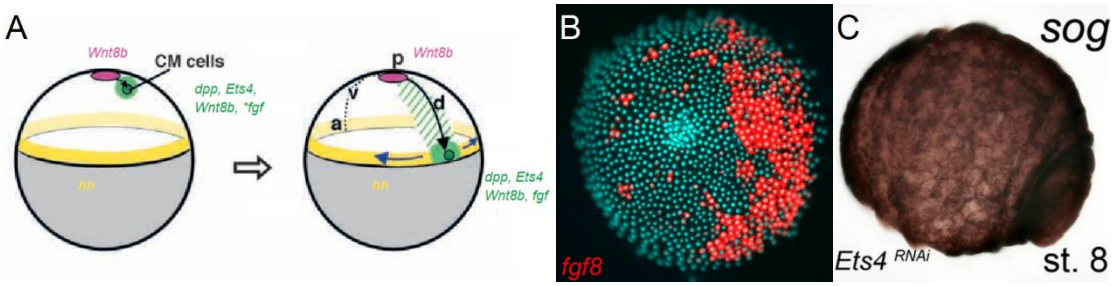

Figure 6. Key factors of the cumulus migration process. A: *dpp* and *Ets4* are expressed in cumulus cells. *Wnt8b* is expressed in the center of the germ disc and in cumulus cells. *Fgf8* is expressed in the ectoderm cells ahead of cumulus cells as they approach the rim. The image is modified after Figure 8 in Akiyama-Oda and Oda, 2003. B: Expression of *fgf8* in the germ disc at the beginning of cumulus migration. From Wang et al., 2023. C: *Ets4* RNAi embryos show no DV axis formation and develop into tube-shaped structures at later stages. The ventral marker gene sog is expressed in most regions of the embryo. From Figure 3, Pechmann et al., 2017. Similar phenotypes were observed in dpp RNAi, ptc RNAi, and fgf8 RNAi embryos.

Although the *Ets4* gene is found in other animals, it is not regarded as the primary developmental factor. It contains an Ets domain and belongs to the Ets transcription family (Hollenhorst et al., 2011; Wei et al., 2010). Genes from this family appeared early in evolution and are typically involved in the formation of specific organs (WASYLYK et al., 1993). In mice and flies, Ets family genes are implicated in controlling/regulating cell adhesion and cell movement processes. Recent studies also suggest that genes with the Ets domain may be associated with the longevity of multiple species (Dobson et al., 2019).

There are a few examples of genes with the Ets domain that function in early developmental stages. In Hydra, Ets-related transcription factors are expressed in the head region and are considered part of the pioneer transcription factors involved in establishing head patterning (Reddy et al., 2020). Another example is in sea urchin, the maternally expressed Ets4 is considered a major determinant in regulating early-expressed genes and may trigger the onset of zygotic transcription along with its downstream targets (Marlétaz et al., 2023).

Aim of the thesis

This thesis aimed to get a better understanding for the role of Ets4 in the early development of spiders, how and why it influenced the establishment of the animal body axis, and whether there were underlying general principles guiding these observations.

To achieve this, in this thesis, I began with a comparison between WT and *Ets4* RNAi embryos, focusing on morphological qualities, as well as gene expression in the primary thickening and cumulus regions. RNA-seq and in situ hybridization were employed to identify potential downstream genes of Ets4, followed by further investigation using RNAi for selected genes to explore their functions.

Based on the current findings, *Ets4* and its potential downstream genes were likely to influence the process of primary thickening formation (gastrulation/invagination) and cumulus migration by regulating cytoskeleton, cell adhesion, and cell movement functions. The differential expression of *Ets4* in cells, could represent an early sign of asymmetry in the radially symmetrical germ disc, which leads to the asymmetric expression of *fgf8* genes in germ disc cells. This asymmetry in turn guided the orientation of cumulus migration in subsequent stages. Many developmental genes, including those from the Hh, Wnt8b, and Dpp pathways, were regulated either directly or indirectly by Ets4. The

movement of the cumulus resulted in the division of the germ disc into several regions, with cells in each region receiving varying types and amounts of signaling. As a consequence, the AP and DV axes of the animal were primarily established, leading the animal into a bilateral period.

In addition, a more detailed description of *Pt* development from 11 to 41 hours after embryo laying (Hael) was provided, and I collected a reliable list of gene expressions in the primary thickening region at stage 4, which could be useful for further investigation.

2 Material and Methods

1. Animal culture

Parasteatoda tepidariorum (common house spider) were cultured in plastic vials with soil at 18°C in a day-night cycle of 12-12 hours in the lab. They were fed once a week with fly (Drosophila melanogaster, wingless) or cricket (Gryllus bimaculate, fed with fish food). Each cocoon contained around 100-400 embryos. Observation of the embryos were under Dissection Microscope (ZEISS) and embryos were placed on Halocarbon oil (H8898-80ml, Sigma). Developmental embryonic stages were classified in reference to (Mittmann and Wolff, 2012).

Long-lab culture could cause problem in development of part of the progeny. It was tested to keep spiders in cold temperature (4°C) for three months to mimic natural winter condition. But the embryos of the offsprings were not significantly improved. In addition, local spiders were crossed with the ones from other labs (Munich lab and Gießen lab) and from the wild, which proved to be very effective.

In cases of mite pollution in the batch, spiders were switched to clean wells. The old wells were frozen for more than 2 days, cleaned, and put into incubator at 65°C for more than 2 days before use.

It was observed that spider embryos could develop in PBS (under the surface) till stage 13, but they would not hatch in liquid.

2. Fixation method

2.1 Embryo fixation for in situ hybridization and HCR staining

Traditional fixation. Embryos were dechorionated in glass dish by dripping 100% Klorix. After several minutes, klorix were removed and the embryos (floated in klorix before) were washed with ddH_2O once. Then they were transferred into a scintillation vial containing the fixative (3.5 ml PBS +0.5 ml 37% formaldehyde + 4 ml heptane), and the fixation lasted for several hours to overnight at RT on the shaker. The fixative was later removed as complete as possible and the embryos were washed with PEMT, 80% PEMT-20% MeOH, 60% PEMT-40% MeOH, 50% PEMT-50% MeOH, and 25% PEMT-75% MeOH for 5 minutes in each medium. PEMT could be replaced by PBST. The embryos were transferred to Eppendorf tube and incubate in 100% MeOH for 30min at RT, and later store at -20°C. Remove the vitelline membrane with forceps and needles, and the embryos were ready for in situ hybridization.

Heat fixation. The idea was firstly used in other organism and relatively new in spider research. Embryos were dechorionated in glass dish by dripping 50% Klorix. After 1-2 minutes, all the Klorix were removed and the embryos (sank in klorix before) were washed with ddH_2O once. Then they were transferred into Eppendorf tube with only 50µl of H_2O left. Set the electronic incubator to 95-99°C and drop H_2O in one well of the incubator. Put the Eppendorf tube in that well for 90 seconds and immediately put the tube on ice for 60 seconds. Add MeOH to the Eppendorf tube and put the tube back on ice. The embryos could be stored in MeOH at -20°C for months. Before use, the vitelline membranes were removed, and the embryo were fixed in 50% PBST- 50% formaldehyde for at least 2 hours in room temperature on wheels. After the fixation, the embryos were washed in PBST, 80%

PBST-20% MeOH, 60% PBST-40% MeOH, 50% PBST-50% MeOH, and 25% PBST-75% MeOH for 5 minutes in each medium. And the embryos could be directly used for in situ hybridization or stored in -20°C. I also tested to fix first and remove the vitelline membrane later, that still worked, but with many scratchy backgrounds.

In most in situ hybridization experiments in this thesis, *P. tepidariorum* embryos before stage 7 were fixed in heat fixation method, and late-stage embryos were fixed in the tradition fixation method.

In HCR staining, only heat fixed embryos were used. But not followed by formaldehyde fixation, embryos were fixed in Clark fixative for 1 hour. Longer time was tested, and 1 hour seems to be the optimal.

2.2 Embryo fixation for antibody staining

Traditional methods. First steps were the same as steps in the traditional fixation method for in situ hybridization, just use EtOH instead of MeOH to reduce background in antibody staining.

New methods. First steps were similar to the early steps in the traditional fixation method for in situ hybridization. Instead of show shaking in fixative overnight, rigorously shaking the embryos in fixative for half an hour to one hour. Later, gradually change the medium from PEMT or PBST to EtOH as the traditional methods. The latter methods seemed to have higher sensitivity than the former one in early-stage embryos.

3. Primer list

	gene	number	sequence	start	stop
AP-1	Rab7a	g23439 Fw	TGG AGA CTC AGG TGT TGG AAA G	304	325
		g23439 Rev	TGG CTA ATG CCA GCG ATA AAC	1954	1934
		g23439 T7Fw	G TAATACGACTCACTATAGGG TCT ATC GAG GTG CAG ACT GC	492	511
		g23439 T7Rev	G TAATACGACTCACTATAGGG TTT ACC AAA TGC CAT CGA ACC AA	1330	1308
AP-2	uncharacterized	g6152 Fw	CGA TGC TCA AGT GCA GAA CC	265	284
		g6152 Rev	TTT GGC TAG GAG CTG CGG TA	1371	1352
		g6152 T7Fw	G TAATACGACTCACTATAGGG CCC TCC TTT TGC TAA TCT CGC	299	319
		g6152 T7Rev	G TAATACGACTCACTATAGGG TCT TTG GGT GAC AGT GTT GGA	1207	1187
AP-3	uncharacterized	g16318 Fw	CTA CAA AAA TCC GTG GCG AAA TTC G	9	33
		g16318 Rev	ATA TCC AGT CTT CAG GAG AAC TTG G	665	641
		g16318 T7Fw	G TAATACGACTCACTATAGGG GAA AAT TTC CCC TTA CAC GTT GAG	49	72
		g16318 T7Rev	G TAATACGACTCACTATAGGG CAG GAG AAC TTG GAA TGA ATG CAA G	653	629
AP-4	dopamin receptor 2	g16752 Fw	CAG TGG CAA GAG AGC CCT AC	56	75
		g16752 Rev	ACA ACT TGG CGA AAT CTG CG	1031	1012
		g16752 T7Fw	G TAATACGACTCACTATAGGG TCA TAG CGT CTC TTG CCA CG	98	117
		g16752 T7Rev	G TAATACGACTCACTATAGGG ACG CGT ATA TCA CGG GGT TC	937	918
AP-5	Mid1ip1	g22926 Fw	AAC GCC CTA GGC GAT TGT C	103	121
		g22926 Rev	CAG AGG CTG CTT CGA TTT CC	906	887
		g22926 T7Fw	G TAATACGACTCACTATAGGG TGG ATT TGT GAA GCC ACC TCA	128	148
		g22926 T7Rev	G TAATACGACTCACTATAGGG CTG CTT CGA TTT CCT CCT GGT	900	880
AP-6	BTB/POZ and MATH domain -containing protein 4	g23307 Fw	GGC GTT TTT CGA ATT CCT CCG	261	281
		g23307 Rev	ATC CCG ATG TTG GTC TGC AA	1096	1077
		g23307 T7Fw	G TAATACGACTCACTATAGGG CTC CGA CCA CTT CAT CGC T	277	295
		g23307 T7Rev	G TAATACGACTCACTATAGGG GGA ACC TCA TAC CTG ACG GC	999	980

Twist	Twist	Twist for 1	CGA CCG AGA AAA AGG AAG CG	246	265
		Twist rev 1	GGG TGT CTT TGA GAT GCC CA	1159	1140
		Twist rev 2	TAA TAC GAC TCA CTA TAG G CCA AAC CAT GGC TCA GGA CA	1038	1019
Ets4	Ets4	Ets4 T7 Fw	G taa tac gac tca cta tag gg gta gtc ttg aac ttc agt tat c		
		Ets4 T7 Rev	G taa tac gac tca cta tag gg gtc tga agt aat ctt ctg ata g		

1	g22384.t1	g22384 Fw	GTA CTA AGT GCC AAT TCA GCG G	16	37
		g22384 rev 1	GAG CAA AAT ACA TCA CAC GAT AAT G	482	512
		g22384 rev 2	G TAATACGACTCACTATAGGG CAC GAT AAT GTT CAC AAT ATA ACA G	470	446
2	g27753.t1	g27753 Fw	GTC TAT CAA ATC GGA CAA CTG AG		
		g27753 rev 1	GTA GTT ACA AAT AAG GTT CTT GGT C	921	902
		g27753 rev 2	G TAATACGACTCACTATAGGG GCC ACA TCT TGG GCT TAT CCT	916	896
		g27753-T7Fw	G TAATACGACTCACTATAGGG CAG TTG TTC CAT TTA CAG AGC C	140	161
3	g6760.t1	g6760 Fw	GGT GGA AAC TAG CTC TGG GC	229	248
		g6760 rev 1	GGC GAG AAA CAA TGA TGG GC	1435	1416
		g6760 rev 2	G TAATACGACTCACTATAGGG CAA CCT CGG CAG AGT TGT CT	1373	1354
4	g5179.t2	g5179 Fw	GAC TGT GGT GAA GGG GAC AG	1240	1259
		g5179 rev 1	TCC ATG TCA ATC CCC GCA AA	2378	2359
		g5179 rev 2	G TAATACGACTCACTATAGGG AGC TGA TCG CAC AGC TTC AT	2270	2251
5	g9727.t1	g9727 Fw	AGA TGG TTT AAA CTC TGC GGA A	9	30
		g9727 rev 1	AAA GCT TTG CTC CGG ATA TCT T	1000	979
		g9727 rev 2	G TAATACGACTCACTATAGGG ACA GTT CAC TGA GTC ACA TTT GC	976	954
		g9727 T7 Fw	G TAATACGACTCACTATAGGG CTC TGC GGA AAT TGC GAT TTA TG	21	43
6	g15186.t1	g15186 Fw	ACT TTA ACG GGG GTT TCC CTT	20	40
		g15186 rev 1	ACG ATG TCT GCA GCA CAA GA	937	918
		g15186 rev 2	G TAATACGACTCACTATAGGG CTC ACC AAC CCA CTG ACC AA	896	877
		g15186.t1 Fw-2	CGG TTC CAC CAA GTG AAG AAG T	154	175
7	g17398.t1	g17398 Fw	CGC GTA GAA AGT GTA AGT TTC	3	23
		g17398 rev 1	GAA CAC TTT GAA AAC ATG ACA CG	733	755
		g17398 rev 2	G TAATACGACTCACTATAGGG CTT TGA AAA CAT GAC ACG TGA G	729	750
8	g4731.t1	g4731 Fw	TCT TCA GAT CAG GTC CGG CT	139	158
		g4731 rev 1	CTG TGG GAT CTT CCT GCA CC	1250	1231
		g4731 rev 2	G TAATACGACTCACTATAGGG CGG TGG TAG GAG TGT CAG GA	1222	1203
		g4731-T7 Fw	G TAATACGACTCACTATAGGG CTG CTG AAG AGT ACA GAC AGC TC	432	454
9	g19992.t1	g19992 Fw	CAC CAG TGC AGA AAG ACA TA	33	52
		g19992 rev 1	TGT TCC CTG CAA TGA TCT TG	995	976
		g19992 rev 2	G TAATACGACTCACTATAGGG CTG TAA GCT TCT GGT TGA TAT TG	900	878
		g19992-T7Fw	G TAATACGACTCACTATAGGG GTT GAA CGT GAT ACG AGA AAA TTC	105	128
10	Itpka	g11911 fw	CTT CGC ACA TCA CTT CAG TTA G	69	90
		g11911 rev	TCA CAG ATA GTG AAA GGA CAC GA	1416	1394
		g11911 T7-rev	G TAATACGACTCACTATAGGG GAG TGA TGC TTA CAC CTT CTG GT	1255	1233
		g11911-Fw-2	GTC AAC AAG GCT TGC CCT GAT	427	447
		g11911-T7Fw	G TAATACGACTCACTATAGGG CTT ACC CTT CTG CAG CTA TTG GC		
11	Peter Pan/SWI 4	g760-2 fw	GCT CTA CTC ACA GCA GTA CAC A	51	72
		g760-2 rev	ACT GGC GTA TAG CAC TTT TCT CA	1157	1135
		g760-2 T7-rev	G TAATACGACTCACTATAGGG TCT CAG AAG CTA TGT TCC CTC T	1139	1118
12	proline rich protein 4	g11258 fw	GCA CTA CGT TCC CGT ACC AA	363	382
		g11258 rev	TCT TGT CTT CAC CAA CGC CA	1642	1623
		g11258 T7-rev	G TAATACGACTCACTATAGGG CAC CGG TGG GAT CAA GTT CT	1582	1563
13	dynamin-1	g12002 fw	GAG GGA AAG GAC CAT TGG AGT	700	720
		g12002 rev	GCA GCC AAT TGC AAC ACC TT	1900	1881
		g12002 T7-rev	G TAATACGACTCACTATAGGG TCG CTG TTG AGT TCT CCC AA	1853	1834
		g12002 T7-fw	G TAATACGACTCACTATAGGG GGT GTG GTG AAT AGA AAT GAC ACT G	806	830
14	protein lethal (2) essential for life	g14129 fw	CAC GCT GTT TCC ATG GTA A	8	27
		g14129 rev	GAC AAC ATA ATG CTT TAT CAC AGG	841	819
		g14129 T7-rev	G TAATACGACTCACTATAGGG CAG GTA TTA TAA TTC CAA ACG GG	838	861
		g14129 T7-fw	G TAATACGACTCACTATAGGG GGA GAA AAT TCT GGA TAA CAG C	38	59
15	RF_0381	g1767 fw	AGC AGT GCA ACA TTT TCA CGA	113	133
		g1767 rev	TGT TTC GCC TTC ATC CCA CA	1175	1156
		g1767 T7-rev	G TAATACGACTCACTATAGGG CAG GAT GCC AGC ATC TCG AA	1110	1091
		g1767 T7-fw	G TAATACGACTCACTATAGGG GAAGGTGTTTCACCAGACGAACC	180	202
16	Ras related protein Rab34	g10703-2 fw	GTT TCA AAA TGT GAA ATG CTC AGG C	7	28
		g10703-2 rev	AGC CTC ATT TTC TGT CAA TT	420	401
		g10703-2 T7-rev	G TAATACGACTCACTATAGGG GTC AAT TTA TAA GCA GAA TTC GC	407	385
17	autophagy related protein 8f	g18439 fw	TTG GGT CTC AAT CTT CAA CC	6	25
		g18439 rev	TCA TTT TTC ATC ACC ATT GAA GG	691	669
		g18439 T7-rev	G TAATACGACTCACTATAGGG ACC ATT GAA GGA TTT TTT GGA TG	679	657
		g18439 fw-2	CCG CCA TGC TGT AAC TAA TAC	147	167
18	DRG1	g23069 fw	GAT GGC CAG AAC TCA GCG TA	165	184
		g23069 rev	CCT CCG CCG GAA TCT CTT TC	1245	1226

		g23069 T7Rev	G TAATACGACTCACTATAGGG CAG ATG AAC CCC AAA CTA AAG CA	1147	1125
19	ZIC-4 (opa)	g12202 fw	TGA ACC ACT TCT CCG TGG AC	167	186
		g12202 rev	TGA GAC CCC GTC AGA AGA CA	1357	1338
		g12202 T7Rev	G TAATACGACTCACTATAGGG ACA GGA TTC GGA ACT GGA GC	1304	1285
		g12202 T7Fw	G TAATACGACTCACTATAGGG GAG TCC AGG TCA CCA AGC TAA C	216	237
20	ADGRL1	g9493 fw	AGC CAA TAT TTA TGG GCA GAA TGC	1353	1376
		g9493 rev	GCG AGA CCA TAG TAC CAG GC	2378	2359
		g9493 T7Rev	G TAATACGACTCACTATAGGG AAG GCC CAA CAG ATG GTA GC	2294	2275
21	uncharacterized	g20989 fw	CTC TGA TAT TGC GCC TCA GTG G	8	29
		g20989 rev	GTA ATA TTT CGT GCT CAG GCA CAG G	684	660
		g20989 T7Rev	G TAATACGACTCACTATAGGG AGG CAC AGG AAC CAT TGA AGG	668	648
		g20989 T7Fw	G TAATACGACTCACTATAGGG GCC TCA GTG GTT AAT GAC CAT G	20	41
22	ZFPL1	g6237 fw	CAT ACT CCG GAA GTC CGA TGA	226	246
		g6237 rev	GCC ATC CCT TGA ACA CAC TG	1348	1329
		g6237 T7Rev	G TAATACGACTCACTATAGGG TCG AAG ACG ACG AAG TGC TG	1292	1273
23	ZNF423	g14296-2 fw	CCC TTA TCT GAT GCG GAT GCT	222	242
		g14296-2 rev	GCG GTA AGG GAT AGG TCG TC	1294	1275
		g14296-2 T7Rev	G TAATACGACTCACTATAGGG GTG CAG ACG GGC TCA TTA CT	1252	1233
		g14296-2 T7Fw	G TAATACGACTCACTATAGGG CTC CTA CAC GAT TGG GGT GAC		
24	uncharacterized	g3789 fw	AAT TAT ATC CCG TCC CGC ACA	77	97
		g3789 rev	TTC GCG ACA AAG AAT CAG CC	1177	1158
		g3789 T7 Rev	G TAATACGACTCACTATAGGG GGC ATT TAG ACG ACC GGG TA	1155	1136
25	uncharacterized	g1978 fw	GAG CTG GGA TTG GAT AGA TCT GG	5	27
		g1978 rev	CTC CAA TCC AGC ATA GTT TGC AC	592	570
		g1978 T7Rev	G TAATACGACTCACTATAGGG CCA GCA TAG TTT GCA CTT TGA TCT T	585	561
26	uncharacterized	g4422 fw	GGT GTA AAG CGA TGG ACT TCC T	59	80
		g4422 rev	CCT TCG TCT TTA CGG CAT CTT C	898	877
		g4422 T7Rev	G TAATACGACTCACTATAGGG AGG AGC AAC TTT AGA GGC CAA	858	838
		g4422 T7Fw	G TAATACGACTCACTATAGGG GGC TTG TTG GCC AAT GGA AAA		
27	uncharacterized	g9731 fw	AGT GCA GTT AAA ATT TTC CGA ACC T	33	57
		g9731 rev	ACA TTC ATC GTT CTT CAA AAA GCA	939	916
		g9731 T7Rev	G TAATACGACTCACTATAGGG TCA AAA AGC AAA ATC CTA TGG GTC	925	902
		g9731 T7Fw	G TAATACGACTCACTATAGGG GGT CAA CTC TAC TCC TTC TAT TTG		
28	uncharacterized	g592 fw	TGG TGC AGT GCT TTA AGT ATG G	32	53
		g592 rev	GTG CAC GTG AAT GCT CTA TTC T	1019	998
		g592 T7Rev	G TAATACGACTCACTATAGGG TCC AAT ATC TTT GAG GCA GCG	984	964
		g592 T7Fw	G TAATACGACTCACTATAGGG CAC TGG GAA ACC TTT GCC AC		
29	uncharacterized	g1983 fw	GTG AAG AAA AGG ATA CCA CAA AGC	124	147
		g1983 rev	GCA TTC CTC ATG AAA GTA AAG TCA C	698	674
		g1983 T7Rev	G TAATACGACTCACTATAGGG CAC TTT TTT CAG CAG ACA TCA AAC	676	653
30	uncharacterized	g22667 fw	TGG AGC ATT CAT AGC AGG TGT	46	66
		g22667 rev	AGC TCC TCT ACG TGA TCC TT	968	949
		g22667 T7Rev	G TAATACGACTCACTATAGGG AAC TGT ACC AGT AGT CGC AGG	874	854
		g22667 T7Fw	G TAATACGACTCACTATAGGG GGC TTG TTG GCC AAT GGA AAA		
31	BMP10	g16925 fw	AGC GTC TTT ATA CTG AGT GGT CA	255	277
		g16925 rev	ATC GAC ATC CAC AGC TAC TTG C	1160	1139
		g16925 T7Rev	G TAATACGACTCACTATAGGG TCG TCT GAG TCA TCG AAC AAC A	1104	1083
32	ptc	g14374 fw	CTA CGA CCC GAC AGC GAT TT	99	118
		g14374 rev	ATG GAG CAA CAA CCC AGT CC	1381	1362
		g14374 T7Rev	G TAATACGACTCACTATAGGG AAC ACC TGC CAC TCC AAT CC	1334	1315
33	Wnt8b	g5617 fw	TGG AAT CAG CAG CAT GGT CTC	693	713
		g5617 rev	TGC ATT TAA CAT CGC AAC ACC A	1628	1607
		g5617 T7Rev	G TAATACGACTCACTATAGGG GCA TTT GCA GAC ACT CTC CAC	1597	1577
		g5617 T7Fw	G TAATACGACTCACTATAGGG GCA GCA GAA AGA GGT ATG GAG G	776	797
34	INTS2	g26532 fw	TGC TGT GCC GAT TAG TTG CT	474	493
		g26532 rev	GGT CGC TGG CCA AAA TTG AT	1865	1846
		g26532 T7Rev	G TAATACGACTCACTATAGGG GCC TGG TAA AAC TGG GTG GA	1588	1569
35	ABHD11	g9721 fw	GTG AGA TTG AAT TCA CCA CAA TTG C	4	28
		g9721 rev	CAG GCA AAT CTT AAA TTC CAA TCA C	1101	1077
		g9721 T7Rev	G TAATACGACTCACTATAGGG CAT GAA GAA TTG TTT CAC ACA GAG C	908	884
36	ABHD11	g9726 fw	AGC TGC TTG GGA GTT TGG TA	42	61
		g9726 rev	CAT TGC AGC TTT GCT TAG TGA GC	990	1012
		g9726 T7Rev	G TAATACGACTCACTATAGGG GAC AGC GTT GAT TTT CTC TCC	919	939
37	ABHD11	g9729 fw	AGG AAA CTT TGT GAA GTC TTG CAG	16	39
		g9729 rev	GCT CTT GCT AAT TTC ACT GGC	945	925

		g9729 T7Rev	G TAATACGACTCACTATAGGG GAA CCT CCT TCA AAC TCA ACG A	890	869
38	ABHD11	g23929-2 fw	GCT CTA GAA GAC CTA GAG AAA CAC C	775	799
		g23929-2 rev	CGC CAA TTG TCT TAG CCA GTT CA	1657	1635
		g23929-2 T7Rev	G TAATACGACTCACTATAGGG CTC AGC AAC AAA AAT GTG TGA TCC	1626	1603
		g23929-2 rev-2	TCA GCA GGC ATC TCA GCA AC	1637	1618
39	ABHD11	g3607 fw	GGC TAG AAG CGT AAG TTT TCA TCA C	61	85
		g3607 rev	TAG GAC TAC ACG AGT TTA CTG G	1074	1053
		g3607 T7Rev	G TAATACGACTCACTATAGGG CGG TTG TAG CTC TGC ATT TGG	865	845
40	Ppaf2	g3137 fw	TGT TCT GCA CTG TTG AGC ATT TT	11	33
		g3137 rev	TGC AGT ATT TCG CAG ATC TCT TG	855	833
		g3137 T7Rev	G TAATACGACTCACTATAGGG TGA ACT TGT GAA GAC GTG TGT	834	814
		g3137 fw-2	CTG CAG AGC GCA GGT AGA TAA	231	251
		g3137 rev-2	CCA AGA CAC TAG TCC GGC AA	1215	1196
		g3137 T7Rev-2	G TAATACGACTCACTATAGGG CAC CCT TGC ATG TGT CTT GC	1147	1128
41	Anxa1	g8154 fw	TGA ACC CAG CTT TTA CGG TGA	217	237
		g8154 rev	ATT CTT ACG AGA GAC CAG CCT	1135	1115
		g8154 T7Rev	G TAATACGACTCACTATAGGG AGA CCA GCC TTA AAA CTG GCA TA	1124	1102
		g8154 T7Fw	G TAATACGACTCACTATAGGG GCT TGC GAA TGC TTC GAA AAT CG	239	261
42	Lici1	g13559 fw	ATC TTA GCT GCT GGG GAG AA	86	105
		g13559 rev	GCC GCT TTC GAA CCA AAT GT	903	884
		g13559 T7Rev	G TAATACGACTCACTATAGGG TTG GAG AGA ATT TGG CGG GC	873	854
		g13559 T7Fw	G TAATACGACTCACTATAGGG GCA TGG TGA TTC TTT TAC CAC ACC	113	136
43	uncharacterized	g16068 fw	AAT TCA GTA ACG AAG TTA TTC TGC T	70	94
		g16068 rev	TGC AAA CAA ATT TAA TGC CAA ATC T	895	871
		g16068 T7Rev	G TAATACGACTCACTATAGGG GCC AAA TCT CGA AAA GAA TTT ACA A	879	855
44	orthopedia-like	g16467 fw	ATG CTG AAT AAC CTG CAC GGC	20	40
		g16467 rev	AGA ATT GGG AAC CAG CTG GG	825	806
		g16467 T7Rev	G TAATACGACTCACTATAGGG ACC AGC TGG GAA GAC ACT TG	815	796
45	ac	g27206 fw	TGG CTT CCT TGA CGC TTC TG	233	252
		g27206 rev	TCC GTA GCC AAC TCA GGT CC	1119	1100
		g27206 T7Rev	G TAATACGACTCACTATAGGG CCA ACT CAG GTC CCA GCA ATA	1112	1092
46	uncharacterized	g2548 fw	GAC TTA GGA GTA CAA AAC CGT GGC	5	28
		g2548 rev	TGT AAA GCG AAA ATA TAT TCG CCG C	639	615
		g2548 T7Rev	G TAATACGACTCACTATAGGG GCC GCA TCT AAG ACA ATG TCT GA	619	597
47	uncharacterized	g15602 fw	GCA TTG CAG AAA TAA TCA GCT TGA G	44	68
		g15602 rev	ATG CAC TCA ATT TCT CTC TAA GC	663	641
		g15602 T7Rev	G TAATACGACTCACTATAGGG CCA GAC AAT ATA TAC AAG GCG TCC	627	604
		g15602 T7Fw:	G TAATACGACTCACTATAGGG GCA GAA ATA ATC AGC TTG AGG TTT G	49	73
48	VSP	g26402 fw	TCC CCA AGA ATT CGC TGA ACC	381	401
		g26402 rev	TAT GGG CAA ACC GTG AGT CT	1698	1679
		g26402 T7Rev	G TAATACGACTCACTATAGGG GGC CAA GCT TTG TTG TTT GC	1253	1234
49	uncharacterized	g4424 fw	ACT GCT GCT CAA TCT TTC CGA	328	348
		g4424 rev	AGT CCC GGA TTT TCC TTG CC	1616	1597
		g4424 T7Rev	G TAATACGACTCACTATAGGG AGT GGC AAC TGT CTT CTC GC	1404	1385
		g4424 T7Fw	G TAATACGACTCACTATAGGG GTC CAG TTG GGA GTG ATT CCA C	539	560
50	uncharacterized	g15442 fw	AGC ACG ACC CAC AAA AAT GT	436	455
		g15442 rev	GTG CTT CGA CGA TGA CTG GA	1649	1630
		g15442 T7Rev	G TAATACGACTCACTATAGGG TCG TAA TCC TGG TCT CGT TCG	1626	1606
51	uncharacterized	g5051 fw	GTA ATT CCA ATA AAC TGA GGA TGC C	14	38
		g5051 rev	GTT CGA TGT AGC ATT AAA TGG GAA GC	611	586
		g5051 T7Rev	G TAATACGACTCACTATAGGG TCT TTC GAA GCC ATG CCT TTC	555	535
52	uncharacterized	g4425 fw	TAG TGC GGC ATG CAA AGA GA	650	669
		g4425 rev	CGA GGG CTC CGG ATA AAC AA	1835	1816
		g4425 T7Rev	G TAATACGACTCACTATAGGG TAT GCG TGA GAG AGG GAG CA	1582	1563
53	golgin	g19878 fw	AGC AGC CAG ATT TTG CCA GA	481	500
		g19878 rev	CTG CAG AGT CTC TTT CAT CCG T	1423	1402
		g19878 T7Rev	G TAATACGACTCACTATAGGG GCT GCA ATT TTT TGC TCT TGC AGA T	1397	1373
54	ltv1	g22997 fw	ACG CTT GAA CAT GAG TGG GT	504	523
		g22997 rev	TCA TTG CTT GGG TTT GTT GGA	1620	1600
		g22997 T7Rev	G TAATACGACTCACTATAGGG AGT TGA AGC TAC AGA GAC AGC A	1469	1448
55	Clca4a	g11056 fw	ACG GCC TCC AGA AAC CTA AG	451	470
		g11056 rev	GAT GGG TAA GCA CTG CCA CA	1682	1663
		g11056 T7Rev	G TAATACGACTCACTATAGGG TGT CCT TTG CTG TTG CGA TG	1408	1389
		g11056 T7Fw	G TAATACGACTCACTATAGGG GGC GAC CAT TAT TTT CGC CAA C	565	586
56	uncharacterized	g14078 fw	CGA GCG TTC TCC TCA TGA CAG	6	26

		g14078 rev	CAC ATT ACA ATT AAA ATA GGT TGC C	594	570
		g14078 T7Rev	G TAATACGACTCACTATAGGG CCA TAT TGA GCC GAT ATT TTT GAC C	465	441
57	uncharacterized	g18398 fw	GCT TAC AGT GCA ACA GCT TCT	310	330
		g18398 rev	AAC TGC AGG AAT CCT CTG ACG	1274	1254
		g18398 T7Rev	G TAATACGACTCACTATAGGG CAG TCG AAC AAG CAA CCT GTG	1221	1201
58	ncRNA,uncharacterized	g26430 fw	GCG GGA TTG CAA ATA TTG ATA GCA C	81	105
		g26430 rev	ATA CCC CAT CCA AAC ATA TTC CCA	842	819
		g26430 T7Rev	G TAATACGACTCACTATAGGG TCT CAA TTT TAA CAC CCC ATT CTC C	755	731
		g26430 T7Fw	G TAATACGACTCACTATAGGG GCA CTT CAC TAT CAG TAA TGT TC	102	124
59	uncharacterized	g10678 fw	GTA CAA TGC ATC AAC GGC GA	224	243
		g10678 rev	ACG CTT GAT AAT GGC TTC TTA TCC	1113	1090
		g10678 T7Rev	G TAATACGACTCACTATAGGG CCA ATA AAG CCA GCA GTT TTT CG	987	965
60	uncharacterized	g3565 fw	TGG AGA CGT TGC GTA TGA CA	258	277
		g3565 rev	GAG CGC AAA CCG TCA TTC AG	1421	1402
		g3565 T7Rev	G TAATACGACTCACTATAGGG GCA TCG TGA CAA ACC AGA CG	1279	1260
61	FMO5	g15065 fw	CCG CGG ATT ACG ACG ATA CT	536	555
		g15065 rev	TTG AAT TGT GTG GCG TGG TC	1476	1457
		g15065 T7Rev	G TAATACGACTCACTATAGGG TTT GCC AGC CAT GTG CAA AG	1377	1358
62	uncharacterized	g10660 fw	CGT CTG ACT CTT CCA CGA ACC	190	210
		g10660 rev	CTA CGC GAT TTC CCC CAC TC	1036	1017
		g10660 T7Rev	G TAATACGACTCACTATAGGG TCA GCA AGT CTT TCC CTG AGC	985	965
63	uafA	g10890 fw	TCA TCC GGC AGA ATT GCC TA	910	929
		g10890 rev	TTT CGA ACC CAA GCA TTC GC	1924	1905
		g10890 T7Rev	G TAATACGACTCACTATAGGG GTA CAG GCG TTT CGA GCC AT	1896	1877
64	uncharacterized	g11980 fw	TCA GTG TGA TAC CAA CGG CA	289	308
		g11980 rev	GCG CCG AAT AGT GAT GGG A	1296	1278
		g11980 T7Rev	G TAATACGACTCACTATAGGG ACA AGA GAG CTG GTG TAT CGC	1200	1180
65	uncharacterized	g1984 fw	TAC ATA ATC AGT TAC GAT ACC CAG C	8	32
		g1984 rev	CAG AAA TTG TGT GAA ATG TGC GT	674	652
		g1984 T7Rev	G TAATACGACTCACTATAGGG CAT GGT TGA CCC TAC TCA GC	590	571
66	uncharacterized	g20358 fw	AGT CTA CGT CAT CCG CTT GC	124	143
		g20358 rev	TGG TAT GCT GTC ATC TGG CAA	1093	1073
		g20358 T7Rev	G TAATACGACTCACTATAGGG ATG CCG TTG TTC GAG CTC AC	951	932
67	uncharacterized	g7529 fw	AGT GTT GAA AAA GAG TCG GGA GAT	275	298
		g7529 rev	AGT TGC TTC CCC TTG ACT CC	1123	1104
		g7529 T7Rev	G TAATACGACTCACTATAGGG ATG CGA GCT TTT AGC CTG GT	1077	1058
68	uncharacterized	g14945 fw	GAC TCT ACA GGC TTA CTG CTC C	221	242
		g14945 rev	ACA AGT CCA ACA AAG GCG TG	1306	1287
		g14945 T7Rev	G TAATACGACTCACTATAGGG AAC TCC GTT TCC AAC AGG CT	1248	1229
69	uncharacterized	g25745 fw	TAA TGC CGT GGG TGC AAG AT	202	221
		g25745 rev	GTC TTG CGT CGT GCC ATT TT	1237	1218
		g25745 T7Rev	G TAATACGACTCACTATAGGG GTC TTC GTG TGA TCG CCT CT	1099	1080
70	CAH1	g10648 fw	GCA GCG CCC TCT TTA TTG GA	327	346
		g10648 rev	CCG TTC ATA GGT TGA ACA ACT CTG C	1265	1241
		g10648 T7Rev	G TAATACGACTCACTATAGGG CGT CGC AGA TCT CAG CAG AA	1204	1185
72	DAB2ip	g20070 fw	ACA CCA GTG CTG GGT ATT CG	101	120
		g20070 rev	TGC GAC ACT CAT GGA ACA CT	1391	1372
		g20070 T7Rev	G TAATACGACTCACTATAGGG TGG GGT CAA CCT CAC AAT CG	1253	1234
73	KLC1	g65 fw	GCG TCT ATT CAA ATG GAA AGG GAA	300	323
		g65 rev	GGT GTT TTA ACA GTT GGT AGA GAT T	1372	1348
		g65 T7Rev	G TAATACGACTCACTATAGGG AGA TGC TAG GTT ATC TCT GGC	1241	1221

S-A-1	Numb	g26621 Fw	AGT ACC TTG GCT GTG TCG AAG	342	362
		g26621 Rev	AGC AAA ATT TGG ACT CGC CC	1417	1398
		g26621 T7Rev	G TAATACGACTCACTATAGGG GGC CAA CCA TTC TTC AGC TC	1234	1215
S-A-2	Creld1	g259 Fw	AAC GAC AAA ATC CTG TGC GA	359	378
		g259 Rev	TCT TTG GTC CTG GTC CTC TAC A	1104	1083
		g259 T7Rev	G TAATACGACTCACTATAGGG TGG TCC TGG TCC TCT ACA ATG A	1100	1079
S-A-3	Creld2	g7589 Fw	GGT GGT GAT GCA TCT TGG GA	415	434
		g7589 Rev	GTT GTT GGC TAA CAG CCA GTG	1371	1351
		g7589 T7Rev	G TAATACGACTCACTATAGGG ACC CCC GTG ATT GGT TTT CT	1330	1311
S-A-4	Creld2	g7590 Fw	AAG GTG GTG ATG CAT CTT GGG	260	280
		g7590 Rev	GAT CGC TTA TCC CAT TCA CCC A	1166	1145
		g7590 T7Rev	G TAATACGACTCACTATAGGG GCA ATG AAC ATG TGT CGT CGA A	1091	1070

S-A-5	EgfR	g18901 Fw	ACC AAT GGG CGT ATG TCT GT	218	237
		g18901 Rev	AGG TCC ATC ACA GGC AAC AC	1096	1077
		g18901 T7Rev	G TAATACGACTCACTATAGGG AAG TTC GAA CAC AGG CAC CA	1043	1024
S-A-7	GSK3	g9959 Fw	CAG TAA GCA ATC GTC GCA GC	345	364
		g9959 Rev	CAT CCC ACC AGA ACT GGC AT	1515	1496
		g9959 T7Rev	G TAATACGACTCACTATAGGG TGT GCA CAG GCT TGT AGA GG	1310	1291
		g9959 T7Fw	G TAATACGACTCACTATAGGG GCC TAG TTT TAC GGG AAT CAA GAC	363	386
S-A-9	GSK3	g25394 Fw	TCT TGC AAG GAA GGT GGC AA	213	232
		g25394 Rev	AAT AAC ATC AGG GGC AGC GG	1349	1330
		g25394 T7Rev	G TAATACGACTCACTATAGGG GAG AAC AGG CTT GGA GAG GG	1134	1115
		g25394 T7Fw	G TAATACGACTCACTATAGGG ATG TCA TTG CCA CTC CTG GG	241	260
S-A-10	Cyclin A1 like	g2080 Fw	AAA GGG CTC CTT TGT CGC TT	308	327
		g2080 Rev	CCA CAT CAC GCG CTT TGT TA	1300	1281
		g2080 T7Rev	G TAATACGACTCACTATAGGG TCG AGC GTA TAC CCC GTC AT	1250	1231
S-A-11	cyclinB	g8469 Fw	TGC TGA GGA AAC CTT TGC GT	215	234
		g8469 Rev	TCC AGC ATA CTT CGT GTG GAC	1209	1189
		g8469 T7Rev	G TAATACGACTCACTATAGGG ATA CTT CGT GTG GAC TGC CT	1203	1184
S-A-12	Cyclin E1	g7775 Fw	AGT TGC GAA AAC ACA CCC AC	625	644
		g7775 Rev	ACT ACT TTG TGG CGG AGT CA	1662	1643
		g7775 T7Rev	G TAATACGACTCACTATAGGG CCA GCA GTG TGC GTC TGT AT	1562	1543
S-A-13	cdk1	g11601 Fw	GAG GGT GTC CCT TCA ACTGC	275	294
		g11601 Rev	AAG CTG CCA GTG CCG ATA TT	995	976
		g11601 T7Rev	G TAATACGACTCACTATAGGG TGC CAG TGC CGA TAT TCG TT	991	972
S-A-14	myc binding protein	g26862 Fw	GTC AGA CAA ATC AGC TGC GAA A	7	28
		g26862 Rev	ACC AAC TGC AGT AAT TAA AGG CAA	789	766
		g26862 T7Rev	G TAATACGACTCACTATAGGG AAA TAT TGT GGT GTT GGC GAC G	754	733
S-A-15	Dennd4a	g2908 Fw	CCT AAG CAG AGC GAG TAC GG	2835	2854
		g2908 Rev	CAC CTT GCT GCC AGT TTT CC	3954	3935
		g2908 T7Rev	G TAATACGACTCACTATAGGG GAG AAC CTT CCT CGG ACG AC	3745	3726
S-A-16	Pik3r1	g14960 Fw	GAG TCA CAC GTT GCT CCG TC	939	958
		g14960 Rev	AGG CGT TGT AAG GTT CAG CA	2200	2181
		g14960 T7Rev	G TAATACGACTCACTATAGGG GAC AGA GCA AAA TCC CCG GT	2117	2098
S-A-18	Pik3r1	g26883 Fw	TGT GAC GAA TGC CTG GGA TG	714	733
		g26883 Rev	TTT CCC AAG GTG GAC GAA GA	1713	1694
		g26883 T7Rev	G TAATACGACTCACTATAGGG TAT TGC AAG CGG CAA ACA CG	2553	2572
S-A-19	Pik3c3	g3457 Fw	AGG CAT TCA CAA CTC GAT GG	374	393
		g3457 Rev	GGC CGG AAA GCC ACT TTC TA	1521	1502
		g3457 T7Rev	G TAATACGACTCACTATAGGG TGG GTG GGT AAA CTG TGG TG	1251	1232
S-A-20	AMPK subunit alpha-2	g3112 Fw	AAT GGC GGA GAA AGG ACA GT	161	180
		g3112 Rev	AGG TGG ACT AGA AGC CCA GT	1232	1213
		g3112 T7Rev	G TAATACGACTCACTATAGGG CGA TTG CCA ATT GGT CGT GT	1143	1124
S-A-21	HIF-1alpha	g18646 Fw	CTC AAC CTG GCC ACC AGT AA	486	505
		g18646 Rev	CAA CAG CTC ACT GTC CGA TG	1457	1438
		g18646 T7Rev	G TAATACGACTCACTATAGGG GCT CGG AGA GAT CGT TTG GA	1409	1390
		g18646 T7Fw	G TAATACGACTCACTATAGGG GCA CAT CCC CAG TCC ACT TT	508	527
S-A-23	Idh2	g4961 Fw	ATT ATG GCA CTG ATC GCC GT	245	264
		g4961 Rev	GAT TGC CAT CCA GCT TTG CT	1303	1284
		g4961 T7Rev	G TAATACGACTCACTATAGGG GGC ACA CTA GAA CAC TGG TCA	1147	1127
S-A-24	Idh3a	g9466 Fw	TCC CGG AGA TGG AAT CGG AC	343	362
		g9466 Rev	TGA ACT CTG AAC ACT TTG CAC G	1292	1271
		g9466 T7Rev	G TAATACGACTCACTATAGGG CAA GTC GGC TGT CCT TAC CT	1264	1245
S-A-25	Idh3g	g14882 Fw	CAC AGC TCA GGC TGA CCA TC	292	311
		g14882 Rev	GCT TGG GAA TAG GAT GCG CT	1359	1340
		g14882 T7Rev	G TAATACGACTCACTATAGGG GTT TGC TGT GCC ACC AAG AT	1285	1266
S-A-26	Idh3g	g20634 Fw	GTC CCT GGA GTT GTT GAA AGC	4	24
		g20634 Rev	CAC AGT CTT ATC AAC AGC ATC ACC	528	505
		g20634 T7Rev	G TAATACGACTCACTATAGGG CAG TCT TAT CAA CAG CAT CAC CAA T	526	502
S-B-1	Snip1	g4437 Fw	TCA AGT GAA AAC AGG CGG TTG	106	126
		g4437 Rev	CCG GGA GCT GTA ACC AAA CT	915	896
		g4437 T7Rev	G TAATACGACTCACTATAGGG GTG GAT CGA CGC GAT TGT TG	859	840
S-B-2	Idh1	g8458 Fw	ACA GTG TGG ACC TGT AGT TGA	246	266
		g8458 Rev	CCA GCT TCA ATA GTT TCC ACG C	1340	1319
		g8458 T7Rev	G TAATACGACTCACTATAGGG GCA CGA TGA GCC AAA CCT CT	1262	1243
S-B-3	AKT interactin protein	g7505 Fw	CTG ATG AGC TCA GCT ACT GC	404	423
		g7505 Rev	TGC ATC CAC GAG AGA CCA TT	1080	1061

		g7505 T7Rev	G TAATACGACTCACTATAGGG ACG AGA GAC CAT TGC TTG AAC T	1073	1052
S-C-1	asph	g13107 Fw	AAC AGG AAA ACC GTG GTG GG	724	743
		g13107 Rev	AGT TGC CAA TAA ATG GTG CCG	1723	1703
		g13107 T7Rev	G TAATACGACTCACTATAGGG ATG GTG CCG CCA GTA GTA AA	1711	1692
S-C-2	Ctnnb1	g2387 Fw	CGT ATC AAG TTC CCC GAC CA	442	461
		g2387 Rev	AAT CTG GAG CAC ACG CTG TT	1692	1673
		g2387 T7Rev	G TAATACGACTCACTATAGGG CCA CCT TCA AGG CGA CGT AA	1604	1585
S-C-3	Sox2	g11061 Fw	CAG GGG GTC TAG ATC CGT CA	418	437
		g11061 Rev	GAG AGA GGG GCA TTG TAC CAG	1482	1462
		g11061 T7Rev	G TAATACGACTCACTATAGGG GGG TCT GAT GCA TCG TTT TGG	1402	1382
S-C-4	cdk2	g9226 Fw	GGA GAA GGC ACA TAC GGT GTT	133	153
		g9226 Rev	GGA TGT GCA AGT GCT CGT TT	953	934
		g9226 T7Rev	G TAATACGACTCACTATAGGG GGC AAT CTG CTC TCG GGT T	929	911
S-C-5	AKT	g4339 Fw	AAA TTG GCG TCC TCG CTA CT	443	462
		g4339 Rev	ACC ACC TCC AAG CCT CTT TT	1559	1540
		g4339 T7Rev	G TAATACGACTCACTATAGGG AAT GGC AAC CGT CCA CAC AT	1420	1401
S-C-6	Prkc2	g19182 Fw	CGG TGG ATT TAC GTC CGA CA	234	253
		g19182 Rev	GGC CTG TAG GAA AGA ATC GCT	1298	1278
		g19182 T7Rev	G TAATACGACTCACTATAGGG ACA GAA AGG GGT GAG GTA TGC	1239	1219
S-C-7	mTOR	g25455 Fw	AGT TGG CAG CCT ATG CCA TT	532	551
		g25455 Rev	AAG AGG CAG TCA ACG ATG GG	1734	1715
		g25455 T7Rev	G TAATACGACTCACTATAGGG AAA AGC AGC CAG TCG AGG AA	1385	1366
S-C-8	Rictor	g9316 Fw	GTT CGC GCC ACC ATT TTT CT	234	253
		g9316 Rev	CGC ATT GCT TCC TTG CGT AT	1744	1725
		g9316 T7Rev	G TAATACGACTCACTATAGGG TCA GTC CCA GTG AGC ACT TT	1162	1143
S-C-9	PTEN	g12581 Fw	TAT CCA CTG CAA AGC GGG AA	1101	1120
		g12581 Rev	GCT TCA CAA GCG TCC CAA TC	1985	1966
		g12581 T7Rev	G TAATACGACTCACTATAGGG ACA AGC GTC CCA ATC GTC AT	1980	1961
S-C-10	MAPK14	g2738 Fw	GGT CAG GAG CTT ACG GTC AA	248	267
		g2738 Rev	ATA AGG CTC TGC AAT CGG CT	1125	1106
		g2738 T7Rev	G TAATACGACTCACTATAGGG TGC GTT AGA TAG GGA TGG GC	1085	1066
S-C-11	MAPK1	g27558 Fw	AAG TCT TTG AAG TCG GAC CCC	287	307
		g27558 Rev	ACA AGT TCT TTC AAG CGC TCC	1277	1257
		g27558 T7Rev	G TAATACGACTCACTATAGGG ATG GTT CTT CAG CTA CAG GCT	1222	1202
S-C-12	MAPK1	g27557 Fw	AGT CTT TGA AGT CGG ACC CC	94	113
		g27557 Rev	ACA GTC TCA TGA TGG GCG AA	856	837
		g27557 T7Rev	G TAATACGACTCACTATAGGG TGA TGG GCG AAC AAG AAC AAC	847	827

H1	EIF3D	g27822 fw	TTC ATT TTG TGC CCC CGG TA	115	134
		g27822 rev	ACC AGA AGT TCT AGG GTC CCA	1289	1269
		g27822 T7 rev	G TAATACGACTCACTATAGGG TCA ACT CCA CAC CAT CTC CC	1188	1169
I1	aos /EGFR	g839 fw	GGG TGA CGT TGA TGC TCG TA	250	269
		g839 rev	TCC GGA TTC GTC TTG GTT CG	1220	1201
		g839 T7 rev	G TAATACGACTCACTATAGGG GTA GGT CGA GCA TGG GAA GG	1201	1182
I2	TSG101	g2715 fw	ATG CCG CAG GAA ACA TTT GAT	149	169
		g2715 rev	GGA AAG TGA TCG CAC ATG CTT	1348	1328
		g2715 T7 rev	G TAATACGACTCACTATAGGG AGA GGA GCT GGT GCT ACA AC	1218	1199
I3	DLL1	g25248 fw	CGG ACG TCA GTT GTT CAG GA	375	394
		g25248 rev	AAA GGC AGG AGG GCA TAC AC	1519	1500
		g25248 T7 rev	G TAATACGACTCACTATAGGG CCA CTC GGT CCA TCA ACA CA	1491	1472
I4	ALDH1A1	g2991 fw	GAG ACC AGG CTG ATG TGG AAA	517	537
		g2991 rev	CGC ATT CAA GTT TGG CTC CT	1461	1442
		g2991 T7 rev	G TAATACGACTCACTATAGGG TCG TCG ATC TGA GGT CCT TG	1393	1374

BMP-1	BMP and activin membrane-bound inhibitor homolog	g18541 fw	ACT GTT AAG GCT GAT GTT CGG T	216	237
		g18541 rev	ACG TCA GAC TCT TAC CAC CAA	1063	1043
		g18541 T7Rev	G TAATACGACTCACTATAGGG GAT TCA AAT GGA CCC GGA CAT	1039	1019
BMP-2	BMP and activin membrane-bound inhibitor homolog	g17346 fw	TCA GCG ATG TGA CAA TCG GA	294	313
		g17346 rev	CCT TCG GCA ACT ACA CAA TAG C	1103	1082
		g17346 T7Rev	G TAATACGACTCACTATAGGG TTT TGC ACC AAG TTC CAG CA	1052	1033
BMP-3	cv-2 (Bmper)	g2323 fw	TGC AGG GAT GGT CAG GTA GA	1449	1468
		g2323 rev	GTT GAA GAG TTC GGG CGT TG	2649	2630

		g2323 T7Rev	G TAATACGACTCACTATAGGG AAG GGC AAT CAT CCA CAG GT	2535	2516
		g2323 T7Fw	G TAATACGACTCACTATAGGG CAAATTACATGCCCAGCAGGAC	1515	1494
BMP-4	p60A/BMP7	g13706 fw	TGG CCG GCA ACA AAG TAT TC	239	258
		g13706 rev	ATC AGG CAC TTA TTG CGG G	1252	1234
		g13706 T7Rev	G TAATACGACTCACTATAGGG CTT ACT CAG TGA CAC CCA CAT GAT	1192	1169

Oda-1	G protein-activated inward rectifier potassium channel 3-like	g5417 fw	CAC CAA ATG TTC GAC CGT CC	420	439
		g5417 rev	CGA GTA ACT CAC AGC CCT CG	1542	1523
		g5417 T7Rev	G TAATACGACTCACTATAGGG TAC TCG CGA GCA CTA CAC AG	1490	1471
Oda-2	uncharacterized/transcription factor COE1	g1125 fw	TGG CTG CTG TTT CAG AGG AT	169	188
		g1125 rev	ACC ATC AAT GAG ACG CCA AAC	725	705
		g1125 T7Rev	G TAATACGACTCACTATAGGG AAT GAG ACG CCA AAC CAT GT	719	700
Oda-3	SLIT-ROBO Rho GTPase-activating protein 1	g2394 fw	CAT TGC ACA AAG ACC GCA CA	1662	1681
		g2394 rev	CTC TCG ATC GAT GCC GTG AA	2919	2900
		g2394 T7Rev	G TAATACGACTCACTATAGGG ACT ACT GCT GCT TGT CCG TC	2670	2651
Oda-4	rhoGEF domain-containing protein gxcJ-like	g15443 fw	GTG TTT GTC TCC GAC GTC CT	390	409
		g15443 rev	TGG GTG GGT GAG TCA GGT AA	1524	1505
		g15443 T7Rev	G TAATACGACTCACTATAGGG TGC AAG GTT TCC ATG GCA GG	1399	1380
Oda-5	uncharacterized LOC107452121	g4530 fw	AGA GGG AAT GCT GAA ACA CG	415	434
		g4530 rev	ATC CTT CCA CAT TTC GCC GTA	1139	1119
		g4530 T7Rev	G TAATACGACTCACTATAGGG TCC ACA TTT CGC CGT AGT TGA	1134	1114
Oda-6	nuclear receptor subfamily 2 group E member 1-like	g794 fw	ATT CTT GCG ATG GGT GTG CT	354	373
		g794 rev	GAT CGT GAA CCG CTG CTA CA	1298	1279
		g794 T7Rev	G TAATACGACTCACTATAGGG AGA CCT GTT GCA CAG CGT AA	1080	1061
Oda-7	homeobox protein Hox-B4a-like	g1787 fw	GCG TGG ATA CGG CAC AAA AT	155	174
		g1787 rev	CCC ATC TTT GCT GCT CTC GT	1005	986
		g1787 T7Rev	G TAATACGACTCACTATAGGG GCT GCT CTC GTG ACT AAG TGT	996	976
Oda-8	roundabout; homolog 3	g10604 fw	CCT ACG TCC AGC GTA CTG AC	820	839
		g10604 rev	AAC ACG TCC TCT CGA AAC CC	2217	2198
		g10604 T7Rev	G TAATACGACTCACTATAGGG CAC TGC AAA ACA GCG GTC TC	2162	2143
Oda-9	uncharacterized LOC107443364	g17172 fw	TTA TGA GGC TGC GAG GCT AC	33	52
		g17172 rev	TAG GAA CTC CGA CAA CGC AC	497	478
		g17172 T7Rev	G TAATACGACTCACTATAGGG GCA CAC CCT TGC TGA CCA TA	481	462
Oda-10	plexin-B	g17369 fw	GAA CGA TGG CCA AGA CTG GA	449	468
		g17369 rev	TCA GCA CTC CAT CCC CTG TA	1786	1767
		g17369 T7Rev	G TAATACGACTCACTATAGGG CTC GCA GCA AAC ACT CCA AC	1445	1426
Oda-11	growth arrest-specific protein 1	g9575 fw	CAG GCT AAC CGT TGG AGG TT	246	265
		g9575 rev	TTG CTC TGA TGT CCA CCA CC	1308	1289
		g9575 T7Rev	G TAATACGACTCACTATAGGG TTG AGC AGG ACG TTG CTT GA	1243	1224
		g9575 fw-2	CAGAGCACGGCGAAGATTGT	500	519
Oda-12	uncharacterized LOC107444955	g886 fw	TCC TAG AGC CCT ATG TGC GT	92	111
		g886 rev	CGG CGT TCA ACA CAT CAT CC	1225	1206
		g886 T7Rev	G TAATACGACTCACTATAGGG AGT CTT TGC TCA TGG CGT CT	1069	1050
Oda-13	uncharacterized LOC107446454	g19176 fw	AACGGTCGCAACAACTGATGA	161	181
		g19176 rev	TTTGCAGAATTTTCGCAGGC	611	592
		g19176 T7Rev	G TAATACGACTCACTATAGGG GCAGAATTTTCGCAGGCAAAG	608	588
Oda-14		g22384 T7Rev	already designed		
Oda-15	uncharacterized protein DDB_G0290685 -like, transcript variant X3	g14890 fw	TCC TAC CCG TGG TGA TCG AA	113	132
		g14890 rev	GCC GTT TTG CCA ACC AAG AT	944	925
		g14890 T7Rev	G TAATACGACTCACTATAGGG ATT TCC GCC ATT CTG CTG GA	890	871
Oda-16	heterogeneous nuclear ribonucleoprotein A/B-like, transcript variant X1	g15130 fw	TCA CCA AAG GCG ATT CAC CC	165	184
		g15130 rev	TAA TAT CCA CCA TAT GCT CC	593	574
		g15130 T7Rev	G TAATACGACTCACTATAGGG ACC ATA TGC TCC ACC ATA TG	585	566
Oda-17	receptor-type tyrosine-protein phosphatase alpha, transcript variant X1	g16957 fw	CAG ACA TCG CCA TGG ACA AC	157	176
		g16957 rev	ACC ACA TTT GCA TTC CCC GA	1002	983
		g16957 T7Rev	G TAATACGACTCACTATAGGG CCA ACA CTC ATC TCG TCG CT	965	946
Oda-18	E3 ubiquitin-protein ligase PDZRN3	g23798 fw	AAA GAA GCA ATC GTT CCG GC	253	272
		g23798 rev	CCT GAA CCA CTG CTC ACG TA	1239	1220
		g23798 T7Rev	G TAATACGACTCACTATAGGG GAG CGG CCA TTT CTT TGT CC	1162	1143
Oda-19	uncharacterized LOC107441350	g27267 fw	GTT CCG GAG GTA AGT TGG GC	140	159
		g27267 rev	TCT TAT TGA TGG GCA GTG CG	605	586

		g27267 T7Rev	G TAATACGACTCACTATAGGG CAC AGG TTC TTG ACC TGA GGG	575	555
Oda-20	glutathione S-transferase Mu	LOC107449800 fw	GGG ATT TAC GAG GTC TTG GAG A	322	343
		LOC107449800 rev	AAT GGG CTA GTG GTC CAA CA	915	896
		LOC107449800 T7Rev	G TAATACGACTCACTATAGGG TGG TCC AAC AAT TGG CCA TC	905	886
Oda-21	slit homolog 2 protein-like	LOC107439100 fw	TTT TAC GCG GTC GTT TCA GC	582	601
		LOC107439100 rev	CAT TGG GTT CCG CGC ATT TT	1467	1448
		LOC107439100 T7Rev	G TAATACGACTCACTATAGGG TTT GCC CTC CGG AAA ACG AT	1439	1420
Oda-22	tyrosine-protein phosphatase 10D-like	g2169 fw	GCC TCA TGG ACA CCG AGA TT	269	288
		g2169 rev	TGA TTG TCC CAA ATC GGC GT	1195	1176
		g2169 T7Rev	G TAATACGACTCACTATAGGG GAC AGA CTG CTG TCG GTG AT	1108	1089
Oda-23	**uncharacterized LOC107440592	g27105 F	Tgc caa gaa ccg aaa gca	431	448
		g27105 R	Tgg cac agg aat agg aag	1080	1063
		g27105 T7Rev	G TAATACGACTCACTATAGGG CGA GAG AAT GTG GAG GAA GG	1058	1039
Oda-24	**8.6 kDa transglutaminase substrate-like	g1540 F	Ctt agc cac gat cgt tct tc	152	171
		g1540 R	Ttg tca tca ggg act tct ga	451	432
		g1540 T7Rev	G TAATACGACTCACTATAGGG TCA GGG ACT TCT GAA TAT GG	445	426
Oda-25	** slit homolog 1 protein-like	g17108 F	Ctg cgc aag aac ctt caa ca	982	1001
		g17108 R	Gtt cca ctg gta atc caa gg	1782	1763
		g17108 T7Rev	G TAATACGACTCACTATAGGG CCA CTT CAT TCT GCA ATC AC	1744	1725
Oda-26	**proclotting enzyme	g17419 F	Act acg atg agt cct cgt ca	510	529
		g17419 R	Agt ttc tgg tca acc agt cc	1086	1067
		g17419 T7Rev	G TAATACGACTCACTATAGGG CCA GTC CAA AAA TTC TGT CAC	1073	1053

Nodal	Nodal modulator 3	nm3_F	GTT CAA GCA GTT TCG AGC CG	1634	1653
		nm3_R	TGA CCA GGT CCC AAT CCA GT	2770	2751
		nm3_T7R	G TAATACGACTCACTATAGGG CCA TTG TGT CAA GCG GGG TA	2601	2582

Gene	Number	Primer	Sequence
EGFP		*PUC57_EGFP_for	CTC AGA ATA AAC GCT CAA C
EGFP		*PUC57_EGFP_rev	CTG GAT TGG GAA CTA ACT
EGFP		BamHI-EGFP-Fw	ATAT GGATCC ATG GTG AGC AAG GGC GAG
EGFP		NotI-EGFP-Rev	ATAT GCGGCCGC TTA CTT GTA CAG CTC GTC CAT G
Ets4	g4238	*pUC57egfp_ets4_ad_for	GAC GAG CTG TAC AAG GGA
Ets4	g4238	*pUC57egfp_ets4_ad_rev	GAT GGA TGT GTG AGT GGG
Ets4	g4238	BamHI-Ets4-Fw	ATAT GGATCC ATG CAG ACG TGT GCT CCC
Ets4	g4238	NotI-Ets4-Rev	ATAT GCGGCCGC TTA ATG GAT GTG TGA GTG GGA AC
Twist	g14287	*pUC57_twist_for	GCT TCC TTG TTC TTT TTG C
Twist	g14287	*pUC57_twist_rev	TGT TCT TGA GGC TGG TTT
Twist	g14287	BamHI-twi-Fw	ATAT GGATCC ATG GGC ATA CTT CCA TGT GG
Twist	g14287	NotI-twi-Rev	ATAT GCGGCCGC TTA GGA GGG GTG TCT TTG AG

Primer	Sequence
**Pet32_for_s-tag	CGA ACG CCA GCA CAT GGA CA
**Pet32_rev T7 terminator	GCT AGT TAT TGC TCA GCG G
**T7 universal primer	TAA TAC GAC TCA CTA TAG GG
**M13F (-40)	GTT TTC CCA GTC ACG AC
**M13R (-24)	AAC AGC TAT GAC CAT G

Purpose	Primer	Sequence
Fragment amplification	*Pt-twi-Fw	CAT CAA CCT CAA GAT CTT AGT ATT C
Fragment amplification	*Pt-twi-Rev	GAG TTC ATG GGT CAG GTA GG
Guide RNA 1	*Pt-twi-gRNA1	GAT TCA AGC AGC AGC TCA TCA GG
Guide RNA 2	*Pt-twi-gRNA2	GCA ATG AAG GAA CTT TAC GGC GG

Guide RNA 3	*Pt-twi-gRNA3	GTT ATC CGT CTC AGA CTC TCT GG
For gRNA transcription	*Pt-twi-gRNA1-F	TAATACGACTCACTATAG ATT CAA GCA GCA GCT CAT C
For gRNA transcription	*Pt-twi-gRNA1-R	TTCTAGCTCTAAAAC GAT GAG CTG CTG CTT GAA T
For gRNA transcription	*Pt-twi-gRNA2-F	TAATACGACTCACTATAG CAA TGA AGG AAC TTT ACG G
For gRNA transcription	*Pt-twi-gRNA2-R	TTCTAGCTCTAAAAC CCG TAA AGT TCC TTC ATT G
For gRNA transcription	*Pt-twi-gRNA3-F	TAATACGACTCACTATAG TTA TCC GTC TCA GAC TCT C
For gRNA transcription	*Pt-twi-gRNA3-R	TTCTAGCTCTAAAAC GAG AGT CTG AGA CGG ATA A
For gRNA transcription	*Pt-twi-gRNA4-F	TAATACGACTCACTATAG TCT TCC CAG AGC GTT TGA GA
For gRNA transcription	*Pt-twi-gRNA4-R	TTCTAGCTCTAAAAC TCT CAA ACG CTC TGG GAA GA
For sequence	*Pt-twi-g2-Seq-F	GCT CAT CAG GAG ATC CAC AG
For sequence	*Pt-twi-g2-Seq-R	GTG TCT TTG AGA TGC CCA TGC
For sequence	*Pt-twi-g3-Seq-F	ATG ACT TCG GAA ATT GAC TGG AAC
For sequence	*Pt-twi-g3-Seq-R	CTG GAT TCG TCT TAA CGT AAT TAT C
For sequence	*Pt-twi-g3-Seq-F2	GAG AAT TAC GTT AAG ACG AAT C
For sequence	*Pt-twi-g3-Seq-new-F1	GAC TTC TTA TTG GTC CAT ACT T
For sequence	*Pt-twi-g3-Seq-new-F2	CAG TAA CGT ACT AGT AAA CGT AC
For sequence	*Pt-twi-g3-Seq-new-R1	AAA TTT CTT ACC TGC TGG AC
For sequence	*Pt-twi-g3-Seq-new-R2	TCT AAA GGT ACT GAG TTG TTT C
For sequence	*g4 seq F/Pt-twi-g3-Seq-F	ATG ACT TCG GAA ATT GAC TGG AAC
For sequence	Pt-twi-g4-Seq-R1	GCT TCC TTT TTC TCG GTC GGA
For sequence	Pt-twi-g4-Seq-R2	TTT CCT GGG ATT CTG GAT TCG T

Primer	Sequence
*Pt-hh-Fw	GGTACACCCATAAATGCCGTCAGTTGAG
*Pt-hh-Rev	GTATATTCATGACAAGCGCCAGATCACACC
*Pt-fgf8-Fw	CATCTCTTCGCTCTCCGCGC
*Pt-fgf8-Rev	GAATGCTCGTGCAAAGAGAGTG
*Pt-dof–Fw	GAAATGGCTCCTGTCGACGTTAC
*Pt-dof–Rev	CAATACTGGAACAGGTTGAGCTG
*Pt-fgf1-Fw	GTGGATAGAGGCATACCGAGT
*Pt-fgf1-Rev	CGGAACACCTCTACGGAACG
*Pt-FGFR1-Fw	GACATATGCTGAGGAAGATAATAG
*Pt-FGFR1-Rev	CAAACGTTATTTGAATCTGAATC
*Pt-FGFR2-Fw	GTCACAGTCATTTTAGGCTTG
*Pt-FGFR2-Rev	CAGTGTACATCTCCTGAGGTAC
*g5611-Fw	CAGGTTACTACAGATTGCCTCC
*g5611-Rev	GCACTTTCGTTCGTATTCATAG
*T7-g5611-Fw	GTAATACGACTCACTATAGGGCTAGCGTACCTGTGT
*T7-g5611-Rev	GTAATACGACTCACTATAGGGGCCAGTCCCCAGC
*T7-Pt-fgf8-off1-Fw	GTAATACGACTCACTATAGGGCTCCGCGCTGCGGC
*T7-Pt-fgf8-off1-Rev	GTAATACGACTCACTATAGGGCGCCTCAATAGTGGAGC
*T7-Pt-fgf8-off2-Fw	GTAATACGACTCACTATAGGGGTGTGTCTATTCAAAGAAGG
*T7-Pt-fgf8-off2-Rev	GTAATACGACTCACTATAGGGGGATGATGAGAGATCTATAG

*From Matthias. **Published paper from other labs

4. Molecular cloning

4.1 Total RNA extraction, gel electrophoresis, and production of cDNA

Total RNA was extracted from embryos to analyse transient gene expression by quantification of transcripts.

Traditional Trizol method. 50-100mg of embryos or tissues were homogenise in 250µl of Trizol in a 1.5ml Eppendorf tube with a pestle. Later another 750ul Trizol was added and the mixture was centrifuged at 4°C, 12000g for 15 min. The supernatant was transferred into fresh tube and incubated for 5 minutes at RT. The sample was mixed with 0.2ml chloroform and shaken vigorously by hand for 15 seconds. After another incubation of 3 minutes, the sample was centrifuged at 4°C, 12000g for 15 min, and appeared in two phases. The upper aqueous phase was transferred to a fresh tube (rather less than more) and added with 0.5 ml isopropanol. After incubation at RT for 10min, the mixture was centrifuged at 4°C, 12000g for 10 min to remove supernatant. Pellet was washed with 75% EtOH, vortexed, and centrifuged at 4°C, 7500g for 5 min. The RNA pellet was air dry for 5 minutes, and the pellet could be dissolved in 50µl RNA-free water, even heat to 60°C for 10 minutes if necessary.

1ul of the final sample could be tested in gel electrophoresis. In gel test, most samples were loaded to 1% agarose gel and running in 1x TAE buffer. For very small fragment, 2% gel were prepared. Generally, the electrophoresis was taken at 135 Volt for 15-20 minutes. Sample DNA was illuminated by Ethidium Bromide and detected by UV light from Bio-RAD Molecular Imager Gel Doc XR+. DNA marker: Smart ladder 200bp-10kb, MW-1700-10, Eurogentec.

A recent and more precise way to extract total RNA was based on Quick-RNA FFPE Kit (R1008, Zymo Research). Vitelline membranes were removed from embryos, and embryos were mixed with 2x Digestion buffer, proteinase K, and DNase/RNase-Free water for incubation at 55°C for 1 to 4 hours. After the digestion, the tube was incubated at 65°C for 15 minutes, mixed with RNA lysis buffer, and centrifuged to remove debris. The supernatant of the sample would mix with 1 volume of EtOH in a new tube and added to column for purification. After several step of preparation and washing, the total RNA would be eluted. I used this method extract total RNA from dissected part of embryos and sent for sequencing analysis.

With extracted total RNA, a cDNA library could be established with SuperScript VILO cDNA synthesis Kit (11754-050, Invitrogen). A 20µl mixture reaction could be set up as follows:

5x VILO Reaction Mix	4µl
10x SuperScript Enzyme Mix	2µl
RNA (up to 2.5µg)	xµl
RNase free water	to 20µl

The tube was incubated at 25°C for 10 minutes and 42°C for 60 minutes. The reaction was terminated by incubation at 85 °C for 5 minutes. The total volume of the sample could be added to 100 µl in total. And the sample stored at -20°C before use.

4.2 Genome DNA extraction and DNA clean

Genome DNAs were extracted from embryos and could be used as template for further analysis. Two tested methods could satisfy this requirement.

One way was to use the lysis step on Quick-RNA FFPE Kit (mentioned in section 4.1), with digestion buffer and proteinase K from the kit. After that, use DNA Clean & Concentrator™ kit (D4004 and

D4006, Zymo Research) to purify DNA from the mixture. DNA containing solution were mixed with binding buffer from the kit and bind to column. After several steps of washing, purified DNA were collected after elution. Later the sample could be used as template for PCR reaction to investigate target region in the genome.

Another way was to use the Quick-DNA^{TM}Tissue/Insect Microprep Kit (D6015, Zymo Research).

4.3 Amplification of fragment of DNA via PCR and gel extraction

I operated the PCR (polymerase chain reaction) to amplify DNA fragment of a template. Different polymerase, with consideration for accuracy and cost were chosen. And the annealing temperature Tm, the elongation time t, could both be calculated with input of the primer sequence in NEB website (https://tmcalculator.neb.com/#!/main). In each polymerase reaction, the details were as follows:

25µl Reaction (Advantage GC 2 Polymerase, kit #639119)

16.5µl H_2O		
0.5µl dNTPs (10mM each)	96°C 2min	
5µl 5xbuffer	96°C 30 second	
0.75µl Fw Primer (10-20µM)	Tm 30 second	34x
0.75µl Rev Primer (10-20µM)	72°C elongation time	
1µl cDNA (or other template)	72°C 5min	
0.5µl Advantage GC 2 Polymerase	12°C ∞	
25 µl Total		

25µl Reaction (Pfusion Polymerase, SM0530s, NEB)

17µl H_2O		
0.5µl dNTPs (10mM each)	98°C 2min	
5µl 5x Pfu buffer	98°C 10 second	
0.75µl Fw Primer (10-20µM)	Tm (42-72°C) 30 second	34x
0.75µl Rev Primer (10-20µM)	72°C t (10-30s/kb)	
1µl cDNA (or other template)	72°C 10min	
0.25µl Pfu Polymerase	10°C ∞	
25 µl Total		

25 µl Reaction (Taq Polymerase, SM0267S, NEB)

~20µl H_2O	
0.5µl dNTPs (10mM each)	95°C 30sec

2.5µl 10x Taq buffer	95°C 15-30 second	
0.5µl Fw Primer (10µM)	Tm (45-68°C) 15-60 second	29x
0.5µl Rev Primer (10µM)	68°C t (1min/kb)	
variable cDNA (or other template)	68°C 5min	
0.125µl Taq Polymerase	10°C ∞	
25µl Total		

25µl Reaction (Q5 Polymerase, SM0491S, NEB)

~16µl H_2O		
0.5µl dNTPs (10mM each)	98°C 30sec	
5µl 5x Q5 buffer	98°C 5-10 second	
1.25µl Fw Primer (10µM)	Tm (50-72°C) 10-30 second	24-34x
1.25µl Rev Primer (10µM)	72°C t (20-30s/kb)	
variable cDNA (or other template)	72°C 2min	
0.25µl Q5 Polymerase	10°C ∞	
25µl Total		

Products of PCR reaction were detected in gel electrophoresis.

For some sample, gel extraction was used to purify DNA of target size after electrophoresis. The process was taken with Zymoclean™ Gel DNA Recovery Kit (D4002) in the following procedure: to excise DNA fragment, add 3 volumes of ADB buffer, incubate at 37-55°C for 5-10 minutes until the gel slice to completely dissolve, use column from the kit to centrifuge, wash, and elute DNA to clean Eppendorf tubes.

4.4 digestion and ligation

In order to construct target fragment into favoured vectors, a traditional method was the cut-ligation process, and it was used in protein purification experiments. The process was to firstly digest both fragment and vector with the same restriction endonuclease, then to ligate the fragment and vector. The digestion reaction at 37°C overnight with reagents as follows:

	Ets4 fragment	pET32a
BamHI	0.8µl	1 µl
NotI	0.8 µl	1 µl
DNA	~850ng, 8 µl	1000ng, 2 µl
10xCutSmart Buffer	4 µl	5 µl
H_2O	26 µl	41 µl
Total	40 µl	50 µl

The ligation reaction. The amount of insert and fragment could be calculated with NEB tools (https://nebiocalculator.neb.com/#!/ligation). And the reaction mixture as follows:

10x T4 buffer	2µl
Vector	500ng, 1 µl
Insert fragment	1 µl
H_2O	5µl
T4 ligase	1 µl
Total	20 µl

The ligation product could be used for transformation.

On the purpose of simply clone target fragment into vector for sequencing and storage, a series of kits were used to directly connect fragment to common vectors, without the first digestion with restriction endonuclease. The disadvantage for this relatively easy method was: fragments could ligate to the vector in both directions.

Kits: TOPO TA Cloning Kit for sequencing pcr4-TOPO vector (45-0030, Invitrogen), TOPO TA Cloning Kit pCR 2.1-TOPO Vector (45-0641, Invitrogen), Zero Blunt TOPO PCR cloning kit pCR-Blunt II-TOPO vector (45-0265, Invitrogen). The reaction system of these kits were relatively similar. So here only list one reaction as an example:

Gel extraction product (fragment)	2µl
Salt solution	0.5µl
PCR II Blunt TOPO vector	0.5 µl
H_2O	5µl
Total	20 µl

The reaction would take place for 1 hour at RT or ON at 4-16°C, and the product could process to transformation.

4.5 transformation

Preferred constructs could be absorbed into bacteria for amplification. And a general protocol worked well to transform DH5α (T3009, Zymo Research) and Top10 (C404003, Invitrogen) competent cells. ~50µl competent cells were thraw on ice and added with 3µl ligation product. After incubation on ice for 30 mins, the tube was heat shocked at 42°C for 30 seconds, then put back to ice for 1 minutes. 500µl SOC medium (gift for buying competent cells) was prewarmed to RT and added to the tube. And the tube would be shaken for 1 hour at 800rpm at 37°C and poured on LB-agar plates with proper antibiotics (depend on the construct) for overnight culture at 37°C.

For protein expression, vector with target protein sequence was transformed to BL21 (CMC0014, Sigma-Aldrich™) and BL21lys (70236-3, Millipore) cells. Transformation of BL21lys cells was exactly the same as the above protocol. Transformation of BL21 cells was similar but different in certain parts: the heat shock was 42°C for 45 seconds, then 2 minutes on ice, used 960µl Expression Recovery Medium instead of SOC medium for incubation, and shake at 250rpm for 1 hour. Also, the culture plate was LB-Lennox or YT plate instead of LB-plate.

4.6 colony PCR and mini prep

After transformation and overnight culture of the plates, if there were colonies growing, sometimes I set colony PCR to detect if target constructs were indeed taken in bacteria. The reaction could be of 10 µl system with polymerase mentioned above, or with the REDTaq Polymerase (R2648, Sigma) system as follows:

10µl Reaction

5µl H_2O	94°C 30sec	
0.125µl Fw Primer (10-20µM)	94°C 30 second	
0.125µl Rev Primer (10µM)	Tm 30 second	24x

variable template	72°C t
5µl Red Taq mixture	72°C 2min
10 µl Total	10°C ∞

The samples were tested in gel electrophoresis. And if they were at the right size, single colonies were inoculated in culture medium with appropriate antibiotics. In some other cases I directly picked colonies and skipped the colony PCR step.

After 8-12 hours of culturing, plasmids could be prepared from bacteria medium. I generally used Zyppy™Plasmid Miniprep Kit (D4036, Zymo Research) for prep small number of plasmids. Certain amount of bacteria medium was collected and centrifuged to get cell body mass. After lysis with Lysis buffer, and neutralize with Neutralization Buffer, cellular internal contents were collected via centrifuge and purified by column in several steps. In the last step, plasmids were eluted in elution buffer to clean Eppendorf tubes. They could be stored at -20°C or could be send with primers for sequencing.

4.7 Preserve bacteria and bacteria stock at -80°C

Bacteria with transformed constructs, could be preserved in cold-proof tube (72.692, SARSTEDT) with 750µl 80% Glycerol (15514-011, Invitrogen) and 750µl bacteria culture medium. The mixture was quickly mixed and directly frozen at -80°C. Before use, the tube was not to thraw, but to quickly flipped with tips on the top (slightly soft because of starting to melt in short period) and re-frozen at -80°C. The tip could be then inoculated with appropriate culture medium.

Most constructs in the lab were preserved in form of plasmid, and they would be transformed into bacteria if required. Constructs in BL21 and BL21lys cells were preserved in -80°C, for experiment of protein purification.

4.8 sequencing

DNA and RNA samples were sent to commercial company for sequencing.

I relied on Eurofins Genomics for Sanger sequencing of DNA samples. Each sample was in 10µl volume in total. With different prediction size of the DNA sample, the amount varied.

Type of the sample	DNA sample	Primer (1x)	H_2O
Plasmid DNA	250-500ng	25pmol	to 10µl
Purified DNA, 150-300bp	5ng	25pmol	to 10µl
Purified DNA, 300-1000bp	25ng	25pmol	to 10µl
Purified DNA, 1000-3000bp	50ng	25pmol	to 10µl

Sequencing results were analysed with Software Geneious (version 2023.0.4).

RNAseq samples were prepared as described in section 4.2, and sequenced at the Cologne Center for Genomics, using a paired-end 2 x 150nt approach on the Illimuna NovaSeq platform. Details on processing and normalizing of the data was on section 13 of this chapter.

5. probe synthesis, whole mount in situ hybridization and microscopy sample preparation

5.1 probe synthesis

Templates for probes were produced by PCR reaction, of normal Forward primer, and Reverse primer with an extra T7, T3 or Sp6 promoter sequence. For higher accuracy, polymerase could choose Advantage Taq, and the reaction was described in section 4.3.

After the reaction, the product was purified by DNA clean kit. (Section 4.2)

According to the design of the experiments, probe could be labelled with Dig or Fluorescent antibody. And RNA polymerase could be T7, T3, SP6, or other polymerase. The setting of the reaction was similar in these cases as follows:

6 µl	Purified template
1 µl	10x transcription buffer (11465384001, Roche)
1 µl	RNase inhibitor (03335402001, Roche)
1 µl	Dig-RNA labelling mix (11277073910, Roche), or Fluorescein RNA labelling mix (11685619910, Roche)
1 µl	T7 RNA polymerase (10881767001, Roche), or T3 RNA polymerase (11031163001, Roche), or Sp6 RNA polymerase (10810274001, Roche)

The reaction was taken place at 37°C for 2 hours, and single strand RNA probes were precipitated with a mixture of:

90 µl	H_2O
45 µl	7.8M ammonium acetate
450 µl	100% EtOH

RNA could be precipitated for 1 hour to overnight. The sample was centrifuged at pre-cooled equipment for 20 minutes at maximal speed at 4°C. And all the supernatant was removed. The sample was later washed with 1 ml of 75% EtOH, and again centrifuged for 10 minutes at maximal speed at 4°C. Carefully removed (even shortly spin with apparatus) all the liquid, the sample was air dry and added with 100 µl H_2O to dissolve. 5 µl of the probe solution could be used for detection by gel electrophoresis. And the probe could be stored at -20°C or -80°C.

5.2 Traditional method of in situ hybridization

Most in situ samples in this thesis were based on the traditional method. And most of the washing steps were by rotating samples in a wheeler at room temperature, unless specifically stated.

Before the experiment, embryos of the right type, stage, and amount were collected and vitellin membranes were removed properly. For heat fixed embryos, it is vital to make sure that embryos were fixed in formaldehyde after vitellin membrane preparation.

Embryos were in MeOH before the experiment. They were washed in 50% MeOH-50% PBST, 25% MeOH-75%PBST, PBST for three times and 50% PBST-50% Hyb-B, subsequently. Each washing step lasted for 5 minutes. After incubated in 500µl Hyb-B for 5 minutes at 65°C, the embryos were incubated in 500µl Hyb-A for 1 hour or longer at 65°C. Buffer in the tube was carefully removed and the embryos were added with 45-48 µl Hyb-A and 2-5 µl probe. The sample was incubated at 65°C overnight.

Embryos were washed with 500µl Hyb-B for 10 minutes and 30 minutes at 65°C in the next day, and later in 50% PBST-50% Hyb-B for 10 minutes at RT, followed by several more washes in PBST. The sample was then incubated in blocking solution for at least 30 minutes, seconded by incubation in antibody solution of anti-Dig (anti-Digoxigenin-AP Fab fragments, 11093274910, Roche) or anti-Flu (Anti-Fluorescein-AP Fab fragments, 11426338910, Roche) with a final dilution of 1:2000 in PBST for 2 to 3 hours. After that, the embryos were washed with PBST for 10 minutes twice and 30 minutes twice and washed at 4°C overnight.

Fresh AP staining buffer (0.1M Tris PH9.5, 0.05M $MgCl_2$, 0.1M NaCl, 0.001 20% Tween-20) was to prepare at the third day with a volume of roughly 5.5 ml x {the number of samples}. The Embryos were washed for 3 times in the staining buffer for 5 minutes and incubated with NBT/BCIP (11681451001, Roche) solution with a concentration of 20µl per ml in staining buffer in dark. The samples were later checked from time to time, and stopped when the staining is specifically strong with little or less background. Samples were washed in PBST of 5 times for 10 minutes to stop the staining and preserved at 4°C for longer time.

Certain types of dye were used for marking nucleus before images of the in situ hybridization samples were taken in the microscope, such as Sytox (s7020, Invitrogen, working concentration 1:50000) and DAPI (4',6'-diamidin-2-phenylindol, vectashield, vector laboratories, working concentration 1:2000).

5.3 Double in situ hybridization

With both Dig-labelled and Flu-labelled probes, it was possible to detect the two probes at the same time.

Both probes were added at the same time in Hyb-A buffer in the first day. After antibody incubation on the second day, one probe was firstly stained with NBT-BCIP buffer, washed in PBST, and incubated with inactivation buffer in 20 minutes for 3 times. The sample would then repeat the process of blocking and antibody incubation with a different type of antibody. The order of the antibody staining could work in both way: it could be anti-DIG first and anti-Flu second, or the other way around. In the fourth day the second probe was detected with substrate INT/BCIP (11681460001, Roche), in a working concentration of 5 µl/ml in staining buffer.

5.4 urea buffer in situ

The protocol was based on paper (), and the method was meant to do in situ hybridization without toxic formamide. Most procedure was in the staining of this protocol was similar to the traditional in situ hybridization staining, except (1) use urea-hybridization buffer instead of traditional ones, (2) minor change in time of incubation, and (3) working temperature at 58°C not 65°C in hybridization buffer incubation and the wash steps before and after probe hybridization.

This method worked with probes of strong expression, not weak ones. It seems to be at lower sensitivity comparing to the traditional method.

5.5 microscopy sample preparation

Most in situ hybridization images in this thesis was taken on whole amount embryos. In special cases, embryos were flattened on slides (AAAA000001##12E, Thermo Scientific) in 50-70% glycerol, and carefully deprived of yolk by tools with tip of human eye lashes. A coverslip (DV40009, Menzel Gläser; 631-0146, VWR international) was later embedded and the images could be observed in

microscope of higher magnification. Most of these steps were operated with dissecting microscope (IFE 01092, ZEISS).

6. probe synthesis, HCR

6.1 probe and probe synthesis for HCR test

This experiment is a rescue solution for not being able to produce Ets4 and Twist antibody. The experiment was suggested by Matthias Pechmann, who also designed and ordered the probes.

6.2 HCR staining

Heat fixed embryos were fixed in Clark fixative for one hour. And if longer time of storage is required, embryos could be preserved in MeOH.

Embryos were washed in PBST for 3 times at room temperature, and in 200µl probe hybridization buffer for 30 minutes at 37°C. Embryos were incubated in 100 µl probe hybridization buffer at a concentration of 0.4pmol for each probe at 37°C overnight.

On the second day, the embryos were removed of hybridization solution, and washed in 1ml probe wash buffer for 15 minutes for 4 times at 37°C, as well as 1 ml 5x SSCT for 5 minutes for 2 times at RT. Meanwhile, 6pmol (2µl of 3µM) of hairpin h1 and h2 were prepared separately and processed heat shock, for heat at 95°C for 90 seconds and cool to RT in dark for 30 minutes. Embryos were incubated with 1ml of amplification buffer for 10 minutes at RT. And after the hairpins were ready, probes were added with snap-cooled h1 and h2 hairpins to 100µl of amplification buffer at room temperature. The incubation lasted overnight at RT.

On the third day, the embryos were washed in 5xSSCT twice at RT, and stained in DAPI-SSCT with a concentration of 1:2000. With one more wash in 5xSSCR, the sample could be used for imaging.

I tested to reuse the probe hybridization buffer, and hairpin amplification buffer, by carefully collecting the old one and storing in -20°C. The second staining worked, but with weaker signals. I also tested to prepare probe wash buffer and amplification buffer in the lab, and they worked.

6.3 sample preparation

HCR samples were kept in the form of whole amount embryos and embedded into 70% glycerol on a slide. Several embryos could be planted on the same slides, and if possible, with target tissue facing upwards. Sample were covered by coverslip and imaged with a microscope (see section 10).

7. dsRNA synthesis, pRNAi and embryonic injections

7.1 dsRNA synthesis

Double strand RNA was synthesized with MEGAscript T7 Transcription Kit (AMB13345, Invitrogen), with template of target fragment from PCR reaction, using template with T7 promotor in both forward and reverse primers, as described in section 4.3.

4 µl	dsRNA template
4 µl	H_2O

2 µl	buffer
2 µl	ATP, CTP, GTP, UTP
2 µl	T7 enzyme mix

The mixture was incubated at 37°C for 4 hours to overnight. Later, a reaction was set for precipitation of dsRNA as follows, and the tube was at -20°C to -80°C from 1 hour to overnight.

20 µl	dsRNA synthesis reaction mix
30 µl	H_2O
30 µl	LiCl (provided in the kit)

The sample was precipitated at 14000rpm at 4°C for 15 minutes. All the supernatant was removed, and 1ml 75% EtOH was added to wash the pellet. After a second precipitation at 14000rpm at 4°C for 15 minutes, the pellet was air dry for 5 minutes, and 30µl H_2O was added to dissolve the pellet. The sample could be even heat up to 70 °C for 10 minutes. Later, the dsRNA solution could be stored at -20°C, or directly used for RNAi injection.

A 1:10 dilution of dsRNA sample was prepared to measure the concentration, or test on a gel.

7.2 Injection device, pRNAi injection, embryonic injection, and time-lapse images

Injection needles were pulled with MODEL P-2000, in the program: HEAT 325, FIL 4, VEL 50, DEL 255, PULL 150 and WP. Injector JFE-0250 was to equip the needles and could be used in injections of both animal adults and embryos. Tip of the needle was cut off carefully before use.

Adult females of *P. tepidariorum* were injected every second day, for four times, with 2µl dsRNA of concentration usually between 2-3 µg/µl. Water or dsRNA injections were used as a control. For each type of dsRNA, I usually have at least two replicates.

After the fourth injection, female spiders were fed with cricket, and crossed with male spiders. The progeny of the spiders would be carefully collected, examined, and recorded.

To tracing the development of RNAi embryos, a time-lapse video could be set, with embryos lining up and attached to lumox dish 35 (94.6077.331, SARSTEDT AG), by heptane glue, and immersed in Halocarbon oil (H8898-80ml, Sigma). Light source came from top or bottom of the samples.

Figure 8. Injection devices

8. CRISPR/Cas9 synthesis and cutting assay, single embryo DNA extraction, and data analysis

8.1 gRNA design, CRISPR/Cas9 synthesis and cutting assay.

Primers were designed and ordered.

Both forward and reverse gRNA primers were diluted and mixed from 20μM stock to 0.3μM final concentration of target oligonucleotide mix.

PCR reaction was set and performed, with the GeneArt Precision gRNA synthesis Kit (A29377, Invitrogen)

10.5μl H_2O	98°C 10 second	
12.5μl Phusion High-Fidelity PCR Master Mix (2x)	98°C 5 second	
1μl Tracr Fragment+T7 Primer Mix	55°C 15 second	32x
1μl 0.3μM Target F1/R1 oligonucleotide mix	72°C 1min	
25μl Total	4°C ∞	

The product was detected in 1-2% gel. If the products were at the right size (100bp and with lower primer band, perhaps), a reaction for in vitro transcription could be set, and incubated at 37°C for 2-3 hours. 1μl of DNase I was added into the reaction mix and incubated at 37°C for 15 minutes.

8 μl	NTP mix (100 mM each of ATP, GTP, CTP, UTP)
6 μl	gRNA DNA template (PCR product from above reaction)
4 μl	5x TranscriptAid Reaction Buffer

2 µl	TranscriptAid Enzyme Mix

Later the sample was purified with the same kit, with a series washing steps, into nuclease-free water. The concentration is measured with Nanodrop 2000, and the size of the product is detected with gel electrophoresis.

To test if the product could be digested by Cas9 enzyme as expected, an in vitro cutting assay is prepared, with samples of sgRNA-Cas9+, sgRNA+Cas9-, and sgRNA+Cas9+. Cas9 enzyme and buffer was from TrueCut Cass9 Protein v2 (A36498, Invitrogen).

200ng	Template (PCR or vector containing the sgRNA target seq
300ng	sgRNA, in a concentration of 200ng/µl
300ng	Cas9, in a concentration of 200ng/µl
1 µl	10x Cas9 Reaction Buffer (NEB)
x µl	RNase-free Water
10 µl	Total

The samples were incubated at 37°C for 1-2 hours and loaded in 2% gel for detection.

8.2 injection, observation, preserve embryo and imaging.

sgRNA and Cas9 protein were injected in the same concentration as in vitro experiment, into early-stage embryos, to detect the function of target gene during development. *P. tepidariorum* embryos at late st.1 was selected and prepared as described in section 7.

Embryonic injection was in principle similar to injection on adults, but with even thinner needles (same program, less cut before use) and much less reagents in each injection. The injection was implanted in two steps, first to poke a tiny hole in the embryo, and second to inject. The procedure helped to remove the internal pressure. And the injected embryos were therefore neighboured by a tiny floating ball of yolk or other embryonic substances. Similar injection method was also used in injection of fluorescent dye at mid-late st.1 embryo, for tracing the development process to analysis anterior-posterior axis formation.

After the injection, embryos were observed or set with time-lapse images to record the process of development. If a special embryo was noticed, it could be carefully removed from the plate to single Eppendorf tube, with heptane. After several times of washing with ddH_2O, the abnormal embryo could be immediately analysed or preserved at -80°C.

8.3 Single embryo DNA extraction for detection of CRISPR individuals

Abnormal embryos from crispr injection were selected and washed, and later they were digested to extract DNA as described in section 4.2. After cleaning with a kit, the DNA could be used as template to amplify the target region with a PCR reaction (section 4.3, Pfu polymerase). The primers for this PCR reaction were different from primers for producing gRNA. Provided the size of the PCR products was as expected, the fragment could be recovered by gel in electrophoresis and later sent for sequencing.

PCR products that showed a double peak or messy part in the sequencing result figure of the target region, was ligated to vector with protocol described in section 4.4. And the plasmid was later transformed to bacteria. The different adjustments of the genome in the target region, produced from crispr-Cas9 injection, were therefore separated, and amplified into single colonies. The colonies could be inoculated in culture medium, prepared for plasmid, and detected by sequencing.

9. microscopy and image processing

In this thesis, images of embryos from whole mount in situ hybridization, and time-lapse images were operated with Axio Zoom. Several buttons (bright light, controller, fluorescent light source, and computer) were switched on, and the software "Zen" were opened. The samples were prepared on glass dish under normal bright light source or transmitted light from above and adjusted to the desirable focus. For taking z-stack images, the software was under category "acquired", and the samples were altered to be right in the middle of the view with proper white balance and exposure time in bright field, as well as with proper exposure time and z stack positions in fluorescent channel. I usually took 7 slides for images of *P. tepidariorum* embryos, that was around ~30µm height between slides. For take time lapse images, plates of samples were glued to the surface, and certain time intervals were set to program image taking. If there were multiple views, different titles could be set. Individual z-stack or centre position was selected, with similar setting method for exposure time as in image taking. In most time lapse images, I used transmission light from to take images for early developmental stages, and normal light for late developmental stages.

Samples from Antibody staining were captured on V16 with AxioCam 506 colour camera. Embryos were on slides instead of in glass dish. Most settings were similar to that of Axio Zoom in taking images. For multiple fluorescent channels, each channel should be checked with exposure time individually. Also, in this microscope, I took around 15-20 slides for single embryos, that was around 10µm height intervals between slides.

Embryos from HCR staining were imaged on a LSM700 (Zeiss). Before that, samples could be checked at lower magnificent with V16 firstly, to see if the position and status of embryos on the slides were good enough for imaging in confocal microscope. The software zen was in a slightly different edition comparing to the computer of Axio Zoom, and it started with choosing program type: Acquired→smart start→choose wavelength→apply smart start. In the HCR images of this thesis, the settings were about these values: 647nm 2.0, gain=730; 594nm 2.0, gain=681; DAPI 3.0, gain=693; pinhole=1AU (x2), X·Y=1024x1024, Averaging=2. In the settings, track 1=647nm, and track 2=594nm & DAPI channel. For each sample, images were taken at 10 times as well as 40 times objective camera. A quick search to set z-stack position was performed before imaging in both cameras.

10x camera, quick live scan	zoom=1, untick track 1, speed=9, scan to set first & last z position
10x camera, experiment	set z=15 (10-20µm interval), tick track 1, speed=7
40x camera, quick live scan	zoom=0.5, untick track 1, speed=8, scan to set first & last z position
40x camera, experiment	set z=50 (1-3µm interval), tick track 1

Files of z-stack images from Axio Zoom and V16, were rendered with Helicon Focus (version 8.2.2), contrast adjusted with Adobe Photoshop (23.0.1), and composited into montage images, movie, or 3D images with Fiji (ImageJ, 1.54). Some images show interference of 647nm light, and certain slices were adjusted with red contrast to reduce the influence.

Images from LSM700 were extracted in Fiji. After adjusting contrast and brightness in each channel, they were merged back into one three-channel-stack as the "original image" of the embryo.

Meanwhile, I manually coloured the cell nucleus with “pencil tool” and “paintbrush tool” of the software, on DAPI channel, according to the expression level of certain genes, on each z stack. The manually paint DAPI channel were merged with the other two channels, and considered as the “coloured image” of the embryo, and further to produce 3D video with a plugin function in Fiji. I also counted and recorded cell nucleus number of each gene expression type to analyze.

10. RNAseq sample and data analysis

10.1 RNAseq sample dissection, data processing and volcano images with R

With forceps and needles, certain parts of embryos were dissected and carefully moved to a clean buffer dish for wash, before they were collected in Eppendorf tubes for total RNA extraction (section 4.1). The samples were sent for sequencing (section 4.8), and the reads were adapted, threshold trimmed with fastp (Chen et al., 2018). Comparing to transcriptome data of *P. tepidariorum* (Posnien et al., 2014) with Kallisto (Bray et al., 2016), the reads were later analysed with Degust (David Powell, 2015, drpowell/degust v3.2.0 Zenodo).

RNAseq data was downloaded from Degust website with method of “EdgeR” of reads of three replicates in both conditions. There were 32187 transcripts in total, and each transcript was informed of effective length, Fold2change, FDR, Average expression, and P value. The total number was based on the transcripts number of reference transcriptome (Posnien et al., 2014).

With the complete gene expression data, Volcano images could be made with R studio (R version 4.2.2; R studio version 2022.12.0) with package “EnhancedVolcano” (DOI: 10.18129/B9.bioc.EnhancedVolcano)

10.2 List of genes selected from RNAseq data.

Several different methods of selecting genes from RNAseq data set were tested: different cut-off value of Fold2Change, different cut-off value of FDR or p-value, different cut-off value of average expression, etc. Many genes were therefore selected based on various merits. As our major confirmation for gene expression method was in situ hybridization, I use criteria that might better choose potential differential genes with the sensitivity of this experiment, assuming the RNAseq data was real, reliable, and indeed reflect actual RNA expression level in embryos of the stage, after the experimental process of cDNA transcription, amplification, sequencing, and bioinformatic process of data processing. The genes after step 3 were used for later annotation and analysis and the list was considered as “Selected gene list”.

	Purpose	Action
Step 1	To remove gene with “No expression”	Calculate “Min” of all 6 reads (2 sample, 3 replicates each), and sort. Then remove the genes with Min {6 reads}<2
Step 2	To remove genes with “similar expression level” in two types of embryos	Sort the list by F2C. For genes with F2C<0, remove genes with Min {dsRed 3 reads}-Max {Ets4 3 reads}≤1
		For genes with F2C<0, remove genes with Min {Ets4 3 reads}-Max{dsRed 3 reads}≤1
Step 3	To remove genes that meet the two above requirements but weird in certain aspects	Make heatmap of all the genes (100x13) to check if expression of replicates in the same sample are dramatically different.

Heatmap images were made with R package “pheatmap” (version 1.0.12, Author Raivo Kolde)

10.3 gene annotation and homology in mouse and fly

Genes in the selected list, were firstly blasted on NCBI website (https://blast.ncbi.nlm.nih.gov/Blast.cgi?PROGRAM=blastn&PAGE_TYPE=BlastSearch&LINK_LOC=blasthome) and recorded. The results were in three types: certain gene of *Parasteatoda tepidariorum,* uncharacterized gene of *P. tepidariorum*, no significant result or of gene in other organisms. Genes of the latter two types were also blasted on Uniprot (https://www.uniprot.org/), and the result was also recorded if they were recognized as genes in other type of spiders.

To better understand the function of the selected *P. tepidariorum* genes, I searched for homology of the genes in mouse (Mus musculus) and fly (*Drosophila melanogastor*) dataset. The recorded gene names were searched in Uniprot, Alliance (https://www.alliancegenome.org/), and Flybase (https://flybase.org/). The name and ID of theses homology genes were recorded, and the list of these genes were considered as “homology of selected gene list”.

10.4 go analysis and pathway analysis.

Go analysis was implanted with the name of genes in “homology of selected gene list”, through annotated database of fly (org.Dm.eg.db) and mouse (org.Mm.eg.db) in R. The program “enrichGO” automatically enriched and analysed the function of fly and mouse genes on the aspects of biological process, molecular function and cellular component.

Similarly, with the name of homology genes and the Fold2Change value for the “homology of selected gene list”, I performed pathway analysis using “gseKEGG” in R program. And the results were also in two versions: of fly and mouse.

I also tried to analyse pathway in a lower standard manually, by downloading images of critical pathways in kegg (https://www.genome.jp/kegg/pathway.html), and searched for the name of every gene in the image to check if they were also in the “Selected gene list”.

Tested pathways: Notch signalling pathway, Hh signalling pathway, Hh (fly) signalling pathway, wnt signalling pathway, NF-κB signalling pathway, TGF-BETA signalling pathway, JAK-STAT signalling pathway, PI3K-AKT signalling pathway, Ras signalling pathway, mTOR signalling pathway, FOXO signalling pathway, MAPK signalling pathway, MAPK (fly signalling pathway), HIF-1 signalling pathway, AMPK signalling pathway, VEGF signalling pathway, HIPPO signalling pathway, HIPPO (fly) signalling pathway, Insulin signalling pathway, Ubiquitin mediated proteolysis, Complement and coagulation cascade, ERBB signalling pathway, EGFR tyrosine kinase signalling pathway, Dorsal-ventral axis formation, apoptosis signalling pathway, Embryonic stem cell pluripotency pathway.

10.5 manually analysis on gene function

Based on literature, and important kegg pathway images, I listed important genes in cellular process of proliferation, metabolism, migration, differentiation, and apoptosis. Comparing of this list to the “Selected gene list”, genes in the intersection parts were recorded and analysed with more detail annotation information, to summarize the possible role this gene played in the corresponding cellular process.

The results were 5 excel tables, and each table contained information of RNAseq data of relevant genes.

10.6 gene network, other analysis from online bioinformatic tools

Online tools “String” (https://string-db.org/cgi/input?sessionId=bohZAb4HSTZb&input_page_show_search=on) was used to identify network of RNAseq differential expression genes. The input were fly homology of the *P. tepidariorum* genes.

11. protein purification, antibody production, SDS-PAGE and Western Blot

11.1 purification of Ets4 protein

I tried to purify Ets4 protein in the lab. The gene fragment (pointer domain only, without homeodomain) was inserted to expression vector Pet32a, and the plasmid was transformed into Bacteria strain BL21 as described in section 4.5 and stored at -80°C as described in section 4.7. Buffers in these experiments were most filtered in 0.2μm filter (PN 4433, Life Sciences), and stored at 4°C.

Firstly, I performed test run for IPTG induction. 10 ml BL21-Pet32a-Ets4 bacteria were inoculated and cultured at 37°C till A_{550}=0.5-1. 2ml bacteria medium was transferred to Eppendorf tube as zero-time sample. The remaining medium was added with 1M IPTG and continued to grow with aeration. 2ml bacteria medium was collected at 1h, 2h, 4h, and ON, these samples were centrifuges at maximal speed at RT for 1 min, resuspended with SDS-loading dye (50 mM Tris-Cl pH 6.8, 100 mM dithiothreitol, 2% w/v SDS electrophoresis grade, 0.1% bromophenol blue, 10% v/v glycerol, 5% beta-Me), and heated at 95°C for 5 minutes. Samples were detected with SDS-PAGE. Later, more tests were operated on different induction condition of IPTG concentration (0.5M and 1M), temperature (26°C and 37°C), and induction time.

Secondly, I tested if the potential Ets4 (Pointer domain) protein was soluble or insoluble in BL21-Pet32a-Ets4 bacteria. Small-scale of BL21-Pet32a-Ets4 bacteria were inoculated and collected after IPTG induction for 4 hours at 37°C. The cells were incubated on ice in lysis buffer (Ph=8 50mM Tris, 100mM NaCl, 1mM DTT, 1mM lysozyme, 1mM PMSF, and DNaseI), and the cell lysate was centrifuged at 20000g at 4°C for 30 minutes to separate supernatant (soluble cell contents) and pellets (in soluble, such as inclusion bodies). Samples were detected by SDS-SAGE.

Thirdly, I tried small-scale purification on His-tag protein by Ni-NTA beads (Ni-NTA Agarose, 30210, Qiagen). Beads were washed in PBS and centrifuged at 500g at RT for 3 minutes to remove supernatant. The beads mixed with cell lysate (as described in last paragraph) and incubated on ice for 20 minutes. The mixture was centrifuged at 500g at RT for 3 minutes, and the supernatant after this centrifuge, as well as beads plus pellet were separately heat at 95°C for 5 minutes with SDS-loading dye. Samples were detected in SDS-SAGE and Western Blot.

Later, large-scale purification on Hig-tag protein by Ni-NTA beads were performed. 1L of BL21-Pet32a-Ets4 bacteria were inoculated and cultured until A_{550}=0.5-1, then induced with 1M IPTG at 37°C for 4 hours. Cells was harvest by centrifuge at 5000g, at 4°C for 15minutes. The sample could be directly used for further step (most time) or stored at -80°C. The pellet is resuspended into 10ml lysis buffer (Ph=8 50mM Tris, 500mM NaCl, 15% Glycerol, 10mM Imidazole, PMSF, lysozyme), and aliquot into Eppendorf tubes for sonicatation (Sonifier II W-450 Branson) at 80% duty cycle, power 9 for 14 minutes. All the supernatant was collected into one falcon tube and added DNaseI to 0.1mg/ml, $MgCl_2$ to 1mM, PMSF 1/100 final concentration. The sample was centrifuged at 22000g at

4°C for 30 minutes. Meanwhile 1ml Ni-NTA resin was washed with water and binding buffer (50mM Na_3PO_4, 500mM NaCl, 20mM Imidazole), and centrifuged at 1000g for 10s to save the pellet. Also, the column (Polypropylene Columns, 1ml, Qiagen, 34924; Pierce centrifuge columns, 10ml Prod #89898) was cleaned with ddH_2O and binding buffer for three column volume each. Beads and Cell lysate were incubated at 4°C for 1 hour, and the mix was loaded to column. After a series of washing with binding buffer, his-Ets4 protein was eluted with Elution buffer (50mM Na_3PO_4, 500mM NaCl, 250mM Imidazole) and collected in Eppendorf tubes. The sample was measured by nanodrop and dialyzed overnight (Dialysis tubing, 32mm x 20mm, D0530-100FT, Sigma-aldrich). I also tested to further concentrated the purified protein with centrifugal filter tube (Centrifugal Filter units, Amicon Ultra 4ml 10kD, UFC801024, Millipore; Centrifugal Filter units, Amicon Ultra 15ml 50kD, UFC905008, Millipore), but there was a lot of loss in protein amount. Intermediate product of the whole process, and the final protein samples were detected in SDS-SAGE and Western Blot.

The final products were from SDS-PAGE tests. After de-staining, correct size bands of His-Ets4 protein in 6% SDS-PAGE gel were cut off and collected in Eppendorf tubes. The samples were washed in H_2O for several times, weighted, and temporarily stored at 4°C. 8 tubes of ~100mg Ets4-protein-containing gel pieces were sent out to commercial company (Eurogentec, www.eurogentec.com) for antibody production.

11.2 antibody production

Antibody production was carried out by a commercial company Eurogentec, with purified Ets4 protein sample in SDS-PAGE gel from us. The protein was purified by the company and injected into two rabbits for several times in two months of different quantities to produce rabbit-antibody again Ets4 protein. The blood sample from rabbits before and after different injections were collected and sent to us. Also, after a purification process carried out by the company. I got final sample of purified Ets4 antibody.

In a different project, I sent out sequence of twist gene of *P. tepidariorum* to company (ProteoGenix, www.proteogenix.science),and got purified antibodies of mouse against pt-twist.

11.3 SDS-PAGE, Western Blot and antibody staining

SDS-PAGE. SDS-polyacrylamide gels were manually prepared from 30%polyacrymide, Ph=8.8 1.5M Tris buffer, Ph=6.5 0.5M Tris buffer, 10% SDS, 10% Ammonium persulfate, and TMEMD, with separating gel in 10% or 6%, stacking gel in 5%, and combs of 1.0mm. Marker (Perfect Protein Marker, 15-150kDa, 69149-0.5ml, Millipore; Color Protein Standard Broad Range, #P7712S, Biolabs) and samples were loaded to wells of 20-25µl in volume. Electrophoresis was carried on at 90V until all samples passing the stacking gels and changed to 110-120V. The gels were stained in Coomassie staining buffer for several hours at RT, then de-stain with methanol: acetic acid solution several times at RT. The gels could be imaged by smartphone or Bio-RAD Molecular Imager Gel Doc XR+ and preserved in 10% Glycerol at 4°C for several months.

Western Blot. SDS-PAGE gels were transferred into NC membrane (porablot NCP, 0.45µm, 741280, macherey-nagel) in a cassette with sponge and filter paper under 100V for 1 hour. The transfer buffer (5 mM Tris, 192 mM glycine, and 20% methanol) was pre-cold at 4°C and an icebox was put in the back of the apparatus. The membrane could be stained in Ponceau S to aid in cutting of the membrane, and the staining could be washed off with 0.1M NaOH and H_2O. The membrane was blocked in blocking solution (5% milk in PBST, or 5% BSA in PBST), and incubated in 1st antibody at different concentrations (Rabbit mAb, Cell Signaling Technology, Inc.; 1:1000 for Monoclonal Anti

polyHistidine antibody, H1029, #0000090863, Sigma; 1:1000 for pre-immune serum of rabbits; 1:1000 for intermediate blood samples of rabbits after injection of Ets4 protein, 1:100-1:1000 for purified rabbit anti Pt-Ets4 antibody; 1:100 for purified mouse anti Pt-twist antibody) in 1% milk of PBST. After 4 times of wash in PBST for 10 minutes, the membrane was incubated in 2nd antibody (1:5000, anti-mouse HRP, or anti-rabbit HRP) 1:5000 of 1% milk, in PBST for 45 minutes, then washed again in PBST for 4 times for 10 minutes. The membrane was detected in staining buffer (WesternSure PREMIUM Chemiluminescent Substrate, 926-95000, LI-COR) and imaged by C-Digit LI-COR.

Antibody staining (Immunostaining). Embryos of interested stage were collected and prepared to remove vitelline membrane. After washed in 50% EtOH-PBST and 25% EtOH-PBST for 5 minutes, the embryos were washed in PBST for 3 times of 5 minutes and blocked in blocking solutions (10 mg/ml BSA, 5% NGS in PBST) for 1 to 5 hours, and incubated in 1st antibody in blocking solutions overnight, at various concentrations (1: 2000 for Phospho-Smad1/5, Ser463/465, 41D10, Rabbit mAb, Cell Signaling Technology, Inc.; 1:50 for Cleaved Caspase, D175, 9661s, cell signalling; 1:1000 for β-catenin, C2206, Sigma; 1:200 to 1:10000 of pre-immune rabbits serum before injection of Ets4 protein; 1:75 to 1:10000 of intermediate rabbits serum during injection of Ets4 protein; 1:10, 1:100 and 1:1000 for purified rabbit anti Pt-Ets4 antibody; 1:10, 1:100 or 1:1000 for pre-immune mouse serum before injection of mouse protein; 1:10 or 1:100 for purified mouse anti Pt-Twist antibody). Embryos were washed in PBST for 3 times every 5 minutes and for 4 times every 30 minutes, then blocked in blocking solution for 1 hour. The samples were incubated in 2nd antibody in blocking solution for 2 hours for Alkaline Phosphatase antibody, and for overnight for fluorescent antibody in various concentrations (1:2000 for Anti-Rabbit IgG alkaline Phosphatase antibody produced in goat, A3687, Sigma; 1: 2000 for Anti-Mouse IgG Alkaline Phosphatase antibody produced in goat, A3562, Sigma; 1:400 for Alexa 647 Fluor goat anti-rabbit IgG, A21245, Invitrogen; 1:400 for Alexa 488 Fluor goat anti-rabbit IgG, A11008, Invitrogen). Samples were washed in PBST for 3 times every 5 minutes and for 4 times every 30 minutes, before detection. For samples with alkaline phosphatase antibody as 2nd antibody, they were detected in staining buffer (0.1M Tris PH9.5, 0.05M $MgCl_2$, 0.1M NaCl, 0.001 20% Tween-20) by NBT/BCIP (11681451001, Roche) solution with a concentration of 20µl per ml in dark. Staining was stopped by washing in PBST of 3 times for 5 minutes and samples were preserved at 4°C or directly took image by microscope. For samples with fluorescent antibody as 2nd antibody, they were detected with microscope under proper source of emitting light. Nucleus of the embryos could be stained by Sytox (s7020, Invitrogen, working concentration 1:50000) and DAPI (working concentration 1:2000) before microscopy. A few test runs were also performed with this experiment: test run to absorb anti Pt-Ets4 antibody in fixed st.2 *P.tepidariorum* embryos before the antibody was used as primary antibody, in the aim of reducing unspecific binding; test run to change PBST into PBS-0.5% Triton X-100; and tests to change different concentration for 1st antibody.

12. Other

The writing of the Introduction, Result and Discussion part, were with the help of ChatGPT(version 3.5 and 4.0) to check grammar mistakes.

3 Results Chapter I: Morphological Observations on Early Development of WT and *Ets4* RNAi embryos in *Parasteatoda tepidariorum*

1. The normalization of developmental time.

The development of *Parasteatoda tepidariorum* (*Pt*) is typically highly synchronized among embryos within the same cocoon, particularly during the early stages of development. Fourteen stages of embryonic development were classified (Mittmann and Wolff, 2012, supplementary Figure 1) based on the characteristics of key developmental events. The time range post-egg laying at 25℃ (hours after egg laying, hael) was recorded. This classification system was widely accepted and commonly used to describe *Pt* development.

To achieve a more precise analysis of early developmental stages, and to compare multiple samples from different sources, minimizing the influence of developmental conditions such as temperature and individual variation among animals, I proposed a normalization process to standardize *Pt* embryo development using a series of continuous time-lapse images. This method would enable us to describe the *Pt* development with an hourly resolution.

For videos of new embryos, I recorded the number of frames corresponding to at least two key events. Since this study focused on early development, the key events identified are: reaching the 32-cell stage, completion of germ disc contraction, and initiation and termination of cumulus migration. Using the frame counts, the actual developmental time between these events was calculated. Concurrently, the time intervals for the same events as described by Mittmann and Wolff (2012) could be calculated. A ratio was then computed comparing the actual development time to the hours after egg laying (hael) developmental time. This ratio allowed for the normalization of all other frames in the video to "hael time".

For example, the video Movie 13-3 (Figure 1, c1, c2, c3, c4) was imaged at 15-minute intervals. Frame 1 showed the embryo at the 32-cell stage, and frame 82 showed the initiation of cumulus migration. The actual developmental time between these two events was calculated as

$$(82 - 1) * 15\text{min} = 20\text{h}15\text{min}$$

According to Mittmann and Wolff (2012), the corresponding "hours after egg laying" (hael) times for these events were 11 hael and 31 hael, respectively. Thus, the hael developmental time between these events was

$$31 - 11 = 20\ hael$$

The ratio of actual developmental time to hael developmental time is therefore

$$\frac{20h15min}{20hael} = 1.01\frac{hour}{hael}$$

This ratio is considered consistent within the same video. To calculate the hael time for a random frame in video 13-3, such as frame ***70***, the formula would be:

$$(\mathbf{70} - 1) * \frac{15min}{1.01} + 11\ hael = 28hael \qquad \text{or} \qquad 31\ hael - (\mathbf{70} - 1) * \frac{15min}{1.01} = 28hael$$

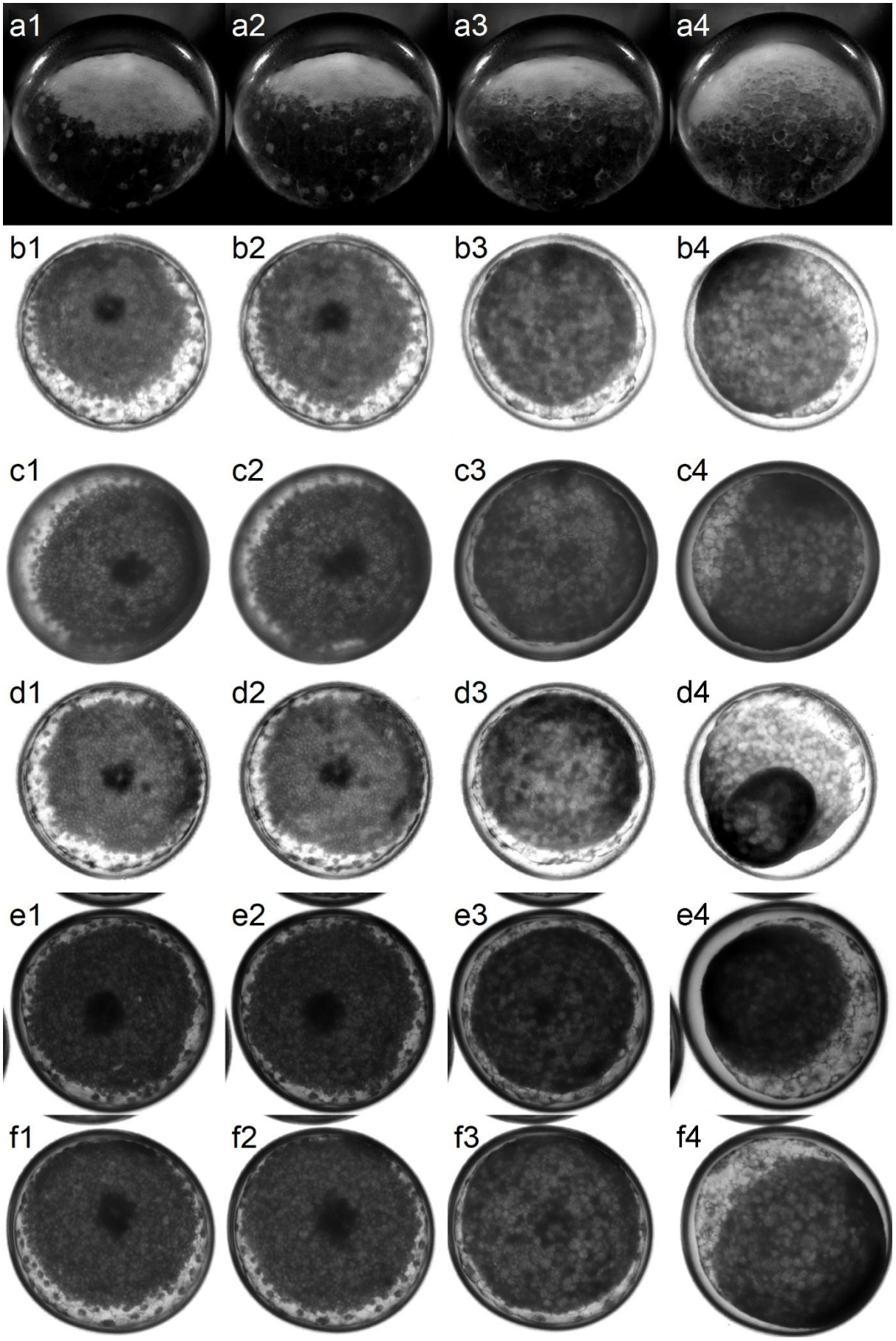
a1
a2
a3
a4
b1
b2
b3
b4
c1
c2
c3
c4
d1
d2
d3
d4
e1
e2
e3
e4
f1
f2
f3
f4

Figure 1-1. Montage image of WT and *Ets4* RNAi embryo at 28, 31, 41 and 52 hael. A1, A2, A3, A4: frame 137, 161, 241 and 329 of Supplementary Movie 1, Pechmann et al., 2016. B1, B2, B3, B4: frame 43, 61, 121 and 187 of Movie 1, Pechmann et al., 2017. C1, C2, C3, C4: frame 70, 82, 122 and 166 of WT video Movie 13-3. D1, D2, D3, D4: frame 31, 49, 109, and 175 of Movie 1, Pechmann et al., 2017. E1, E2, E3, E4: frame 14, 20, 40, and 50 of *Ets4* RNAi video 1-44. F1, F2, F3, F4): frame 14, 20, 40 and 50 of *Ets4* RNAi video 2-44. A1, B1, C1, D1, E1, F1: 28 hael. A2, B2, C2, D2, E2, F2: 31 hael. A3, B3, C3, D3, E3, F3: 41 hael. A4, B4, C4, D4, E4, F4: 52 hael.

Using this method, it would bd possible to normalize all developmental times in *Parasteatoda* to standard "hours after egg laying" (hael) at 25°C. This allowed for the comparison of samples from different sources at the same hael time (supplementary Table S1-1, S1-2). Figure 1-1 showed wild-type (WT) and *Ets4* RNAi embryos at 28, 31, 41, and 52 hael. Some embryos were from previously published studies (Figure 1-1 row A, B, D), while others were newly videotaped (Figure 1-1 row C, E, F). After the normalization procedure, the same types of embryos resembled each other at the same hael time. Different types of embryos exhibited similarities at the first two time points but diverged at the two later time points.

Subsequently, I quantified the cell count in the video to determine the total number of cells at standardized hael time for WT embryos (Figure 1-2). At 18 hael, the germ disc comprised approximately 300 cells, increasing to about 500 cells by 22 hael. This data was corroborated by alternative estimations: tracing selected cells (supplementary Figure S1-1), counting their progeny (supplementary Figure S1-2), and calculating the average division time of germ cells (supplementary Figure S1-3).

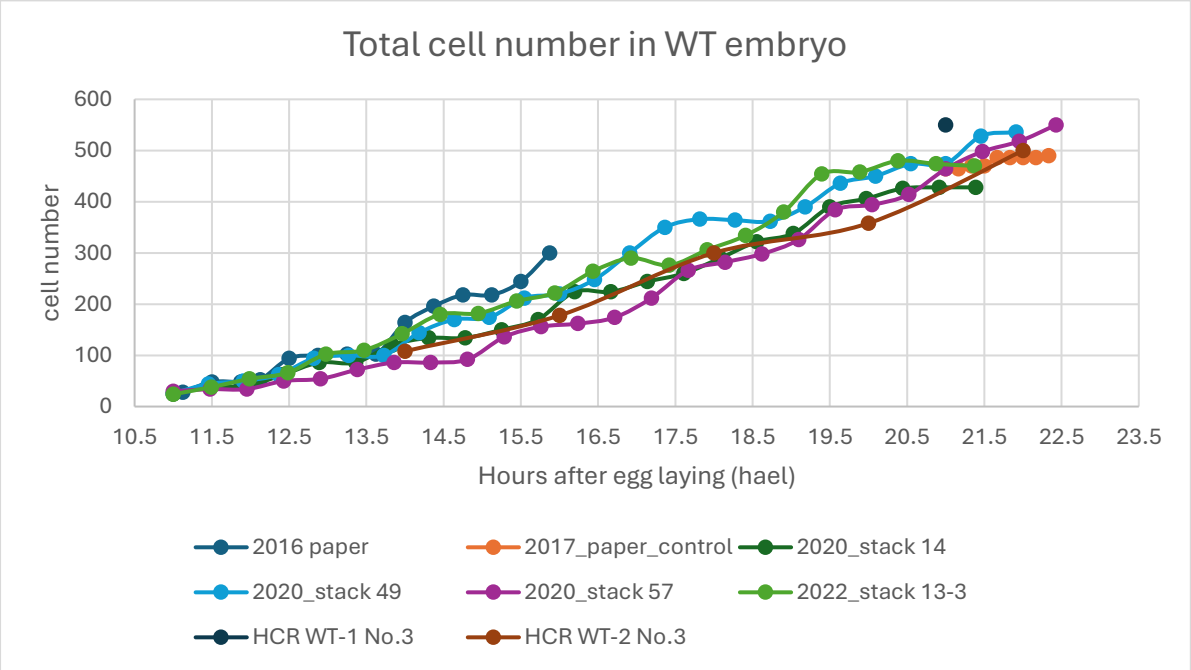

Figure 1-2. Cell counts in WT Embryos from 11 to 24 hael.

Supplementary Figure S1-4 illustrated the total cell number in *Ets4* RNAi embryos from 21 to 23 hael. Comparison shows that, at 21 to 23 hael, the WT germ disc cell number was slightly greater than that of the *Ets4* RNAi embryos at the same time point (supplementary Figure S1-5).

2. The definition of primary thickening region.

The primary thickening referd to the central region of the germ disc during stages 3 to 4 of development. From movies showing the embryonic development of *Pt* embryos, it was evident that the primary thickening undergoes continuous development, with an increasing number of cells contributing to its enlargement over time (supplementary Figure S1-6). Our research primarily focused on this region. The cumulus was a cluster of cells derived from primary thickening and was characterized by its migration at stage 5.

To clarify the concept, I defined the "primary thickening region" as the inner part within a border delineated by 26 cells at 24 hael in the WT *Pt* embryo (Figure 1-3, A3). At earlier stages, the primary thickening region was defined as the area encompassed by the ancestors of these 26 cells at 24 hael (Figure 1-3, A1, A2). Staining images at 24 hael as well illustrate this region within the border of 26 cells (Figure 1-3, B1, B2, B3). Figure 1-3, B3 demonstrates that all cells beneath the ectoderm were contained within this 26-cell border.

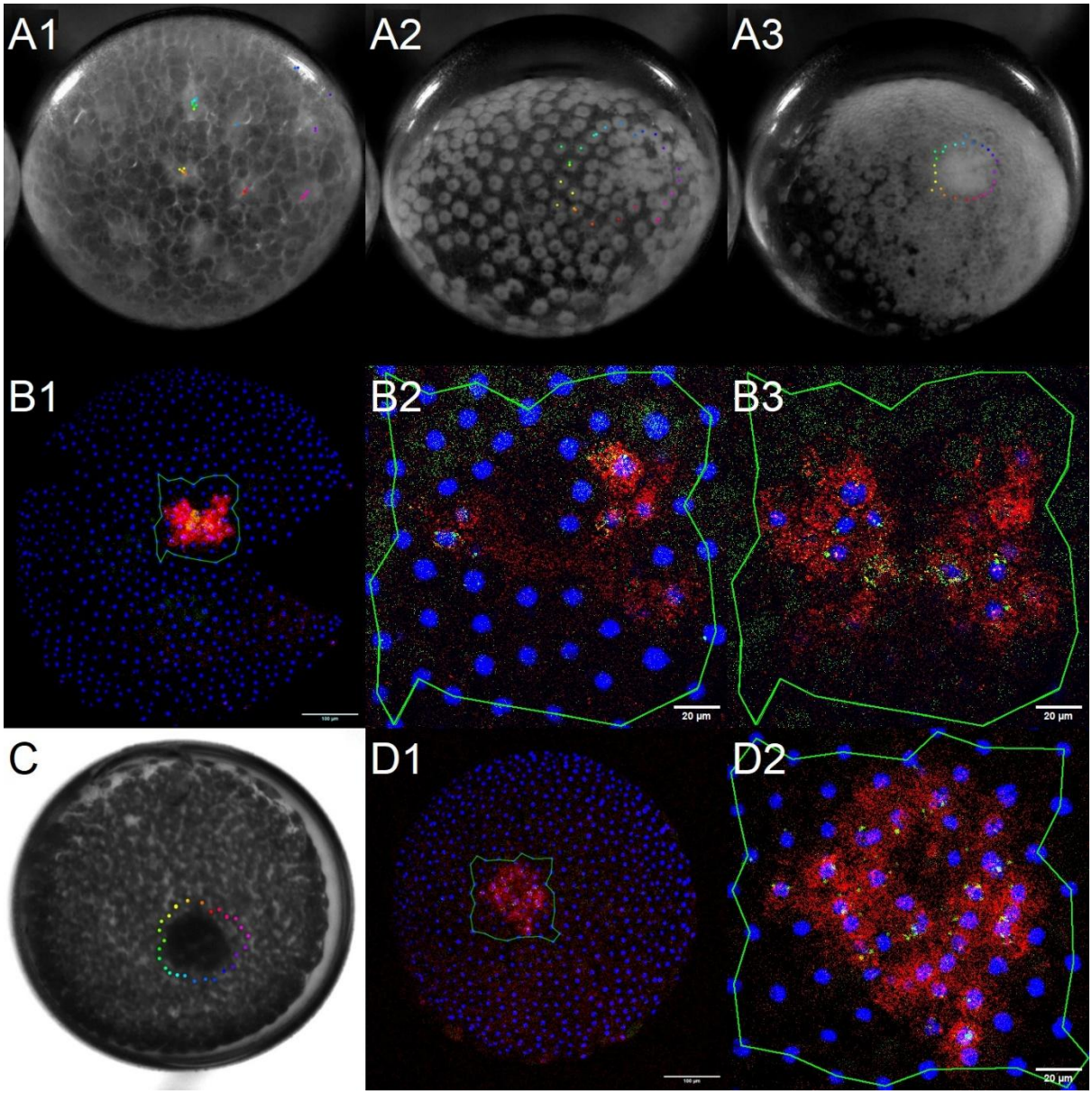

Figure 1-3. 26-cells-region of WT and *Ets4* RNAi embryos. A1, A2, and A3: WT embryo. Frame 1,58 and 116 of Supplementary Movie 1, Pechmann et al., 2016, of, at hael 11, 17.75 and 24.5. Primary thickening region is

artificially defined and marked in A3, and traced frame by frame in the video to A1. B1, B2 and B3: WT embryo at 24 hael. B1: 10x. B2 and B3: 40x. B2: ectoderm of the region. B3: inner layer with largest area. C: *Ets4* RNAi embryo, frame 4, No.1-21, at 23 hael. D1 and D2: *Ets4* RNAi embryo at 23 hael. D1: 10x. D2: 40x, z project. Green lines passing through and linked 26 cells, with the same cells in three images. HCR staining. Blue: Dapi. Red: *fuchi*. Green: *Ets4*.

The size of the 26-cell region measured approximately 19,000-20,000 μm² at 21 to 23 hael, reducing to 16,000-17,000 μm² by 26 hael (Figure 1-3, B2, B3; supplementary Table S1-3).

The primary thickening region of *Ets4* RNAi embryos was defined using methods analogous to those described previously (Figure 1-3, C and D1). All inner cells located within the 26-cell region up to at least 24 hael (Figure 1-3, D2).

I conducted cell counting within the 26-cell region (Figure 1-4) of WT embryos, using bright-field videos from 11 to 19 hael, and a series of HCR staining images from 18 to 26 hael. All samples were normalized to a standard "hael" time. The overlapping results around 18 hael indicated alignment between cell counts obtained from both sources.

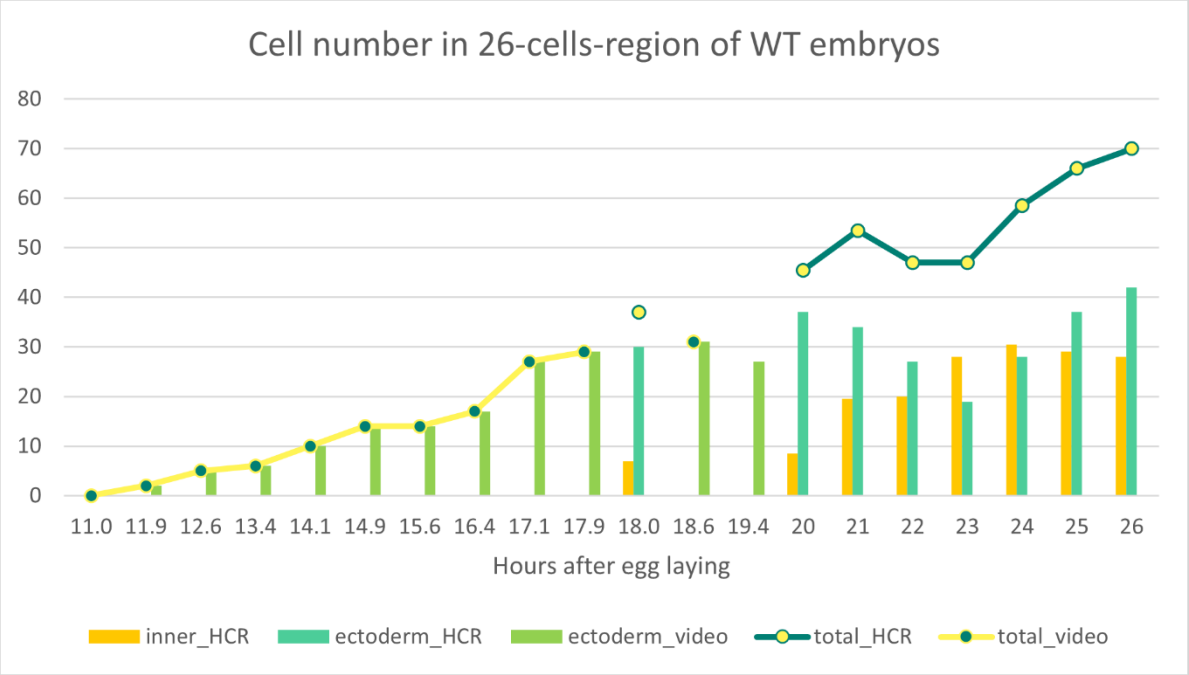

Figure 1-4. Number of cells in 26-cells-region. 11-19.4 hael counts are cell counting of Supplementary Movie 1, Pechmann et al., 2016 (Figure 1-3 A1-A3). 18-26 hael counts are of average number of ectodermal, inner and total cells in 26-cells-region of HCR samples.

Comparing the cell growth rate in the primary thickening region (Figure 1-4) to the complete germ disc region of WT embryos (Figure 1-2, supplementary Figure S1-3), it became evident that the cells within the primary thickening region proliferated at a similar rate to those in the rest of the germ disc region (supplementary Figure S1-7). The visually greater density observed in the primary thickening region was thus primarily a result of faster contraction.

Cell counts were also conducted within the 26-cell region of *Ets4* RNAi embryos. Due to limited samples, counts were available only for 21 to 25 hael. Within this range, the total cell number in the primary thickening region of *Ets4* RNAi embryos was found to be similar to that in WT embryos (supplementary Figure S1-8).

3. Definition of types of cells in the primary thickening.

Previous research identified several specific genes expressed in the primary thickening region, including *dpp*, *Ets4*, *fuchi*, *fascin*, *hb*, *twist*, etc. (Akiyama-Oda and Oda, 2003; Yamazaki et al., 2005; Schwager et al., 2009; Pechmann et al., 2017; Iwasaki-Yokozawa et al., 2022). In our study, I performed HCR staining to detect the expression of *Ets4* and *fuchi* genes. Due to the high sensitivity of the experiment, I distinguished three types of gene expression levels in the results: nascent transcripts (na+), weak expression, and strong expression.

In the primary thickening region of WT embryos, four distinct cell populations were identified based on varying expression levels of *fuchi* and *Ets4* during early developmental stages (Figure 1-5): the cells showed nascent transcripts of both *fuchi* and *Ets4* genes, but no cytoplasm expression (*fuchi* $^{na+}$ *Ets4* $^{na+}$ cell; Figure 1-5 A); the cell showed weak expression of both genes in cytoplasm (*fuchi*$^{+}$*Ets4*$^{+}$ weak; Figure 1-5, B); the cell showed strong expression of both genes (*fuchi*$^{+}$*Ets4*$^{+}$; Figure 1-5, C1, C3, D, E1, D2); and the cell showed strong expression of *fuchi* but no expression of *Ets4* in the cytoplasm (*fuchi*$^{+}$*Ets4*$^{-}$ cell; Figure 1-5, C1, C3, D, E1, E2)

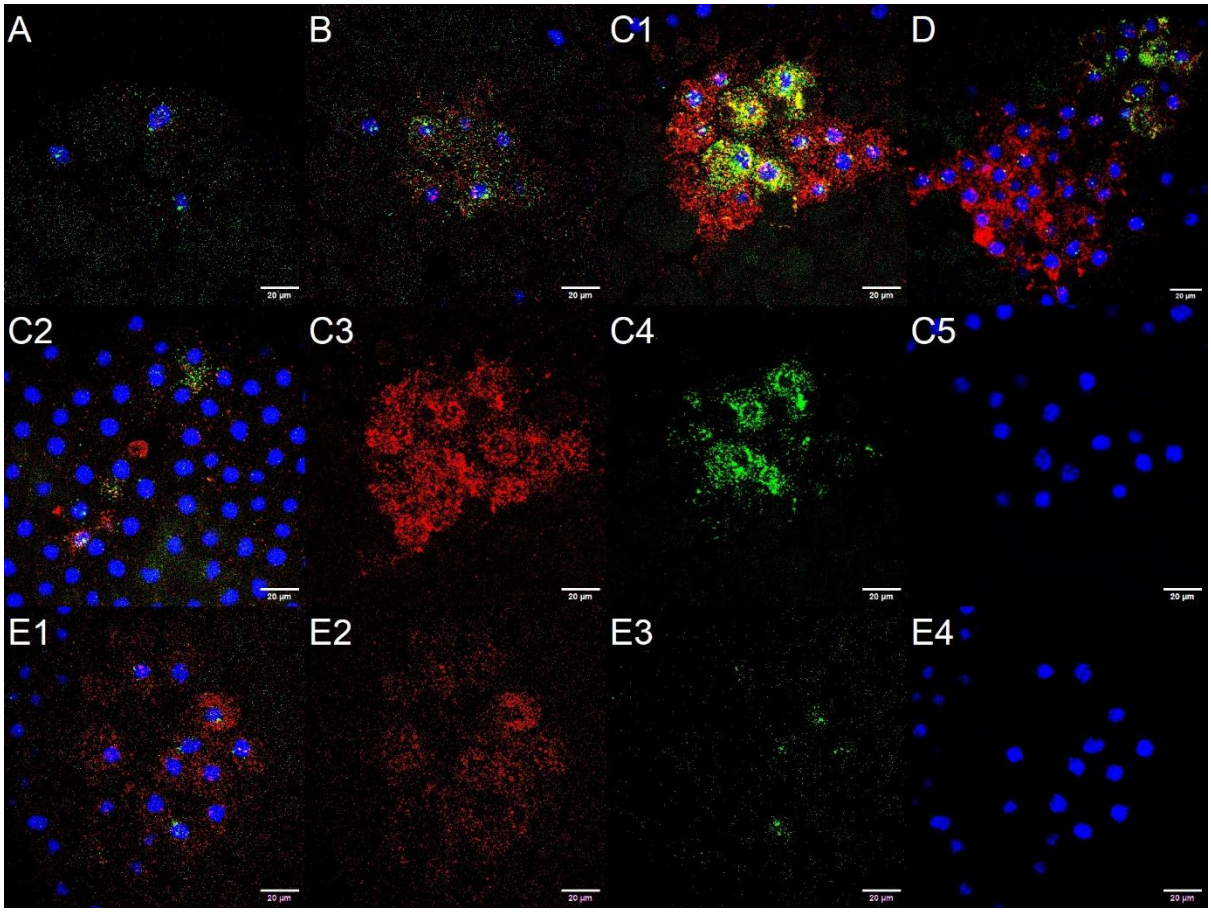

Figure 1-5. Different types of cells. A. *fuchi* $^{na+}$*Ets4* $^{na+}$ cells, WT sample, at 16 hael. B. *fuchi*$^{+}$*Ets4*$^{+}$(weak) cells, WT sample at 20 hael. C1, C2, C3, C4, an C5: WT sample at 26 hael. C1: inner layer. C2: ectoderm. C3, C4, and C5: three splitting channels of C1. D. WT sample at 35 hael. E1, E2, E3, E4: *Ets4* RNAi embryo at 27 hael. E1: inner layer. E2, E3, E4: three splitting channels of E1. 40x. HCR staining. Blue: Dapi. Red: *fuchi*. Green: *Ets4*.

There were more possible combination of *fuchi* and *Ets4* expression in cells. However, Between 22 and 30 hael, in the primary thickening region of WT embryos, the following observations were made: (1) all inner cells expressed *fuchi*; (2) all *Ets4*$^{+}$ cells were also co-expressed *fuchi* (Figure 1-5, C1, C3, C4). In addition, a distinction was observed between *fuchi*$^{+}$*Ets4*− cells with and without nascent *Ets4* transcripts at different development time (Figure 1-5 C1, D). Furthermore, the majority of ectoderm cells (Figure 1-5, C2) did not express *fuchi*, and none were observed to express *Ets4*.

In *Ets4* RNAi embryos, no *Ets4*$^{+}$ cells were detected, confirming the efficacy of the RNAi technique employed. All inner cells within the primary thickening primary thickening region were *fuchi*$^{+}$*Ets4*$^{-}$ cells (Figure 1-5, E1, E2, E3). A distinction was observed between these cells based on the presence or absence of nascent *Ets4* transcripts (Figure 1-5, E1). The cell types observed in the primary thickening region of WT and *Ets4* RNAi embryos, in reference to the expression of *fuchi* and *Ets4*, were summarized in supplementary Table S1-4.

Based on the previously defined cell types, I conducted cell counts for each type within the primary thickening region of WT embryos from 14 to 39 hael (Figure 1-6, supplementary Figure S1-9, S1-10, S1-11, S1-12, S1-13, S1-14).

In summary, there are approximately 15 *fuchi*$^{+}$*Ets4*$^{+}$ (weak) cells observed at 18-20 hael (Figure 1-6 B, supplementary Figure S1-9, S1-10). From 21 to 27 hael, the primary thickening region comprised around 10 *fuchi*$^{+}$*Ets4*$^{+}$ cells and 20-30 *fuchi*$^{+}$*Ets4*$^{-}$ cells (Figure 1-6, supplementary Figure S1-11). With around 10 cells, the number of *fuchi*$^{+}$*Ets4*$^{+}$ cells remained stable until the migration stage. Meanwhile, *fuchi*$^{+}$*Ets4*$^{-}$ cell number increased to 40-50 in one cocoon and remain consistent at 20-30 in another cocoon (Figure 1-6, supplementary Figure S1-12, S1-14).

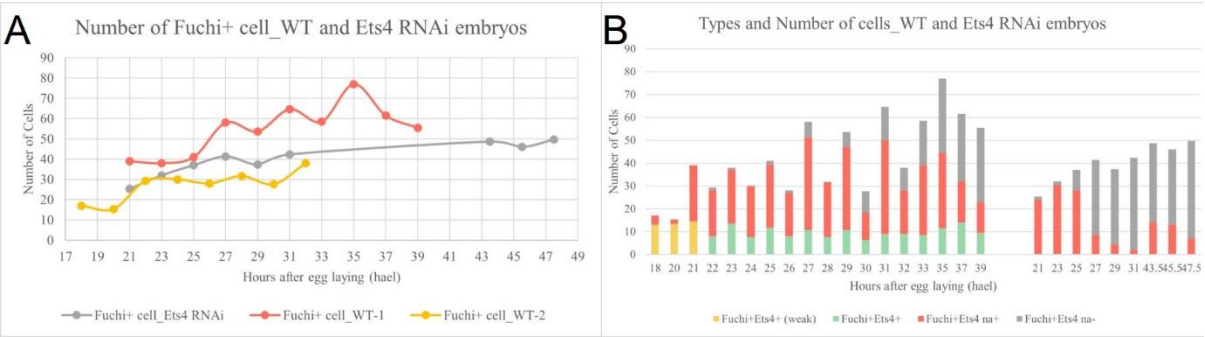

Figure 1-6. Counts of different types of cells at 14-49 hael based on HCR images from supplementary Figure S1-9 to Figure S1-18. A: total counts of *fuchi*$^{+}$ cells at 18 to 35 hael in WT embryos, and at 21 to 49 hael in *Ets4* RNAi embryos. B: *fuchi*$^{+}$*Ets4*$^{+}$ and *fuchi*$^{+}$*Ets4*$^{-}$ cells counts in both WT and *Ets4* RNAi embryos. *fuchi*$^{+}$*Ets4*$^{-}$ cells are further classified into *fuchi*$^{+}$*Ets4* $^{na+}$ and *fuchi*$^{+}$*Ets4* $^{na-}$ cells.

Similar cell number counting was performed in *Ets4* RNAi embryos from 21 to 31 hael (Figure 1-6, supplementary Figure S1-15, S1-16, S1-18). The total number of *fuchi*$^{+}$ cells in *Ets4* RNAi embryos fall between the counts observed in two different WT cocoon embryos at the same time points (Figure 1-6, supplementary Figure S1-19). This variation was not considered significant and was likely due to sample variations.

These results confirmed the findings in Section 2, where I compared the primary thickening cell numbers between WT and *Ets4* RNAi embryos at 21-26 hael (supplementary Figure S1-8).

I summarized the information regarding cell types and counts of different cell types in WT and *Ets4* RNAi embryos from stages 2 to 5, illustrated in a schematic image (Figure 1-7). In WT embryos,

fuchi na^{+}*Ets4* na^{+} cells initially increased gene expression and transited into *fuchi*$^{+}$*Ets4*$^{+}$(weak) cells around 18 hael. By 22 hael, these cells further differentiated into *fuchi*$^{+}$*Ets4*$^{+}$ and *fuchi*$^{+}$*Ets4*$^{-}$ cell types, which subsequently progressed into more specialized states.

Conversely, in *Ets4* RNAi embryos, no *Ets4*$^{+}$ cells were observed. The number of *fuchi*$^{+}$ cells increased around 21 hael and remained stable for the next 20 hours.

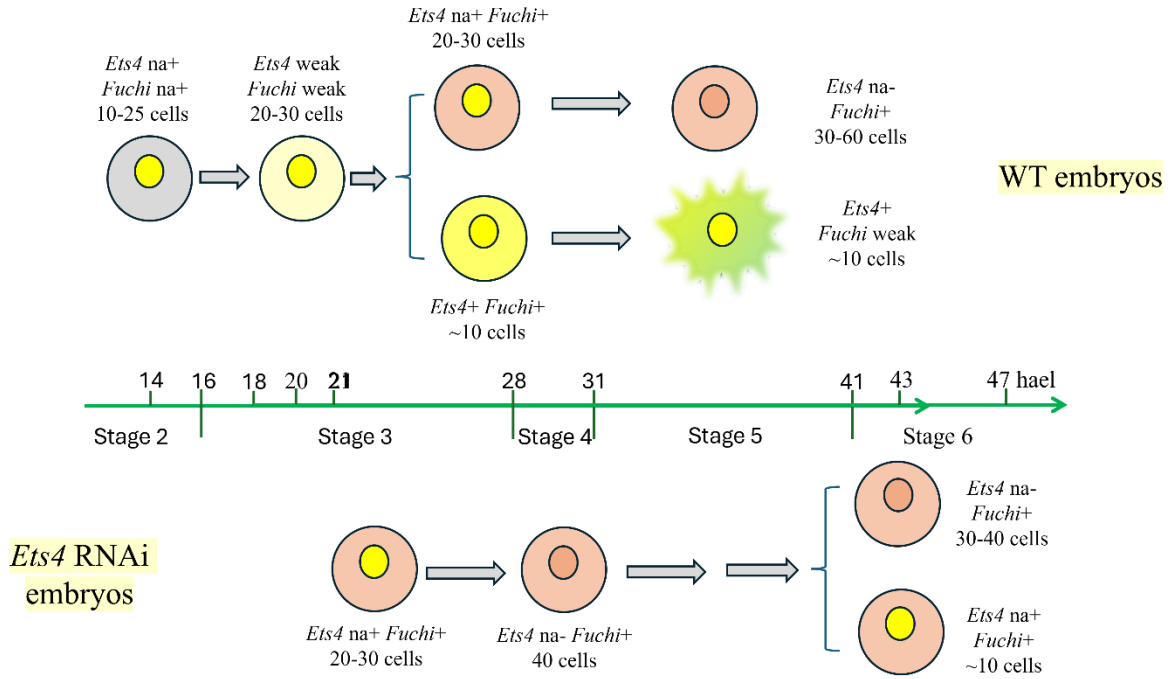

Figure 1-7 A combined schematic image of cumulus cell lineage with WT and *Ets4* RNAi embryos. WT embryos are from 14 to 39 hael, and *Ets4* RNAi embryos are from 21 to 31 and 43 to 47 hael. Cells are marked with dual cycles representing nucleus and cytoplasm. *fuchi* expression is indicated in red colour and *Ets4* expression in green, and co-expression of *fuchi* and *Ets4* expression in red. Cytoplasmic expression is marked in the large outer cycle, while nascent transcripts are denoted in the smaller inner cycles. The image also includes development stages, timetable, important events of WT and *Ets4* RNAi embryos.

4. First asymmetry event: embryonic and extraembryonic division. Invagination.

After 11 hael in *Pt* development, the majority of cells were localized at the embryo surface, with an absence of inner cells. In exceptionally rare instances, a single cell was observed positioned centrally within the embryo (supplementary Figure S1-20).

The first morphologically observable event marking cell differentiation in spider was the division of embryonic and extraembryonic cells at stage 2. Embryonic cells concentrated towards the center, excluding yolk, leading to an increase in cell density over time (Pechmann et al., 2016). In contrast, the extraembryonic region exhibited decreasing cell density.

Around the initiation of contraction, cells in the center of the embryonic region (future germ disc) repositioned themselves from the ectoderm to positions beneath the surface previously occupied by yolk. This process ultimately resulted in the formation of a multi-layered structure in the central area of the germ disc, known as the "primary thickening". The movement of cells into the inner layer was referred to as "invagination".

Recent studies reported that the primary thickening region consistently localizes opposite to the polar bodies in early-stage embryos (Wang and Pechmann, 2024). This spatial arrangement was observed in both WT (supplementary Figure S1-21) and *Ets4* RNAi embryos (supplementary Figure S1-22). Polar bodies, products of primary oocyte meiosis, became discernible at stage 1 of fertilized embryos (Mittmann and Wolff, 2012). Notably, the nuclei of polar bodies were significantly smaller than those of zygote cells and the cells were surrounded by *fuchi*$^{+}$ cells in the extraembryonic region (Iwasaki-Yokozawa, 2022; supplementary Figure S1-23).

Cell tracing analyses revealed that the primary thickening progenitors originated from 5 to 6 cells at the 32-cell stage, with the site of invagination located centrally within this region (Figure 1-8). Although this observation was consistently confirmed across multiple samples, the underlying mechanisms remained unclear.

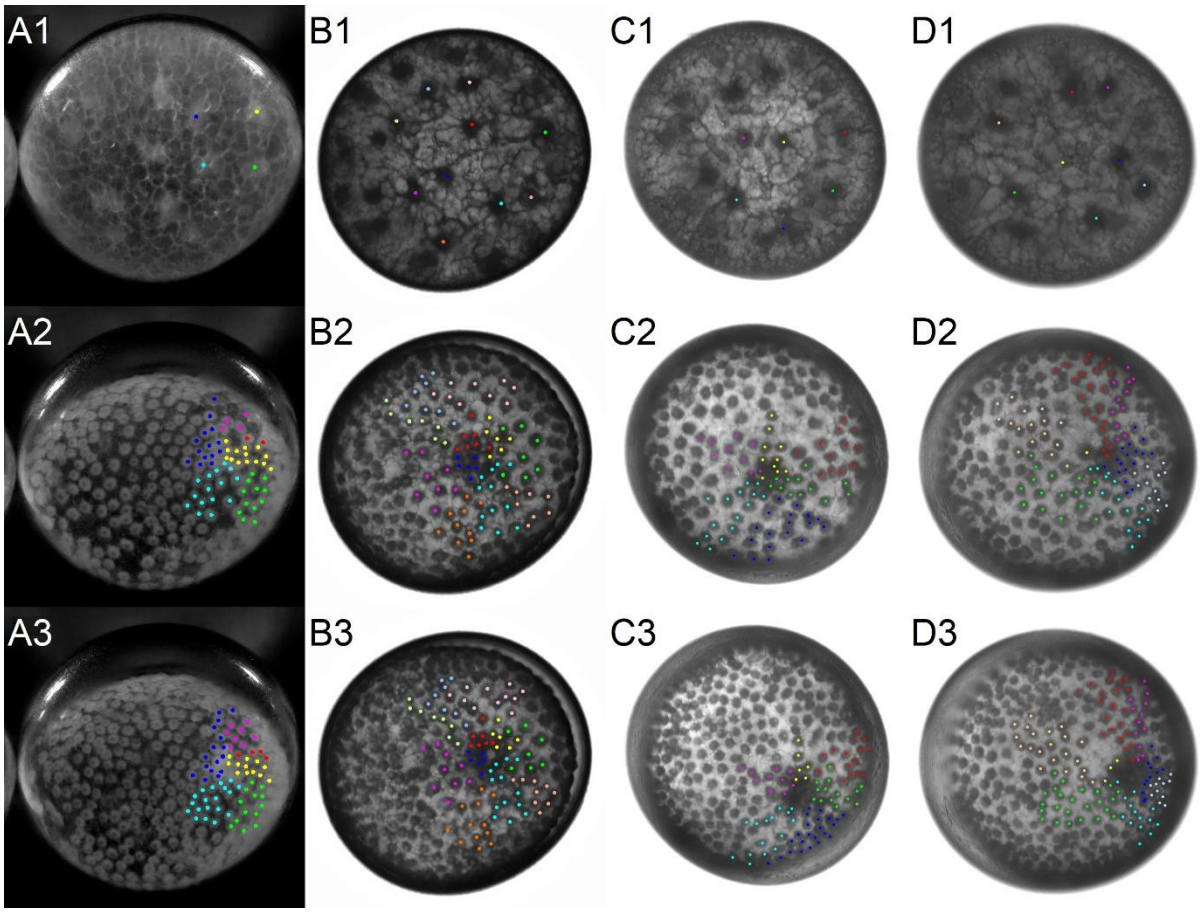

Figure 1-8. Lineage tracing of primary thickening cells in WT embryos from 11 to 21 hael. Progenies of the same cell at 11 hael, are marked in the same colour, unless the cells move out of view or cannot be distinguish in overlapping regions. A1, A2 and A3: from supplementary movie 1, Pechmann et al., 2016. B1, B2, and B3: from WT stack 87. C1, C2 and C3: from WT stack 2-2. D1, D2, and D3: from WT stack 13-4. A1, B1, C1, and D1, around 32-cell stage, at 11 hael. A2, B2, C2 and D2: initiation of invagination, last image before observing cell internalize, around 18 to 20 hael. A3, B3, C3 and D3: Around 20 to 21 hael.

Additionally, as mentioned previously, all inner cells within the primary thickening region at stages 3-4 exhibit *fuchi* expression, with some cells also expressing *Ets4*. In most embryos, the primary thickening region was the sole area where cells co-express both genes. Additionally, in all embryos examined, only one region undergone the process of "invagination" within the germ disc, consistently located at the center.

Figure 1-9 presented time-lapse images illustrating *fuchi-Ets4* co-expression regions at 14 hael (A1, A2, A3) and 16 hael (B1, B2, B3), as well as the invagination site observed between 18-22 hael (C1, C2, C3, D1, D2, D3, E1, E2, E3).

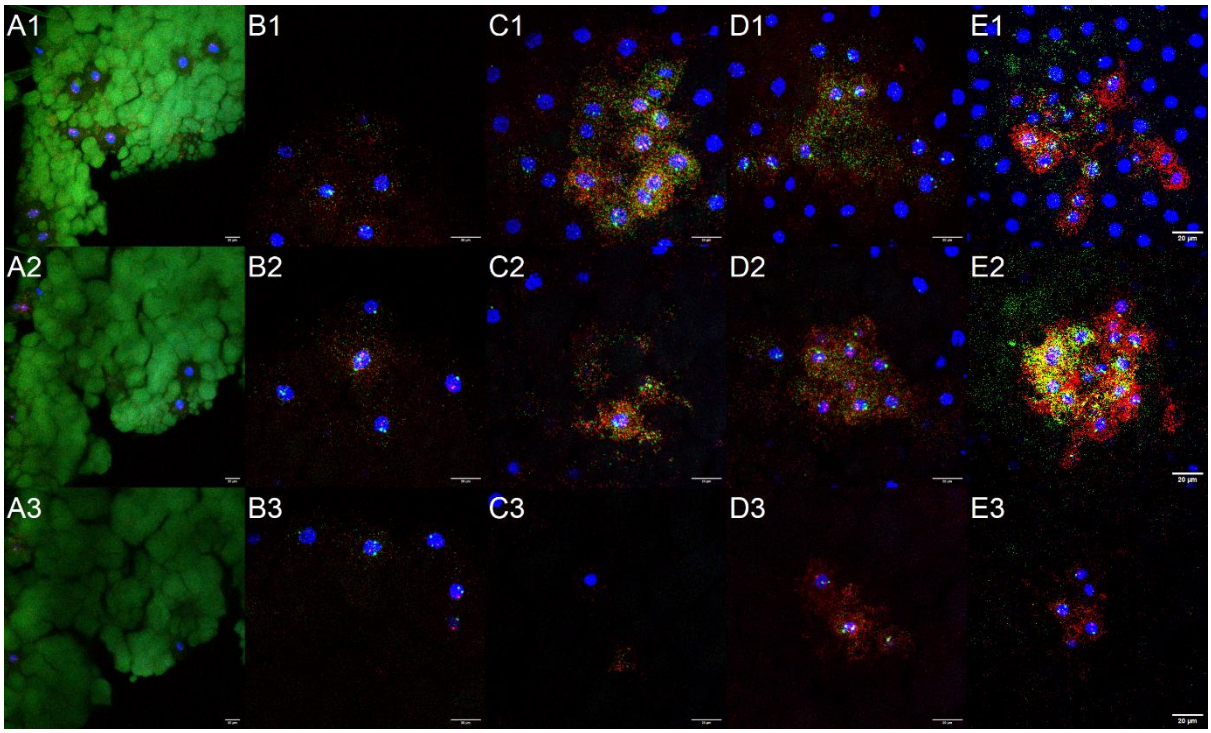

Figure 1-9. Invagination process. A1, A2 and A3: WT-2 0h e5, max z-stack images of slices 11-22, 23-34 and 35-46, 14 hael. B1, B2 and B3: WT-2 2h e9, max z-stack image of slices 5-16, 17-28 and 29-40, 16 hael. C1, C2 and C3: WT-2 4h e5, max z-stack images of slices 14-21, 22-29 and 30-37, 18 hael. D1, D2 and D3: WT-2 6h e4: max z-stack images of slices 15-26, 27-38 and 39-50, 20 hael. E1, E2 and E3: WT-2 8h e1 max z-stack images of slices 2-8, 9-15, and 23-29 (16-22 not shown), 22 hael. HCR staining. Blue: Dapi. Red: *fuchi*. Green: *Ets4* (It is auto-fluorescent signal in yolk in A1, A2 and A3).

By 14 hael, clusters of 10-20 *fuchi* na$^+$*Ets4* na$^+$ cells were observed, arranged in a single layer. There was minimal difference observed in gene expression levels among these cells (Figure 1-9, A1, A2, A3).

At 16 hael, the region still contained several *fuchi* na$^+$*Ets4* na$^+$ cells arranged in a single layer. However, some cells exhibited higher expression levels of both genes and could be identified as *fuchi*$^+$*Ets4*$^+$(weak) cells (Figure 1-9, B1, B2, B3. Figure 1-5, B).

Invagination was observed to initiate at 18 hael, when several *fuchi*$^+$*Ets4*$^+$(weak) cells located in two or three layers beneath the ectoderm. Additionally, more *fuchi*$^+$*Ets4*$^+$(weak) cells were observed in the ectoderm, surrounding a hole which appears to be the previous location of the current inner cells, identified as the blastopore (Figure 1-9, C1, C2, C3).

Two hours later, the majority of *fuchi*$^+$*Ets4*$^+$(weak) cells repositioned in the inner layer, and the blastopore enlarged (Figure 1-9, D1, D2, D3).

During the period from 18-20 hael, there were approximately 10-20 *fuchi*$^+$*Ets4*$^+$(weak) cells in total (Figure 1-6).

From 22 hael onwards, *Ets4*$^+$ cells were exclusively found in the inner layer. Cells that previously exhibited weak expression levels now transitioned into cells with strong expression of *Ets4* and *fuchi*

genes. These cells further differentiated into either *fuchi*$^{+}$*Ets4*$^{+}$ or *fuchi*$^{+}$*Ets4*$^{-}$ cells. The total cell number within this region increased to approximately 30-40 cells.

During this period, the blastopore gradually shrunk in size and eventually closed completely around 27 hael (supplementary Figure S1-11).

Supplementary Table S1-5 summarized the counts of different types of cells during the invagination process. Analysis of cell number and average nuclear volume changes indicated that the majority of cells involved in invagination undergo division between 18 and 21 hael, coinciding with the observed time span of invagination (supplementary Figure S1-24).

A comparative analysis was conducted between WT and *Ets4* RNAi embryos at 21 and 23 hael, as depicted in Figure 1-10. Despite the absence of *Ets4*$^{+}$ cells in *Ets4* RNAi embryos, there were minimal differences observed in the invagination process between both types. Total cell numbers, distribution across layers, cell locations, and developmental processes at the same time points exhibited remarkable similarity (Figure 1-10, A4 and C4, B4 and D4, A5 and C5, B5 and D5, A6 and C6, B6 and D6). In *Ets4* RNAi embryos, cell division within the primary thickening region also continued during the invagination process (supplementary Figure S1-25), as in WT embryos (supplementary Figure S1-24).

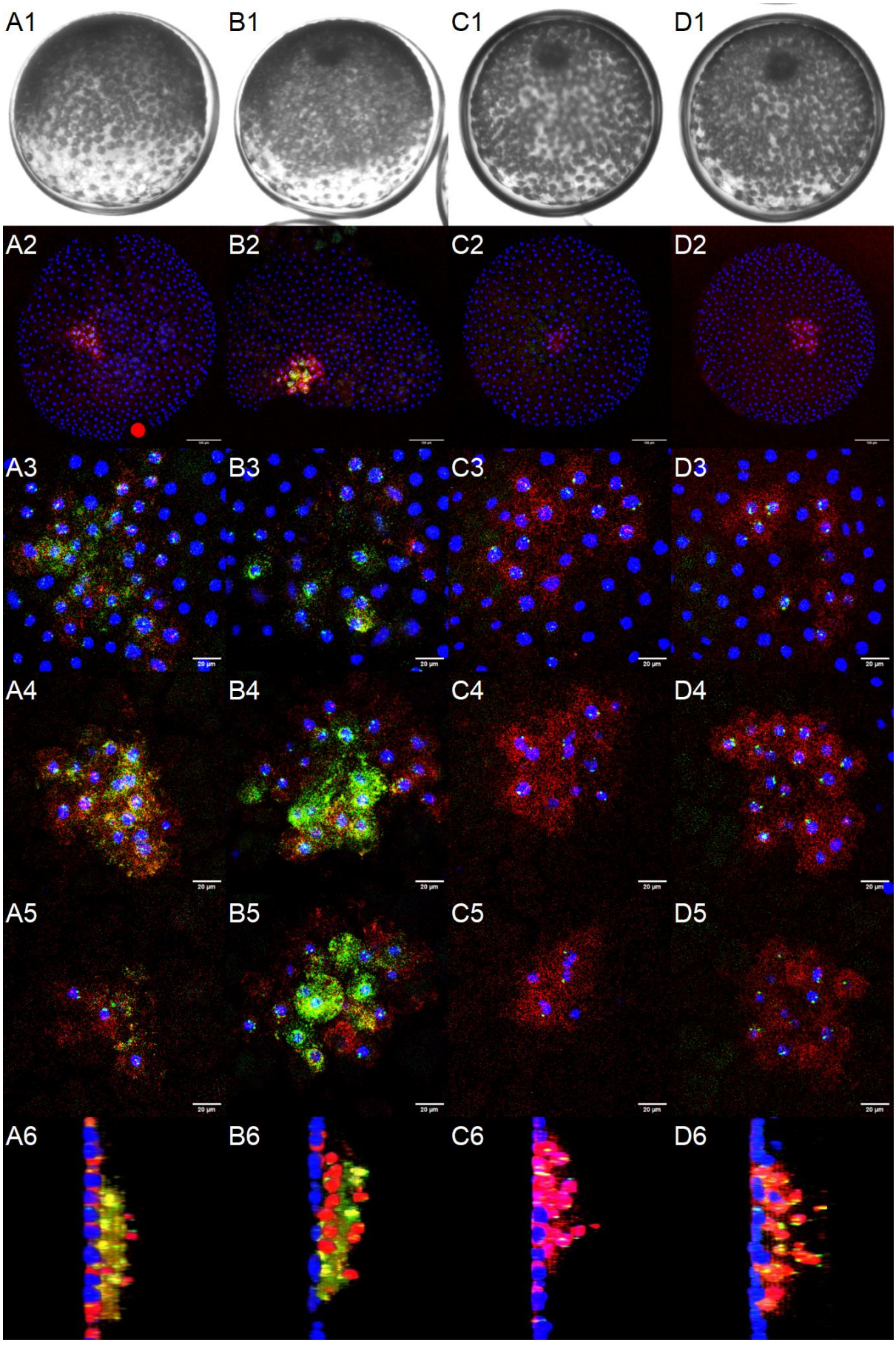
A1
B1
C1
D1
A2
B2
C2
D2
A3
B3
C3
D3
A4
B4
C4
D4
A5
B5
C5
D5
A6
B6
C6
D6

Figure 1-10. Comparison of WT and *Ets4* RNAi embryos at invagination process. A1, A2, A3, A4, A5, and A6: WT-1 0h e4, 21 hael. B1, B2, B3, B4, B5 and B6: WT-1 2h e4, 23 hael. C1, C2, C3, C4, C5 and C6: *Ets4* RNAi 0h e3, 21 hael. D1, D2, D3, D4, D5 and D6: *Ets4* RNAi 2h e1, 23 hael. A1, B1, C1 and D1: bright field image of embryo from the same cocoon. A2, B2, C2, and D2: AVG-z-stack, 10x. A3, A4 and A5: AVG z-stack of frame 2-7, 8-13, and 14-19. B3, B4, and B5: AVG z-stack of frame 3-11, 12-20, and 20-28. C3, C4 and C5: AVG z-stack of frame 3-9, 10-16, and 17-23. D3, D4 and D5: AVG z-stack of frame 3-9, 10-16, and 17-23. A6, B6, C6 and D6: lateral view of 3D model, of respective 40x image. HCR staining. Blue: Dapi. Red: *fuchi*. Green: *Ets4*.

In all examined samples, including video recordings and staining images, only a single invagination site was observed. In rare instances, clusters of 3 to 4 *fuchi*$^{+}$*Ets4*− cells were identified within the germ disc, situated outside the primary thickening region. These clusters were located in the ectoderm and were in close proximity to the primary thickening region. Such occurrences were noted in both WT (supplementary Figure S1-26) and *Ets4* RNAi embryos (supplementary Figure S1-27), with an incidence rate of approximately 1–2% in both groups.

5. Internalized cell differentiate according to *Ets4* expression level

Following invagination, *fuchi*$^{+}$*Ets4*$^{+}$ (weak) cells differentiated into distinct populations: *fuchi*$^{+}$*Ets4*$^{+}$ and *fuchi*$^{+}$*Ets4*− cells (Figures 1-6 and 1-7). This differentiation process was completed at around 24 hael. The transition in gene expression levels occured for 3 hours, roughly between 21 and 24 hael in wild-type embryos (Figure 1-11).

At approximately 22 to 23 hael, *fuchi*$^{+}$*Ets4*− cells and *fuchi*$^{+}$*Ets4*$^{+}$ cells were mixed in the primary thickening region beneath the ectoderm. (Figure 1-11, columns B and C).

A discernible pattern emerged from 24 to 31 hael, in the top view of *fuchi*$^{+}$*Ets4*$^{+}$ and *fuchi*$^{+}$*Ets4*− cell clusters within the primary thickening region. *fuchi*$^{+}$*Ets4*$^{+}$ cells were centrally located and are surrounded in an incomplete manner by *fuchi*$^{+}$*Ets4*− cells, with niches apparent in one or two directions (Figure 1-11, columns D, E, F; supplementary Figure S1-28; Figures S1-11 and S1-12).

The pattern of *fuchi*$^{+}$*Ets4*$^{+}$ and *fuchi*$^{+}$*Ets4*− cell clustering in the primary thickening region was observed across multiple embryos, with variations in the size and number of niches. However, all observed patterns deviated from a radially symmetric arrangement.

It was long believed that the transition from morphological radial symmetry to bilateral symmetry began when a subset of primary thickening cells (cumulus) initiated migration along the radial axes around 31 hael. The precise directional choice of this cell movement remained unclear, as it showed considerable diversity even within the same batch of samples. Recent studies reported asymmetric expression of *fgf8* in germ disc cells 2 to 3 hours before cumulus migration began, with variable and highly dynamic patterns (Wang et al., 2023). In this study, I observed regional asymmetry as early as 24 hael, confined to the primary thickening region. The asymmetrical clustering pattern of *Ets4*$^{+}$ and *Ets4*$^{-}$ cells observed between 24 and 31 hael may represent an early precursor to the subsequent asymmetrical events leading to bilateral symmetry.

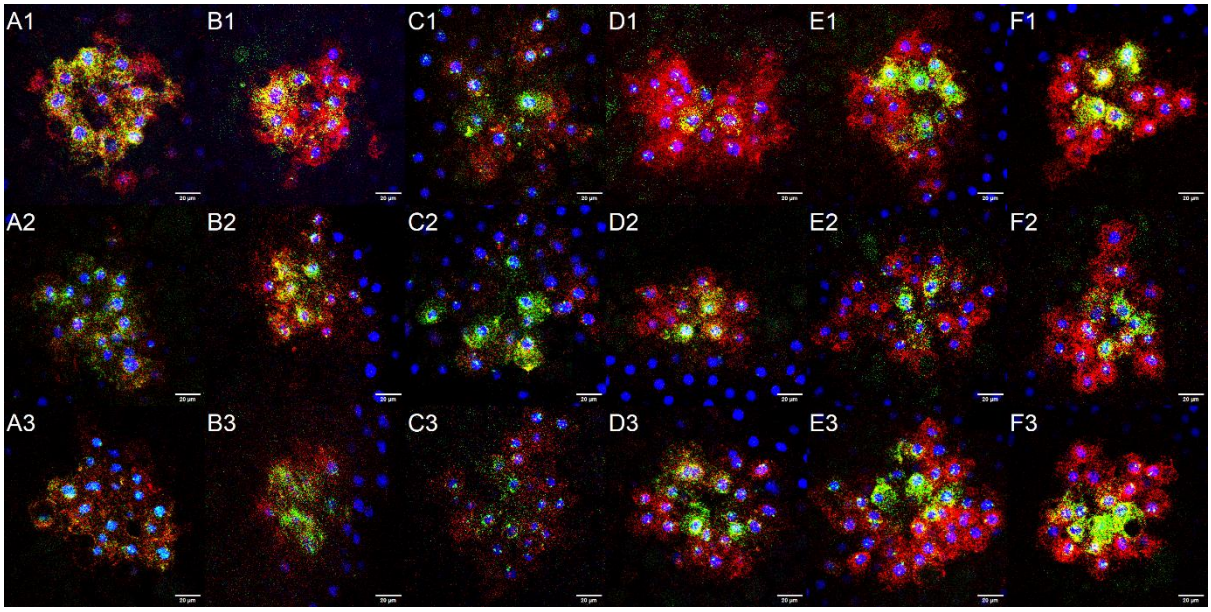

Figure 1-11. Top view of all the centre inner cells of embryos at 21 to 26 hael. AVG z-stack of inner region, 40x. A1, A2 and A3: 21 hael. B1, B2 and B3: 22 hael. C1, C2 and C3: 23 hael. D1, D2 and D3: 24 hael. E1, E2 and E3: 25 hael. F1, F2 and F3: 26 hael. Blue: Dapi. Red: *fuchi*. Green: *Ets4*.

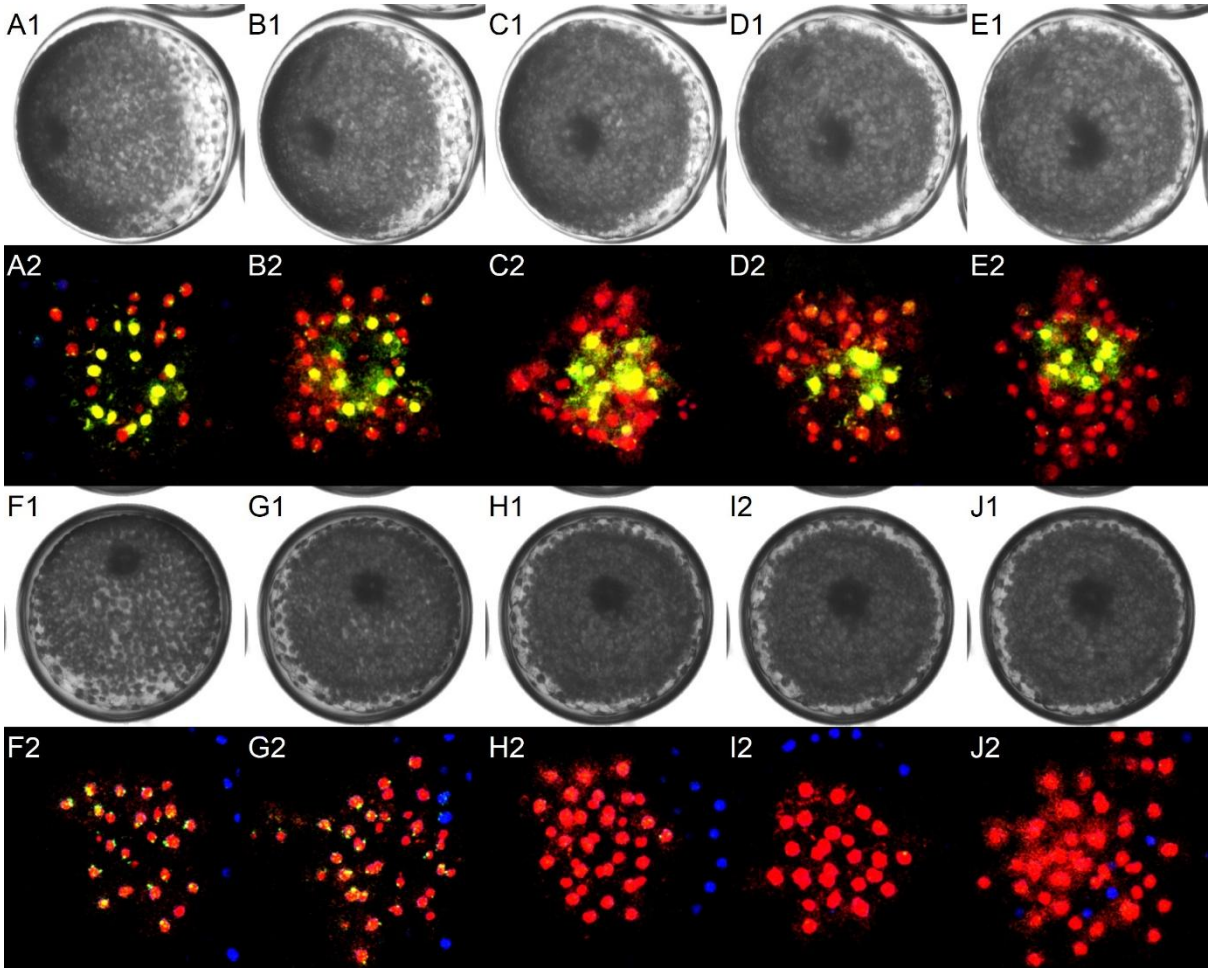

Figure 1-12. Bright field and 3D top view of all the centre inner cells of embryos at hael 23, 25, 27, 29 and 31, of WT and *Ets4* RNAi embryos. A, B, C, D, E: WT embryo. F, G, H, I, J: *Ets4* RNAi embryo. A1, A2, F1, F2: 23 hael. B2, B2, G1, G2: 25 hael. C1, C2, H1, H2: 27 hael. D1, D2, I1, I2: 29 hael. E1, E2, J1, J2: 31 hael. A1 to J1: bright field. A2 to J2: 3D top view of inner cells. 40x images were colours and made into 3D model by Fiji. Blue: Dapi. Red: *fuchi*. Green: *Ets4*.

Figure 1-12 illustrated the relative spatial arrangement of *fuchi*$^{+}$*Ets4*$^{+}$ and *fuchi*$^{+}$*Ets4*$^{-}$ cells within the primary thickening region of WT and *Ets4* RNAi embryos from 23 to 31 hael, as viewed from the top of the embryo. Bright-field images of both embryo types at the same developmental stages showed minimal differences (Figure 1-12, A1–E1, F1–J1).

As depicted in Figure 1-11, the characteristic pattern of *fuchi*$^{+}$*Ets4*$^{+}$ and *fuchi*$^{+}$*Ets4*$^{-}$ cell clustering becomes evident in WT embryos after 23 hael (Figure 1-12, B2–E2). In contrast, *Ets4* RNAi embryos, due to effective RNAi injections, exhibited a complete absence of *Ets4*$^{+}$ cells. Within these embryos, the inner primary thickening cells appeared homogeneously under detection of *fuchi* and *Ets4*, and no sub-cellular clusters were observable under current conditions (Figure 1-12, F2-J2).

In WT embryos at 29 hael, most *fuchi*$^{+}$*Ets4*$^{-}$ cells exhibited nascent transcription of the *Ets4* gene (Figure 1-12, A2–D2). In other samples, the time of nascent transcription of *Ets4* gene in these cells could be later than 35 hael (supplementary Figure S1-11, S1-12, S1-13, S1-14). In contrast, in *Ets4* RNAi embryos, nascent *Ets4* transcription was effectively suppressed by 25 hael in the majority of *fuchi*$^{+}$*Ets4*$^{-}$ cells (Figure 1-12, F2–J2; Figures S1-15 to S1-18).

Supplementary Figure S1-29 presented a schematic illustration depicting the various cell types and their spatial arrangement within WT and *Ets4* RNAi embryos at approximately 27 hael.

6. Second asymmetry event in WT embryo but not in *Ets4* RNAi embryo: Cumulus migration.

Cumulus migration initiated around 31 hael in WT embryos. Figure 1-13 illustrated the types and arrangements of inner cells at this stage. Notably, *Ets4*$^{+}$ cells gradually moved out from the periphery of *fuchi*$^{+}$*Ets4*$^{-}$ cells. This observation, along with the quantification of *Ets4*$^{+}$ cells at various stages, strongly supported the hypothesis that *Ets4*$^{+}$ cells present at earlier stages are the migrating cumulus at stage 5. However, it was also possible that some *Ets4*$^{+}$ cells remained at the center of the germ disc and subsequently downregulate *Ets4* expression.

Supplementary Figure S1-30 presented a comparison of WT and *Ets4* RNAi embryos at approximately 31 hael. Aside from the difference in the level of *Ets4* expression, no significant morphological distinctions were observed between the two embryo types at this stage.

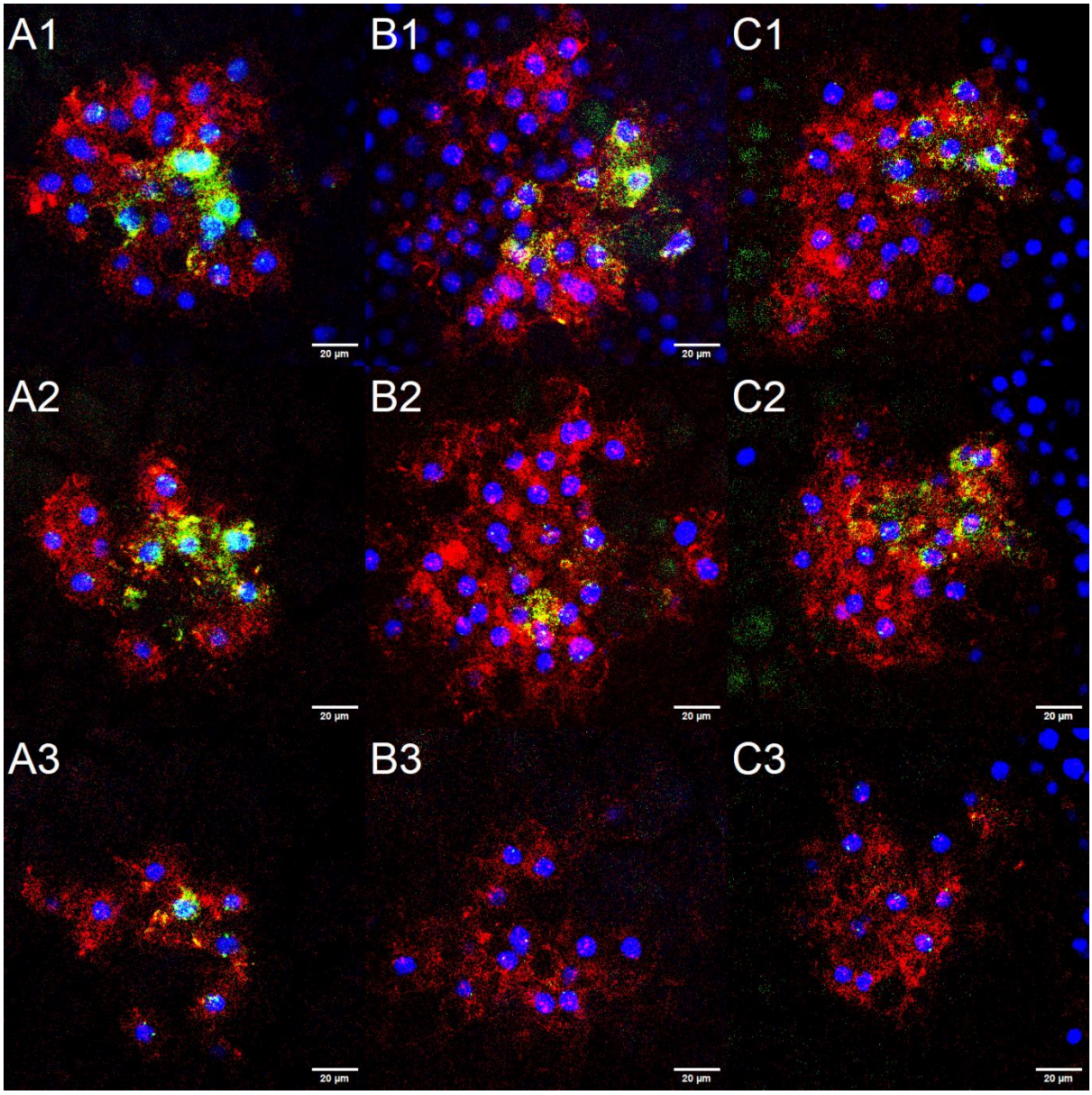

Figure 1-13. Initiation of cumulus migration. A1, A2, A3, B1, B2 and B3: 29 hael. C1, C2 and C3: 33 hael. A1: WT-1 8h e1, slice 7-14. A2: WT-1 8h e1, slice 15-22. A3: WT-1 8h e1, slice 23-30. B1: WT-1 8h e2, slice 8-15. B2: WT-1 8h e2, slice 16-23. B3: WT-1 8h e2, slice 24-31. C1: WT-1 12h e3, slice 6-11. C2: WT-1 12h e3, slice 12-17. C3: WT-1 12h e3, slice 18-23. 40x. Blue: Dapi. Red: *fuchi*. Green: *Ets4*.

At stage 5, cumulus migration was prominently observed (Figure 1-14, supplementary Figure S1-31), with *Ets4*$^{+}$ cells leading the movement, forming a cohesive group of approximately 10 cells (Figure 1-6, supplementary Figure S1-13). A distinct path was established by a scattered arrangement of *fuchi*$^{+}$*Ets4*$^{-}$ cells, extending from the center of the germ disc to the migrating cumulus. However, the precise origin of these *fuchi*$^{+}$*Ets4*$^{-}$ cells along the migration path remained unidentified.

The migration of cumulus was analysed by measuring the radius of the germ disc and the distance travelled by the cumulus (Figure 1-14, A1–A5). From these measurements, the average speed of cumulus migration was calculated to be approximately 23 µm/h.

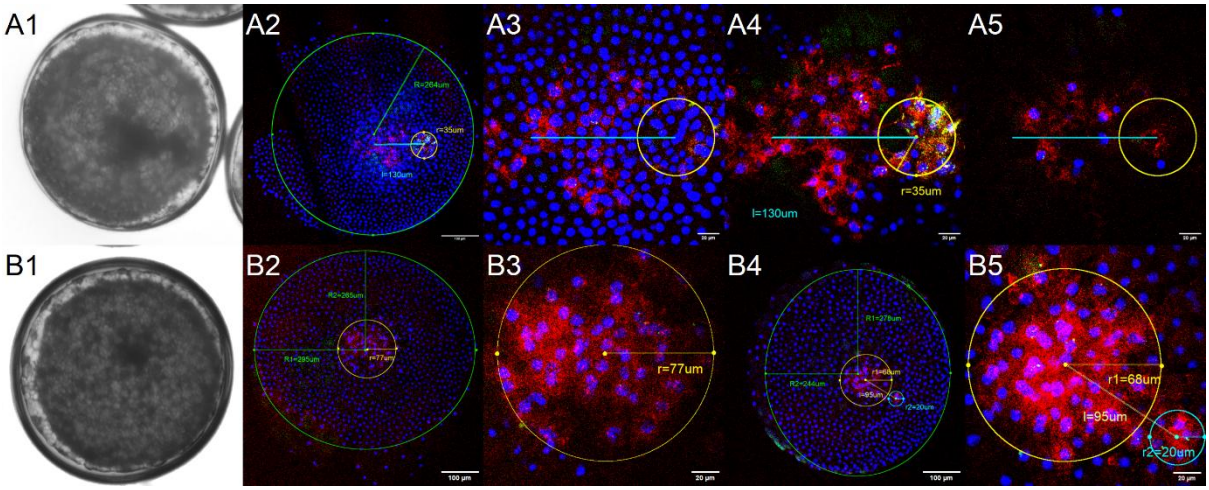

Figure 1-14. WT and *Ets4* RNAi embryo at mid stage 5. A1 to A5: WT embryo, at 39 hael. B1 to B5: *Ets4* RNAi embryo. B1: 39 hael. B2 to B5: 43 hael. A1, B1: bright field. A2, B2, B4: 10x. A3, A4, A5: 40x. AVG z-stack of frame 2-7, 8-13, 14-19 and 20-25, respectively. B3, B5: AVG z-stack, 40x. HCR staining. Blue: Dapi. Red: *fuchi*. Green: *Ets4*.

At stage 5, the inner cells of *Ets4* RNAi embryos exhibited a uniform distribution in all directions (Figure 1-14, B1–B5). Most *Ets4* RNAi embryos at this stage resembled the embryo shown in B2 and B3, displaying radial symmetry without observable directional movement of cell clusters. In rare instances, as depicted in B4 and B5, small groups of cells migrated toward a specific direction at a significantly slower progress compared to WT cumulus (supplementary Figure S1-32; Table S1-6).

In WT embryos, following cumulus migration, specific regions of the germ disc formed a scattered pattern in the inner layer. In contrast, in *Ets4* RNAi embryos at a similar stage, the pattern observed in other regions of the germ disc differs significantly (supplementary Figure S1-33). This comparison suggested the possibility that animal body patterning may be induced by cumulus migration in WT embryos. However, identifying the key factors within cumulus cells responsible for this induction and understanding how this induction was implemented would require further research.

7. Summary

I developed a method to normalize *Pt* developmental videos into standard 25°C developmental time, defined the primary thickening region and categorized cell types based on *fuchi* and *Ets4* gene expression level. Additionally, I quantified cell numbers in various regions and types in WT and *Ets4* RNAi embryos.

The number of primary thickening cells and *fuchi*$^{+}$ cells within the primary thickening region were similar in WT and *Ets4* RNAi embryo types. During the invagination process, the morphology and progression of invagination were comparable between both embryos. A notable difference arose post-invagination: WT embryos developed an asymmetric cell cluster pattern, whereas this pattern was absent in *Ets4* RNAi embryos.

On a cellular level, comparing the inner primary thickening cells of WT and *Ets4* RNAi embryos revealed potential similarities in proliferation processes, with a suggestion that proliferation might be similar or slightly stronger in WT embryos. In WT embryos, differentiation into *Ets4*$^{+}$ and *Ets4*$^{-}$ cells occurred within the primary thickening, whereas *Ets4* RNAi embryos lacked this differentiation.

Furthermore, WT cumulus cells exhibited migration, whereas all the primary thickening cells in the primary thickening region of *Ets4* RNAi embryos did not migrate. The observed differences may lead to the higher energy demand required for biological activities in WT primary thickening cells compared to *Ets4* RNAi embryos, suggesting potential variations in cellular metabolism between the two types.

4 Result Chapter II: RNA Sequencing Analysis and Functional Characterization of Differentially Expressed Genes in Primary thickening Cells of *dsRed* and *Ets4* RNAi Embryos

1. Sample preparation, sequencing, annotation and selection of gene lists

I dissected the primary thickening region of both *dsRed* and *Ets4* RNAi embryos for RNA extraction, as the control and experimental groups, respectively In the *Ets4* RNAi embryos, a deficiency in dorsal-ventral axis formation was observed, as described by Pechmann et al. 2017. (supplementary Figure S2-1). RNA samples were prepared and sequenced as described by Want et al. 2023. Three reads from both WT and *Ets4* RNAi embryos were processed, and analyzed using Degust (David Powell, 2015).

Figure 2-1 B showed the PCA (principle component analysis) dimensions of the six samples. S9, S10, and S11 corresponded to *dsRed* RNAi samples, while S12, S13, and S14 corresponded to *Ets4* RNAi samples. S9 and S10, as well as S13 and S14, were closely clustered. However, S11 and S12 did not cluster closely with the other samples of their respective types.

Possible explanations for this observation included: (1) differences in the developmental stage of the samples, and (2) S12 was derived from two cocoon, and one of the cocoons had lightly higher percentage of WT phenotypes (supplementary Figure S2-1). Therefore, two approaches were considered: analyzing differentially expressed genes from all six samples, or focusing exclusively on four samples (S9, S10, S13, and S14). Both approaches were implemented and tested (Raw data in https://degust.erc.monash.edu/degust/compare.html?code=4665039dc3ef6d89ff40a0616cc74bdd#/).

Figure 2-1 A, presented a volcano plot for all six samples, displaying statistical values calculated using Degust. The plot was generated using R software (EnhancedVolcano) with a Fold2Change threshold of 2 and an FDR threshold of 0.001. In the figure, most genes were labeled with their Augustus number identifiers, while some genes annotated with their gene names. Notably, *Ets4*/spdef, *twist*, *hh*/*shh*, and *btl/fgfr* were prominently displayed, indicating that these genes exhibited high Fold2Change values and low FDR values across all six samples.

Following RNA sequencing, now I had transcriptomic data from six samples, three from *dsRed* RNAi embryos and three from *Ets4* RNAi embryos—yielding a total of 32,187 transcripts. Of all 32,187 transcripts, over 16,000 transcripts had read counts (tpm) greater than 2 in at least one sample, suggesting gene expression in primary thickening region of either WT or *Ets4* RNAi embryos.

However, it was difficult to perform function analysis. The transcriptome was poorly annotated, and although a previous study provided automatic annotations, these annotations contained errors and inconsistencies. Even when the name of a gene was determined, there was a significant likelihood that the gene has not been previously studied in spider embryos. In addition, within the *Pt* genome, there were many “uncharacterized genes”, which were likely unique to the species and lack orthologs in other model organisms.

The number of potentially relevant genes was 16,000, which was too large to annotate manually. An alternative approach was to focus on transcripts with the most significant differential expression between WT and *Ets4* RNAi cells. The selected set of differential transcripts should be sufficiently large to ensure representativeness while remaining manageable enough for manual annotation.

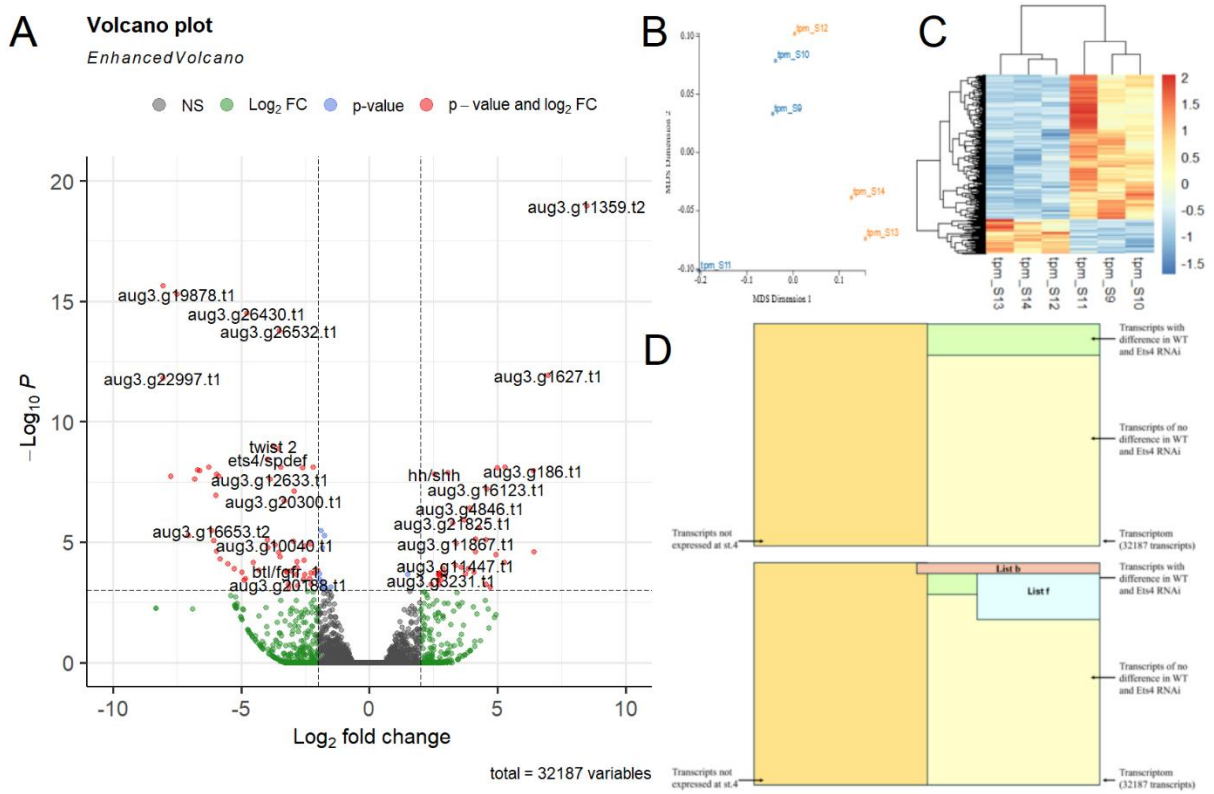

Figure 2-1. Sequence results and selection of gene lists. A**.** Volcano plot generated in R using the EnhanceVolcano package, showing log_2 fold change and false discovery rate (FDR) values for a total of 32,187 transcripts. B. PCA (principal component analysis) plot visualized using the DEGUST website, illustrating the clustering of transcriptomic data. C. Heatmap of the selected differential gene list F. D. Venn diagram showing the number of transcripts related to primary thickening cells at stage 4 in WT (*dsRed* RNAi) and *Ets4* RNAi embryos, highlighting the selection of gene lists B and F.

Various selection methods were tested, and some were detailed in Table 2-1. Lists B and C were chosen based on statistical significance from all six samples or four samples (S9, S10, S13, S14), respectively. While Lists D and E were derived from lists B and C. List F was manually curated, taking into account experimental detection sensitivity and the artificial definition of "difference in expression level" (Table S2-1).

Figure 2-1C presented the heatmap for List F, while the heatmaps for the remaining lists were shown in supplementary Figure S2-3. The heatmap was clustered into two major groups: one containing the three *dsRed* RNAi samples (S9, S10, S11) and the other containing the three *Ets4* RNAi samples (S12, S13, S14). All six transcriptome profiles were visualized as colored blocks, with color intensity representing the read count.

Figure 2-D showed the number of transcripts related to primary thickening cells at stage 4 in WT (*dsRed* RNAi) and *Ets4* RNAi embryos, and the selection of gene lists b and f.

Table 2-1. Selected Lists of Transcripts for Annotation and Biological Function Analysis

List	A1	A2	B	C	D	E	F
Counts of transcripts	32187	32187	200	332	400	133	828
Selection criteria	3 vs 3	2 vs 2	From List A1,	From List A2,	List B U list C	List B ∩ list C	From List A1, Aver expression>2,

			FDR<0.05, Fold2FC>2	FDR<0.05, Fold2FC>2			Differ expression>1, heatmap
Annotation	Auto	Auto	Manual	Manual	Manual	Manual	Manual

I aimed to identify the subsets among Lists B, C, D, E, and F that best represented the differential genes between *dsRed* and *Ets4* RNAi embryos as found in List A. Therefore, all genes in Lists B, C, D, E, and F were manually annotated, to facilitate further functional analysis.

The manual annotation process, included of BLAST search on NCBI (https://blast.ncbi.nlm.nih.gov/) and UniProt (https://www.uniprot.org/blast), and ortholog identification in mouse and fly through UniProt (https://www.uniprot.org/),, Alliance of Genome Resources (https://www.alliancegenome.org/), and Flybase (https://Flybase.org/). Supplementary Figure S2-2 depicted a workflow of the process. This manual annotation method was considered to be more reliable than the published automatic annotations.

I searched for orthologs in both mouse and fly rather than relying on a single model species because I were uncertain which model would be most appropriate. Spiders were more closely related to insects than to mammals from an evolutionary perspective. However, fly presented unique aspects and there is a wealth of research data available in mammals.

As a result, most genes were annotated and identified the homology genes in mouse or fly. Of list F, for example, NCBI BLAST annotated 689 of the 828 transcripts. Among the rest 139 transcripts, 112 were classified as “uncharacterized genes”, 6 were identified as ncRNA, and 21 yielded no results. Following a second BLAST search in UniProt, 44 genes remained unannotated.

2. GO analysis for different gene lists

2.1 GO analysis for selected gene List B.

Gene function analysis was conducted using three methods: GO analysis, pathway analysis, and literature review. The results of these analyses will be discussed in Sections 2, 3, and 4, respectively. This section focuses on the results of the GO analysis for different gene lists, starting with List B.

After manual annotation, most of the 200 transcripts in List B were annotated with mouse and/or fly orthologs. Two separate tables were generated: one listing mouse gene names and the other listing fly gene names, all with the corresponding RNAseq expression data of the original spider transcripts. Each table was independently analyzed using R software to identify functions of the genes, relying on information from previously published results for mouse or fly genes. The functional analysis was categorized into three perspectives: Biological Process (BP), Cellular Component (CC), and Molecular Function (MF). Consequently, six result tables were produced for List B, detailing the related terms for mouse orthologs and fly orthologs in BP, CC, and MF categories. (Figure 2-2).

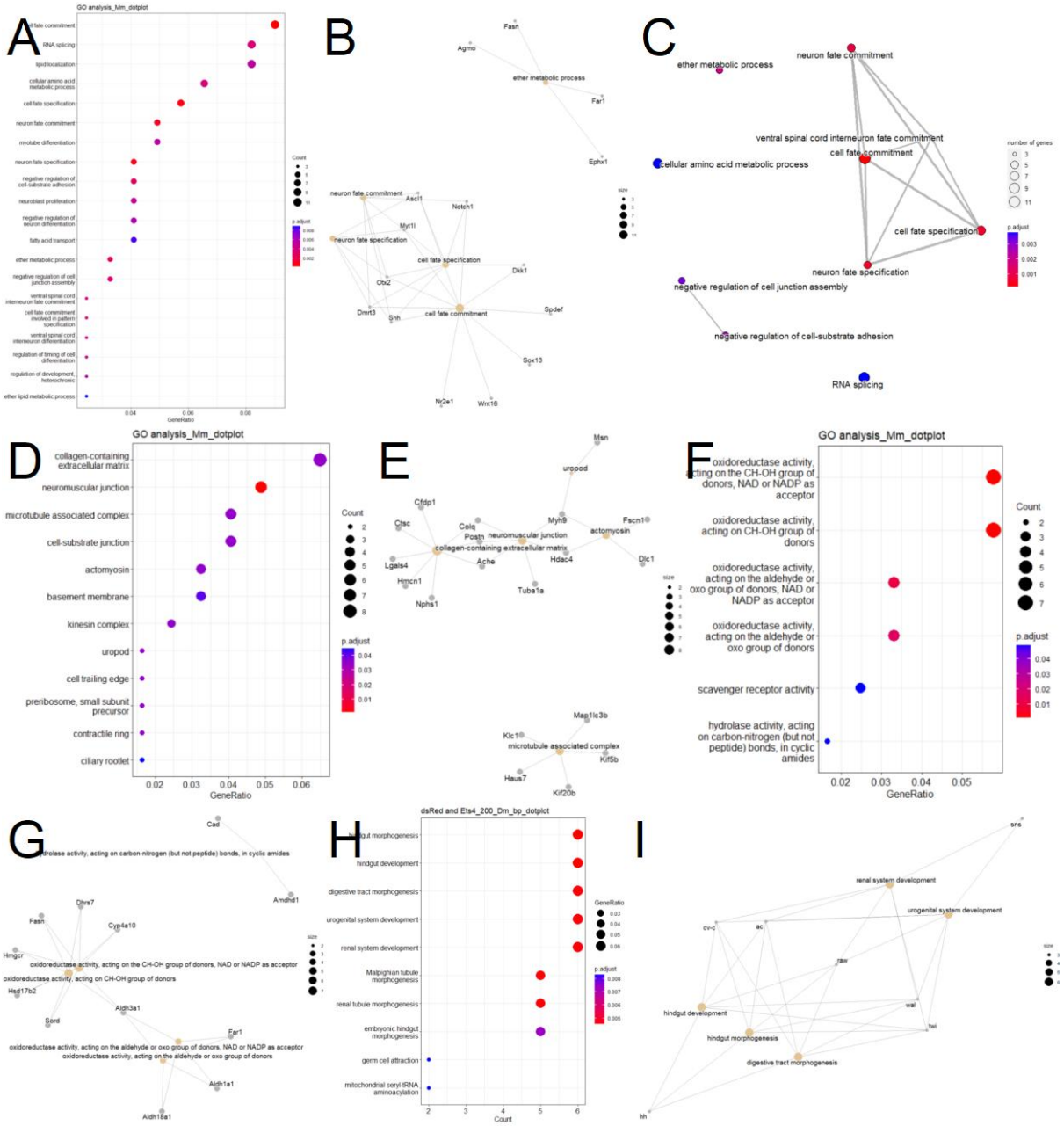

Figure 2-2. GO analysis on biological process (BP), cellular component (CC), and molecular function (MF) of selected gene list B, with ortholog gene lists from mouse (Mm) and fly (Dm). The analysis was performed using R, with results visualized as dotplots (top 20 terms from the analysis), cnetplots (the connections between biological process terms and the associated orthologs from the gene list), and emapplots (relationships of biological terms) for each GO category. A. Dotplot_bp_top20_Mm_gene list B. B. Cnetplot_bp_Mm_gene list B. C. Emapplot_bp_Mm_gene list B. D. Dotplot_cc_Mm_gene list B. E. Cnetplot_cc_Mm_gene list B. F. Dotplot_mf_Mm_gene list B. G. Cnetplot_mf_Mm_gene list B. H. Dotplot_bp_top10_Dm_gene list B. I. Cnetplot_bp_Dm_gene list B.

Figure 2-2 A displayed the top 20 BP terms for mouse ortholog genes from List B. The top three terms with the highest counts of relevant genes are “Cell Fate Commitment”, “RNA Splicing”, and “Lipid Localization”. Other notable terms included “Cell Fate Specification”, “Neural Fate Commitment”, “Myotube Differentiation”, and “Cell Fate Commitment Involved in Pattern Specification”, all of which are associated with cell differentiation. Figure 2-2 B presented a list of genes associated with

the term “Cell Fate Commitment”. Prominent developmental genes such as *Hedgehog* (*shh*) and *Notch* (*notch1*) are included, with the gene *Ets4* also being linked to this term. Figure 2-2 C illustrated the relationships between several cell differentiation terms. The diagram showed interconnected terms related to cell differentiation, as well as connections between two terms specifically related to cell junctions.

The CC analysis of mouse orthologs for List B transcripts yielded fewer terms compared to the BP analysis. Figure 2-2 D highlighted the top three terms with the largest number of relevant genes: “Collagen-Containing Extracellular Matrix”, “Neuromuscular Junction”, and “Microtubule-Associated Complex”. Terms related to cytoskeleton and cell-cell junctions were frequently mentioned across other terms. Figure 2-2 E listed genes associated with these CC terms, including Tubulin and Myosin, both key components of the cytoskeleton, and Fascin, a gene previously associated with primary thickening development.

Figures 2-2 F and G displayed the results of the MF analysis of mouse orthologs for List B transcripts. Key terms identified include “Oxidoreductase Activity”, “NADPH”, and “Hydrolase”. The specific objectives of these terms were unclear.

Figures 2-2 H and I presented the results of the BP analysis for fly orthologs of List B transcripts. The top three BP terms identified were “Hindgut Morphogenesis”, “Hindgut Development”, and “Digestive Tract Morphogenesis”. These terms were only indirectly related to primary thickening cells. Notably, *hh* and *twist* genes were listed as relevant to these processes.

In summary, the GO analysis of mouse and fly orthologs from List B provided valuable insights into the potential functions of the original spider transcripts. The GO analysis from mouse orthologs indicated that the most relevant cellular activities associated with the genes are cell differentiation, cell junction formation, and cytoskeleton processes. The analysis on fly orthologs highlighted developmental processes, but these might be less directly applicable to the target primary thickening cells in spiders.

The discrepancies between the BP analysis resulted for mouse and fly orthologs of List B transcripts, could result from differential annotation, publication bias, and biological differences of the two reference species.

2.2 Comparison of GO analysis for selected gene lists B, C, D, E, and F, with mouse and fly orthologs

Additional Gene Ontology (GO) analyses were conducted on lists c, d, e, and f using R, following the methodology described for list B. For each list, six result tables were generated, and terms with the highest gene counts were illustrated in the corresponding figures. All analyses were performed with a significance threshold of $p = 0.01$, unless otherwise noted. (supplementary Table S2-2, S2-3, S2-4, S2-5, S2-6, and S2-7)

Table 2-2 combined the BP, CC, and MF terms from supplementary Tables S2-1, S2-3, and S2-5, which were generated from mouse orthologs of lists B, C, D, E, and F.

Table 2-2. Summary of GO terms (BP, CC, and MF) for selected gene lists B, C, D, E, and F with mouse orthologs.

list	b	c	d	e	f
gene counts	200	332	400	133	828
Selection criteria	3 vs 3 list, FDR<0.05, Fold2FC>2	2 vs 2 list, FDR<0.05, Fold2FC>2	200 list U 332 list	200 list ∩ 332 list	Aver expression>2, Differ expression>1, heatmap
GO_bp_top 25	Differentiation. Development. Metabolism.cell adjunction	Differentiation. Development. Metabolism.cell adjunction	Differentiation. Development. Metabolism.cell adjunction	Differentiation. Development. Metabolism.	Proliferation. Differentiation. Development. Metabolism.cell adjunction
GO_cc_top 12	cell-matrix junction, kinesin	neuromuscular, kinesin	neuromuscular, kinesin	neuromuscular, microtubule	vesicles. Organelle. Protein complex. Cell polarity
Go_mf_top 10	oxidoreductase activity, scavenger receptor activity	oxidoreductase activity	oxidoreductase activity		RNA processing, protein processing
Ets4	Yes	Yes	Yes	Yes	Yes

From Table 2-2, the GO terms from mouse orthologs across different lists appeared to be in strong agreement. “Differentiation/Development” and “Metabolism” were key terms in BP analysis for all lists. “Cell adjunction” was mentioned in all lists except list E, which had the fewest transcripts. “Proliferation” was mentioned only in list F. The CC analysis of all the lists highlighted cell movement-related components, though the terms varied across different sources. The MF analyses, on the other hand, were with very few terms, making it difficult to summarize and interpret.

In addition, the gene *Ets4* (*spdef*) was present in all these lists, and its related GO terms contributed to the final summary.

Similar to Table 2-2, Table 2-3 combined the BP, CC, and MF terms from supplementary Table S2-3, S2-5, and S2-7, generated from fly orthologs of lists B, C, D, E, and F.

Table 2-3. Summary of GO terms (BP, CC, and MF) for selected gene lists B, C, D, E, and F with fly orthologs.

list	b	c	d	e	f
gene counts	200	332	400	133	828
Selection criteria	3 vs 3 list, FDR<0.05, Fold2FC>2	2 vs 2 list, FDR<0.05, Fold2FC>2	200 list U 332 list	200 list ∩ 332 list	Aver expression>2, Differ expression>1, heatmap
GO_bp	system development, adult system morphogenesis, metabolism	differentiation, AP pattern, system development, adult system morphogenesis, cell movement	cell cycle regulation, AP pattern, system development, adult system morphogenesis, cell movement	system development, adult system morphogenesis, metabolism	differentiation, system development, adult system morphogenesis, cell movement, metabolism, mRNA and protein processing
GO_cc		supramolecular complex	supramolecular complex		division, cell junction, supramolecular complex, PI3K
Go_mf important					RNA and protein metabolism
Ets4	No	No	No	No	No

The BP analysis emphasized “differentiation/system development” and “adult system morphogenesis” across all lists. “Cell movement” was mentioned in terms from lists C, D, and F, while “metabolism” appeared in lists B, E, and F. Terms from lists C and D specifically referred to “AP patterning”, which was not among the top 25 terms in list F but was included in the complete results. Similarly, “cell cycle regulation” from list D was present in the full BP term set for list F; while a related term, “division”, appearing in the top 25 CC terms of list F. Additionally, list F included many terms related to RNA and protein processing.

The CC and MF analyses of fly orthologs from lists B, C, D, and E provided limited information. However, the analysis of list F offered valuable insights, with terms related to “cell cycle”, “cell movement”, and “RNA and protein metabolism” aligning with those identified in the BP analysis of the same list.

Tables 2-2 and Table 2-3 independently summarized the GO analysis results from different lists using mouse and fly orthologs. These transcript lists differed significantly in their selection criteria, gene counts, and heatmap image fit. Nevertheless, to some extent, the analysis results from these gene lists highlighted similar cellular activities, from a summary of the functions of genes in each list.

The reason for this partly lied in the overlap of genes among the different lists. More importantly, because the lists reflected different aspects or stages of the same batch of cellular activities, the differential activity of primary thickening cells between WT and *Ets4* RNAi embryos (Figure 2-1D)—the GO analyses of these lists ultimately led to similar outcomes.

However, all the analyses were based on the top 25 terms, and I was concerned that some terms relevant to the function of primary thickening cells may not always appear among them. Therefore, I examined the full list of terms to obtain additional information.

Among all the lists, List F had the largest number of transcripts (828) and therefore yielded the most terms in the GO analyses. And among the analyses of List F, the BP analysis provided the most interpretable results compared to the CC and MF analyses. Therefore, I focused on the BP analysis terms from List F to interpret the cellular activities in greater detail.

2.3 Manually classification and summary of BP analysis on List F.

The BP analysis of List F produced 383 terms from mouse orthologs and 386 terms from fly orthologs, using a cutoff of p = 0.01. I manually analyzed all these terms, by combining terms with similar meanings and aggregating the related genes.

BP terms from the GO analysis of transcripts in List F were classified according to the terms in supplementary Table S2-8. Table S2-8 included all potentially relevant biological activities across five levels: molecular, cellular, tissue, organ, and organism (including developmental events). The terms were derived from textbooks with two goals in mind: (1) to ensure comprehensive coverage of possible biological activities at each level, and (2) to avoid overlapping among terms within the same level. Each BP term was assigned to the most appropriate manual term across all levels. It was common for multiple BP terms to fit into the same manual term (Table 2-4, supplementary Table S2-9).

Table 2-4. Examples of classification of BP terms of List F to appropriate manual terms from supplementary Table S2-8

A	molecular level	term 1	gene list 1	term 2	gene list 2	term 3	gene list 3
A1	DNA replication						
A2	DNA damage and repair	double-strand break repair	Arid2/Trip12/Epc1/Fancd2/Setmar/Sirt7/Ogg1/Otub2/Trip13/Apbb1/Pbrm1/Rpa1/Smc6/Brca2/Polm/Trrap/Spidr/Dna2/Rad50/Zfyve26	positive regulation of response to DNA damage stimulus	Arid2/Epc1/Setmar/Ino80b/Ddx5/Apbb1/Pbrm1/Spred2/Trp73/Nacc2/Trrap/Spidr/Dhx9	regulation of response to DNA damage stimulus	Arid2/Trip12/Epc1/Setmar/Ino80b/Sirt7/Ogg1/Otub2/Ddx5/Apbb1/Pbrm1/Spred2/Trp73/Brca2/Nacc2/Trrap/Spidr/Dhx9
A3	transposition	entry of viral genome into host nucleus through nuclear pore complex via importin	Kpna2/Kpna6				
A4	chromatine modeling	histone deacetylation	Ctbp1/Hdac4/Kdm5a/Msl3/Mier1/Sirt7/Per2/Prdm5/Pink1	histone H4 acetylation	Ctbp1/Epc1/Msl3/Tcf3/Apbb1/Iws1/Brca2/Trrap	histone modification	Ctbp1/Trip12/Epc1/Flcn/Kat6b/Hdac4/H1f4/Setdb1/Setmar/Kdm4a/Kdm5a/Msl3/Mier1/Myb/Sirt7/Nnmt/Otub2/Pcgf3/Prdm1/Prmt1/Tcf3/Apbb1/Iws1/Glyr1/Usp16/Brca2/Per2/Huwe1/Prdm5/Trrap/Brd1/Pink1/Wdr82

Table 2-4 showed four manual terms at the molecular level (Level A): A1 DNA replication, A2 DNA damage and repair, A3 transposition, and A4 chromatin remodeling. As an example, under manual term A2 (“DNA damage and repair”), there were three BP terms related to this category from the BP analysis of List F. These BP terms were “double-strand break repair”, “positive regulation of response to DNA damage stimulus”, and “regulation of response to DNA damage stimulus”. The related gene lists for these BP terms included 20, 13, and 18 genes, respectively.

A further step was taken to combine the gene lists for the same manual term and remove overlapping genes. For manual term A2 (“DNA damage and repair”), the combined gene list contained a total of 26 genes.

Using this method, 383 BP terms from mouse orthologs and 386 BP terms from fly orthologs of List F were reclassified according to the manual terms. Related genes were combined and counted (supplementary Table S2-9).

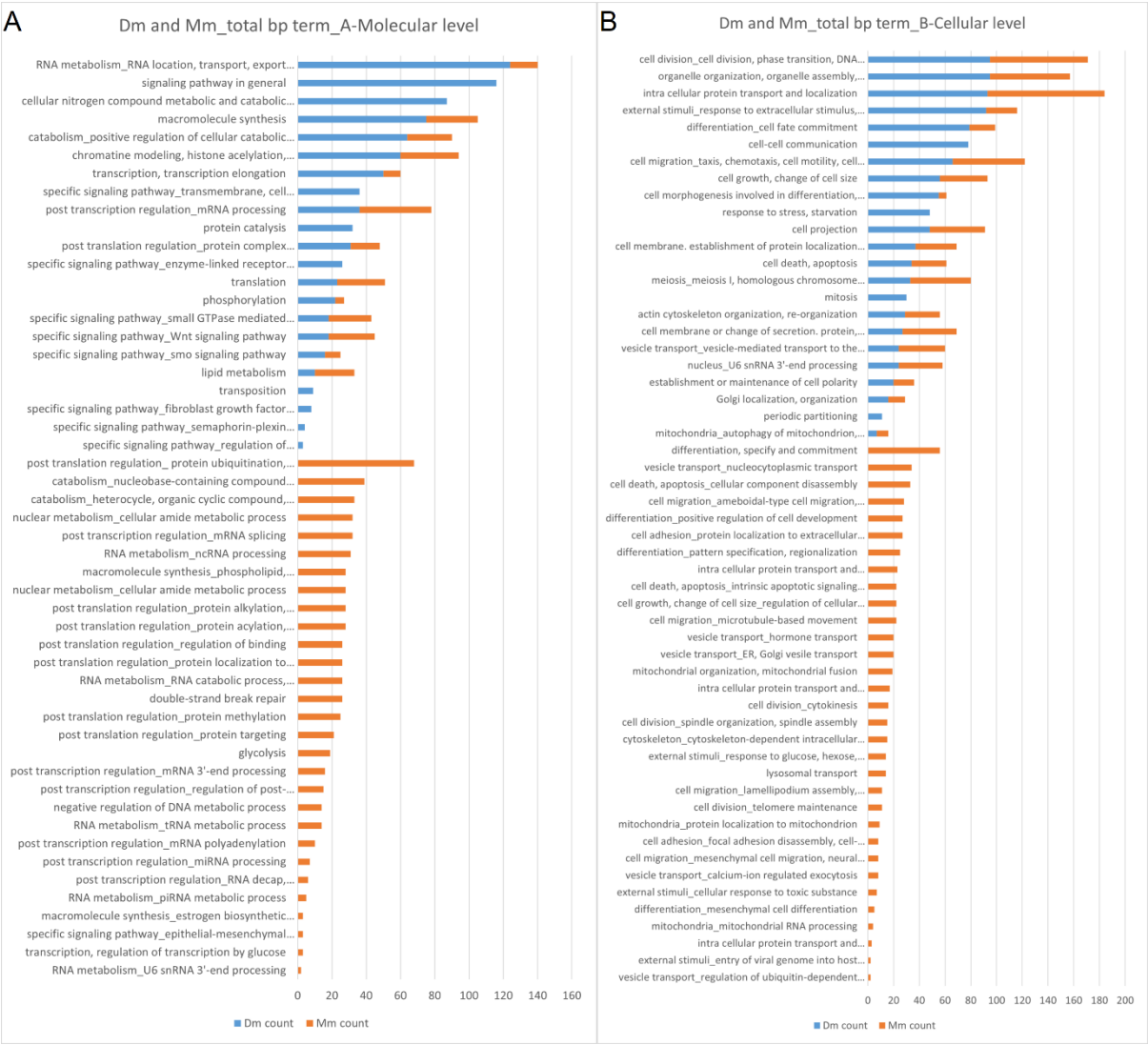

Figure 2-3. Gene counts for different biological activities at the molecular (A) and cellular (B) levels based on mouse and fly orthologs of List F. Gene counts were calculated by manually classifying and combining biological process (bp) terms from automated R analysis of list f, using gene datasets from mouse and fly. The image and detailed gene list are provided in the supplementary Table S2-9.

Figures 2-3 and Figure 2-4 displayed the counts of genes associated with all manually generated biological terms across the five levels. While the number of genes connected to a term did not directly indicate its importance, a higher gene count reduced the likelihood of errors and suggested a stronger confirmation of the term's actual relevance. Also, certain terms were mentioned in only one of the species and will not be discussed further.

Figure 2-3 illustrated the manually generated terms at the molecular (A) and cellular (B) levels. At the molecular level (Figure Y9A), terms from both mouse and fly orthologs predominantly involved DNA and RNA processes (e.g., RNA metabolism, transcription and post-transcription regulation, chromatin remodeling), macromolecule processes (e.g., macromolecule synthesis, catabolism, lipid metabolism), protein processes (e.g., translation and post-translation regulation, phosphorylation), and some signaling pathways (e.g., small GTPase, Wnt, smo).

Figure 2-3 B showed the cellular biological activities of BP terms from the differential genes in List F. The manually generated terms, which included BP terms from both mouse and fly orthologs, were: cell division, cell growth, organelle organization, protein transport and localization, cell membrane,

vesicle transport, cell fate commitment or differentiation, cell migration, cell projection, cytoskeleton, cell polarity, and mitochondria.

Figure 2-4 illustrated the manually generated terms at the tissue (A), organ (B), and organism (C) levels, along with the counts of BP terms from fly and mouse orthologs in List F. At the tissue level (Figure 2-4 A), terms from both mouse and fly orthologs included “epithelium”, “nerve and neuron”, “embryonic stem cell”, and “muscle”. Many other terms were related but vary in detail.

Figure 2-4 B showed the manually generated terms at the organ level. Notably, there was very little overlap between terms from fly and mouse orthologs in this image Terms from both sources included “respiratory system”, “nervous system”, and “circulatory system”, and these terms did not have a large number of related genes. Additionally, BP terms from mouse orthologs included “kidney” and “digestive tract”, while BP terms from fly orthologs included “larval development” and “wing disc”.

Figure 2-4 C showed the terms at the organism level, particularly related to developmental processes. Both mouse and fly BP terms included “Dorsal-Ventral patterning”, “gastrulation”, and “embryo organ morphogenesis”. Additionally, BP terms from fly orthologs mentioned “Anterior-posterior axis”, while mouse orthologs referred to “axis specification” and “mesoderm differentiation”. Most of these terms appeared to be closely related, providing valuable insights into the role of primary thickening cells in body patterning in spiders.

I specifically searched for the gene *Pt-Ets4* (*spdef* / *Ets98B*) across all terms. In the context of mouse orthologs, the gene *spdef* was associated with the terms “cell fate commitment”, “digestive system development”, “digestive tract development”, “respiratory system development”, “respiratory tube development”, and “lung development”. In contrast, no BP terms related to *Ets98B* were found in fly orthologs. Additionally, the gene *Ets97D* was linked to terms such as “positive and negative regulation of transcription”, “response to stress and starvation”, and “regulation of organelle organization”. The relevant terms were detailed in the Table S2-9 (incomplete gene list).

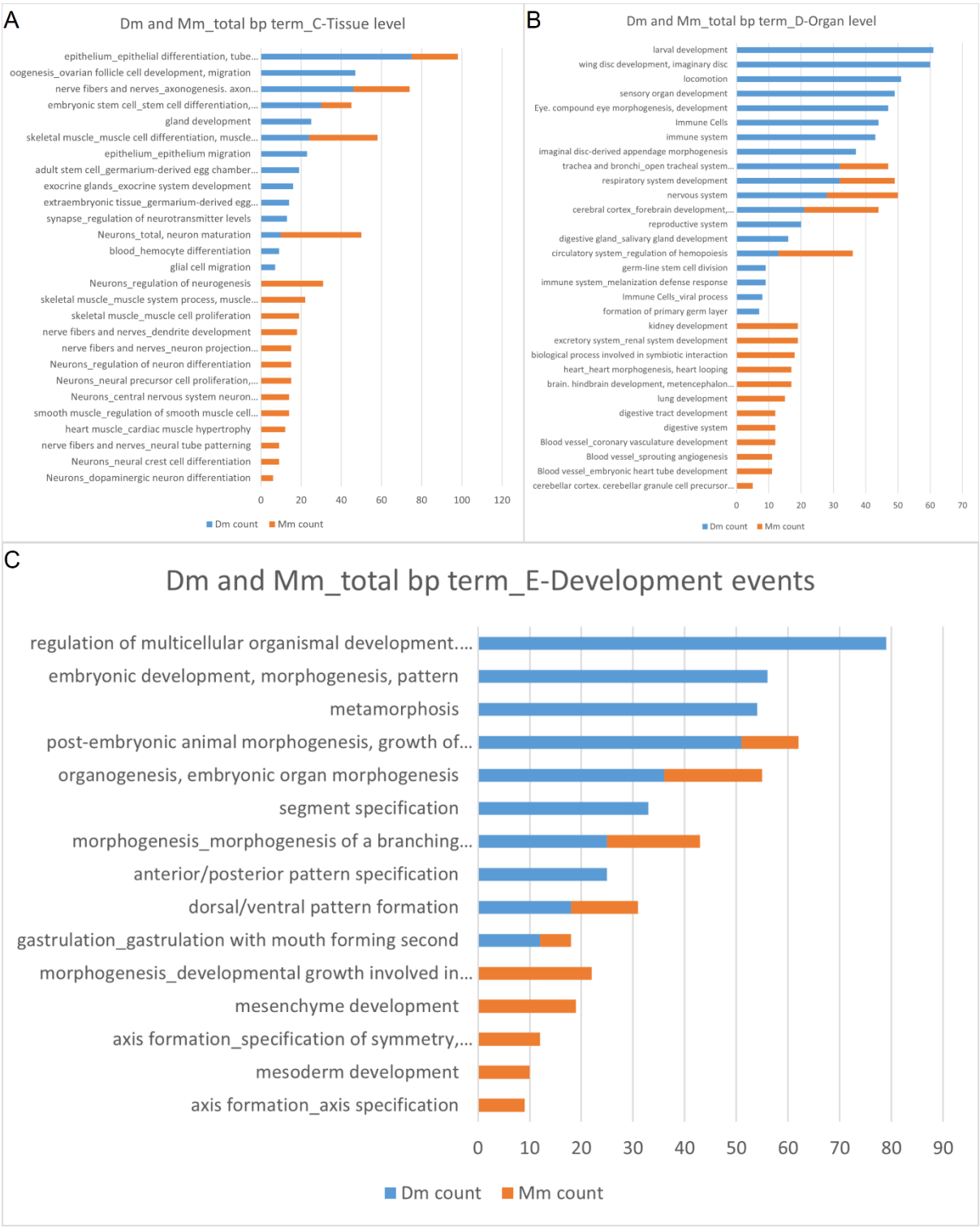

Figure 2-4. Gene counts for different biological activities at the tissue (A), organ/organogenesis (B), and animal/development (C) levels based on mouse and fly orthologs of List F. Gene counts were calculated by manually classifying and combining biological process (bp) terms from automated R analysis of list f, using gene datasets from mouse and fly. The image and detailed gene list are provided in the supplementary table S2-9.

An additional observation from Figures 2-3 and 2-4 was that the results from fly and mouse orthologs showed considerable agreement at the cellular and molecular levels. However, there were notable

differences at tissue and organ levels. The organism level showed a middle ground: while both fly and mouse orthologs mention key developmental events wan general BP terms, some differences remained.

To simplify the results, key terms from both orthologs of List F were selected, summarized, and compiled into a single table encompassing all levels (Table 2-5).

Table 2-5. Summary of biological events at the molecular, cellular, tissue, organ, and organism levels with the highest gene counts in the manual analysis of biological process (BP) terms (mouse and fly orthologs) for List F.

molecular level	cellular level	tissue level	organ level	organism development
metabolism and catabolism	mitochondria, division and apoptosis and metabolism	neuron, neuron related, axon	neural cells	gastrulation
translation and post-translation regulation	protein transport, vesicle, membrane system	muscle	respiratoy tubes	DV apttern
transcription and post-transcription regulation, RNA metabolism	cell polarity, cell shape change	pluripotency cell	blood vessel	struncture shape change, morphogenesis
chromatin modeling	division	epithelium		organogenesis
pathway, smo, wnt, small GTPasse	apoptosis			
	migration			
	differentiation			
	exteral signal, protein transport			

Table 2-5 summarized the manually generated terms across different biological levels. It appeared that many molecular processes were involved, including changes in RNA and protein production, regulation, modification, transport, and consumption, as well as alterations in the synthesis and digestion of organic molecules. A significant directional change was likely associated with cell migration, differentiation, shape change, and division. These processes resembled the differentiation of neural, muscle, pluripotent, or epithelial cells and might relate to specific aspects of system development in neural, respiratory, and blood vessel systems. The gene lists also provided insights into dorsal-ventral patterning, gastrulation, and morphogenesis across different species.

Compared to Tables 2-2 and Table 2-3, which summarized the top 25 terms from Lists B, C, D, E, and F, Table Y2-5 contained most of the key terms from all the tables in a more precise way.

The observation that GO analyses of the same gene list yielded similar results at the cellular and molecular levels across different organisms and supported the validity of our functional analysis approach, which used orthologs in fly and mouse to interpret spider gene functions. It was challenging to assess the terms at other levels and determine the extent to which these conclusions about gene function can be confidently extended to spiders. The actual biological events should be a subset of the potential processes. But this approach still provided valuable insights into understanding the events.

Alternative methods such as pathway analysis, although still based on published gene functions like GO analysis, provided a different perspective on cellular activities. This alternative approach aimed to offer a more comprehensive understanding of the roles of primary thickening cells.

3. Pathway analysis for gene List F.

Previous GO analyses already identified several cell signaling pathways. For example, the PI3K signaling pathway was mentioned as one of the CC terms from fly orthologs of List F. Additionally, the terms “Smo”, “small GTPase”, and “Wnt” were noted as BP terms from both fly and mouse orthologs of List F.

Pathway analysis of the gene set was conducted automatically using R (ggridges), incorporating Fold2Change values of fly and mouse orthologs with a specified cutoff p-value. However, few pathways met the criteria, with the analysis of List F, even with a p-value as high as 0.1 (supplementary Figure S2-4). With only 800 genes, the list was relatively small, making it challenging to identify pathways with a low p-value.

3.1 Manual pathway analysis for List F.

I visualized the pathways using R (pathview), by inputting the names of fly and mouse orthologs for transcripts in List F, along with the Fold2Change values for each transcript. This approach allowed us to highlight genes from our list within the context of various KEGG pathways in fly and mouse, without calculating p-values. Green indicated genes with a Fold2Change smaller than zero, while red indicates genes with a Fold2Change larger than zero. To clarify the concept and avoid any misunderstanding, I would refer to these images as “pathview images” in the following sections.

In total, I obtained approximately 80 pathview images marked with mouse orthologs and around 40 with fly orthologs. The discrepancy in the number of pathways was attributed to differences in the KEGG pathways available for each species (supplementary Table S2-10).

To assess the relevance of certain pathways to our selected differential gene list (List F), these Pathview images were analyzed in several details: the total number of colored genes involved, their distribution (e.g., around the cell membrane, in the cytoplasm, or downstream of the pathway), whether the core gene of the pathway was colored, and whether the changes in colored genes were consistent in either increasing or decreasing pathway activity.

A table summarizing these observations was created and is included in the supplementary Table S2-10. Figure 2-5 displayed the head of this table. Each row represented a different pathway. Pathway images from both fly and mouse were analyzed independently, and comparisons were made between the two species.

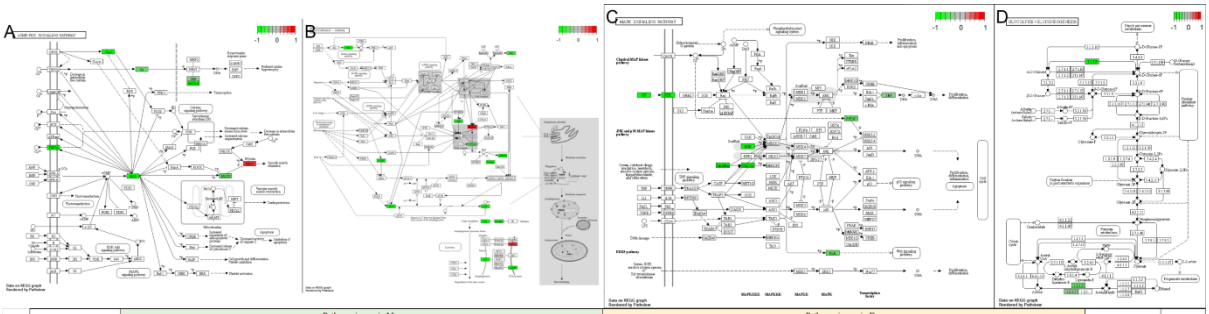

		Pathway image in Mm							Pathway image in Dm								
	Pathway/ analyses of differential genes	total number	number of upstream genes	include key genes of the path or not	form a complete path or not	downstream effects of the related genes	other	conclusion	total number	number of upstream genes	include key genes of the path or not	form a complete path or not	downstream effects of the related genes	other	conclusion	Mm vs Dm	other
22	cGMP-PKG pathway	8	1, but as effect	1 or the 2	close to	muscle	unidirection, up regulation for sm	related, not sure if main								no Dm path	
67	Autophagy-animal	12	not sure	PI3K complex, LC3	middle-late part	Autophagysome, lysosome	Insulin, PI3K, MAPK, AMPK, ULK, mTOR	related or side related	10	not sure	some, no doubt	middle-late part	autophage, lysosome	PI3K, MAPK, mTOR, etc.	related or side related	similar, 6 genes differ	
10	MAPK pathway	8	2	no	no	proliferation, Wnt	phosphatidylinositol, TNF, p53, ras	side related	8	3	no	middle lost	cell shape, pattern	polarity. Various direction	side related	different in pathway	
23	Glycolysis-Glucogenesis	3	very small ratio. Not sure function, not sure if unidirection				metabolism	side related or not.	3	very small ratio. Not sure function, not sure if unidirection				metabolism	side related or not.	same	

Figure 2-5. Manual assessment of the relevance between KEGG pathways and gene List F, and classification based on the assessment. A. The cGMP-PKG signaling pathway. B. The autophagy (animal) pathway. C. The MAPK signaling pathway. D. The glycolysis-gluconeogenesis pathway. Table: head of the assessment table to evaluate the relevance of each pathway to the mouse or fly orthologous genes from list F.

Based on this information, pathways were classified into four types, according to the following criteria (Figure 2-5).

Class I : Highly Related Pathways. At least one complete pathway, or more than 1/4 of all the genes, was colored. All the colored genes consistently regulated the pathway. Key genes of the pathway were colored. Figure 2-5 A showed the pathview image of the cGMP-PKG signaling pathway, in which the colored genes included at least one complete path: PMCA (↓) → PKG (↓) → MLCP (↓) --| MLC (↑). Although the regulation of these colored genes differed individually, they collectively contributed to increasing the downstream of this complete path.

Class II: Related Pathways. Most requirements of Class I were met, but either key genes were not colored, or the colored genes regulated the pathway in different directions. Figure 2-5 B showed the pathview image of the Autophagy (animal) pathway. While many colored genes were present in the pathway, particularly in the lysosome-related section, they did not form a complete path. Additionally, key genes of the pathway, such as ATG genes, were not colored. Moreover, the differentially expressed genes suggested conflicting regulation.

Class III: Weakly Related Pathways. Many genes were colored in the pathway, but they were primarily in peripheral regions and did not coordinate in the direction of change. Figure 2-5 C showed the pathview image of the MAPK signaling pathway, one of the most fundamental pathways in most cells. Eight genes in the image were colored, but they were not positioned centrally or connected within the same processes. A closer examination revealed that most of these genes were also involved in other pathways or biological processes. This suggested that changes in these differential genes might affect cellular activities through other pathways rather than this one.

Class IV: Not Related or Slightly Related Pathways. Less than 5 genes were colored, and they were not in key positions. Figure 2-5 D showed the well-known Glycolysis / Gluconeogenesis pathway. Only three genes were colored in the image.

The classification of pathways was based on their relevance to the list of differential genes (the orthologs of list f). Class I and Class II pathways were more likely to be directly influenced by the changes in expression of the genes in the list. Class III and Class IV pathways could still be regulated by the expression level changes of differential genes, but their statistical impact was smaller compared to Class I and Class II pathways. Additionally, a pathway with few or even no differential genes did not imply it is unimportant in primary thickening cells at this stage. It only meant that this pathway might be equally important or unimportant in primary thickening cells at stage 4 in *dsRed* and *Ets4* RNAi embryos.

There were a total of 62 pathview image, from either mouse or fly, with at least two genes colored. These pathview images were classified into four types. Eight pathways were classified as Class I, 18 as Class II, 28 as Class III, and 16 as Class IV (Table 2-6). In the following sections, I will primarily discuss Class I and Class II pathways.

Table 2-6. Classification of Type I, II, III, and IV Pathways and Their Associated Biological Activities.

Pathway classification		I	II	III	IV
clssification criteria		related process. As least one complete path, or more than 1/4 related genes. Unidirection. With key genes	fits most requirement in I, with no key genes, or with different directions in one path	multiple gene related	2 to 5 genes related
Basical cellular activity	DNA and chromatin			ATP dependent chromatin remodeling, DNA replication	Polycomb repressive complex
	RNA, transcription	Spliceosome	mRNA surveillance	RNA degradation, RNA polymerase	
	protein		Nucleocytoplasmic transport, Ubiquitin mediated protease		Protein processing in endoplasmic reticulum
	membrane system, vesicles	Endocytosis	Lysosome, SNARE interactions in vesicular transport		Endocrine and other factor regulated calcium reabsorption , Synaptic vesicle cycle
general regulation pathway		cGMP-PKG pathway, PI3K-AKT pathway	RAP1 pathway, Ras pathway	Apelin pathway, calcium pathway, circadian entrainment, ERBB pathway, JAK-STAT pathway, MAPK pathway, mTOR pathway	Circadian rhythm, Longevity regulation pathway, Longevity regulation pathway-multiply species, Toll like receptor signaling pathway
movement	cell skeleton, movement protein	Actin cytoskeleton, Motor proteins			Cytoskeleton in muscle cells
	cell-cell interaction, external signals	Axon guidance	Adherens junction, Chemokine, Focal adhesion, Tight junction	Gap junction	
metabolism			FOXO pathway, Glucagon pathway	AMPK pathway, fatty acid degradation, HIF-1 pathway, Inositol phosphate metablism, Insulin pathway, Vitamin digestion and absorption	Glycolysis-Glucogenesis, Oxidative phosphorylation. Pancreatic secretion, VEGF pathway
development, differentiation		Hedgehog pathway	Dorso-ventral axis formation, Notch pathway, Wnt pathway	Hippo pathway, Pluripotency of stem cell	TGF-beta pathway, Osteoblast differentiation
proliferation, apoptosis			Autophagy, Cell cycle		Necroptosis

In Table 2-6, the pathways were organized into the following categories: basic cellular activities, general regulatory pathways, cell proliferation-related pathways, cell migration-related pathways, cell differentiation-related pathways, and cell metabolism-related pathways.

The first category, “basic cellular activities”, included molecular processes such as “mRNA surveillance” (mmu03015), “Spliceosome” (mmu03040, dme03040), “Nucleocytoplasmic transport” (mmu03013), “Lysosome” (mmu04142), “Ubiquitin-mediated proteolysis” (mmu04120), among others. These pathways contributed to various cellular activities, including cell proliferation, differentiation, movement, and metabolism. However, it was challenging to determine the specific impact of these pathways on a particular or universal change in cells. For this reason, I will not further analyze these pathways unless they are clearly involved in a specific process.

Other types of pathways will be discussed in the following sections.

3.2 Cell proliferation-related pathway

To begin with, cell proliferation was defined as “an increase in the number of cells as a result of cell growth and cell division” (NCBI website), including the regulation of this process.

Many other Class I and Class II pathways mentioned key terms such as “cell proliferation”, “cell growth”, and “cell cycle” in their images, often positioned downstream in certain pathways. These pathways included: “Wnt signaling pathway” (mmu04310, dme04310), “PI3K signaling pathway” (mmu04151), “Ras signaling pathway” (mmu04014), “Hh signaling pathway” (mmu04340, dme04341), “FOXO signaling pathway” (mmu04068, dme04068), and “cGMP-PKG signaling pathway” (mmu04022, Figure Y13 A). While the pathway most directly connected to the process of “cell proliferation” is the “cell cycle” pathway (mmu04110), which was classified as a Class II pathway relevant to our differential gene list.

Figure Y14 showed the Pathview and heatmap images of the “cell cycle” pathway.

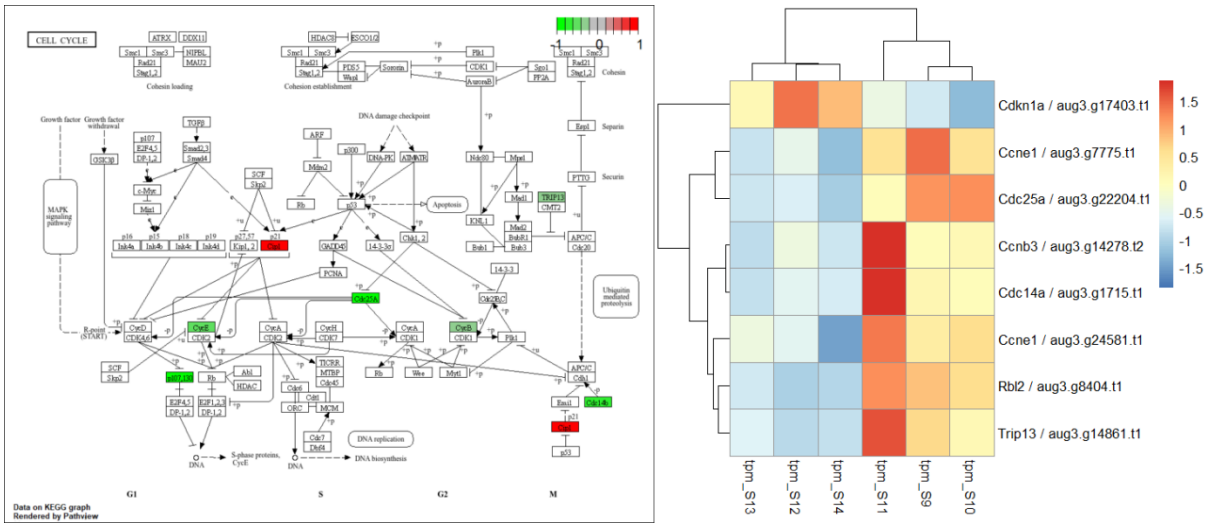

Figure 2-6. Cell cycle Pathway and Heatmap Analysis of Depicted Genes.

In the Pathview image, 7 genes were colored. Genes cip1 (cdkn1a, p21), cycB (ccnb3), and cycE (ccne1) were key genes that reflect the condition of cell division. These colored genes formed paths in the image, particularly in the G1 to S transition phase.

(1) cdkn1a (↑) --|cyclin E (↓) --| (middle factor) →{DNA synthesis S phase protein ↑} & {G1 to S transition↑}

(2) p107,130 (↓) – (middle factor) --| →{DNA synthesis S phase protein ↑} & {G1 to S transition↑},

It appeared that *Ets4* RNAi primary thickening cells exhibited increased synthesis of S phase proteins, thereby promoting the G1 to S phase transition more than WT primary thickening cells.

However, the effect on the S to G2 phase and G2 to M phase transitions was less clear from the list of differential genes. As a result, I could not draw definitive conclusions about these phases' comparison between WT and *Ets4* RNAi embryos.

The heatmap image in Figure Y14 displayed 8 genes, corresponding to the 7 genes in the pathview image, with the exception of two of ccne1. This duplication arose from two transcripts in the spider transcriptome, both annotated as the same gene. In the heatmap, genes were labeled with both their annotated names and original transcript numbers. Some genes were annotated with names differing from those in the pathview image: Cdkn1a is labeled as cip1, Ccne1 as cycE, Ccnb3 as cycB, and Rbf2 as p107. The genes in the heatmap image exhibited distinct expression patterns between the *dsRed* RNAi samples and the *Ets4* RNAi samples. This comparison of read counts (tpm) aligned with the Fold2Change values of the same genes depicted in the pathview image.

3.3 Cell movement-related pathways

Several Class I and Class II pathways were involved in cell movement processes, each addressing different aspects of cellular dynamics. Pathways such as “Regulation of actin cytoskeleton” (mmu04810) and “Motor protein” (mmu04814) focus on motor proteins, actin arrangement, and cytoskeletal dynamics. In contrast, pathways like “Focal adhesion” (mmu04510), “Adherens junction” (mmu04520), “Tight junction” (mmu04530), “Axon guidance” (mmu04360), and “Chemokine

signaling pathway" (mmu04062) were concerned with signaling related to cell-to-cell and cell-to-matrix interactions, as well as external signaling mechanisms.

Several pathways played a role in regulating the aforementioned processes by transducing signals from external sources to internal cellular components, ultimately affecting cell movement, motility, migration, and muscle function. These included the "PI3K-AKT signaling pathway", "Ras signaling pathway", "RAP1 signaling pathway" (mmu04015), and "cGMP-PKG signaling pathway" (smooth muscle relaxation process).

Furthermore, several developmental pathways also influenced cell movement processes (Hh pathway, Wnt pathway). But these pathways will be discussed in Section 3.4.

Additionally, similar to the cell proliferation process, cell migration involved a series of RNA and protein activities. Understanding the specific contribution of these processes to cell movement remained challenging. However, the "Endocytosis" pathway was an exception and was considered closely related to the cell migration process. This pathway will be discussed in this section.

3.3.1 Pathways that directly related cell movement

Figure 2-7 illustrated a combination of pathways, including "Regulation of Actin Cytoskeleton", "Motor Protein", "Focal Adhesion", and "Axon Guidance".

Figure 2-7A presented the pathview and heatmap images of the "Regulation of Actin Cytoskeleton" pathway. The colored genes formed nearly a complete pathway, beginning with the external signal chemokine factor, which activated receptor RTK. This signal then progressed through key cellular factors such as PI3K and Ras, and included actin-related genes like Cdc42, MLCP, MLC, and FAK. The pathway culminated in downstream components like F-actin and myosin. All the colored genes in this pathway were aligned in the same regulatory direction, leading to a unified effect on the pathway's effectors.

The downstream effects of the "Regulation of Actin Cytoskeleton" pathway included actin polymerization, filopodia and lamellipodia formation, focal complex assembly, stress fiber development, and actomyosin assembly and contraction. The data suggested that in *Ets4* RNAi embryos, there was a decrease in F-actin-related components and myosin II, while actomyosin assembly might be increased compared to WT embryos.

Figure 2-7B illustrated the pathway "Motor protein" and the expression of differential genes from list f within this pathway. The image showed components of microtubules and motor proteins connected to microtubules, including Dynein, Dynactin, and Kinesin, as well as Myosin and Actin. Nine differential genes were colored in the image in an organized manner: Genes associated with the plus end of the microtubule, including both components of Kinesin, were colored green, while genes associated with the minus end of the microtubule, including one component of Cytoplasmic Dynein and one gene in Axonemal Dynein, were colored red. In addition, the components of actin, microtubule was colored green, while the gene regulating actin and myosin was colored red.

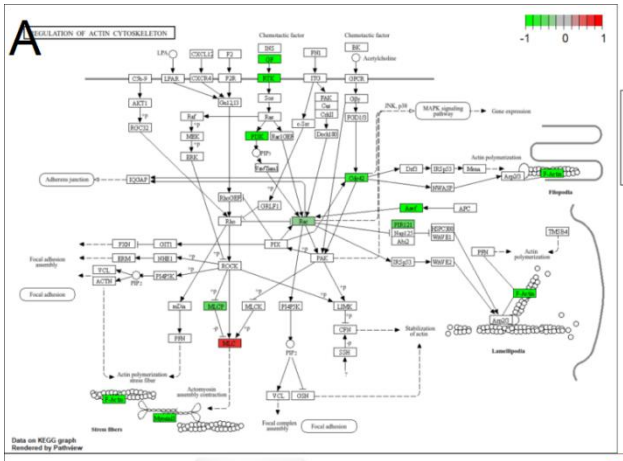
A
REGULATION OF ACTIN CYTOSKELETON
Data on KEGG graph
Rendered by Pathview

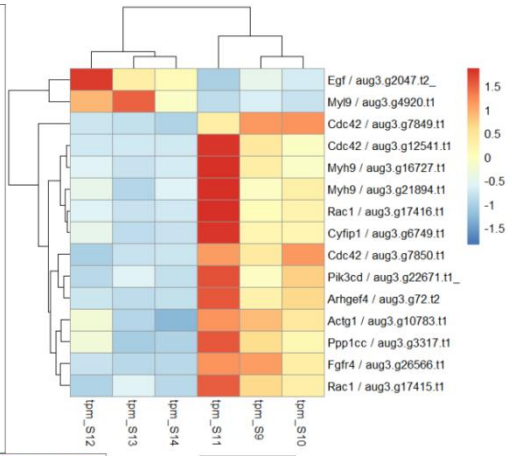
Egf / aug3.g2047.t2_
Myl9 / aug3.g4920.t1
Cdc42 / aug3.g7849.t1
Cdc42 / aug3.g12541.t1
Myh9 / aug3.g16727.t1
Myh9 / aug3.g21894.t1
Rac1 / aug3.g17416.t1
Cyfip1 / aug3.g6749.t1
Cdc42 / aug3.g7850.t1
Pik3cd / aug3.g22671.t1_
Arhgef4 / aug3.g72.t2
Actg1 / aug3.g10783.t1
Ppp1cc / aug3.g3317.t1
Fgfr4 / aug3.g26566.t1
Rac1 / aug3.g17415.t1
tpm_S12
tpm_S13
tpm_S14
tpm_S11
tpm_S9
tpm_S10
1.5
1
0.5
0
-0.5
-1
-1.5

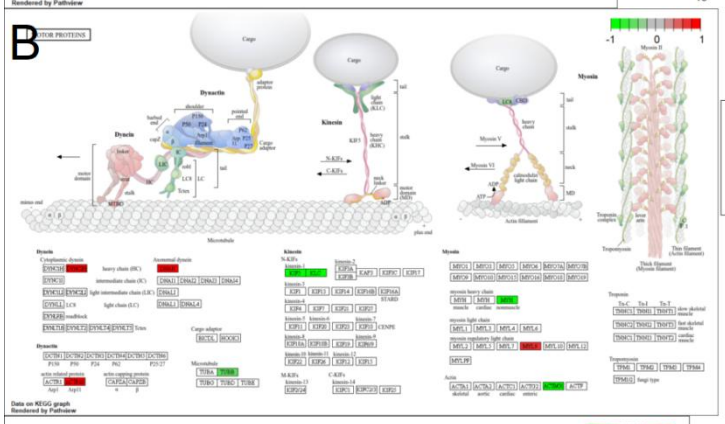
B
MOTOR PROTEINS
Dynactin
Dynein
Kinesin
Myosin
Data on KEGG graph
Rendered by Pathview

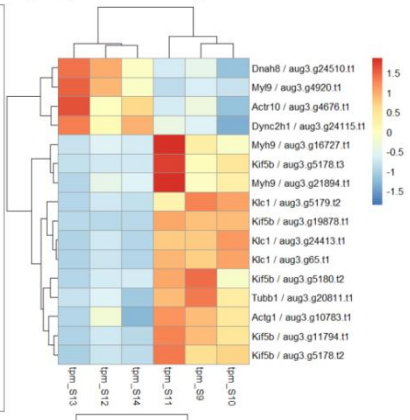
Dnah8 / aug3.g24510.t1
Myl9 / aug3.g4920.t1
Actr10 / aug3.g4676.t1
Dync2h1 / aug3.g24115.t1
Myh9 / aug3.g16727.t1
Kif5b / aug3.g5178.t3
Myh9 / aug3.g21894.t1
Klc1 / aug3.g5179.t2
Kif5b / aug3.g19878.t1
Klc1 / aug3.g24413.t1
Klc1 / aug3.g65.t1
Kif5b / aug3.g5180.t2
Tubb1 / aug3.g20811.t1
Actg1 / aug3.g10783.t1
Kif5b / aug3.g11794.t1
Kif5b / aug3.g5178.t2
tpm_S13
tpm_S12
tpm_S14
tpm_S11
tpm_S9
tpm_S10
1.5
1
0.5
0
-0.5
-1
-1.5

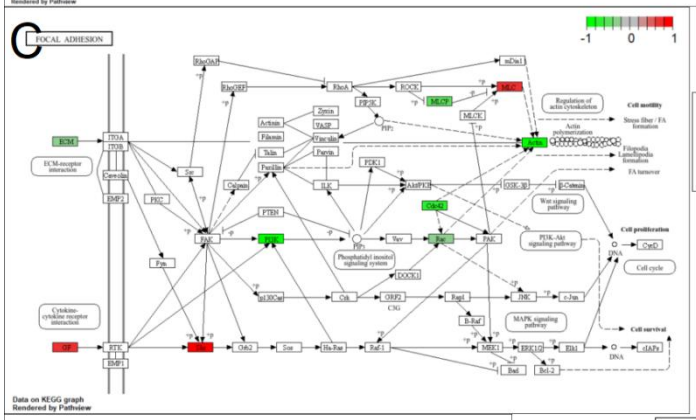
C
FOCAL ADHESION
Data on KEGG graph
Rendered by Pathview

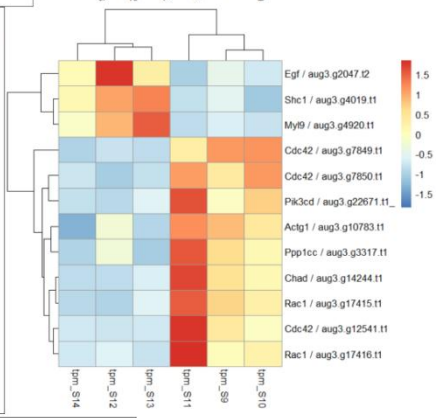
Egf / aug3.g2047.t2
Shc1 / aug3.g4019.t1
Myl9 / aug3.g4920.t1
Cdc42 / aug3.g7849.t1
Cdc42 / aug3.g7850.t1
Pik3cd / aug3.g22671.t1_
Actg1 / aug3.g10783.t1
Ppp1cc / aug3.g3317.t1
Chad / aug3.g14244.t1
Rac1 / aug3.g17415.t1
Cdc42 / aug3.g12541.t1
Rac1 / aug3.g17416.t1
tpm_S14
tpm_S12
tpm_S13
tpm_S11
tpm_S9
tpm_S10
1.5
1
0.5
0
-0.5
-1
-1.5

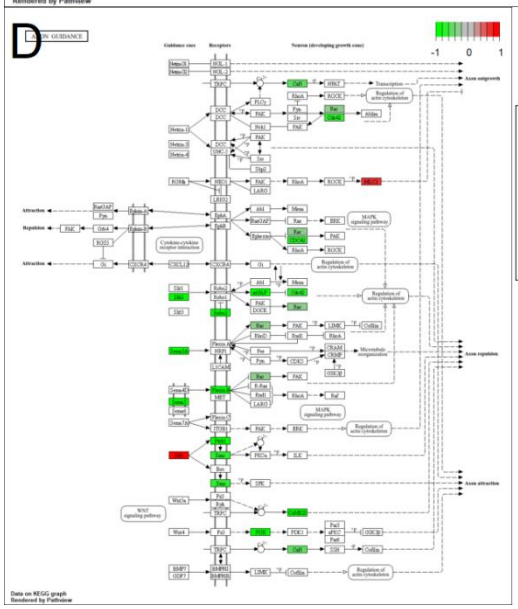
D
AXON GUIDANCE
Data on KEGG graph
Rendered by Pathview

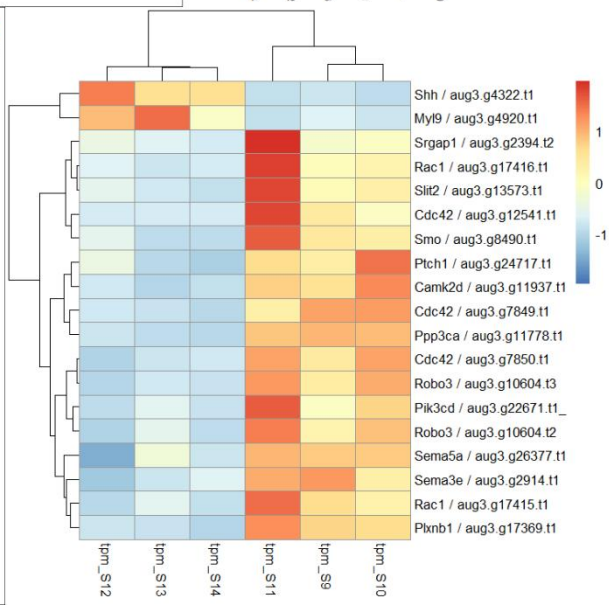
Shh / aug3.g4322.t1
Myl9 / aug3.g4920.t1
Srgap1 / aug3.g2394.t2
Rac1 / aug3.g17416.t1
Slit2 / aug3.g13573.t1
Cdc42 / aug3.g12541.t1
Smo / aug3.g8490.t1
Ptch1 / aug3.g24717.t1
Camk2d / aug3.g11937.t1
Cdc42 / aug3.g7849.t1
Ppp3ca / aug3.g11778.t1
Cdc42 / aug3.g7850.t1
Robo3 / aug3.g10604.t3
Pik3cd / aug3.g22671.t1_
Robo3 / aug3.g10604.t2
Sema5a / aug3.g26377.t1
Sema3e / aug3.g2914.t1
Rac1 / aug3.g17415.t1
Plxnb1 / aug3.g17369.t1
tpm_S12
tpm_S13
tpm_S14
tpm_S11
tpm_S9
tpm_S10
1
0
-1

Figure 2-7. Actin cytoskeleton (A), Motor protein (B), Focal adhesion (C), and Axon guidance (D) Pathways and Heatmap Analysis of Depicted Genes.

In the cytoskeleton hypothesis for explaining mammalian cell movement during “crawling motion”, rapid actin polymerization at the leading edge of the cell facilitated forward movement, while microtubules at the lagging part of the cell help maintained direction and stability. This coordination between actin and microtubules enabled the cell to move effectively and in the correct direction.

If considered within this migrating cell model, the pathview image of the “motor protein” pathway indicated that a reduction in cell movement ability at the front and a diminished orientation ability at the back of primary thickening cells in *Ets4* RNAi embryos compared to WT embryos.

Figure 2-7 C presented the “Focal adhesion” pathway, where nine genes were highlighted. Seven of these nine differentially expressed genes were also marked in the “Regulation of actin cytoskeleton” pathway (Figure Y15 A). These genes were situated in similar cellular locations and were involved in similar downstream activities.

Figure 2-7 D illustrated the “Axon guidance” pathway, which was involved in the process by which neurons extend axons to reach their target locations during neural development.

This pathway ranked third in gene count among all pathways analyzed, with “Endocytosis” and the “Wnt signaling pathway” being first and second, respectively. It included 14 colored genes in the Pathview image.

Among these colored genes, three pairs of signals and receptors were identified: Hh & Ptc & Smo, Silt & Robo, and Sema & Plexin B. Additionally, the cytoplasmic signal transduction of most pathways involves the genes Rac and/or Cdc42, which were also implicated in regulating the actin cytoskeleton in the 'Regulation of actin cytoskeleton' and 'Focal adhesion' pathways.

3.3.2 Pathways that regulate cell movement

In the last section, Several pathways were discussed which primarily involved in cell movement and the regulation of the cytoskeleton. Several pathways, including the “Regulation of actin cytoskeleton” (Figure 2-7 A), “Focal adhesion” (Figure 2-7 C), as well as “Ras signaling pathway” (Figure S2-5), featured the pathway “PI3K → Rac → actin organization”.

The pathview image of the “PI3K-AKT signaling pathway” in Figure 2-8 shows 13 colored genes, included the core factor PI3K. However, although actin organization was mentioned in the image, no genes related to this process were colored, and the “PI3K → Rac → actin organization” path was not highlighted in this image (Figure 2-8).

Additionally, differentially expressed genes included several signals and receptors: GF & RTK, G protein and G protein receptor, as well as BCAP and related FGF, FGFR, although these were not depicted in the image. The colored genes were also associated with downstream cell activities such as glucose metabolism, cell cycle regulation, cell survival, and protein synthesis.

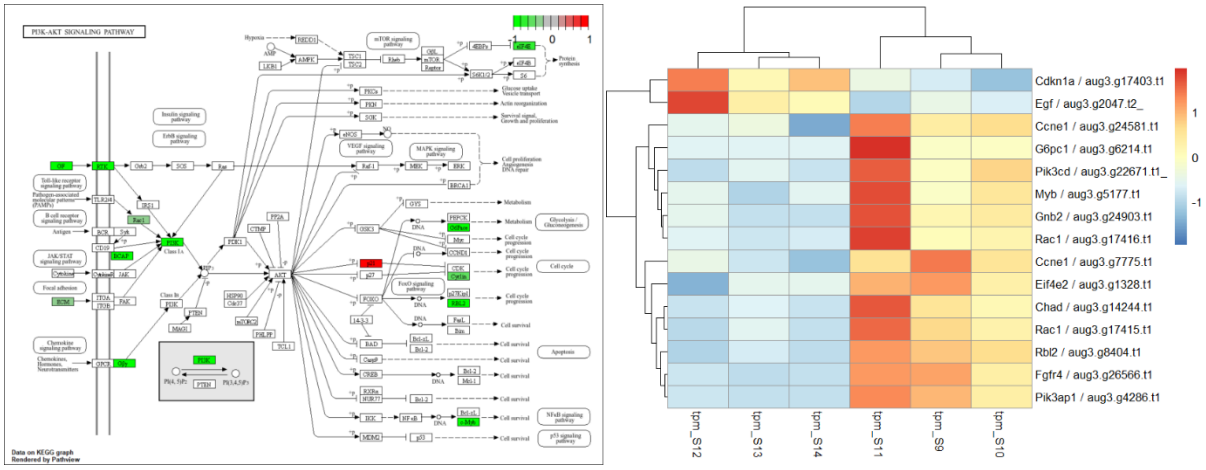

Figure 2-8. PI3K signalling Pathway and Heatmap Analysis of Depicted Genes.

A plausible explanation suggested that the PI3K pathway as one of the key regulators of cytoskeleton regulation. However, among all the potential downstream cellular activities regulated by this pathway, cytoskeleton regulation may not be the most common effect in the majority of cells that maintain this pathway.

A manual pathway (Figure 2-9) was created using Microsoft PowerPoint to visually integrate the information of differential expressed genes connected to pathway "PI3K → Rac → actin organization", from five pathview images: "Regulation of Actin Cytoskeleton" (Figure 2-7 A), "Focal Adhesion" (Figure 2-7 C), "Axon Guidance" (Figure 2-7 D), "PI3K-AKT Signaling Pathway" (Figure 2-8), and "Ras Signaling Pathway" (Figure S2-5).

Figure 2-9 constructed pathway depicting key elements involved in cell movement, along with a heatmap image showing the differential expression of related genes from list f. The differential expression genes identified in the Pathview images are depicted in black text. And essential genes that were not part of the differential expression gene list but were crucial to the pathway were also incorporated, marked in grey text.

Figure 2-9 integrated data from several pathways and could be summarized into one primary pathway:

Signal → Receptor → other factor → PI3K → downstream factors, including Rac, Cdc42 → downstream effect, including cytoskeleton organization, cell movement regulation.

Six signal-receptor pairs were highlighted: GF-RTK (from "Regulation of actin cytoskeleton", "Focal adhesion", "PI3K-AKT signaling pathway", and "Ras signaling pathway"), ECM (from "Focal adhesion" and "PI3K-AKT signaling pathway"), Slit-ROBO (from "Axon guidance"), Sema-Plexin B (from "Axon guidance"), GPCR-Gβr (from "PI3K-AKT signaling pathway" and "Ras signaling pathway"), and Netrin1-DCC (from "Axon guidance").

The downstream components of the manually depicted pathway in Figure 2-9 primarily focused on the actin cytoskeleton. This pathway also integrated aspects of cell proliferation and metabolism, derived from the "PI3K-AKT signaling pathway" pathview image.

Figure 2-9 incorporated a large number of differential genes in a closely connected manner, which may reflect potential differences in cytoskeleton organization and other cellular activities contributing to cell movement between WT and *Ets4* RNAi embryos.

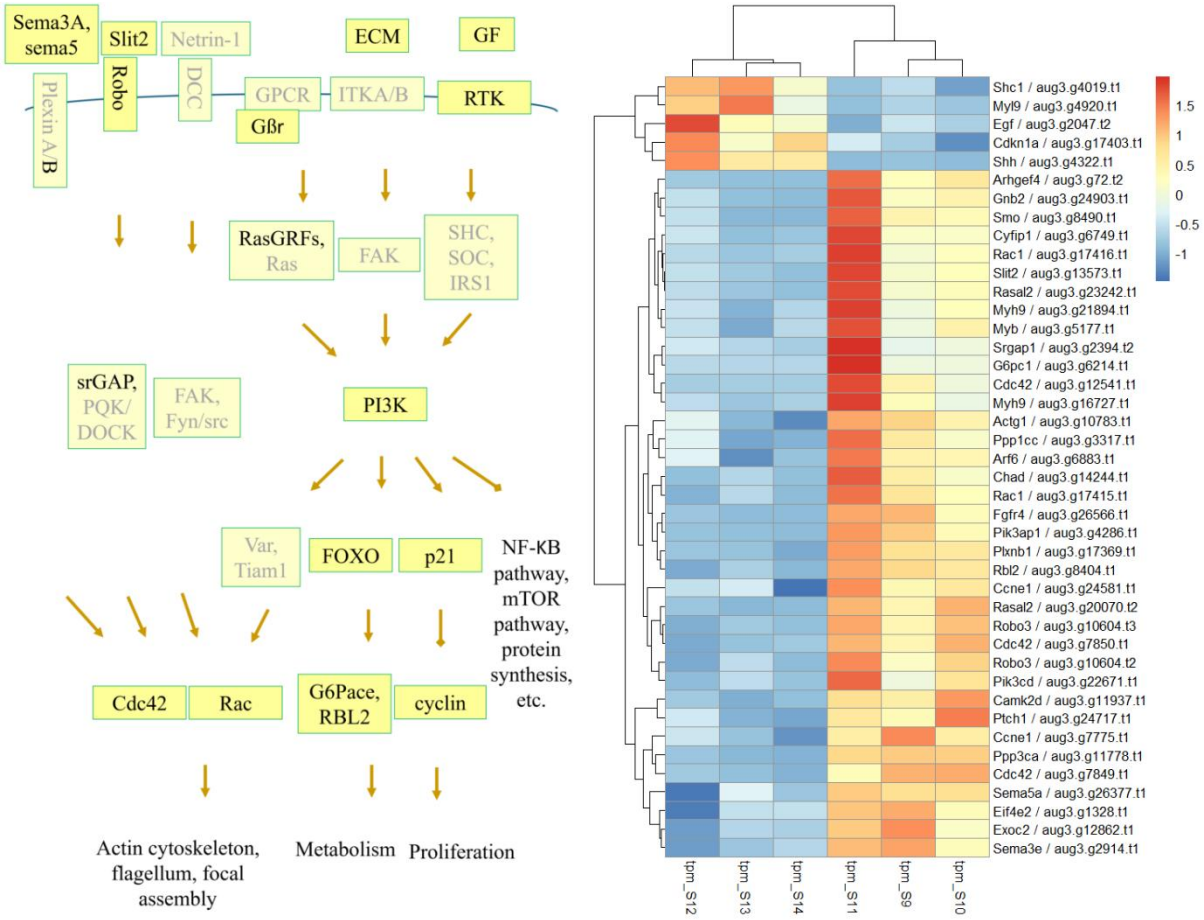

Figure 2-9. Manually constructed cell movement-related Pathway and Gene Heatmap. The pathway is integrated of several pathways, involving Actin Cytoskeleton (Figure 2-7 A), Focal Adhesion (Figure 2-7 C), Axon Guidance (Figure 2-7 D), PI3K-AKT Signaling Pathway (Figure 2-8), and Ras Signaling Pathway (Figure S2-5). The pathway image was manually drawn in PowerPoint. The heatmap, generated using R (pheatmap), combines gene sets from these five pathways. Gene names are provided in the format "Mm ortholog gene name / *Pt* Augustus number".

3.3.3 Endocytosis pathway

The "Endocytosis" pathway describes a complex vesicular transport process involving several stages. It begins with the generation of vesicles from the cell membrane, which then merge with early or late endosomes. Within these endosomes, some contents of the original vesicles are subjected to digestion in a low pH environment, while other components are incorporated into new vesicles. These new vesicles are then returned to the membrane, completing the cycle.

This pathway was long considered related to cell movement, explaining the cell membrane system involved in extending 'feet' to the front of the cell during crawling. In our pathway analysis, the 'Endocytosis' pathway standed out due to its inclusion of the highest number of differentially expressed genes among all pathways analyzed.

Figure 2-10 presented the pathview image for the "Endocytosis" pathway. Most of the genes associated with the membrane and vesicle recycling to the membrane were shown in green, while the genes localized to late endosomes and multivesicular bodies were predominantly red. This suggested the primary thickening cells of *Ets4* RNAi embryo on average, would possess less outer membrane

and more inner membrane, compared to WT embryos. A reduced surface area of the cells reflected reduced attachment to the surroundings, or less “feet” to move.

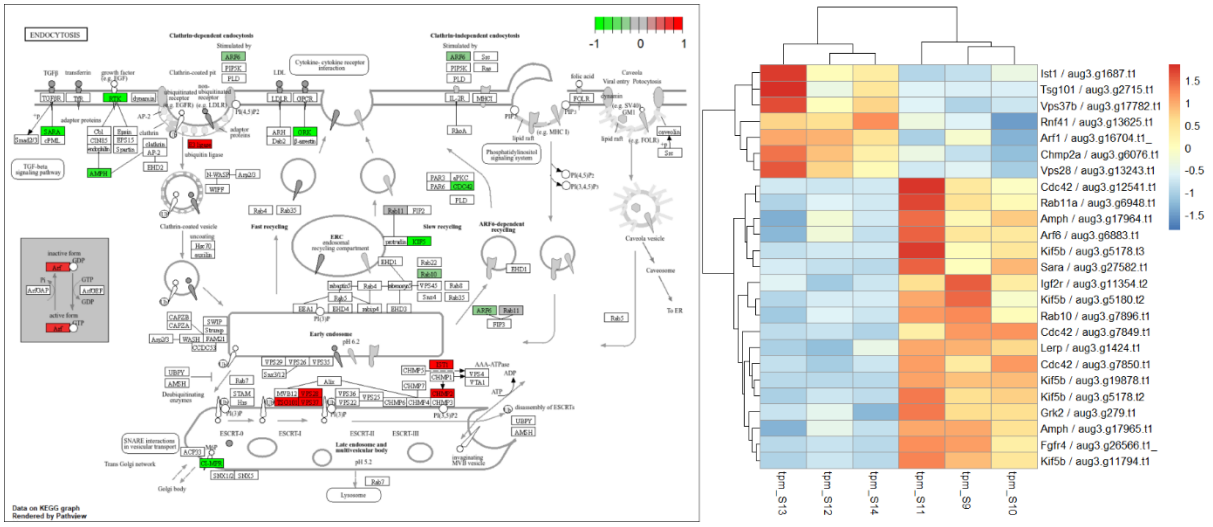

Figure 2-10. Endocytosis Pathway and Gene Heatmap Analysis.

A similar observation was noted in the “Motor protein” pathway (Figure Y15 B). Here, differential expression genes related to kinesin, which operated at the microtubule plus end, were depicted in green, indicating higher expression in WT primary thickening cells compared to *Ets4* RNAi embryos. Conversely, genes associated with dynein, functioning at the microtubule minus end, were shown in red, reflecting lower expression in WT primary thickening cells relative to *Ets4* RNAi embryos. Consequently, in primary thickening cells of *Ets4* RNAi embryos, microtubules were dynamically reduced in the front direction and cell propulsion were undermined.

Although it remained possible that the observed connection between differential expression genes and their locations could be coincidental, it was more likely that it reflected a genuine pattern. This connection suggested that *Ets4* RNAi primary thickening cells were undergoing a process of adjusting their movement dynamics. The differential expression of genes associated with various aspects of cell movement, such as vesicle trafficking and cytoskeleton organization, indicated a reconfiguration in the movement processes of these cells.

3.4 Cell differentiation-related pathways

In the KEGG database, developmental-related pathways could be broadly categorized into two types. The first type included pathways named after key developmental factors, such as the “Hh signaling pathway”, “Wnt signaling pathway”, “Notch signaling pathway”, “TGF-beta signaling pathway”, and “Hippo signaling pathway”. The second type encompassed pathways that described specific developmental events, including “Dorso-ventral axis formation”, “Regulation of pluripotency of stem cells”, and “Osteoblast differentiation”.

In this section, I will focus on the “Hh signaling pathway”, “Wnt signaling pathway”, “Notch signaling pathway” because these Class I and Class II pathways demonstrated a close relevance to the differential expression gene list.

Previous study showed that at stage 4, *hh* was expressed in extraembryonic and germ disc rim cell (Akiyama-Oda and Oda, 2010), *Wnt8b* in the primary thickening region (Janssen et al., 2021), and *Delta* in the extraembryonic region (Oda et al., 2007).

I would also examine the “TGF-beta signaling pathway”, given that *dpp* was identified as a marker gene for primary thickening cells (Akiyama-Oda and Oda, 2003). Additionally, *dpp* was highlighted as a key factor in establishing dorsal-ventral axis in *Pt* (Akiyama-Oda and Oda, 2006).

The “Hh signaling pathway” differed between mouse and fly, resulting in two versions of the Pathview image, each based on the mouse and fly orthologs from list f. (Figure 2-11).

Figure Y19 A illustrated the “Hh signaling pathway” in mouse. The key components of the pathway—Hh, Ptc, and Smo—were all highlighted in the image. Additionally, three other differential expression genes were colored, comprising a significant portion of the entire pathway image. Genes located inside the cells were depicted in green, while the Hh gene outside the membrane was shown in red. Figure 19 B depicted the “Hh signaling pathway” in fly. Key factors of this pathway—Hh, Smo, and Ptc—were marked in color, along with one additional gene. Similar to the mouse version, Hh was shown in red, while the inner cellular factors were depicted in green. The heatmap images for both mouse and fly versions confirmed the color coding based on the Fold2Change values, visualizing the reads for all samples of these genes.

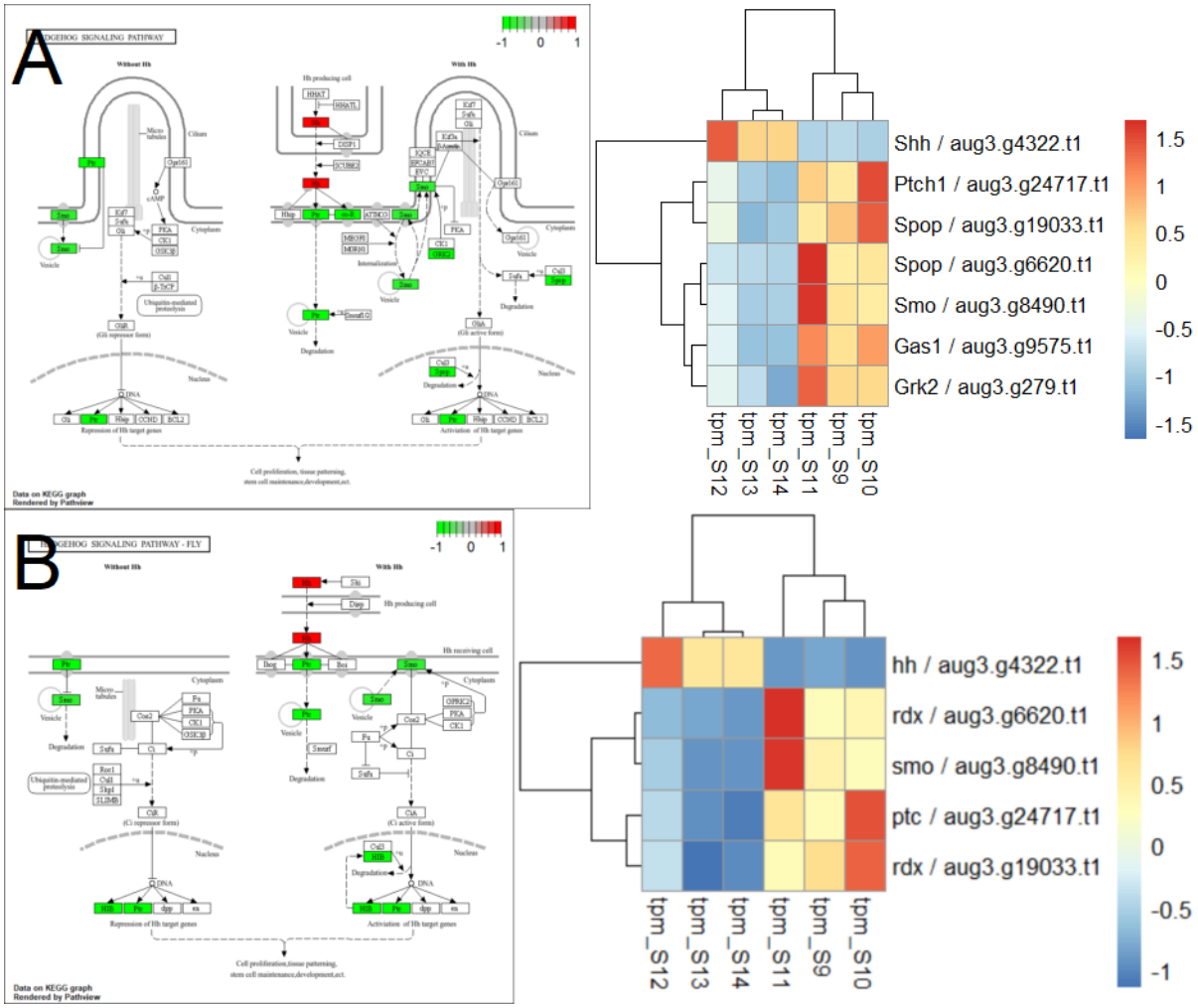

Figure 2-11. Hedgehog Pathway from mouse (A) and fly (B) and Gene Heatmap Analysis.

In both “Hh signaling pathways”, Hh itself was upregulated in *Ets4* RNAi primary thickening cells, while the inner cellular components responsible for signal reception were downregulated. This suggested that in WT embryos, the primary thickening region predominantly functioned as a receptor

for the Hh signal. In contrast, in *Ets4* RNAi embryos, this region appeared to act more as a source of the Hh signal, while internal respond to the signal are diminished.

Figure 2-12 presented a combined image of the “Wnt signaling pathway”, “Notch signaling pathway”, and “TGF-beta signaling pathway”, along with the expression of genes from list f within these pathways.

Figure 2-12 A presented a combined view of the “Wnt signaling pathway” using orthologs from both mouse and fly. While the pathways were conceptually the same for both species, differences in gene annotation led to variations in the colored genes within the pathview images. This pathway encompassed three distinct sub-pathways: the Wnt canonical pathway, the planar cell polarity pathway, and the Wnt/Ca^{2+} pathway. Each sub-pathway involved different Wnt proteins and functions in various cell types.

In the Wnt canonical pathway, a total of 9 differential expression genes were identified, including the core factor Wnt. These genes were primarily located in two areas: the signal-receptor components near the cell membrane and the transcriptional regulation components inside the nucleus. All these differential expression genes showed lower expression levels in *Ets4* RNAi embryos compared to WT embryos. This pathway may impact the regulation of the “Cell cycle” and “Adherens junction” pathways.

In the Wnt planar cell polarity pathway, 5 differential genes were highlighted, primarily at the cell membrane and within the cytoplasm. It is challenging to determine the overall effect of these genes on the regulation of this pathway. The relevant processes associated with this pathway include the “cytoskeleton”.

In the Wnt/Ca^{2+} pathway, only 2 genes were highlighted.

Overall, the Wnt canonical pathway appeared to be the most relevant to primary thickening cells among the three Wnt pathways, as it involved the highest number of differential expression genes, which were interconnected and regulated accordingly. In *Ets4* RNAi embryos, primary thickening cells might exhibit reduced ability to both send and receive Wnt signals comparing to WT embryos, which led to diminished downstream effects on cell cycle regulation and cell adhesion.

Figure Y20 B displayed the differential expression of genes in the Notch signaling pathway. Four genes were highlighted, excluding the core factors Notch and delta. *Delta* (*g12734*) was included in list b, showing higher expression in *Ets4* RNAi samples compared to *dsRed* RNAi samples. Even considering this, it remained challenging to determine whether the entire pathway was up- or down-regulated in *Ets4* RNAi embryos relative to WT.

Figure Y20 C presented the Pathview image of the TGF-beta signaling pathway. It was quite surprising that only three differential expression genes were marked in the Pathview image, with one of them being more related to proliferation (p107, Rbf2). Notably, the signaling factor dpp itself was not colored. This finding echoed a previous in situ hybridization experiment, which also showed *dpp* expressed in a similar pattern in primary thickening cells of both WT and *Ets4* RNAi embryos (Pechmann et al., 2017).

I examined other key factors of the TGF-beta signaling pathway through the transcriptome analysis. The genes *Pt-smad/Smad4* (g16672.t1, g16672.t2) and *Pt-mad* (g26552) all exhibited high expression levels across all six samples, with no significant differences between WT and *Ets4* RNAi embryos. This suggested that the production of Dpp and the response to Dpp were at similar levels in primary thickening cells of both WT and *Ets4* RNAi embryos.

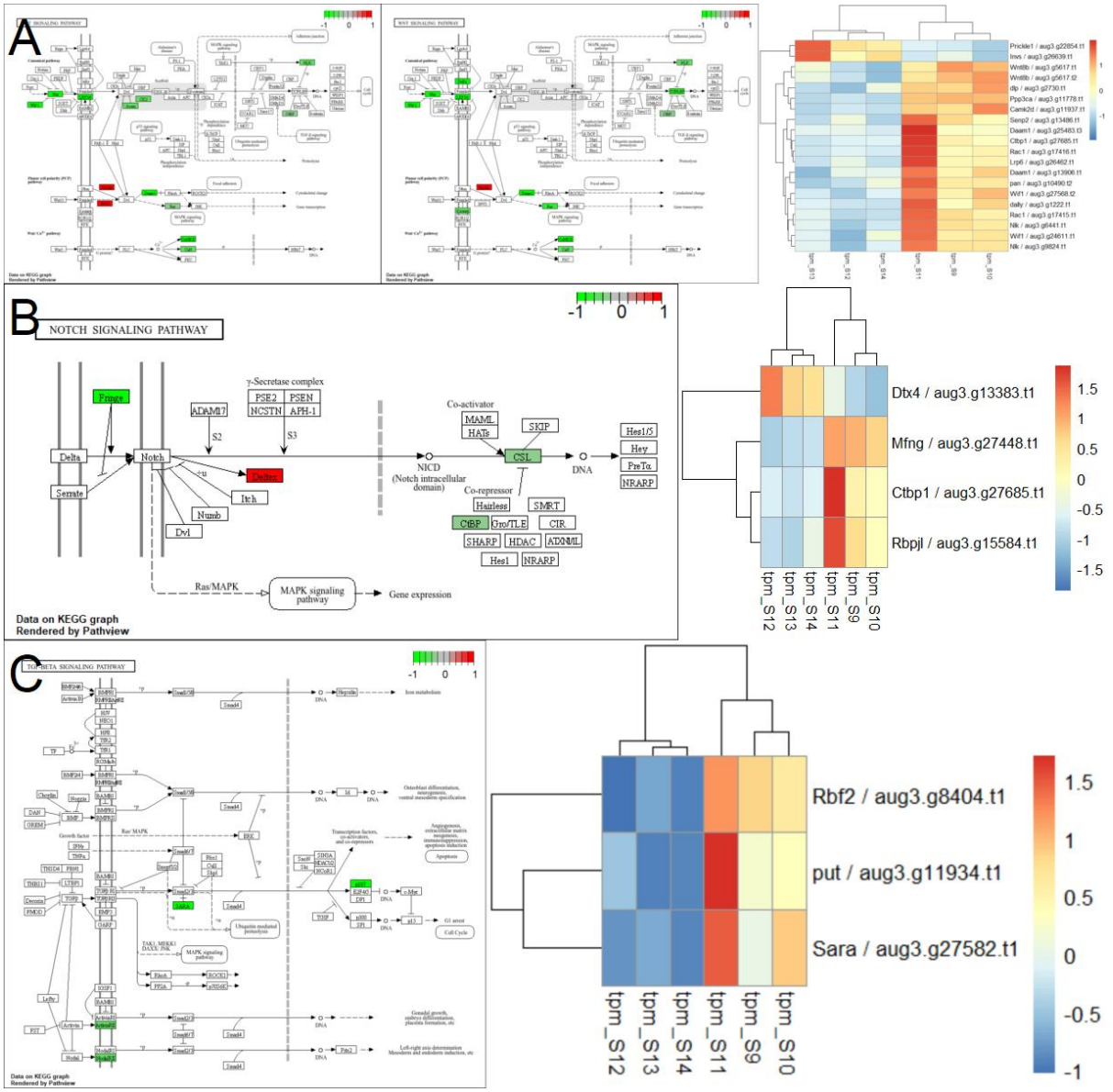

Figure 2-12. Wnt (A), Notch (B) and TGF-β (C) signalling Pathways and Gene Heatmap Analysis.

The “Dorso-ventral signaling pathway” in fly was only partially related to the differential expression gene list, specifically regarding the production of mRNA for Grk (Figure S2-6 A).

Key factors essential for maintaining stem cell pluripotency and self-renewal, such as Oct4, Nanog, and Sox2, were not present in the differential gene list. Therefore, the “signalling pathway in regulating pluripotency of stem cells” (Figure S2-6 B) might not be present in spiders. Nonetheless, primary thickening cells regulated several developmental pathways similar to stem cells.

3.5 Cell metabolism-related Pathways

I analyzed a subset of the pathways related to cell metabolism. Figure 2-5 D depicted the ten steps of glycolysis, pyruvate oxidation, and the TCA cycle. Among these, only three genes were marked in the image, representing two different sub-pathways. All three genes were involved in reversible processes.

Figure S2-7 combined the Pathview images of the following pathways: “FoxO signaling pathway” (A), “Glucagon signaling pathway” (B), “Fatty acid degradation” (C), and “Inositol phosphate metabolism” (D). The "Glucagon signaling pathway" suggested that glucose transport and glucose reduction processes might differ in expression levels between primary thickening cells of WT and *Ets4* RNAi embryos. Differential expressions were observed in the pathways related to "fatty acid degradation" and "inositol phosphate metabolism" between the two embryo types; however, limited understanding of these processes precluded further analysis.

4. Function analysis of differential expression genes with other methods.

Additional information was consulted from other sources (textbooks, review papers, articles, other websites, etc.) to further analyze gene expression in primary thickening cells of WT and *Ets4* RNAi embryos.

4.1 Cell proliferation related analysis with other methods: Cyclins and CDKs.

The most well-known genes related to proliferation were cyclins and cyclin-dependent kinases (CDKs). I identified these genes in the *Parasteatoda* genome and examined their expression levels in the complete RNAseq dataset (Figure S2-8).

Most of these genes exhibited low expression levels. Notably, *Cdk8*, *Cdk9*, and *Cdk12* were highlighted for their higher expression and significant Fold2Change values. These genes were annotated as playing roles in transcriptional regulation.

4.2 Cell migration related analysis with other method

A schematic illustration from Ridley et al., 2003 (Figure 2-13 A), provided the key steps involved in crawling motion, and outlines the essential factors that contribute to this cellular activity.

I conducted an auto-annotation of the transcriptome to identify the Augustus numbers for each gene listed in Figure 2-13A. Using these Augustus numbers, I then searched the RNA-seq data to obtain read counts (tpm) for each transcript. With the RNA-seq data, I identified genes showing differential expression in the primary thickening region of WT and *Ets4* RNAi embryos, using the selection criteria of list F. For each queried gene, multiple transcripts were typically found with the same annotation. It was however, not yet know if they were paralogs, or alternative splicing products.

Figure 2-13 B illustrated the counts of transcripts for 21 genes from Figure 2-13 A. Grey indicated the counts of transcripts with low expression in both *dsRed* and *Ets4* RNAi samples, green represented the counts of transcripts with similar expression levels in *dsRed* and *Ets4* RNAi samples, and yellow signified the counts of transcripts with differential expression between *dsRed* and *Ets4* RNAi samples.

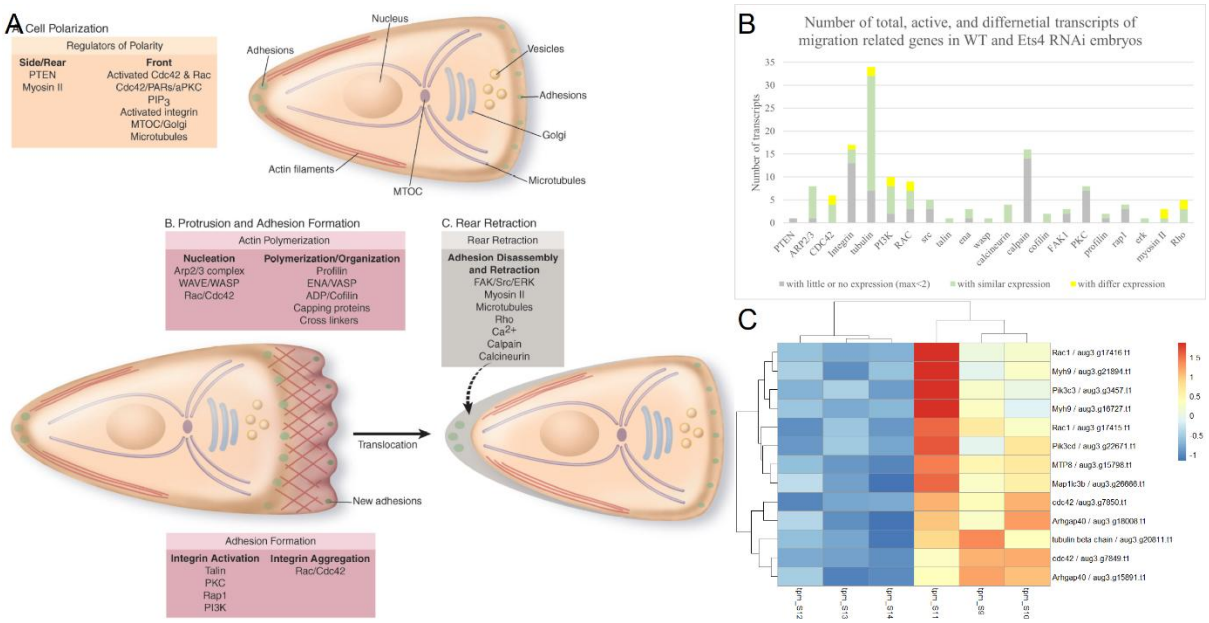

Figure 2-13. Analysis of Migration Pathways and Associated *Pt* Genes. A. Diagram illustrating cell migration by crawling and key genes involved in this process (Ridley et al., 2003). B. Count of *Pt* genes from the total transcripts based on auto-annotation data. Transcripts were classified into three categories: no expression (reads of all 6 samples < 2), no difference (difference between maximum and minimum reads < 2), or with difference (difference between maximum and minimum reads > 2). C. Heatmap of genes classified as "with difference" from panel B.

In the results, 20 of the 21 genes, excluding the PTEN gene, had at least one transcript with a read count exceeding 2, as indicated by green and yellow coloring in Figure Y24 B. Among these 20 genes, most exhibited similar expression levels in *dsRed* and *Ets4* RNAi samples. Only 7 genes displayed transcripts with differential expressions between the two embryo types.

For these 7 genes, differential expression transcripts often occupied a small portion. For example, the tubulin gene showed 7 transcripts in grey, indicating low expression across all samples; 25 transcripts in green, reflecting high but similar expression levels in both *dsRed* and *Ets4* RNAi samples; and only 2 transcripts in yellow, denoting differential expression between *dsRed* and *Ets4* RNAi samples.

Analysis of the current results suggested that (1) Key genes in the cell crawling movement model were present and expressed in spider, either in WT or *Ets4* RNAi embryos. Thus support the hypothesis that cumulus movement in spider was similar to mammalian crawling cells. (2) Most cytoskeleton-related genes were expressed at similar levels in primary thickening cells of both WT and *Ets4* RNAi embryos, with only a small proportion of transcripts specifically involved in cytoskeleton functions for cell movement.

4.3 Development and cell differentiation related analysis with other methods.

Cumulus migration direction was hypothesized to be influenced by the asymmetric expression of FGF, which may create a gradient that guides the directional movement of these cells by regulating cellular responses to environmental cues (Wang et al., 2023). The KEGG website did not feature an FGF-specific pathway. However, the Biotechne website provided a comprehensive view of the FGF signaling pathway. I manually cross-referenced the genes from the differential expression list (list f) with this pathway image (Figure 2-14).

It is observed that FGF8 and FGFR were present among the differential expression genes, alongside PI3K, FOXO, and STAT5. However, mTOR, JAK, the majority of STAT genes, and most genes in the MAPK pathway were not included in this list.

In *Ets4* RNAi embryos at stage 4, both FGF factors and relevant downstream genes were downregulated compared to WT embryos, resulting in a general impairment in both sending and receiving FGF signals.

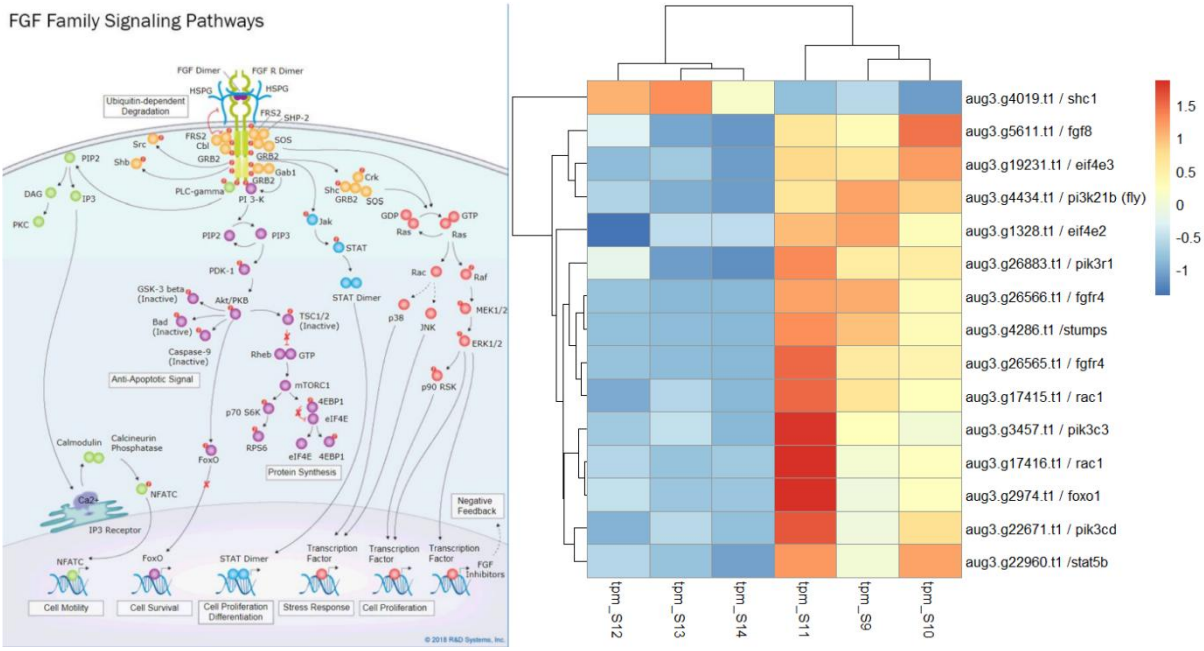

Figure 2-14. FGF Family Signalling Pathway and Heatmap of Related Genes. FGF signalling pathway diagram from Biotechne (https://www.rndsystems.com/pathways/fgf-signaling-pathways). Genes related to this pathway were identified and manually checked for their presence in list F.

Research on induced cells (iPSCs, iN, etc.) provided lists of specific genes involved in the induction and differentiation of various cell types (Xu et al., 2015). A search for mouse induced programming factors was conducted using automatic annotation of the spider transcriptome, and the results were analyzed to infer possible changes in the differentiation direction of primary thickening cells between WT and *Ets4* RNAi embryos. As a result of the gene research, most mouse programming factors identified in induced cell differentiation experiments, were not found in the spider transcriptome with auto annotation. The involvement of iPSC reprogramming genes such as *Ascl1* and *Myt1l* suggested a differential neural differentiation pathway in primary thickening cells between WT and *Ets4* RNAi embryos (Figure S2-9).

In Figure S2-10, the schematic diagrams illustrated that Ascl1 played a crucial role in neural cell induction. Additionally, Ascl1 can interacted with Myt1l to regulate the Notch signaling pathway, highlighting its significant role in differentiation. Robo and Slit were previously identified as components of the “axon guidance” pathway and associated with promoting cytoskeleton arrangement, could be interpreted as functioning in both cell movement and cell (neural directional) differentiation in WT but not *Ets4* RNAi embryos.

4.4 Other analysis on cell metabolism

A search for glycolysis and TCA cycle-related genes in the RNA-seq reads showed that more than half of the transcripts for glycolysis and TCA cycle enzymes were expressed in both WT and *Ets4* RNAi primary thickening cells. Furthermore, only a small proportion of these transcripts exhibited differential expressions between *Ets4* RNAi and WT samples.

5. Summary: function of differential expression genes in cellular activities

Analysis using different methods, primarily based on differential expression genes, currently suggested the following differences in cellular activities between the primary thickenings of WT and *Ets4* RNAi embryos:

Cell migration was more active in primary thickening cells of WT embryos compared to *Ets4* RNAi embryos. The number of differentially expressed genes associated with GO terms relevant to cell migration was substantial. Many of these differentially expressed genes were related to pathways involved in regulating the cytoskeleton, motor proteins, or endocytosis processes. It was suggested that the regulatory process might largely depend on PI3K signaling pathways. In WT embryos, primary thickening cells appeared to be in a preparatory phase for movement, potentially analogous to the mammalian cell crawling model, whereas *Ets4* RNAi embryos did not show this preparation. However, the differences in cell movement between the two embryo types may involve only a small subset of the total cytoskeleton-related transcripts. The similar expression levels of the remaining cytoskeleton-related transcripts might be involved in maintaining the cellular skeleton system.

Cell differentiation process was active in primary thickening cells of both WT and *Ets4* RNAi embryos, suggesting that primary thickening cells could play different roles in the two cases. Differential expressed genes in WT and *Ets4* RNAi primary thickening cells were strongly associated with the Hh signaling pathway, and related to the Wnt signaling pathway, FGF signaling pathway, among others. Other differentiation processes might be involved, with neural key factors potentially regulating the actin cytoskeleton in processes such as axon guidance, but not necessarily leading to the production of functional neurons.

Cell proliferation process involved many differentially expressed genes from list f, and several genes associated with the cell cycle pathway, in influencing the G1 to S transition between WT and *Ets4* RNAi embryos. However, most cyclin and CDK genes exhibited similar expression levels in *dsRed* and *Ets4* RNAi samples, suggesting that while cell cycle processes might be relevant, they may not account for the major differences observed between primary thickening cells of the two embryo types.

Cell metabolism: GO analysis revealed that many organic compounds associated with differential expression genes may vary significantly between primary thickening cells of the WT and *Ets4* RNAi embryos. While there were some differences observed in glucose metabolism, the differences were relatively minor and constituted only a small portion of the overall metabolic process. Due to lack of understanding in the results, no firm conclusion was made to summary the whole activity in general.

5 Result Chapter III: Gene expression in primary thickening cells of WT and *Ets4* RNAi embryos

This chapter presented in situ hybridization images of genes at stages 4 and 5 in spider *Parasteatoda tepidariorum*. The aim was to identify genes specifically expressed in the primary thickening and cumulus regions. Functional analysis of these genes provided insights into primary thickening, cumulus cells, and the early developmental processes of *Parasteatoda tepidariorum*.

Overall, my expression analysis in combination with a review of the available literature identified expression pattern for 212 early expressed genes in WT embryos, including 133 novel genes and 79 previously reported genes (Table S3-1). Primary screening excluded genes without specific staining in primary thickening or cumulus at stages 4 and 5, resulting in 113 genes. Among these, 24 were previously published, while 89 represented either novel genes or genes with new expression pattern at germ-disc stages. Of the 113 genes, 57 exhibited staining in *Ets4* RNAi embryos at stage 4. This subset included 10 published genes and 47 novel genes or genes with updated staining patterns. In this chapter, I presented these images and provide an initial interpretation of the observed staining patterns.

1. In situ hybridization of genes in WT embryos

1.1 In situ hybridization of genes at stage 4 in WT embryos

The expression of 113 genes was analyzed, at stage 4 WT embryos. In addition to previously published genes, new genes were selected for various reasons. Some were identified as differentially expressed in *Ets4* RNAseq data, primarily following List C (Result Chapter II, Table 2-1). Others were derived from RNAseq results of genes that showed regional expression at stage 1 (unpublished), while some represented general housekeeping genes involved in fundamental cellular pathways.

Of the 113 genes, 75 exhibited specific staining in the primary thickening region. Of these 75 genes with specific primary thickening expression, 23 were previously published (supplementary Figure S3-1). The remaining 52 genes with new specific expression in the primary thickening region were shown in Figures 3-1, 3-2, and 3-3. Among these genes, *cv-2*(A)*, opa* (M), and *Wnt8b* (S) were previously published with expression pattern at stages later than stage 4 (Kanayama et al., 2011; Leite et al., 2024; McGregor et al., 2008), while the remaining genes unstudied.

Figures 3-1, 3-2, and 3-3 show that most genes exhibited staining in the primary thickening region, as well as in other germ disc cells. *Cv-2, Itpka, L(2)efl, RF_038, Znf423, Wnt8b* and *Clca4a* were exceptions, with staining limited to primary thickening cells (Figure 3-1 A, H, I, J, N, S; Figure 3-2 A). Similar observations were made from supplementary Figure S3-1 of the published genes *dpp, fascin, ptc, Ets4*, *hb, twist, fuchi*, and *Fgfr1*, appeared to be expressed only in the primary thickening region, while *fkh, vasa, piwi, kcnj9, Ebf1, Srgap1, fgf8*, and *dof* showed expression in cells outside the primary thickening region.

While technical factors could account for some of the expression patterns, the differences could also be derived from earlier variation in expression. The expression of 44 genes at stage 2 was available in supplementary material. Of these, 32 genes were ubiquitously expressed in all cells (supplementary Figure S3-2, S3-3), while the remaining 12 genes were expressed in specific regions of the embryos (supplementary Figure S3-4).

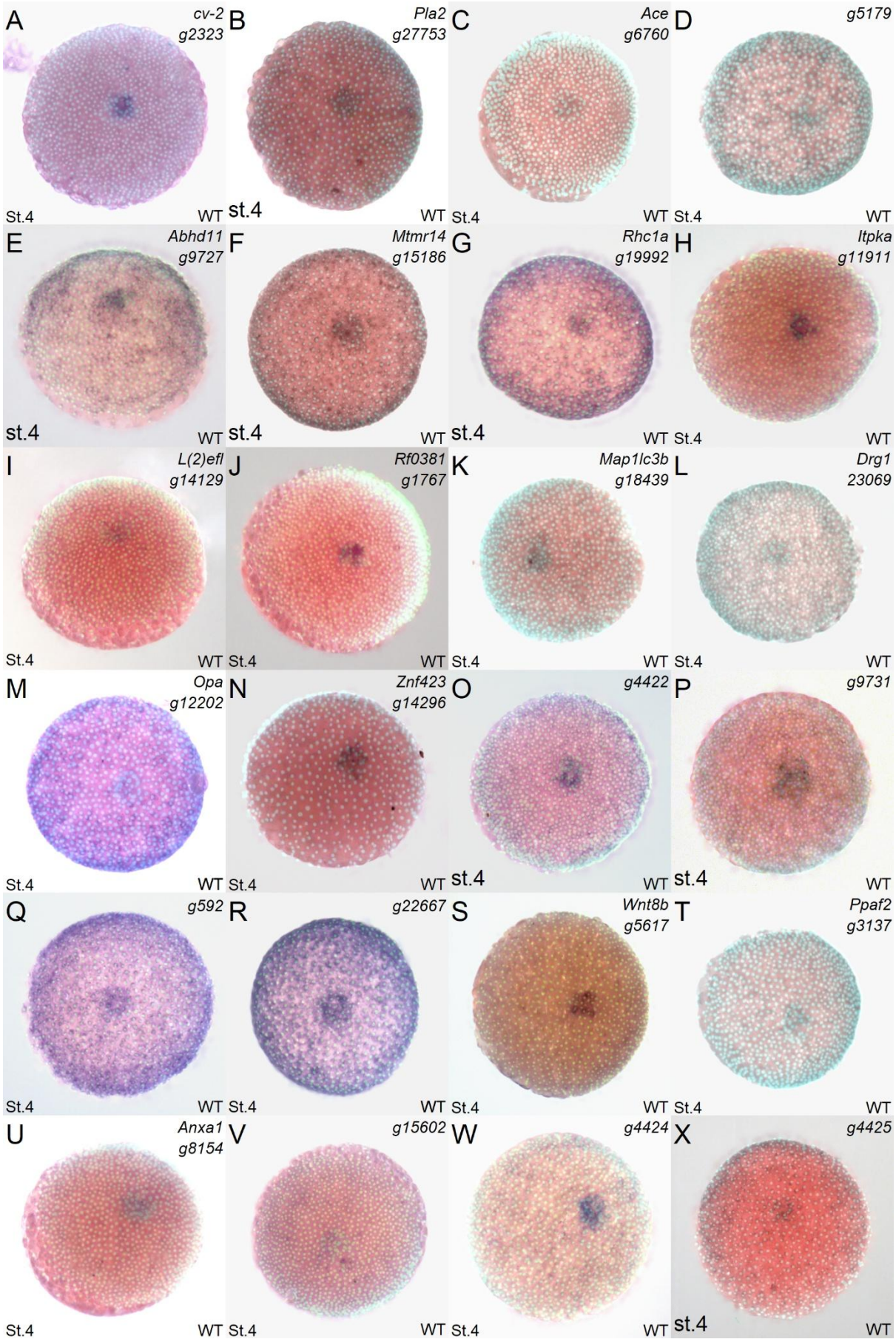
A
cv-2
g2323
St.4
WT
B
Pla2
g27753
st.4
WT
C
Ace
g6760
St.4
WT
D
g5179
St.4
WT
E
Abhd11
g9727
st.4
WT
F
Mtmr14
g15186
st.4
WT
G
Rhc1a
g19992
st.4
WT
H
Itpka
g11911
St.4
WT
I
L(2)efl
g14129
St.4
WT
J
Rf0381
g1767
St.4
WT
K
Map1lc3b
g18439
St.4
WT
L
Drg1
23069
St.4
WT
M
Opa
g12202
St.4
WT
N
Znf423
g14296
St.4
WT
O
g4422
st.4
WT
P
g9731
st.4
WT
Q
g592
St.4
WT
R
g22667
St.4
WT
S
Wnt8b
g5617
St.4
WT
T
Ppaf2
g3137
St.4
WT
U
Anxa1
g8154
St.4
WT
V
g15602
St.4
WT
W
g4424
St.4
WT
X
g4425
st.4
WT

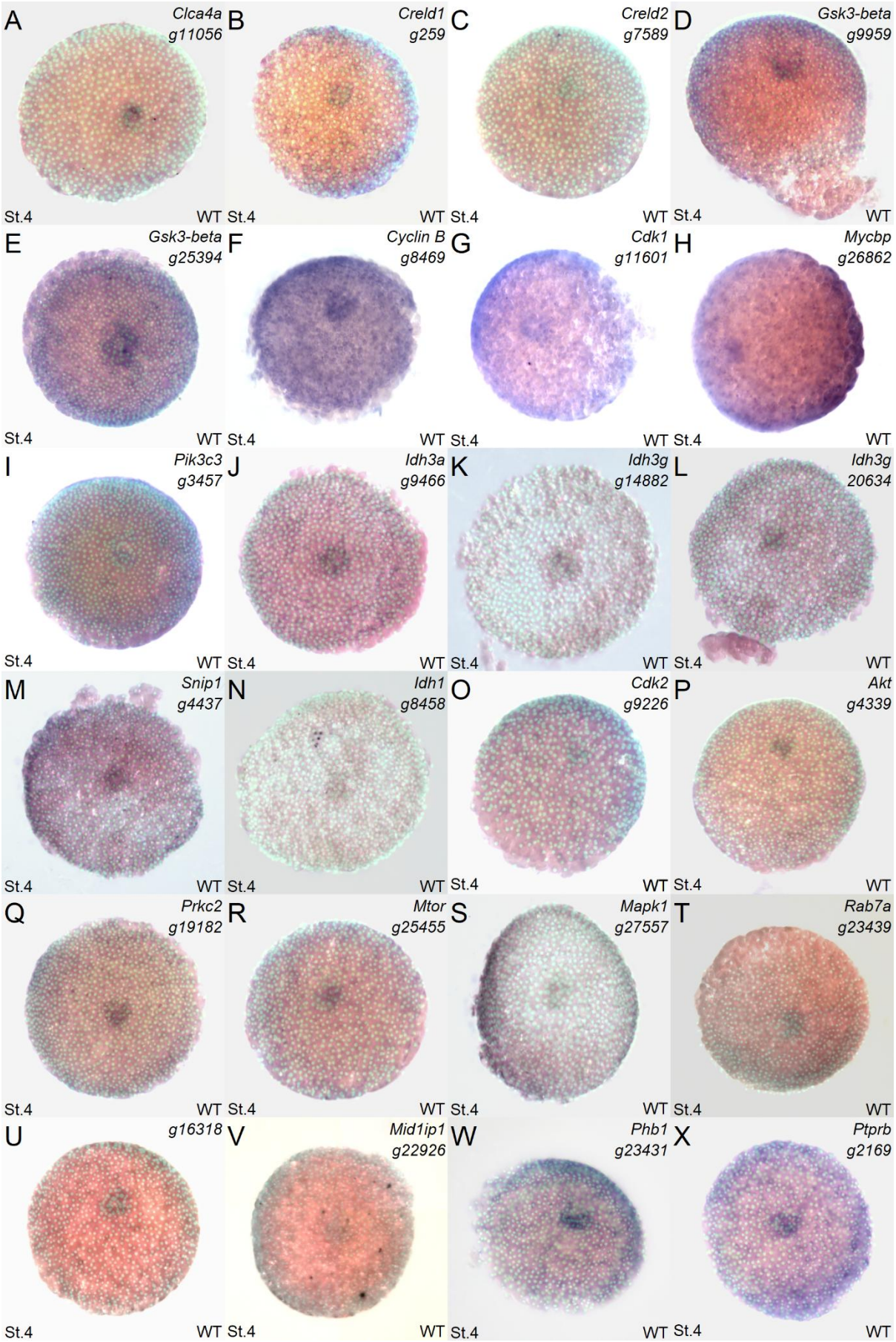
A
Clca4a
g11056
St.4
WT
B
Creld1
g259
St.4
WT
C
Creld2
g7589
St.4
WT
D
Gsk3-beta
g9959
St.4
WT
E
Gsk3-beta
g25394
St.4
WT
F
Cyclin B
g8469
St.4
WT
G
Cdk1
g11601
St.4
WT
H
Mycbp
g26862
St.4
WT
I
Pik3c3
g3457
St.4
WT
J
Idh3a
g9466
St.4
WT
K
Idh3g
g14882
St.4
WT
L
Idh3g
20634
St.4
WT
M
Snip1
g4437
St.4
WT
N
Idh1
g8458
St.4
WT
O
Cdk2
g9226
St.4
WT
P
Akt
g4339
St.4
WT
Q
Prkc2
g19182
St.4
WT
R
Mtor
g25455
St.4
WT
S
Mapk1
g27557
St.4
WT
T
Rab7a
g23439
St.4
WT
U
g16318
St.4
WT
V
Mid1ip1
g22926
St.4
WT
W
Phb1
g23431
St.4
WT
X
Ptprb
g2169
St.4
WT

Figure 3-1. In situ hybridization images of genes that show specific expression in the region of the primary thickening at stage 4 WT embryos (a). Genes shown: *cv-2, Pla2, Ace, g5179, Abhd11, Mtmr14, Rhc1a, Itpka, L(2)efl, RF_0381,Map1lc3b, Drg1,opa, Znf423, g4422, g9731, g592, g22667, Wnt8b, Ppaf2, Anxa1, g15602, g4424*, and *g4425*. Sytox/brightfield overlay.

Figure 3-2. In situ hybridization of genes that show a specific expression in the primary thickening region at stage 4 WT embryos (b). Genes shown: *Clca4a, Creld1, Creld2 g7589, Gsk3b g9959, Gsk3b g25394, CyclinB, Cdk1, Mycbp, Pik3c3, Idh3a, Idh3g g14882, Idh3g g20634, Snip1, Idh1, Cdk2, Akt, Prkc2, Mtor, Mapk1 g27557, Rab7a, g16318, Mid1ip1, Phb1*, and *Ptprb*. Sytox/brightfield overlay.

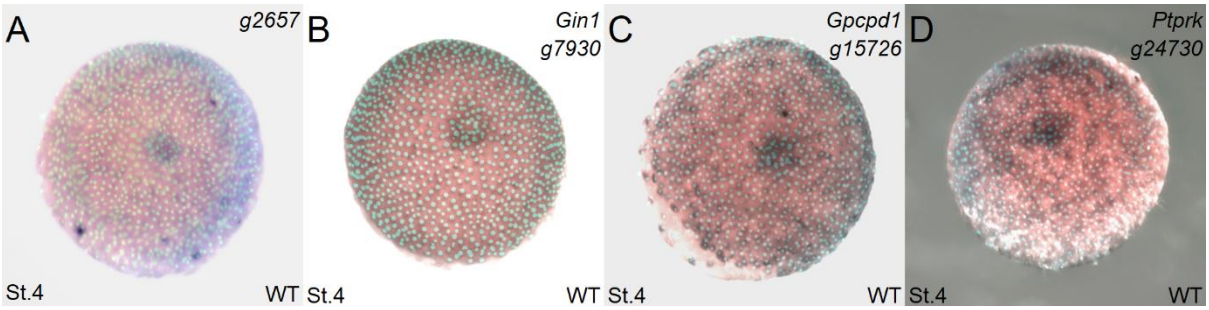

Figure 3-3. In situ hybridization images of genes with specific staining in the primary thickening region at stage 4 in WT embryos (c). Genes shown: g2657, Gin1, Gpcpd1, and Ptprk. Sytox/brightfield overlay.

It was observed that some genes showing expression at stage 2 were also expressed in both the primary thickening region and other regions of the germ disc—such as *Pla2*, *Abhd11 g9727*, *Mtmr14*, and *Ppaf2*. While other genes were de novo synthesized during stage 3 specifically in primary thickening cells, like *Ets4*, *Itpka, RF_0381*, and *Znf423* (supplementary Figure S3-5).

For most published genes, such as *dpp* and *fkh* (supplementary Figure S3-1), the expression at stage 2 were not clear, which making it challenging to determine whether the observed patterns also apply to these genes. The *fuchi* gene presented a classification challenge. While it was clearly expressed in part of the embryo at stage 2, specifically in the extraembryonic region, its expression in the embryonic region was confined to future primary thickening cells from late stage 2 to early stage 3 (Iwasaki-Yokozawa et al., 2022, and Result Chapter I, Figure 1-9, supplementary Figure S1-14). Considering only the embryonic region, *fuchi* appeared to have a late onset and was expressed exclusively in the primary thickening region, similar to *Ets4*.

In total, only a limited number of genes were analyzed, and it remained uncertain whether these observations apply to all genes involved in the early development of *Parasteatoda*.

Of the 113 genes which expression were analyzed at stage 4 WT embryos, 38 genes showed no primary thickening expression at the stage (supplementary Figure S3-6, S3-7). Among the listed genes, *hh* and *delta* expression were previously published (Oda et al., 2010, Oda et al., 2007), with both genes being expressed at the border region between the embryonic and extraembryonic parts of the embryo at early stages. Expression pattern of *hh* at stages 2, 3, and 4 in WT embryos were provided in the supplementary Figure S3-8 and S3-9. In their study, Oda and colleagues mentioned the genes *g15443* and *Radil*, but the expression of the genes was not published (Akiyama-Oda et al. 2022). The remaining genes in the list were unstudied, so far.

1.2 In situ hybridization of genes at stage 5 in WT embryos

Among the genes expressed in the primary thickening region at stage 4 in WT embryos, their expression patterns at stage 5 differed. Many genes showed no expression, while others exhibited

staining in the rim region. Of particular interest were the genes expressed in the cumulus region, which could generally be categorized into two main types.

1. Some genes showed staining exclusively in the cumulus region. Figure 3-4 presented eight genes of this category. The expression of *Ets4*, pMad, *fgf8*, and *cv-2* were described previously (Pechmann et al., 2017, Oda et al., 2003, Wang et al., 2023, and Leite et al., 2024), while *Itpka, RF_0381, g592*, and *g22667* were newly identified genes. Of these, three (*g592, g22667*, and *RF_0381*) were uncharacterized, with no homologs identified in common model organisms through NCBI BLAST, suggesting they were likely spider-specific genes.

Based on Figure 3-4, five genes exhibited expression exclusively in the cumulus region (*Ets4*, *dpp* related protein pMad, *cv-2, Itpka* and *RF_0381*). *Fgf8* was expressed in the frontal portion of cumulus cells as well as in some other germ disc cells. Genes *g592* and *g22667* showed staining along the cumulus migration path. Notably, the staining patterns of *fgf8, g592*, and *g22667* displayed certain variability across different staining samples.

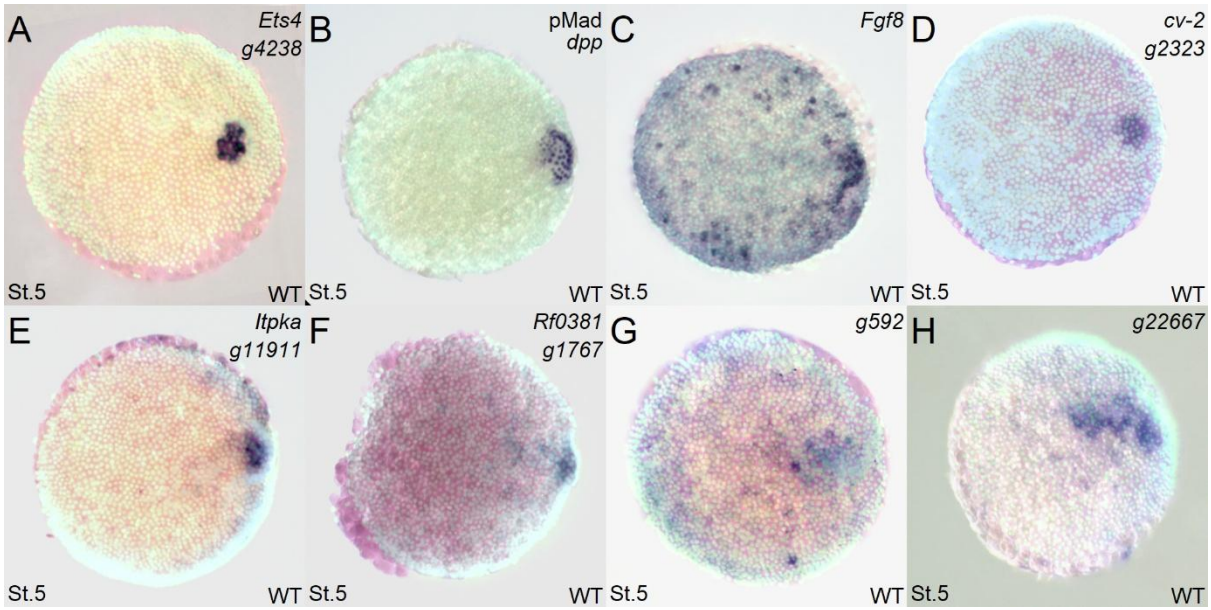

Figure 3-4. In situ hybridization images of genes with specific staining in cumulus region at stage 5 in WT embryos (a). Genes shown: *Ets4*, *fgf8, cv-2, Itpka, Rf_0381, g592, g22667*, and antibody staining of pMad. Sytox/brightfield overlay.

2. Some genes showed staining in both the cumulus region and the rim region of the germ disc. Figure 3-5 displayed expression of these genes. Among them, *dof* and *fuchi* showed expression at stage 5 (Wang et al., 2023, Iwasaki-Yokozawa et al., 2022), while Wnt8b was previously published with expression pattern from other stages (McGregor et al., 2008). *Znf423, Clca4a, Snip1, Prkc2, Pten, Rab7a*, and *Gpcpd1* are newly identified genes.

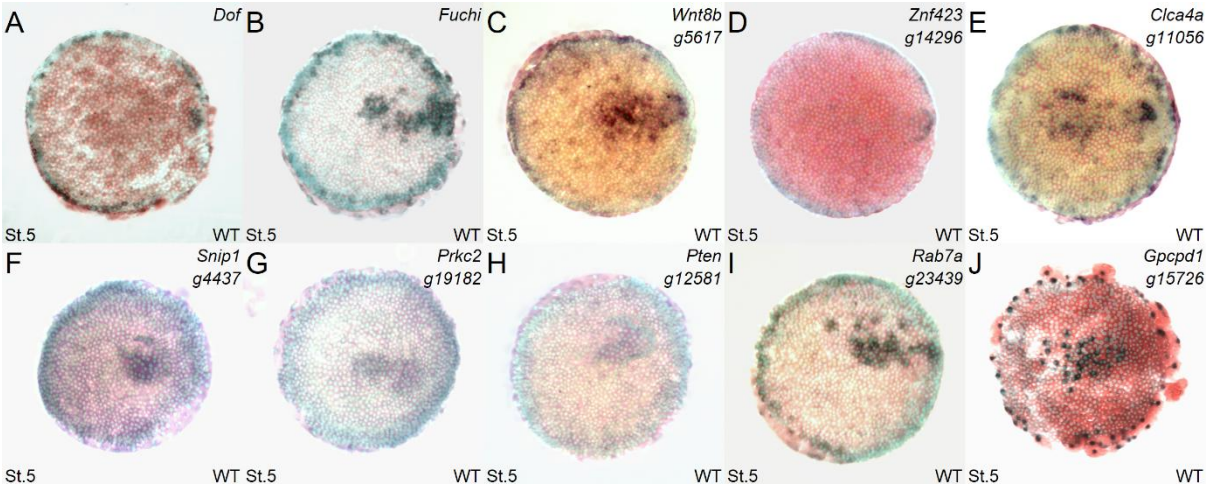

Figure 3-5. In situ hybridization images of genes with specific staining in cumulus region at st.5 in WT embryos (b). Genes shown: *dof, fuchi, Wnt8b, Znf423, Clca4a, Snip1, Prikc2, Pten, Rab7a*, and *Gpcpd1*. Sytox/brightfield overlay.

In Figure 3-5, *dof* and *Znf423* showed staining in both the cumulus region and the rim region. The other eight genes exhibited staining in the cumulus migration path cells and rim cells. Among these, *Clca4a* was unique, as it appeared to be expressed in cells surrounding the cumulus migration path rather than in the migration path cells themselves.

The cumulus migration path and the rim of the germ disc were distinct in their cell differentiation activities. By stage 5, the rim region began to express anterior marker genes, while the cell migration path expresses dorsal markers. However, these regions shared similarities, including high cell density and active cell proliferation compared to other parts of the germ disc. Additionally, the cells in these regions exhibited increased movement in the subsequent stages of germ disc formation. Genes expressed in both regions may therefore play roles in these processes.

1.3 Observed gene expression patterns from stage 2 to 5 in WT Parasteatoda development

In situ hybridization experiments were conducted with the genes mentioned above at various developmental stages. Expression pattern for 63 of the 113 genes were available for stages 2, 4, and 5. Based on the expression of these genes from stage 2 to stage 5, four main expression patterns were observed (Figure 3-6):

Type I: Genes that showed expression at stage 2, exhibited specific staining in the primary thickening region at stage 4, and were expressed in cumulus-related regions at stage 5 (Figure 3-7, Figure 3-8).

Type II: Genes that showed expression at stage 2, exhibited specific staining in the primary thickening region at stage 4, but did not show expression or exhibit expression in regions unrelated to the cumulus at stage 5 (Figure 3-9, Figure 3-10).

Type III: Genes that showed expression at stage 2, but had no expression or exhibited expression in regions unrelated to the primary thickening at stage 4 (Figure 3-11, Figure 3-12).

Type IV: Genes that showed no expression at stage 2, but exhibited specific staining in the primary thickening region at stage 4 (Figure 3-13).

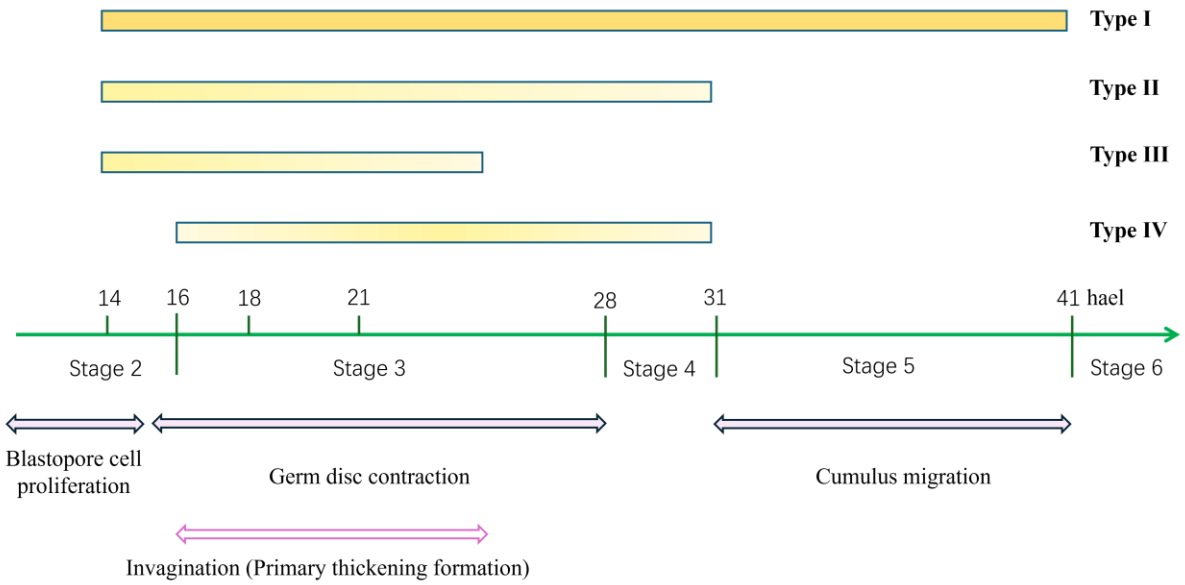

Figure 3-6. Gene expression pattern types I, II, III, and IV, and key events in early development of *Parasteatoda*. Type I: Genes are expressed at stage 2, show expression in the primary thickening region at stage 4 as well as in cumulus-related regions at stage 5. Type II: Genes are expressed at stage 2, show expression in the primary thickening region at stage 4, then either show no expression or expression unrelated to the cumulus region at stage 5. Type III: Genes are expressed at stage 2 and show no expression at stage 4, or the expression is not visible in primary thickening-related regions. Type IV: Genes are expressed after stage 2 and show specific primary thickening expression at stage 4. At stage 5, the expression of these genes is variable and thus is not depicted in the image.

This classification of gene types was primarily based on gene expression in the primary thickening and cumulus regions. While it did provide a comprehensive or strictly exhaustive description of all genes involved in early embryo development, it served well for addressing key questions related to the formation of the primary thickening region, cumulus cell specification, initiation of cumulus migration, and the establishment of the new axis.

Additionally, the expression for some genes at later stages were identified as well (supplementary Figure S3-10 to S3-14). Some of these special staining patterns were included in the following combining image (Figure 3-7 to Figure 3-13) but would not be discussed here.

Figures 3-7 and 3-8 showed the expression of Type I genes at stages 2, 4, 5, and germ band stages. A total of 17 genes were included, such as *g592, g22667, Creld2 g7589, Gsk3b g9959, Gsk3b g25394, Cyclin B, Pik3c3, Idh3a, Idh3g g14882, Snip1, Akt, Prkc2, Mapk1 g27557, Rab7a, Ptprb, Gpcpd1*, and *Ptprk*. Among these, two genes, *g592* and *g22667*, were uncharacterized. Additionally, a large portion of the genes were involved in general cellular pathways, including *Creld2, Gsk3b, Cyclin, Pik3c3, Idh, Akt*, and *Mapk1*.

Most Type I genes were expressed at similar levels in all cells at stage 2, while a few, such as *Gsk3b g25394, Akt, Prkc2*, and *Mapk1 g27557* (Figure 3-7 E1, Figure 3-8 B1, C1, D1), showed higher expression levels in certain regions. Additionally, it remained unclear whether this regional differential expression pattern results from initially ubiquitous expression at an earlier timepoint, followed by uneven consumption in specific areas.

All Type I genes were expressed in the primary thickening region, as well as in other cells of the germ disc region at stage 4. At stage 5, all Type I genes were expressed in the cumulus migration path. And except for the two uncharacterized genes *g592* and *g22667*(Figure 3-7 A1, B1), the rest also showed expression in the rim area at this stage.

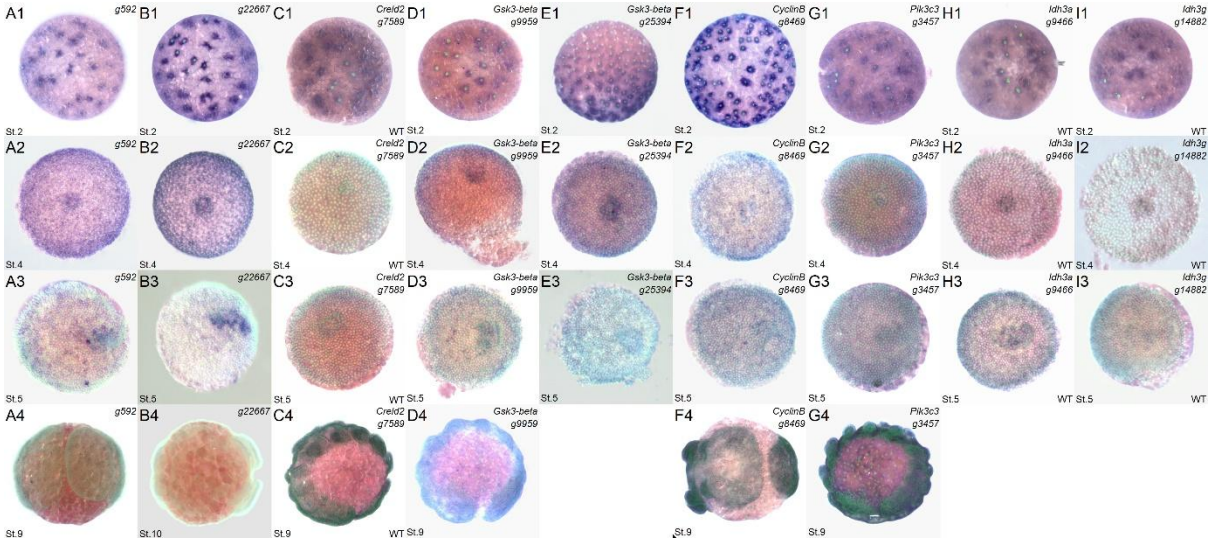

Figure 3-7. Gene expression pattern type I (a). In situ hybridization images of gene *g592, g22667, Creld2 g7589, Gsk3b g9959, Gsk3b g25394, Cyclin B, Pik3c3, Idh3a*, and *Idh3g g14882* at stage 2, 4, 5, and 9 in WT embryo. Sytox/brightfield overlay.

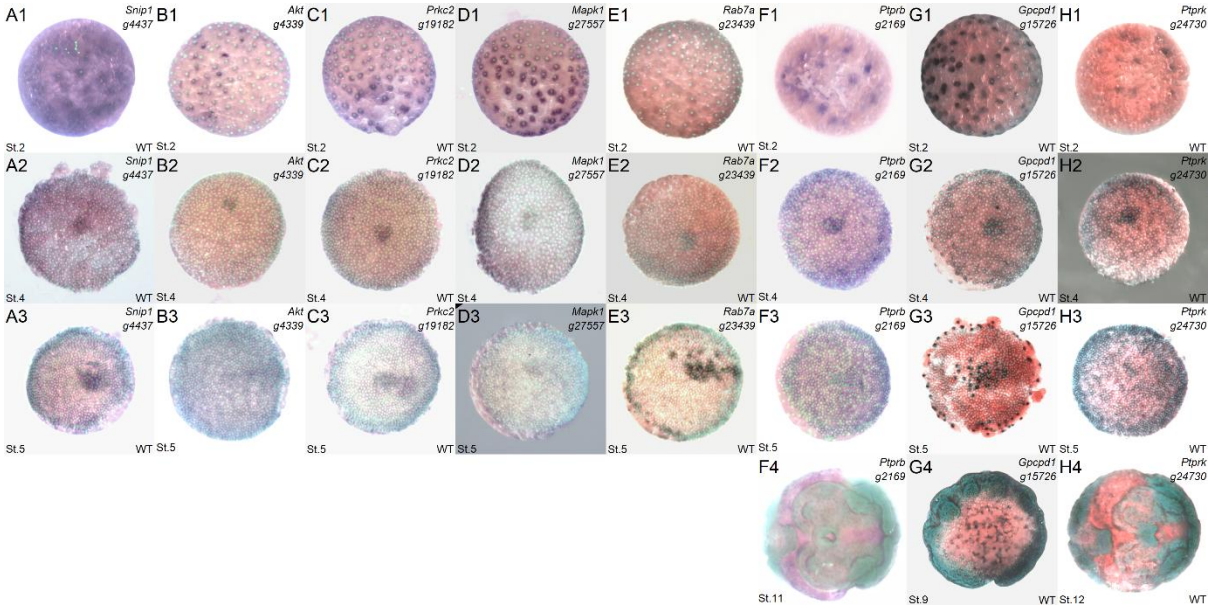

Figure 3-8. Gene expression patten type I (b). In situ hybridization images of gene *Snip1, Akt, Prkc2, Mapk1 g27557, Rab7a, Ptprb, Gpcpd1*, and *Ptprk* at stage 2, 4, 5 and 8 in WT embryo. Sytox/brightfield overlay.

Figures 3-9 and 3-10 showed the expression pattern of Type II genes at stages 2, 4, 5, and the germ band stage. A total of 16 genes were included in the images: *Pla2, Abhd11 g9727, Mtmr14, Rhc1a, g4422, g9731, Ppaf2, Anxa1, g4424, g4425, Creld1, Idh1, g16318, Phb1, g2657,* and *Gin1*. Nearly half of these genes were uncharacterized and may be unique to spider.

All Type II genes showed expression in cells at stage 2, mostly in a ubiquitous manner. At stage 4, all these genes were expressed in the primary thickening region. Most Type II genes were also expressed in other cells of the germ disc.

Most genes of this type showed no expression in the germ disc at stage 5. A few genes, such as *Ppaf2, g16318*, and *Gin1* (Figure 3-9 G1, Figure 3-10 E1, H1), stained in the rim region. This suggested the possibility of further subdividing this gene type. Based on the current images, it appeared that the majority of these genes do not exhibit specific staining at stage 9. If this holds true, it suggested that at least some of these genes functioned specifically in early stages and did not participate in later development.

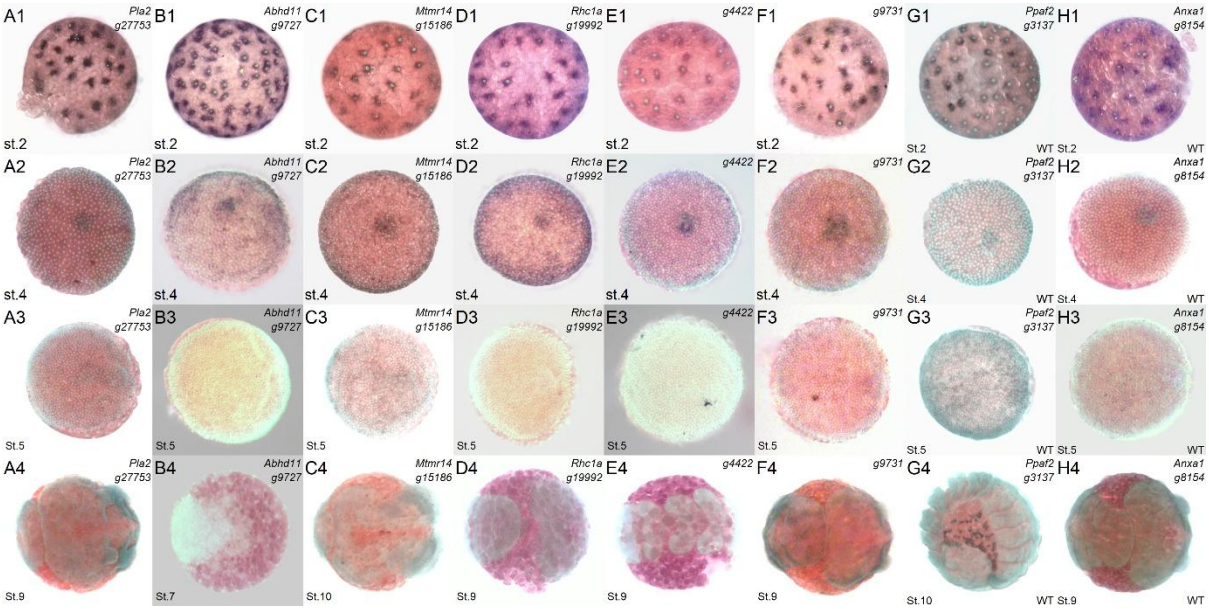

Figure 3-9. Gene expression pattern type II (a). In situ hybridization images of gene *Pla2, Abhd11 g9727, Mtmr14, Rhc1a, g4422, g9731, Ppaf2*, and *Anxa1* at stage 2, 4, 5 and 9 in WT embryos. Sytox/brightfield overlay.

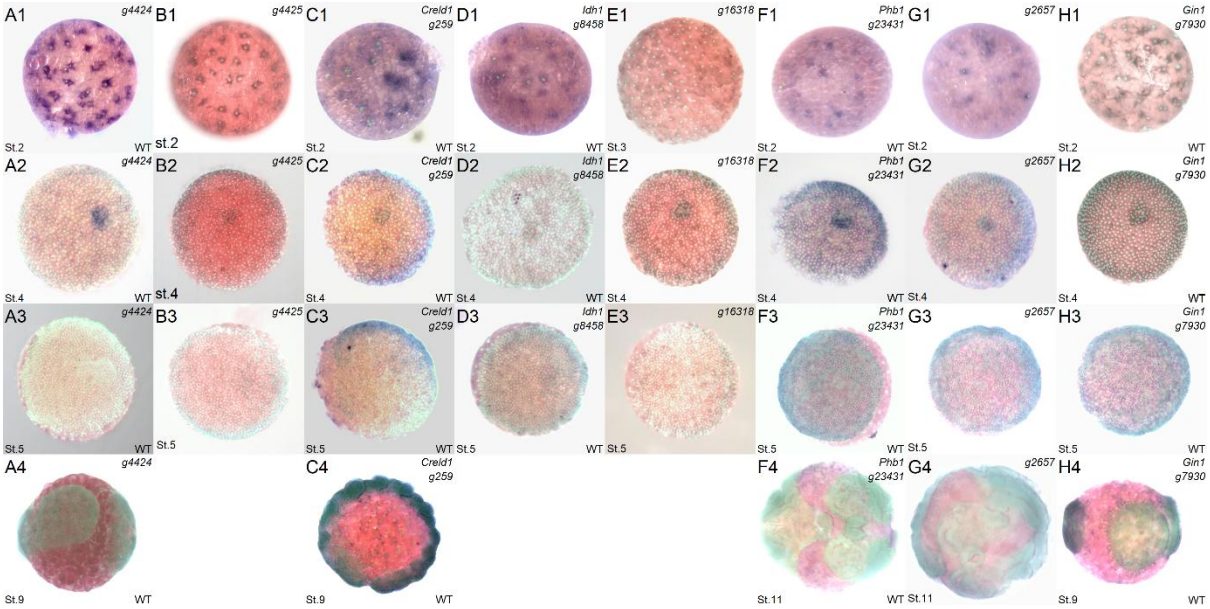

Figure 3-10. Gene expression pattern type II (b). In situ hybridization images of gene *g4424, g4425, Creld1, Idh1, g16318, Phb1, g2657*, and *Gin1* at stage 2, 4, 5, and 9 in WT embryos. Sytox/brightfield overlay.

Figure 3-11 and Figure 3-12 showed genes with expression pattern type III. The images included 19 genes, such as *delta, hh, CaM, g3789, Abhd11 g9726, Numb, Creld2 g7590, Egfr, Cyclin A1, Pik3r1 g26883, Hif, Ampk, Idh2 g4961, Aktip, Asph, Sox2, Mapk1 27558, Incenp*, and *g16165*. This list was a mix of genes with varying functions, including uncharacterized genes (*g3789, g16165*), general pathway genes (*Creld2, Egfr, Cyclin A1, Pik3r1, Hif, Ampk, Idh*), and key developmental factors (*delta, hh, Numb, Sox2*).

Type III genes also showed early expression at stage 2, mostly in a ubiquitous manner. However, genes like *delta, hh, Hif*, and *Mapk1 g27558* (Figure 3-11 A1, B1; Figure 3-12 A1, G1) might exhibit regional, differential expression. Previous studies shown that *delta* (Oda et al., 2007) and *hh* (Oda et al., 2010) stained in the extraembryonic side of the embryo. *Mapk1 g27558* may follow a similar pattern. *Hif* (Figure 3-12 A2, supplementary Figure S3-21) on the other hand, was difficult to interpret from the expression images; it could only be concluded that there are more cells with higher expression of *Hif* compared to those with low expression.

Type III genes did not exhibit expression in the primary thickening at stage 4. Most of these genes showed no expression in the germ disc at all. However, genes like *hh, g3789, Numb, Cyclin A1, Hif* and *g16165* (Figure 3-11 B2, D2, F2, I2; Figure 3-12 A2, I2), did show expression in other germ disc cells. Specifically, *hh* (Figure 3-11 B2) was expressed in the rim cells of the germ disc.

The expression of type III genes varied significantly at stage 5. Some were expressed ubiquitously in germ disc cells, while others were localized to specific regions such as the cumulus migration path, dorsal opening region, and rim region. This variability suggested that type III genes could be further classified into more accurate subtypes.

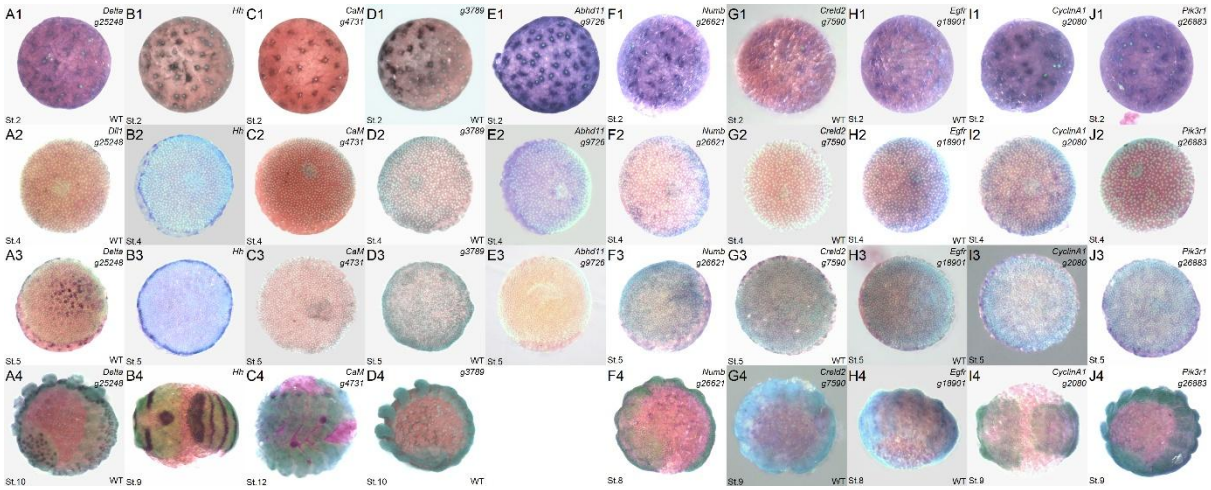

Figure 3-11. Gene expression pattern type III (a). In situ hybridization images of gene *delta, hh, CaM, g3789, Abhd11 g9726, Numb, Creld2 g7590, Egfr, Cyclin A1*, and *Pik3r1 g26883* at stage 2, 4, 5, and 9 in WT embryos. Sytox/brightfield overlay.

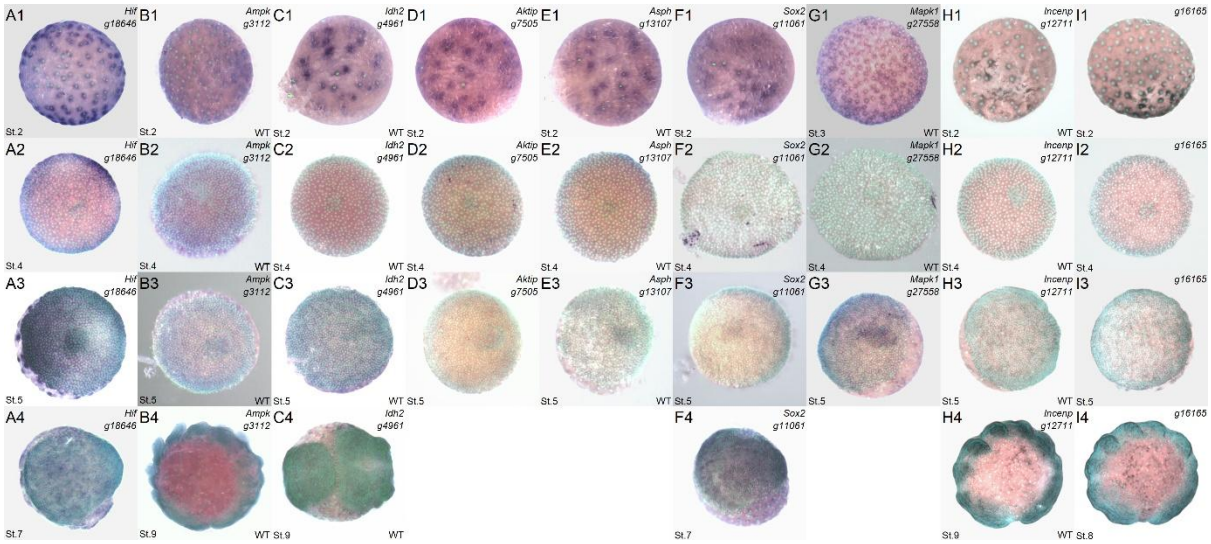

Figure 3-12. Gene expression pattern type III (b). In situ hybridization images of gene *Hif, Ampk, Idh2 g4961, Aktip, Asph, Sox2, Mapk1 g27558, Incenp*, and *g16165* at stage 2, 4, 5, and 9 in WT embryos. Sytox/brightfield overlay.

Figure 3-13 showed genes of expression pattern type IV. There were 12 genes of this type, including *Ets4, fuchi, Itpak, L(2)efl, RF_0381, opa, Znf423, ptc, Wnt8b, Clca4a, twist,* and *hb*. Among them, *opa, ptc, Wnt8b*, *twist* and *hb*, were conserved developmental genes across many species and were published as key factors in spider (Oda et al., 2010, McGregor et al., 2008, Yamazaki et al., 2005, Pechmann et al., 2017, Schwager et al., 2009). *Fuchi* belonged to the Gata family, which was consistently involved in early development (Iwasaki-Yokozawa et al., 2022). *Ets4* was essential for the integrity and initiation of cumulus migration (Pechmann et al., 2017). It was a transcription factor by nature, as was *Znf423*. *Itpka* and *Clca4a* might be involved in several pathways, particularly in inositol-related regulation. *L(2)efl* played a vital role in flies, with functions related to muscle processes and potential effects on mortality during development. *RF_0381*, however, did not have identified orthologs in flies or mice and might be a species-specific gene in spider.

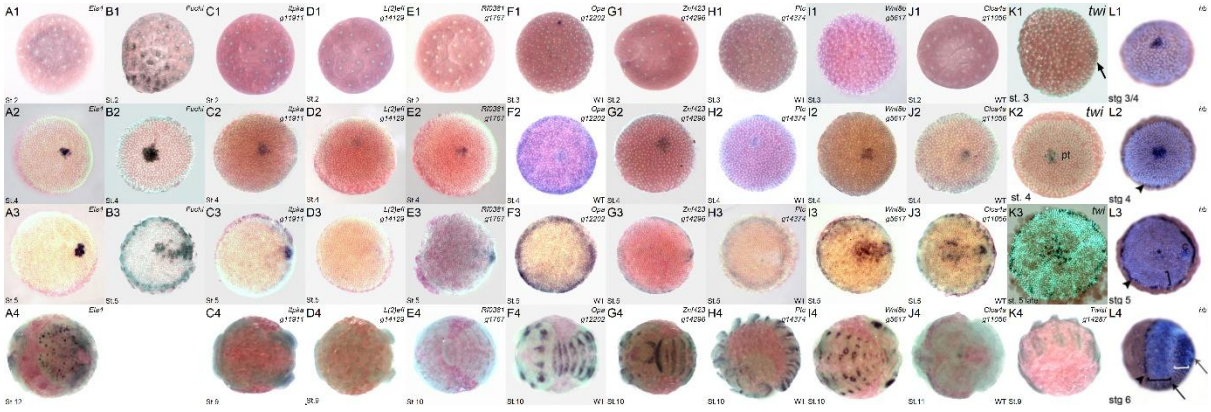

Figure 3-13. Gene expression pattern type IV. In situ hybridization images of gene *Ets4,fuchi, Itpka, L(2)efl, RF_0381, opa, Znf423, ptc, Wnt8b, Clca4a*, *twist* and *hb* at stage 2, 4, 5 and 9 in WT embryos. The staining image of Twist at stage 3, 4 and 5 were from Pechmann et al., 2017. Sytox/brightfield overlay.

Except for *fuchi* (Figure 3-13 B), the remaining 11 genes of type IV showed no expression in the embryo at stage 2. At stage 4, these genes were expressed exclusively in the primary thickening region, with no expression observed in other regions of the germ disc.

Fuchi showed few expressions at stage 2 based on in situ hybridization images. The expression of nascent *fuchi* transcripts was observed in the primary thickening region and extraembryonic cells at this stage (Result Chapter I, Figure 1-9 A1-A3, B1-B3). Expression of the *fuchi* gene was evident in these two regions at both stage 3 and stage 4. On the embryonic side, it was expressed exclusively in the primary thickening region within the germ disc.

Most of the 12 genes showed expression at stage 5. *Ets4*, *Itpka, RF_0381*, *Znf423,* and *hb* (Figure 3-13 A3, C3, E3, G3, L3), were specifically expressed in the cumulus region, while *fuchi, Wnt8b*, and *Clca4a* (Figure 3-13 B3, I3, J3) were expressed in cells surrounding the cumulus migration path. *Twist* (Figure 3-13 K3) exhibited a dotted pattern in the center of the germ disc at stage 5, and was also expressed in the rim cells of the germ disc. *Opa* and *ptc* (Figure 3-13 F3, H3) were exclusively expressed in the cells of the rim of the germ disc.

From the perspective of the embryo, it initiated Type I, II, and III genes before stage 2, then generally shut off Type III genes while opening Type IV genes at stage 3. Subsequently, Type II genes were closed before stage 5. The concept of opening and closing specific sets of genes in a coordinated manner provided valuable insights into how the embryo organizes such a wide range of activities sequentially and in an orderly fashion within a relatively short period of time.

This classification approach also provided a clearer way to analyze the functions of genes that might be involved in specific events. It appeared that all key developmental events involved a combination of spider-specific genes, pathway genes and conserved developmental genes. However, it was not yet possible to describe in detail the coordinated regulation of groups of genes involved in these events, or how combination of different functional genes contributed to a specific developmental process.

2. In situ hybridization of genes in *Ets4* RNAi embryos

2.1 In situ hybridization of genes at stage 4 in *Ets4* RNAi embryos.

Ets4 RNAi embryos were generated through parental RNAi injection (Pechmann et al., 2017). The *Ets4* RNAi embryos appeared morphologically normal until stage 4, with a similar process of germ disc formation and primary thickening invagination. However, instead of initiating cell migration, the cumulus cells dissociated and dispersed in different, thus resulted in a deficiency of dorsal field formation, which led to the establishment of a tube-like embryo. However, most of the embryos recovered from the tube shape and formed a wild type like germ band at stage 9.

I performed in situ hybridization with 57 genes in *Ets4* RNAi embryos at stage 4. Of these, 10 genes were previously published (Pechmann et al., 2017, Wang et al., 2023), while the other 47 genes were newly analyzed in the course of this thesis (Table S3-2).

Figure 3-14 and supplementary Figure S3-15 consisted of genes with specific staining in the primary thickening region of *Ets4* RNAi embryos at stage 4, including *dpp, fascin, fuchi, fkh, fgf8, delta, hh, Mtmr14, g4422, g592, g22667, Creld1, Creld2 g7589, Gsk3b g9959, Gsk3b g25394, Cyclin B, Pik3c3, Hif1a, Idh2, Idh3g g14882, Snip1, Idh1, Asph, Cdk2, Akt, Prkc2*, and *Mapk1 g27557*.

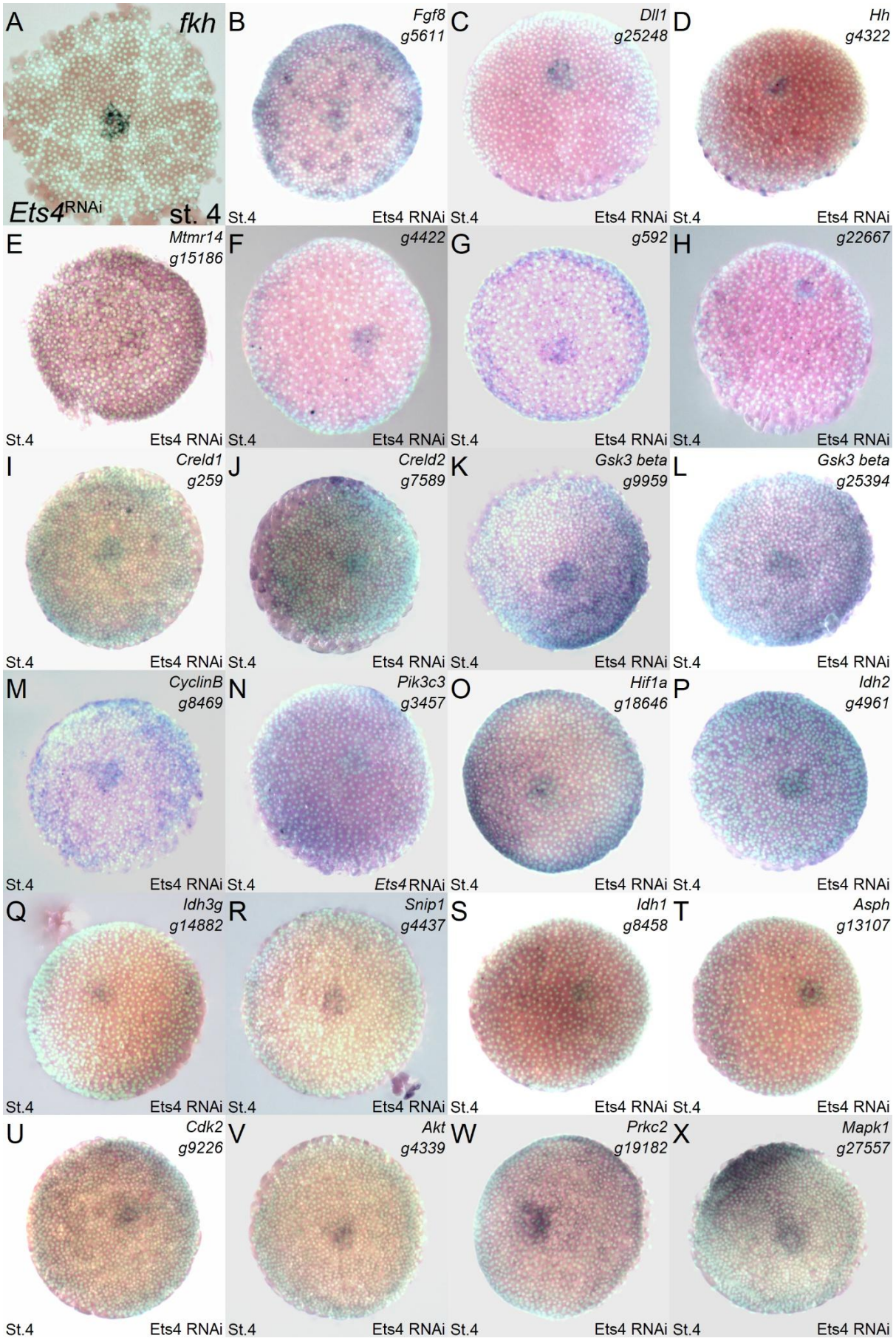
A
fkh
Ets4RNAi
st. 4
B
Fgf8
g5611
St.4
Ets4 RNAi
C
Dll1
g25248
St.4
Ets4 RNAi
D
Hh
g4322
St.4
Ets4 RNAi
E
Mtmr14
g15186
St.4
Ets4 RNAi
F
g4422
St.4
Ets4 RNAi
G
g592
St.4
Ets4 RNAi
H
g22667
St.4
Ets4 RNAi
I
Creld1
g259
St.4
Ets4 RNAi
J
Creld2
g7589
St.4
Ets4 RNAi
K
Gsk3 beta
g9959
St.4
Ets4 RNAi
L
Gsk3 beta
g25394
St.4
Ets4 RNAi
M
CyclinB
g8469
St.4
Ets4 RNAi
N
Pik3c3
g3457
St.4
Ets4 RNAi
O
Hif1a
g18646
St.4
Ets4 RNAi
P
Idh2
g4961
St.4
Ets4 RNAi
Q
Idh3g
g14882
St.4
Ets4 RNAi
R
Snip1
g4437
St.4
Ets4 RNAi
S
Idh1
g8458
St.4
Ets4 RNAi
T
Asph
g13107
St.4
Ets4 RNAi
U
Cdk2
g9226
St.4
Ets4 RNAi
V
Akt
g4339
St.4
Ets4 RNAi
W
Prkc2
g19182
St.4
Ets4 RNAi
X
Mapk1
g27557
St.4
Ets4 RNAi

Figure 3-14. In situ hybridization images of genes with specific staining in the primary thickening at stage 4 in *Ets4* RNAi embryos. Genes shown: *fkh, fgf8, delta, hh, Mtmr14, g4422, g592, g22667, Creld1, Creld2 g7589, Gsk3b g9959, Gsk3b g25394, Cyclin B, Pik3c3, Hif1a, Idh2, Idh3g g14882, Snip1, Idh1, Asph, Cdk2, Akt, Prkc2*, and *Mapk1 g27557*. The staining image of *Fkh* is from Pechmann et al., 2017. Sytox/brightfield overlay.

I currently did not have an in situ hybridization image showing *fuchi* expression in Ets4 RNAi embryos at stage 4. However, images from HCR staining were available in Results Chapter I, supplementary Figure S1-18, which displayed the gene expression in the primary thickening region.

I lacked the expression pattern of most of these genes at stage 2 in Ets4 RNAi embryos. Therefore, it was challenging to determine whether exclusive expression in the primary thickening correlates with the late initiation of gene expression, as observed in WT embryos.

Supplementary Figure S3-16 showed the expression of the other 30 genes, with no or weak expression in the primary thickening region in *Ets4* RNAi embryos at stage 4. The list of these genes included: *Ets4, Hb, twist, Fgfr1, dof, sog, ptc, cv-2, Pla2, Abhd11 g9727, Itpka, L(2)efl, RF_0381, opa, Znf423, g9731, Wnt8b, Anxa1, Lici1, g4424, Clca4a, Numb, Creld2, Egfr, Cyclin A1, Pik3r1 g26883, Ampk, Aktip, Sox2*, and *Mapk1 g27558*.

Within the list, the expression pattern of *Ets4, hb, twist, Fgfr1, dof*, and *ptc* were published previously. However, for *ptc*, a new image was used, taken at a slightly earlier stage than the previously published ones, and the staining result differs from the published expression. Additional experiments would be required to obtain clearer, time-lapse staining for this gene. The expression of *cv-2* and *sog* were reported in different embryos or at different stages in Ets4 RNAi embryos. The rest of the genes were newly identified and analysed (supplementary Figure S3-16).

In the list of genes with or without primary thickening expression in *Ets4* RNAi embryos at stage 4, there were developmental genes, pathway-related genes, and spider-specific genes in both categories. There were no obvious differences in the types of genes that made up the two lists.

2.2 In situ hybridization staining of genes at stage 5 in *Ets4* RNAi embryos.

Stage 5 of *Ets4* RNAi embryos differed morphologically from stage 5 of WT embryos for the lack of cumulus migration. The embryonic region remained in the shape of a germ disc, which lasted for approximately 10 hours, which was roughly the same duration as the cumulus migration process in WT embryos. Later, the central region of the germ disc grew upwards, until the embryonic region transformed from a tube-like structure.

Several criteria were used to assess an *Ets4* RNAi embryo at stage 5: (1) the embryo remained in a germ disc shape, with no central growth; (2) there was a higher overall nucleus density; and (3) the central region was not the only area with multiple cells layers.

This helped to distinguish *Ets4* RNAi embryos at stage 5 from those at stages 4 and 6. However, stage 5 of *Ets4* RNAi embryos lasted for about 10 hours. During such a prolonged period, gene expression may vary, and it was difficult to differentiate between the early and late stages of stage 5 based on morphology alone. As a result, the expression of genes at this stage might not capture the fine details.

Figure 3-15 showed in situ hybridization image at stage 5 in *Ets4* RNAi embryos for 15 genes, including *Ets4, Numb, Egfr, Cyclin A1, Hif1a, Idh2, Idh3g g14882, Snip1, Idh1, Aktip, Asph, Sog, Sox2, Cdk2*, and *Akt*. The list included many pathway-related genes as well as some development-related genes.

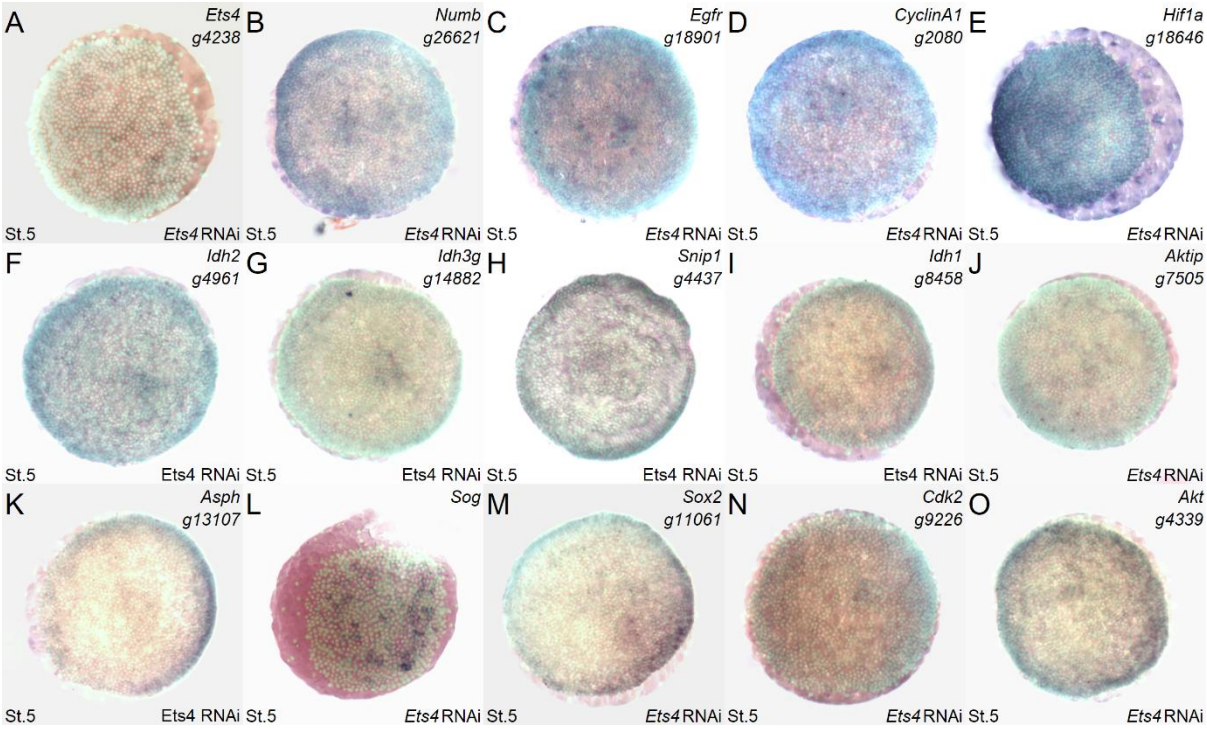

Figure 3-15. In situ hybridization images of genes at stage 5 in *Ets4* RNAi embryos. Genes shown: *Ets4, Numb, Egfr, Cyclin A1, Hif1a, Idh2, Idh3g g14882, Snip, Idh1, Aktip, Asph, Sog, Sox2, Cdk2*, and *Akt*. Sytox/brightfield overlay.

Most of the stained images in Figure 3-15 exhibited radial symmetry, reflecting the morphology of the embryo. *Ets4* showed either no expression or expression in only a few distinct cells. *Numb, Egfr, Cyclin A1, Hif, Idh2, Idh1, Aktip, Cdk2*, and *Akt* (Figure 3-15 B, C, D, E, F, I, J, N, O) displayed specific staining in the central region and rim of the germ disc. *Idh3g g14882* (Figure 3-15 J) was expressed in the central region but not in the rim region. *Sog* expression was localized in discrete areas of an inner cycle, surrounding the central part.

A combination of gene expression at stage 4 and 5 in *Ets4* RNAi embryos was provided in supplementary Figure S3-17.

The expression of *engrail, sog*, and *twist* in *Ets4* RNAi embryos at the tube stage was published in Pechmann et al., 2017, and the results were repeated and confirmed. However, no new expression pattern for other genes were obtained. Additionally, there were no expression images available for later stages, when most of the embryos recovered from the tube shape and appeared similar to wild-type morphology.

Due to the lack of expression pattern for most genes at stage 2 and tube stage, it was difficult to combine gene expression data from different stages and summarized the expression patterns in *Ets4* RNAi embryos as in WT embryos.

3. Comparison of gene expression in WT and *Ets4* RNAi embryos

3.1 Comparison of gene expression in primary thickening region of WT and *Ets4* RNAi embryos at stage 4

Section 1.1 of this chapter presented in situ hybridization images of 113 genes in WT embryos at stage 4, and section 2.1 included 57 genes in *Ets4* RNAi embryos at stage 4. In combination, there were 57 genes showing expression pattern from both types of embryos. By comparing the staining of genes in the primary thickening region of WT and *Ets4* RNAi embryos, these genes could be categorized into one of the four sub-groups: 23 genes in D1, 7 in D2, 16 in N1, and 11 in N2 (Table S3-3).

D1 (Differential expression gene group 1): Genes that showed specific expression in the primary thickening region at stage 4 in WT embryos, but not in *Ets4* RNAi embryos. Alternatively, gene expression in *Ets4* RNAi embryos was significantly weaker compared to WT embryos (Figure 3-16, Figure 3-17).

D2: Genes that showed specific expression in the primary thickening region at stage 4 in *Ets4* RNAi embryos, but not in WT embryos. Alternatively, gene expression in WT embryos was significantly weaker compared to *Ets4* RNAi embryos (Figure 3-18).

N1 (Non-differential expression group 1): Genes that were specifically expressed in the primary thickening at stage 4 in both WT and *Ets4* RNAi embryos, with similar expression levels (supplementary Figure S3-18).

N2: No specific expression in the primary thickening region was observed at stage 4 in either WT or *Ets4* RNAi embryos (supplementary Figure S3-19).

Figure 3-16 and Figure 3-17 showed the expression of genes from group D1, in the germ disc region of WT and *Ets4* RNAi embryos. There were a total of 23 genes. Of these, 19 genes in Figure 3-16 show specific expression in the primary thickening region of WT embryos, but not in *Ets4* RNAi embryos. The remaining 4 genes in Figure 3-17 showed expression in both embryos, but the expression was much stronger in WT embryos than in *Ets4* RNAi embryos.

Figure 3-16 showed comparative staining in WT and *Ets4* RNAi embryos for the genes *Ets4, hb, Fgfr1, dof, twist, cv-2, Pla2, Abhd11, Itpka, L(2)efl, Rf_0381, opa, Znf423, g9731, ptc, Wnt8b, Anxa1, g4424* and *Clca4a*. The expression of *Ets4, hb, Fgfr1, dof* and *twist* were published previously, while the rest of the genes were newly analysed during this study.

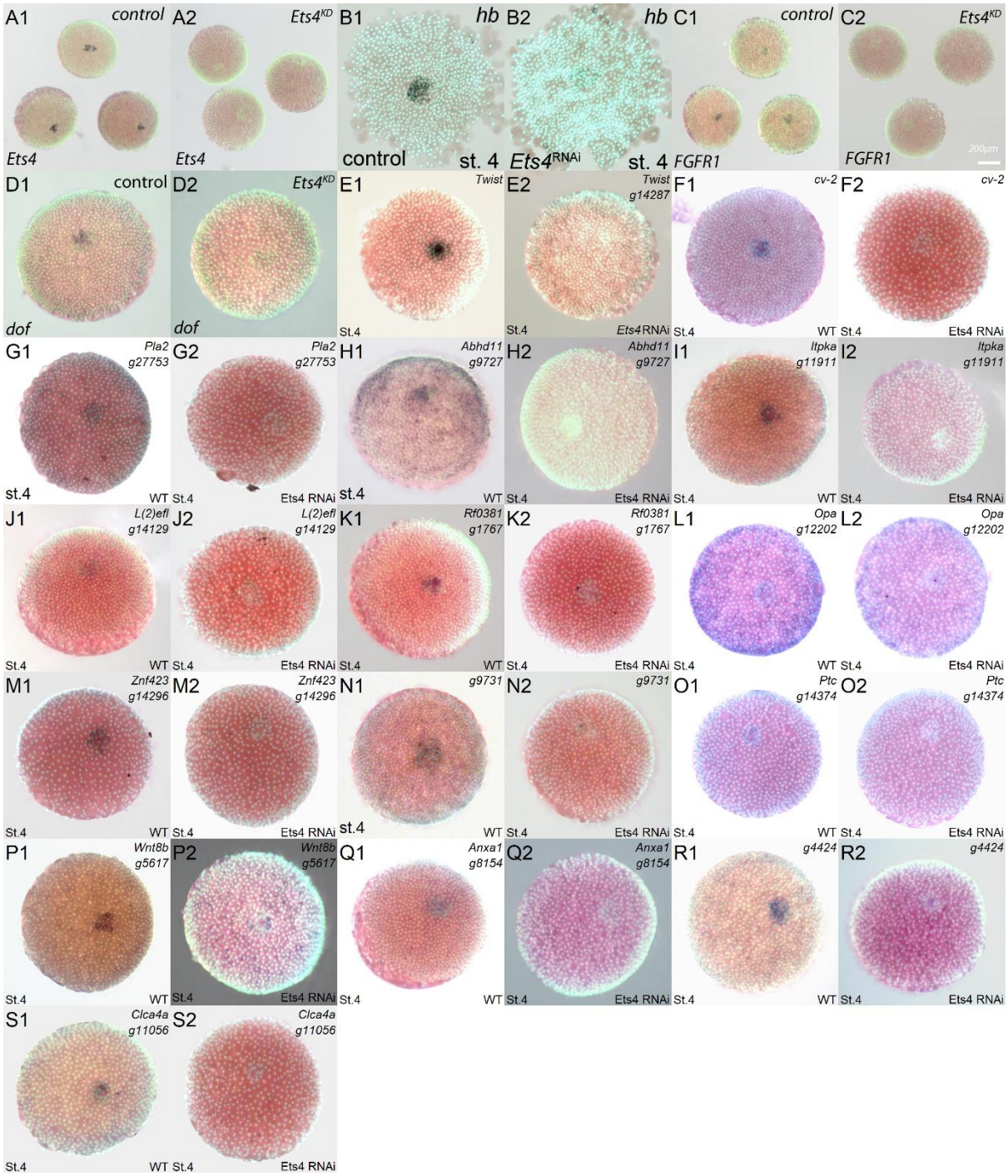

Figure 3-16. Comparison of in situ hybridization images of D1 genes in germ disc at stage 4 of WT and *Ets4* RNAi embryos (a). List of genes: *Ets4, hb, Fgfr1, dof, twist, cv-2, Pla2, Abhd11, Itpka, L(2)efl, Rf_0381, opa, Znf423, g9731, ptc, Wnt8b, Anxa1, g4424*, and *Clca4a*. The expression image of *hb* were from Pechmann et al., 2017. And the in situ hybridization image of *Ets4, Fgfr1, dof* were taken from Wang et al., 2023. Sytox/brightfield overlay.

Figure 3-17 compared the in-situ hybridization images in the germ disc at stage 4 of WT and *Ets4* RNAi embryos for the genes *fascin, fgf8, Mtmr14*, and *g22667*. There was specific staining in the primary thickening region of both embryos, but the expression in WT embryos was much stronger than in *Ets4* RNAi embryos.

It was not common practice to use staining image from in situ hybridization experiments in a quantitative manner, as many factors could affect the results. The conclusions drawn from comparisons in Figure 3-17 were based on the size of the staining area in the primary thickening region, which appeared much smaller in *Ets4* RNAi embryos than in WT embryos. Therefore, the expression level in the primary thickening region of *Ets4* RNAi embryos was considered weaker than in WT embryos.

The expression pattern of *fgf8* at stage 4 in *Ets4* RNAi embryos closely resembled the expression pattern observed at stage 5 in WT embryos. However, the expression of other genes at stage 4 in *Ets4* RNAi embryos (Figure 3-16, Figure 3-17) did not exhibit a similar pattern. Therefore, this similarity was not a characteristic of *Ets4* RNAi embryos in general, but may represent a specific regulatory pattern for *fgf8*.

These 23 genes in group D1 included general developmental genes and spider-specific genes. It seemed that these genes were highly likely to be influenced, either directly or indirectly, by the *Ets4* gene, as indicated by the expression image. However, the precise mechanisms and timing of this influence remained unclear and require further investigation.

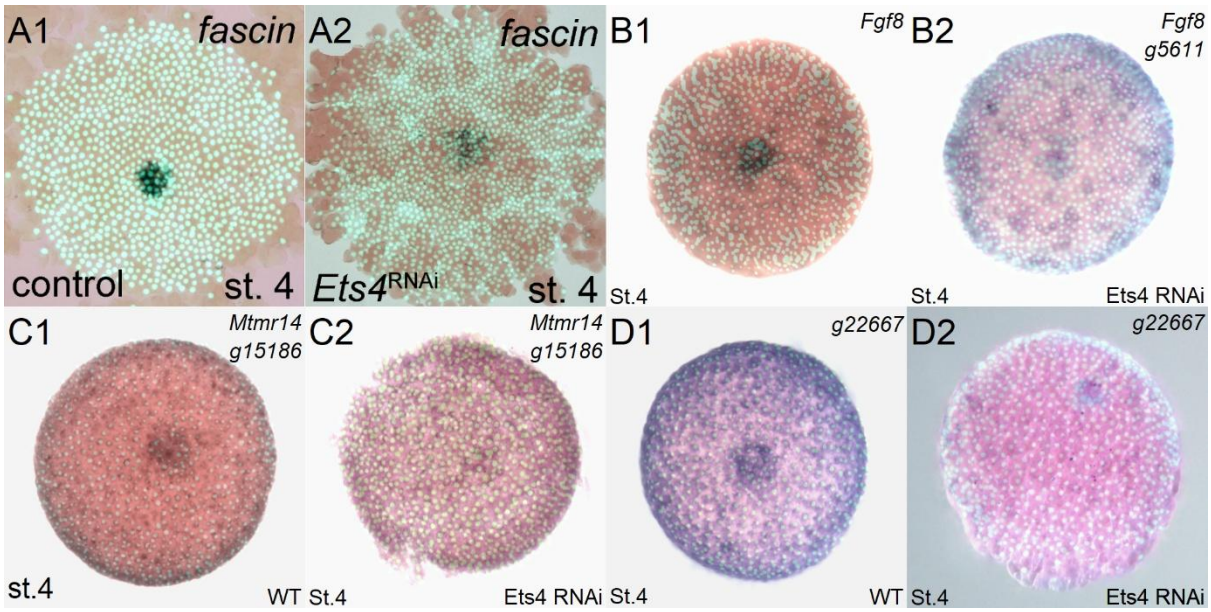

Figure 3-17. Comparison of in situ hybridization images of D1 genes in germ disc at stage 4 of WT and *Ets4* RNAi embryos (b). List of genes: *fascin, fgf8, Mtmr14*, and *g22667*. The expression image of *fascin* were from Pechmann et al., 2017. Sytox/brightfield overlay.

Figure 3-18 showed in situ hybridization images of D2 genes in the germ disc at stage 4 in WT and *Ets4* RNAi embryos. Genes in this group include *hh, delta, Idh2, Hif1a, Asph, Cdk2, and Mapk1 g27557. Hh, delta*, and *Idh2* (A, B, C) show specific staining in the primary thickening region of *Ets4* RNAi embryos but did not show expression in WT embryos. On the other hand, *Hif1a, Asph, Cdk2*, and *Mapk1 g27557* (D, E, F, G) displayed weaker expression in WT embryos.

From the images, it seemed that these genes were inhibited by the *Ets4* gene or *Ets4*-related genes in WT embryos. *Hh, delta*, and *Asph* were involved in developmental processes, while the other genes primarily functioned in general pathways.

Hh and *delta* (Figure 3-18 A, B) also expressed in the rim of the germ disc and in extraembryonic cells in both WT and *Ets4* RNAi embryos. There might be differences in the expression of genes between the two types of embryos, but I will not discuss this here any further.

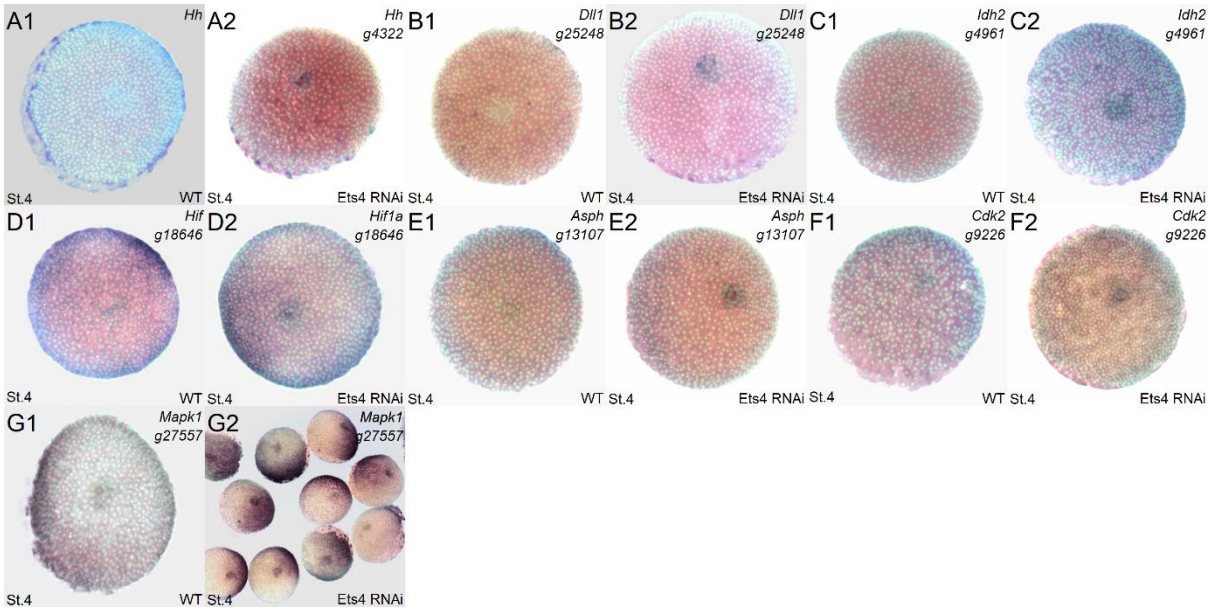

Figure 3-18 Comparison of in situ hybridization images of D2 genes in germ disc at stage 4 of WT and *Ets4* RNAi embryos. List of genes: *hh, Delta, Idh2, Hif1a, Asph, Cdk2*, and *Mapk1 g27557*.Sytox/brightfield overlay.

Genes in group N1 showed similar expression in the primary thickening region at stage 4 of both WT and *Ets4* RNAi embryos. These genes included *fkh, dpp, fuchi, g4422, g592, Creld1, Creld2 g7589, Gsk3b g9959, Gsk3b g25394, Cyclin B, Pik3c3, Idh3g g14882, Snip1, Idh1, Akt*, and *Prkc2*. They were primarily associated with general cellular pathways, but also included some spider-specific genes and a few developmental genes, such as *dpp*. The expression of N1 genes in both WT and *Ets4* RNAi embryos were provided in Fig.S3-18, based on in situ hybridization images. The image for *fuchi* was from Result Chapter I, supplementary Figure S1-19, of HCR staining.

Genes in group N2 showed no expression in the primary thickening region at stage 4 of both WT and *Ets4* RNAi embryos. However, these genes exhibited specific staining at other developmental stages in either WT or *Ets4* RNAi embryos, indicating that the probe is functional. These genes included *sog, Lici1, Numb, Creld2 g7590, Egfr, Cyclin A1, Pik3r1 g26883, Ampk, Aktip, Sox2*, and *Mapk1 g27558*, which were mainly associated with general cellular pathways. A few developmental genes were also included (Fig. S3-19).

Genes in groups N1 and N2 might be independent of *Ets4* and *Ets4*-related genes. It was also possible that these genes were involved in complex regulatory processes with *Ets4*, but the net result of gene expression remained unchanged due to multiple regulatory pathways. Until more evidence supports the latter case, I will initially treat these genes as unrelated to *Ets4* genes.

3.2 Comparison of gene expression in WT and *Ets4* RNAi embryos at stage 5

Stage 5 germ disc in WT and *Ets4* RNAi embryos resembled each other in terms of the morphology of the germ disc. However, a key distinction was that cumulus migration occurred in WT embryos but not in *Ets4* RNAi embryos. Therefore, in WT embryos, stage 5 represented an intermediate stage transitioning from radial symmetry to bilateral symmetry, while in *Ets4* RNAi embryos, the germ disc maintained radial symmetry.

Figure 3-19 presented a comparison of gene expression at stage 5 between WT and *Ets4* RNAi embryos. This included in situ hybridization staining of the genes *fascin, Ets4, Numb, Egfr, Cyclin A1,*

Hif1a, Idh2, Idh3g g14882, Snip1, Idh1, Aktip, Asph, Sox2, Cdk2, and *Akt*, as well as antibody staining for pMad, which was downstream of *dpp*.

Out of the 16 genes, 10 exhibited specific staining in the cumulus-related region in WT embryos (pMad*, fascin, Ets4, Hif1a, Idh2, Idh3g g14882, Snip1, Asph, Cdk2*, and *Akt*; Figure 3-19 A1, B1, C1, G1, H1, I1, J1, M1, O1, P1). In *Ets4* RNAi embryos, 4 of these 10 genes (pMad*, Ets4, Snip1*, and *Asph*; Figure 3-19 A2, C2, J2, M2) showed no expression in the germ disc, while the remaining 6 genes showed specific expression in the center of the germ disc. Interestingly, the first 4 genes were more related to development, while the latter 6 genes were associated with general pathways of cell proliferation and cell metabolism. It was still unclear whether this pattern was a common feature for all genes expressed in the cumulus region at stage 5 in WT embryos.

The expression in the central region of the germ disc was generally similar between WT and *Ets4* RNAi embryos for all these genes. However, *fascin, Cyclin A1, Hif1a, Snip* and *Asph* (Figure 3-19, B, F, G, J, M) were exceptions. All these genes showed expression in the rim region in both WT and *Ets4* RNAi embryos, and the expression patterns appeared similar in both embryo types, with exceptions of pMad*, fascin*, and *Ets4* (Figure 3-19, A, B, C) expression.

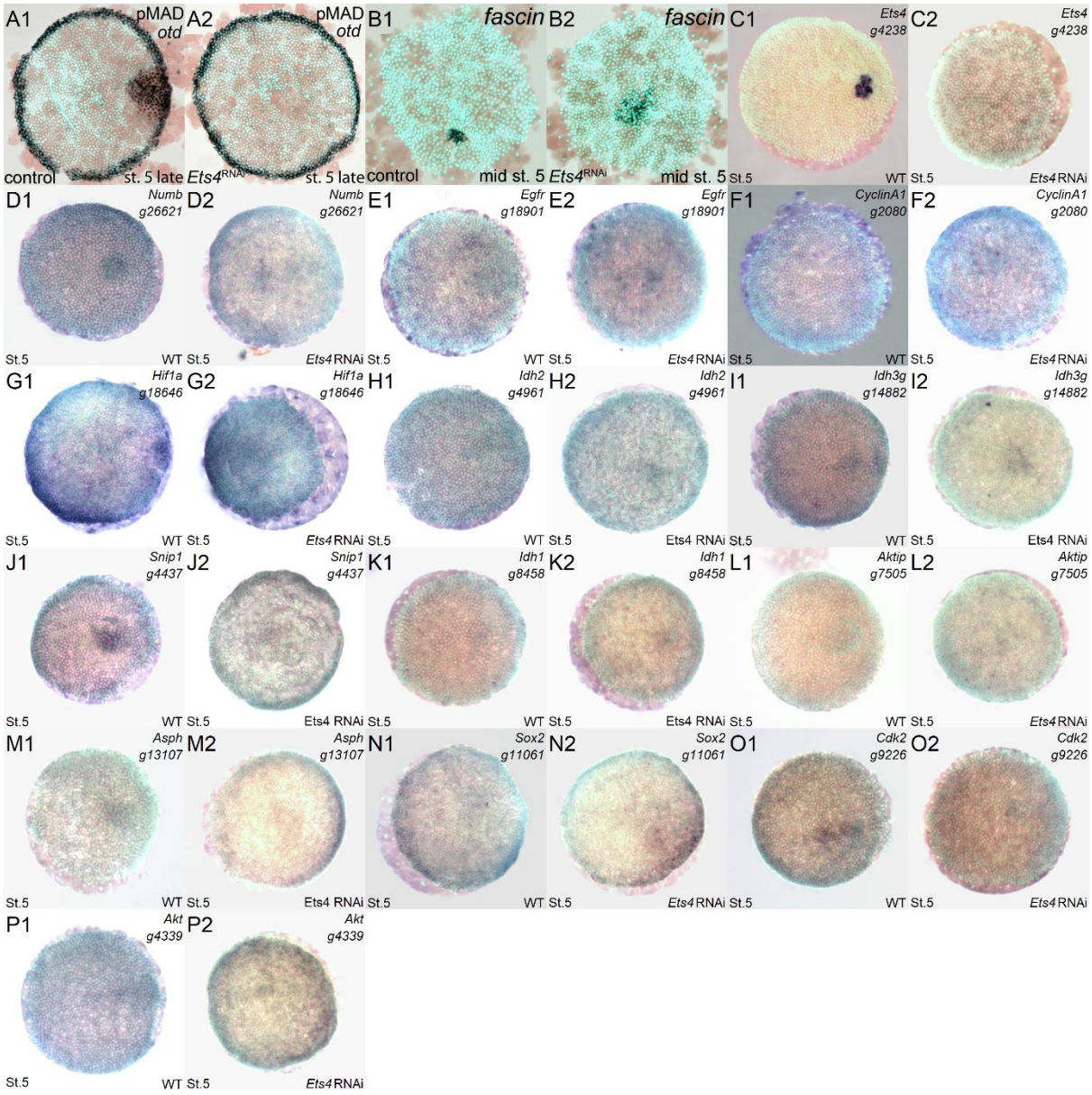

Figure 3-19. Comparison of the expression pattern of WT and *Ets4* RNAi embryos at stage 5. Genes shown: pMad (antibody), *fascin, Ets4, Numb, Egfr, Cyclin A1, Hif1a, Idh2, Idh3g g14882, Snip1, Idh1, Aktip, Asph, Sox2, Cdk2, Akt*. The antibody staining of pMad was from Pechmann et al., 2017. Sytox/brightfield overlay.

Supplementary Figure S3-20 showed a combined image of the expression pattern of the genes at stages 4 and 5, in both WT and *Ets4* RNAi embryos.

3.3 Gene expression in *Ets4* RNAi embryo of Type I, II, III, IV genes in WT embryos.

In section 1.3, 63 genes were classified into 4 types based on their expression from stage 2 to 5 in WT embryos. Of these 63 genes, 46 were identified with expression pattern in *Ets4* RNAi embryos. A series of combination image was prepared with expression of genes at stage 2, 4, and 5 in WT embryos and stage 4 of Ets4 RNAi embryos for comparison, in the order of Type I, II, III, and IV, respectively (Figure 3-20, Figure 3-21, Figure 3-22, Figure 3-23).

Figure 3-20 showed a combination of in situ hybridization images for Type I genes at stages 2, 4, and 5 of WT embryos, and stage 4 of *Ets4* RNAi embryos. The images included 12 of the 17 genes mentioned in section 1.3 (Figures 3-7, 3-8).

Type I genes were selected as genes with ubiquitous or regional expression at stage 2, primary thickening expression at stage 4, and cumulus-related expression at stage 5 in WT embryos. In stage 4 *Ets4* RNAi embryos, all the genes in these combined image showed specific expression in the primary thickening region.

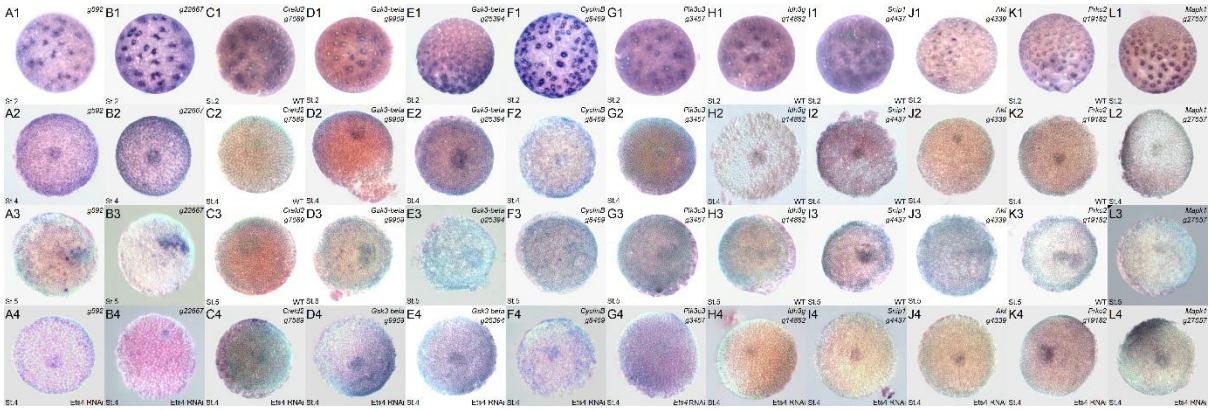

Figure 3-20. Combination of in situ hybridization images of Type I genes at stage 2, 4, 5 of WT embryos, and at stage 4 of *Ets4* RNAi embryos. The list of genes include: *g592, g22667, Creld2 g7589, Gsk3b g9959, Gsk3b g25394, Cyclin B, Pik3c3, Idh3g g14882, Snip1, Akt, Prkc2*, and *Mapk1 g27557*. Sytox/brightfield overlay.

Figure 3-21 showed combined images of Type II genes at stages 2, 4, and 5 in WT embryos, and at stage 4 in *Ets4* RNAi embryos. The figure included 9 of the 16 genes mentioned in section 1.3 (Figure 3-9, Figure 3-10).

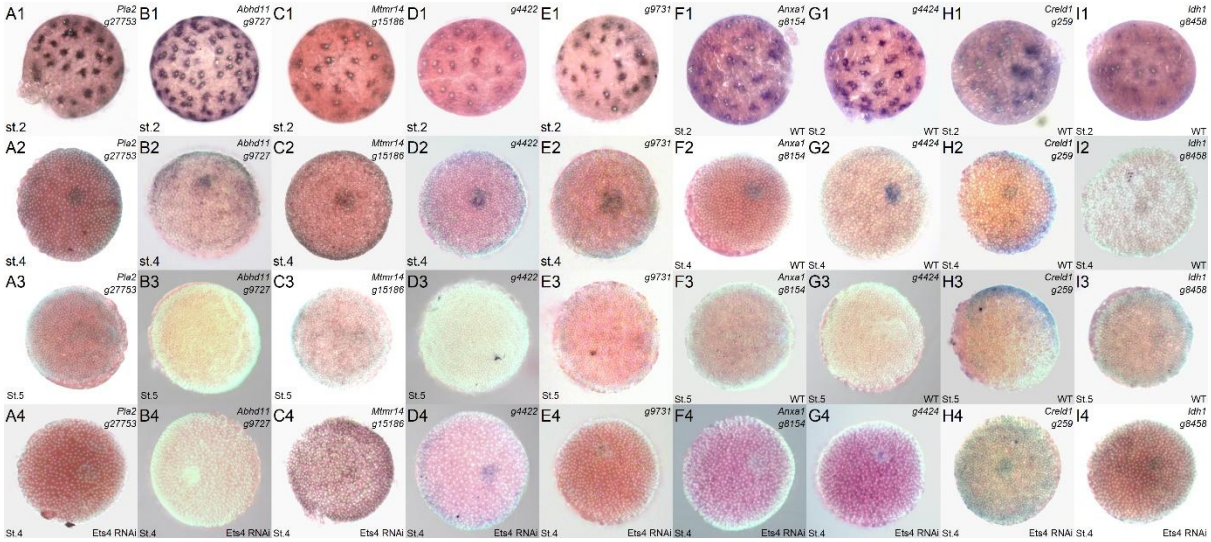

Figure 3-21. Combination of in situ hybridization images of Type II genes at stage 2, 4, 5 of WT embryos, and at stage 4 of *Ets4* RNAi embryos. List of genes including: *Pla2, Abhd11 g9727, Mtmr14, g4422, g9731, Anxa1, g4424, Creld1*, and *Idh1*. Sytox/brightfield overlay.

Type II genes were classified as genes that showed expression at stage 2 and had primary thickening expression at stage 4, but did not exhibited expression or cumulus-related expression at stage 5 in WT embryos. In *Ets4* RNAi embryos, the staining patterns for these genes varied. Of the genes in this group, 5 (*Pla2, Abhd11 g9727, g9731, Anxa1, g4424*; Figure 3-21, A, B, E, F, G) showed no expression in the primary thickening region, while 4 genes (*Mtmr14, g4422, Creld1, Idh1*; C, D, H, I) displayed specific staining in the primary thickening region. This classification did not seem to coordinate with the differential expression of Type II genes at stage 9.

Figure 3-22 showed the expression of Type III genes at stage 2, 4, and 5 in WT embryos, and at stage 4 in *Ets4* RNAi embryos. It included 14 of the 19 genes mentioned in section 1.3 (Figures 3-11, 3-12).

Type III genes were selected as genes with expression at stage 2, but no expression or no primary thickening-related expression at stage 4 of WT embryos. At stage 5, the expression of these genes was variable.

Of the 14 Type III genes in Figure 3-22, 9 genes had no specific primary thickening expression in *Ets4* RNAi embryos, including *Numb, Creld2 g7590, Egfr, Cyclin A1, Pik3r1 g26883, Ampk, Aktip, Sox2, Mapk1 g27558* (Figure 3-22, C, D, E, F, G, H, K, M, N). Another 5 genes showed specific staining in the primary region at stage 4 in *Ets4* RNAi embryos, including *delta, hh, Hif, Idh2*, and *Asph* (Figure 3-22, A, B, I, J, L). This subdivision did not reflect the differences in the expression of Type III genes at stage 5.

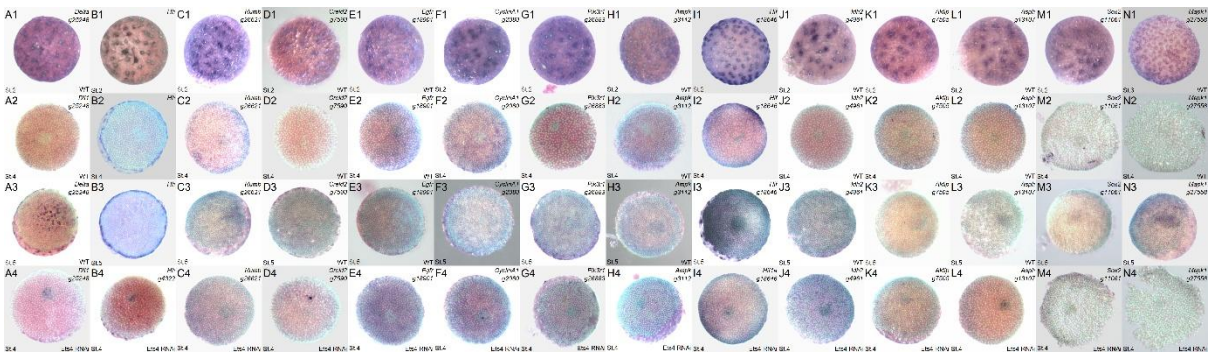

Figure 3-22. Combination of in situ hybridization images of Type III genes at stage 2, 4, 5 of WT embryos, and at stage 4 of *Ets4* RNAi embryos. List of genes including: *delta, hh, Numb, Creld2 g7590, Egfr, Cyclin A1, Pik3r1 g26883, Ampk, Hif, Idh2, Aktip, Asph, Sox2*, and *Mapk1 g27558*. Sytox/brightfield overlay.

Figure 3-23 presented Type IV genes and their expression at stage 2, 4, and 5 in WT embryos, and at stage 4 in *Ets4* RNAi embryos. All of the 12 genes mentioned in section 1.3 were included in the figure. *Fuchi* was shown a HCR staining instead of regular colorimetric in situ hybridization staining.

Genes in Type IV had no expression at stage 2 but showed specific staining in the primary thickening region at stage 4 in WT embryos. Most of these genes also exhibited cumulus-related expression at stage 5. 11 of the 12 genes in the list showed no expression in *Ets4* RNAi embryos. However, *fuchi* was expressed in approximately the same number of primary thickening cells at stage 4 in *Ets4* RNAi embryos as in WT (Result Chapter I, Figure 1-6).

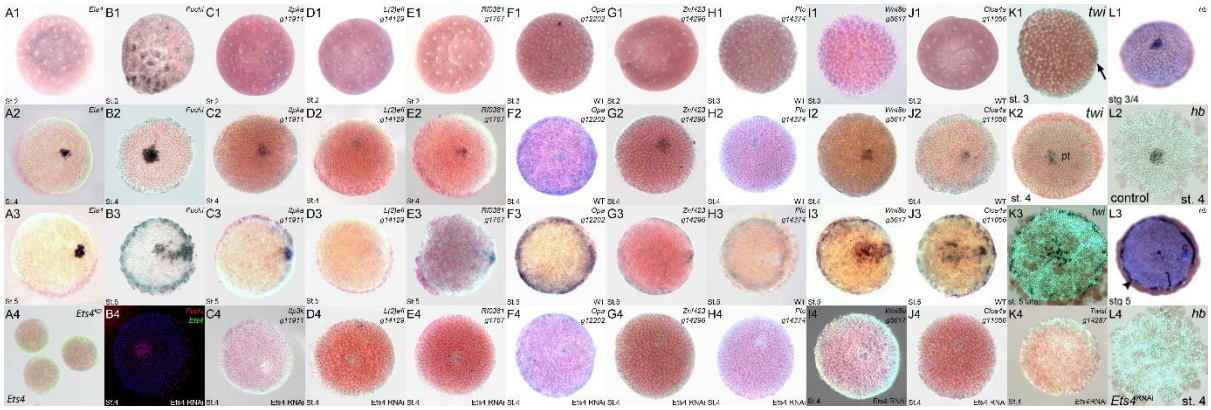

Figure 3-23. Combination of in situ hybridization images and HCR image, of Type IV genes at stage 2, 4, 5 of WT embryos, and at stage 4 of *Ets4* RNAi embryos. Genes shown: *Ets4, Itpka, L(2)efl, RF_0381, opa, Znf423, ptc, Wnt8b, Clca4a, twist*, and *fuchi*. Sytox/brightfield overlay.

To summarize, Type I genes uniformly exhibited similar primary thickening expressions at stage 4 in both WT and *Ets4* RNAi embryos. In contrast, most Type IV genes displayed distinctly different primary thickening expressions between WT and *Ets4* RNAi embryos. For Type II and Type III genes, the results were mixed, with roughly half showing similar primary thickening expressions and half differing. This information offered insights into the functional role of the *Ets4* gene within the broader regulatory network of animal development.

Supplementary Table S3-4 was listed to link gene types (I, II, III, IV) and developmental events in both WT and *Ets4* RNAi embryos, suggesting the relationships between different types of genes, and their potential developmental outcomes.

Additionally, the in situ hybridization experiment of *Hif* at stages 3 and 4 in WT embryos revealed uneven expression patterns in certain embryos, and similar cases were observed in the *Mapk1 g27557* (supplementary Figure S3-21). Both genes showed expression in a seemingly more asymmetric manner in *Ets4* RNAi embryos. It was unclear whether the observed asymmetry is randomly generated or represents an early indication of future asymmetric events. Furthermore, the expression patterns was not yet fully confirmed.

4. Comparison the results from in situ hybridization experiments and RNAseq analysis.

4.1 Chi-Square (X^2) Tests of RNA-Seq Reads and In Situ Hybridization Staining Results

Previous sections provided information regarding whether certain genes are expressed in the primary thickening region at stage 4 in WT and *Ets4* RNAi embryos, and if there were differences in gene expression between the two embryos. Similar conclusions could also be drawn from Result Chapter II, which presents RNA-seq reads from primary thickening cells of three WT replicates and three *Ets4* RNAi replicates.

To address whether the conclusion from the two methods, RNAseq and in situ hybridization, agreed with each other, the Chi-square (X^2) test was used. This statistical test was typically employed to evaluate the accuracy of predictions by comparing predicted values with actual values. The website http://www.mdtserver.com/rfiles/4ft-chisq.htm was used to calculate the X^2 with Yates' continuity correction (Table S3-2).

Table 3-1 X^2 calculation of correlation in expected images and RNAseq reads

	WT	Ets4 RNAi	list B	list F
NN	23	25	27	21
NY	15	5	0	6
YN	11	12	21	14
YY	64	15	9	16
Total	113	57	57	57
X2	23.083	7.8056	7.4948	4.5651
Df	1	1	1	1
p value	1.55E-06	0.005208	0.006188	0.03263

As a result, comparison of the two methods, with the results from both in situ hybridization and RNAseq readings for determining gene expression in the primary thickening region at stage 4 in WT embryos were highly consistent. This suggested that the results from the two methods reliably supported each other.

Following a similar approach, I compared the results from in situ hybridization experiments and RNAseq reads in *Ets4* RNAi embryos, and selected differential gene list B and F.

The results from in situ hybridization and RNAseq reads regarding whether a gene was expressed in the primary thickening region at stage 4 in *Ets4* RNAi embryos still showed strong agreement. However, the correlation was not as robust as in WT embryos, possibly due to greater variability between the *Ets4* RNAi embryos compared to the WT embryos.

And in general, list B and list F provided reliable criteria for determining whether a gene was differentially expressed in the primary thickening region of WT and *Ets4* RNAi embryos at stage 4, based on the gene expression results from in situ hybridization experiments. Moreover, when comparing the two, list B appeared to be more reliable than list F.

4.2 Expression of genes of two pathways, from in situ hybridization experiment and RNAseq

For more vivid examples of the agreement between the two methods, I combined the RNAseq reads of certain genes with their in situ hybridization staining images. As mentioned in Result Chapter II, the PI3K-AKT signaling pathway and the Hh signaling pathway were two key pathways discussed, which were likely involved in regulating cell migration and cell differentiation, respectively.

Therefore, I selected the genes that were relevant to these two pathways and were also included in the in situ gene list (the 113-gene list).

Supplementary Figure S3-22 showed the PI3K-AKT pathway. A total of 22 genes from the in situ gene list, were highlighted in red, grey, or green, representing the Fold2Change values of each gene from RNAseq data. Heatmap images were also generated for these genes and divided into two categories: genes located near the cell membranes and the remaining genes. The in situ hybridization images of 16 genes in both WT and *Ets4* RNAi embryos at stage 4 were presented, and of the rest 6 genes in only WT embryos. The expression images were roughly arranged in order of the genes' position within the pathway, from the extracellular region to the inner cellular region.

12 of the genes showed consistent expression in both WT and *Ets4* RNAi embryos, matching the color markings in the Pathview images (*fgf8, Fgfr1, Egfr, dof, Pik3c3, Akt, Gsk3b g9959, Gsk3b g25394, Mapk1 g27557, Mapk1 g27558, Cdk2, fkh*). However, 4 of the genes exhibited discrepancies between the actual expression pattern and the color marking in the Pathview image (*Pik3r1 g26883, Cyclin A1, Cyclin B, Ampk*). Despite these exceptions, I could conclude that, for the majority of genes involved in this pathway, the Pathview image based on RNAseq reads closely corresponded to the actual staining patterns observed in the embryos.

Supplementary Figure S3-23 showed a combination of the pathview image, heatmap image, and expression images of relevant genes from the Hh signaling pathway. The genes included *hh, ptc, opa (Zic4, GliA), Gsk3b g9959, Gsk3b g25394*, and *dpp (Bmp4)*, and were analyzed in both WT and *Ets4* RNAi embryos. More images for the expression of *hh* and *delta* were provided in supplementary Figure S3-9.

For the six genes of the Hh signaling pathway, the results from in situ hybridization were consistent with the coloring of the genes in the pathview image and with the gene expression levels shown in the heatmap image.

In conclusion, most genes in the two pathways exhibited similar expression levels in both RNAseq reads and in situ hybridization images. This section reaffirmeed the conclusions of the X^2 test from Section 4.1, presenting the results in a more straightforward manner. Based on the agreement between the two methods, I expected to extend the conclusion to a larger scale. For example, genes with high RNA-seq reads were more likely to show expression when tested by in situ hybridization, assuming a certain level of reliability.

6. Summary

The expression pattern of 113 genes at stage 4 of WT embryos were provided, encompassing data from both previously published studies and new experiments. Additionally, images of 63 genes at stages 2, 4, and 5 in WT embryos were presented and categorized into four distinct expression patterns (I, II, III, and IV). Uncharacterized or spider-specific genes were present in all four types of gene expression patterns.

Additionally, expression images of 57 genes at stage 4 of *Ets4* RNAi embryos were presented, derived from both previous publications and new experiments. These images were compared with expression pattern of the corresponding genes in WT embryos at the same developmental stage, allowing for the identification of genes exhibiting differential or similar expression patterns in the primary thickening region between the two embryo types.

It was noteworthy that genes classified as expression types I and IV exhibited a relatively uniform, or nearly uniform, response in the *Ets4* knockout condition. This observation provided new insights into

the role of *Ets4*, as well as a broader understanding of gene regulatory mechanisms during animal development.

A comparison was made on the gene expression results in the primary thickening region at stage 4, through in situ hybridization staining and RNAseq data analysis. Overall, the consistency between the two experimental approaches supported the reliability of both methods.

6 Result Chapter IV: RNA interference experiments to investigate the function of genes in the primary thickening region

RNA interference (RNAi) was a widely used method for studying gene function. This technique involved knocking down a target gene and observing the effects of its loss to infer its original function. RNAi was used in Parasteatoda research for nearly two decades, with a well-established protocol and numerous publications based on this method, significantly advancing our understanding of *Parasteatoda* development.

I used the pRNAi (parental RNAi) method to investigate the function of approximately 30 genes that are involved in the early steps of *P. tepidariorum* development. All of these genes were expressed in the primary thickening region at stage 4 in WT embryos, and some were regulated by the Ets4. Through that, I hope to enhance our understanding of the gene regulatory network in the region.

The results of seven RNAi experiments were described in this chapter; these were considered more reliable or were supported by more videos and images. The targeting genes including *RF_0381*, *g4422*, *cv-2 (crossveinless 2, Bmper)*, *twi*, *Abhd11 g9727*, *Itpka*, and *Znf423*. The order of the subsections was determined by the stage at which the first phenotype appeared in each RNAi embryo during development.

Each subsection consisted of three parts: (1) the expression of the target gene in WT and *Ets4* RNAi embryos; (2) records and statistical analysis of RNAi experiments, an assessment of experimental reliability, and results presented in the form of videos and images; (3) the inferred function of the target gene in WT embryo development based on the collected data. The subsections in this part were relatively independent. Comparisons and summaries of different RNAi results will be presented in the section 8.

1. *RF_0381* RNAi

1.1 Expression of *RF_0381* gene in WT and *Ets4* RNAi embryos.

The spider transcript g1767 was annotated as a 'putative ankyrin repeat protein RF_0381' in NCBI, with no homologous gene identified in mouse or fly. However, homologous genes of *RF_0381* were present in the African social velvet spider, wasp spider, and several other invertebrates. In plants, such as beans, homologous genes were involved in the metabolism of guanosine tetraphosphate, protein localization in chloroplasts, and the regulation of the JNK cascade (OrthoDB website).

In common house spider, *RF_0381* was not detected at stage 2 in WT embryos based on *in situ* hybridization images (Result Chapter III, Figure 3-13, E1). The gene's transcripts were first observed at stages 3–4, exclusively in the primary thickening region, and later in migrating cumulus cells at stage 5 (Figure 3-13, E2, E3). In Chapter III, this gene was classified as a Type IV gene.

In *Ets4* RNAi embryos, no expression of *RF_0381* transcripts were detected in the primary thickening region at stage 4, suggesting that the *RF_0381* gene may act downstream of *Ets4* (Result Chapter III, Figure 3-23, E4).

1.2 *RF_0381* RNAi experiment and characteristics of *RF_0381* RNAi embryos.

Only one batch of *RF_0381* RNAi experiments was conducted, and both spiders injected with *RF_0381* dsRNA lived for over a year, which the survival time of most WT and RNAi spider was around six months after reaching adulthood or the first injection. However, it was still unknown whether the prolonged survival of the *RF_0381* RNAi spider was a result of the *RF_0381* dsRNA injection.

The RNAi injection yielded seven cocoons from these spiders. Based on initial observations, only a small portion of RNAi embryos resembled WT-like phenotype, while the majority arrested at stage 2. A third group of RNAi embryos halted development at the germ disc stage (supplementary Figure S4-1).

From supplementary Figure S4-1, it could be seen that in the second and third cocoons, more than half of *RF_0381* RNAi embryos arrested development before stage 2 (in red colour). The proportion of RNAi embryos that halted development at the germ disc stage was much smaller, ranging from around 10–30% across different cocoons (in yellow). The ratios of the different types of embryos were comparable between the two spiders.

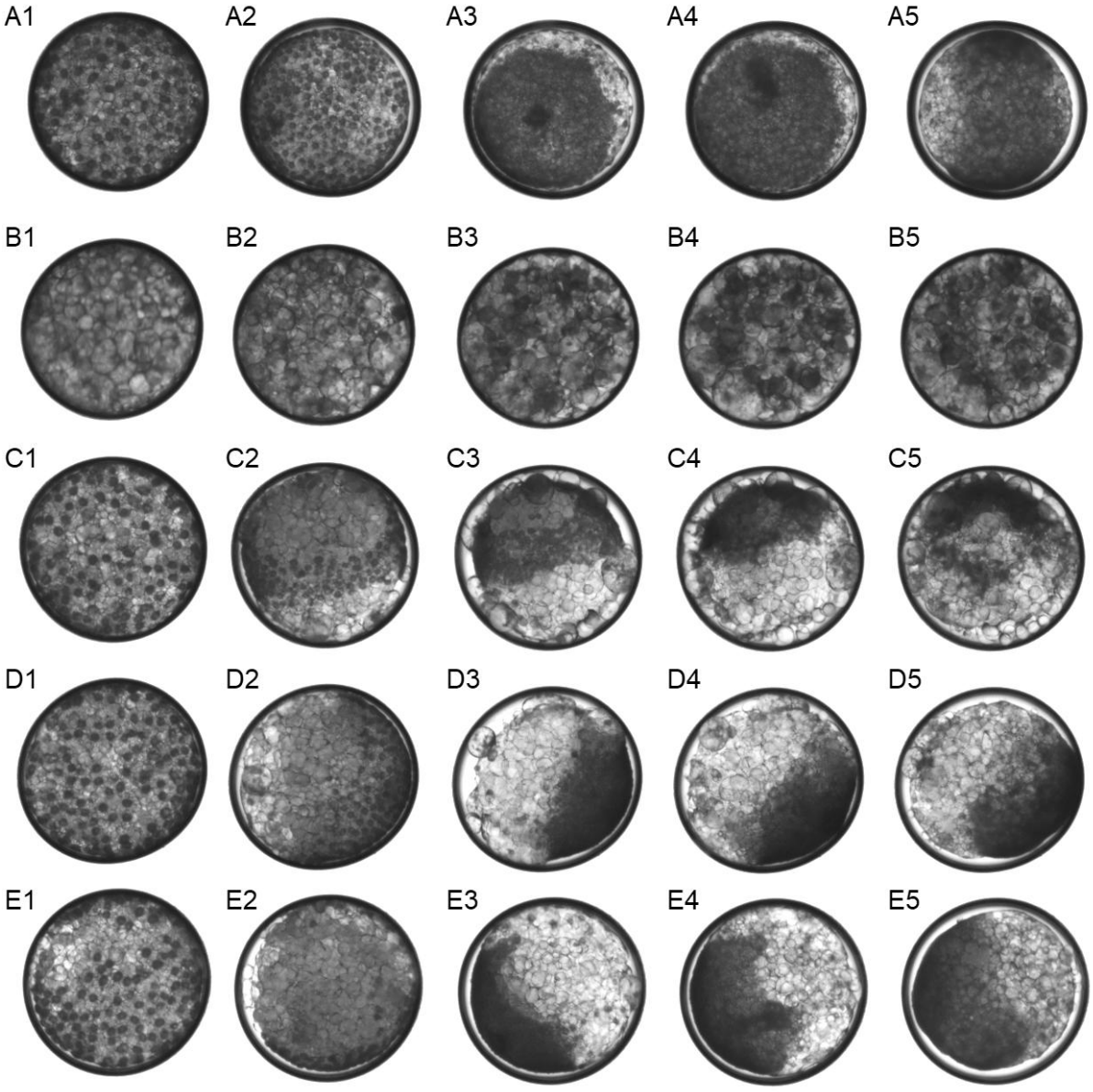

Figure 4-1. The major phenotype of *RF_0381* RNAi embryo is a defect in cell movement at stage 1. A. WT like *RF_0381* RNAi embryo. No cell loss was observed at stage 2. B, C, D, E: *RF_0381* RNAi embryo with varying degrees of cell loss at stage 2. A1, B1, C1, D1, D1: frame 1, Hael 18, stage 2/3. A2, B2, C2, D2, E2: frame 10, Hael 22, stage 3. A3, B3, C3, D3, E3: frame 25, Hael 29, stage 4. A4, B4, C4, D4, D4: frame 40, Hael 36, stage 5. A5, B5, C5, D5, E5: frame 78, Hael 53, stage 7.

Sixty embryos from cocoon 15-2 C3 were captured in time-lapse images for better observation. As shown in Figure 4-1, this cocoon may not exhibit the strongest RNAi injection effect but was more likely to be in the process of recovering from the injection.

In the video of cocoon 15-2 C3, 36 out of 60 embryos arrested development before stage 2. Among these embryos, only a portion of the surface region exhibited cell nuclei, and the location of the nucleus-positive region varied greatly among different embryos. The regions lacking cells (and nuclei) were unable to form the corresponding embryonic or extra-embryonic structures during later development. Additionally, the early cleavages seemed to be affected, and there were lots of membrane rupture leading to free floating yolk granules.

Figure 4-1 showed several *RF_0381* RNAi embryos with varying degrees of uneven distribution of cells at stage 2. A1–A5 represent WT-like embryos, which exhibited no cell loss in the observed area at stage 2. This embryo later formed a germ disc, similar to WT embryos. Furthermore, the developmental timing of each stage was comparable to that of WT embryos after standardization (method described in Chapter I, section 1, Hael calculations in the supplementary Table S4-1).

The *RF_0381* RNAi embryo in images B1–B5 exhibited very few cells in the observed area. The embryo could not form any cellular structures at later stages and subsequently leaked yolk. Embryos in images C1–C5, D1–D5, and E1–E5 showed partial cell loss at stage 2. At later stages, there was a loss of the germ disc region (C2–C4, E2–E4) or a loss of extraembryonic cells (C2–C4, D2–D4, E2–E4) in these embryos.

Embryos with minimal cell loss at an earlier stage were able to proceed with WT-like development (E1–E5) at a rate similar to that of WT-like embryos (A1–A5). In contrast, embryos with extensive cell loss could not form a germ disc and were unable to develop a germ band (C1–C5, D1–D5).

In the video, 4 out of 60 *RF_0381* RNAi embryos arrested development at around stage 5, exhibiting concentric contraction of the entire germ disc.

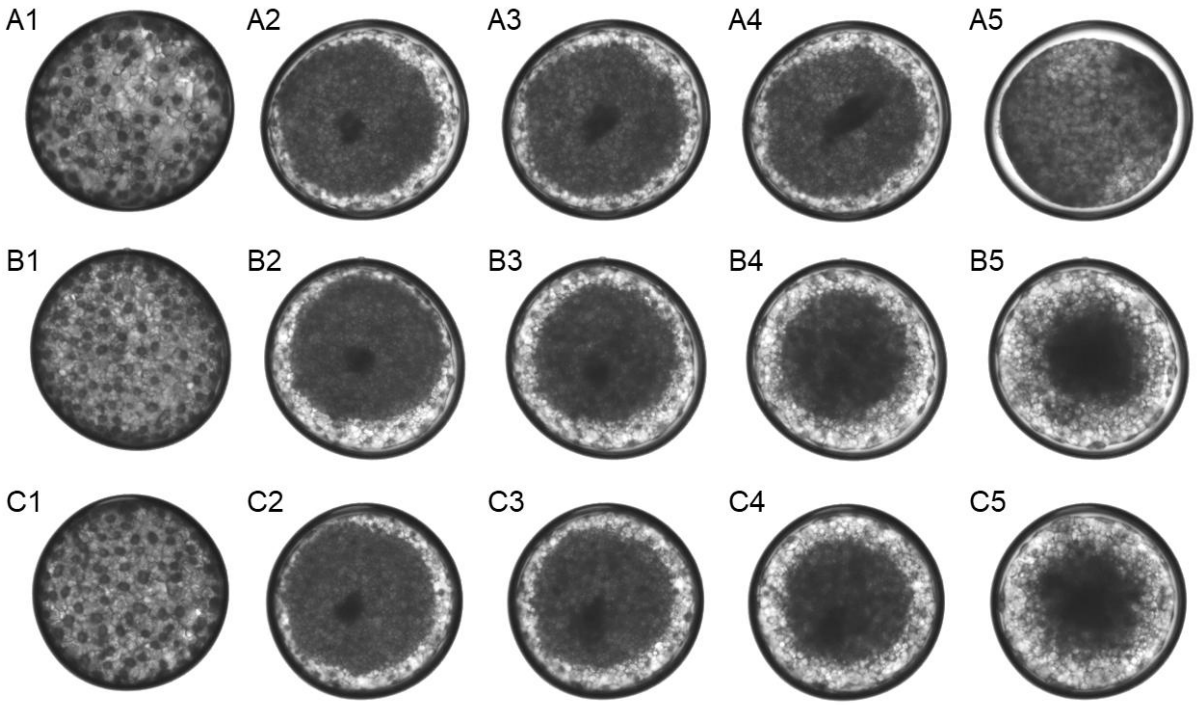

Figure 4-2. A minor phenotype of *RF_0381* RNAi embryos is germ disc contraction at stage 5. A, *RF_0381* RNAi embryo exhibiting WT-like development until the germ band stage. B and C: *RF_0381* RNAi embryos showing germ disc contraction at stage 5. A1, B1, C1: frame 1, Hael 18, stage 2/3. A2, B2, C2: frame 30, Hael 31.5, stage 4/5. A3, B3, C3: frame 35, Hael 34, stage 5. A4, B4, C4: frame 40, Hael 36, stage 5. A5, B5, C5: frame 78, Hael 53, stage 7.

Figure 4-2 showed three *RF_0381* RNAi embryos: one with WT-like development (A1–A5) and two exhibiting contractions at stage 5 (B1–B5, C1–C5). Until the early stages of stage 5, there were no distinct differences among the three embryos (A2, B2, C2). The embryo in B3 showed minimal or no cumulus migration, while the embryos in A3 and C3 were in the midst of cumulus migration. Shortly thereafter, the germ discs of embryos B and C contracted towards the centre (B4, B5, C4, C5) and could not progress further in development, unlike embryo A (A4, A5).

Twenty of the 60 embryos formed a germ band, similar to WT embryos.

1.3 Analysis the function of gene *RF_0381* based on *RF_0381* RNAi experiments.

The major phenotype of *RF_0381* RNAi embryos was the uneven distribution of cell nuclei at stage 2, which could be a defect of early cleavages, cell movement, or rupture of membrane systems. The arrangement of cell nuclei was in a variety of patterns, sometimes in specific regions, and other times in scattered, non-adjacent areas. This suggested that during stages 1/2 cell division or movement of different regions was relatively independent and not influenced by neighbouring regions. The observation confirmed the recent finding that cell specification occurs very early in development (Wang and Pechmann, 2024). From the timing, this phenotype may be caused by a maternal deficiency of the RF_0381 protein.

A small portion of *RF_0381* RNAi embryos exhibited contraction at stage 5 in a radial-symmetric pattern, regardless of the cumulus migration condition of the embryo. That could be a secondary defect resulting from defects at stage 2 or related to the loss of *RF_0381* gene expression in the primary thickening region during stages 3-4. Both hypotheses require further confirmation.

2 *g4422* RNAi

2.1 Expression of *g4422* gene in WT and *Ets4* RNAi embryos.

The spider gene *g4422* was identified as an uncharacterized gene in NCBI, and no homologous genes were reported. However, it was annotated as a chitin-binding domain-containing protein in other spider species in UniProt, with a coverage of 37.1%.

In WT embryos, the *g4422* gene was detected in most cells at stage 2, while at stage 4 it is primarily expressed in cells of the primary thickening region. No expression of this gene was detected at stage 5 (Result Chapter III, Figure 3-9 E1 to E4). Based on this information, the *g4422* gene was classified as a type II gene in Chapter III.

In *Ets4* RNAi embryos, *g4422* was also expressed in the primary thickening region at stage 4. Therefore, it was considered to be not regulated by Ets4 (Result Chapter III, Figure 3-21, D4).

2.2 *g4422* RNAi experiment and characteristics of *g4422* RNAi embryos.

I conducted only one batch of pRNAi experiments for the *g4422* gene with three spider. All of these spider produced embryos that were clearly neither spherical nor ellipsoidal. The ratio of irregularly shaped embryos was consistently high, usually exceeding 85% in C3. Since irregularly shaped embryos were rarely observed in WT embryos, it was almost certain that this phenotype is a result of *g4422* knockdown.

Time-lapse images of 31 embryos from cocoon 26-2 C3 were analyzed. Four embryos were roughly spherical in shape, while the remaining 27 embryos were not. From the video, it could be observed that the non-round shape appeared as early as stage 1 (Figure 4-3).

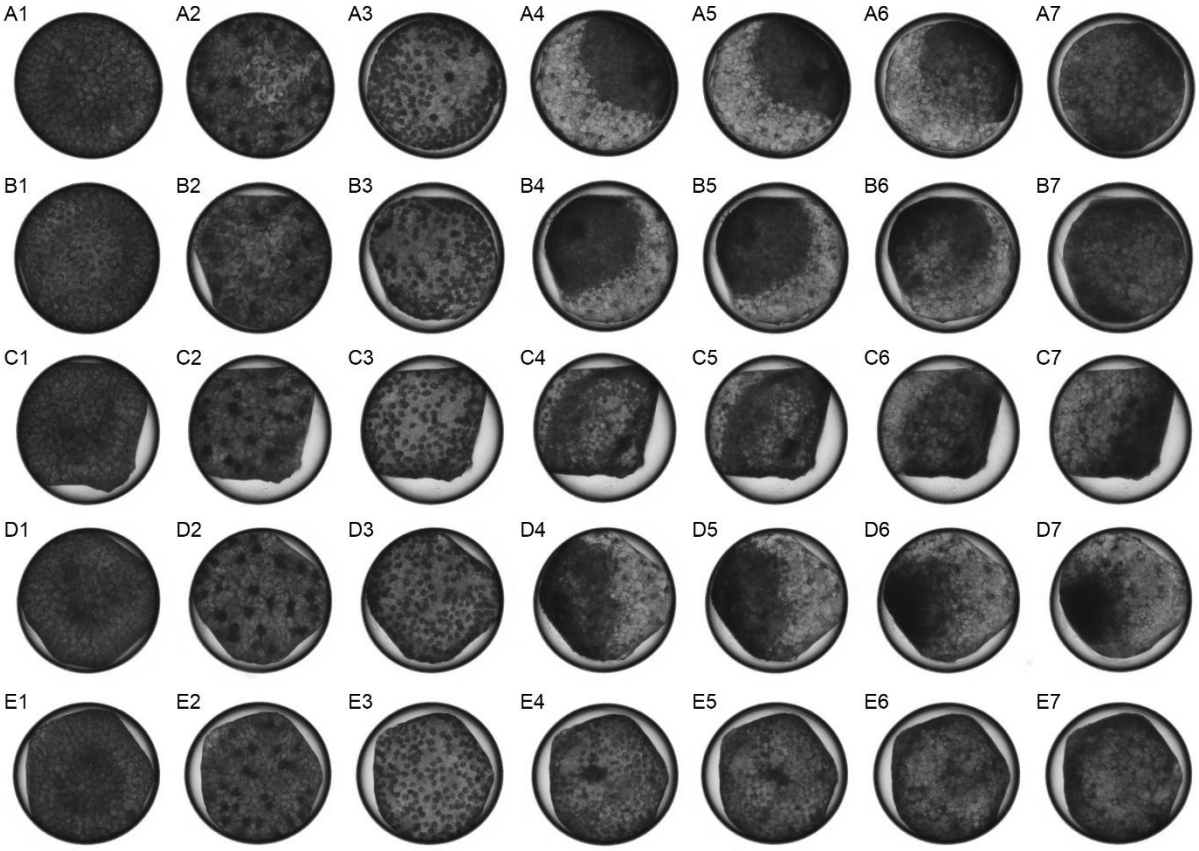

Figure 4-3. Development of *g4422* RNAi embryos. A1-A7: WT like *g4422* RNAi embryo tp to the germ band stage, video 1-4. B1-B7, C1-C7, D1-D7, E1-E7: *g4422* RNAi embryo with a non-roundish shape, from video 8-2, video 1-3, video 5-3, and video 7-3, respectively. A1,B1, C1, D1, E1, frame 5, Hael 7, stage 1. A2, B2, C2, D2, E2: frame 16, Hael 11, stage 1/2. A3, B3, C3, D3, E3, frame 35, Hael 18, stage 2/3. A4, B4, C4, D4, E4, frame 63, Hael 28, stage 3/4. A5, B5, C5, D5, E5, frame 71, hael 31, stage 4/5. A6, B6, C6, D6, E6, frame 99, Hael 41, stage 5/6. A7, B7, C7, D7, E7: frame 137, Hael 54.7, stage 7.

Figure 4-3 showed the early development of five *g4422* RNAi embryos: one in a spherical shape (A1-A7) and four in a non-spherical shape (B1-B7, C1-C7, D1-D7, E1-E7). The latter four embryos began transitioning from a spherical to a non-spherical shape starting at stage 1 (C1, D1, E1) or stage 2 (B1), which may result from regional attachment of the vitelline membrane to the outer membrane of the embryo. This attachment may either be maintained (C7, D7) or lost (B7, E7) at later stages, while the embryo's shape remained non-spherical (B7, C7, D7, E7). Additionally, the non-spherical shapes of the *g4422* RNAi embryos were distinct and vary from one another.

It is noteworthy that in WT embryos, the detachment of the vitelline membrane from the outer embryo membrane occurred around 16 Hael at stage 2, when the volume of the embryo generally shrunk. A similar process was observed in WT-like *g4422* RNAi embryos (A1-A3). However, the inner space between the two membranes was observed earlier in other *g4422* RNAi embryos (B2, C2, D2, E2). Judging by the details, it was not a neat and complete detachment, but rather showed many blurry areas in between, suggesting it could be a detachment of the inner layer of the vitelline membrane.

Another observation regarding the *g4422* RNAi embryos was that almost all of their germ discs, including those in WT-like *g4422* RNAi embryos, exhibited an uneven distribution of cells, with some areas having large holes (Figure 4-3, A3, B3, C3, D3, E3). Some of these holes were later covered by cell movement (A4, B4), allowing the embryos to proceed to develop into a normal germ band (A7, B7), at a rate comparable to that of WT embryos (Hael calculation in supplementary Table S4-1).

However, other embryos maintained the holes until stage 4 (C4, D4, E4), developed more slowly, and were unable to form a germ band (C7, D7, E7).

Additionally, none of the *g4422* RNAi embryos in the video exhibited rotation of the germ disc by stage 4.

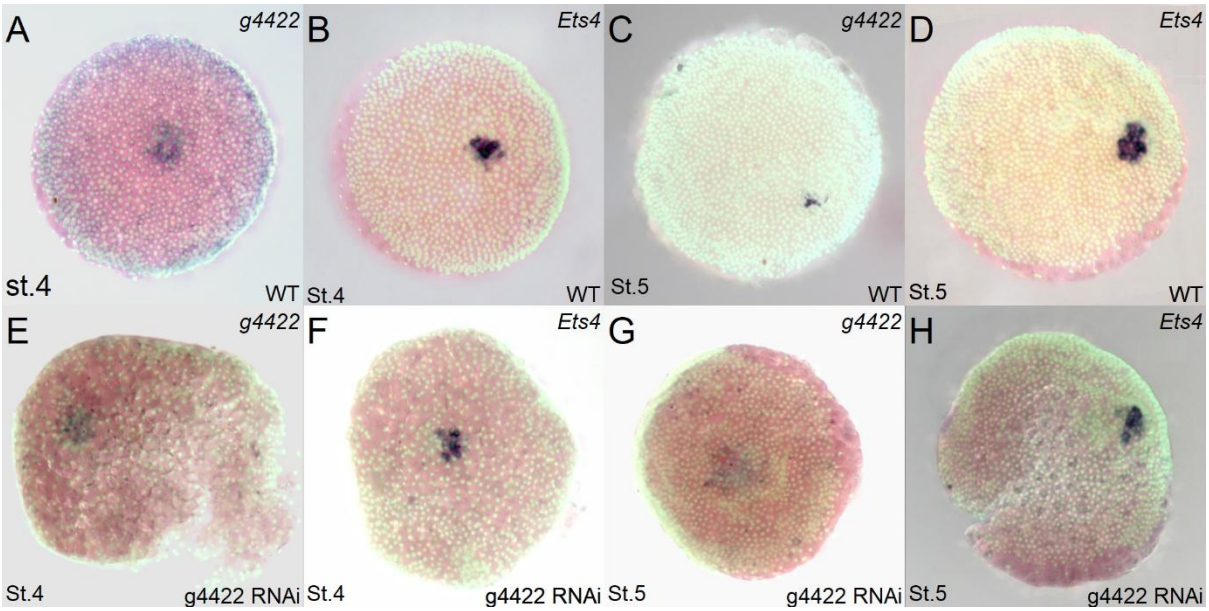

Figure 4-4. Expression of gene *g4422* and *Ets4* at stage 4 and 5 in WT and *g4422* RNAi embryo. A, B: WT embryo at stage 4. C, D: WT embryo at stage 5. E, F: *g4422* RNAi embryo at stage 4. G, H: *g4422* RNAi embryo at stage 5. A, C, E, G: *g4422* expression. B, D, F, H: *Ets4* expression.

Figure 4-4 showed *in situ* hybridization staining in *g4422* RNAi embryos (E-H). Most of the embryos (E-G) exhibited a non-spherical shape, in contrast to the WT embryos (A-D). Additionally, the cells in the *g4422* RNAi embryos at stage 4 (E, F) displayed an uneven distribution, as observed in the video images (Figure 4-3, C4, D4, E4).

Gene *g4422* was expressed in the primary thickening region at stage 4 in both WT and *g4422* RNAi embryos (A, E), indicating that the RNAi embryo represented a knockdown case, not a knockout. *Ets4* was expressed in the primary thickening region at stage 4 in both WT and *g4422* RNAi embryos (B, F), and in the cumulus region in both WT and *g4422* RNAi embryos (D, H), showing no significant difference in expression patterns between the two types of embryos.

2.3 Analysis the function of gene *g4422* based on *g4422* RNAi experiments.

The video showing the development of *g4422* RNAi embryos revealed abnormalities, including non-spherical embryo shape, uneven arrangement of germ disc cells, and a lack of germ disc rotation. The *in situ* hybridization of *g4422* RNAi embryos corroborated the first two observations.

The non-spherical shape and lack of rotation in g4422 RNAi embryos may result from a defect in the membrane region, possibly due to the improper detachment of the inner layer of the vitelline membrane. If this was the case, the g4422 gene may play a role in maintaining the integrity of the vitelline membrane. Furthermore, the uneven distribution of the germ disc could be a consequence of earlier defects in the embryo's shape changes or the absence of g4422 expression during stage 2.

The *g4422* gene was expressed in the primary thickening region of both WT and *Ets4* RNAi embryos, while the *Ets4* gene was expressed in the primary thickening region of both WT and *g4422* RNAi embryos. It was highly likely that these two genes function independently of each other.

3 *cv-2* RNAi

3.1 Expression of *cv-2* gene in WT and *Ets4* RNAi embryos.

In other species, the *cv-2* protein interacted with and inhibits the function of BMP (dpp) protein in cell differentiation or developmental processes.

In P. tepidariorum, the *cv-2* gene was expressed in the primary thickening region at stage 4 (Chapter III, Figure 3-1 A), in the cumulus region at stage 5, and in the dorsal region/boundary between the embryonic and extraembryonic regions from stages 8 to 12 (Leite et al., 2024). The expression pattern of the gene at stages 2, 6, and 7 was currently unknown.

In *Ets4* RNAi embryos, the *cv-2* gene was not detected in the primary thickening region at stage 4. Therefore, it was considered to be downstream of the *Ets4* gene.

3.2 *cv-2* RNAi experiment and characteristics of *cv-2* RNAi embryos.

I conducted one batch of *cv-2* RNAi experiments with two spiders, which produced progenies that stopped development at the germ disc stage. The lethality rate of embryos from the first spider was much higher than that from the second. However, the results had not been fully confirmed due to the lack of replicates.

I had time-lapse images of the development of 25 embryos from cocoon *cv-2*-2 C2. All embryos exhibit varying degrees of abnormality compared to WT embryos at different stages of development. Ten of the 25 embryos stopped development at the germ disc stage.

Figure 4-5 illustrated the development of three *cv-2* RNAi embryos, two of which stop development at the germ disc stage (B1-B4, C1-C4). At stages 4/5, the germ discs in images B1 and C1 displayed multiple areas with darker coloration. In contrast, the germ disc of the embryo in image A1 showed only one such area, corresponding to the primary thickening region. This suggested that the embryos in images B1 and C1 may possessed multiple regions with inner cells at this stage.

At stage 5, the embryo in A1 exhibited migration of cumulus cell clusters towards the rim of the embryo (A2). This process led to the dorsal opening at the rim of the germ disc, allowing the embryo to develop into a germ band (A4). In contrast, the multiple darker regions in the embryos shown in B1 and C1 sent out mobile cells migrating in different directions (B2, C2). Some of these mobile cells migrated towards the rim of the germ disc, while others did not. The germ discs of these embryos did not open at any peripheral position; instead, they contracted towards the center of the germ disc (B4, C4).

However, alternative explanation for the defects of embryo development in B1-B4 and C1 to C4, suggested irrelevance to dsRNA injections. Statistics on development of WT embryos revealed that 6.3% embryo (n=412) were mal formed during development (Wang and Pechmann, 2024), most of which exhibited abnormalities before and during germ disc stage. Similar case may occur in this batch of cv-2 RNAi embryos, and more replicates would help for further understanding.

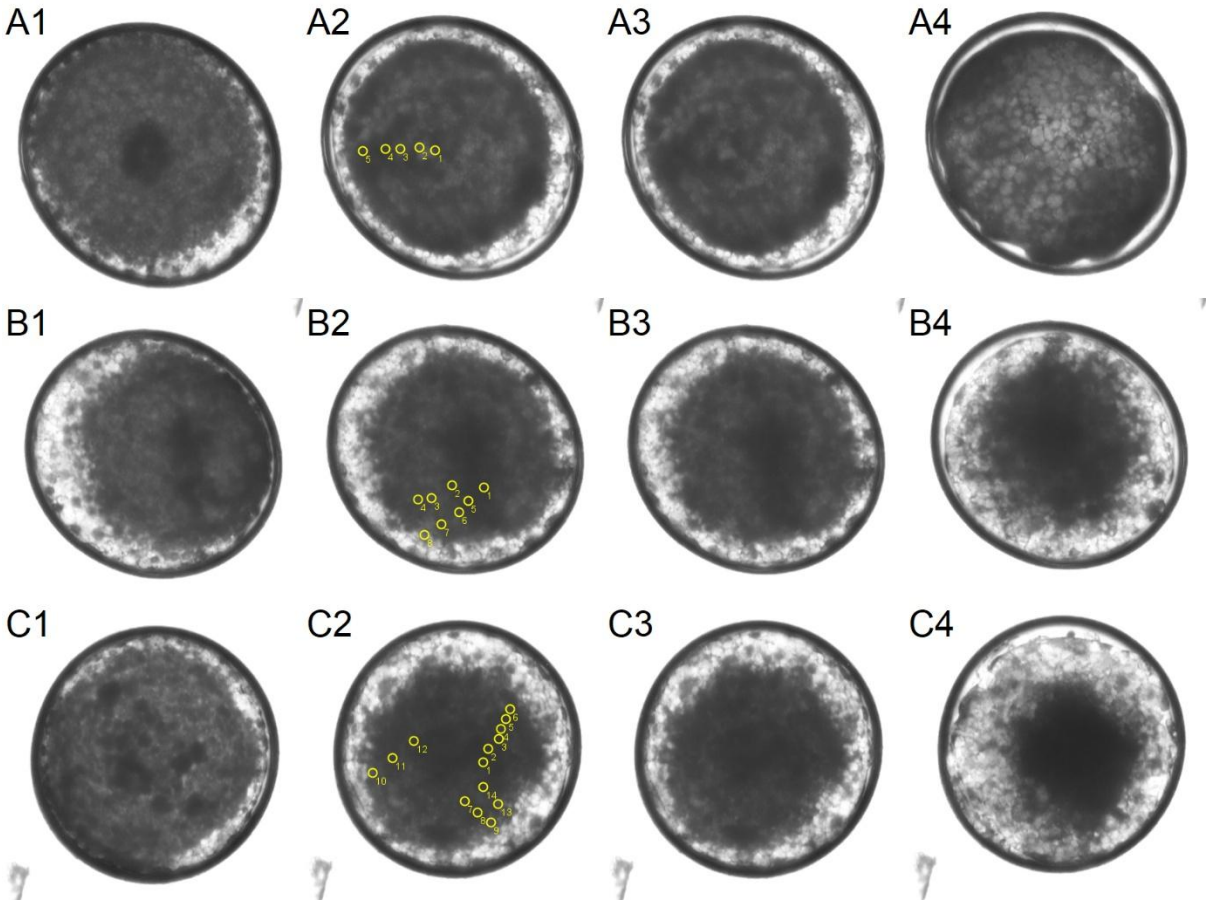

Figure 4-5. *cv-2* RNAi embryos that stop development at germ disc stage. A1-A4, embryo developing similarly to WT embryos at the germ disc stage. From *cv-2* RNAi video 5-4, of frame 15, 35, 35 and 87. B1-B4 and C1-C4, embryos that stop development at the germ disc stage. B1-B4 are from *cv-2* RNAi video 2-2, of frame 20, 35, 35, and 87. C1-C4 are from *cv-2* RNAi video 1-3, of frame 17, 35, 35, 87. A1, B1, C1: stage 4/5. A2, B2, C2: traces of migrating cells from A1 to A3, B1 to B3, and C1 to C3, overlaid in image A3, B3 and C3. A3, B3, C3: stage 5/6. A4, B4, C4: Hael 66, stage 8.

The remaining 15 of the 25 *cv-2* RNAi embryos in cocoon *cv-2*-2 C2 all formed a germ band. There were no distinguishable differences in the development of these embryos compared to WT embryos at stages 4 to 5. However, at stage 6, the dorsal opening angle of these *cv-2* RNAi embryos was smaller than that of WT embryos.

Figure 4-6 showed the development of one WT embryo (A1-A5) and three *cv-2* RNAi embryos (B1-B5, C1-C5, D1-D5) from stage 4 to stage 8. The time taken for each stage of *cv-2* RNAi embryos was similar to that of WT embryos after standardization (Hael calculation in the supplementary Table S4-1).

At stage 6, the largest opening angle of the WT embryo (A3) was more than 270°, causing the germ disc to fold into a triangle. In contrast, at the same stage, the largest opening angle of the *cv-2* RNAi embryos is around 210° (B3) and, in some cases, as small as 90° (C3, D3).

cv-2 RNAi embryos in images B3, C3, and D3 did not open further at later stages. Instead, they elongated in the frontal direction, driven by the cells at the center of the germ disc, which would later form the posterior region (B4, C4, D4), similar to the WT embryo (A4). These *cv-2* RNAi embryos successfully formed germ bands, which appeared broader compared to the WT embryo at stage 8 (A5, B5, C5, D5). It was still unclear whether this will affect further development.

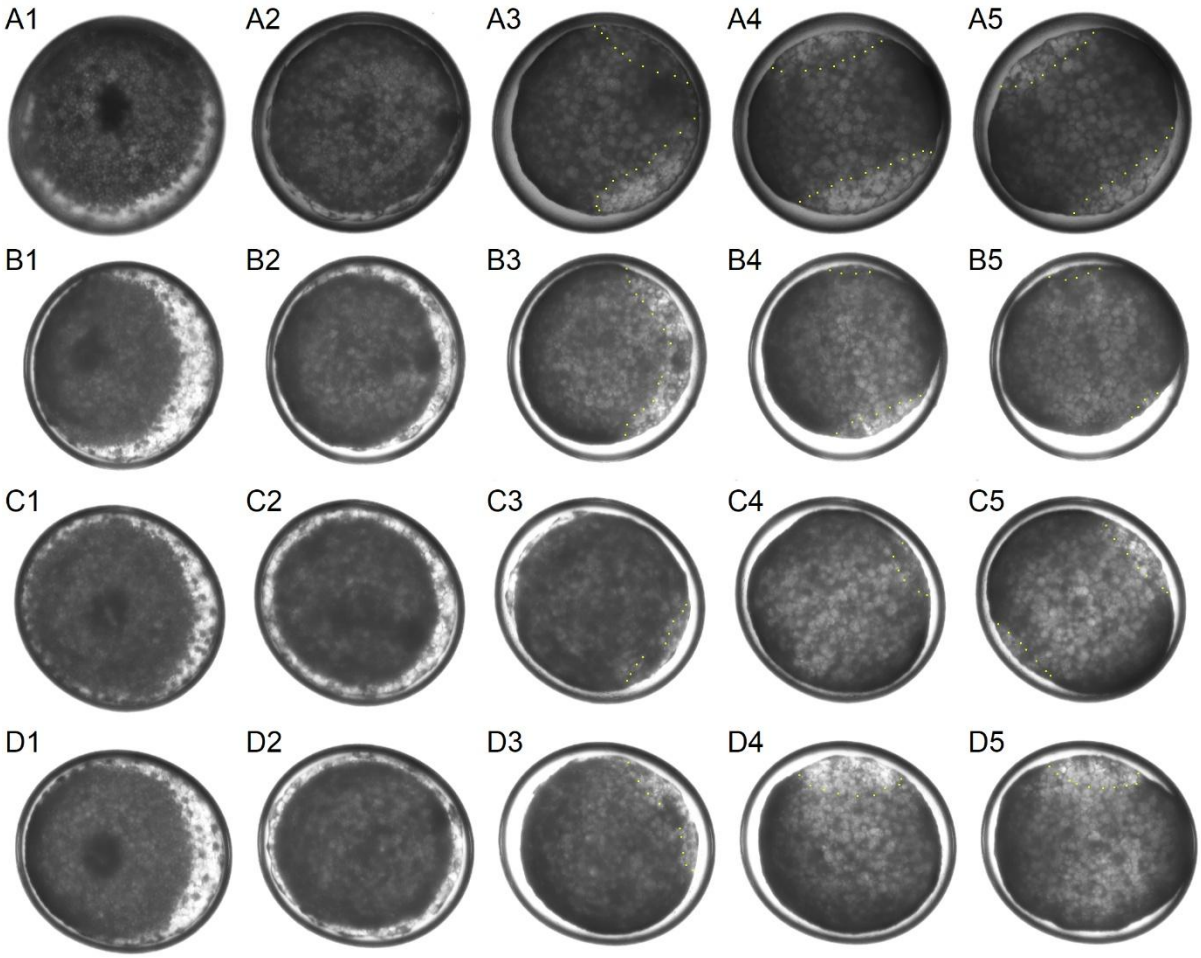

Figure 4-6. *cv-2* RNAi embryos exhibit a smaller angle during the dorsal opening process. A1-A5: WT embryo from 2022 video 13-3, of frame 75, 115, 155, 175, and 191, respectively. B1-B5, C1-C5, D1-D5: *cv-2* RNAi embryo, from video 2-3, 5-5, and 5-3. B1, C1, D1: frame 15. B2, C2, D2: frame 35. B3, C3, D3: frame 54. B4, C4, D4: frame 65. B5, C5, D5: frame 75. A1-D1: Hael 30, stage 4/5. A2-D2: Hael 40, stage 5/6. A3-D3: Hael 50, stage 6/7. A4-D4: Hael 55, stage 7/8. A5-D5: Hael 60, stage 8. Yellow dot lines in A3-A5, B3-B5, C3-C5, and D3-D5 mark the border of embryonic-extraembryonic region of the embryo.

3.3 Analysis of the function of gene *cv-2* based on *cv-2* RNAi experiments.

The reason why *cv-2* RNAi embryos that contracted at the germ disc stage fail to proceed to the germ band stage was not yet fully confirmed or understood. If this observation was reliable, it may suggest that *cv-2* functions in maintaining a single invagination site within the germ disc.

cv-2 RNAi embryos with a smaller dorsal opening angle showed a restricted ability for cell movement along the migration path and in other regions of the germ disc. That agreed with previous understanding on the function of cv-2 in regulating BMP signaling, which was necessary for dorsal opening process (Akiyama-Oda and Oda, 2006). However, further experiments were necessary to draw more definitive conclusions.

4 *Twi (twist)* RNAi

4.1 Expression of gene *twi* in WT and *Ets4* RNAi embryos.

The *twi* gene was a key developmental gene in animals, commonly regarded as a marker for mesodermal cells. It played a crucial role in the differentiation of several tissue types.

In spider development, the *twi* gene (aug3.g14287.t1) was expressed as early as stage 3 in the primary thickening region, continuing in the same region at stage 4 (Pechmann et al., 2017). At stages 5 and 6, *twi* expression was observed in cells at the rim of the germ disc and some central regions. The gene's expression pattern gradually evolved into a segmental pattern through stages 7, 8, and 9 (Yamazaki et al., 2005). Additionally, both studies reinforced the connection between *twi* expression and mesodermal derivation.

In *Ets4* RNAi embryos, the *twi* gene was not detected in the primary thickening region at stage 4. Additionally, exogenous expression of the *Ets4* gene promoted the expression of *twi*, strongly supporting the hypothesis that *Ets4* acted upstream of *twi* at this stage (Pechmann et al., 2017).

4.2 *twi* RNAi experiments.

Attempts to knock out the *twi* gene (aug3.g14287) were ongoing for several years. A recent publication by Iwasaki-Yokozawa et al. (2022), reported in the supplementary files, that no significant differences were observed between *twi* RNAi embryos and WT embryos.

Based on an updated genome annotation, Matthias Pechmann (MP), found a new Pt-twist annotation (NM_001323807.1) which was used, in combination with the previous annotation, to produce a longer fragment that was used for an additional knockdown approach of Pt-twist via RNAi. The RNAi experiment with new *twi* dsRNA, produced embryos with noticeable differences compared to WT embryos. The gene analysis, experimental design, and molecular cloning for this experiment were all carried out by MP.

4.3 Characteristics of *twi* RNAi embryos.

4.3.1 General information

The *twi* RNAi experiment was conducted over several batches (supplementary Figure S4-2). A small portion of the *twi* RNAi embryos displayed a tube-like shape around stage 7, resembling the phenotype of *Ets4* RNAi embryos at the same stage (Pechmann et al., 2017). Many of these tube-shaped embryos recovered in later stages and formed a germ band, similar to WT embryos.

The ratio of tube-shaped *twi* RNAi embryos appeared to be related to the quality of the cocoon. In some cocoons of poor quality (e.g., *twi*-1, not listed), the proportion of tube-shaped embryos is quite high, accompanied by an increased death rate. I selected five RNAi spider that produced high-quality first cocoons. The cocoons from these spider were collected and embryonic phenotypes were statistically analysed. On average, the ratio of tube-shaped embryos in these cocoons was around 10%, with a maximum of 30% (supplementary Figure S4-2).

Via time-lapse recording, I analysed more than 400 embryos from five cocoons of four different *twi* RNAi *P. tepidariorum* females (*twi*-6 C3, *twi*-6 C4, *twi*-12 C3, *twi*-13 C3, and *twi*-14 C5). To record the abnormalities in the *twi* RNAi embryos, most RNAi embryos were compared to the development of WT embryos (Table 4-1). These abnormalities included issues with the germ disc formation process (such as holes and irregular shapes), the primary thickening region (delayed formation, relatively small size, not centrally located, and multiple multi-cellular regions), stage 4 abnormalities (excessive length, failure of the germ disc to rotate to the frontal view), cumulus-related abnormalities (multiple mobile cells, no movement, weak migration path), stage 6 abnormalities (germ disc contraction,

posterior region growing upwards during dorsal opening, and tube-shaped embryos), as well as abnormalities in the germ band (too narrow or too broad), among others.

These features reflected the outcome of *twi* dsRNA injection and the specificity of different batches of spider.

Table 4-1 listed the abnormalities found in the developmental videos of different batches of *twi* RNAi embryos. It was clear that various batches of *twi* RNAi embryos exhibited certain levels of specificity.

Four abnormalities were present in all batches of videos, highlighted in yellow or green in the table. The terms marked in yellow represent phenotypes of "primary thickening formation delay" and "stage 4 duration longer than 3 Hael", which were observed in most *twi* RNAi embryos across all batches. The green color highlighted the phenotypes "no cumulus migration at stage 5" and "tube formation or posterior upgrowth during dorsal opening". The ratio of these phenotypes exceeded 10% in all *twi* RNAi video batches, and these two phenotypes were often observed in the same embryo at different stages. I believed these abnormalities are a direct result of *twi* gene knockdown during embryo development, and I will discuss them further in later sections.

Some phenotypes were observed at a high ratio in certain batches of *twi* RNAi embryos but not in all. These are marked in red in Table 4-1. The list included "germ disc slight contraction at stage 5/6" and "delay in development at stage 7", among others. Given our doubts that these phenotypes may be more related to the specificity of the spider rather than just the dsRNA injections, I will not discuss these observations further.

Table 4-1 Abnormalities in *twi* RNAi embryos during early development stages

cocoon		Twist-6 C3	Twist-6 C4	Twist-12 C3	Twist-13 C3	Twist-14 C5
stage of video		stage 3 to 10	stage 2 to 10	stage 4 to 8	stage 2 to 8	stage 4 to 5
number of embryos		6	99	99	100	hundreds
counts of embryos		6	50	20-36	20-36	22
(phenotype ratio)						
stage 3-4, germ disc region	germ disc with holes	some very severe	some	2/36	25%	50%
	strange shape of germ disc	not found	some	not found	not obvious	most roundish
stage 3-4, primary thickening region	primary thickening formation delay	high ratio	most	(not knowing)	high ratio	(not knowing)
	primary thickening too small	1/6	9/29	no	6.25%	no
	primary thickening not in center	yes, because of holes	9/29	2/35	not obvious	1/22
	several multi layered regions	1/6	1/29	4/35	25%	3/22
stage 4, germ disc	stage 4 longer than 3 hael	all	all	all	all	all
	some germ disc not in frontal view	2/6	42%	1/36	20%	a few
stage 5, primary thickening and cumulus	multiple moveable cells	2/6	1%	1/36	5%	2/22
	cumulus path too weak to tell, or no cell migration (tube phenotype)	4/6	some	*2/20*	33%	4/22
stage 6	germ disc contraction	2/6	52%	*2/20*	70%	30%
	tube or with posterior growth	2/6 or 0	32%	30%	25%	(4/22)
stage 7 and later	germ band too narrow or too broad	2/6 too narrow	not found	most OK	some	(not knowing)
	strong delay in stage 7	50%	40%	no	half	(not knowing)

4.3.2 Hael calculation in different batches of *twi* RNAi embryos and the timing of stage 4.

A method was introduced in Chapter I (section 1) for standardizing the development time of WT embryos from various sources to the timing in Mittmann and Wolff, 2012. This method was based on the assumption that the time cost of each stage of different WT embryos is proportionate in most cases. So far, I did not find strong evidence to contradict this assumption, at least not during embryonic development stages 2-8, Hael 11-70.

RNAi embryos could be a different case. Although I performed a similar standardization process for *RF_0381* RNAi (section 1), *g4422* RNAi (section 2), and *cv-2* RNAi (section 3) embryos, and found that the time cost of their developmental processes is similar to that of WT embryos, this was not the case for *twi* RNAi embryos. I could not identify a single ratio that would align the actual development time of *twi* RNAi embryos with the Hael time intervals of WT embryos at stages 2, 3, 4, 5, 6, 7, and 8. A closer analysis revealed that the actual time cost of *twi* RNAi embryos at stages 2 to 4 and 5 to 8 is similar to the Hael time in WT embryos, while the time cost between stages 4 and 5 in *twi* RNAi embryos was much longer than in WT embryos.

To be precise, I counted the total number of cells in frame 2-10 of a selected embryo from *twi*-6 C4 (scene 3, No.4-2; counting result in supplementary Table S4-2), and compared this result with the total cell count from a WT embryo from Pechmann, 2016, which was at a similar angle in the view. Through this comparison, I determined that frame 2 of this *twi* RNAi embryo corresponds to 12 Hael.

Meanwhile, during the development of the same *twi* RNAi embryo, I observed that frames 50 and 70 correspond roughly to stages 4/5 and 5/6, respectively. Therefore, I identified them as Hael 31 and Hael 41. This meant that these two frames, and one actual development hour of this embryo, are approximately equivalent to 1 Hael. Using this ratio, I calculated that frames 13 and 32 correspond to Hael 18 and Hael 28. Similarly, frames 102, 135, 153, and 174 correspond to Hael 56, Hael 76, Hael 86, and Hael 96. Images of the embryos in these frames confirmed the calculation results (Figure 4-7 D).

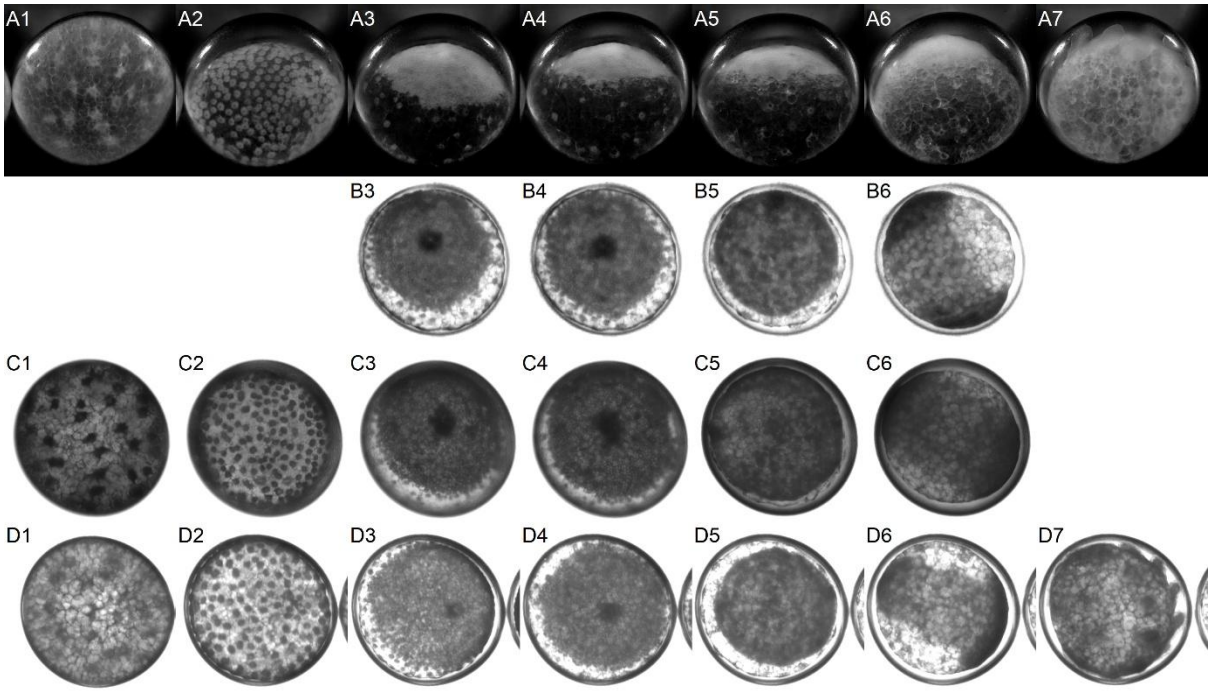

Figure 4-7. Development of three WT embryos (A1-A7, B3-B6, C1-C6) and one *twi* RNAi embryo. A1-A7, WT embryo from Pechmann, 2016. B3-B6, WT embryo from Pechmann et al., 2017. C1-C6: WT embryo, No. 2022 13-3. D1-D7: Twist-6 C4, s3 4-2. A1, C1, D1: Hael 12, stage 2. A2, C2, D2: Hael 18, stage 2/3. A3, B3, C3, D3: Hael 28, stage 3/4. A4, B4, C4, D4: Hael 31, stage 4/5. A5, B5, C5, D5: Hael 41, stage 5/6. A6, B6, C6, D6: Hael 56, stage 6/7. A7, D7: Hael 76, stage 8/9. Frame numbers of each image were in supplementary Table S4-1.

Figure 4-7 showed images of stage 2, stage 2/3, stage 3/4, stage 4/5, stage 5/6, stage 6/7, and stage 8/9 from three WT embryos (A1-A7, B3-B6, C1-C6) and one *twi* RNAi embryo (D1-D7). The images of the *twi* RNAi embryo at these stages were in similar developmental conditions as the WT embryos at the same stages. Images of the *twi* RNAi embryo at stages 9/10 and 10/11 also resembled the images

of WT embryos from Mittmann and Wolff, 2012. Therefore, I considered the Hael calculation for this embryo in the video to be reliable.

For a WT embryo at 25°C, stage 3 lasted around 10 hours (from Hael 18 to Hael 28), and stage 4 lasted around 3 hours (from Hael 28 to Hael 31). The *twi* RNAi embryo shown in Figure 4-7 D has frame 13 corresponding to Hael 18, frame 32 to Hael 28, and frame 50 to Hael 31. The interval between frames in the video is 30 minutes. This meant the embryo spends approximately 9.5 hours (from frame 13 to 32) in stage 3, and 9 hours in stage 4 (from frame 32 to 50). By comparison, the duration of stage 3 in this *twi* RNAi embryo was similar to that of WT embryos, while the duration of stage 4 was much longer.

Figure 4-8 showed 25 embryos from the same cocoon of *twi* RNAi embryos, at frames 13 (A), 32 (B), and 50 (C). It could be observed that all embryos across the frames are synchronized in their development: in image B, all the embryos already formed a fully shaped and tightly arranged germ disc, while in image C, no cumulus movement was observed in any of the embryos,. In summary, these embryos all took 9.5 hours for stage 3 and 9 hours for stage 4.

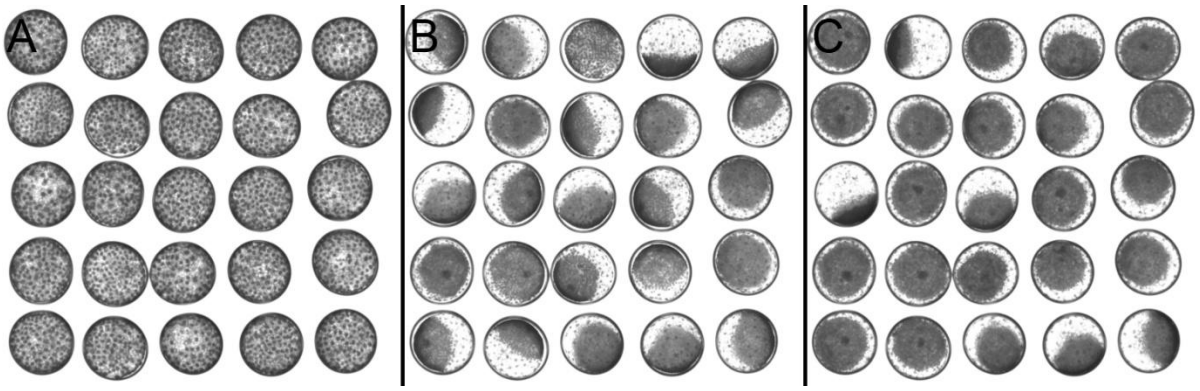

Figure 4-8. Image for 25 embryos in Twist-6 C4 scene 3. A: frame 13, Hael 18, stage 2/3. B: frame 32, Hael 28, stage 3/4. C: frame 50, Hael 31, stage 4/5.

Using the same method, I calculated the Hael for other batches of *twi* RNAi embryos (see Supplementary Table S4-1). Supplementary Figure S4-3 was a montage image showing one WT embryo and five *twi* RNAi embryos at Hael 28, 31, and 41. These *twi* RNAi embryos were from different RNAi injection batches. The analysis confirmed that the embryos in each image correspond to the respective stages. However, counting from the number of frames, stage 4 of the WT embryo took 3 hours, while the *twi* RNAi embryos took 12, 9, 5(+), 5.5, and 7 hours, respectively. Figure S4-4 in the supplementary document, illustrated the same issue in a different format. In summary, all batches of twi RNAi embryos in our current experiments showed a longer stage 4 duration than WT embryos.

4.3.3 *twi* RNAi embryos exhibit a delayed initiation of the invagination process.

In Chapter I section 1, I traced the cells in the primary thickening region of WT embryos from stage 2 to stage 3, which led to two findings: (1) primary thickening cells were derived from multiple cells at the 32-cell stage, and (2) the first appearance of cell disappearance (invagination) in this region typically occurred around 18-19 Hael.

A similar method was applied to analyze *twi* RNAi embryos. Figure 4-9 showed images of the last frame of each embryo before cell disappearance (invagination). The embryos included three WT embryos (A1-A4, B1-B2, C1-C2), and six *twi* RNAi embryos from two batches (*twi*-6 C4: D1-D2, E1-E2, F1-F2; *twi*-13 C3: G1-G2, H1-H2, I1-I2). All embryos were in the frontal view, allowing for

the observation of the entire primary thickening formation process. For better comparison, I also included images of each embryo at 28 Hael (stage 4).

For the three WT embryos, the time of the pre-invagination frame was 18.5 Hael (A1), 18.75 Hael (B1), and 19 Hael (C1). In contrast, for the *twi* RNAi embryos, the pre-invagination frames occurred at 21 Hael (D1), 21 Hael (E1), 21.5 Hael (F1), 24.5 Hael (G1), 24.5 Hael (H1), and 28.5 Hael (I1). This indicated a noticeable delay in invagination in the *twi* RNAi embryos compared to the WT embryos. Furthermore, the extent of this delay differed between batches of *twi* RNAi embryos (D1, E1, F1 versus G1, H1, I1).

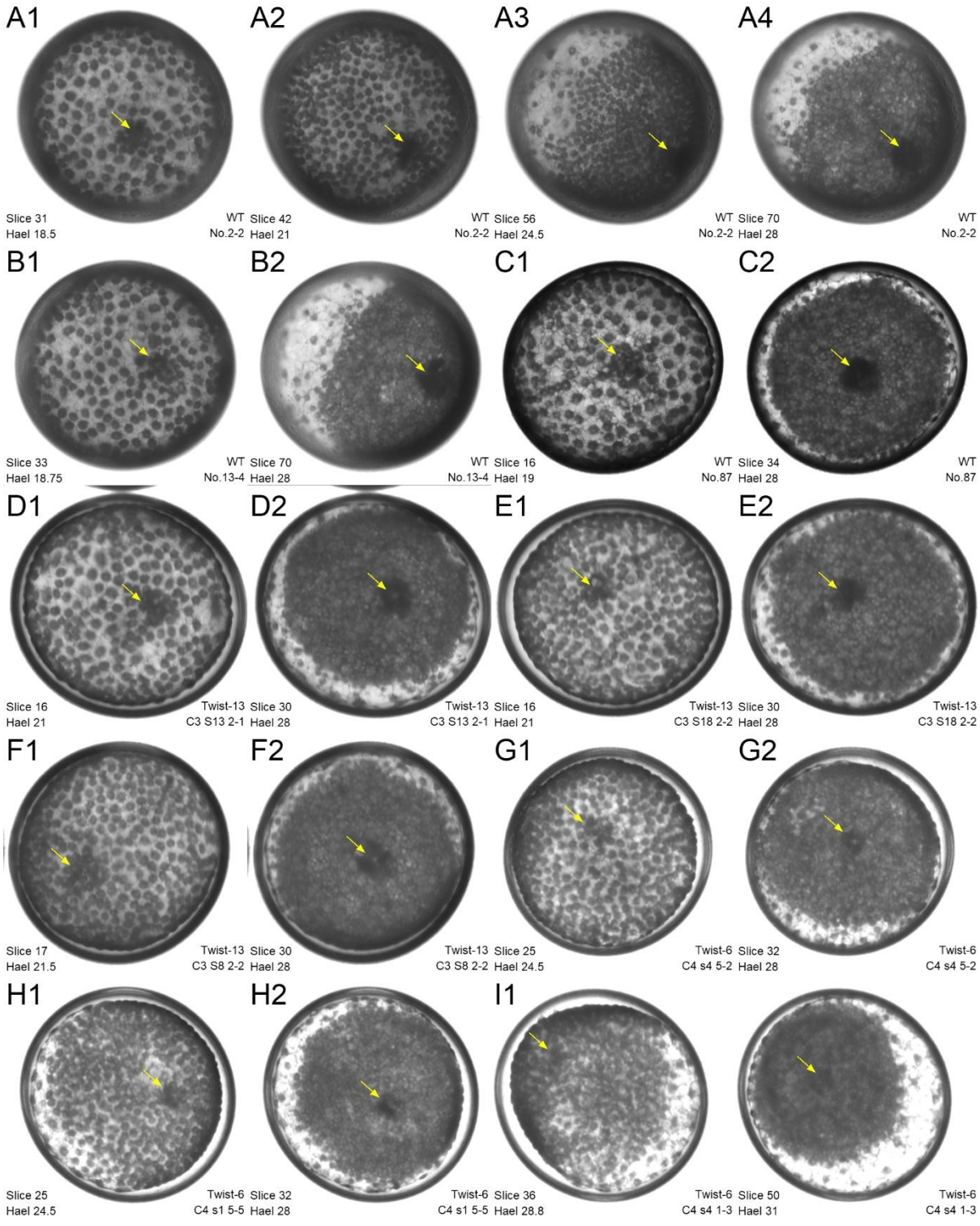

Figure 4-9. Time of the invagination process in WT and *twi* RNAi embryos. A1-A4, B1-B2, C1-C2: WT embryos. D1-D2, E1-E2, F1-F2: *twi* RNAi embryo from Twist-13 C3. G1-G2, H1-H2, I1-I2: *twi* RNAi embryo from Twist-6 C4. A1, B1, C1, D1, E1, F1, G1, H1, I1: last frame before cell disappear (invagination). A4, B2, C2, D2, E2, F2, G2, H2: frame of embryos at 28 Hael. A2: frame of the embryo at 21 hael. A3: frame of the embryo at 24.5 hael. I2: frame of the embryo at 31 hael. Frame number and Hael time is marked in the image. Arrow: primary thickening region.

The embryo in I1 is the latest *twi* RNAi embryo to showed invagination as observed. The invagination site for this embryo occurred at 28.5 Hael. This meant that while most embryos in the same batch reached stage 4, this particular embryo still had a single-layered germ disc. However, the embryo eventually formed a small primary thickening region at stage 5 (I2) and continued to develop normally in later stages, ultimately reaching the germ band stage.

Figure 4-9 also showed the cell density of other germ disc cells. *twi* RNAi embryos at around 21 Hael (D1, E1, F1) exhibited similar cell density to WT embryos at 21 Hael (A2). Similarly, *twi* RNAi embryos at around 24 Hael (G1, H1) had comparable cell density to WT embryos at 24 Hael (A3). This suggested that other regions of the germ disc were not significantly affected by the delayed initiation of primary thickening formation in *twi* RNAi embryos.

All *twi* RNAi embryos formed a normally appearing primary thickening region around 28 Hael, despite the delayed initiation (D2, E2, F2, G2, H2, I2). Some *twi* RNAi embryos (G2, I2) displayed a smaller primary thickening region compared to WT embryos, while others (D2, F2) did not. I attributed this variation to spider-specific factors and will not discuss it further.

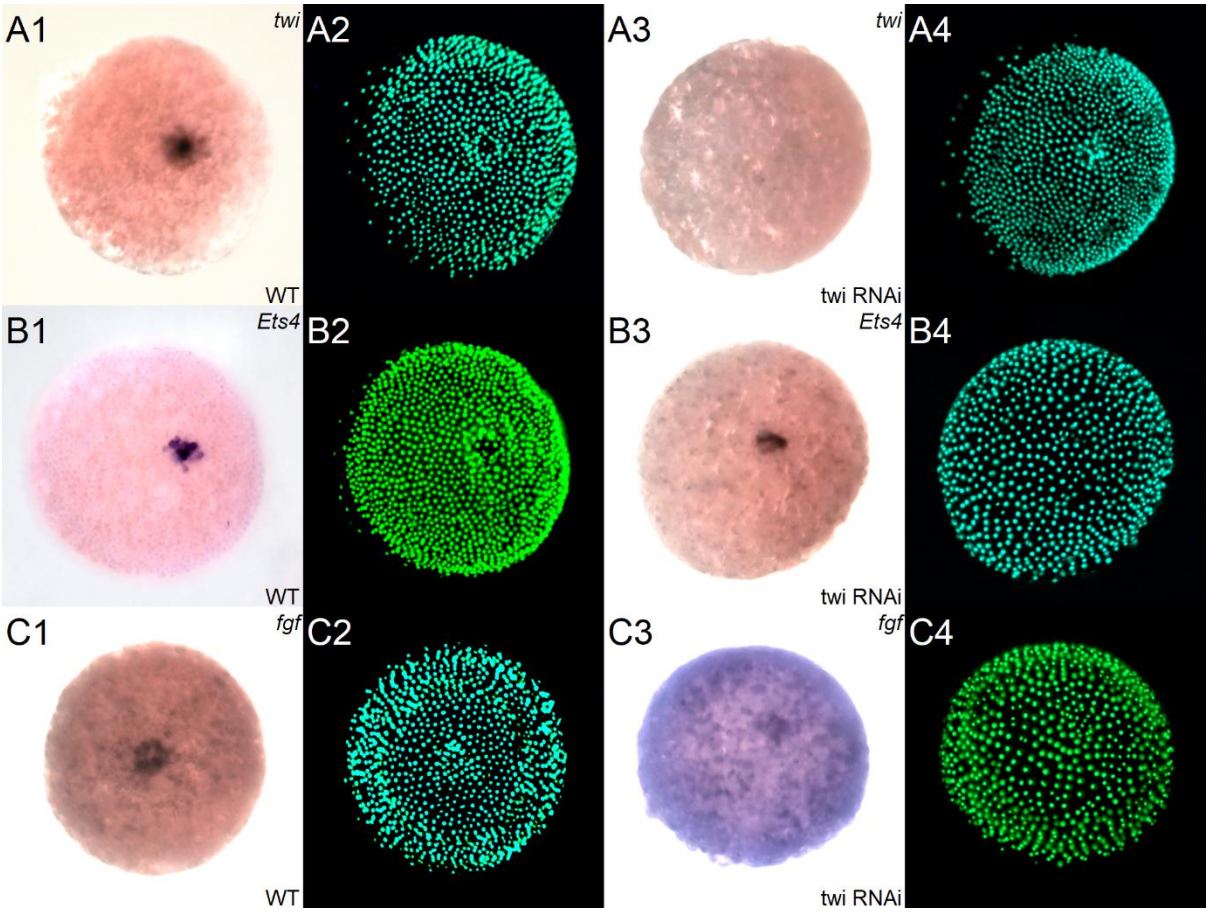

Figure 4-10. Expression of gene *twi*, *Ets4*, *fgf8* in WT and *twi* RNAi embryo at stage 4. A1-A2, B1-B2, C1-C2: WT embryo. A3-A4, B3-B4, C3-C4: *twi* RNAi embryo. A1-A4: *twi*. B1-B4: *Ets4*. C1-C4: *fgf8*. A2, B2, C2, A4, B4, C4: sytox.

In some *twi* RNAi embryos, I also observed that the primary thickening region was smaller or delayed in its congregation process. Figure 4-10 showed the expression for the genes *twi* (A1-A4), *Ets4* (B1-B4), and *fgf8* (C1-C4) in WT (A1, A2, B1, B2, C1, C2) and *twi* RNAi (A3, A4, B3, B4, C3, C4) embryos. The Sytox staining of both types of embryos (A2, A4, B2, B4, C2, C4) offered a clearer view of the primary thickening region. Some *twi* RNAi embryos in these images showed a primary thickening region that is difficult to discern (B4, C4).

Figure 4-10 also showed that the *twi* gene was not detected in *twi* RNAi embryos (A3), confirming the reliability of the RNAi experiment. The expression of *Ets4* and *fgf8* was similar in both WT and *twi* RNAi embryos (B1, B3; C1, C3).

In addition, there was some extra information regarding the process of primary thickening formation. Firstly, the primary thickening region of some *twi* RNAi embryos originated from fewer cells at the 32-cell stage, or even just a single cell at the 32-cell stage (Supplementary Figure S4-5). Secondly, HCR staining suggested that *Ets4*+ cells in *twi* RNAi embryos were neither closely connected to each other nor located within the surrounding *Ets4*- cells, with the total number of *Ets4*+ cells even being fewer than five (Supplementary Figure S4-6). Thirdly, multiple inner cells were observed in some *twi* RNAi embryos at stages 3-4, with only one of the multiple inner regions showing *Ets4*+ expression (Supplementary Figure S4-7, S4-8). This phenomenon was also observed in WT embryos (Chapter I, section 4, supplementary Figure S1-26) at a ratio of approximately 1/60, while in *twi* RNAi embryos, the ratio was around 1/29. These observations were made from one or two batches of *twi* RNAi embryos. As of now, I could not confirm whether these conclusions apply to all *twi* RNAi embryos.

4.3.4 Some *twi* RNAi embryos, which lacked cumulus migration, developed into radially-symmetric, tube-like structures.

As stated in Table 4-1, 10-35% of *twi* RNAi embryos across all batches exhibited no cumulus migration or delayed cumulus migration at stage 5, while the remaining embryos resembled WT embryos.

Figure 4-11 showed several selected *twi* RNAi embryos (B1-B4, C1-C4, D1-D4, E1-E4) at stages 5 to 6, along with one WT embryo (A1-A4) and one *Ets4* RNAi (F1-F4) embryo for comparison. The *twi* RNAi embryos in B1-B4 and C1-C4 displayed a WT-like process of cumulus migration at stage 5 (B1-B2, C1-C2) and the opening of the germ disc at stage 6 (B3, C3). The embryo in C4 also showed upward growth of the posterior region during dorsal opening, which contrasted with the WT embryo (A4) and the *twi* RNAi embryo in B4.

The *twi* RNAi embryos in D1-D4 and E1-E4 showed no cell movement from the primary thickening region at stage 5 (D1, D2, E1, E2). From the beginning of stage 6, some cells from the primary thickening region began to move in various directions (D3, E3), and both embryos grew upwards into a tube-like structure simultaneously (D4, E4). This was slightly different from the development observed in *Ets4* RNAi embryos in F1-F4. These embryos typically exhibited a dispersal of cells from the primary thickening region (cumulus) during the first half of stage 5 (F2). The outgrowth of the posterior region in *Ets4* RNAi embryos also began at stage 6 (F3, F4), forming a tube-like structure similar to the *twi* RNAi embryos (Pechmann et al., 2017).

I did not yet understand the differences between *twi* RNAi embryos that showed cumulus migration and those that do not. It seemed that the size of the primary thickening region was not a determining factor. For example, the primary thickening region in the embryo shown in B1 was quite small but eventually migrates along a clear path (B3), while in embryos D1 and E1, the primary thickening region was large, yet no cell migration was observed in later stages (D2, E2).

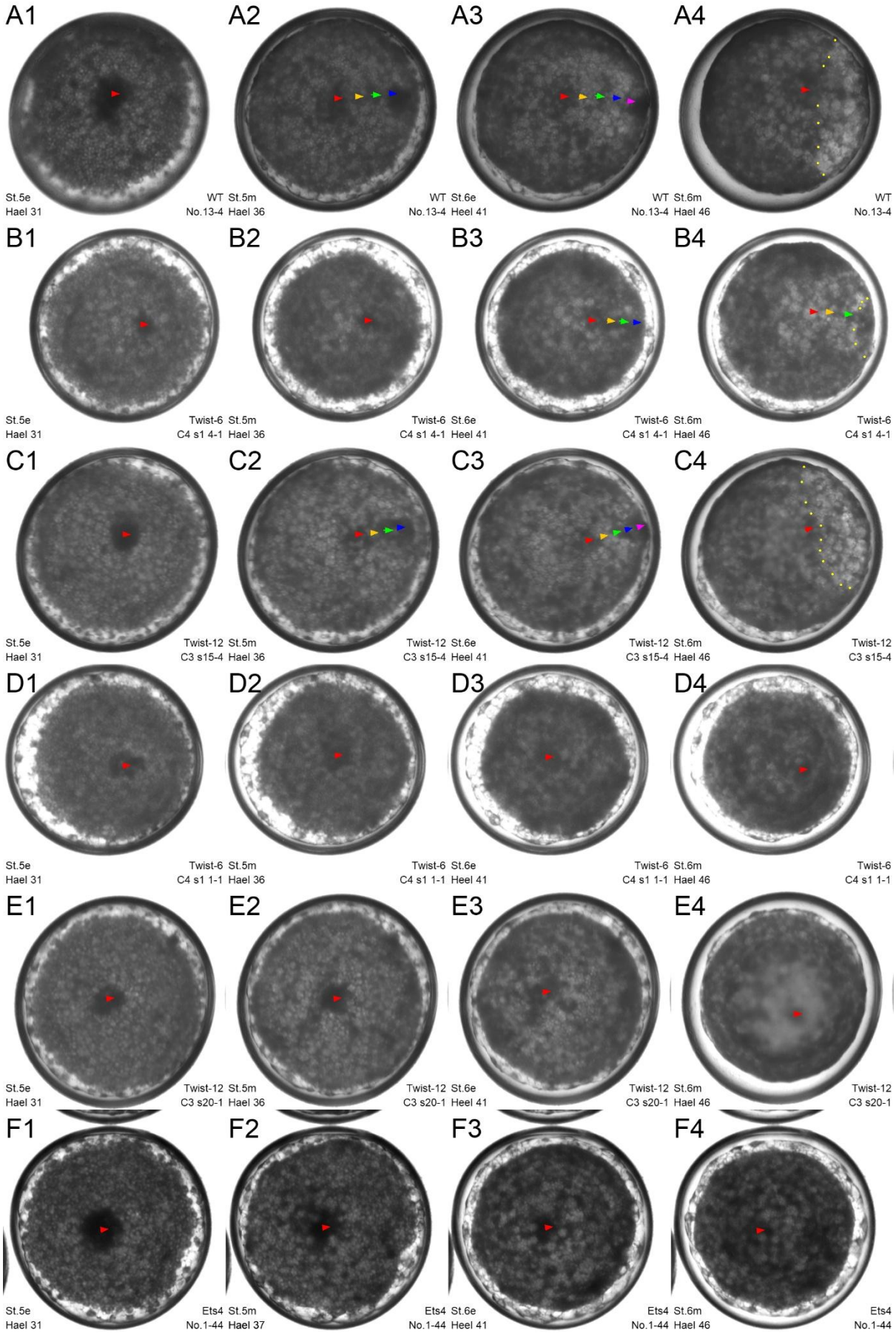
A1
St.5e
Hael 31
WT
No.13-4
A2
St.5m
Hael 36
WT
No.13-4
A3
St.6e
Heel 41
WT
No.13-4
A4
St.6m
Hael 46
WT
No.13-4
B1
St.5e
Hael 31
Twist-6
C4 s1 4-1
B2
St.5m
Hael 36
Twist-6
C4 s1 4-1
B3
St.6e
Heel 41
Twist-6
C4 s1 4-1
B4
St.6m
Hael 46
Twist-6
C4 s1 4-1
C1
St.5e
Hael 31
Twist-12
C3 s15-4
C2
St.5m
Hael 36
Twist-12
C3 s15-4
C3
St.6e
Heel 41
Twist-12
C3 s15-4
C4
St.6m
Hael 46
Twist-12
C3 s15-4
D1
St.5e
Hael 31
Twist-6
C4 s1 1-1
D2
St.5m
Hael 36
Twist-6
C4 s1 1-1
D3
St.6e
Heel 41
Twist-6
C4 s1 1-1
D4
St.6m
Hael 46
Twist-6
C4 s1 1-1
E1
St.5e
Hael 31
Twist-12
C3 s20-1
E2
St.5m
Hael 36
Twist-12
C3 s20-1
E3
St.6e
Heel 41
Twist-12
C3 s20-1
E4
St.6m
Hael 46
Twist-12
C3 s20-1
F1
St.5e
Hael 31
Ets4
No.1-44
F2
St.5m
Hael 37
Ets4
No.1-44
F3
St.6e
Heel 41
Ets4
No.1-44
F4
St.6m
Hael 46
Ets4
No.1-44

Figure 4-11. Development of WT (A1-A4), *twi* RNAi (B1-B4, C1-C4, D1-D4, E1-E4), and *Ets4* RNAi (F1-F4) embryos at stage 5 to stage 6. B1-B4 and D1-D4: embryo from *twi*-6 C4. C1-C4 and E1-E4: embryo from *twi*-12 C3. A1, B1, C1, D1, E1, F1: 31 hael, stage 4/5. A2, B2, C2, D2, E2: 36 hael, stage 5. F2: 37 hael, stage 5. A3, B3, C3, D3, E3, F3: 41 hael, stage 5/6. A4, B4, C4, D4, E4, F4: 46 hael, stage 6. Red arrowhead: primary thickening region or posterior region. Orange, green, blue and magenta arrow head: cumulus migration path. Yellow dot: border of embryonic and extraembryonic region.

So far, all *twi* RNAi embryos observed with no cumulus migration developed into tube-like structures. *twi* RNAi embryos with delayed cumulus migration (B2) or those exhibiting an upward growth of the posterior region during stage 6 along with dorsal opening (C4) could be considered intermediate or mild phenotypes of the process. However, I am still uncertain about the ratio of these types of embryos.

Figure 4-12 showed *in situ* hybridization images at stage 5 of *twi* RNAi embryos with cumulus migration (A2-D2) and those without the process of cumulus migration (A3-D3). In both types, the expression of the *twi* gene was weak or difficult to discern (A2, A3). Compared to the expression in WT embryos (A1), the *twi* gene was effectively knocked down in the *twi* RNAi embryos at this stage.

In *twi* RNAi embryos with cumulus migration, *Ets4* expression was detected in the cumulus cells (B2), similar to WT embryos (B1). *fgf8* expression was found in the frontal cells ahead of the migrating cumulus, as well as in other germ disc cells (C2), similar to WT embryos (C1). Additionally, *sog* expression formed a ring shape in the germ disc, with an opening directed towards the cumulus migration path in this type of *twi* RNAi embryo (D2), as seen in WT embryos (D1).

In *twi* RNAi embryos that showed no cumulus migration, *Ets4*+ cells were primarily located at the center of the germ disc (B3). *fgf8* expression was observed in other regions of the germ disc (C3), and *sog* was expressed in a complete ring-shaped region with no opening (D3). All three genes displayed different expression patterns in the no-migration type of *twi* RNAi embryos compared to WT embryos. Specifically, the differences in expression patterns were observed in: the cumulus itself (B1, B3), the region ahead of the cumulus cells (C1, C3), and the region adjacent to the migration path (D1, D3). Expression in other regions of the germ disc remained similar in *twi* RNAi embryos and WT embryos (C1, C3; D1, D3).

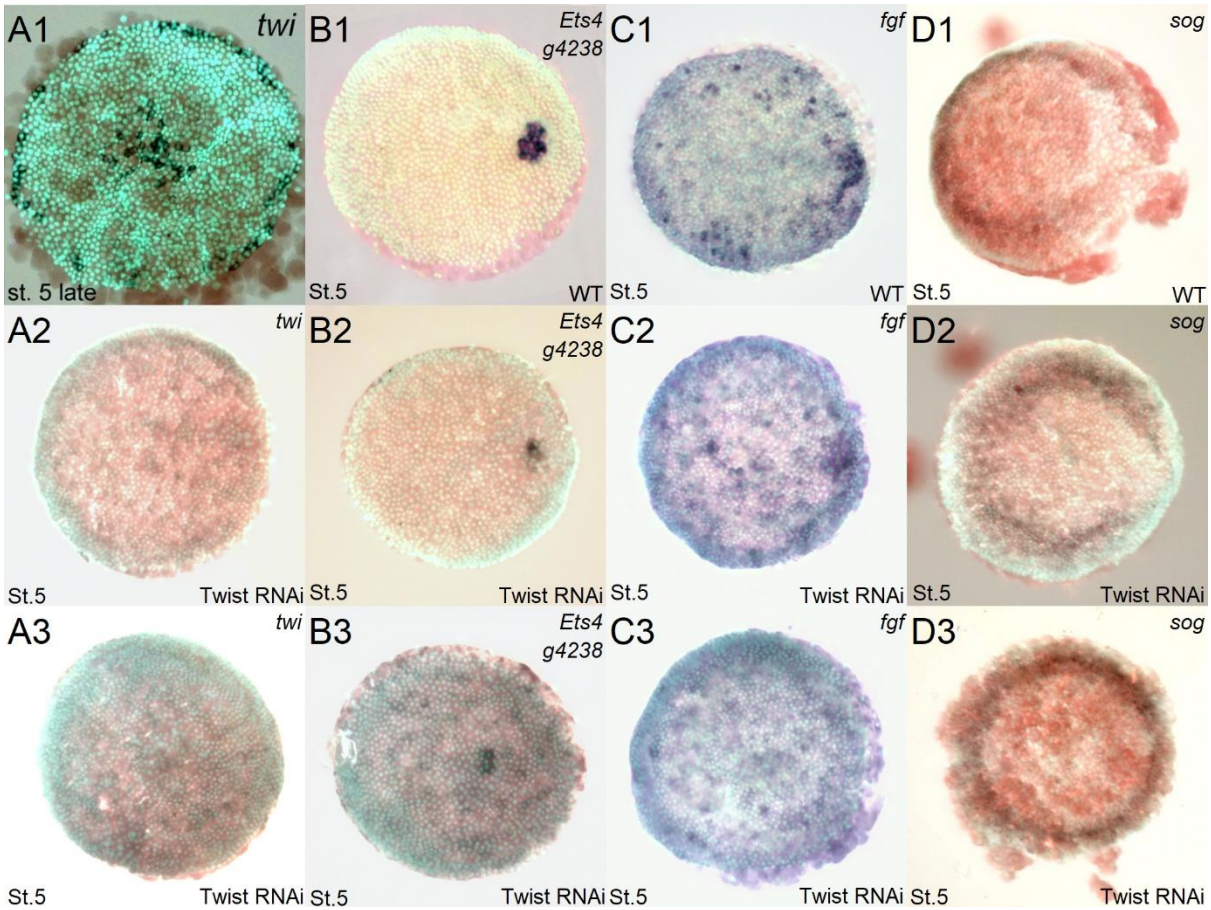

Figure 4-12. Expression of *twi*, *Ets4*, *fgf8* and *sog* in WT and *twi* RNAi embryos at stage 5. A1, B1, C1, D1: WT embryo. A2, B2, C2, D2: *twi* RNAi embryo with cumulus migration. A3, B3, C3, D3: *twi* RNAi embryo without cumulus migration. A1-A3: *twi*. B1-B3: *Ets4*. C1-C3: *fgf8*. D1-D3: *sog*.

From Figure 4-12 B1-B3, it appeared that the *Ets4*+ cell cluster is smaller in both types of *twi* RNAi embryos compared to WT embryos. This suggested a reduced number of cumulus cells, which may or may not be able to migrate, in *twi* RNAi embryos at stage 5.

In addition, WT embryos and *twi* RNAi embryos with cumulus migration exhibited bilateral symmetry in their gene expression patterns (*twi*, *Ets4*, *fgf*, *sog*) at stage 5. In contrast, *twi* RNAi embryos with no cumulus migration maintain radial symmetry at this stage.

In situ hybridization images showed that the *twi* RNAi tube was segmented in a radially symmetric manner (Figure 4-13, A3, B3) and expressed the gene *sog* weakly and ubiquitously (B3). This resembled the characteristic of a “ventral tube”, similar to the *Ets4* RNAi tube (Pechmann et al., 2017, Figure 4-13 B2) and the *fgf* RNAi tube (Wang et al., 2023) at this stage. Further comparisons will be discussed in Discussion section. The *twi* gene was expressed weakly in *twi* RNAi embryos at the tube stage.

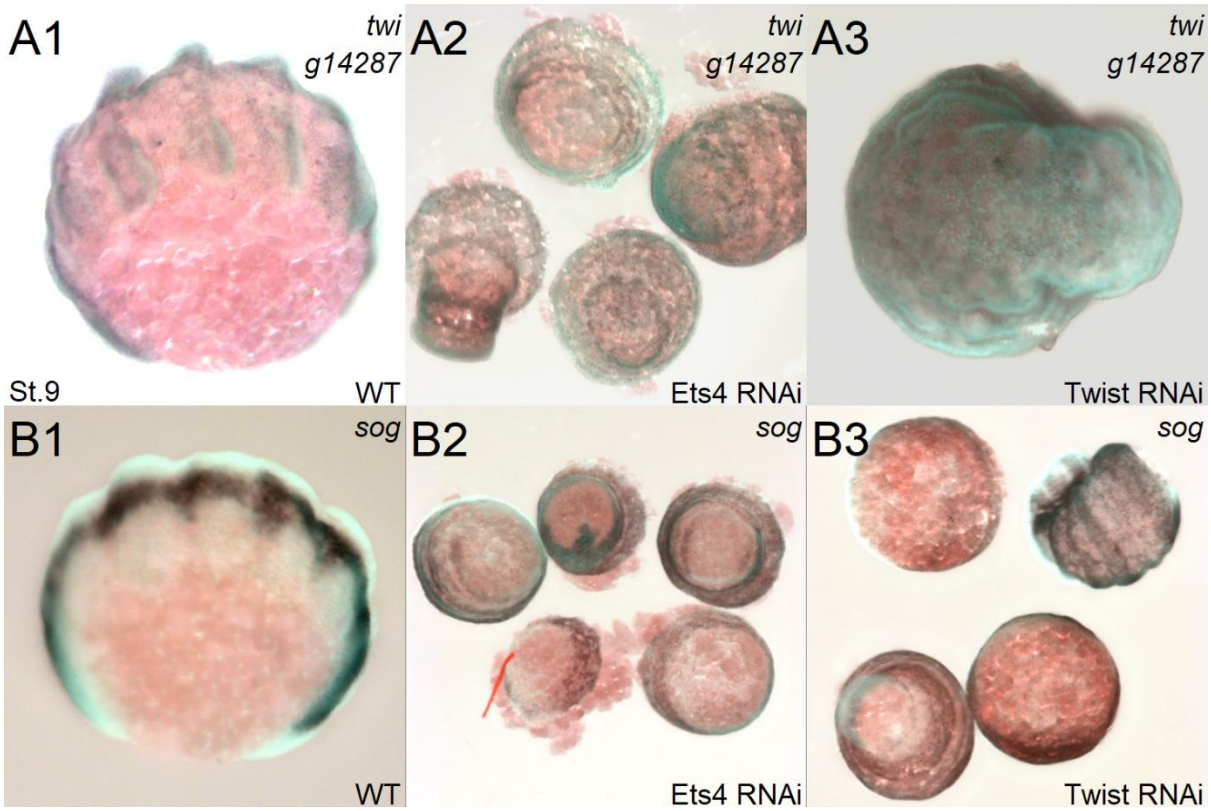

Figure 4-13. Expression of *twi* and *sog* in WT, *Ets4* RNAi tube, and *twi* RNAi tube. A1, B1: WT embryo at stage 8 and stage 9. A2, B2: *Ets4* RNAi tube. A3, B3: *twi* RNAi tube. A1-A3: *twi*. B1-B3: *sog*.

4.4 Summary of observations in *twi* RNAi embryos and analysis of the function of *twi*.

RNAi experiments targeting new dsRNA of the *twi* gene produced embryos with a tube phenotype at a low rate. Although different batches of *twi* RNAi embryos exhibited various specificities, they consistently showed a delayed initiation of invagination at stage 3, elongation at stage 4, and 10-30% inhibition of cumulus migration at stage 5, leading to the formation of a tube. It remained unclear whether these observations are independent cases or a cause-and-effect relationship.

It appeared that only by 21 hael, or even 24 hael, could enough primary thickening-relevant cells cluster tightly enough in *twi* RNAi embryos. The current hypothesis was that the loss of the *twi* gene might impair cell adhesion, invagination or the differentiation process from *fuchi* na+ *Ets4* na+ cells to *fuchi* (weak), *Ets4* (weak) cells.

As a consequence, it was reasonable to assume that the cell arrangement in the primary thickening region may differ between *twi* RNAi embryos and WT embryos. Possible defects in cell adhesion, the number and location of $Ets4^{+}$ and $Ets4^{-}$ cells, and responses to external signals may prolong stage 4 and impair the movement of cumulus cells under *twi* knockdown conditions. In extreme cases, a small proportion of *twi* RNAi embryos exhibited defects in cumulus migration. Additional experiments were needed to gain a better understanding.

5 *Abhd11* RNAi

5.1 Expression of *Abhd11 g9727* in WT and *Ets4* RNAi embryo.

In other species, the gene *Abhd11* was associated with certain developmental diseases, as well as the expansion and differentiation of embryonic stem cells. In vitro experiments suggested that this protein was involved in the hydrolysis of DAG (diacylglycerol) and may regulate lipid metabolism.

Of the spider transcriptome, transcript *g9721*, *g9726*, *g9727*, *g9729*, *g23929.t2*, *g3607* were annotated as *Abhd11*. The expression patterns of these transcripts in WT embryos varied. *Abhd11 g9727* was expressed ubiquitously at stage 2, then in primary thickening cells and some other germ disc cells at stage 4 (Fig. XXX). No expression for this gene was detected at stages 5 and 7. It was classified as a type II gene in Chapter III (Chapter III, Figure 3-9, B1 to B4).

The *Abhd11 g9727* gene was not expressed in the primary thickening region of *Ets4* RNAi embryos at stage 4 (Chapter III, Figure 3-21, B4). Therefore, this gene was considered to be downstream of the *Ets4* gene.

5.2 *Abhd11 g9727* RNAi experiment and characteristics of *Abhd11* RNAi embryos.

I performed only one batch of RNAi injection for the *Abhd11 g9727* gene, using two spiders. The fourth cocoon from both spiders showed holes in the germ disc at stages 3 to 4 (Figure 4-14 C, D), with a penetration rate of approximately 50%. These embryos showed no differences compared to WT embryos in later developmental stages.

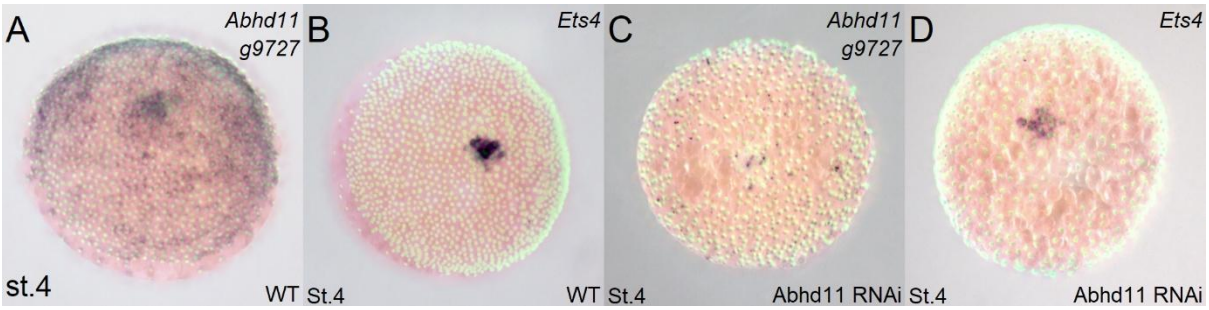

Figure 4-14. Expression of gene *Abhd11 g9727* and *Ets4* in WT and *Abhd11* RNAi embryo at stage 4. A, B: WT embryo. C, D: *Abhd11* RNAi embryo. A, C: *Abhd11*. B, D: *Ets4*.

Figure 4-14 showed no expression of *Abhd11 g9727* in the *Abhd11* RNAi embryos, confirming the successful knockdown of the gene. The *Ets4* gene was expressed in the primary thickening region of the *Abhd11* RNAi embryos, similar to its expression in WT embryos.

5.3 Analysis on the function of gene *Abhd11 g9727* based on *Abhd11* RNAi experiments.

It appears that the loss of *Abhd11 g9727* led to incomplete formation of the germ disc, though the effect is mild and non-lethal. The holes in the germ discs may result from defects in cell proliferation, cell adhesion, yolk exclusion, or other processes. Additional experiments were needed to confirm these observations and investigate the underlying mechanisms further.

The *in situ* hybridization images suggested that *Abhd11 g9727* is regulated by Ets4 in the primary thickening region around stage 4. Given that *Ets4* was activated at stage 3, the expression of *Abhd11 g9727* at stage 2 was likely controlled by other genes or pathways.

6 *Itpka* RNAi

6.1 Expression of gene *Itpka* in WT and *Ets4* RNAi embryo.

In other species, the *Itpka* (*Itpkb*) gene was associated with inositol phosphate metabolism and functions in the regulation of phosphorylation. It may influence various relevant cell signaling processes in spider embryos.

In *P. tepidariorum*, *Itpka* was detected starting at stage 3 in the primary thickening cells. It was expressed in migrating cumulus cells at stage 5. The gene was classified as a type IV gene in Chapter III. No expression was detected at stage 8, though some regions in the appendages may express *Itpka* at stage 9 (Chapter III, Figure 3-13, C1 to C4).

In *Ets4* RNAi embryos, *Itpka* was not expressed at stages 3, 4, and 5 (Chapter III, Figure 3-23, C4). This suggests that *Itpka* was a downstream gene of *Ets4* in the primary thickening region.

6.2 *Itpka* RNAi experiment and characteristics of *Itpka* RNAi embryos.

I conducted multiple batches of *Itpka* RNAi injections, involving at least six spiders. The first cocoon typically produced embryos in good condition, with a high ratio of WT-like embryos, while embryos from the third and fourth cocoons tended to cluster together. The most common and notable phenotype in *Itpka* RNAi embryos was defects in the germ band, which was either too short, too narrow, or exhibits an abnormal rotation angle. Additionally, some other defects were observed in specific batches of *Itpka* RNAi embryos, which were listed in Supplementary Table S4-3.

The development of 96 embryos from the *Itpka*-8 C3 cocoon was recorded in time-lapse images from stage 3 to stage 8. Embryos from this spider exhibited a slightly higher ratio of severe phenotypes compared to the average.

Figure 4-15 showed images of one WT embryo (A1-A6) and three *Itpka* RNAi embryos (B1-B6, C1-C6, D1-D6) from stages 5 to 8. Additional images of these three *Itpka* RNAi embryos at stages 8 to 9 could be found in Supplementary Figure S4-9. For clarity, all embryos were rotated so that the cumulus migration was oriented towards the 12:00 direction.

The WT embryo in Figure 4-15 shows a symmetrical process of dorsal opening from stage 6 (A2-A6). Cells along the symmetric axis move forward in unison, while cells off the axis move at the same speed as their mirror counterparts. Different regions of the entire germ disc coordinate their movement, ensuring the embryonic region remains bilaterally symmetric.

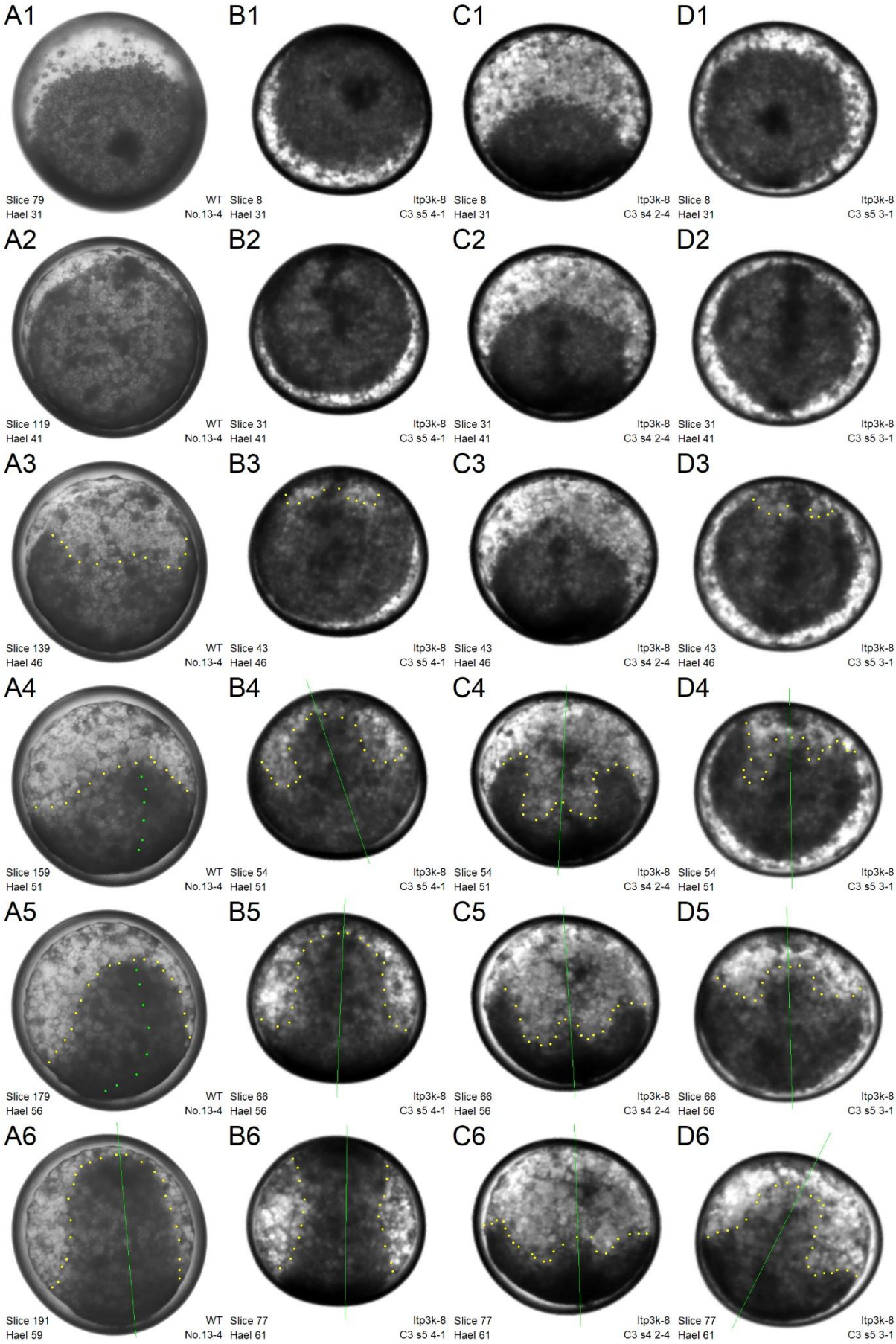
A1
Slice 79
Hael 31
WT
No.13-4
B1
Slice 8
Hael 31
Itp3k-8
C3 s5 4-1
C1
Slice 8
Hael 31
Itp3k-8
C3 s4 2-4
D1
Slice 8
Hael 31
Itp3k-8
C3 s5 3-1
A2
Slice 119
Hael 41
WT
No.13-4
B2
Slice 31
Hael 41
Itp3k-8
C3 s5 4-1
C2
Slice 31
Hael 41
Itp3k-8
C3 s4 2-4
D2
Slice 31
Hael 41
Itp3k-8
C3 s5 3-1
A3
Slice 139
Hael 46
WT
No.13-4
B3
Slice 43
Hael 46
Itp3k-8
C3 s5 4-1
C3
Slice 43
Hael 46
Itp3k-8
C3 s4 2-4
D3
Slice 43
Hael 46
Itp3k-8
C3 s5 3-1
A4
Slice 159
Hael 51
WT
No.13-4
B4
Slice 54
Hael 51
Itp3k-8
C3 s5 4-1
C4
Slice 54
Hael 51
Itp3k-8
C3 s4 2-4
D4
Slice 54
Hael 51
Itp3k-8
C3 s5 3-1
A5
Slice 179
Hael 56
WT
No.13-4
B5
Slice 66
Hael 56
Itp3k-8
C3 s5 4-1
C5
Slice 66
Hael 56
Itp3k-8
C3 s4 2-4
D5
Slice 66
Hael 56
Itp3k-8
C3 s5 3-1
A6
Slice 191
Hael 59
WT
No.13-4
B6
Slice 77
Hael 61
Itp3k-8
C3 s5 4-1
C6
Slice 77
Hael 61
Itp3k-8
C3 s4 2-4
D6
Slice 77
Hael 61
Itp3k-8
C3 s5 3-1

Figure 4-15. Development images of WT and *Itpka* RNAi embryos from stage 5 to stage 8. A1-A6: WT embryo, No. 13-4. B1-B6, C1-C6, D1-D6: *Itpka* RNAi embryo, No. s5 4-1, s4 2-4, s5 3-1. A1, B1, C1, D1: 31 Hael, stage 4/5. A2, B2, C2, D2: 41 Hael, stage 5/6. A3, B3, C3, D3: 46 Hael, stage 6. A4, B4, C4, D4: 51 Hael, stage 6/7. A5, B5, C5, D5: 56 Hael, stage 7/8. A6, B6, C6, D6: around 61 Hael, stage 8. Yellow dots mark the boundary of embryonic-extraembryonic region. Green dots and green lines mark the symmetric axis of the embryo.

Some *Itpka* RNAi embryos (B1-B6) exhibited a similar symmetry to that seen in WT embryos. They also took the same amount of time at different stages, similar to WT embryos (as shown in the supplementary Table S4-1). Out of the 36 embryos in the video with a clear view of the dorsal opening process, 7 embryos fall into this category.

Most *Itpka* RNAi embryos in this video resembled the embryos shown in images C1-C6 and D1-D6. Both embryos were bilaterally symmetric at stage 5 (C1-C3, D1, D2). However, at stage 6, cells on the two sides of the germ disc moved at different speeds (C5, C6, D4-D6). This results in the loss of bilateral symmetry and even led to the formation of an asymmetric germ band (Supplementary Figure S4-9 B6, C6). Supplementary Figures S4-10 and S4-11 provided additional images of *Itpka* RNAi embryos exhibiting defects in the symmetry of cell movement at stage 6. In some embryos, one side of the germ disc leads, rather than the posterior region, led the future germ band (Supplementary Figure S4-10 C4).

These *Itpka* RNAi embryos typically spent much longer at stages 6 and 7 compared to WT embryos or WT-like *Itpka* RNAi embryos (Figure 4-15, C6, C6). Additionally, the yolk regions of many *Itpka* RNAi embryos appeared disorganized.

The expression of *Itpka* RNAi embryos from stage 7 to stage 9 provided a clearer view of the defects in germ band formation in these embryos.

Figure 4-16 and Supplementary Figure S4-12 showed the expression of the genes *Itpka*, *hh*, *otd*, *opa*, *sog*, *twi*, and *Wnt* in WT and *Itpka* RNAi embryos at stages 7 to 10. In general, the *Itpka* RNAi embryos at this stage exhibited obvious abnormalities in the size and shape of the germ band, including regional rotation (Figure 4-16 I4), asymmetry (Figure 4-16 B2, Supplementary Figure S4-12 B2, F2), being too short (Figure 4-16 A2, C2, I2, Supplementary Figure S4-12 E2), being too long (Figure 4-16 F2, Supplementary Figure S4-12 D2), head and tail not attaching (Supplementary Figure S4-12 G2, D2), being too narrow (Supplementary Figure S4-12 F2), uneven broadness (Supplementary Figure S4-12 H2), and uneven expression of genes in body segments (Figure 4-16 D2).

In addition, even the WT-like *Itpka* RNAi embryos showed a delay in splitting the left and right sides around stage 9. Figure 4-16 C1, C2; E2, E3; and I3, I4 showed a pair of WT and *Itpka* RNAi embryos at approximately the same stage. When the gene expression splited into two sides in WT embryos, the expression in *Itpka* RNAi embryos remained connected. This delay was observed in the anterior (C1, C2), middle (E2, E3), and posterior (I3, I4) regions of different *Itpka* RNAi embryos.

Previous publications showed a similar phenotype in *sog* RNAi embryos, which was considered a delay in the development of ventral midline-related structures, referred to as a 'dorsalized' germ band. The expression of *sog* and *otd* in the germ band of *Itpka* RNAi embryos suggested that a similar phenomenon might be occurring (Figure 4-16 F1, F2; G1, G2).

Moreover, the very posterior segment of many *Itpka* RNAi embryos showed differences compared to WT embryos (Figure 4-16 C1, C2; E1, E4), which could be a secondary effect following the germ band defects. Additionally, the yolk granules in some *Itpka* RNAi embryos were unusually large, and

a few extraembryonic cells can be observed in this region, which differed from WT embryos (Figure 4-16 A2, Supplementary Figure S4-12 A2, C2)

In summary, the germ band of *Itpka* RNAi embryos exhibited numerous abnormalities in size, shape, and gene expression across different segments. Some *Itpka* RNAi embryos showed a delay in the formation of ventral structures. Additionally, the extraembryonic region may also be affected.

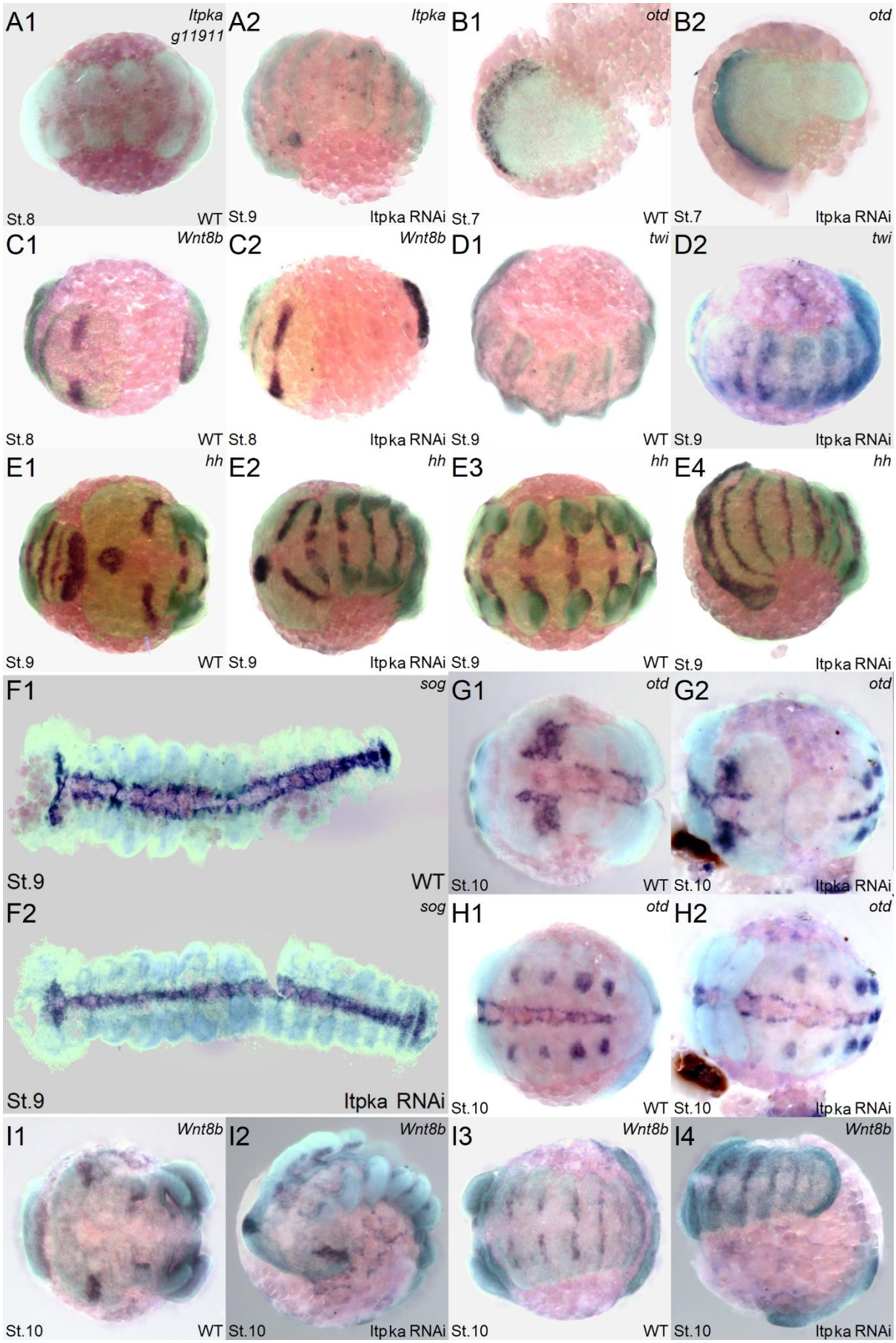
A1
Itpka g11911
St.8
WT
A2
Itpka
St.9
Itpka RNAi
B1
otd
St.7
WT
B2
otd
St.7
Itpka RNAi
C1
Wnt8b
St.8
WT
C2
Wnt8b
St.8
Itpka RNAi
D1
twi
St.9
WT
D2
twi
St.9
Itpka RNAi
E1
hh
St.9
WT
E2
hh
St.9
Itpka RNAi
E3
hh
St.9
WT
E4
hh
St.9
Itpka RNAi
F1
sog
St.9
WT
F2
sog
St.9
Itpka RNAi
G1
otd
St.10
WT
G2
otd
St.10
Itpka RNAi
H1
otd
St.10
WT
H2
otd
St.10
Itpka RNAi
I1
Wnt8b
St.10
WT
I2
Wnt8b
St.10
Itpka RNAi
I3
Wnt8b
St.10
WT
I4
Wnt8b
St.10
Itpka RNAi

Figure 4-16. Expression of gene *Itpka*, *hh*, *otd*, *opa*, *sog*, *twi* and *Wnt8b* in WT and *Itpka* RNAi embryo at stage 7 to stage 10. A1, B1, C1, D1, E1, E3, F1, G1, H1, I1, I3: WT embryo. A2, B2, C2, D2, E2, E4, F2, G2, H2, I2, I4: *Itpka* RNAi embryo. A1-A2: *Itpka*. B1-B2, G1-G2, H1-H2: *otd*. C1-C2, I1-I4: *Wnt8b*. D1-D2: *twi*. E1-E4: *hh*. F1-F2: *sog*.

At an earlier stage, 40 out of 96 *Itpka* RNAi embryos in the video did not rotate the germ disc to the frontal view at stage 4 (Supplementary Figure S4-13). This rate was higher than that observed in WT embryos. Some *Itpka* RNAi embryos also showed a certain level of unevenness in the nucleus distribution within the germ disc (Supplementary Figure S4-14). Additionally, *in situ* hybridization images of *Itpka* RNAi embryos at stage 4 often displayed numerous unspecific staining dots (Supplementary Figure S4-15), which may result from a disorganized yolk region.

However, most *Itpka* RNAi embryos (87 out of 96) developed to the germ band stage, with the majority progressing through all developmental stages in a time frame similar to that of WT embryos (Supplementary Table S4-1). The gene expression patterns of *Ets4*, *Wnt8b*, *Clca4*, and *hh* in *Itpka* RNAi embryos at stage 4 were comparable to those in WT embryos (Supplementary Figure S4-15). Notably, only *Itpka* gene expression was absent in *Itpka* RNAi embryos, confirming the effectiveness of the gene knockdown.

6.3 Analysis the function of gene *Itpka* based on *Itpka* RNAi experiments.

In WT embryos, the *Itpka* gene was expressed in the primary thickening region from stage 3 to 4 and in the cumulus region at stage 5. It was surprising that *Itpka* RNAi embryos exhibited severe germ band defects at a very high penetration rate. It was almost certain that the loss of the *Itpka* gene in cumulus cells disrupted the unified and coordinated movement of surrounding cells along the cumulus migration path during the dorsal opening process in later stages. However, the molecular mechanism underlying this effect remained unknown.

The delay in ventral structure formation at stage 9 in some *Itpka* RNAi embryos could be a secondary effect of abnormal germ band formation or a distinct new effect. Additionally, *Itpka* was highly likely to play a role in yolk or embryonic-extraembryonic connections, as well as in embryo production, potentially preventing embryos from clustering.

7 *Znf423* RNAi

7.1 Expression of gene *Znf423* in WT and *Ets4* RNAi embryos.

In other species, the gene *Znf423* was expressed in the nucleus and functions as a transcription factor. It may associate the downstream genes in the BMP pathway, regulating cell proliferation, differentiation, and maturation during the development of certain neural tissues.

In spider, the *Znf423* gene was expressed in the primary thickening region at stages 3 and 4. At stage 5, its expression was observed in cumulus cells and at the rim of the germ disc. From stages 8 to 9, *Znf423* was detected in a segmental pattern across multiple segments, including both anterior and posterior regions. At stages 9 and 13, it was expressed at the tips of appendages. The expression pattern of *Znf423* at stages 6 and 7 remained unknown (Result Chapter III, Figure 3-13, G1 to G4).

The *Znf423* gene was not detected in *Ets4* RNAi embryos at stage 4 (Result Chapter III, Figure 3-23, G4), suggesting that it was regulated by Ets4.

7.2 *Znf423* RNAi experiment and characteristics of *Znf423* RNAi embryos.

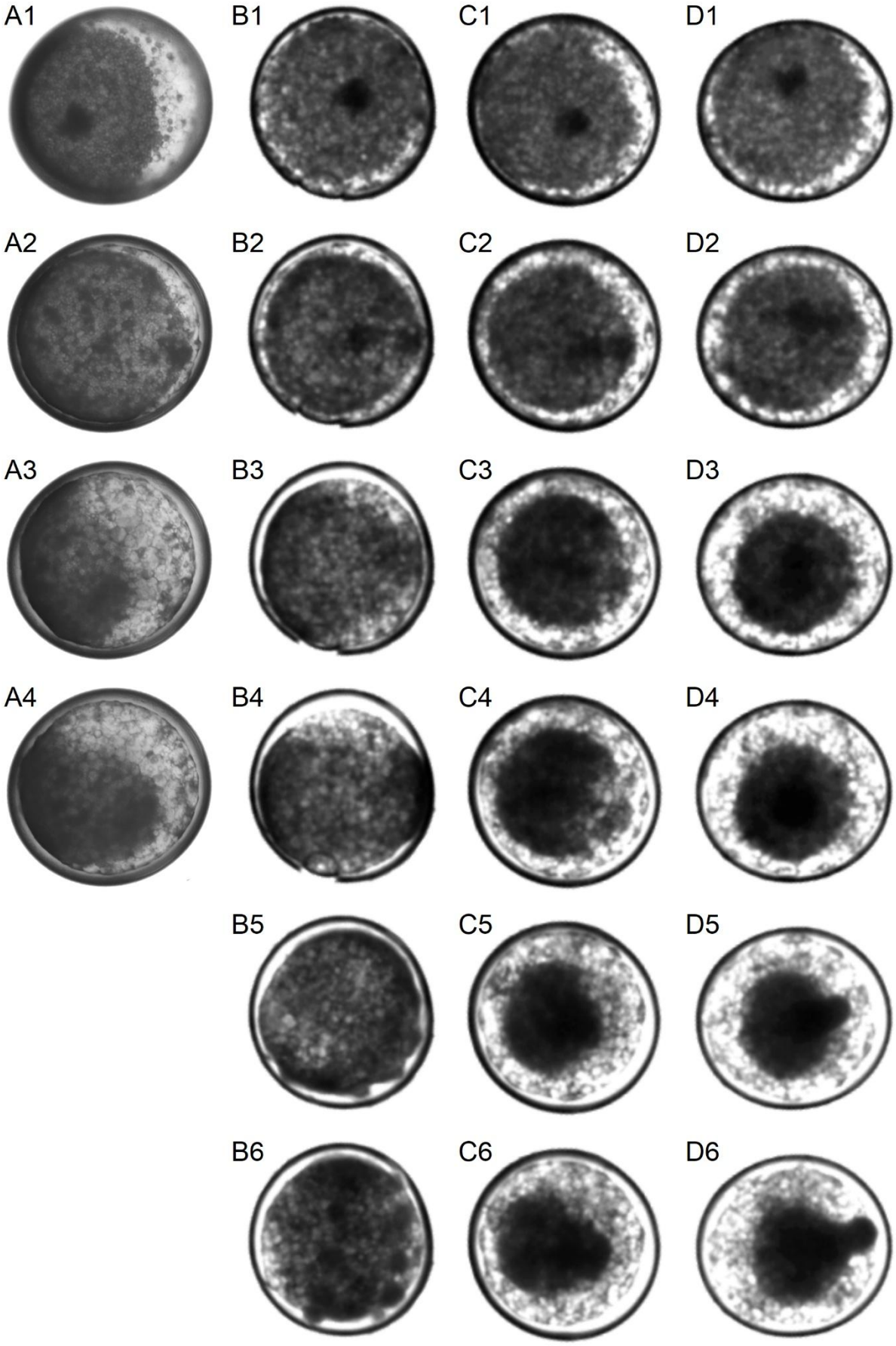
A1
B1
C1
D1
A2
B2
C2
D2
A3
B3
C3
D3
A4
B4
C4
D4
B5
C5
D5
B6
C6
D6

Figure 4-17. Development images of WT and *Znf423* RNAi embryos at stage 4 to stage 10. A1-A4: WT embryo, No. 13-4. B1-B6, C1-C6, D1-D6: *Znf423* RNAi embryo, No. s1 1-2, S1 2-1, s2 3-3. A1-A4: frame 79, 119, 159, 179, respectively. B1, C1, D1: frame 23. B2, C2, D2: frame 46. B3, C3, D3: frame 69. B4, C4, D4: frame 80. B5, C5, D5: frame 126. B6, C6, D6: frame 149. A1, B1, C1, D1: Hael 31. A2, B2, C2, D2: Hael 41. A3, B3, C3, D3: Hael 51. A4, B4, C4, D4: Hael 56. B5, C5, D5: Hael 76. B6, C6, D6: Hael 86. All the embryos were rotated in the position with cumulus migrate to the right, for better comparison.

I conducted a single batch of *Znf423* RNAi injections and recorded observations from cocoons of two spider. Most RNAi embryos exhibited a WT-like development process, while some embryos died at the germ disc stage. A small percentage of RNAi embryos showed germ disc contraction at stage 5, which later developed into a small tube.

Besides the lack of replicates, our current *Znf423* RNAi experiment results were incomplete. The videos and *in situ* hybridization images in this section were from the 5th cocoon of spider *Znf423*-1. In the video, 44 out of 64 embryos were WT-like, 18 out of 64 formed small tubes, and 2 out of 64 had other defects. The lethal type of *Znf423* RNAi embryos recorded in earlier cocoons was mostly absent.

Figure 4-17 showed a WT embryo (A1-A4) and three *Znf423* RNAi embryos (B1-B6, C1-C6, D1-D6) from stage 4 to stage 10. The *Znf423* RNAi embryo in images B1-B6 showed a development process resembling the WT embryo, with a similar time cost for each developmental stage (Supplementary Table S4-1).

The other two *Znf423* RNAi embryos progressed at the same pace of development until stage 5/6, with cumulus migration processes similar to WT embryos (C1, C2, D1, D2). However, the germ discs of these two embryos contracted towards the central region, and the embryos slowly grew upwards (C3-C6, D3-D6). This tube was quite different from the tubes formed in *Ets4* RNAi or *twi* RNAi embryos. It was smaller in size, and the highest positions of some embryos were even detached from the yolk region (D6).

It was difficult to discern from the video images the differences between the latter two *Znf423* RNAi embryos and WT embryos at stages 3 and 4. Additionally, the *Znf423* RNAi embryo in image C1-C6 showed a clear dorsal opening process, while the embryo in image D1-D6 showed no or only subtle opening of the germ disc. This suggested that the germ disc opening is not a key factor in the formation of the small tube.

Supplementary Figure S4-16 showed that gene *Znf423* was not or only weakly expressed in *Znf423* RNAi embryos at stage 4, confirming the effect of the knockdown experiment. The image also displays the expression of genes *Znf423*, *Ets4*, *hh*, *ptc*, and *opa* in both WT and *Znf423* RNAi embryos at stage 4. No obvious difference in the expression pattern of these genes was observed. It remained unclear whether the *Znf423* RNAi embryos were indeed WT-like at stage 4, or if differences existed that our detection failed to capture, either due to using an incorrect probe or missing embryos with more severe phenotypes.

In addition, *in situ* hybridization images of *Znf423* RNAi embryos at stages 5 and 6 were missing so far.

Figure 4-18 showed the gene expression of the small tube formed by *Znf423* RNAi embryos (A2, B2, C2, C3, D). These small tubes were fixed when the WT-like *Znf423* RNAi embryos of the same cocoon were at stage 10, but they resembled stage 6 or stage 7 WT embryos a lot by morphology and gene expression (B1, B2; C1, C2).

Znf423 RNAi tubes showed a nice segmental division along the anterior and posterior axis (B2, C2, C3, D). However, the posterior region of the small tube appeared thicker than other regions and

always detaches from the yolk (A2, B2, C3, D). However, I did not have specific *in situ* hybridization images for posterior marker genes to explore further differences.

There were some detailed differences in gene expression in the anterior region. *hh* was expressed as two segmental stripes in WT embryos (B1), while only one expression stripe is observed in the *Znf423* RNAi tube, which showed more segments in the posterior region of the embryo (B2). *ptc* was expressed in two semi-ring regions near the rim in WT embryos (C1), whereas in the *Znf423* RNAi tube, there was only one semi-ring region expressing the gene (C2). This could be a "defect in stripe splitting" described in previous publications (Kanayama et al., 2011, Pechmann et al., 2009).

I did not know if the dorsal-ventral division of the tube in *Znf423* RNAi embryos was similar to that of WT embryos. Additionally, there was no expression of the *Znf423* gene in the two types of *Znf423* RNAi embryos until stage 8 (C1-C3).

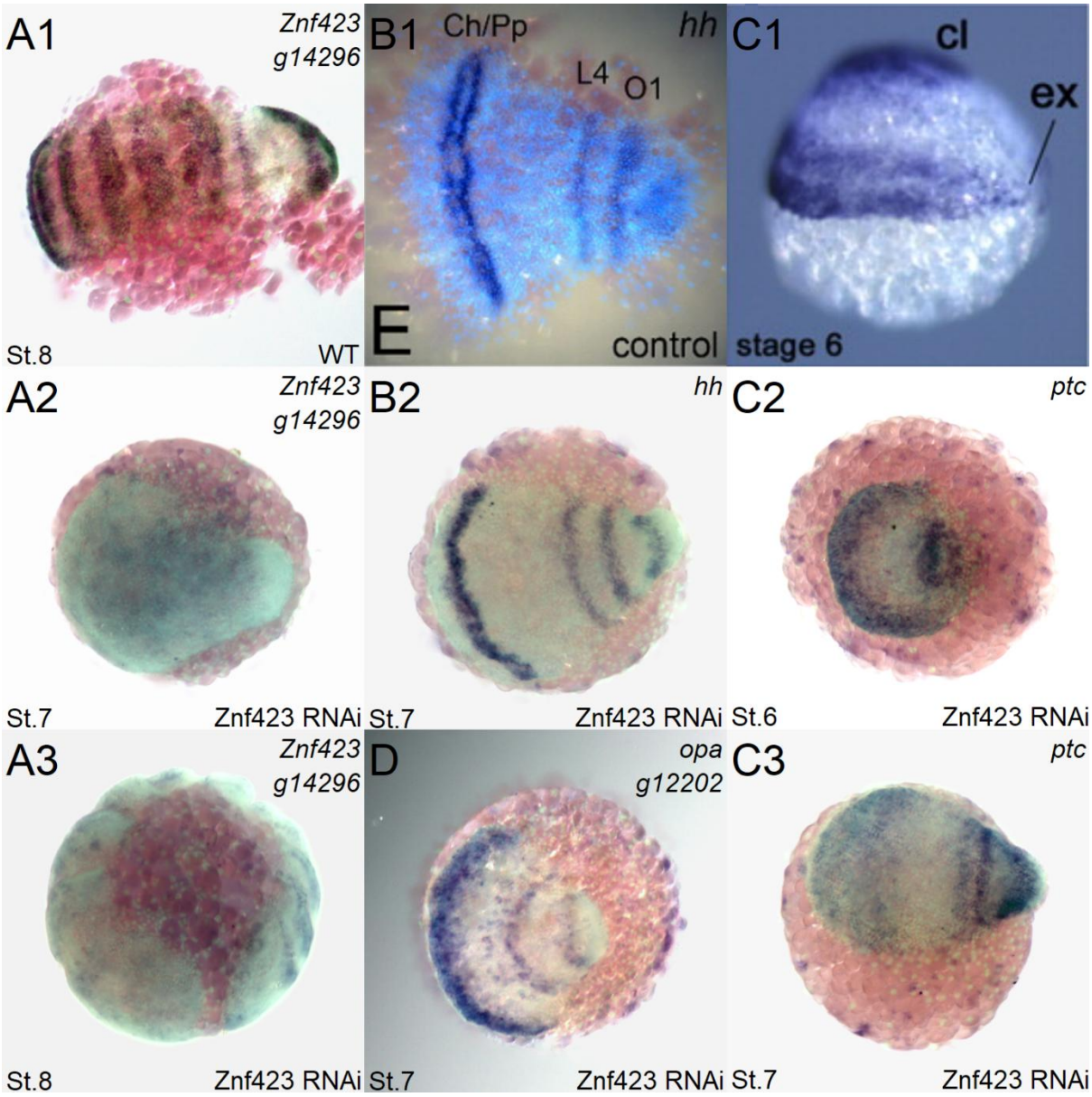

Figure 4-18. Expression of gene *Znf423*, *hh*, *ptc*, and *opa* in WT and *Znf423* RNAi embryos at stage 6 to stage 8. A1, B1, C1: WT embryo. B1: from Pechmann et al., 2009. C1: from Akiyama-Oda and Oda, 2010. A2, B2, C2, C3, D: *Znf423* RNAi embryo, small tube. A3: *Znf423* RNAi embryo, WT-like, at stage 8. A1-A3: *Znf423*. B1-B2: *hh*. C1-C3: *ptc*. D: *opa*.

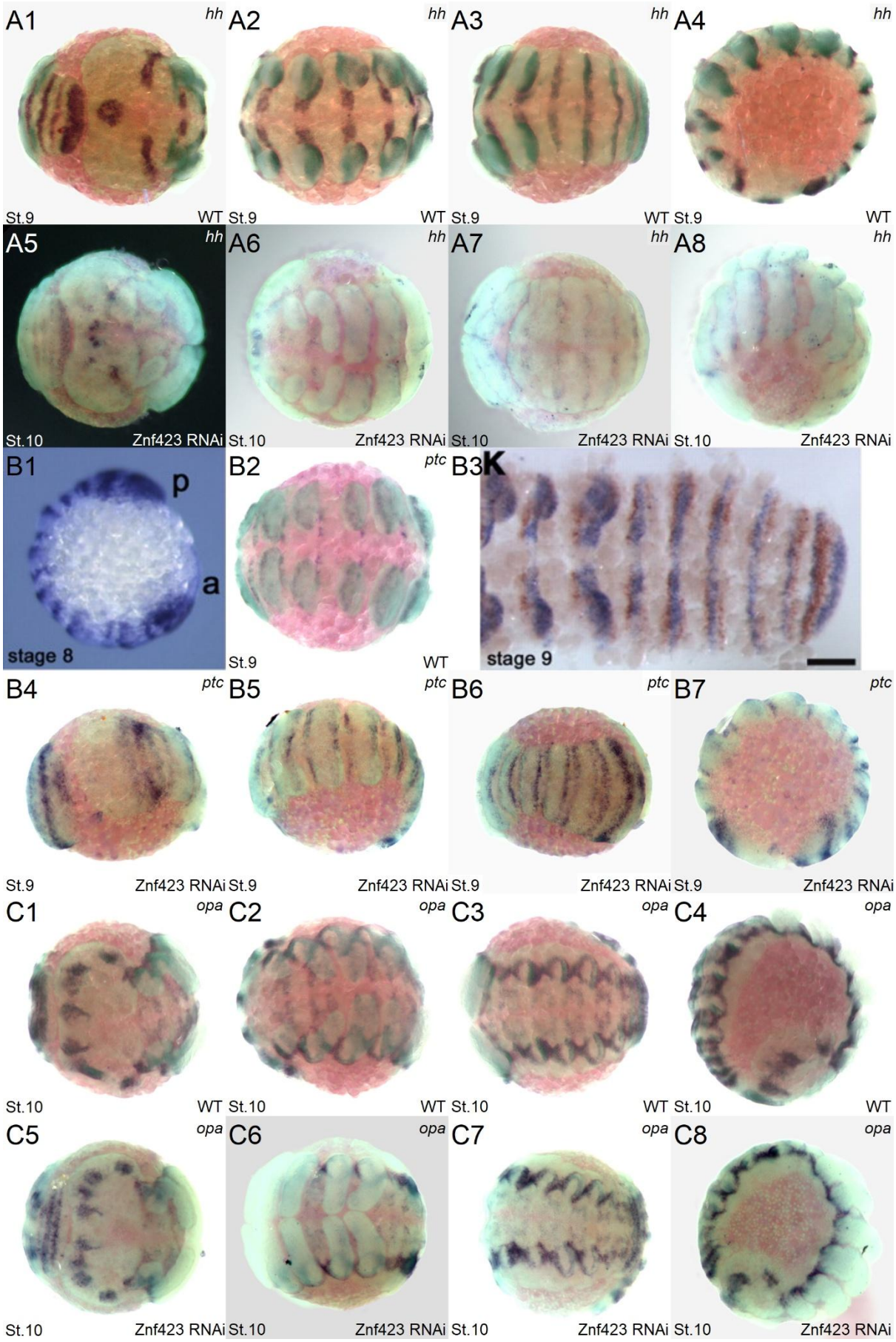
A1
hh
St.9
WT
A2
hh
St.9
WT
A3
hh
St.9
WT
A4
hh
St.9
WT
A5
hh
St.10
Znf423 RNAi
A6
hh
St.10
Znf423 RNAi
A7
hh
St.10
Znf423 RNAi
A8
hh
St.10
Znf423 RNAi
B1
p
a
stage 8
B2
ptc
St.9
WT
B3
K
stage 9
B4
ptc
St.9
Znf423 RNAi
B5
ptc
St.9
Znf423 RNAi
B6
ptc
St.9
Znf423 RNAi
B7
ptc
St.9
Znf423 RNAi
C1
opa
St.10
WT
C2
opa
St.10
WT
C3
opa
St.10
WT
C4
opa
St.10
WT
C5
opa
St.10
Znf423 RNAi
C6
opa
St.10
Znf423 RNAi
C7
opa
St.10
Znf423 RNAi
C8
opa
St.10
Znf423 RNAi

Figure 4-19. Expression of gene *hh*, *ptc*, and *opa* in WT and *Znf423* RNAi embryo at stage 9 to 10. A1-A4, B1-B3, C1-C4: WT embryo. B1 and B3: from Akiyama-Oda and Oda, 2010. A5-A8, B4-B7, C5-C8: *Znf423* RNAi embryo. A1-A8: *hh*. B1-B7: *ptc*. C1-C8: *opa*.

More *Znf423* RNAi embryos in this cocoon formed a germ band similar to WT embryos. No obvious defects were found in the embryos until stage 10 (Figure 4-17, B1-B6). Figure 4-19 showed the expression of *hh*, *ptc*, and *opa* in WT and WT-like *Znf423* RNAi embryos at stages 9 and 10.

The expression of the *hh* gene followed a similar pattern in both WT and *Znf423* RNAi embryos in most regions of the embryo (A2-A4, A6-A8). However, in the anterior region, *hh* was expressed around the stomodeum in the WT embryo (A1, Feitosa et al., 2017), while in the *Znf423* RNAi embryo, the gene was expressed in a half-cycle shaped region (A5). This suggested that certain patterning processes were distorted in the *Znf423* RNAi embryos.

The expression of the *ptc* gene may also be missing in the anterior region of the *Znf423* RNAi embryo (B1, B4). In other parts of the embryo, the expression patterns of *ptc* in WT and *Znf423* RNAi embryos were generally similar (B2, B3, B5, B7). Additionally, the germ band in the *Znf423* RNAi embryo showed uneven broadness (B6), suggesting some developmental defects in this region.

The expression of the *opa* gene in the *Znf423* RNAi embryo was similar to that in WT embryos.

The anterior region of the *Znf423* RNAi embryo showed some abnormalities based on the expression patterns of the *hh*, and *ptc* genes in this region. However, it was unclear how these abnormalities, if they indeed exist, might affect the development of the embryo in subsequent stages. Additionally, it would be beneficial to have more replicates to confirm these conclusions.

7.3 Analysis the function of gene *Znf423* based on *Znf423* RNAi experiments.

The *Znf423* RNAi experiment had limited replicates, and the analysis was based on a cocoon of embryos with mild phenotypes. Additionally, the fixation of the samples was of incomplete stages. This indicated a significant space for improvement and raises questions about the current conclusions. Nevertheless, I hope that these results can contribute to a part of the future comprehensive understanding.

So far, I observed two types of *Znf423* RNAi embryos. One type was shaped like a small tube contracted from the germ disc after stage 5, closely resembling stage 7 WT embryos. The other type of *Znf423* RNAi embryos developed like WT embryos up to stage 10. No obvious differences were observed in the development video of these embryos. In both types of *Znf423* RNAi embryos showed the anterior region shows certain abnormalities compared to WT embryos, which suggested that the *Znf423* gene played a role in the formation of segments in the anterior region after stage 6.

8. Summary of new RNAi phenotypes.

8.1 Summary of new RNAi experiments.

The results of 7 RNAi experiments were discussed (Supplementary Figure S4-17). Among these experiments, 4 results were considered more reliable (2.1 *RF_0381* RNAi, 2.2 *g4422* RNAi, 2.4 *twi* RNAi and 2.6 *Itpka* RNAi), and 3 results were considered less reliable (2.3 *cv-2* RNAi, 2.5 *Abhd11* RNAi, and 2.7 *Znf423* RNAi). These judgments were made based on the specificity of the phenotypes observed and the number of replicates conducted in each experiment.

Figure 4-20 displayed the information of WT and 4 new RNAi experiments, which were considered to have more reliable results in a tree image. The developmental events were noted with the

corresponding time scale, and events for each type of embryo were represented with the same color. Some RNAi embryos required multiple columns to depict different types of phenotypes. Effects observed during non-embryonic periods, such as cocoon production or spider lifespan, were not included in these images.

In Figure 4-20, the key events marked for *RF_0381* RNAi embryos included two columns: one depicting the type of embryo with cell movement defects at stages 1-2, and the other showing a contraction at stage 6. The key events for *g4422* RNAi embryos started with abnormalities in embryo shape at stages 1-2, and in the following stages, embryos exhibited various developmental problems thereafter. *twi* RNAi embryos showed a delay in the invagination process at stage 3, which might explain the prolonged stage 4. Some of the embryos displayed a lack of cumulus migration and formed a large tube expressing the ventral marker gene. *Itpka* RNAi embryos exhibited major abnormality during the dorsal opening process, where cells from different positions no longer move at the same coordinated speed. This resulted in an asymmetric, malformed germ band.

Furthermore, supplementary Figure S4-18 showed a combined image of tree diagram of 12 types of RNAi embryos at stages 3 to 7, including some published RNAi embryos, some new and reliable RNAi embryos, and WT embryos. Two types of phenotypes were exhibited in different RNAi embryos, of tube-like structure at stage 6 in *Ets4* RNAi, *ptc* RNAi, *fgf* RNAi, *twi* RNAi, and *dpp* RNAi embryos; and germ disc contraction from stage 5 to stage 6 in *vasa* RNAi, *hh* RNAi, *RF_0381* RNAi, and *Delta* RNAi. The tube-like structure are discussed in section 3 of the Discussion Chapter.

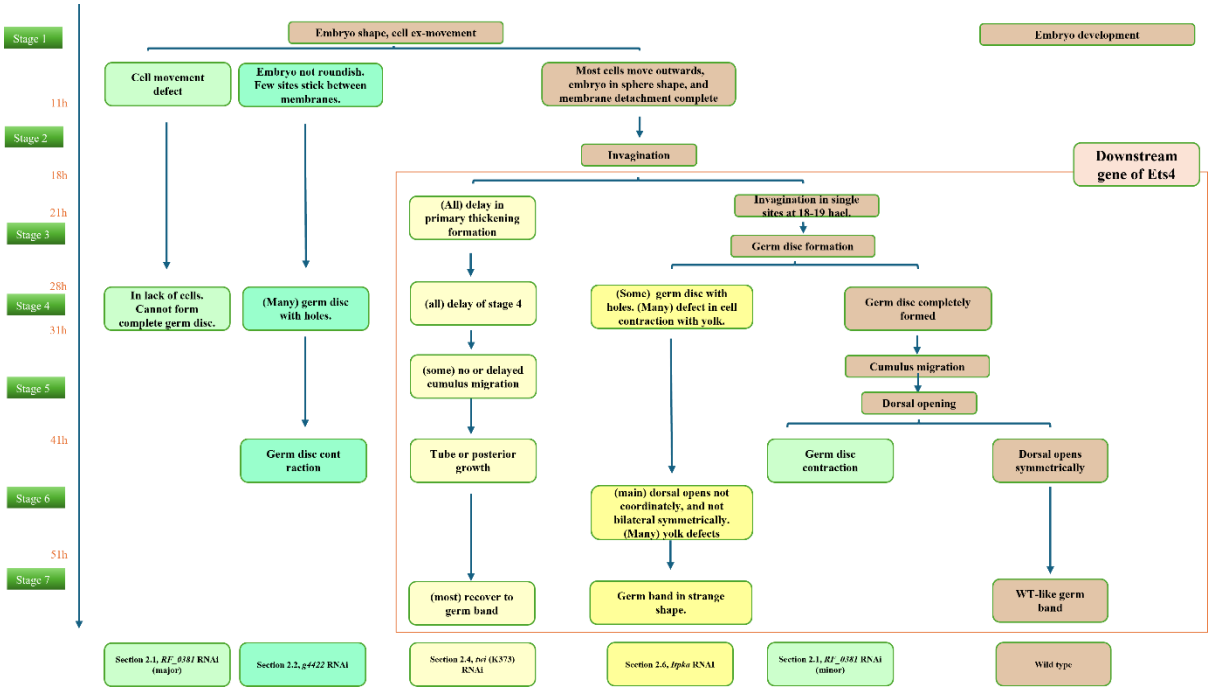

Figure 4-20. Key development event observed in WT, *RF_0381* RNAi, *g4422* RNAi, *twi* RNAi and *Itpka* RNAi embryo from stage 1 to stage 7.

8.2 Classification of genes based on gene expression and RNAi phenotypes of each class.

In Chapter III, genes were classified into four types based on their expression in the primary thickening region at stages 2 to 5 in WT embryos. *RF_0381*, *twi*, *Itpka*, and *Znf423* are all Type IV genes, while *g4422* and *Abhd11 g9727* are Type II genes. The classification of *cv-2* was unclear due to the lack of its expression at stage 2.

Chapter III also compared the expression of some genes in the primary thickening region at stage 4 in WT and *Ets4* RNAi embryos. *RF_0381*, *cv-2*, *twi*, *Abhd11 g9727*, *Itpka*, and *Znf423* were all

expressed in WT embryos, but not in *Ets4* RNAi embryos. Therefore, they were considered downstream of the *Ets4* gene. The gene *g4422* was expressed in both WT and *Ets4* RNAi embryos, and was considered independent of the *Ets4* gene.

Therefore, the Type IV genes, or the downstream genes of *Ets4* in the primary thickening region, were more likely to regulate the following processes: invagination (*twi*, *cv-2*), cumulus migration (*twi*, *cv-2*), dorsal opening (*cv-2*, *Itpka*), and animal patterning (*RF_0381*, *twi*, *Znf423*). Some abnormalities, such as inhibition of cumulus migration and tube formation, were observed in *Ets4* RNAi embryos, while most other phenotypes (invagination, dorsal opening defects, and contraction) were not observed in *Ets4* RNAi embryos.

RF_0381 and *g4422* genes may also contribute to developmental abnormalities at stages 1-2, while *Znf423* may play a role in anterior defects. These functions were likely unrelated to gene expression in the primary thickening and cumulus region.

8.3 Classification of genes by gene function, and RNAi phenotype of each class.

The genes *cv-2*, *twi*, *Abhd11 g9727*, and *Znf423* played roles in development across various species. *twi* was a marker for mesodermal differentiation, while *Abhd11* may promote the differentiation of embryonic stem cells. *cv-2* and *Znf423* both regulated the BMP pathway. Neither *cv-2* RNAi nor *Znf423* RNAi resembled *dpp* RNAi in spider. However, there were some similarities: both *cv-2* RNAi embryos (mild phenotype) and *dpp* RNAi embryos exhibited defects in dorsal opening, while both *Znf423* RNAi embryos (small tube) and *dpp* RNAi embryos showed upward growth in the posterior region.

The genes *RF_0381*, *Abhd11*, and *Itpka* were involved in metabolism or cell signaling. *RF_0381* regulated guanosine tetraphosphate and the JNK cascade. *Abhd11* may regulated DAG hydrolysis and lipid metabolism, while *Itpka*, as part of inositol phosphate metabolism, may be regulated by PI3K and influence various cell-signaling processes. However, there was still insufficient information to compare and link the phenotypes observed in the RNAi experiments of these genes. The gene *g4422* may function in chitin binding, but its role during the embryonic stage remained unclear.

In addition, spider-specific genes such as *RF_0381* and *g4422* showed a high level of abnormality at stages 1-2 in their corresponding RNAi embryos. However, this was not a general trend. Rhc1a, g592, and g22667 were also spider-specific genes, yet the RNAi experiments targeting these genes closely resembled WT embryos in developmental progression (not shown).

9. Summary

This chapter primarily focused on the results from RNA interference experiments. Seven new RNAi experiments (*RF_0381* RNAi, *g4422* RNAi, *cv-2* RNAi, *twi* RNAi, *Abhd11* RNAi, *Itpka* RNAi, and *Znf423* RNAi) were presented and interpreted. And a summary of the RNAi phenotypes and the role of these genes within the regulatory network was analyzed.

So far, I believed that Type IV genes, or genes downstream of *Ets4*, played critical roles in processes such as invagination (*twi*, *cv-2*), cumulus migration (*twi*, *cv-2*), dorsal opening (*cv-2*, *Itpka*), and animal body patterning (*RF_0381*, *Znf423*). The defects observed in *Ets4* RNAi embryos were included in the list of abnormalities seen in RNAi embryos of *Ets4* downstream genes, but the abnormalities in *Ets4* RNAi embryos did not account for all the abnormalities observed in RNAi embryos of downstream *Ets4* genes.

7 Discussion

1 The invagination of primary thickening cells in *Parasteatoda tepidariorum* (*Pt*): detail description, related molecules, and mechanisms

1.1 Description of invagination process based on new experimental results

During the early stage of *Pt* development, a group of blastopore-related cells internalize and become the primary thickening of the spider embryo (Mittmann and Wolff, 2012). This process is also referred to as a gastrulation process. After the blastopore closes, the cells in the region are considered to constitute the primary thickening region, from which the cumulus cells originate.

A 2015 study on different types of spiders suggested that primary thickening cells and cumulus cells may be of different types, and that the mechanisms separating them could vary among spider species (Edgar et al., 2015). In 2022, the Oda group found that the *fuchi* gene is expressed 15 hours after egg laying (hael) in the presumptive embryonic pole (Iwasaki-Yokozawa et al., 2022). More recently, a study suggested that the center of the germ disc was consistently located opposite the polar bodies (Wang and Pechmann, 2024).

In Result Chapter I of the Results section of this thesis (section 1, Figure 1-1, supplementary Table S1-1), a method was introduced to standardize the timing across different sources of videos and time-series images of fixed embryos. This approach improved our understanding of the gastrulation/invagination process (Figure 5-1). The results of germ disc cell counting presented in this chapter were similar to those reported in previous studies at the same developmental stage, including studies by Akiyama-Oda and Oda (2003),Schwager, Meng, et al., (2015), Pechmann et al. (2016), and Iwasaki-Yokozawa et al. (2022), as well as Mittmann and Wolff (2012), which were used as a methodological reference of the approach.

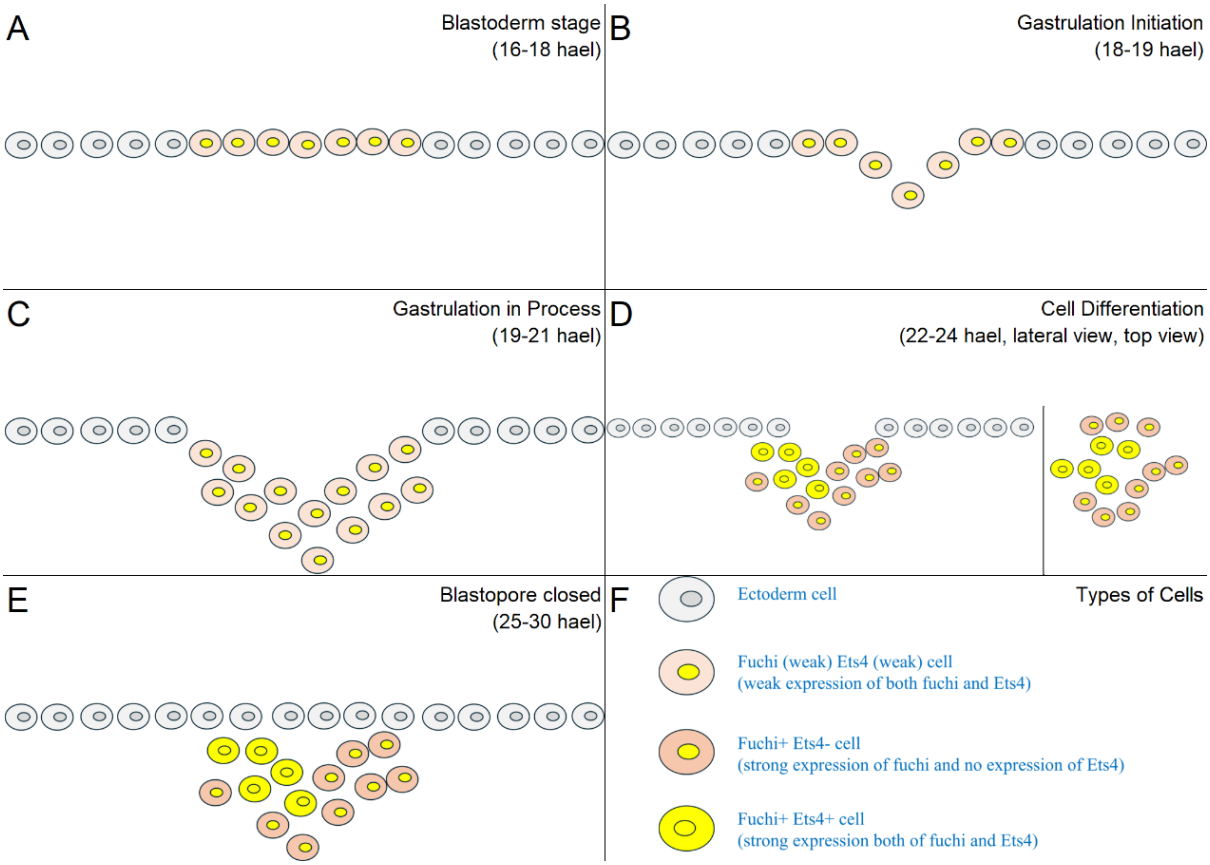

Figure 5-1. Schematic drawing of *Pt* invagination process. A. before invagination. B. initiation stage. C. Process of cell internalization. D. differentiation of internalized cells. E. Blastopore closed. F. Legend for different cell types. Since the image is drawn in lateral view, the number of cells shown in the primary thickening region represents approximately half the number of cells actually counted.

Figure 5-1 showed that the invagination process occurred between 18 to 22 hael (A, B, C, F). The sum of internalized cells formed an inverted cone shape (B, C, D, E). Most of these cells co-express *fuchi* and *Ets4* weakly during invagination (B, C), but later differentiated into either *Ets4*$^{+}$ or *Ets4*$^{-}$ cells (D, E). The *Ets4*$^{+}$ cells cluster together and were surrounded by *Ets4*$^{-}$ cells in the first several layers beneath the ectoderm (D, E). All internalized cells showed strong expression of the *fuchi* gene at this stage (D, E).

The blastopore was formed as a result of cell internalization and became most prominent around 21 hael (B, C). Neighboring ectodermal cells filled the gap through cell rearrangements or proliferation. By 25 hael, the ectoderm was completely restored (D, E). Most of these newly formed ectodermal do not express *Ets4* or *fuchi*.

Additional details about the process were as follows:

The future blastopore-related cells, or primary thickening-related cells, weakly expressed *fuchi* and *Ets4* at 18 hael, which may be traced back to nascent transcript expression of both genes as early as 14 hael. There were approximately 10 such cells at this stage, and the number increased to 15–25 following a cell division at 16 hael. From 18 hael onward, *fuchi* and *Ets4* expression became detectable in the cytoplasm, which was also the onset of invagination. Table 5-1 provided a comprehensive overview of the timing of key events during the early stages of *Pt* embryogenesis, including invagination process, based on the timing annotations from videos and images from Result Chapter I.

Table 5-1: a timeline of key early developmental events in *Pt* embryos

Hael	Region	Events
14	Germ disc centre	*fuchi* $^{na+}$*Ets4* $^{na+}$ cell (supplementary Figure S1-9, Figure 1-9)
14	Extraembryonic region	*fuchi* $^{na+}$ cells (supplementary Figure S1-23)
14-15	Extraembryonic region	The breakdown of specific cell-cell contacts may indicate the onset of germ disc contraction (Figure 1-23 A2 to A4)
16	Total embryo	The reduction of the total volume of the embryo initiate (Table S5-1)
18	Germ disc centre	*fuchi*$^{+}$*Ets4*$^{+}$ (weak), invagination starts (suppl. Figure S1-10, Figure 1-9)
18	Extraembryonic region	polar body in the middle of *fuchi*$^{+}$ cells (supplementary Figure S1-23)
24	Total embryo	The total volume of the embryo stabilizes (Table S5-1)
24	Germ disc centre	Differentiation of *Ets4*$^{+}$ and *Ets4*$^{-}$ cells, and the emergence of an asymmetric pattern in the primary thickening region (Figure 1-11)

There were, however, additional features of the invagination site. Cell tracing in this region showed that the future primary thickening consisted of the progeny of 5 to 6 cells that were present at the 32- or 64-cell stage, and the invagination appeared to occur at the center of these cells.

From the initiation of the invagination process, the internalized cells were observed to form multiple layers (B), which may suggest a sudden displacement of a small region of cells from the surface. It was unclear whether the yolk in the original region beneath the site was consumed or displaced. During the invagination process, at least some of the cells undergo division, resulting in an increase in the total number of *fuchi*/*Ets4*-related cells to 30–40.

In addition, the analysed embryos rarely showed cells with multiple multicellular regions in the germ disc. Only in a few cases (2%) small clusters of cells (3 or 4) showed *fuchi*$^{+}$/*Ets4*$^{-}$ expression outside the primary thickening region, and all of these cells were located in the ectodermal cell layer. This suggested a mechanism that prevents the formation of multiple primary thickening regions in the germ disc during *Pt* development.

1.2 Potential regulatory factors that drive the invagination of primary thickening cells

Current studies were not conclusive regarding the key factors involved in the invagination process. However, it was known that the absence of several critical genes, which were expressed in the primary thickening region, did not appear to lead to defects in primary thickening formation. These genes included *fuchi* (Iwasaki-Yokozawa et al., 2022), *dpp* (Akiyama-Oda and Oda, 2006), *ptc* (Akiyama-Oda and Oda, 2010), *Ets4* (Pechmann et al., 2017), and *fgf8* (Wang et al., 2023).

Chapter I of the Results section of this thesis provided a more detailed comparison of WT and *Ets4* RNAi embryos at different time points (Figure 1-10). As a result, no differences were observed in the invagination process or in the number of related cells. This observation further confirmed that *Ets4* is not a determining factor in this process.

Chapter IV of the Results section presented some RNAi embryos with abnormalities in the invagination process. It suggested that *twist* may influence the congregation of cells in the primary thickening region before invagination (supplementary Figure S4-6). It was observed in Drosophila ventral furrow formation process, that *twist* functioned in mesoderm invagination process (Gheisari et al., 2020). This suggested the early invagination process of *Pt* may also involve *twist*. On the other hand, *cv-2*, an antagonist of *dpp*, was related to the site selection for invagination (Figure 4-5). However, some of the results required further validation and replication.

The supplementary results in Chapter III (Figure S3-4) included a list of genes that were differentially expressed in the embryonic and extraembryonic regions at stages 1 and 2, including *GSK3beta* and *hh*. It was possible that some of these genes were involved in determining the location of the polar body or the primary thickening region and in the establishment of the embryonic–extraembryonic division at later stages.

1.3 Selection of the invagination site

Previous publications and new results suggested that the site of invagination has three key features: (1) it was opposite the polar bodies; (2) At the 32-cell stage, it was located at the center of a cluster of 5 to 6 cells, and remains centrally positioned within their progeny at later stages; and (3) it involved 15 to 25 cells, all of which weakly expressed both *fuchi* and *Ets4*.

This did not appear to be a coincidence, and it was particularly difficult to explain the opposite position of the polar bodies relative to the future primary thickening region.

According to Suzuki (1995), when the sperm entered the oocyte, the egg was a primary oocyte at telophase, located within the yolk granule and its own cytoplasm. This indicated that the first meiotic division was not yet completed, and all three polar bodies were not formed. The polar bodies became visible in the embryo starting from stage 1, and the invagination process began at the end of stage 2. There was a possibility that the movement of the polar body from the interior to the exterior surface, the movement of the sperm from the exterior to the interior, and the selection of future invagination site, were somehow related.

Hypotheses were proposed with differences in the timing and spatial arrangement of events. However, due to the lack of direct evidence, the details remained unknown.

1.4 Possible mechanisms for the invagination process

Edgar et al. (2015) suggested that the gastrulation/invagination process results from differential adhesion among cells, and I supported this idea. Earlier research introduced the "differential adhesion hypothesis," which proposed that changes in adhesion molecules altered the surface forces of cells (Foty & Steinberg, 2005), leading to the formation of boundaries during development (Duguay et al., 2003; Fagotto, 2014). As an example, the development of the central neural tube in mice involves an invagination process in which the internalized cells possessed different types and amounts of adhesion molecules compared to the cells on the surface. Cadherin was one of the well-known adhesion molecules.

A previous study from the Oda lab identified two types of cadherin in *Pt*, both of which belong to an ancient type of cadherin (Sasaki et al., 2017). The homologs of this type of cadherin in *Drosophila* possessed more cadherin domain repeats, suggesting the possibility of diversified adhesion (Nishiguchi & Oda, 2021).

In Chapter II of the Results section, cadherin was expressed at high levels in the primary thickening region of both WT and *Ets4* RNAi embryos. This seemed to align with the observation that there is no direct difference in the invagination process between the two types of embryos. However, there were no research on the specific types and amounts of cadherin expressed in *fuchi*$^{+}$*Ets4*$^{+}$ cells and *fuchi*$^{+}$*Ets4*$^{-}$ cells to date. Therefore, the link between invagination and the specificity of cell adhesion remained unclear.

1.5 Detailed description of germ disc formation and some related genes.

The formation of the germ disc occurs when embryonic cells moveed toward the center of the germ disc (or away from the direction of the polar body) around stage 3. It was reported that, during this movement, cells excluded yolk to reduce their size (Pechmann, 2016).

In Chapter I of the Results section, a more detailed description of the process was provided.

Around stage 2, each cell division took approximately half an hour. The process of germ disc contraction began around the same time that the invagination process starts (18 hael) and continued until 26-27 hael, when the germ disc reached its smallest size. Between 26 and 29 hael, in most embryos, the germ disc rotated to a position facing upwards. At this point, there were approximately 1,000 cells in the complete germ disc."

From at least 14 to 23 hael, the proliferation rate of cells in the primary thickening region was similar to that of cells in other regions of the germ disc (Result Chapter I, supplementary Figure S1-7). However, the cells in the primary thickening region were closer to each other, making them appear more condensed.

In Chapter IV of the Results section (Figure 4-8, supplementary Figure S4-3, S4-4), *twi* RNAi embryos showed a delay in invagination, while the germ disc at 18-23 Hael showed no difference at stage 3. This suggested that the formation of the germ disc at this stage was more a result of "pushing" from the extraembryonic region. While some *cv-2* RNAi embryos, with multiple inner cell regions and a non-round shape of the germ disc, suggested that germ disc formation also requires "pulling" forces from the primary thickening region. It also suggested that between 18 and 23 hael, the "pushing" force is the dominant force. Several RNAi embryos exhibited minor defects in germ

disc formation. The target gene in these RNAi experiments may play a role in this process and warrants further analysis (supplementary Figure S5-1).

2 Migration of the cumulus in *Pt*: description, regulatory factors, and mechanisms

2.1 Cell differentiation in the primary thickening region and the formation of the cumulus

As mentioned in section 1.1, it was newly observed that shortly after invagination (18-21 hael), cells in the region with weak expression of *fuchi* and *Ets4* differentiate into two types of cells with different levels of *Ets4* expression. This process occurred from 21 to 24 hael. There were approximately 10 *fuchi*$^{+}$*Ets4*$^{+}$ cells and about 25-30 *fuchi*$^{+}$*Ets4*$^{-}$ cells in the primary thickening region. In some batches of embryos, the number of *fuchi*$^{+}$*Ets4*$^{-}$ cells increased to 40-55 before stage 4.

The arrangement of cells in the region was quite interesting (Figure 5-1 D). If to consider the ectoderm as the “ground floor” and the inner cells as “underground layers”, and name as -x layers counting downward from the ground floor, *fuchi*$^{+}$*Ets4*$^{+}$ cells were located in the central region of layers -1 to -3 and were closely connected to each other. *fuchi*$^{+}$*Ets4*$^{-}$ cells were positioned around the edges of layers -1 to -3 and in layers -4 and -5. However, the cycle of *fuchi*$^{+}$*Ets4*$^{-}$ cells was incomplete. In one or two areas, *fuchi*$^{+}$*Ets4*$^{+}$ cells occupied the most external position in all the layers (Figure 5-1 D, Figure 5-2 A2, A3, A4). This was no longer a radial arrangement of cells.

Most of the *fuchi*$^{+}$*Ets4*$^{-}$ cells also showed expression of nascent transcripts of the *Ets4* gene at stages 3 and 4, and even during the first few hours of stage 5.

After the migration of the cumulus begins, the inner region at the center of the germ disc consisted solely of *fuchi*$^{+}$*Ets4*$^{-}$ cells, while the migrating cumulus was composed of approximately 10 cells, all of which were *fuchi*$^{+}$*Ets4*$^{+}$ cells. The similarity in cell number and gene expression strongly suggested that the *Ets4*$^{+}$ cells at stages 3 and 4 were the cumulus cells at stage 5, and the *Ets4*$^{-}$ cells were the later center cells.

2.2 Regulatory factors and mechanisms of the cell differentiation in primary thickening

The differentiation of cells in the primary thickening region was a new finding. So far, the most directly related phenotype to this process was observed in some *twist* RNAi embryos, where the number of *Ets4*$^{+}$ cells is reduced, and the location of these cells shifted to the peripheral region of the inner layer. This suggested that the *twist* gene played a role in the process.

A hypothesis regarding the differentiation process was based on the arrangement of cells. Given the total number of cells, approximately 30-40, in the primary thickening region beneath the ectoderm at around 22-25 hael, and the fact that these cells generally form an inverted cone shape, there must be around 10 cells in the center and around 20-30 cells in the surrounding area. This corresponded exactly to the number of *Ets4*$^{+}$ and *Ets4*$^{-}$ cells, which were located in the inner and surrounding regions, respectively. Therefore, the differentiation of *Ets4*$^{+}$ and *Ets4*$^{-}$ cells may result from their location. More precisely, it was possible that the concentration of a certain factor was higher in the inner region, inducing the differentiation of *Ets4*$^{+}$ cells, while the situation may differ in the outer region.

This hypothesis was based on the assumption that there was little to no cell movement in the region after invagination, which remained uncertain. However, if the hypothesis was correct, several candidates for the "key factors" could be identified based on current knowledge: *dpp* (Akiyama-Oda and Oda, 2003), *Ets4* (Pechmann et al., 2017), *fgfr1*, *dof* (Wang et al., 2023), *cv-2*, *RF_0381*, and *Itpka* all showed expression in *fuchi*$^{+}$*Ets4*$^{+}$ cells, but not in *fuchi*$^{+}$*Ets4*$^{-}$ cells at stage 5. Additionally,

all of these genes showed expression in the primary thickening region at stages 3 and 4. It was plausible that these genes exhibited distinct expression patterns prior to the migration of the cumulus.

In addition, in the primary thickening region of WT embryos, most *Ets4* $^{na+}$ cells (*fuchi*$^{+}$*Ets4*$^{-}$ cells) ceased the nascent transcription of *Ets4* after the *Ets4*$^{+}$ cell cluster (cumulus) left the center, around 37 hael. In *Ets4* RNAi embryos, which lacked *Ets4*$^{+}$ cells, most *Ets4* $^{na+}$ cells stopped expressing *Ets4* between 27-31 hael. This suggested that *Ets4* expression in cells could promoted the transcription of the *Ets4* gene through a positive feedback mechanism. If this is the case, the key factor may be the *Ets4* gene itself. No further investigation on this issue was conducted to date.

2.3 *Pt* cumulus migration

The cumulus migration process in *Pt* development occurred when cumulus cells moved along a random/selected radius beneath the ectoderm, from the center of the germ disc towards the periphery. This process took place between 31 and 41 hael (Holm, 1952; Mittmann and Wolff, 2012).

In Result Chapter I of this thesis, it was found that the migrating cumulus cells are all *fuchi*$^{+}$*Ets4*$^{+}$ cells (Figure 1-13). These cells are closely positioned to each other at all stages, with an average of 10 cells. The shape of the cell cluster varies considerably, including spherical, arrowhead, and tangential shapes, among others. In some embryos, the cells in the upper layer of the cumulus are more closely aligned towards the front, while in others, the opposite is observed. It is unclear whether the relative position of the cells within the cluster changes during migration.

At stage 5, the germ disc contains 1,000-2,000 cells, with approximately 20 cells within one radius. The radius of the germ disc is 250-300 μm, and the radius of the cumulus is approximately 35 μm. Cell movement takes approximately 10 hours. As a result, the movement speed of cumulus is around 21.5-26.5 μm/h, corresponding to the passing of about two germ disc cells every hour.

In the region just passed by the cumulus cells, newly divided *fuchi*$^{+}$*Ets4*$^{-}$ cells are scattered along the path beneath the ectoderm, creating a region of higher cell density under the microscope. The source of these cells is not yet known.

2.4 Regulatory factors of cumulus migration

There have been many studies on *Pt* cumulus migration to date. While the loss of the *ptc* gene results in a static cumulus with no movement (Akiyama-Oda and Oda, 2010) loss of the *Ets4* gene causes a dispersion of the cumulus cell cluster (Pechmann et al., 2017). In *hh* RNAi, *fuchi* RNAi, and *fgf8* RNAi embryos, approximately one-third of the embryos exhibit defects in the cumulus migration process (Iwasaki-Yokozawa, 2022; Akiyama-Oda and Oda, 2010; Wang et al., 2023). A typical phenotype observed when cumulus migration is completely or partially disrupted is that the embryo maintains radial symmetry and grows along the anterior-posterior (AP) axis, forming a ventralized, tube-like structure. This occurs in *ptc* RNAi, *Ets4* RNAi, and *fgf8* RNAi embryos. However, although *dpp* RNAi (Akiyama-Oda and Oda, 2006) embryo exhibits a similar phenotype, the cumulus migration is not affected.

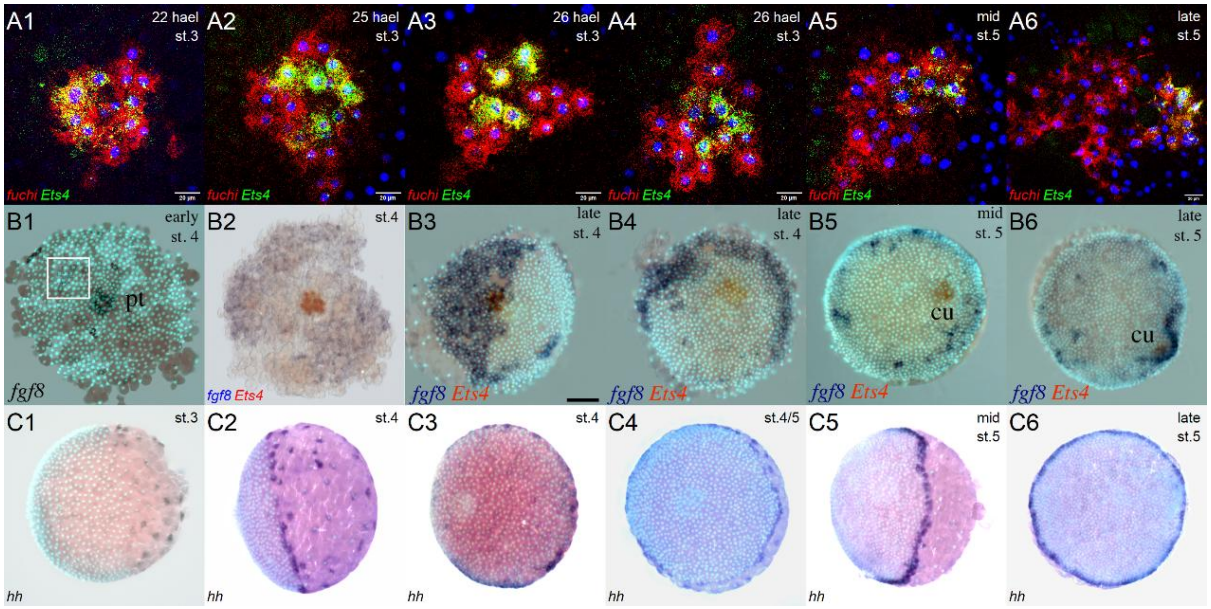

Figure 5-2. Expression of *fuchi* and *Ets4* (A1-A6), *Fgf* (B1-B6, originally from Wang et al., 2023), and *hh* (C1-C6) from stage 3 to stage 5 in WT embryos.

Of these genes, *dpp*, *ptc*, *Ets4*, and *fuchi* are expressed in the primary thickening region from stage 3 to stage 4. *hh* is expressed in the rim region of the germ disc (Figure 5-2 C1, C2, C3, C4). These genes all exhibit radially symmetric expression patterns. *Fgf8* is expressed in the primary thickening region at stage 3, and by late stage 4 to early stage 5 (stage 4/5), it is expressed only in a subset of germ disc cells. These cells are asymmetrically arranged, with rapid turnover and considerable variability among different samples (Wang et al., 2023; Figure 5-2 B2, B3, B4). Previous research suggests that the direction of cumulus migration is influenced by the *fgf8* expression pattern (Wang et al., 2023).

In this thesis, Result Chapter III (section 1.3, Figure 3-6 to 3-13) lists many genes that show expression in the primary thickening region at stage 4 (types I, II, IV), or in the cumulus region at stage 5 (types I, IV). These genes may play a role in the initiation or regulation of cumulus migration.

In Result Chapter IV (section 4, Table 4-1, Figure 4-11 to 4-13), I observed that in 10-30% of *twist* RNAi embryos, the cumulus remains at the center of the germ disc instead of migrating. These embryos grow upwards into a tube shape, suggesting that the *twist* gene influences the cumulus migration process.

The most significant outcome comes from the comparison of the transcriptomes of primary thickening cells at stage 4 in WT and *Ets4* RNAi embryos, as presented in Result Chapter II (Table 2-2, 2-3, 2-6; Figure 2-3, 2-7 to 2-10, 2-13). As the differentially observed morphology of the two types of embryos, are the completeness of the cumulus and the migration of the cumulus. The differentially expressed genes are likely key regulators of both processes. Approximately 800 genes were identified with differential expression levels, and the reliability of the screening was confirmed through in situ hybridization experiments and statistical analysis.

A large number of the selected genes were found to be associated with various processes related to cell migration, cytoskeleton dynamics, and cell adhesion. These processes include the endocytosis pathway, axon guidance pathway, focal adhesion pathway, actin cytoskeleton pathway, motor protein pathway, and others. Many of the selected genes were also connected to key developmental processes, such as the Hedgehog (Hh) pathway, Wnt pathway, Notch pathway, and dorso-ventral (DV) axis

formation pathway. Additionally, several cellular regulation processes were highlighted, including the Ras pathway, PI3K pathway, cGMP-PKG pathway, FOXO pathway, nucleocytoplasmic transport, mRNA surveillance, spliceosome activity, ubiquitin-proteasome system, and lysosomal functions. Interestingly, most genes involved in cell proliferation processes exhibited similar expression levels in the primary thickening regions of both WT and *Ets4* RNAi embryos and were not included in the list of differentially expressed genes.

The analysis provides a direct explanation for the differences in cell activity between primary thickening cells in WT and *Ets4* RNAi embryos. It also presents a list of genes that may be involved in the cumulus migration process.

2.5 Possible mechanisms for *Pt* cumulus migration

There are two types of cell movement: amoeboid and crawling. The former is faster, with a speed of around 5 minutes per cell length, and is generally not associated with focal adhesion. The latter is slower, moving at several μm/min, and is typically linked to focal adhesion (Dormann & Weijer, 2006). Based on the speed and the genes discussed in sections 2.3 and 2.4, the cumulus migration is more similar to the crawling type of cell movement. Additionally, given the number of cells migrating together, this is a case of congregated cell movement, not individual cell movement.

Congregated cell movement in the development of other species, such as the collective cell migration in the mouse neuronal system, can be described as follows: Environmental signals (e.g., fibronectin, morphogens, signals connected to the extracellular matrix, paths produced by adhesion factors, and chemotaxis cues) bind to the transmembrane proteins of the leading cells, determining the direction of movement through signal transduction. Other cells follow the leading cells, maintaining the integrity of the cell cluster through innate features, including the appropriate levels and types of adhesion molecules and cytoskeleton proteins. During migration, temporary adhesion complexes are formed between the moving cells and the surrounding cells, involving the regulation of cytoskeleton proteins like actin and the turnover of the cell membrane system (Geiger & Yamada, 2011; Scarpa & Mayor, 2016; Swaney et al., 2010; Theveneau et al., 2010; Tojima et al., 2010).

If the basic mechanism of cumulus migration in *Pt* is similar to the mouse neural cell migration process, the relevant details of this process could be analyzed and presented as follows:

(1) Signal transduction and directional decision

Sections 2.1 and 2.2 discussed the asymmetric pattern of $Ets4^{+}$ and $Ets4^{-}$ cells in the primary thickening region, which precedes the asymmetric expression of *fgf8* in the germ disc cells. Interestingly, in some embryos, the primary thickening cell pattern, when expanded along the radius, resembles the *fgf8* staining pattern observed in some samples. For example, in Figure 5-2 A2 and A3, the central pattern of cells may extend into regions similar to those seen in *fgf* staining in B2 and B3. The varying surrounding patterns of $Ets4^{-}$ and $Ets4^{+}$ cells in earlier stages, with different niche sizes or varying degrees of opening, could be linked to the *fgf8* expression pattern, which display different sizes and shapes across the germ disc region.

A hypothesis is proposed based on this comparison: $Ets4^{+}$ cells, rather than $Ets4^{-}$ cells, may release certain signaling factors that disperse from the center towards other regions of the germ disc. Cells that receive these signaling factors would then express *fgf8* at a later stage.

Signals released by the $Ets4^{+}$ cells could include Fgf8 protein and other factors related to cell movement. This deduction is based on the observation that primary thickening cells express *fgf8* at stage 3 rather than at stages 4 or 5. Furthermore, more than half of the *fgf8* RNAi embryos still exhibit cumulus migration similar to WT embryos. Additionally, in *hh* RNAi embryos, which lack *fgf8*

expression at stage 5, more than half also demonstrate normal cumulus migration, confirming the deduction that Fgf8 may not be the only signal for cumulus movement. Also, it suggests *hh* may play a direct role in regulating *fgf8* expression in the germ disc cells as discussed in Wang et al., 2023.

The germ disc cells receive signals that prompt them to produce Fgf8. This possibility is supported by auto-regulation observed in other species. Thus, a causal link is built between the different relative positions of *Ets4*$^{+}$ and *Ets4*$^{-}$ cells in primary thickening region at stage 3 to stage 4, and the varying expression of Fgf8 at stages 4/5 in the germ disc cells.

Additionally, Fgf8 expression either spans the entire region along the radius (as seen in B2, B3) or is localized to regions near the rim (as in B4, B5, B6). This pattern suggests that Fgf8 expression is turned off sequentially, from the center to the rim with in a short period of time. This rapid turnover of expression is mentioned in Wang et al. (2023), and is also observed in the development of other species (Bökel and Brand 2013; Balasubramanian & Zhang, 2016). Furthermore, this process requires the presence of Hh.

The expression of *fgfr1* and *dof* genes at this stage is observed exclusively in *Ets4*$^{+}$/cumulus cells, indicating a specific response to Fgf8 signals from the germ disc region at stages 4/5. As a result, cumulus cells create a path within the germ disc, possibly with some redundancy, and at least two waves of signals disperse throughout the area. This seems to prepare the cells for the upcoming migration process.

This hypothesis is illustrated in schematic drawings in Figure 5-3. It depicts the asymmetry pattern in the primary thickening region from stages 3 to 4 (A), the Hh gradient starting at stage 4 (B, Akiyama-Oda et al., 2022), the asymmetric expression of Fgf in the germ disc cells at stages 4/5 (C, D, E), and the subsequent cell migration process (F, G).

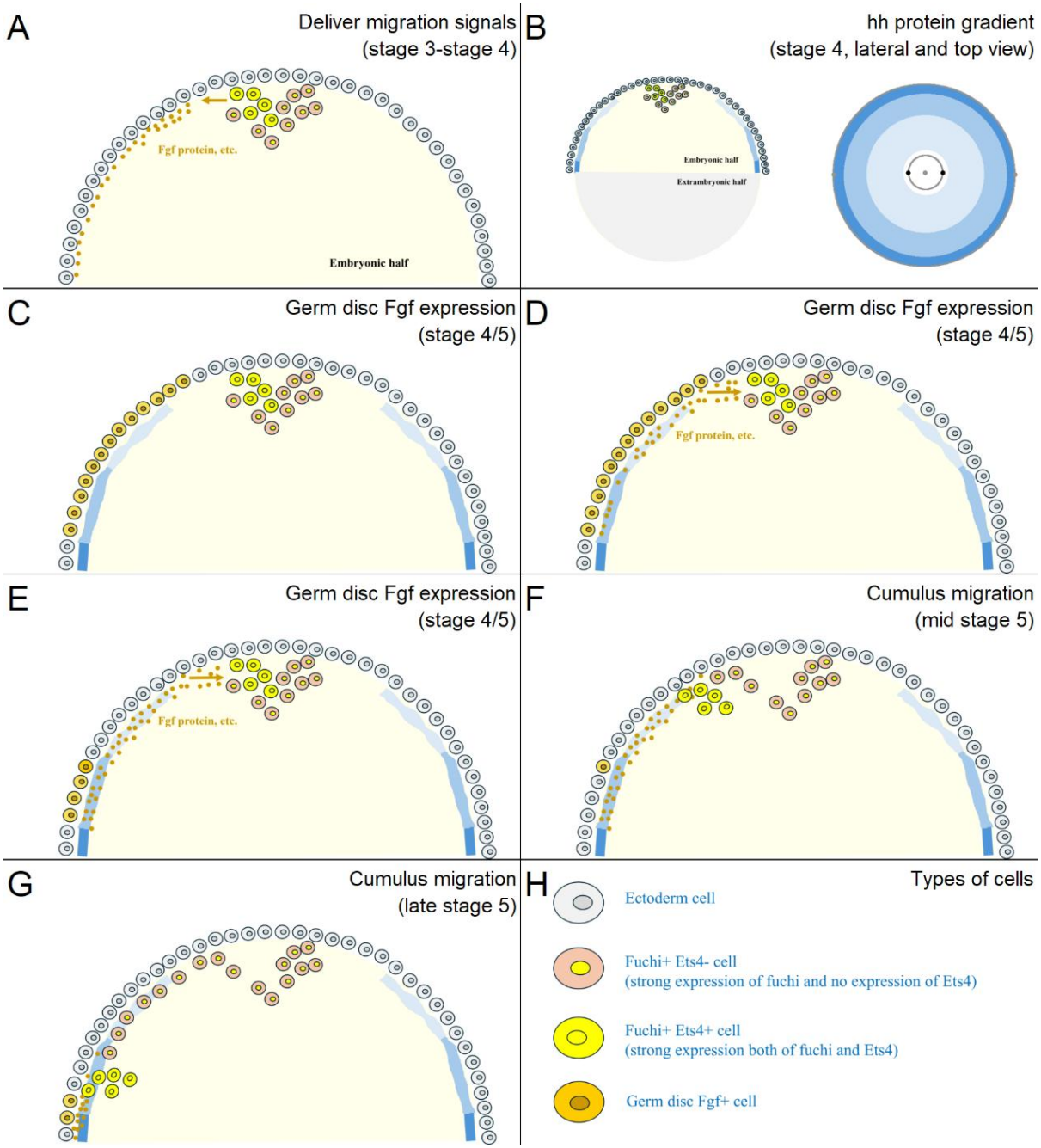

Figure 5-3. Hypothesis on the cause-and-effect link between the asymmetric arrangement of *Ets4*$^{+}$ and *Ets4*$^{-}$ cells and the asymmetric expression of *fgf* in the germ disc region, explaining the morphology and gene expression observed in cumulus migration process. A. Asymmetric distribution of *Ets4*$^{+}$ and *Ets4*$^{-}$ cells in the primary thickening region at stages 3 to 4. The *Ets4*$^{+}$ cells send out movement-related signals, including Fgf8 protein. B. Hh gradient forms in the germ disc at stage 4. C. At stages 4/5, the primary thickening cells stop expressing *fgf8*. D. At stages 4/5, the germ disc cells begin to express *fgf8*, and the protein disperses towards the primary thickening region. E. At stages 4/5, *fgf8* expression is turned off in the germ disc cells closer to the center, while cells near the periphery continue to express the gene. F. Mid stage 5, the cumulus initiates migration toward the germ disc regions where *fgf8* was previously expressed. Most regions of the germ disc have turned off *fgf8* expression. G. Late stage 5, the cumulus migrates toward the rim of the germ disc. *fgf8* expression is induced in the ectoderm cells ahead of the cell cluster's direction of movement. H. Types of cells.

The *fgf8* expression near the rim region at late stage 5 is likely induced by the Hh gradient originating from the rim. In some *hh* RNAi embryos, the cumulus exhibits a winding movement and fails to reach the rim, suggesting that Hh signaling is crucial for guiding the cumulus to its destination. This guidance may occur through the induction of Fgf signals ahead of the migrating cell cluster.

Additionally, to explain the observation in *twist* RNAi embryos using the above hypothesis: some embryos exhibit fewer and less clustered *Ets4*$^{+}$ cells in the primary thickening region, which may result in fewer signals being sent out and a reduced ability to respond. This could lead to a deficiency in cumulus migration.

(2) The migration process of cumulus cells

A detailed description of the movement of mouse neural cells during development involves the cycling of the cytoskeleton and cell membrane system. At the front, new attachments are made with neighboring cells or extracellular structures in the form of a temporary adhesion complex. Within the cell, the cytoskeleton or membrane elongates towards the front, while actin filaments in the lagging direction contract. Microtubules and related proteins stabilize the structure and help with directional decisions. A RhoA-Rac1 gradient on both sides of the cell regulates actin dynamics (SenGupta et al., 2021).

As mentioned in Section 2.4, the *Ets4* gene may influence numerous pathways related to the regulation of the cytoskeleton and membrane systems. As discussed in Result Chapter II (Figure 2-7 to 2-9), these processes could be regulated by the PI3K pathway. Furthermore, in Result Chapter III (supplementary Figure S3-22), Fgf8 and several other genes were linked to this pathway, potentially reflecting the core components of cell activity during that time.

Therefore, the movement of the cumulus/*Ets4*$^{+}$ cells may follow a process similar to that of mouse neural cells. At least at the genetic level, all the necessary genes are expressed at high levels at the right time and in the appropriate cells. However, direct evidence to confirm this presumption is still lacking.

However, there are two distinctions: First, during cumulus migration, a scattered path is formed behind the moving cells by *fuchi*$^{+}$*Ets4*$^{-}$ cells (Figure 5-2, A5, A6). The source of these cells remains unclear. Second, the cumulus cells move beneath the ectoderm, in an area that was originally occupied by yolk. This process likely involves the metabolism of yolk during cumulus migration, though this aspect is not well understood.

(3) Developmental/differentiation regulation during cumulus migration.

It is known that cumulus cells express the *Wnt8b* and *dpp* genes, while along their migration path, Fgf8 and Hh proteins are passed through at different stages. As a result, the movement of the cumulus cells inevitably involves both sending and receiving signals, which could induce cell differentiation in various directions. This process will be discussed in more detail in section 5.

Summary: A hypothesis is proposed to link the asymmetric expression of the *fgf8* gene in the germ disc to the *Ets4*$^{+}$ / *Ets4*$^{-}$ cell pattern in the primary thickening region at earlier stages. The hypothesis also outlines potential functional pathways regulating the cytoskeleton and membrane systems, which are driven by downstream genes of *Ets4*. Hh signaling is considered, and the observations from relevant RNAi embryos (*hh* RNAi, *Ets4* RNAi, *fgf8* RNAi, and *twist* RNAi) align well with the hypothesis. No significant contradictions have been identified so far.

For further validation of the hypothesis, the following experiments could be designed: (1) Expression of Fgf8 protein at stages 4 and 5: Investigate whether Fgf8 protein indeed acts as a signaling molecule to attract and initiate cumulus migration. (2) Identification of migration-related factors: From the differential gene list of *Ets4* RNAseq, identify potential factors related to migration. The protein corresponding to these factors should show asymmetric expression, and its pattern should closely resemble the Fgf8 protein expression pattern in the same sample. (3) Analysis in *ptc* RNAi embryos: Since *fgf8* expression in *ptc* RNAi embryos is in a ring-like pattern near the center of the germ disc, if the hypothesis is correct, *ptc* RNAi embryos should exhibit a radially symmetric arrangement of $Ets4^{+}$ and $Ets4^{-}$ cells in the primary thickening region. This arrangement can be detected. (4) *fgf8* mRNA/protein injection: If *fgf8* mRNA or protein is injected into a specific radius of *fgf8* RNAi embryos at stages 4/5, the cumulus might be directed to migrate toward that region.

3 *Pt* dorsal opening process, the formation of DV axis, and tube phenotype in RNAi embryos

The dorsal opening process occurs after the migration of the cumulus. Through this process, the radially symmetrical germ disc transforms into a bilaterally symmetrical germ band. The anterior–posterior axis is established, and the dorsal–ventral axis is primarily formed, as illustrated in Figure 3 of the Introduction.

This thesis primarily focuses on the earlier developmental stages. However, a few observations suggest potential involvement in the dorsal opening process. In particular, *Itpka* and *cv-2* RNAi embryos exhibit aberrant or reduced cell movement during dorsal opening. Both genes are downstream targets of *Ets4* and are expressed in cumulus cells during their migration. These findings suggest that *Ets4*, along with its downstream effectors, may influence dorsal opening as an extension of their role during cumulus migration.

As shown in Figure 5 of the Introduction, some RNAi embryos exhibit a tube phenotype, characterized by radial symmetry without formation of the dorsal–ventral axis, while elongating along the anterior–posterior axis during stages 5 to 7. These RNAi embryos including *dpp* RNAi (Akiyama-Oda and Oda, 2006), *ptc* RNAi (Akiyama-Oda and Oda, 2010), *Ets4* RNAi (Pechmann et al., 2017), *fgf* RNAi (Wang et al., 2023), and *twi* RNAi embryos (section 4, Result Chapter IV of this thesis). A comparison between the five tube-related RNAi embryos and WT embryos is presented in in Table 5-2. Additionally, the target genes of these RNAi experiments (*dpp*, *ptc*, *Ets4*, *fgf*, *twi*) all show expression in the primary thickening region at stage 4 in WT embryos.

Table 5-2 Comparison of WT embryo and five tube phenotype RNAi embryo in cumulus condition and axis formation

	Cumulus migration	central cell disperse at st.5	Dorsal opening at st.6	Anterior-Posterior axis	Dorsal-Ventral axis	Penetration rate	Reference
WT	Yes	No	Yes	germ disc rim→center of the germ disc	Germ disc region adjacent to dorsal field→germ disc	NA	
dpp RNAi	Yes	No	No	germ disc rim→center of the germ disc	NA	Not known	Akiyama-Oda and Oda, 2006
ptc RNAi	No	No	No	center of the germ disc→germ disc rim	NA	>90%	Akiyama-Oda and Oda, 2010
Ets4 RNAi	No	Yes	No	germ disc rim→center of the germ disc	NA	>90%	Pechmann et al., 2017
fgf8 RNAi	No	No	No	germ disc rim→center of the germ disc	NA	20-40%	Wang et al., 2023
twi RNAi	NO	No	No	germ disc rim→center of the germ disc	NA	10-30%	section 4, Result Chapter IV

Previous publication on RNAi phenotypes discussed why the DV axis could not be established in the individual RNAi embryos: *dpp* RNAi embryos exhibit cumulus migration but are unable to open the dorsal region of the germ disc or promote differentiation of the relevant dorsal field cells. *ptc* RNAi inhibits cumulus migration, and the embryo opens the dorsal region at the position of unmoved cumulus cells, at the center of the germ disc. The embryo remains its radial symmetry. In *Ets4* RNAi embryos cumulus cells disperse. Due to the lack of directional migration of cells, the DV axis is not established. Localized BMP signalling is missing. *Fgf8* RNAi embryos lack the asymmetric arrangement of the cell movement signal *fgf8*. In 20-40% of *fgf* RNAi embryos, the cumulus cells

remain at the center of the germ disc, preventing the opening of the region, and the embryo remains radially symmetric.

As discussed in Section 4 of Chapter IV (Results), *twi* RNAi embryos show a delayed initiation of invagination at early stages, suggesting a role for *twi* in cell adhesion. Some *twi* RNAi embryos exhibit isolated *Est4*$^{+}$ cells in the primary thickening region, with fewer cells compared to WT embryos. This suggests that *twi* may also function in the differentiation of *Ets4*$^{+}$ cells. The current hypothesis proposes that primary thickening cells in *twi* RNAi embryos have defects in cell adhesion as well as in the number and organization of *Ets4*$^{+}$ cells. These defects may impair the congregation of cumulus cells, their response to external signals, or their movement. In extreme cases, a small proportion of *twi* RNAi embryos exhibit defects in cumulus migration.

Recently, I observed a similar delay in invagination in at least some batches of fgfs RNAi embryos (Supplementary Figures S5-2 and S5-3), and a supplementary explanation for this phenotype is proposed: The reduction of *fgf* signaling in the primary thickening region at stage 3 may alter internal cell adhesion and congregation in *fgf* RNAi embryos. As a result, the embryo may have a cumulus with loose cell connections at stage 5. Considering previous findings that fgf8 serves as a directional signal guiding cumulus movement, these factors may act together to impair cumulus cell migration to some extent.

If the hypothesis is correct—that the tube phenotypes observed in both *twi* and *fgf* RNAi embryos result from defects in cell adhesion, it provides a plausible explanation for why only a subset of *fgf* and *twi* RNAi embryos exhibit the tube phenotype. Furthermore, it also explains why the tube phenotype occurs at a higher frequency in *fgf* RNAi embryos compared to *twi* RNAi embryos, as the former also shows defects in signal transduction.

Figure 5-4 shows a schematic representation of the mechanisms underlying dorsal opening or tube formation in WT (A), *dpp* RNAi (B), *ptc* RNAi (C), *Ets4* RNAi (D), *fgf* RNAi (E), and *twi* RNAi (F) embryos. As discussed, the mechanism for *dpp* RNAi, *ptc* RNAi and *Ets4* RNAi are supported by more evidence. whereas the mechanism for *fgf* RNAi and *twist* RNAi remain to be proven.

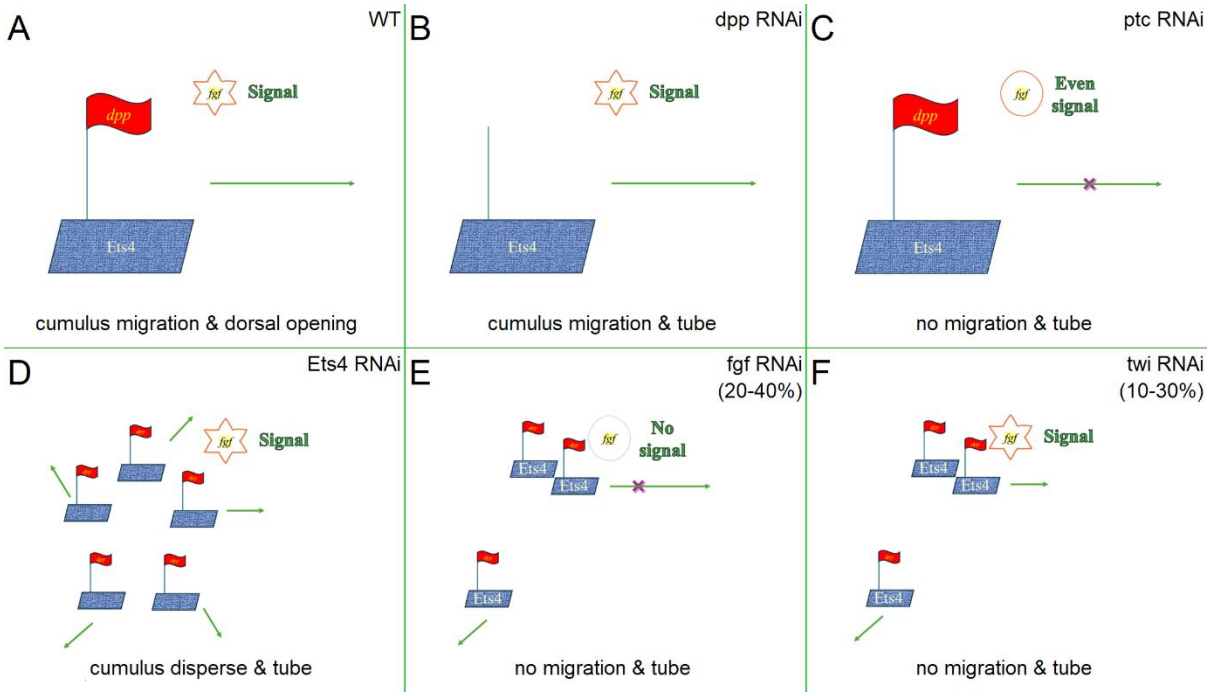

Figure 5-4. Schematic drawing illustrating the possible status of cumulus cells and the resulting dorsal–ventral axis formation in WT (A), *dpp* RNAi (B), *ptc* RNAi (C), *Ets4* RNAi (D), *fgf8* RNAi (E), and *twi* RNAi (F)

embryo at stage 5 to stage 6. Red flag: *dpp*. Blue floor (pieces): congregated cumulus cells, generally numbering around 10, characterized by *Ets4* expression. Orange Star: movement related signals, directional in WT. Signal factor including Fgf. Green arrow: process or inhibition of cell movement.

4 The Role of *Ets4* in early embryonic development of *Parasteatoda tepidariorum*

4.1 The Role of *Ets4* in development and cell activities of *Pt*, based on previous publications and new experimental results

The *Pt-Ets4* gene was first identified by Pechmann et al. (2017), showing expression in the primary thickening region at stages 3 and 4, and in the cumulus at stage 5. *Ets4* has been reported to function upstream of *twist* and *hb*, and its ectopic expression promotes cell invagination and migration. Knockdown of *Ets4* disrupts the integrity of the cumulus, leading to severe abnormalities in dorsal-ventral (DV) axis formation and altered body patterning. Further study (Wang et al. 2023) has shown that *Ets4* regulates the expression of *Fgfr1* and its downstream gene *dof*.

This thesis builds upon previous research by examining the morphological characteristics of primary thickening cells from stage 3 to stage 5 in both wild-type (WT) and *Ets4* RNAi embryos. A comparative transcriptomic analysis was conducted on primary thickening cells at stage 4 in both conditions. Additionally, over 50 genes were analyzed using in situ hybridization, and a subset of *Ets4* downstream genes were selected for functional investigation through RNA interference (RNAi) experiments. These studies generated a range of findings, some of which have been discussed in earlier sections. This section will specifically summarize the results relevant to the role of *Ets4* in early embryonic development.

At the morphological level, several consistent observations were made. First, cells involved in the invagination process consistently exhibit weak *Ets4* expression prior to movement. Second, primary thickening cells are clearly differentiated into two distinct populations based on *Ets4* expression levels, with these populations arranged asymmetrically within the primary thickening region. Finally, a direct correlation was observed between *Ets4* expression and cell migration: all migrating cumulus cells are $Ets4^{+}$ cells, and conversely, all $Ets4^{+}$ cells participate in the migration process.

At the level of cellular activity, several conclusions can be drawn regarding the role of *Ets4*.

(1) *Ets4* and its downstream genes are strongly implicated in the regulation of the cytoskeleton, membrane dynamics, and other processes associated with cell movement. This conclusion is well-supported by RNA-seq data, aligns with morphological observations, and is partially validated through in situ hybridization experiments. While the hypothesis that $Ets4^{+}$ cells may secrete signaling molecules to promote cell migration remains speculative, it is not contradicted by the available data.

(2) *Ets4* may play a critical role in regulating cell adhesion processes. Cells expressing *Ets4* are actively involved in key developmental events such as invagination, primary thickening cell differentiation, and cumulus migration—all of which depend on dynamic regulation of cell–cell and cell–tissue adhesion. Additionally, the involvement of ETS domain-containing factors in cell adhesion regulation suggests that *Ets4* may perform a similar regulatory function in *Parasteatoda tepidariorum*.

(3) *Ets4* influences the expression of multiple developmental regulatory genes (supplementary Figure S5-4). It acts upstream of key factors such as *twist*, *hb*, *wnt8b*, and several components of the *fgf* signaling pathway, while repressing the expression of *hh* and *delta*. The *dpp* gene appears to be regulated independently of *Ets4* and vice versa (Pechmann et al. 2017). However, some *dpp*-related genes, such as *cv-2*, may function downstream of *Ets4*, suggesting an indirect connection between *Ets4* activity and *dpp*-related pathways.

(4) *Ets4* may also be involved in the regulation of metabolic processes, particularly those related to yolk consumption. However, current knowledge on this potential role is limited.

(5) It is suggested that *Ets4* is not directly related to genes involved in cell proliferation. This conclusion is supported by cell number counting of both WT and *Ets4* RNAi embryos, transcriptome comparisons between the two embryo types, and in situ hybridization experiments of relevant genes.

4.2 Genes upregulated or downregulated in *Ets4* RNAi embryos

Ets4 is a transcription factor by nature. However, there is limited information regarding the specific genes directly regulated by *Ets4* in *Parasteatoda tepidariorum* (*Pt*).

More than 800 genes were identified based on differential expression in the primary thickening cells of WT and *Ets4* RNAi embryos. Additionally, over 20 genes were confirmed through in situ hybridization experiments conducted on both types of embryos.

Among the differentially expressed genes, those showing higher expression in WT embryos are involved in four main cellular processes: Cell congregation, as well as the initiation and spatial localization of the invagination process (*twist, fgf8, cv-2*); cumulus migration (*twist, fgf8, cv-2, Fgfr1, Dof, L(2)efl, RF_0381, Clca4a*); cell movement in the dorsal opening process (*Itpka, cv-2*); and cell differentiation (*RF_0381, Znf423, hb, twist, opa, ptc, Wnt8b*). The first three processes can be further categorized into functions related to adhesion, cytoskeleton, and cell movement.

These potential downstream genes of *Ets4* exhibit diverse expression patterns. Some are ubiquitously expressed at stage 2 and later in the primary thickening region at stages 3 and 4, while others are only expressed in the primary thickening region starting from stage 3. This suggests that, at least for some genes, there are additional regulatory factors involved aside from *Ets4*.

The genes that are expressed at higher levels in *Ets4* RNAi embryos may be inhibited by *Ets4* in the primary thickening region. These include *hh* and *delta*, both of which function in cell differentiation. Both genes are expressed at stage 2 in the extraembryonic region but show no expression in the primary thickening region at stages 3 and 4.

In addition, several differentially expressed genes remain unclassified due to a lack of understanding regarding their functions. These include *g9731*, *Anxa1*, *g4424*, *Mtmr14*, *g22667*, *Idh2*, *Hif1a*, *Asph*, *Cdk2*, *Mapk1*, *g27557*, and *fascin*.

4.3 Potential regulator of *Ets4*.

There are several observations that may suggest the upstream regulators of the *Ets4* gene.

It was discussed in section 2.2 that the Ets4 protein may promote the transcription of the *Ets4* gene either within the cell itself or in neighboring cells. It appears that cells with higher expression of *Ets4* are able to maintain this expression, while cells with lower *Ets4* expression tend to shut down transcription earlier.

In *twis*t RNAi embryos, some samples show very few $Ets4^{+}$ cells in the primary thickening region. This could be a result of reduced and delayed cell aggregation in the region prior to invagination, or it may indicate a regulatory feedback loop between *Ets4* and *twist*, as *Ets4* is upstream of *twist*.

In other species, Fgf signaling may trigger the activation of ERK, which enters the cell nucleus and phosphorylates specific transcription factors, including genes from the Pea3/Etv4 subfamily (Raible &

Brand, n.d.; Willardsen et al., 2014). It is possible that a similar process occurs in *Pt* cumulus cells, which also respond to Fgf signaling.

In addition, as supplementary to Result Chapter III (Figure S3-4), several genes show differential expression between the embryonic and extraembryonic regions at stage 2, including *Gsk3b*, *Rnf141*, *Hif1a*, *g19182*, *Creld1*, and others. The timing of their differential expression aligns with the initiation transcription of *Ets4* and *fuchi* gene in the primary thickening region, suggesting that some of these genes could be key factors in the process.

5 The formation of anterior-posterior (AP) and dorsal-ventral (DV) axes in *Pt*, along with the associated gene regulatory network (GRN), and cell lineage map

Figure 3 of the introduction provides an overview of axis formation in *Pt*, while Figure 5 and 6 highlights some of the key factors involved in this process, including *dpp*, *hh*, and *fgf8*.

The expression of *Wnt8b* (Figure 3-23, I1 to I4) at the germ disc stage was not shown in detail. It has not been discussed alongside other key factors. Additionally, prior research and review articles have typically treated the formation of the anterior-posterior (AP) and dorsal-ventral (DV) axes independently, rather than together. These points represent new insights and will be addressed in this section.

Supplementary Figure S5-5 summarizes the types of cells and the marker genes expressed by each cell type in *Pt* from stage 2 to stage 6 of development. The two columns on the right list the presence of secreted factors (Hh, Fgf8, Wnt8b, and Dpp) in different cells, based entirely on analysis rather than actual experimental results.

Wnt, Hh, and Fgf proteins are all associated with lipids, enabling them to function as long-distance morphogens during development in various species. Among these, Hh has been extensively studied in *Pt*, and it is assumed in function in the entire germ disc. Evidence for that lies in the expression of *fgf8* in *hh* RNAi embryos, when aberrant is throughout the entire germ disc region (Wang et al., 2023). Additionally, Hh expression follows a gradient pattern, rather than being evenly distributed across the germ disc. This is supported by the series of ring-shaped expressions of downstream genes of *hh*, such as *ptc*, *sog*, and *otd* (Akiyama-Oda and Oda, 2003, 2010; Pechmann et al., 2008). The 2022 study from the Oda group aligns with this view, utilizing the Hh gradient to explain the arrangement of ectodermal cells along the anterior-posterior (AP) axis, based on single-cell sequencing analysis (Akiyama-Oda et al., 2022).

The asymmetric and highly variable pattern of *fgf8* expression in the germ disc does not seem to have a strong impact, as all embryos develop into well-formed bilateral structures. While the exact details of the process remain unclear, it appears that whether or not fgf is expressed does not significantly affect the future differentiation decisions of germ disc cells in the non-cumulus path region. Therefore, Fgf will not be treated as a primary patterning factor in subsequent discussions.

The understanding of the Wnt gene in *Pt* is still at a preliminary stage. There are multiple wnt genes identified in *Pt* (Janssen et al., 2021), but only *Wnt8b* is expressed during the germ disc stage. The Result Chapter III of this thesis provides the expression pattern of Wnt8b at stage 3, 4, and 5 (Figure 3-1 S, Figure 3-5 C, Figure 3-13 I1 to I4, Figure 3-23 I1 to I4). Research on this gene has primarily focused on later stages, when the germ band is formed (McGregor et al., 2008). Knockdown of *Wnt8b* results in defects in the formation of the caudal region.

Dpp is considered a middle-to-short range morphogen. The downstream protein, Mad, which is phosphorylated (pMad), is expressed in cells along the cumulus migration path at stage 6, just before the dorsal opening begins.

Figure 5-5 illustrate the gene expression (solid color) and protein gradients (triangles) of Wnt8b, Dpp, and Hh at stages 5 and 7, taking into account the considerations mentioned above. Each gene is represented in a different color. Region with multiple gene expression are marked with a combination of the representative colors of the genes.

The image shows that the establishment of the AP axis is influenced by the gradients of Hh and Wnt8b. At stage 5, *hh* is strongly expressed in the rim (anterior) region, while *Wnt8b* is expressed in both the rim (anterior) and center (posterior) regions. By stage 7, both genes are expressed in the anterior and posterior regions, but *Wnt8b* extends further in the posterior. Cells in the germ band could differentiate according to their position within the germ disc, based on the concentration of each morphogen in the area.

The DV axis formation is only linked to the expression of *dpp* in Figure 5-5. Dpp determines the dorsal region, while the rest of the germ disc is specified as ventral. Several other genes were introduced in Result Chapter III, which stain the dorsal region of the germ band, including other Bmp genes and the Bmp inhibitor *cv-2* (supplementary, Figure S3-11). This suggests that a more detailed gene regulatory mechanism of the dorsal region remains to be discovered.

For the RNAi embryos that show defects in body axis formation, the phenotypes can be clearly explained by the absence of morphogens, as shown in the figure. This includes *Wnt8b* RNAi (McGregor et al., 2008), *hh* RNAi (Akiyama-Oda and Oda, 2010), *cv-2* RNAi, and RNAi treatments that produce the tube phenotype (*dpp, Ets4, ptc, fgf* and *twi*) as discussed in Section 3. For these RNAi experiments, the widespread production of fgf8 across the germ disc may be involved. Further investigation is required in these cases, as discussed in Section 2.

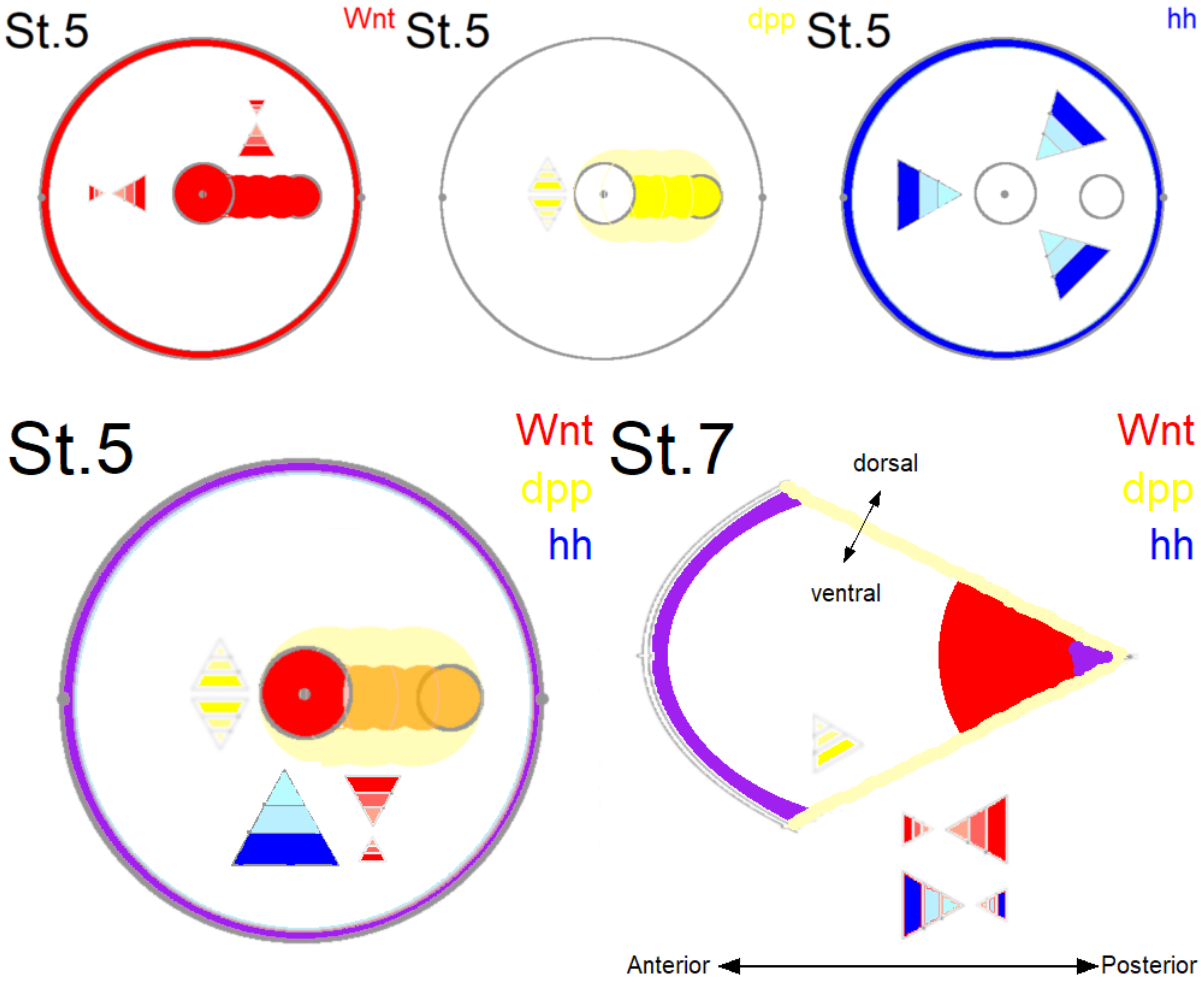

Figure 5-5. Gene expression and protein gradient of Wnt8b, Dpp, and Hh. The protein gradients of dpp and Hh are considered reliable, while the gradient of Wnt8b is a general assumption. The expression patterns of these three genes are shown both individually and in combination at stage 5, with the cumulus (depicted as a round circle) located in the middle of the rim and center of the germ disc. This is compared to the combined expression of the three genes at stage 7. In the figure, gene expression is represented by different colors, while protein gradients are indicated by triangles. Red: *Wnt8b* or Wnt8b. Yellow: *dpp* or Dpp. Blue: *hh* or Hh. Purple: *Wnt8b* and *hh*.

If I consider the developmental events from the perspective of cell differentiation, the information in Figure 5-5 and supplementary Figure S5-5 could also be interpreted as follows: homogeneous cells are programmed into various types of differentiated cells by interacting with different inducers at different times.

Figure 5-6 illustrates this process from this perspective. It depicts the different cells in the embryonic region of *Pt* development from stage 2 to stage 5, with key factors marked in different colors. The timetable is shown on the left. I assume these cells to be homogeneous when they exhibit no morphological differences and have not been detected with in situ hybridization showing distinct gene expression, as per the current research.

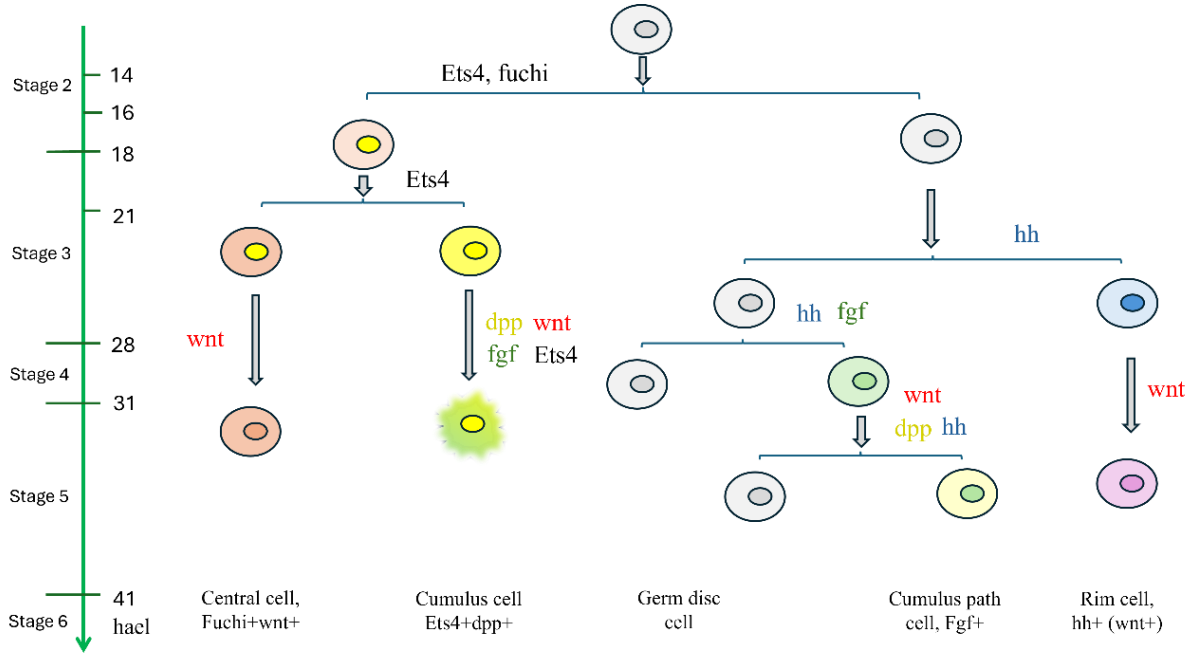

Figure 5-6. Lineage map of cells in the embryonic region of *Pt* development from stage 2 to stage 5, highlighting key factors involved in cell differentiation.

Figure 5-6 shows that at stage 2, the cells are of two types: those expressing *fuchi* and *Ets4*, and those expressing neither gene. The first type will be further divided based on the *Ets4* expression level at stage 3. *Ets4*$^{+}$ cells will later express *dpp*, *Wnt8b*, and *Fgf8* at different time points, while *Ets4*$^{-}$ cells will express *Wnt8b* during the subsequent stages.

Some cells that do not express either *fuchi* or *Ets4* will differentiate under the influence of Hh signaling. These cells will then begin to express *hh* and later, *Wnt8b* at subsequent stages.

The hypothesis presented in section 2.5 is also incorporated here, suggesting that germ disc cells receiving Fgf8 signaling will eventually express *fgf8* themselves. While the general influence of Hh on germ disc cells is mentioned, the potential for different differentiation outcomes based on varying concentrations of these signals has not been discussed.

In general, this lineage map is oversimplified, as it only takes into account a few secreted proteins. Important developmental genes, such as *Notch*, *twist*, *hunchback*, *fascin*, *fkh*, *Egfr*, and others, are not considered in this model.

The current figure is quite unique compared to the cell lineage maps of other species, as it involves the GATA family factor (*fuchi*) and ETS domain factor (*Ets4*) at the initial stage of cell differentiation. There is a possibility that the distinctive developmental process of the spider has co-evolved with these specific key factors, but no evidence supports this claim at present.

Even if I skip the first step and only consider the combination of Wnt, Dpp, Fgf, and Hh in development, no similar trajectory is observed, at least in mouse embryonic stem cell differentiation. This difference may be due to the varying complexities of early developmental stages between species. In the spider (*Pt*), until the establishment of the AP and DV axes (stage 5), the majority of the embryonic region is a single layer with no obvious differentiation into the three germ layers. In contrast, the process in mice is quite different.

In addition, the determination of the polar body-primary thickening axis, or the location of the posterior site, occurs before stage 2. This was discussed in section 1 and summarized in Table 5-1.

6 The evolution of germ disc formation, primary thickening formation and cumulus in chelicerate

The early development of *Parasteatoda tepidariorum* (*Pt*) involves key events such as germ disc formation, primary thickening formation (invagination), and cumulus migration. It is intriguing to explore whether similar processes occur in closely related species and whether differences in the morphology of animal development align with their evolutionary distances.

Figure 5-7 presents a phylogenetic tree of several invertebrate species, primarily chelicerates, whose developmental processes have been studied. The tree is based on data from NCBI Taxonomy and was visualized using the iTOL platform (https://itol.embl.de/).

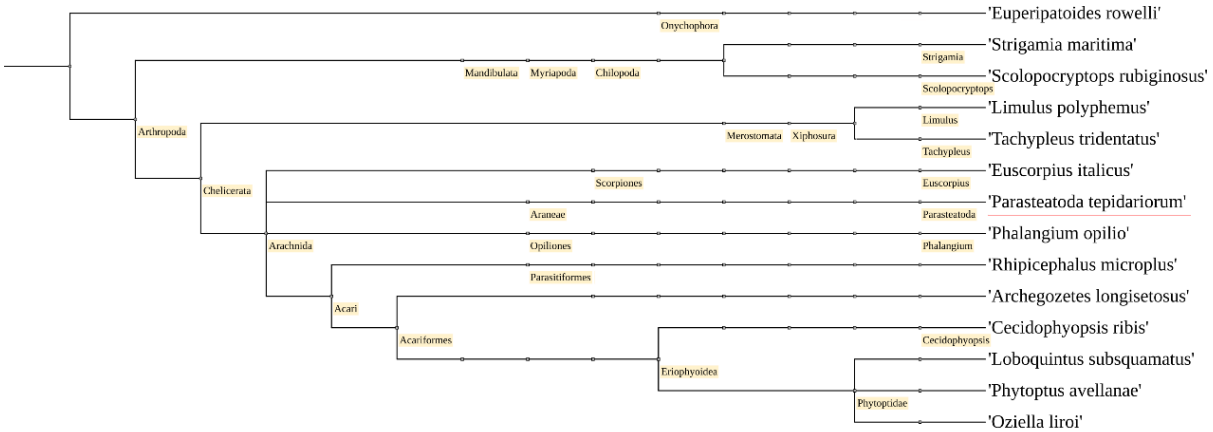

Figure 5-7. Phylogenetic tree of various invertebrate species, with *Parasteatoda tepidariorum* specifically marked by an underline in the image.

In Figure 5-7, *Parasteatoda tepidariorum* (spider) is specially marked. This species belongs to the Araneae class within the Chelicerata subphylum. Other Chelicerata species, such as horseshoe crabs, scorpions, mites, and ticks, are also included. In addition to Chelicerata, some species from the Myriapoda class of Arthropoda are also represented.

I compare the developmental processes of these animals, with a focus on: (1) the formation of the germ disc, its size, and timing; (2) the regional cell invagination process, or gastrulation, or the formation of the blastopore; and (3) whether clusters of cells migrate during early developmental stages. The comparison is summarized in Figure 5-8. As an example, Figure 5-8 combines developmental images from several species to illustrate the key considerations during this comparison.

A1 shows the *Pt* embryo at the blastoderm stage, while A2 depicts the fully formed germ disc of the animal (from Akiyama-Oda and Oda, 2003). A3 provides a lateral view of the primary thickening region, and A4 shows the embryo midway through cumulus migration.

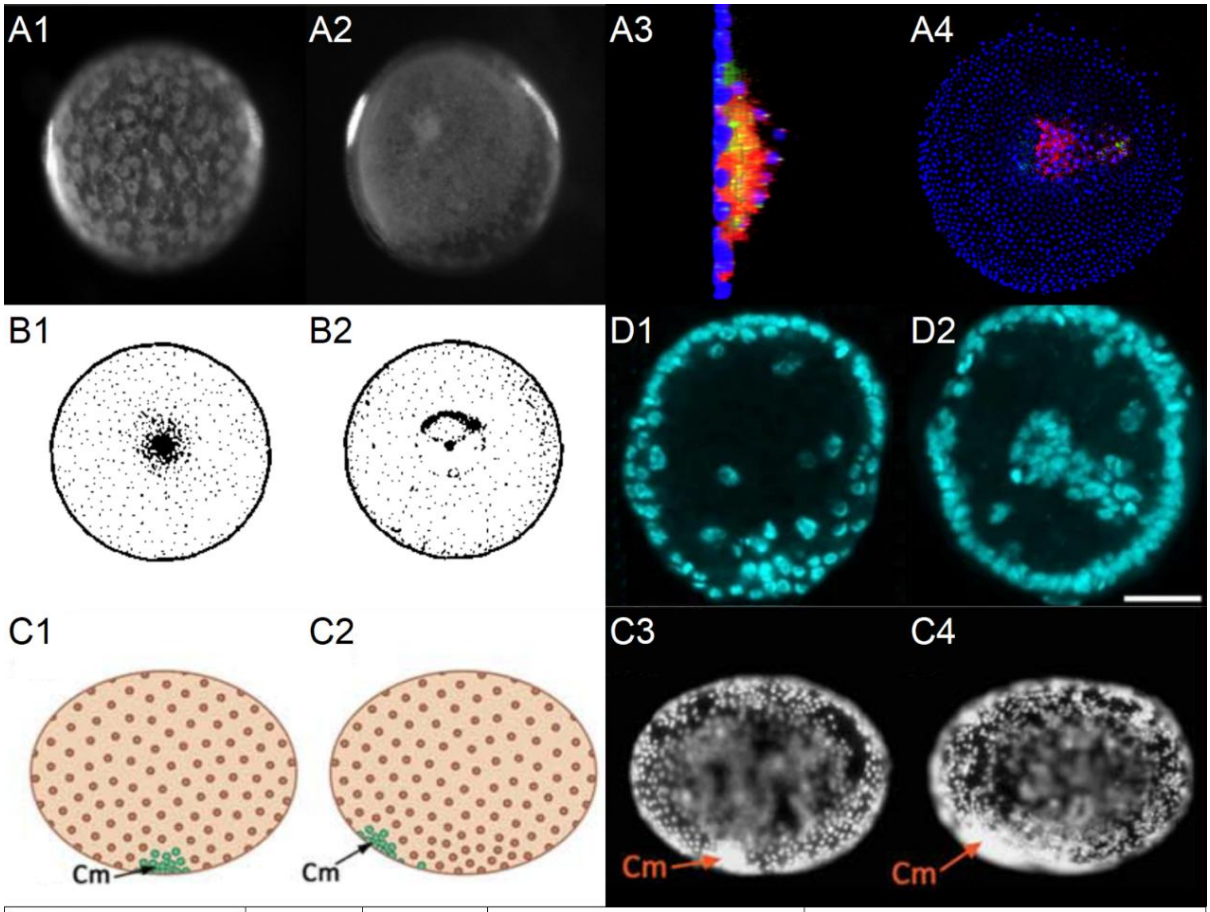

species	germ disc	densed center	cumulus migration	reference
Euperipatoides rowelli	small	Y	not observed (AP related?)	Mayer and Whitington, 2009
Strigamia maritima	complete	Y	not observed	Brena and Akam, 2011
Scolopocryptops rubiginosus	complete	Y	move, but AP related	Sakuma and Machida, 2002
Limulus polyphemus	small	Y	Y, DV related	Sekiguchi, 1960
Tachypleus tridentatus	small	Y	Y, DV related	Yamamichi and Sekiguchi, 1974
Euscorpius italicus	small	perhaps	not knowing	Laurie, 1890
Parasteatoda tepidariorum	complete	Y	Y, DV related	Akiyama-Oda and Oda, 2003
Phalangium opilio	complete	Y	not sure, (DV related?)	Gainett et al., 2022
Rhipicephalus microplus	small	Y	Y, AP related	Santos et al., 2013
Archegozetes longisetosus	complete	perhaps	not knowing	Laumann et al, 2010; Barnett and Thomas, 2017
Cecidophyopsis ribis	complete	Y	differently, penetrate to the other side	Chetverikov and Desnitskiy, 2016
Loboquintus subsquamatus	complete	Y	differently, penetrate to the other side	Chetverikov and Desnitskiy, 2016
Phytoptus avellanae	complete	Y	differently, penetrate to the other side	Chetverikov and Desnitskiy, 2016
Oziella liroi	complete	Y	differently, penetrate to the other side	Chetverikov and Desnitskiy, 2016

Figure 5-8. Selected images depicting the development of *Parasteatoda tepidariorum* (*Pt*; A1, A2, A3, A4), *Tachypleus tridentatus* (*Tt*; B1, B2), *Rhipicephalus microplus* (*Rm*; C1, C2, C3, C4), and *Cecidophyopsis ribis* (*Cr*; D1, D2) are shown. A1 and A2 are from Akiyama-Oda and Oda, 2003, A3 and A4 are from this thesis, and the sources for the remaining images are listed in the table. Additionally, a comparison of species from Figure 5-7 is provided, focusing on aspects of germ disc formation, primary thickening formation, and cumulus migration.

The development of *Tachypleus tridentatus* (*Tt*; B1, B2; horseshoe crab; Yamamichi and sekiguchi, 1974) shows many similarities to the development of *Pt*. B1 depicts the formation of the germ disc in the *Tt* embryo, and B2 shows the opening of the germ disc after cumulus migration. This process closely resembles the development of *Pt* from stages 4 to 7. The main difference is the size of the germ disc, which is much larger in *Pt* and more regional in *Tt*.

Rhipicephalus microplus (*Rm*; C1-C4; ticks; Santos et al., 2013) shows a blastoderm stage similar to *Pt* (C1, C3), with the only difference being the shape of the embryos. Local cell invagination and internalized cells initiate migration, and the future germ band highly depends on this migration process (C2, C4), which is similar to *Pt* in priciple. However, in *Pt*, the germ disc forms as a condensed structure before cumulus movement starts, whereas in *Rm*, the majority of the embryonic cells are relatively loose in structure. Furthermore, the cumulus migration in *Pt* promotes the detachment and movement of ectoderm cells along the path, while in *Rm*, a more condensed structure is formed along the path to become the future germ band, likely due to an increase in cell adhesion. This marks a key difference between the two species.

A very recent study detected pMad expression in a cluster of cells beneath the surface epithelial cells layers at stage 5 of the tick *Ixodes scapularis* (Hinne et al., 2025). This cell cluster is observed at the posterior of the developing germ band in subsequent stages.These findings confirm observations in *Rm* and provide strong evidence that the migrating cell cluster (the cumulus) in ticks also expresses *dpp*, similar to the cumulus cells in *Pt* development.

Cecidophyopsis ribis (*Cr*; D1, D2; eriophyid mites; Chetverikov and Desnitskiy, 2016) also exhibit a blastoderm stage, with certain cells undergoing invagination into the inner region (D1), similar to the invagination process in *Pt*. However, in *Cr*, the internalized cells pass through the entire embryo until it reaches the opposite side (D2), a process that does not occur during *Pt* development. Although, strictly speaking, the internalized cells are also involved in movement, their movement is quite distinct from the cumulus movement in Rm and Pt, where the cell migration path is closely located beneath the ectoderm.

Using a similar method, the development of other species was analyzed and summarized in a table, as shown in Figure 5-8. If a developmental event is similar to that observed in *Pt*, a “Y” is marked; otherwise, an “N” is marked. The species in the table are listed in the same order as in Figure 5-7, and the species discussed in the paragraphs above are highlighted in color.

The comparison highlights the significant diversity in the developmental processes across species. The formation of the blastoderm is widely observed, as is the process where certain regional cells internalize beneath the ectoderm, while the majority of the cells remain on the surface. This process is referred to by different terms in various species, including invagination, gastrulation, primary thickening formation, and blastopore formation.

The formation of the germ disc varies in size among species. Two species in Myriapoda and chelicerate species from Araneae, Opiliones, and Acariformes exhibit large-sized germ discs similar to those in *Pt*, which distinguishes them from other species.

Cell movement after internalization is observed more frequently than expected. While this movement may be primarily related to the formation of the anterior–posterior (AP) axis, the dorsal–ventral (DV) axis, or directed toward the yolk—potentially followed by various cellular activities—this has been demonstrated in comparisons among *Rm*, *Cr*, and *Pt*. It seems highly likely that a conserved “toolkit” for this process exists within the developmental “toolbox” of arthropods.

However, strictly speaking, it has not been proven that all invaginated cells are homologous. Apart from the *dpp* expression observed in the tick *Ixodes scapularis*, there is very limited information available to compare the nature of migrating cells across different species. Therefore, it would be an oversimplification to assume that all invagination and cell movement processes are homologous among species without further research on the topic.

Moreover, in the analysis of the species listed, there is no developmental process resembling the tube-like phenotype observed in *dpp* RNAi, *Ets4* RNAi, etc., in *Pt*. This tube-like phenotype can fully recover; however, the order of DV axis formation and AP axis elongation is altered compared to the

normal development process in *Pt*. Yet, no definitive conclusion can be drawn based on the limited number of species examined in this study.

To briefly answer the earlier question: blastoderm formation and blastopore formation (invagination) are commonly observed, as well the general process of germ disc formation and internal cell movement. However, the size of the germ disc, and the outcome of the cell movement, vary among arthropods. The development of the horseshoe crab shares many similarities with that of spider development, despite horseshoe crabs not being the closest relatives to spiders on the phylogenetic tree. The reliability of this judgment needs further confirmation, and additional molecular comparisons could be conducted.

7 General analysis of gene regulation network, and organization of gene clusters.

The complete transcriptome of *Pt* contains 32,187 transcripts (Posnien et al., 2014). Sequencing data from cells in the primary thickening region of WT or *Ets4* RNAi embryos reveal around 16,000 transcripts with detectable expression levels. Among them, 800 genes were identified as differentially expressed between the two types of embryos. These are large numbers to consider. How do cells coordinate the activity of 10,000 to 20,000 genes? By what mechanism does the reduction in expression of a single gene, such as *Ets4*, lead to changes in nearly 800 other genes? What mechanisms determine which genes are affected and which are not? These are complex and intriguing questions.

Modularity Theory suggests that the development process consists of various modules, each regulating specific aspects of development without influencing the rest (Alcalá-Corona et al., 2021; Carroll, 2008; Jaeger & Monk, 2021; Pereira-Leal et al., 2006). From this perspective, the primary thickening cells in *Ets4* RNAi embryos shut down or regulate the modules associated with *Ets4*, while leaving other modules unaffected.

Further questions: In the *Pt* WT embryos, how many modules are there? What are the molecular representatives of each module? Are they all independent of each other?

Based on the research in this thesis, the current understanding of these questions is as follows:

Genes express in primary thickening region, could be classified in at least four types: expression lasts from stage 2 to stage 5 (I), from stage 2 to stage 4 (II), from stage 2 to stage 3 (III), and from stage 3 to stage 4 (IV).

Firstly, there are distinct groups of genes (as detailed in Result Chapter III, section 1.3 and 3.3), with each group exhibiting different expression patterns, either in specific regions or at different developmental stages. Genes expressed in the primary thickening region can be classified into at least four types: expression lasts from stage 2 to stage 5 (Type I); from stage 2 to stage 4 (Type II); from stage 2 to stage 3 (Type III); and from stage 3 to stage 4 (Type IV).

Secondly, among the genes downregulated with the knockdown of *Ets4*, some belong to type II genes (e.g., *Pla2, Abhd11, g9727, Mtmr14, g9731, Anxa1, g4424*), while others are type IV genes (e.g., *Itpka, L(2)efl, Rf_0381, opa, Znf423, ptc, Wnt8b, Clca4a, twist*, and *hb*). Many genes that are upregulated with the knockdown of *Ets4* belong to type III (e.g., *Delta, hh, Hif, Idh2*, and *Asph*). Most type I genes show a consistent expression pattern in both WT and *Ets4* RNAi embryos.

Thirdly, the function of *Ets4*-related genes includes those involved in cell adhesion, cytoskeleton organization, cell movement, as well as genes related to development and cell differentiation.

Fourthly, based on the RNAi embryo phenotype, it appears that the potential downstream genes of *Ets4*, classified as Type IV, are involved in cell movement and development/cell differentiation. On

the other hand, many potential downstream genes of *Ets4*, classified as Type II, play roles in cell adhesion. These genes also express at stage 2, possibly contributing to germ disc contraction as well.

Fifthly, genes that are expressed at similar levels in both WT and *Ets4* RNAi embryos, potentially independent of *Ets4* and the "*Ets4* module", include those involved in development (e.g., *dpp, fuchi, Gsk3b g9959, Gsk3b g25394*), cell proliferation (e.g., *Cyclin A, Cyclin B*), and others with unclear functions (e.g., *fkh, g592, Creld1, Creld2 g7589, Pik3c3, Idh3g g14882, Snip1, Idh1, Akt*, and *Prkc2*).

In summary, it appears that primary thickening cells organize cellular activities as follows: *Ets4* directly or indirectly influences 800 genes. Among these genes, some are expressed at earlier stages and may also be regulated by other genes, likely involved in cell adhesion. Other genes are expressed at the same stage or later than *Ets4* and in the same location; these genes are associated with cell movement and differentiation. A third group of genes is inhibited by *Ets4* and are not expressed in the primary thickening region of WT embryos. These genes may belong to the *Ets4* module or modules related to it.

Very little is known about the modules independent of the *Ets4* module. I suspect that all genes in Tpye I share this characteristic. So far, it appears that genes associated with cell proliferation belong to this category, along with a variety of other developmental genes.

This understanding is still in its early stages and is far from complete, but it is included here for the sake of completeness in this thesis. In future study, exploring the intriguing gene arrangements, and investigate whether this organization is conserved across species and identifying any differences could provide valuable insights into the evolution of developmental processes.

8. Limitation of the current method, and brief Outlook

This thesis primarily focuses on the early developmental stages of *Parasteatoda tepidariorum*, specifically the processes of the invagination of primary thickening cells, the migration of cumulus cells, as well as the regulatory genes involved in both processes. Since the formation of the AP and DV axes in the developing embryo is closely linked to these events, this study also offers new insights into axis formation.

Additional data and further experimental results will be necessary to validate the current findings and to enhance our understanding. These may include: Tests of transcriptional regulation of gene *Ets4* and by Ets4; Crispr experiments to create transgenic lines for *twist*; further investigation of selected genes from *Ets4* RNA-seq data; including those related to Wnt signaling, cytoskeleton, and adhesion proteins during invagination; testing the hypothesis of signal transduction as discussed in Section 2; detection of cytoskeleton protein expression during cumulus migration to elucidate detailed steps of the process; functional analysis of polar body-related genes; cell culture and in vitro cell migration experiments; studies on metabolism and yolk consumption; literature review on the evolution of development in other chelicerates, among others.

8 References

Akiyama-Oda, Y., Akaiwa, T., & Oda, H. (2022). Reconstruction of the Global Polarity of an Early Spider Embryo by Single-Cell and Single-Nucleus Transcriptome Analysis. *Frontiers in Cell and Developmental Biology*, *10*. https://doi.org/10.3389/fcell.2022.933220

Akiyama-Oda, Y., & Oda, H. (2003). Early patterning of the spider embryo: A cluster of mesenchymal cells at the cumulus produces Dpp signals received by germ disc epithelial cells. In *Development* (Vol. 130, Issue 9, pp. 1735–1747). https://doi.org/10.1242/dev.00390

Akiyama-Oda, Y., & Oda, H. (2006). Axis specification in the spider embryo: Dpp is required for radial-to-axial symmetry transformation and sog for ventral patterning. *Development*, *133*(12), 2347–2357. https://doi.org/10.1242/dev.02400

Akiyama-Oda, Y., & Oda, H. (2010). Cell migration that orients the dorsoventral axis is coordinated with anteroposterior patterning mediated by Hedgehog signaling in the early spider embryo. *Development*, *137*(8), 1263–1273. https://doi.org/10.1242/dev.045625

Akiyama-Oda, Y., & Oda, H. (2020). Hedgehog signaling controls segmentation dynamics and diversity via msx1 in a spider embryo. In *Sci. Adv* (Vol. 6). https://www.science.org

Alcalá-Corona, S. A., Sandoval-Motta, S., Espinal-Enríquez, J., & Hernández-Lemus, E. (2021). Modularity in Biological Networks. In *Frontiers in Genetics* (Vol. 12). Frontiers Media S.A. https://doi.org/10.3389/fgene.2021.701331

Asashima, M., & Satou-Kobayashi, Y. (2024). Spemann-Mangold organizer and mesoderm induction. *Cells and Development*, *178*. https://doi.org/10.1016/j.cdev.2024.203903

Balasubramanian, R., & Zhang, X. (2016). Mechanisms of FGF gradient formation during embryogenesis. In *Seminars in Cell and Developmental Biology* (Vol. 53, pp. 94–100). Academic Press. https://doi.org/10.1016/j.semcdb.2015.10.004

Bökel, C., & Brand, M. (2013). Generation and interpretation of FGF morphogen gradients in vertebrates. In *Current Opinion in Genetics and Development* (Vol. 23, Issue 4, pp. 415–422). https://doi.org/10.1016/j.gde.2013.03.002

Briscoe, J., & Thérond, P. P. (2013). The mechanisms of Hedgehog signalling and its roles in development and disease. In *Nature Reviews Molecular Cell Biology* (Vol. 14, Issue 7, pp. 418–431). Nature Publishing Group. https://doi.org/10.1038/nrm3598

Carroll, S. B. (2008). Evo-Devo and an Expanding Evolutionary Synthesis: A Genetic Theory of Morphological Evolution. In *Cell* (Vol. 134, Issue 1, pp. 25–36). Elsevier B.V. https://doi.org/10.1016/j.cell.2008.06.030

De Robertis, E. M. (2008). Evo-Devo: Variations on Ancestral Themes. In *Cell* (Vol. 132, Issue 2, pp. 185–195). Elsevier B.V. https://doi.org/10.1016/j.cell.2008.01.003

De Robertis, E. M. (2009). Spemann's organizer and the self-regulation of embryonic fields. In *Mechanisms of Development* (Vol. 126, Issues 11–12, pp. 925–941). https://doi.org/10.1016/j.mod.2009.08.004

Dobson, A. J., Boulton-McDonald, R., Houchou, L., Svermova, T., Ren, Z., Subrini, J., Vazquez-Prada, M., Hoti, M., Rodriguez-Lopez, M., Ibrahim, R., Gregoriou, A., Gkantiragas, A., Bähler, J., Ezcurra, M., & Alic, N. (2019). Longevity is determined by ETS transcription factors in

multiple tissues and diverse species. *PLoS Genetics*, *15*(7). https://doi.org/10.1371/journal.pgen.1008212

Dormann, D., & Weijer, C. J. (2006). Imaging of cell migration. In *EMBO Journal* (Vol. 25, Issue 15, pp. 3480–3493). https://doi.org/10.1038/sj.emboj.7601227

Driever, W., & Nusslein-Volhard, C. (1988). A Gradient of bicoid Protein in Drosophila Embryos. In *Cell* (Vol. 54).

Duguay, D., Foty, R. A., & Steinberg, M. S. (2003). *Cadherin-mediated cell adhesion and tissue segregation: qualitative and quantitative determinants*. www.elsevier.com/locate/ydbio

Edgar, A., Bates, C., Larkin, K., & Black, S. (2015). Gastrulation occurs in multiple phases at two distinct sites in Latrodectus and Cheiracanthium spiders. *EvoDevo*, *6*(1), 1. https://doi.org/10.1186/s13227-015-0029-z

Fagotto, F. (2014). The cellular basis of tissue separation. In *Development (Cambridge)* (Vol. 141, Issue 17, pp. 3303–3318). Company of Biologists Ltd. https://doi.org/10.1242/dev.090332

Feitosa, N. M., Pechmann, M., Schwager, E. E., Tobias-Santos, V., McGregor, A. P., Damen, W. G. M., & Nunes da Fonseca, R. (2017). Molecular control of gut formation in the spider Parasteatoda tepidariorum. *Genesis (New York, N.Y. : 2000)*, *55*(5). https://doi.org/10.1002/dvg.23033

Foty, R. A., & Steinberg, M. S. (2005). The differential adhesion hypothesis: A direct evaluation. *Developmental Biology*, *278*(1), 255–263. https://doi.org/10.1016/j.ydbio.2004.11.012

Geiger, B., & Yamada, K. M. (2011). Molecular architecture and function of matrix adhesions. *Cold Spring Harbor Perspectives in Biology*, *3*(5), 1–21. https://doi.org/10.1101/cshperspect.a005033

Genikhovich, G., & Technau, U. (2017). On the evolution of bilaterality. *Development (Cambridge)*, *144*(19), 3392–3404. https://doi.org/10.1242/dev.141507

Gheisari, E., Aakhte, M., & Müller, H. A. J. (2020). Gastrulation in Drosophila melanogaster: Genetic control, cellular basis and biomechanics. In *Mechanisms of Development* (Vol. 163). Elsevier Ireland Ltd. https://doi.org/10.1016/j.mod.2020.103629

Gilbert, S., & Barresi, M. (n.d.). *Developmental Biology* (11th ed.).

Heldin, C.-H., Miyazono, K., & Peter, &. (1997). TGF-signalling from cell membrane to nucleus through SMAD proteins. In *Nature © Macmillan Publishers Ltd* (Vol. 390).

Hilbrant, M., Damen, W. G. M., & McGregor, A. P. (2012). Evolutionary crossroads in developmental biology: the spider Parasteatoda tepidariorum. In *Development (Cambridge, England)* (Vol. 139, Issue 15, pp. 2655–2662). https://doi.org/10.1242/dev.078204

Hinne, I. A., Ciccotti, H. R., Wudarski, J., Pham, M. N., Sharma, A., McVicar, M. M., Faustino, B., Nuss, A. B., Sharma, P. P., & Gulia-Nuss, M. (2025). Early embryonic development in the tick Ixodes scapularis suggests syncytial organization and cellularization before blastoderm formation. *EvoDevo*, *16*(1), 4. https://doi.org/10.1186/s13227-025-00240-y

Hollenhorst, P. C., McIntosh, L. P., & Graves, B. J. (2011). Genomic and biochemical insights into the specificity of ETS transcription factors. *Annual Review of Biochemistry*, *80*, 437–471. https://doi.org/10.1146/annurev.biochem.79.081507.103945

Holm, A. (n.d.). *Holm1952 Spinnenentwicklung*.

Ingham, P. W., & McMahon, A. P. (2001). Hedgehog signaling in animal development: Paradigms and principles. In *Genes and Development* (Vol. 15, Issue 23, pp. 3059–3087). https://doi.org/10.1101/gad.938601

Iwasaki-Yokozawa, S., Nanjo, R., Akiyama-Oda, Y., & Oda, H. (2022). Lineage-specific, fast-evolving GATA-like gene regulates zygotic gene activation to promote endoderm specification and pattern formation in the Theridiidae spider. *BMC Biology*, *20*(1). https://doi.org/10.1186/s12915-022-01421-0

Jaeger, J., & Monk, N. (2021). Dynamical modules in metabolism, cell and developmental biology. *Interface Focus*, *11*(3). https://doi.org/10.1098/rsfs.2021.0011

Janssen, R., Pechmann, M., & Turetzek, N. (2021). A chelicerate Wnt gene expression atlas: novel insights into the complexity of arthropod Wnt-patterning. *EvoDevo*, *12*(1). https://doi.org/10.1186/s13227-021-00182-1

Kanayama, M., Akiyama-Oda, Y., Nishimura, O., Tarui, H., Agata, K., & Oda, H. (2011). Travelling and splitting of a wave of hedgehog expression involved in spider-head segmentation. *Nature Communications*, *2*(1). https://doi.org/10.1038/ncomms1510

Kanayama, M., Akiyama-Oda, Y., & Oda, H. (2010). Early embryonic development in the spider Achaearanea tepidariorum: Microinjection verifies that cellularization is complete before the blastoderm stage. *Arthropod Structure and Development*, *39*(6), 436–445. https://doi.org/10.1016/j.asd.2010.05.009

Leite, D. J., Schönauer, A., Blakeley, G., Harper, A., Garcia-Castro, H., Baudouin-Gonzalez, L., Wang, R., Sarkis, N., Nikola, A. G., Koka, V. S. P., Kenny, N. J., Turetzek, N., Pechmann, M., Solana, J., & McGregor, A. P. (2024). An atlas of spider development at single-cell resolution provides new insights into arthropod embryogenesis. *EvoDevo*, *15*(1). https://doi.org/10.1186/s13227-024-00224-4

Marlétaz, F., Couloux, A., Poulain, J., Labadie, K., Da Silva, C., Mangenot, S., Noel, B., Poustka, A. J., Dru, P., Pegueroles, C., Borra, M., Lowe, E. K., Lhomond, G., Besnardeau, L., Le Gras, S., Ye, T., Gavriouchkina, D., Russo, R., Costa, C., … Lepage, T. (2023). Analysis of the P. lividus sea urchin genome highlights contrasting trends of genomic and regulatory evolution in deuterostomes. *Cell Genomics*, *3*(4). https://doi.org/10.1016/j.xgen.2023.100295

McGregor, A. P., Hilbrant, M., Pechmann, M., Schwager, E. E., Prpic, N. M., & Damen, W. G. M. (2008). Cupiennius salei and Achaearanea tepidariorum: Spider models for investigating evolution and development. In *BioEssays* (Vol. 30, Issue 5, pp. 487–498). https://doi.org/10.1002/bies.20744

Mittmann, B., & Wolff, C. (2012). Embryonic development and staging of the cobweb spider Parasteatoda tepidariorumC. L. Koch, 1841 (syn.: Achaearanea tepidariorum; Araneomorphae; Theridiidae). *Development Genes and Evolution*, *222*(4), 189–216. https://doi.org/10.1007/s00427-012-0401-0

Nishiguchi, S., & Oda, H. (2021). Structural variability and dynamics in the ectodomain of an ancestral-type classical cadherin revealed by AFM imaging. *Journal of Cell Science*, *134*(14). https://doi.org/10.1242/jcs.258388

Oda, H., Iwasaki-Yokozawa, S., Usui, T., & Akiyama-Oda, Y. (2020). Experimental duplication of bilaterian body axes in spider embryos: Holm's organizer and self-regulation of embryonic fields. In *Development Genes and Evolution* (Vol. 230, Issue 2, pp. 49–63). Springer. https://doi.org/10.1007/s00427-019-00631-x

Oda, H., Nishimura, O., Hirao, Y., Tarui, H., Agata, K., & Akiyama-Oda, Y. (2007). Progressive activation of Delta-Notch signaling from around the blastopore is required to set up a functional caudal lobe in the spider Achaearanea tepidariorum. *Development*, *134*(12), 2195–2205. https://doi.org/10.1242/dev.004598

Ornitz, D. M., & Itoh, N. (2015). The fibroblast growth factor signaling pathway. *Wiley Interdisciplinary Reviews: Developmental Biology*, *4*(3), 215–266. https://doi.org/10.1002/wdev.176

Panfilio, K. A. (2022). Plasticity in patterning and gestation at the eco-evo-devo interface. In *Development Genes and Evolution* (Vol. 232, Issues 2–4, pp. 49–50). Springer Science and Business Media Deutschland GmbH. https://doi.org/10.1007/s00427-022-00692-5

Pechmann, M. (2016). Formation of the germ-disc in spider embryos by a condensation-like mechanism. *Frontiers in Zoology*, *13*(1). https://doi.org/10.1186/s12983-016-0166-9

Pechmann, M. (2017). *A novel role for Ets4 in axis specification and cell migration in the spider Parasteatoda tepidariorum*. https://doi.org/10.7554/eLife.27590.001

Pechmann, M. (2020). Embryonic development and secondary axis induction in the Brazilian white knee tarantula Acanthoscurria geniculata, C. L. Koch, 1841 (Araneae; Mygalomorphae; Theraphosidae). *Development Genes and Evolution*, *230*(2), 75–94. https://doi.org/10.1007/s00427-020-00653-w

Pechmann, M., McGregor, A. P., Schwager, E. E., lia Feitosa, N. M., & M Damen, W. G. (2009). *Dynamic gene expression is required for anterior regionalization in a spider*. www.pnas.org/cgi/content/full/

Pereira-Leal, J. B., Levy, E. D., & Teichmann, S. A. (2006). The origins and evolution of functional modules: Lessons from protein complexes. *Philosophical Transactions of the Royal Society B: Biological Sciences*, *361*(1467), 507–517. https://doi.org/10.1098/rstb.2005.1807

Posnien, N., Zeng, V., Schwager, E. E., Pechmann, M., Hilbrant, M., Keefe, J. D., Damen, W. G. M., Prpic, N. M., McGregor, A. P., & Extavour, C. G. (2014). A comprehensive reference transcriptome resource for the common house spider Parasteatoda tepidariorum. *PLoS ONE*, *9*(8). https://doi.org/10.1371/journal.pone.0104885

Prpic, N. M., & Pechmann, M. (2022). Extraembryonic tissue in chelicerates: a review and outlook. In *Philosophical Transactions of the Royal Society B: Biological Sciences* (Vol. 377, Issue 1865). Royal Society Publishing. https://doi.org/10.1098/rstb.2021.0269

Raible, F., & Brand, M. (n.d.). *Tight transcriptional control of the ETS domain factors Erm and Pea3 by Fgf signaling during early zebra®sh development*. www.elsevier.com/locate/modo

Reddy, P. C., Gungi, A., Ubhe, S., & Galande, S. (2020). Epigenomic landscape of enhancer elements during Hydra head organizer formation. *Epigenetics and Chromatin*, *13*(1). https://doi.org/10.1186/s13072-020-00364-6

Roth, S. (2025). Neofunctionalization of Toll Signaling in Insects: From Immunity to Dorsoventral Patterning. *Annual Review of Cell and Developmental Biology Downloaded from Www.Annualreviews.Org. Guest*, *31*, 19. https://doi.org/10.1146/annurev-cellbio-120319

Roth, S., Shira Neuman-Silberberg, F., Barcelo, G., & SchLipbach, T. (1995). cornichon and the EGF Receptor Signaling Process Are Necessary for Both Anterior-Posterior and Dorsal-Ventral Pattern Formation in Drosophila. In *Cell* (Vol. 81).

Saito-Diaz, K., Chen, T. W., Wang, X., Thorne, C. A., Wallace, H. A., Page-Mccaw, A., & Lee, E. (2013). The way Wnt works: Components and mechanism. *Growth Factors*, *31*(1), 1–31. https://doi.org/10.3109/08977194.2012.752737

Santos, V. T., Ribeiro, L., Fraga, A., de Barros, C. M., Campos, E., Moraes, J., Fontenele, M. R., Araújo, H. M., Feitosa, N. M., Logullo, C., & Da Fonseca, R. N. (2013). The embryogenesis of the Tick Rhipicephalus (Boophilus) microplus: The establishment of a new chelicerate model system. *Genesis*, *51*(12), 803–818. https://doi.org/10.1002/dvg.22717

Sasaki, M., Akiyama-Oda, Y., & Oda, H. (2017). Evolutionary origin of type IV classical cadherins in arthropods. *BMC Evolutionary Biology*, *17*(1). https://doi.org/10.1186/s12862-017-0991-2

Scarpa, E., & Mayor, R. (2016). Collective cell migration in development. *Journal of Cell Biology*, *212*(2), 143–155. https://doi.org/10.1083/jcb.201508047

Schwager, E. E., Meng, Y., & Extavour, C. G. (2015). Vasa and piwi are required for mitotic integrity in early embryogenesis in the spider Parasteatoda tepidariorum. *Developmental Biology*, *402*(2), 276–290. https://doi.org/10.1016/j.ydbio.2014.08.032

Schwager, E. E., Pechmann, M., Feitosa, N. M., McGregor, A. P., & Damen, W. G. M. (2009). hunchback Functions as a Segmentation Gene in the Spider Achaearanea tepidariorum. *Current Biology*, *19*(16), 1333–1340. https://doi.org/10.1016/j.cub.2009.06.061

Schwager, E. E., Schönauer, A., Leite, D. J., Sharma, P. P., & McGregor, A. P. (2015). Chelicerata. In *Evolutionary Developmental Biology of Invertebrates 3: Ecdysozoa I: Non-Tetraconata* (pp. 99–139). Springer-Verlag Vienna. https://doi.org/10.1007/978-3-7091-1865-8_5

SenGupta, S., Parent, C. A., & Bear, J. E. (2021). The principles of directed cell migration. In *Nature Reviews Molecular Cell Biology* (Vol. 22, Issue 8, pp. 529–547). Nature Research. https://doi.org/10.1038/s41580-021-00366-6

Suzuki, H. (1995). Fertilization occurs internally in the spider Achaearanea tepidariorum (C. Koc h)'. In *Invertebrate Reproduction and Development* (Vol. 28, Issue 3).

Swaney, K. F., Huang, C. H., & Devreotes, P. N. (2010). Eukaryotic chemotaxis: A network of signaling pathways controls motility, directional sensing, and polarity. In *Annual Review of Biophysics* (Vol. 39, Issue 1, pp. 265–289). https://doi.org/10.1146/annurev.biophys.093008.131228

Theveneau, E., Marchant, L., Kuriyama, S., Gull, M., Moepps, B., Parsons, M., & Mayor, R. (2010). Collective Chemotaxis Requires Contact-Dependent Cell Polarity. *Developmental Cell*, *19*(1), 39–53. https://doi.org/10.1016/j.devcel.2010.06.012

Tojima, T., Itofusa, R., & Kamiguchi, H. (2010). Asymmetric clathrin-mediated endocytosis drives repulsive growth cone guidance. *Neuron*, *66*(3), 370–377. https://doi.org/10.1016/j.neuron.2010.04.007

Wang, R., Leite, D. J., Karadas, L., Schiffer, P. H., & Pechmann, M. (2023). FGF signalling is involved in cumulus migration in the common house spider Parasteatoda tepidariorum. *Developmental Biology*, *494*, 35–45. https://doi.org/10.1016/j.ydbio.2022.11.009

Wang, R., & Pechmann, hias. (n.d.). *Polar bodies serve as a landmark for anteroposterior axis forma4on in spiders*. https://doi.org/doi.org/10.1101/2024.09.30.615744

WASYLYK, B., HAHN, S. L., & GIOVANE, A. (1993). The Ets family of transcription factors. *European Journal of Biochemistry*, *211*(1–2), 7–18. https://doi.org/10.1111/j.1432-1033.1993.tb19864.x

Wei, G. H., Badis, G., Berger, M. F., Kivioja, T., Palin, K., Enge, M., Bonke, M., Jolma, A., Varjosalo, M., Gehrke, A. R., Yan, J., Talukder, S., Turunen, M., Taipale, M., Stunnenberg, H. G., Ukkonen, E., Hughes, T. R., Bulyk, M. L., & Taipale, J. (2010). Genome-wide analysis of ETS-family DNA-binding in vitro and in vivo. *EMBO Journal*, *29*(13), 2147–2160. https://doi.org/10.1038/emboj.2010.106

Willardsen, M., Hutcheson, D. A., Moore, K. B., & Vetter, M. L. (2014). The ETS transcription factor Etv1 mediates FGF signaling to initiate proneural gene expression during Xenopus laevis retinal development. *Mechanisms of Development*, *131*(1), 57–67. https://doi.org/10.1016/j.mod.2013.10.003

Xu, J., Du, Y., & Deng, H. (2015). Direct lineage reprogramming: Strategies, mechanisms, and applications. In *Cell Stem Cell* (Vol. 16, Issue 2, pp. 119–134). Cell Press. https://doi.org/10.1016/j.stem.2015.01.013

YAMAMICHI, Y., & SEKIGUCHI, K. (1974). EMBRYO AND ORGAN CULTURES OF THE HORSESHOE CRAB, TACHYPLEUS TRIDENTATUS. *Development, Growth & Differentiation*, *16*(4), 295–304. https://doi.org/10.1111/j.1440-169X.1974.00295.x

Yamazaki, K., Akiyama-Oda, Y., & Oda, H. (2005). *Expression Patterns of a twist-Related Gene in Embryos of the Spider Achaearanea tepidariorum Reveal Divergent Aspects of Mesoderm Development in the Fly and Spider*.

9 Supplementary Figures and Tables

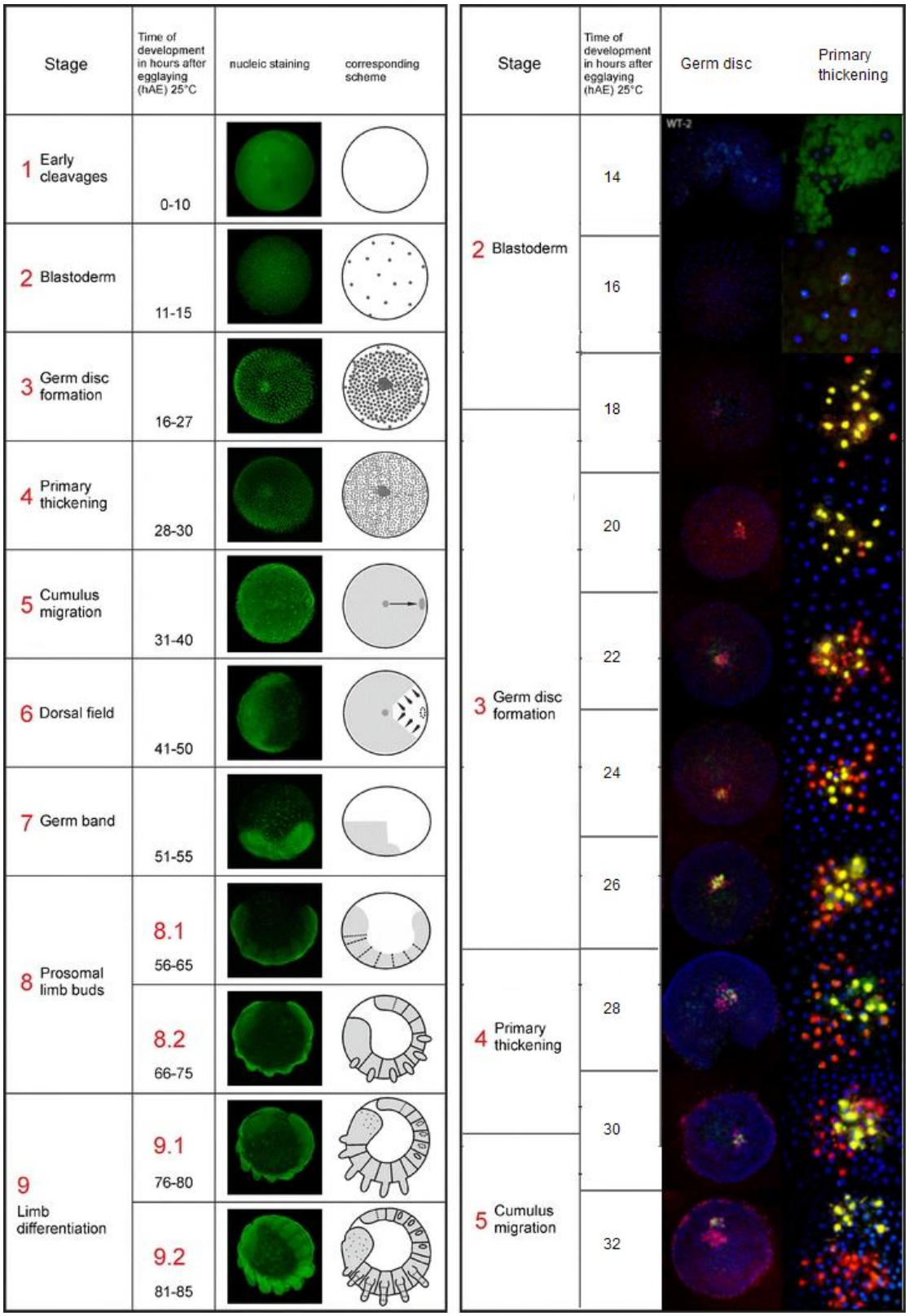

Supplementary Figure 1. Early development of *Parasteatoda tepidariorum*. The left side of the image was modified from Mittmann and Wolff, 2012, while the right side was from the images in Result Chapter I.

(Supplementary Figures and Tables for Result Chapter I)

Table S1-1 number of frames from video, and corresponding hael hours of WT embryos.

Source of video	Frame Interval	11 hael	28 hael	31 hael	41 hael
description		Most nucleus move to the surface; total cell number 32 to 64.	germ disc contracts to the smallest size, facing upwards, rim region stable.	Initiation of cumulus migration.	cumulus reached the rim region, while the migration path has not opened.
2016 paper	10min	1	137	161	241
2017 paper	10min		43	61	121
2020 stack 14	30min	6	42		
2020 stack 49	30min	1	38	45	
2020 stack 57	30min	4	40	46	
2022 stack 13-3	15min	1	70	82	122
HCR WT-1	2h		6h (27hael)	10h	
HCR WT-2	2h		14hh	18h (32 hael)	

Table S1-2. number of frames from video, and corresponding hael hours of Ets4 RNAi embryos.

	First frame	28 hael	31 hael	41 hael	52 hael
2017 paper	23 hael	31	49	109	175
2023 HCR image	21 hael	6h (27hael)	10h		
2023 HCR video 1-44	21.5 hael	14	20	40	62 (50)
2023 HCR video 2-14	21.5 hael	14	20	40	62 (50)
2023 HCR video 2-44	21.5 hael	14	20	40	62 (50)

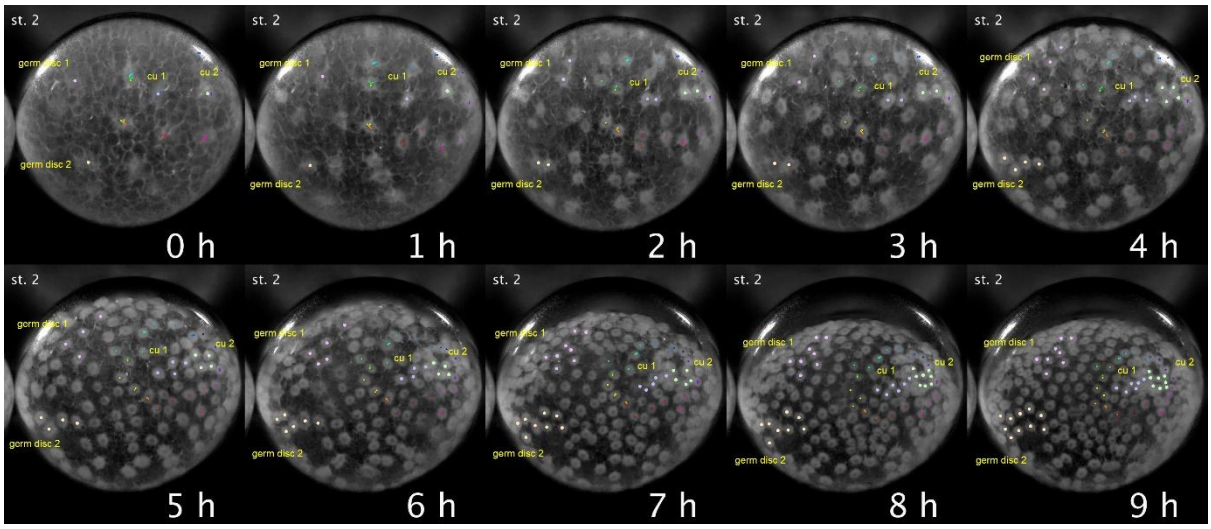

Figure S1-1. Trace of cells in a video. Large dots marked four cell clusters from single cell ancestor. two of germ disc cells, and two of future primary thickening cells. Small dots marked the region of primary thickening. Video were from Pechmann et al., 2016.

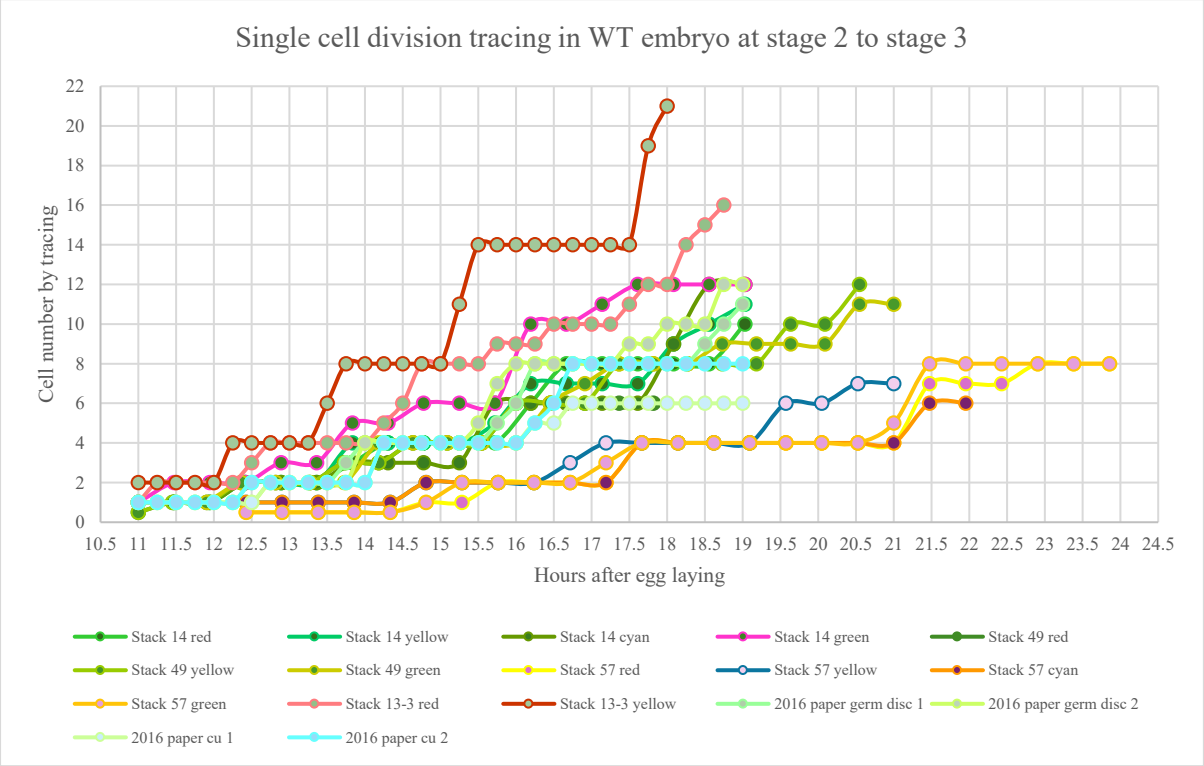

Figure S1-2. Counts of traced cells in WT embryos. Cell tracing were in same process as shown in Figure S1-1, and the tracing stops when some of the progenies were not distinguishable due to rotation of the germ disc, or increase of embryonic cell density. Excel S1-1.

Stage	st.2					st.3									st.4-
Hours after egg laying	11h	12h	13h	14h	15h	16h	17h	18h	19h	20h	21h	22h	23h	24-27h	28h-
Summary of cell divion in germ disc		division n+1													
			division n+2												
					division n+3										
								division n+4							
Total cell number	16-32	32-64		64-128		128.256		256-512							

Figure S1-3. Proliferation of germ disc cells of WT embryos, based on counts of total cell number (Figure 1-2) and counts of traced cells.

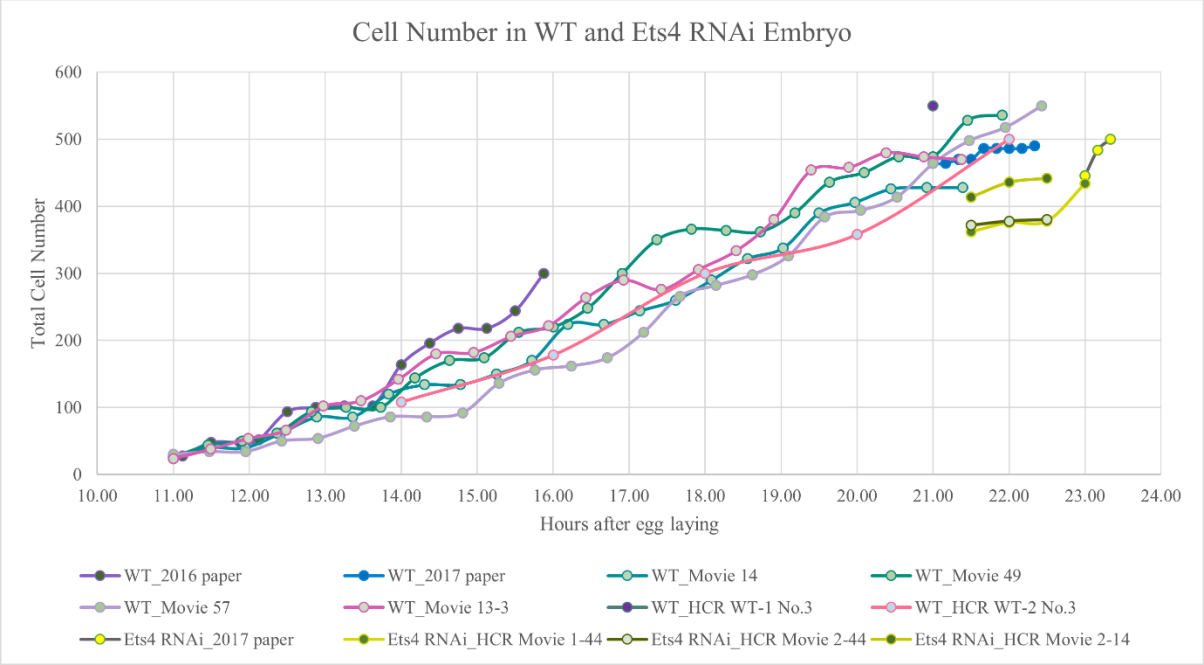

Figure S1-4. Combined cell number at 11 to 24 hael of WT and *Ets4* RNAi embryos. WT samples are coloured in red-blue, and *Ets4* RNAi counts are marked in yellow or green.

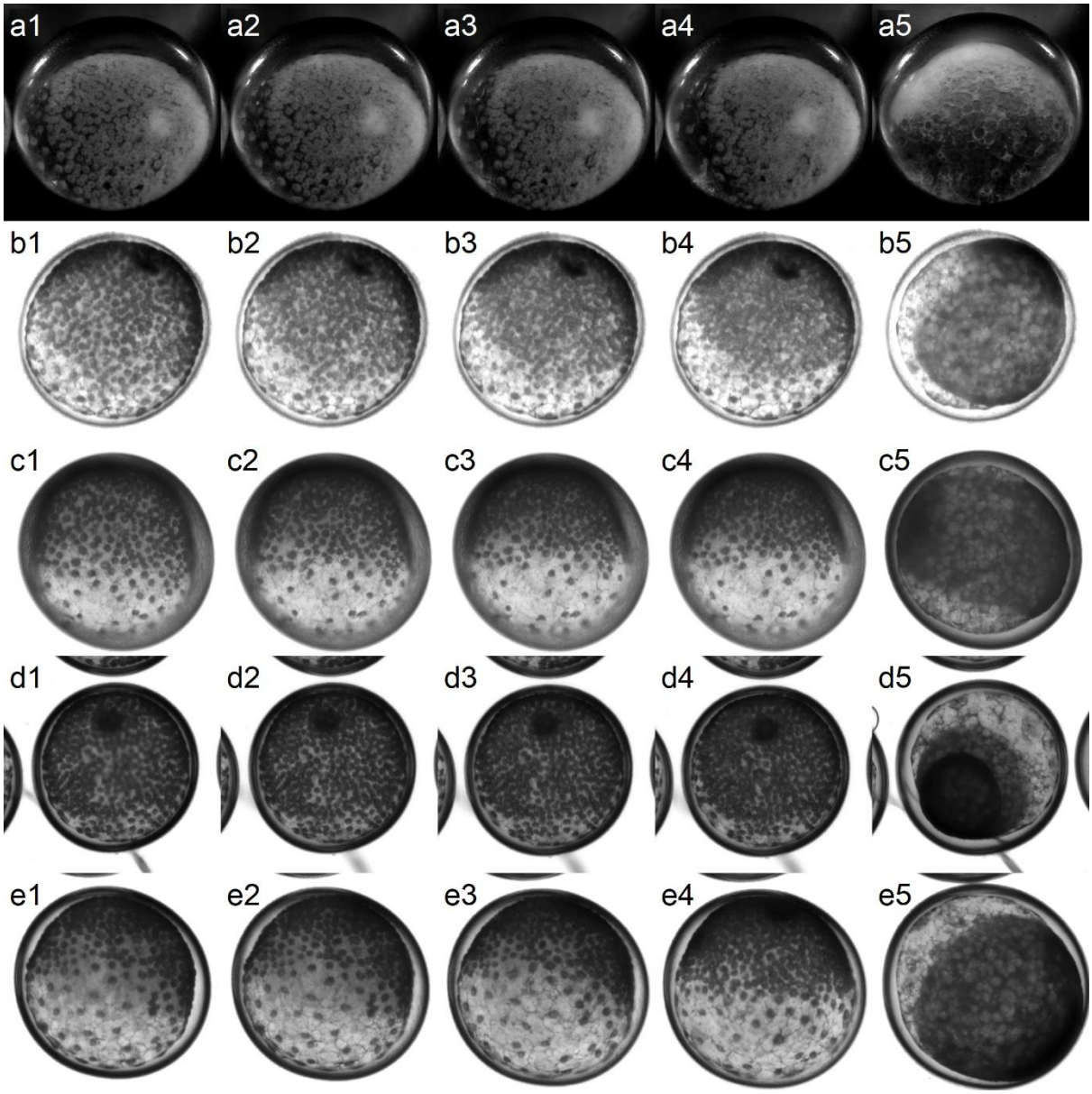

Figure S1-5. Montage image of WT and Ets4 RNAi embryos. A1 to A5: frame 89, 93, 97 and 329 of supplementary video in Pechmann et al., 2016. B1 to B5: frame 4, 7, 10, 13, and 187 of supplementary video from Pechmann et al., 2017. C1 to C5: frame 44, 46, 48, 50 and 166 of WT video stack 13-3. D1 to D5: frame 1, 2, 3, 4, and 50 of Ets4 RNAi video 1-33. E1 to E5: frame 1, 2, 3, 4, 50 of Ets4 RNAi video 2-44. A1, B1, C1, D1, E1: 21.5 hael. A2, B2, C2, D2, E2: 22 hael. A3, B3, C3, D3, E3: 22.5 hael. A4, B4, C4, D4, E4: 23 hael. A5, B5, C5, D5, E5: 52 hael.

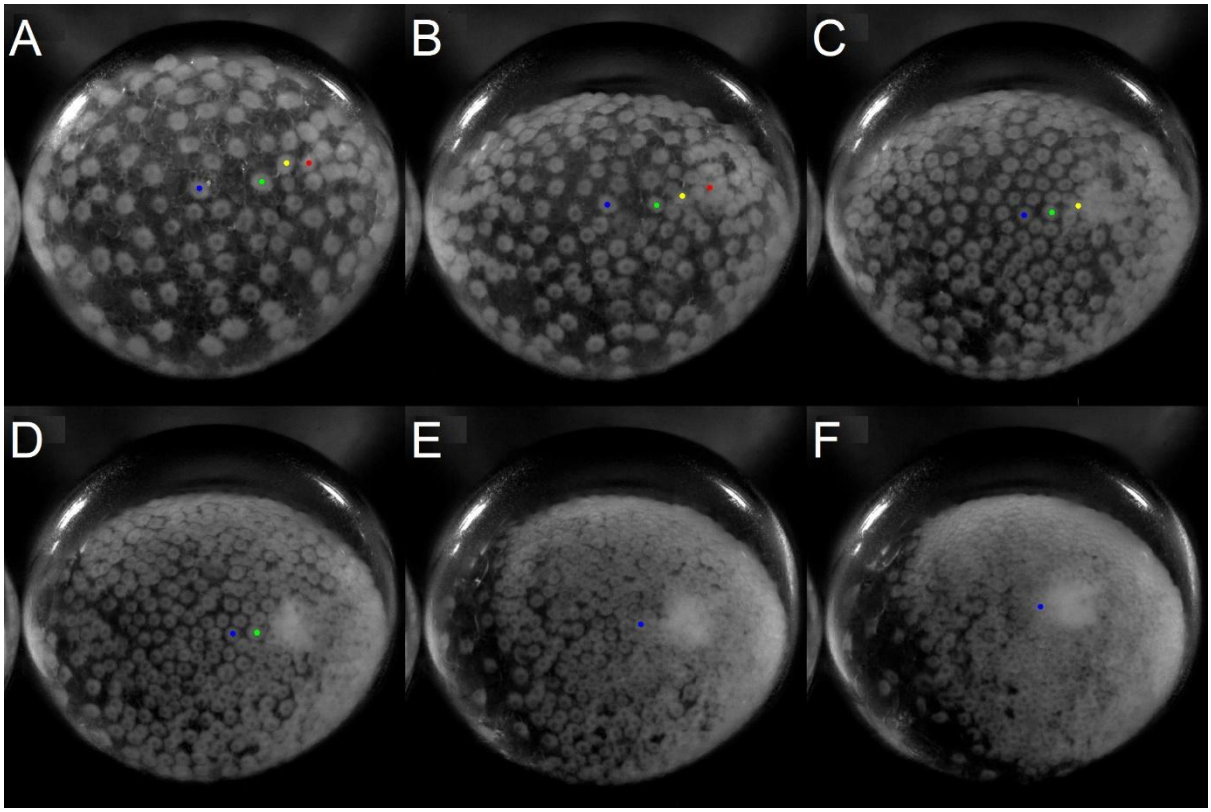

Figure S1-6. Enlargement of primary thickening region during germ disc contraction. Video were from supplementary video of Pechmann et al., 2016. A, B, C, D, E, F: frame 32, 47, 62, 77, 92, 107 of the video, at hael 15 to 24. Four cells and the corresponding ancestor cells are marked and traced in dots of different colour. The tracing of cell is stopped when the cell appears in the centre, overlapped by other cells and could not be clearly observed.

Table S1-3 Area size measurement of the 26-cell region

	sample	hael	Ets4+ cell	Fuchi+Ets4- cell	inner cell number	ectoderm cell number	total cell number	Area (μm^2)	HCR image for measure
1	WT-2 4h No.5	18	13	3	7	30	37	35371.184	10x
2	WT-2 6h No.1	20	12	0	8	29	37	24148.285	10x
3	WT-2 6h No.4	20	14	2	9	45	54	44766.135	10x
4	WT-1 0h No.3	21	15	23	19	38	57	35124.956	10x
5	WT-1 0h No.4	21	14	26	20	30	50	20372.404	10x
6	WT-2 8h No.1	22	7	20	20	27	47	20518.186	10x, 40x
7	WT-1 2h No.1	23	12	24	28	19	47	19351.622	40x
8	WT-2 10h No.1	24	4	27	27	29	56	19036.51	40x
9	WT-2 10h No.7	24	12	23	34	27	61	17944.315	40x, link
10	WT-1 4h No.2	25	9	27	29	37	66	16998.684	40x
11	WT-2 12h No.3	26	8	21	28	42	70	16977.59	10x, 40x

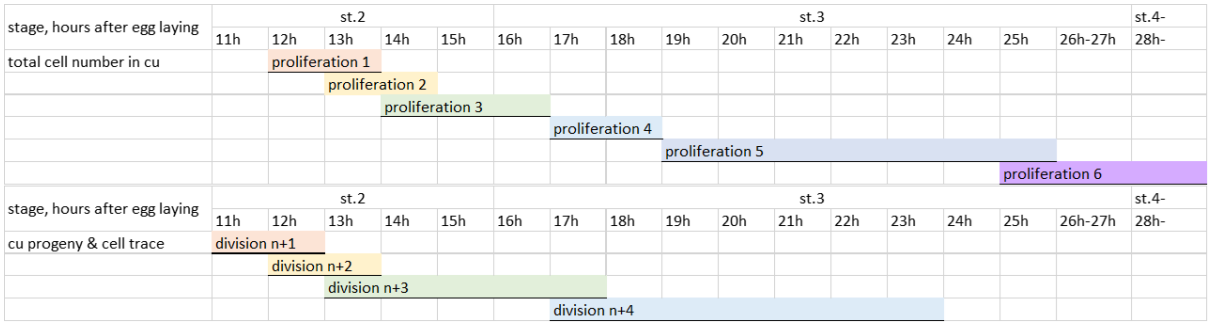

Figure S1-7. Comparison of division of cells in germ disc and primary thickening region in WT embryos. Data on germ disc cell division were from Figure 1-2, Figure S1-2, Figure S1-3. And Data on primary thickening division (26 cell region, Figure 1-3) were from Figure 1-4 and Figure S1-2.

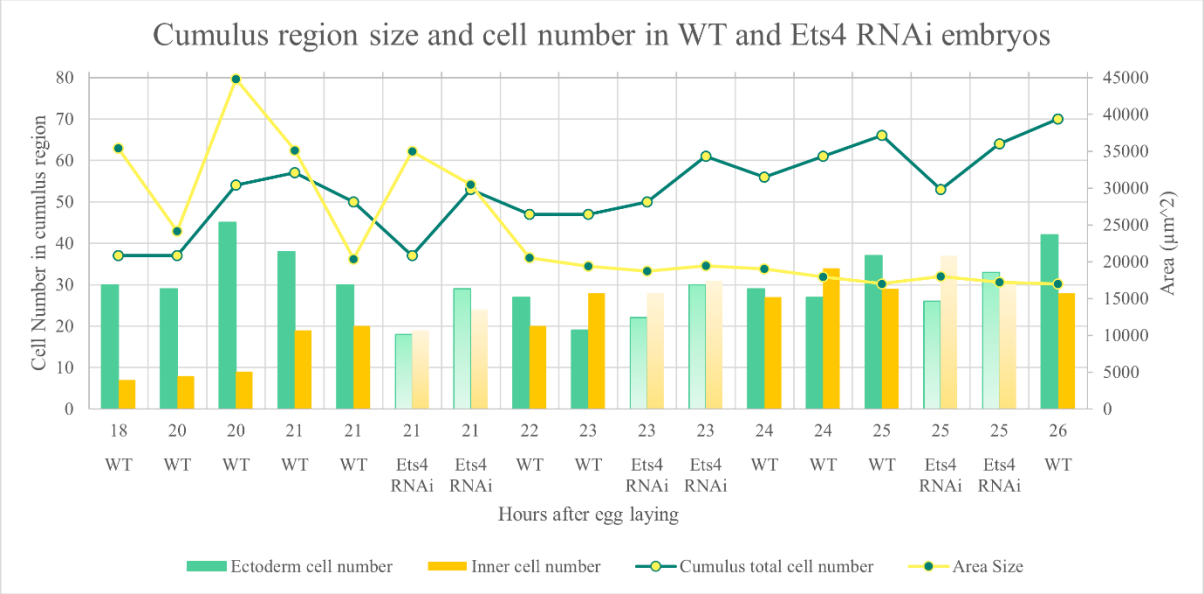

Figure S1-8. Size of 26-cell region in WT and Ets4 RNAi embryos, and the number of cells in the region of both types. Samples are arranged by developmental time (hael). Ets4 RNAi cell counts are in particular marked with gradient colour, while WT counts are in solid colour.

Table S1-4 Types of cells in primary thickening region of WT and Ets4 RNAi embryos

Primary thickening region	WT cell		Ets4 RNAi cell
Beneath the ectoderm	Fuchi+Ets4+		Fuchi+Ets4 na+
	Fuchi+Ets4-	Fuchi+Ets4 na+	
		Fuchi+ Ets4 na-	Fuchi+Ets4-Ets4 na-
On ectoderm	Fuchi-Ets4-		Fuchi-Ets4-

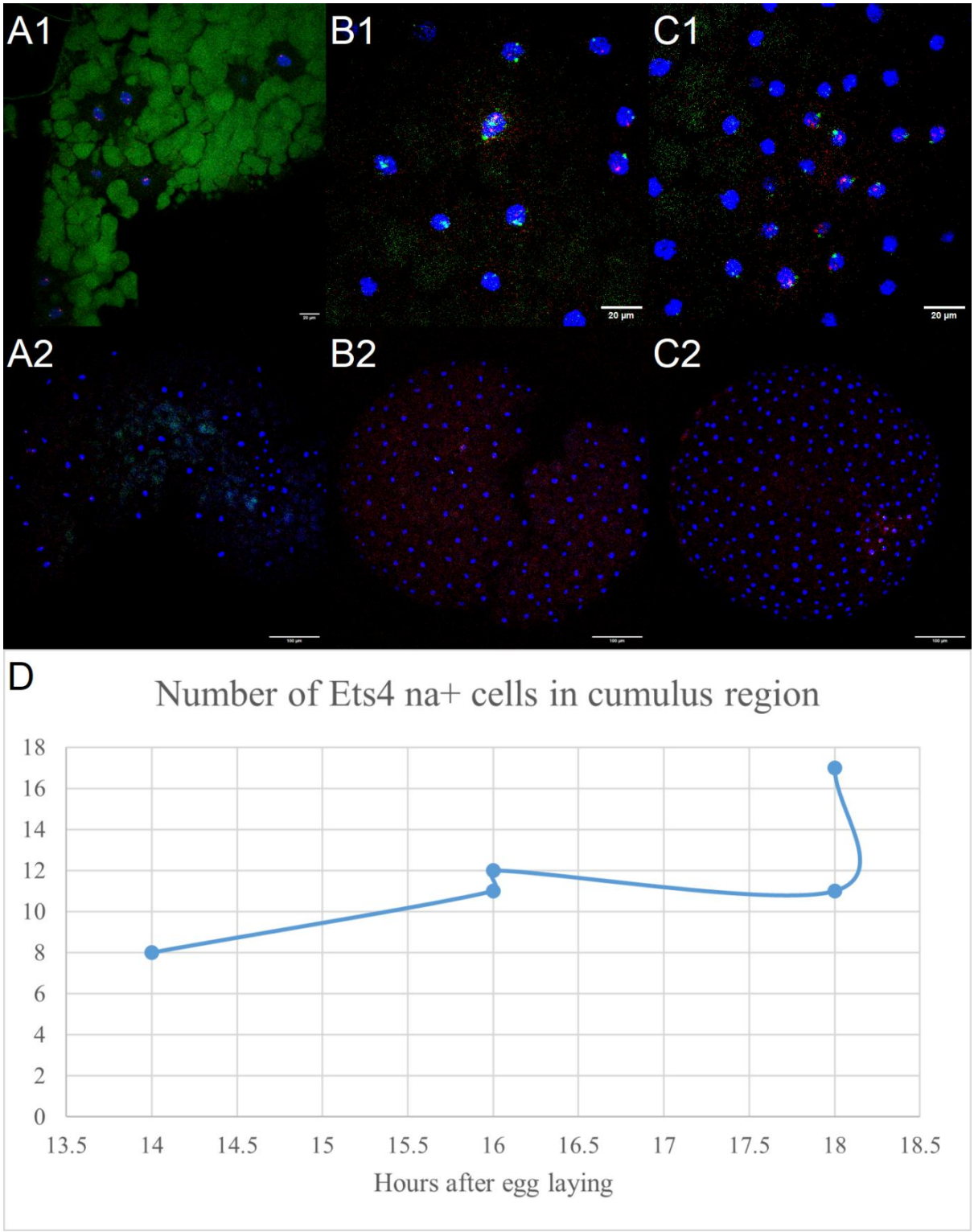

Figure S1-9. Image and cell count of WT embryos at 14, 16 and 18 hael. A1 and A2: 14 hael. B1 and B2: 16 hael. C1 and C2: 18 hael. A1, B1 and C1: 40x AVG z-stack. A2, B2, C2: 10x AVG z-stack image. D: counts of fuchi na+Ets4 na+ cells at 14, 16 and 18 hael. Blue: Dapi. Red: *fuchi*. Green: *Ets4*.

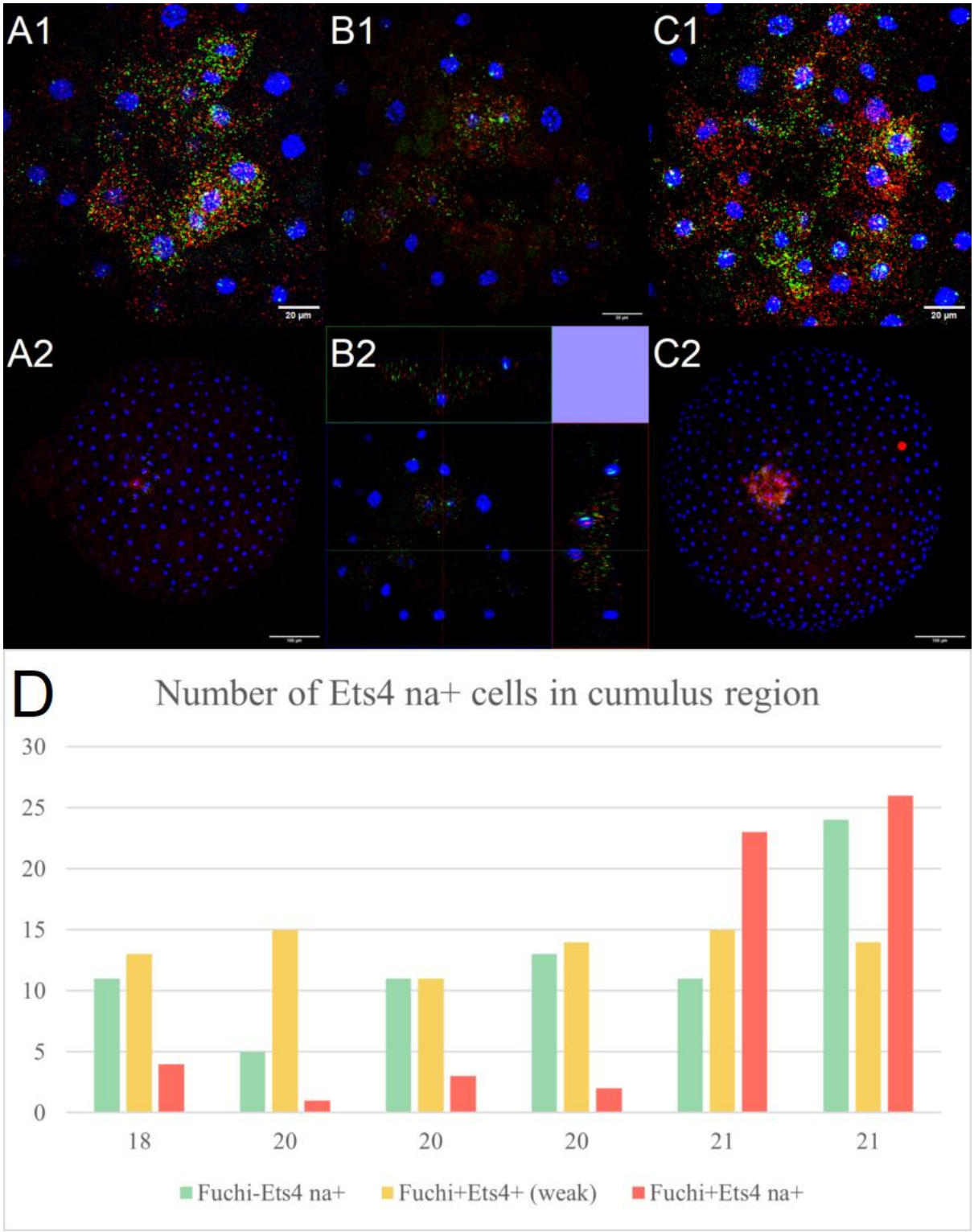

Figure S1-10. Image and cell count of WT embryos at 18, 20 and 21 hael. A1 and A2: 18 hael. B1 and B2: 20 hael. C1 and C2: 21 hael. A1, B1 and C1: 40x, ectoderm. A2 and C2: 10x, z-stack. B2: 40x orthogonal image. D: counts of cells, of Fuchi-Ets4 na+, Fuchi weak Ets4 weak, Fuchi+Ets4 na+ types based on 40x image. Blue: Dapi. Red: *fuchi*. Green: *Ets4*.

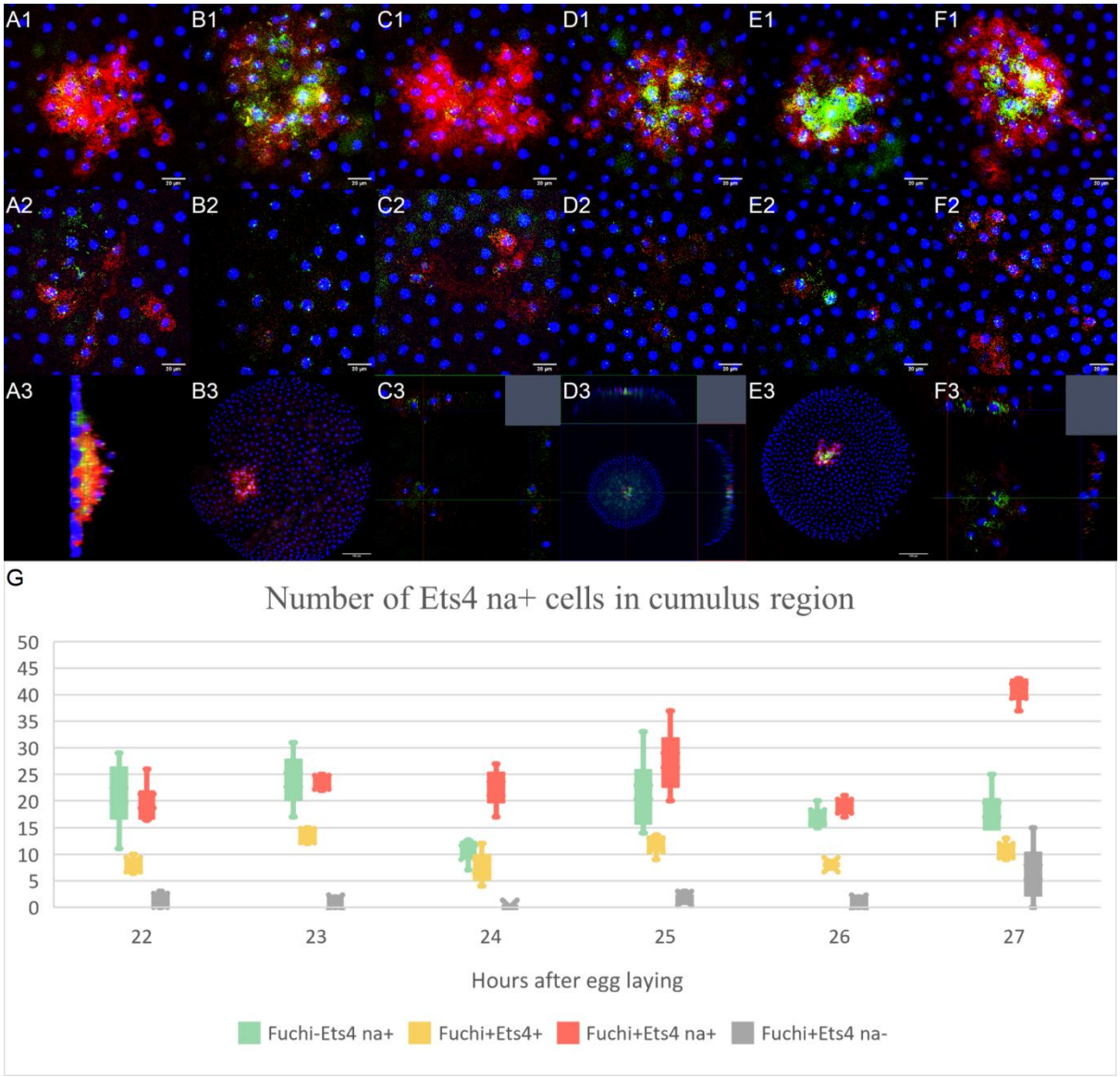

Figure S1-11. Image and cell count of WT embryos at 22, 23, 24, 25, 26 and 27 hael. A1, A2, and A3: 22 hael. B1, B2 and B3: 23 hael. C1, C2 and C3: 24 hael. D1, D2 and D3: 25 hael. E1, E2 and E3: 26 hael. F1, F2 and F3: 27 hael. Samples of A, C, E were from WT cocoon 2, and Samples of B, D, F were from WT cocoon 1. A1, B1, C1, D1, E1 and F1: AVG z-stack, 40x. A2, B2, C2, D2, E2 and F2: ectoderm, 40x. A3: lateral view of 3D model by Fiji. B3 and E3: AVG z-stack, 10x. C3 and F3: orthogonal view, 40x. D3: orthogonal, 10x. G: counts of different types of cells, including fuchi-Ets4 na+, fuchi+Ets4+, fuchi+Ets4 na- and fuchi+Ets4 na+ cells. Blue: Dapi. Red: *fuchi*. Green: *Ets4*.

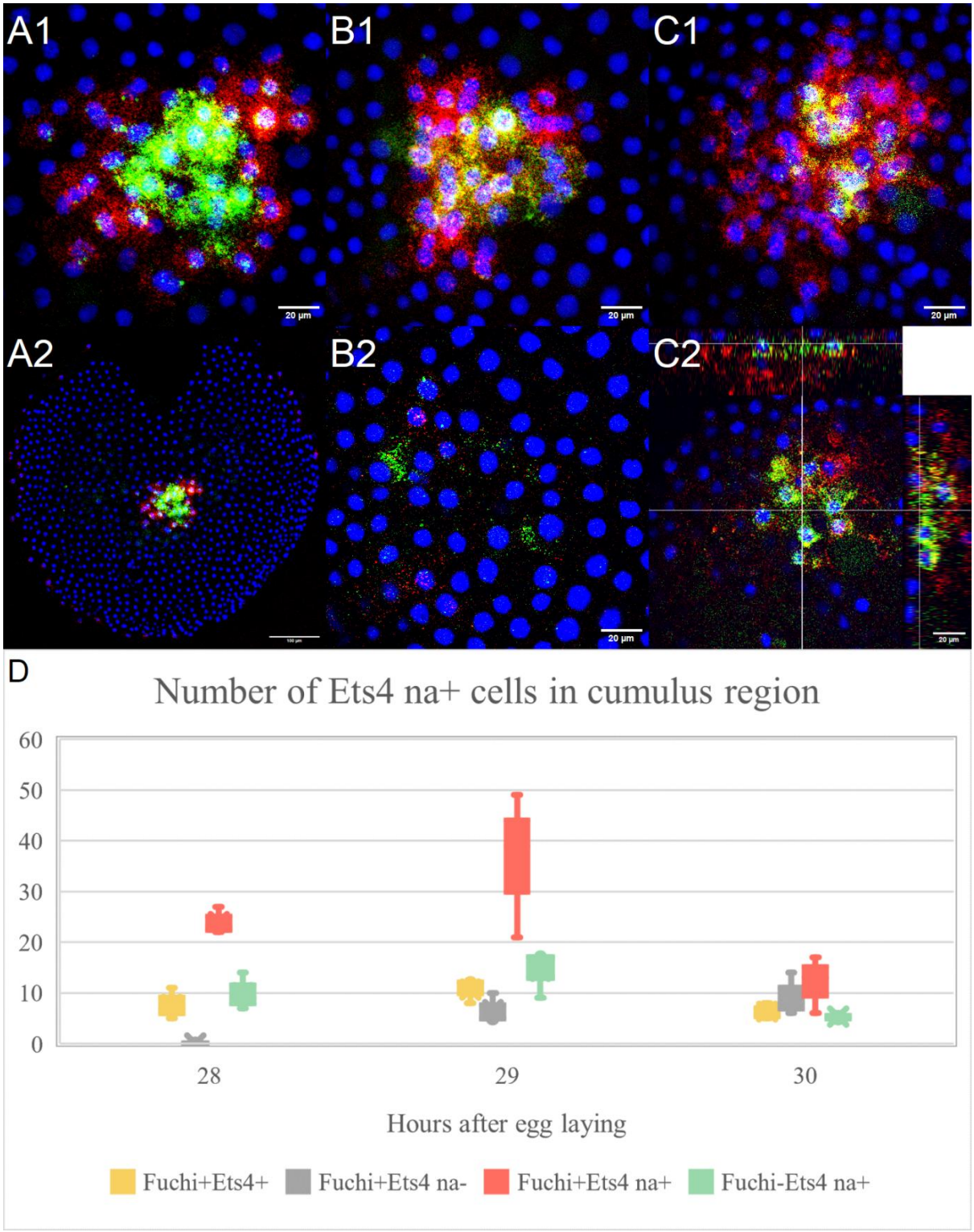

Figure S1-12. Image and cell count of WT embryo at 28, 29, and 30 hael. A1 and A2: 28 hael. B1 and B2: 29 hael. C1 and C2: 30 hael. A and C were from WT cocoon 2, and B were from WT cocoon 1. A1, B1 and C1: AVG z-stack, 40x. A2: AVG z-stack, 10x. B2: ectoderm, 40x. C1: orthogonal view, 40x. D: counts of different types of cells, including fuchi+Ets4+, fuchi+Ets4 na-, fuchi+Ets4 na+, fuchi-Ets4 na+ cells. Blue: Dapi. Red: *fuchi*. Green: *Ets4*.

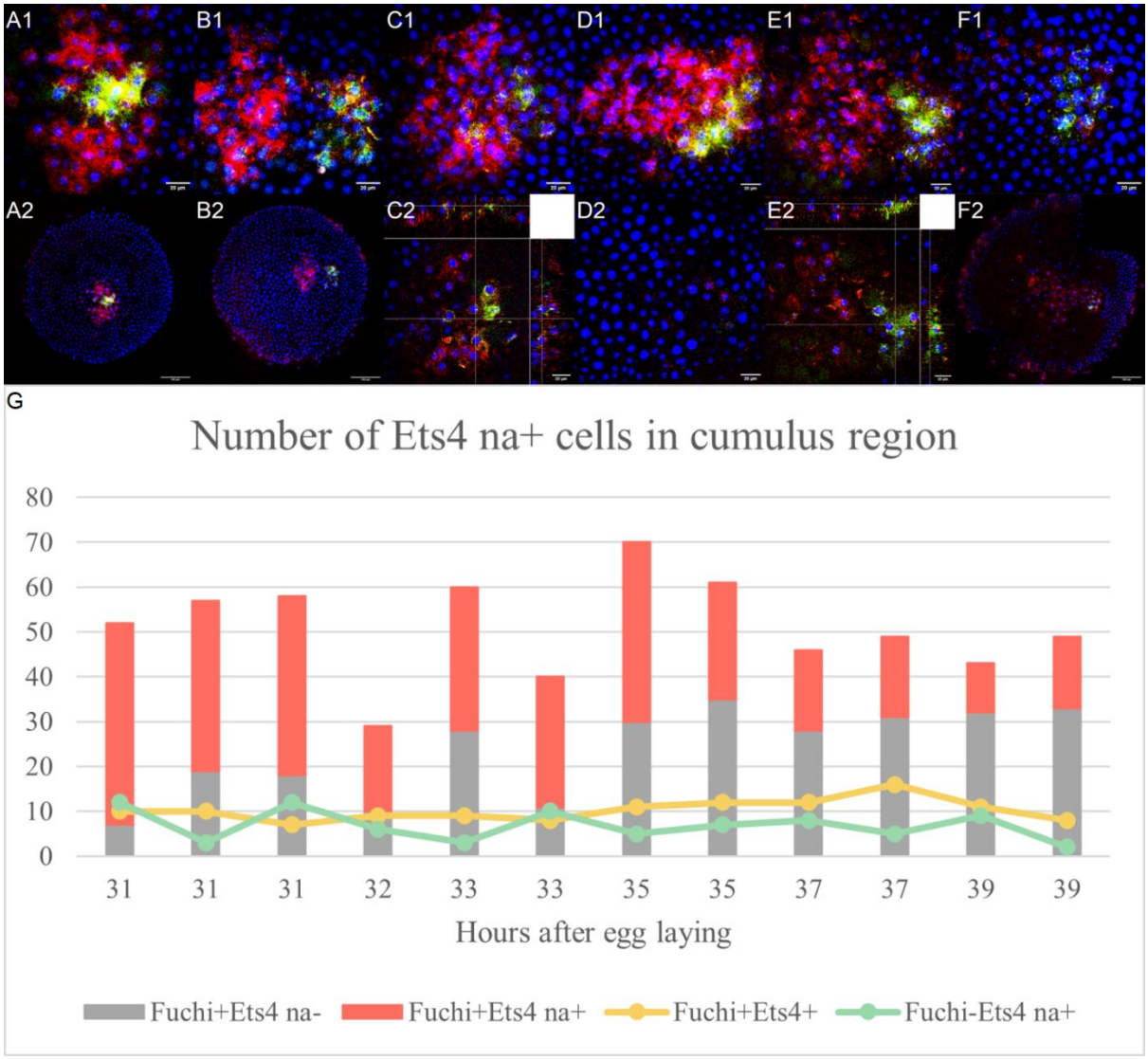

Figure S1-13. Image and cell count of WT embryo at 31, 32, 33, 35, 37 and 39. A1 and A2: 31 hael. B1 and B2: 32 hael. C1 and C2: 33 hael. D1 and D2: 35 hael. E1 and E2: 37 hael. F1 and F2: 39 hael. A, C, D, E, F were from WT cocoon 1, and B were from WT cocoon 2. A1, B1, C1, D1, E1 and F1: AVG z-stack, 40x. A2 and B2: AVG z-stack, 10x. C2 and E2: orthogonal view, 40x. D2: ectoderm, 40x. F2: AVG z-stack, 10x. G: Counts of different types of cells, including fuchi+Ets4 na-, fuchi+Ets4 na+, fuchi+Ets4+, fuchi-Ets4 na+ cells. Blue: Dapi. Red: *fuchi*. Green: *Ets4*.

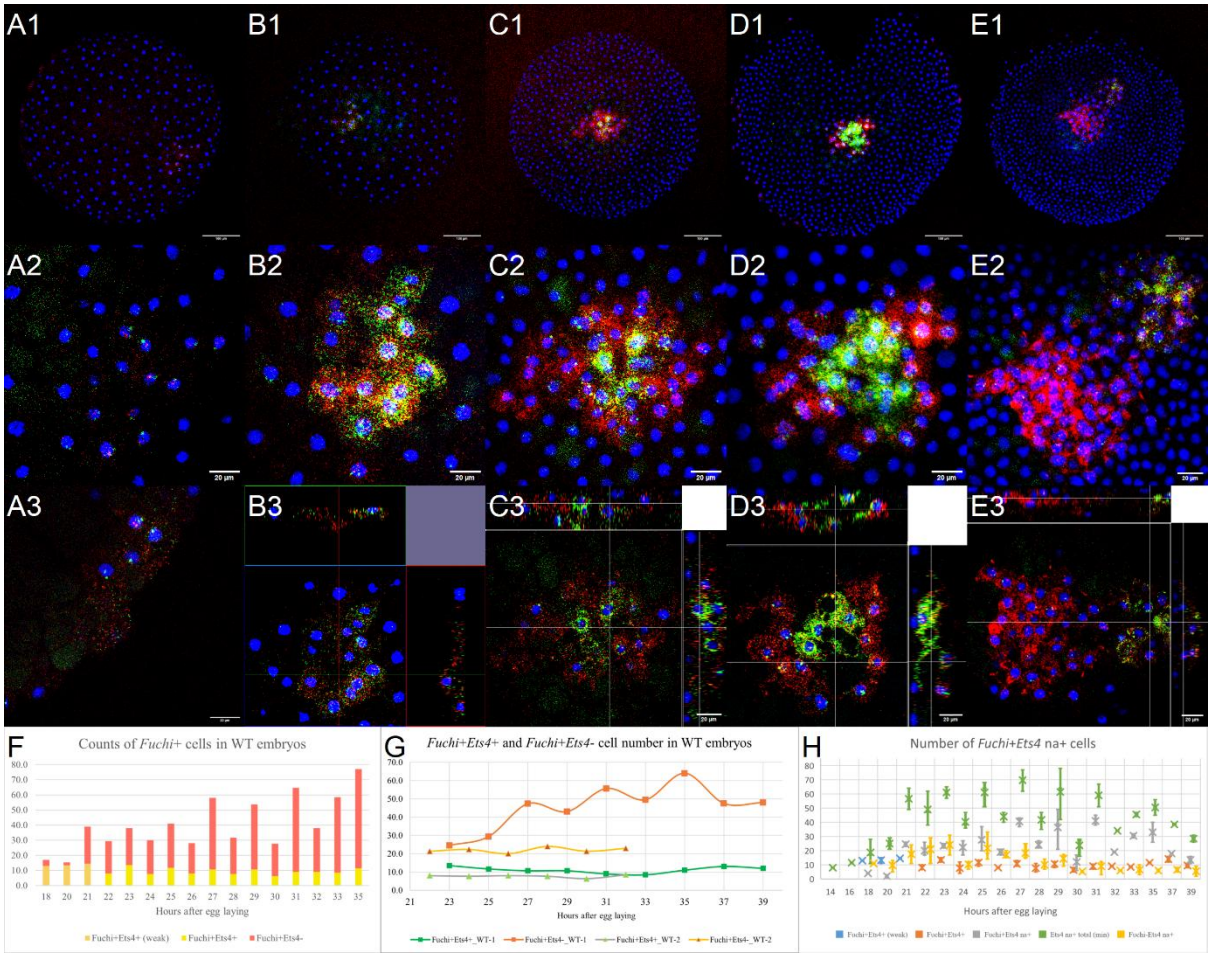

Figure S1-14. Examples of WT embryos at 14-39 hael and counts of different types of cells. A1, A2, and A3: 18 hael. B1, B2 and B3: 18 hael. C1, C2 and C3: 25 hael. D1, D2 and D3: 28 hael. E1, E2 and E3: 35 hael. A1, B1, C1, D1 and E1: 10x AVG z-stack. A2, B2, C2, D2 and E2: 40x AVG z-stack. A3: 40x of hypothetical primary thickening region. B3, C3, D3 and E3: orthogonal view of 40x image. F: Total counts of *Fuchi+Ets4+* and *Fuchi+Ets4-* cells at 18 to 35 hael, including weak and strong expression cells. G: *Fuchi+Ets4+* and *Fuchi+Ets4-* cell counts at 21 to 39 hael, separated by source of cocoons. H: Number of *Ets4* na+ cells at 14 to 39 hael. HCR staining. Blue: Dapi. Red: *Fuchi*. Green: *Ets4*.

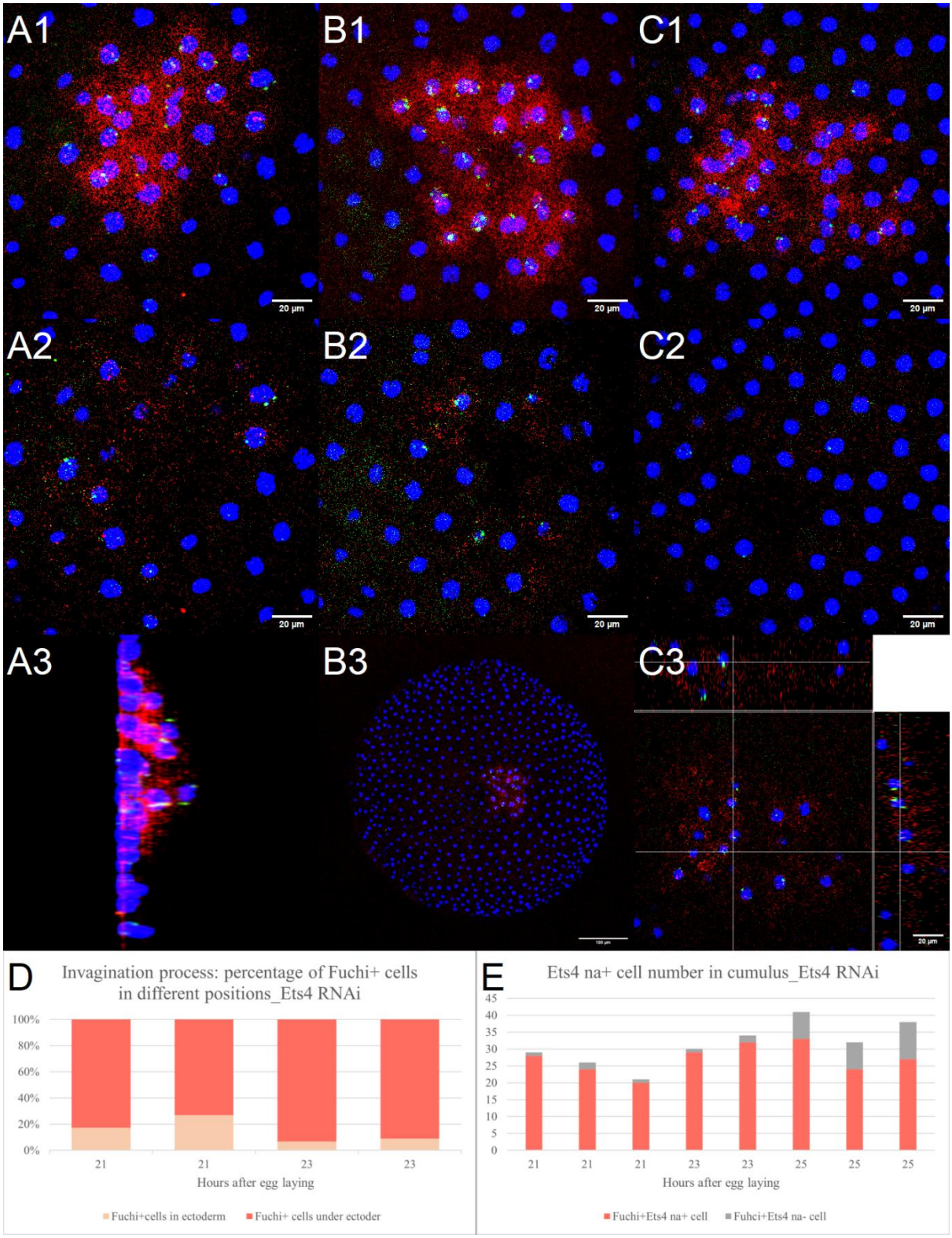

Figure S1-15. Image and cell number of Ets4 RNAi embryos at 21, 23 and 25 hael. A1, A2 and A3: 21 hael. B1, B2 and B3: 23 hael. C1, C2 and C3: 25 hael. A1, B1 and C1: AVG z-stack, 40x. A2, B2 and C2: ectoderm, 40x. A3: lateral view of 3D model by Fiji. B3: AVG z-stack, 10x. C3: orthogonal view. D: counts of ectoderm Fuchi+ cells and inner Fuchi+ cells. E: counts of Fuchi+ Ets4 na+ cells and Fuchi+ Ets4 na- cells in primary thickening region. Blue: Dapi. Red: *Fuchi*. Green: *Ets4*.

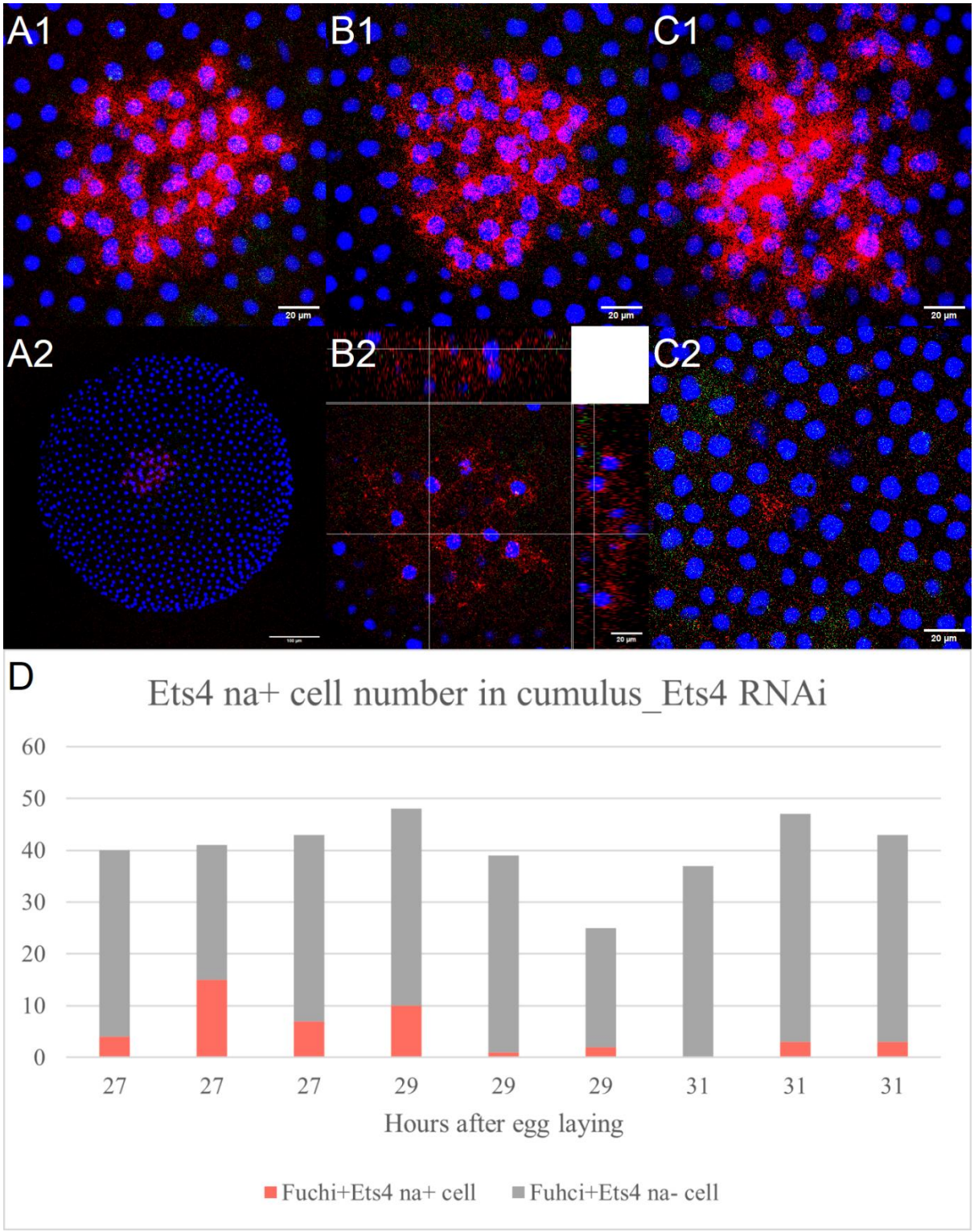

Figure S1-16. Image and cell number of Ets4 RNAi embryos at 27, 29, 31 hael. A1 and A2: 27 hael. B1 and B2: 29 hael. C1 and C2: 31 hael. A1, B1 and C1: AVG z-stack, 40x. A2: AVG z-stack, 10x. B2: orthogonal view. C3: ectoderm, 40x. D: counts of Fuchi+Ets4 na+ cells and Fuchi+ Ets4 na- cells in primary thickening regions. Blue: Dapi. Red: *Fuchi*. Green: *Ets4*.

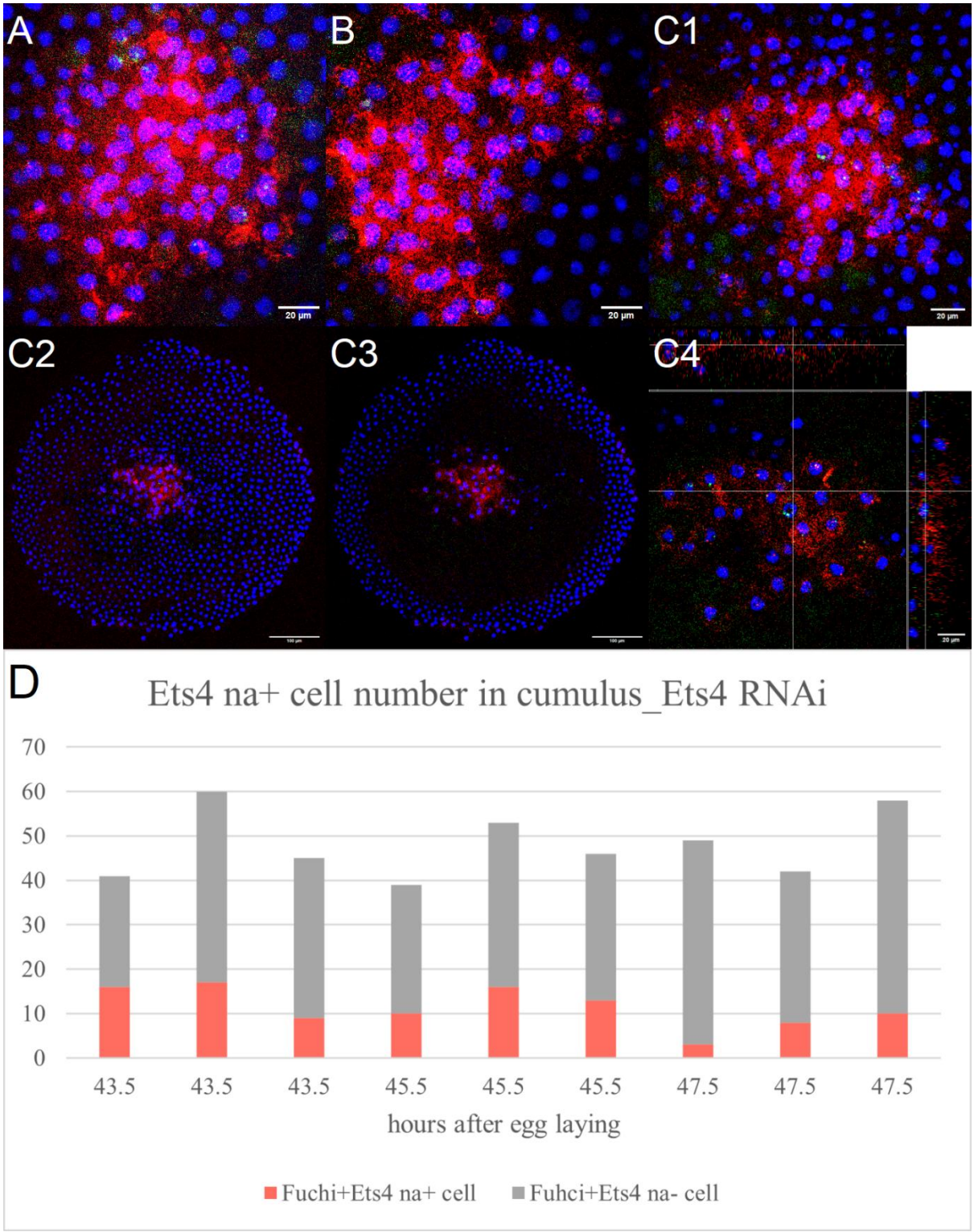

Figure S1-17. Image and cell number of Ets4 RNAi embryos at 43, 45, 47 hael. A: 43.5 hael. B: 45.5 hael. C1: 47.5 hael. A1, B1, and C1: AVG z-stack, 40x. C2: AVG z-stack, 10x. C3: AVG z-stack, 10x . C4: orthogonal view. D: counts of Fuchi+Ets4 na+ cells and Fuchi+Ets4 na- cells in primary thickening region. Blue: Dapi. Red: *Fuchi*. Green: *Ets4*.

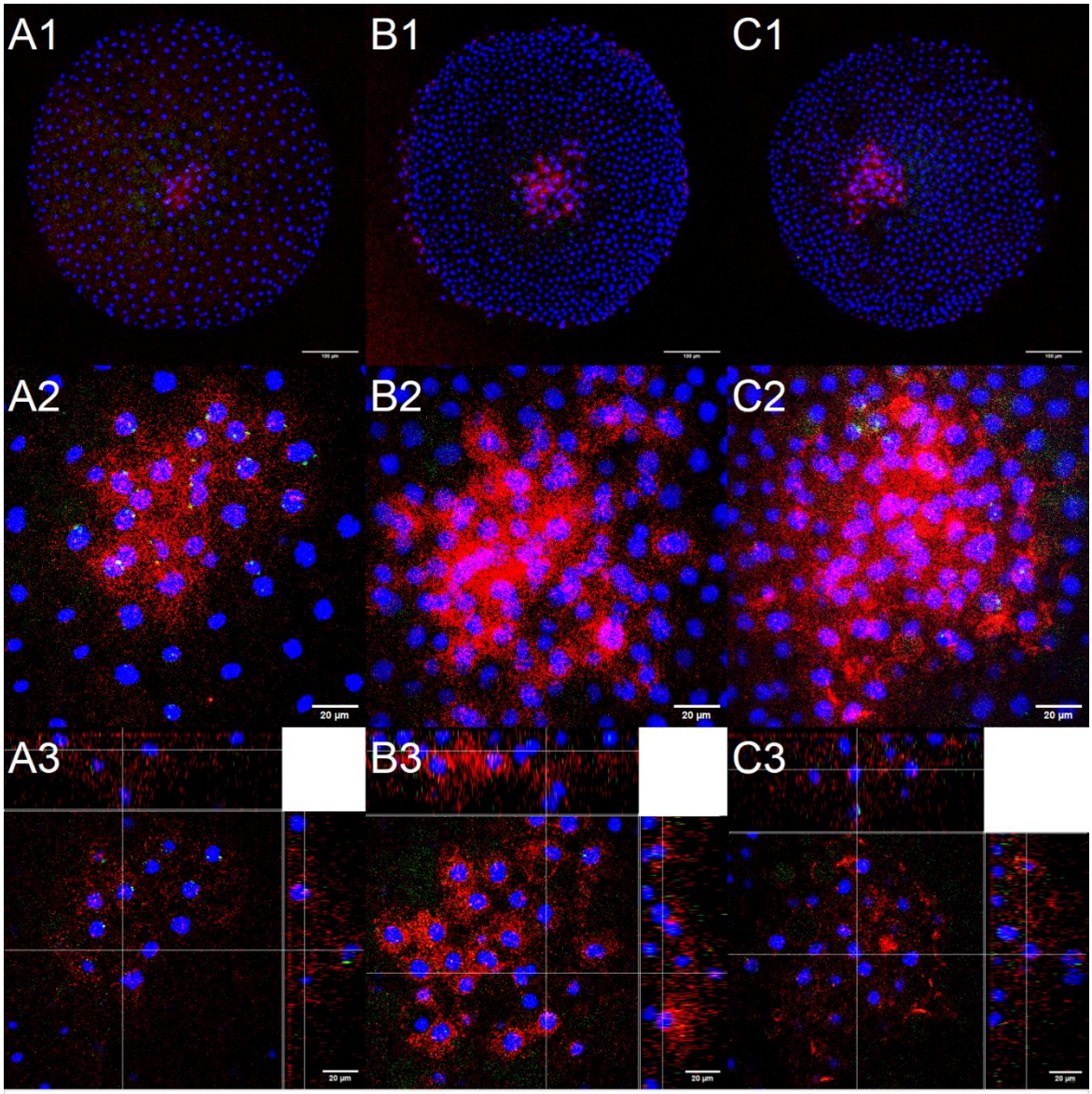
A1
B1
C1
A2
B2
C2
20 μm
A3
B3
C3

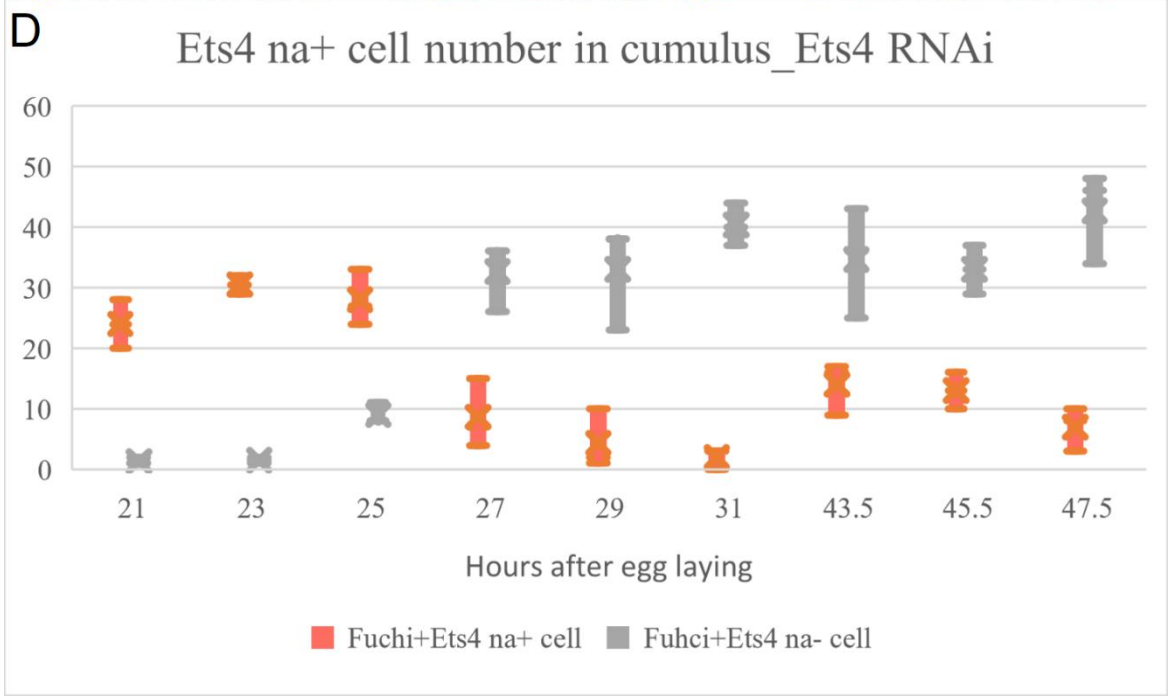
D
Ets4 na+ cell number in cumulus_Ets4 RNAi
60
50
40
30
20
10
0
21
23
25
27
29
31
43.5
45.5
47.5
Hours after egg laying
Fuchi+Ets4 na+ cell
Fuhci+Ets4 na- cell

Figure S1-18. Image and cell number of Ets4 RNAi embryo, at hael 21-31 and 43-47. A1, A2 and A3: 21 hael. B1, B2, and B3: 31 hael. C1, C2 and C3: 43.5 hael. A1, A2, and A3: AVG z-stack, 10x. B1, B2 and B3: AVG z-stack, 40x. C1, C2 and C3: orthogonal view. D: Fuchi+ Ets4 na+ cell number and Fuchi+ Ets4 na- cell number of all the embryos. Blue: Dapi. Red: *Fuchi*. Green: *Ets4*.

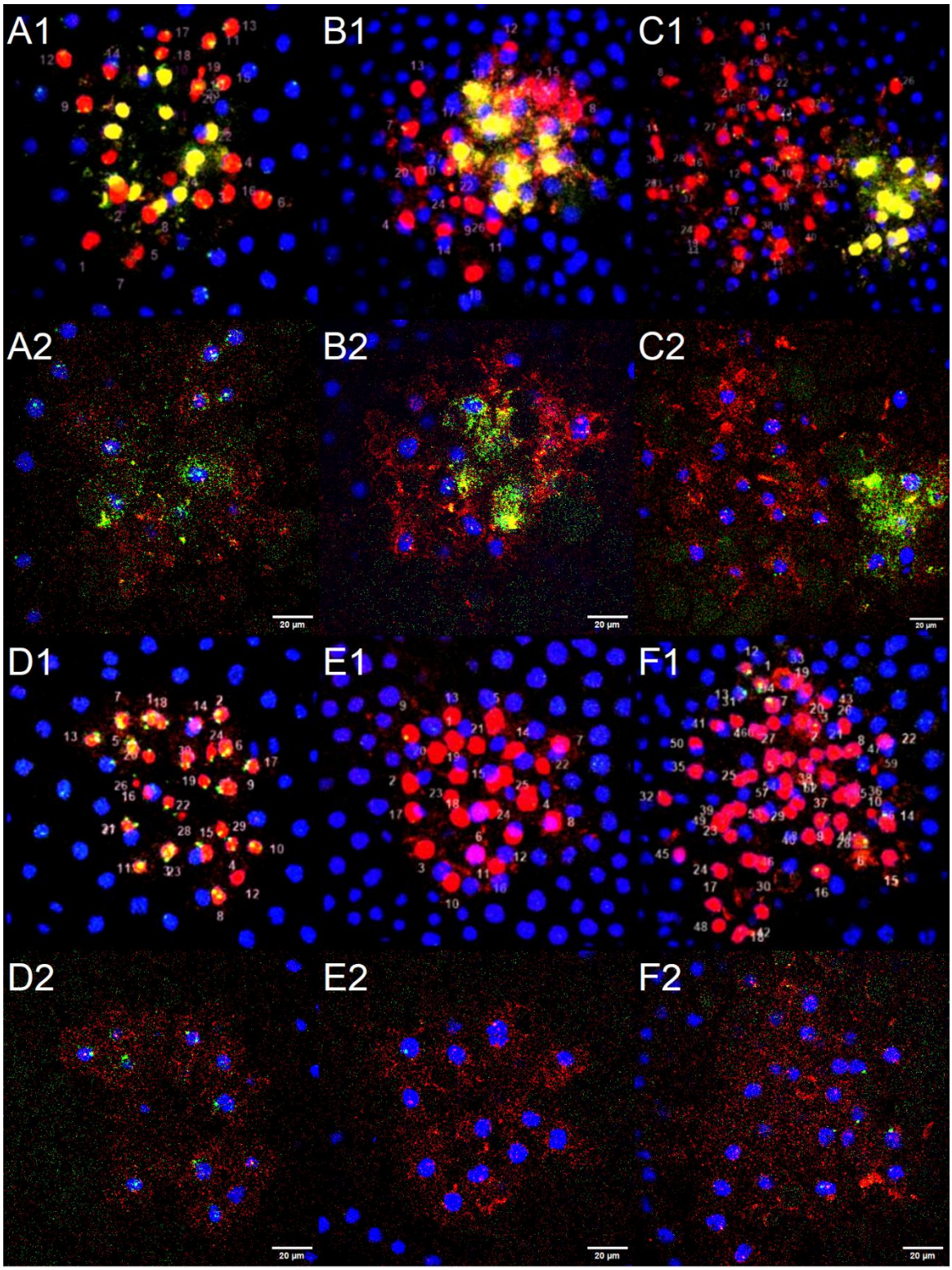

Figure S1-19, top view and inner image of WT and Ets4 RNAi embryos at stage 3, 4, 5. A, B, C: WT embryos. D, E, F: Ets4 RNAi embryos. A1, A2, D1, D2: 23 hael. B1, B2: 30 hael. E1, E2: 29 hael. C1, C2: 37 hael. F1,

F2: 43 hael. A1, B1, C1, D1, E1, and F1: top view of coloured 3D image made by Fiji, 40x. . A2, B2, C2, D2, E2 and F2: AVG z-stack, 40x. Blue: Dapi. Red: *Fuchi*. Green: *Ets4*.

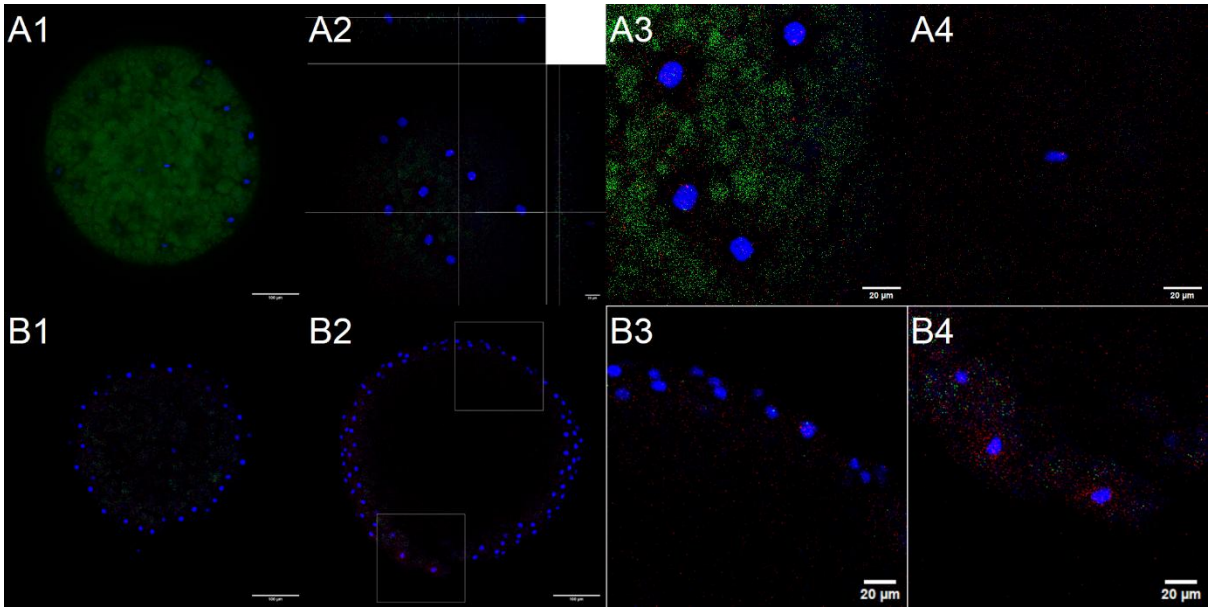

Figure S1-20 Inner cells in early WT Pt embryos. A1, A2, A3 and A4: 14 hael. B1, B2, B3 and B4: 18 hael. A1 and B1: 10x. A2: Orthogonal view, 10x. A3 and A4: max z-stack, 40x. B2: max z-stack,10x. The two boxes regions in B2 are enlarged in B3 and B4. HCR staining. Blue: Dapi. Red: *fuchi*. Green: *Ets4*.

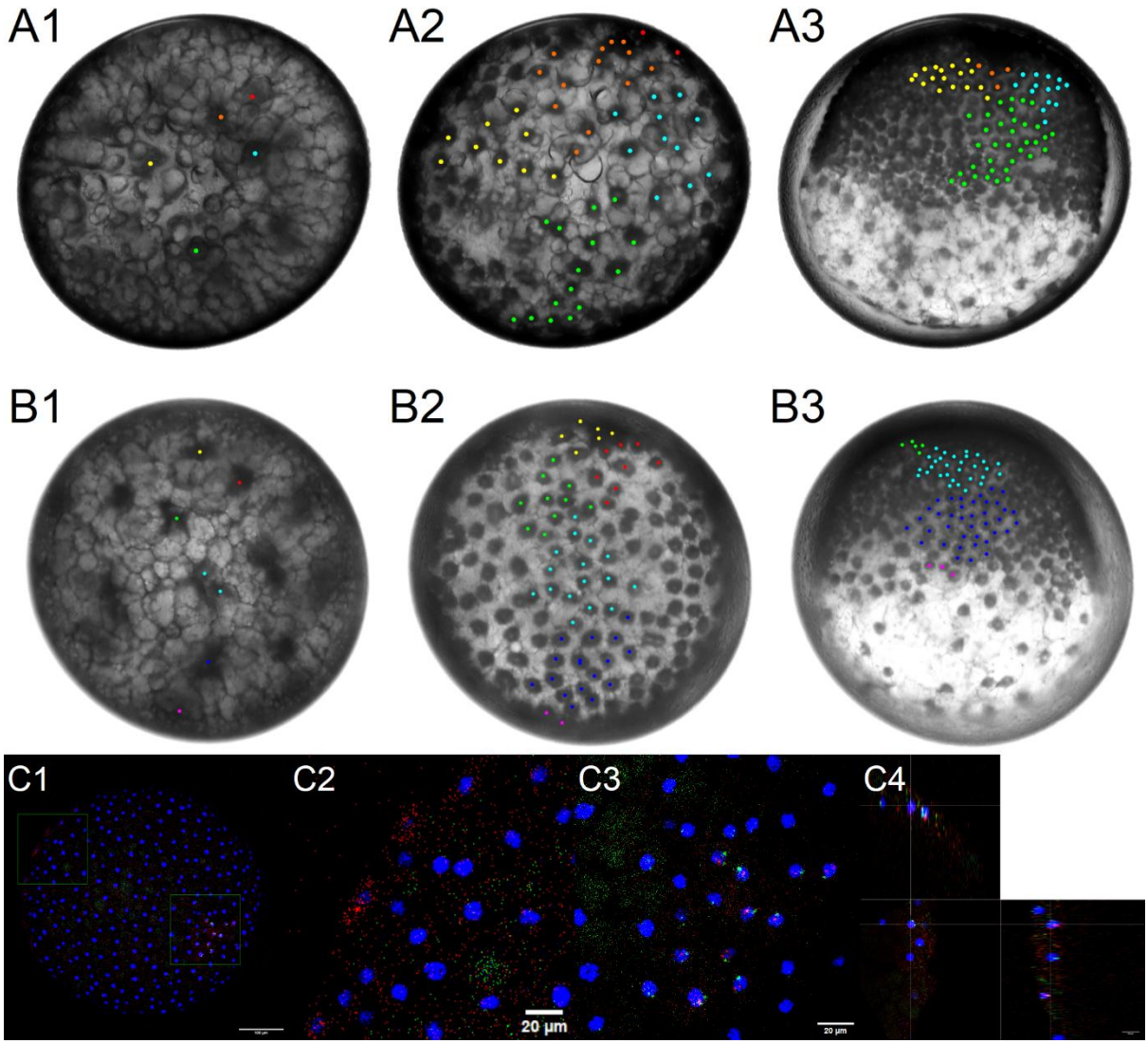

Figure S1-21. Opposite position of polar body and primary thickening region in WT embryos. A1, A2, A3: from WT stack 57. B1, B2, B3: from WT stack 13-3. C1, C2, C3, and C4: 18 hael. A1, B1: 32 cell stage, at 11 hael. A2 and B2: around 17 hael. A3 and B3: at 22 and 23 hael, respectively. Cells are traced from A1 to A3, and B1 to B3. C1: 10x. The two box regions in C1 are enlarged in C2 and C3, of extraembryonic region, and future primary thickening region. C2 and C3: 40x. C4: orthogonal view of C3, after rotation. One cell in deep layer of the embryo. Blue: Dapi. Red: *fuchi*. Green: *Ets4*.

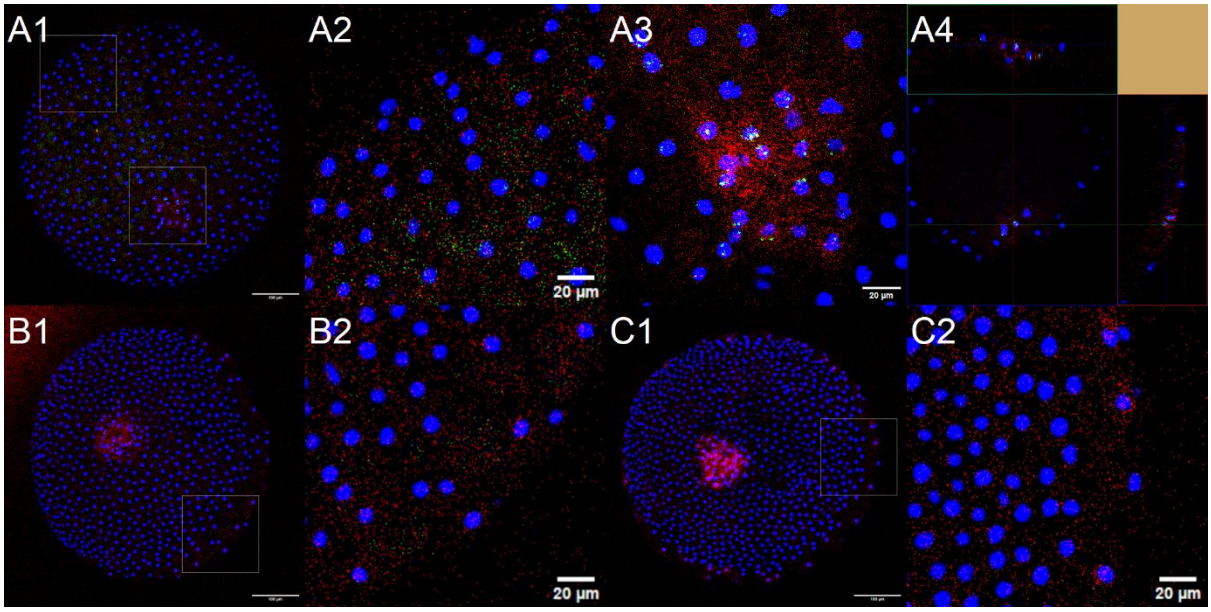

Figure S1-22. Position of primary thickening region and extraembryonic region in Ets4 RNAi embryos. A1, A2, A3 and A4: 21 hael. B1 and B2: 25 hael. C1 and C2: 29 hael. A1, B1 and C1: Max z-stack, 10x. A2, A3, B2 and C2: AVG z-stack, 40x. A2, B2 and C2: extraembryonic region of the box in A1 (upper box), B1 and C1, respectively. A3: centre of the embryonic region of the lower box in A1. A4: orthogonal view, 40x. Blue: Dapi. Red: *fuchi*. Green: *Ets4*.

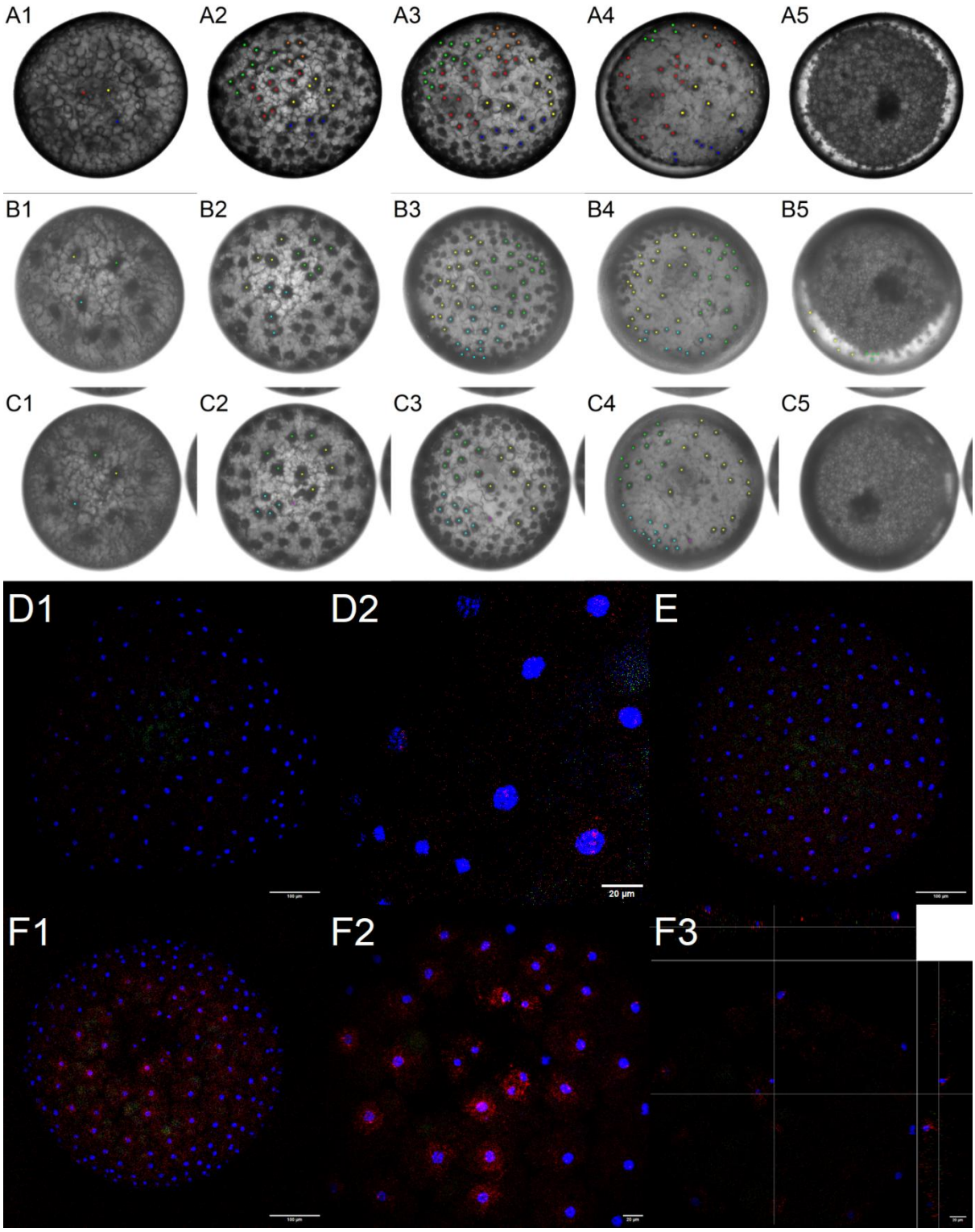

Figure S1-23. Polar bodies and the extraembryonic region in WT embryos. A1, A2, A3, A4 and A5: WT stack 70. B1, B2, B3, B4 and B5: WT stack 24-2. C1, C2, C3, C4 and C5: WT stack 29-3. A1, B1 and C1: 32 cell stage, at 11 hael. A2, B2, and C2: with noticeable broken part within cells, at 14 to 15 hael. A3, B3 and C3: at 18 hael, polar bodies (smaller nuclei) are visible. A4, B4 and C4: around 21 hael, before germ disc rotation initiates. A5, B5 and C5: early stage 5, at 31 hael. Progenies of the same cell are marked in the same colour. D1, D2, E: 16 hael. F1, F2 and F3: 18 hael. D1, E, and F1: max z-stack, 10x. D2 and F2: max z-stack, 40x. F3: orthogonal view of F2. Blue: Dapi. Red: *fuchi*. Green: *Ets4*.

Table S1-5 Sub-steps of invagination process in WT embryos

Time (hael)	14 or earlier	16	18	20	22 or later
Layers in the spot	Single		3	3-4	4 or more
Fuchi and Ets4 expression	Na+	Mainly na+, a few weak	Weak		Strong
Cell number			20-30 cells in total, less than 10 inner cells	20-30 cells in total, all inner cells	
Events	A few na+→weak expression				
		All weak expression, a few internalize			
			All internalize		
				Weak expression→strong	

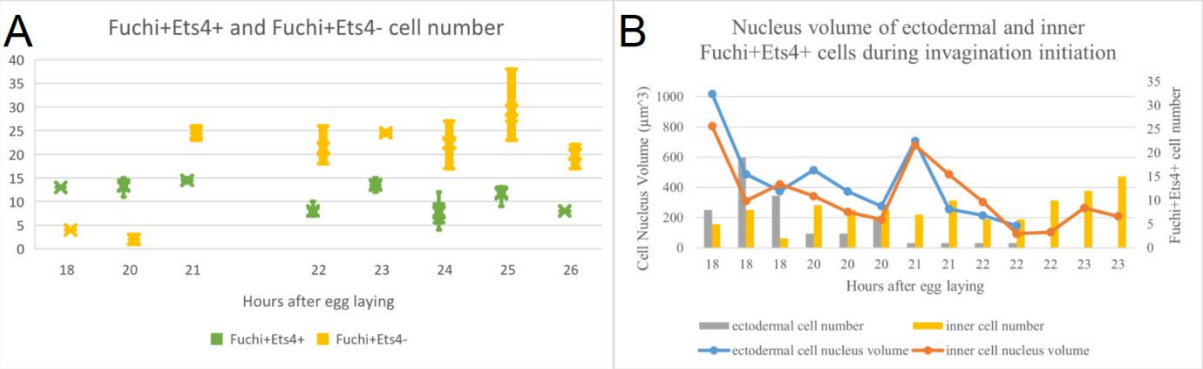

Figure S1-24. Total cell number and average nucleus volumes of fuchi+Ets4+ cells during invagination process in WT embryos, to deduce the timing of cell division. A. Average counts of Fuchi+Ets4+ and Fuchi+Ets4- cells at 18 to 26 hael. B. Average number and nucleus volume of Fuchi+Ets4+ cells at 18 to 23 hael. Volume of nucleus are measured with the help of 3D Objects Counter in Fiji.

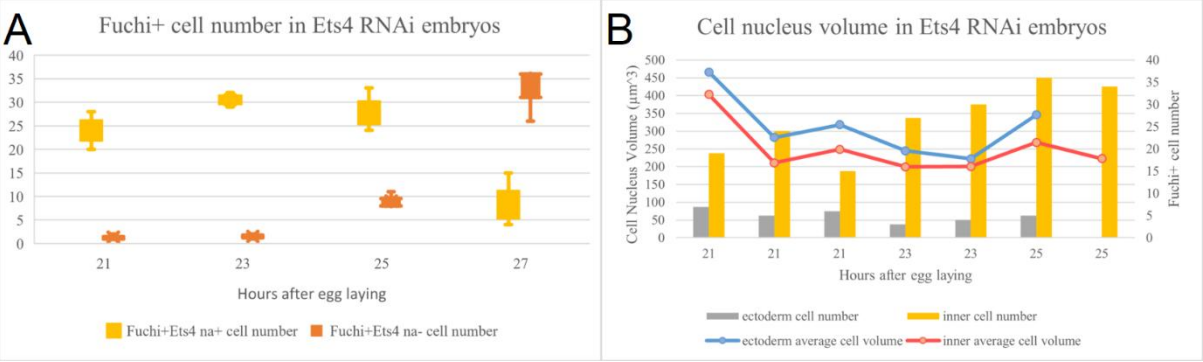

Figure S1-25. Total cell number and average nucleus volumes of cells in Ets4 RNAi embryos. A. Average counts of fuchi+ cells at 21 to 27 hael. B: Average number and nucleus volume of Fuchi+ cells at 21, 23 and 25 hael. Volume of nucleus are measured with the help of 3D Objects Counter in Fiji.

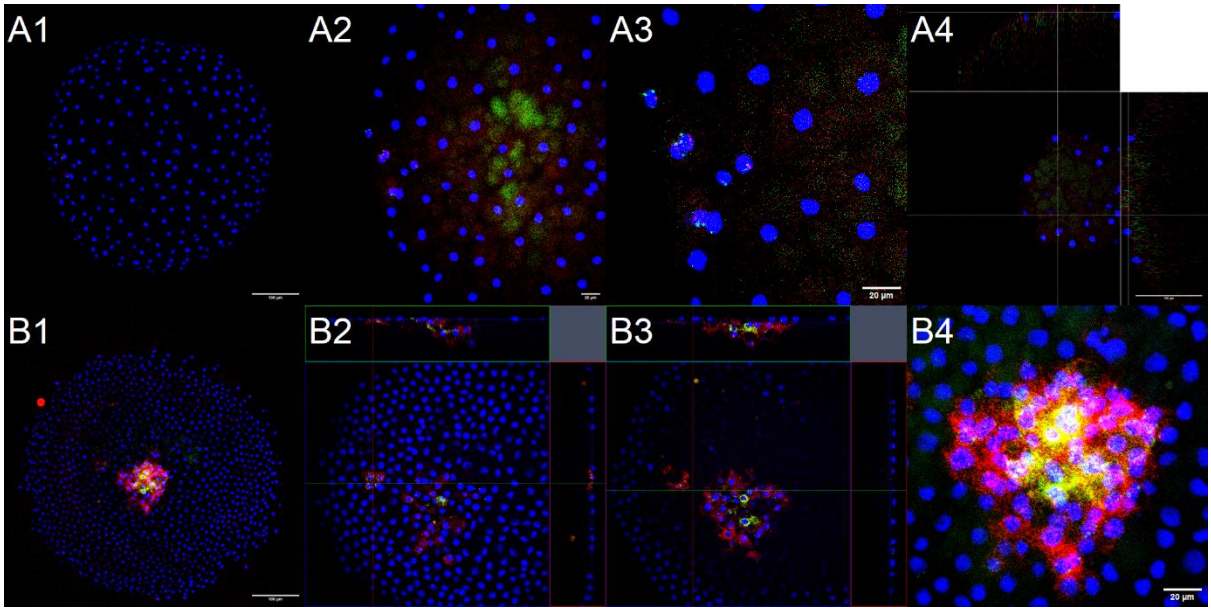

Figure S1-26. WT embryos with extra fuchi+ cell clusters in germ disc. A1, A2, A3 and A4: 18 hael. B1, B2, B3, and B4: 27 hael. A1 and B1: AVG z-stack, 10x. A2, A3, B4: max z-stack, 40x. A4: orthogonal view, 40x. B2 and B3: orthogonal view, 10x. HCR staining. Blue: Dapi. Red: *fuchi*. Green: *Ets4*.

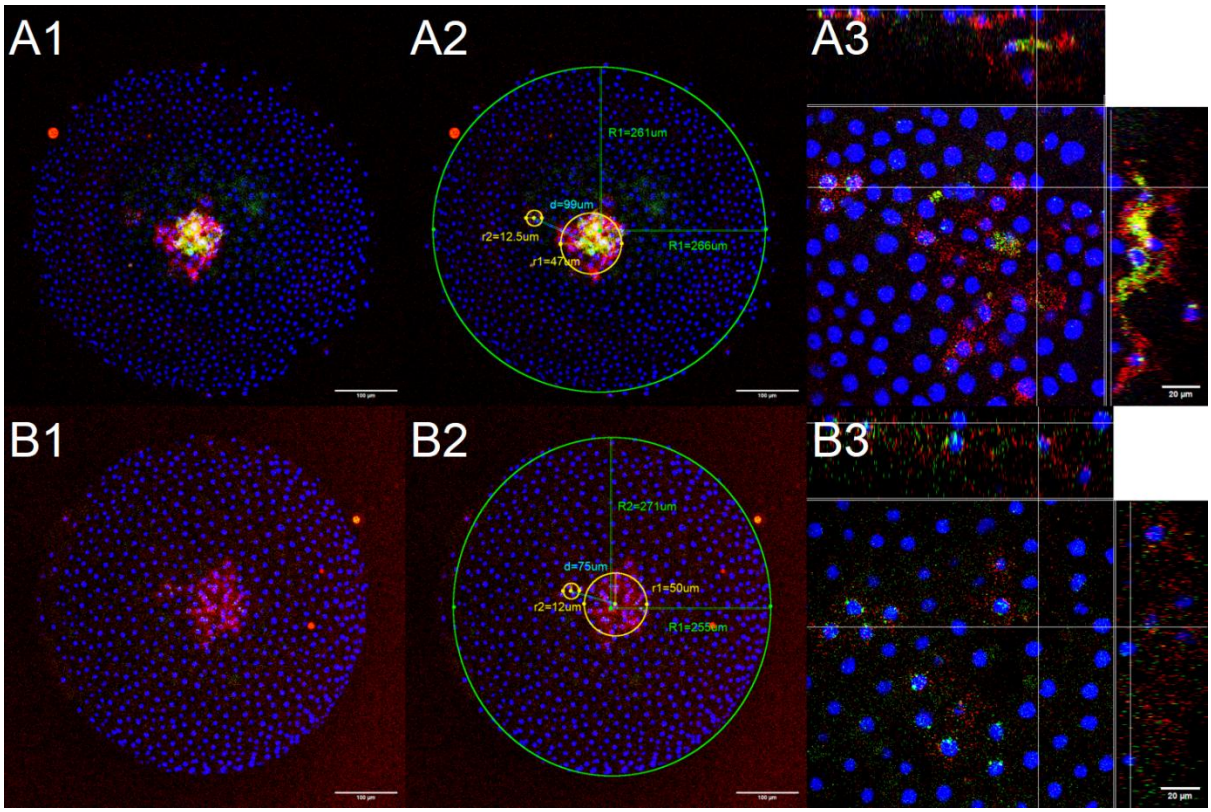

Figure S1-27. Extra fuchi+ cell clusters in germ disc of WT and Ets4 RNAi embryos. A1, A2 and A3: WT embryo, at 27 hael. B1, B2 and B3: Ets4 RNAi embryo, at 25 hael. A1, A2, B1 and B2: AVG z-stack, 10x. A3 and B3: orthogonal view, 40x. HCR staining. Blue: Dapi. Red: *fuchi*. Green: *Ets4*.

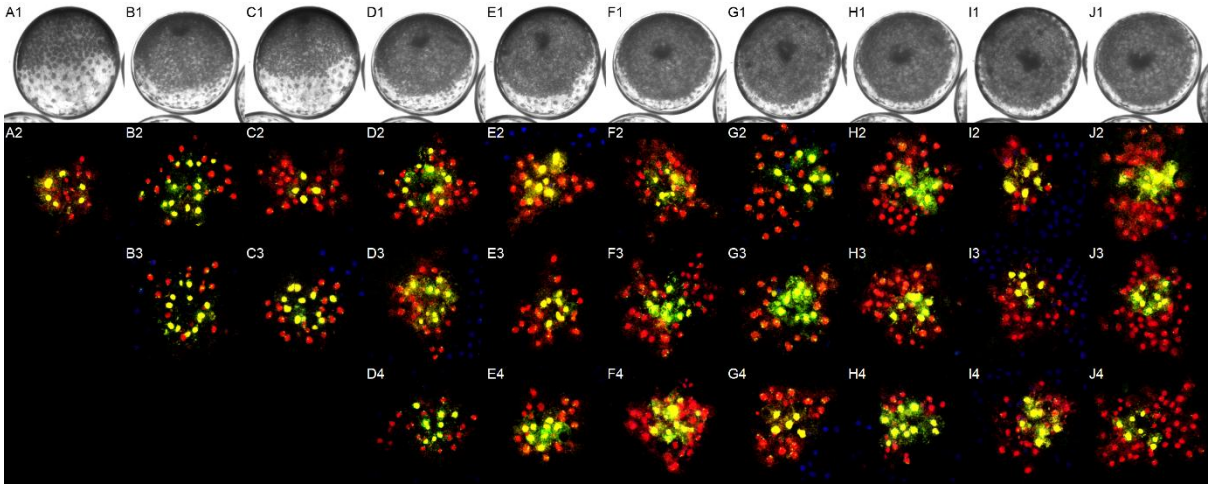

Figure S1-28. Bright field and 3D top view of all the centre inner cells of embryos at 22 to 31 hael. A1 and A2: 22 hael. B1, B2 and B3: 23 hael. C1, C2 and C3: 24 hael. D1, D2, D3 and D4: 25 hael. E1, E2, E3 and E4: 26 hael. F1, F2, F3 and F4: 27 hael. G1, G2, G3 and G4: 28 hael. H1, H2, H3 and H4: 29 hael. I1, I2, I3 and I4: 30 hael. J1, J2, J3 and J4: 31 hael. A1, C1, E1, G1 and I1: bright field image of embryo from WT cocoon 2; at 22, 24, 26, 28 and 30 hael respectively. B1, D1, F1, H1 and J1: bright field image of embryo from WT cocoon 1; at 23, 25, 27, 29 and 31 hael respectively. A2 to J2, B3 to J3 and D4 to J4: 3D top view of inner cells. 40x images were colours and made into 3D model by Fiji. Some images are rotated, to make the migration direction towards right. Red: *fuchi*. Green: *Ets4*.

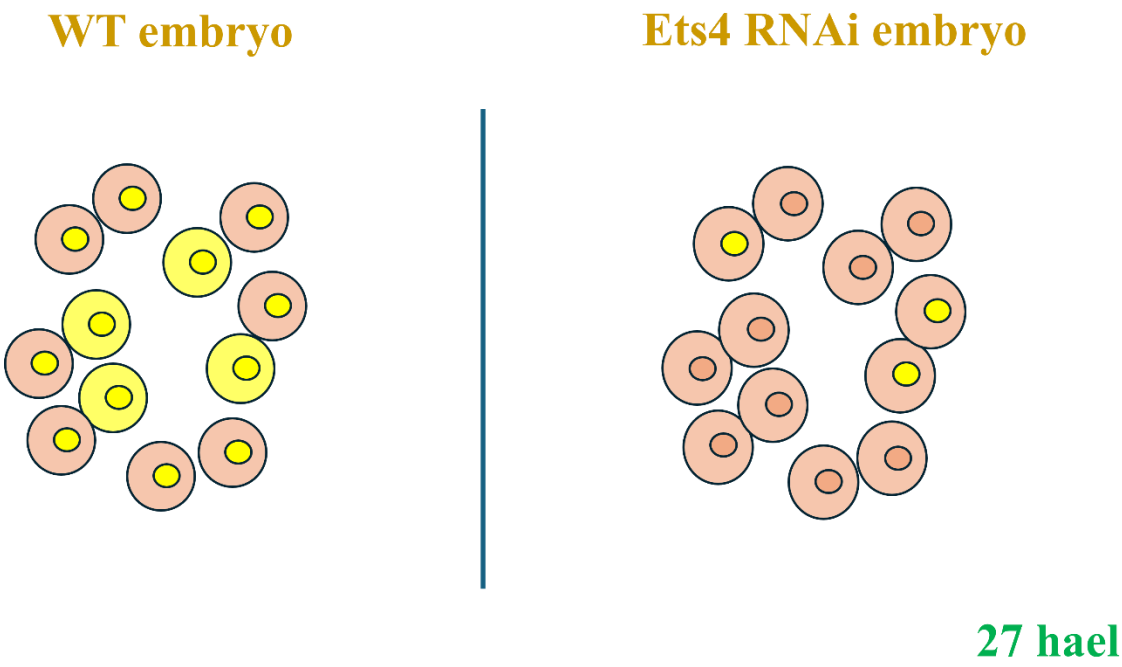

Figure S1-29. Schematic image of cluster of inner cells in top view in WT and Ets4 RNAi embryos at end of stage 3. Cells are marked with two cycles to show nucleus and cytoplasm. Expression in cytoplasm are marked in the large, outer cycle, and nascent transcripts expression are marked in the small inner cycles. Fuchi expression is depicted in red colour and Ets4 expression is in green. A combination of both Fuchi and Ets4 expression is in yellow.

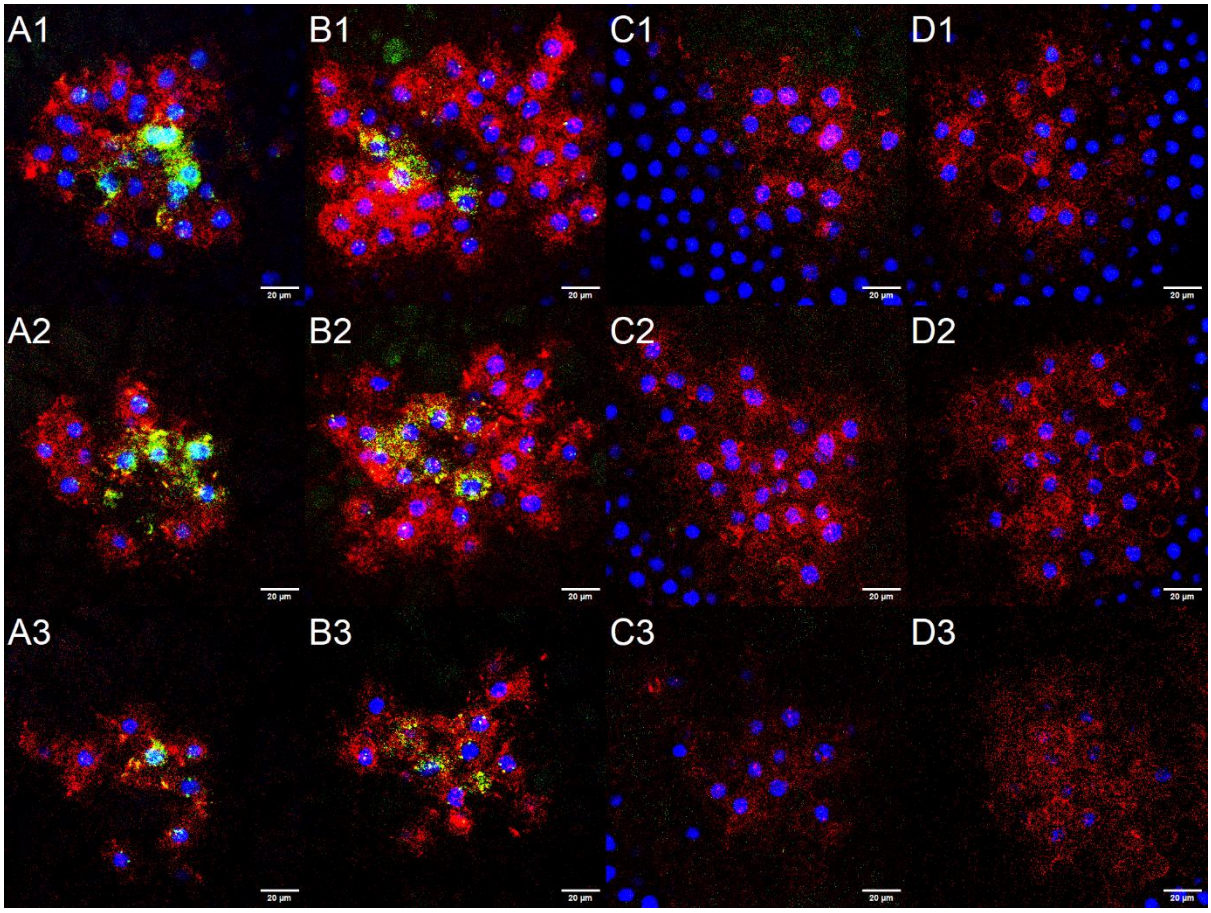

Figure S1-30. Cells in the primary thickening region at around 30 hael in WT and Ets4 RNAi embryos. A1, A2 and A3: WT embryo, 29 hael, AVG z-stack of frames 8-15, 16-23, 24-31. B1, B2 and B3: WT embryo, 31 hael, AVG z-stack of frames 7-13, 14-20, 21-27. C1, C2 and C3: Ets4 RNAi embryo, 29 hael, AVG z-stack of frames 8-14, 15-21, 22-28. D1, D2 and D3: Ets4 RNAi embryo, 31 hael, AVG z-stack of frames, 7-13, 14-20, 21-27. 40x. Blue: Dapi. Red: *fuchi*. Green: *Ets4*.

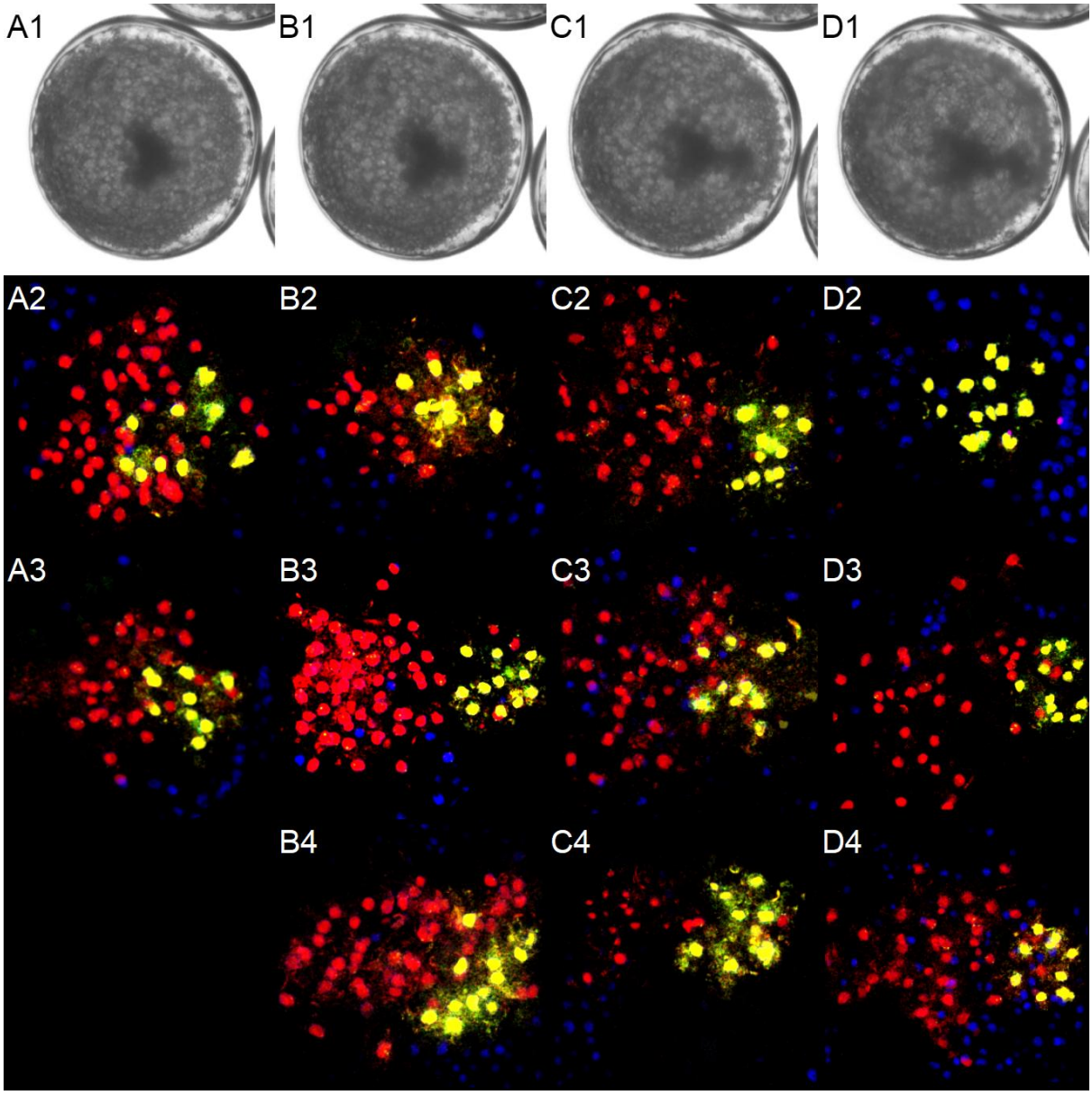

Figure S1-31. Bright field and 3D top view of all the centre inner cells of embryos at 33 to 39 hael. A1, A2 and A3: 33 hael. B1, B2, B3 and B4: 35 hael. C1, C2, C3 and C4: 37 hael. D1, D2, D3 and D4: 39 hael. A1, B1, C1, and D1: bright field image of WT cocoon 1. A2, A3, B2, B3, B4, C2, C3, C4, D2, D3 and D4: 3D top view of inner cells. 40x images were colours and made into 3D model by Fiji. Some images are rotated, to make the migration direction towards right. Red: *fuchi*. Green: *Ets4*.

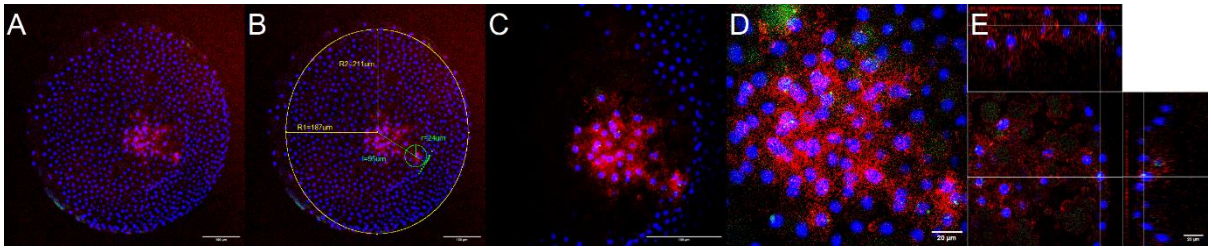

Figure S1-32. Image of Ets4 RNAi embryo with a few cells migrating, at 43 hael. A and B: AVG z-stack, 10x. B: Measurement of the radius of the germ disc, the radius of migrating small cumulus, and the distance of

between the cumulus and germ disc centre. C: AVG z-stack of inner cells, 10x. D: AVG z-stack, 40x. E: orthogonal view of D, rotate for 45°. HCR staining. Blue: Dapi. Red: *fuchi*. Green: *Ets4*.

Table S1-6 Comparison of cumulus migration in WT embryos, and in exceptional Ets4 RNAi embryos

	WT embryos	Ets4 RNAi (only one sample)
Migrating centre	Cluster of cells	Cluster of cells
Migrating cell number	Around 10	8
Migrating cell type	Fuchi+ Ets4+	Fuchi+Ets4 na+
Depth of migrating cells	One to two layers beneath ectoderm	One to two layers beneath ectoderm
Time to arrive middle stage 5	About 32 to 37 hael	43 hael
Other germ disc inner cells	A lot of fuchi+Ets4- cells follows	Not seen

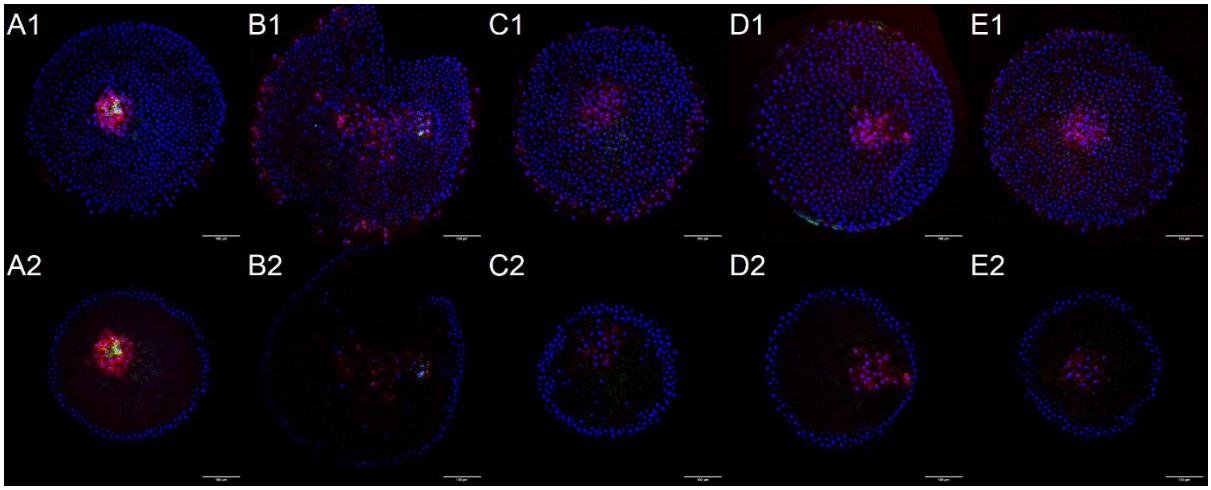

Figure S1-33. Comparison on fuchi-Ets4- cell movement in WT and Ets4 RNAi embryos. A1 and A2: WT embryo, 31 hael. B1 and B2: WT embryo, 39 hael. C1 and C2: Ets4 RNAi embryo, 31 hael. D1 and D2: Ets4 RNAi embryo, 43.5 hael. E1 and E2: Ets4 RNAi embryo, 43.5 hael. A1, B1, C1, D1 and E1: AVG z-stack, 10x. A2, B2, C2, D2 and E2: single frame, 10x. Blue: Dapi. Red: *fuchi*. Green: *Ets4*.

(Supplementary Figures and Tables for Result Chapter II)

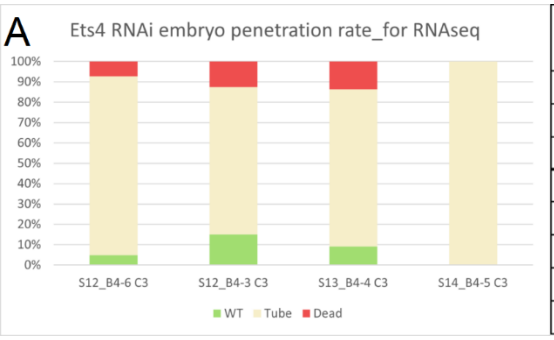

B

	number of embryos	extracted RNA concentration (ng/ul)
S9_dsRed	110	6.6- 18.7
S10_dsRed-4 C3	110	12.5
S11_dsRed-8 C3	110	13
S12_Ets4 RNAi B4-6 C3	90	9.6
S12_Ets4 RNAi B4-3 C3	40	
S13_Ets4 RNAi B4-4 C3	114	18.4
S14_Ets4 RNAi B4-5 C3	130	13.8

Figure S2-1. Penetration Rate of *Ets4* RNAi Embryos and Primary thickening Samples for Sequencing. A. Penetration rate of *Ets4* RNAi embryos for sequencing. Sample 12 (S12) consists of embryos from the third cocoon of B4-6 (Batch 4 No.6) and B4-3 Spiders. Sample 13 is from the third cocoon of B4-4 Spiders, and Sample 14 comes from the third cocoon of B4-5 Spiders. The green color indicates embryos exhibiting wildtype-like morphology at developmental stages 5 to 8. The red color denotes dead embryos, while the light-yellow color represents embryos with no cumulus migration and a tube-like shape at developmental stages 5 to

8. B. For each sample, 110-130 embryos were dissected, with three biological replicates each for dsRed and *Ets4* RNAi embryos. RNA was extracted from each sample, yielding a final concentration of approximately 10-20 ng/µl for sequencing.

A

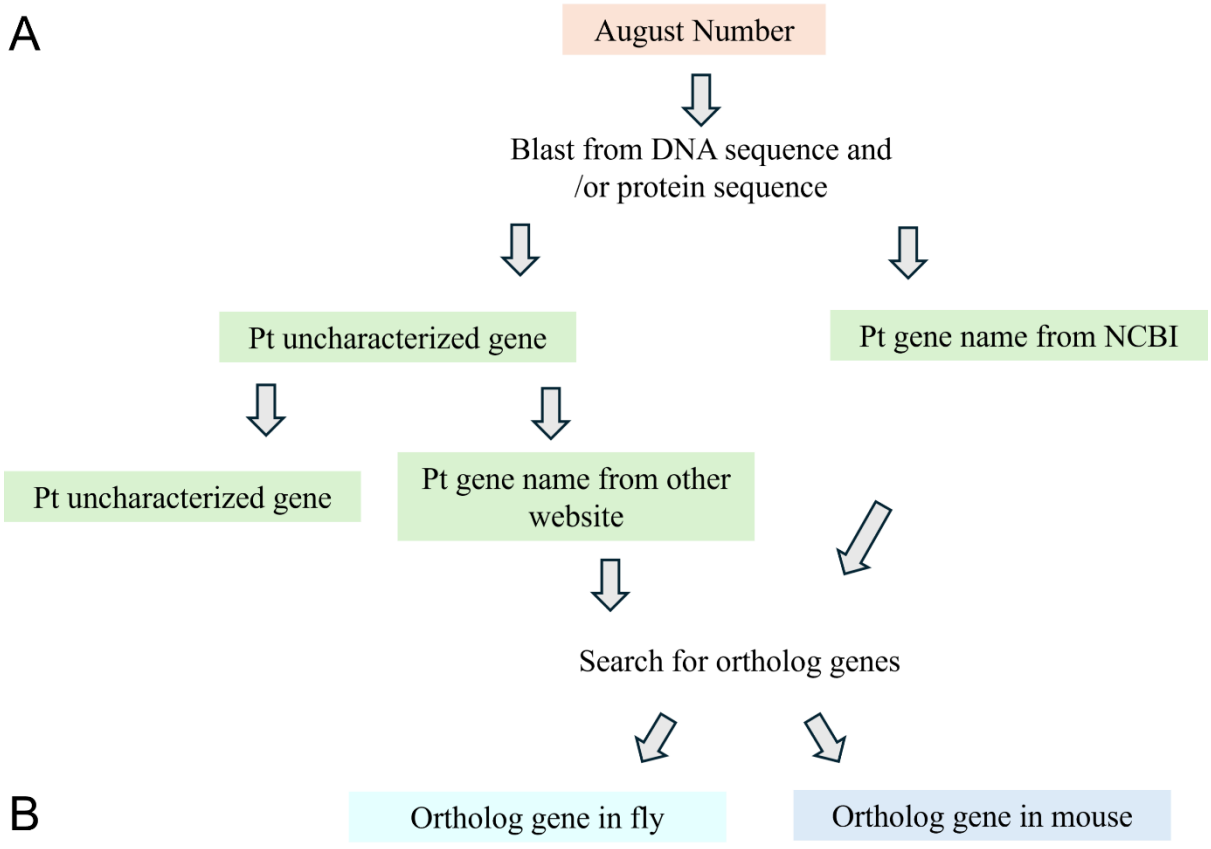

B

Name	Sequence	sprot_Top TrEMBL_T: Pfam	gene_ont	eff_length	3_tpm_S1	3_FDR	3_AveExpr	3_P value	tpm_S9	tpm_S10	tpm_S11	tpm_S13	tpm_S14	tpm_S12	Protein sequence	Parasteatoda gene from NCBI blast	Parasteatoda LOC	fly homology	fly gene ID	mouse homo	UniProt ID	other species	UniProt ID
aug3_g4238.t1	TTACCAGT	ETS4_DRO A0A087TM	PF02198.1	GO:0043	2607.84	-3.97685	3.79E-09	6.647318	1.18E-12	161.599	196.816	241.265	2.20942	3.25887	26.7402	MQTCAPIRVETRPC	SAM pointed domain-containing Ets transcription factor	LOC107451717	Ets98B	FBgn0005659	Spdef	Q9WTP3		
aug3_g1428.t1	ATCTTCCC	TWIST_XEI	Q65YY8	PF00010.2	GO:0046	1258.84	-3.76169	1.01E-09	4.792967	2.52E-13	43.2936	63.0725	43.2093	0.866768	0.794551	7.6629	MDNYVRTNPLNLP	twist-related protein 2-like	LOC107440133	twi	FBgn0003900	Twist2	Q90D30	TCM_000472	A0A0610H43
aug3_g2334.t1	TTCGAATC					53.1938	-3.53695	1.36E-09	9.684165	3.81E-13	1213.71	1428.11	2433.99	70.4555	103.874	186.478	MKCMSTFDLGKGP	E3 ubiquitin-protein ligase ATL59	LOC107450101	Zip89		Dzip3	Q7TPV2	DZIP3 ligase	A0A7L2A7K5
aug3_g1767.t1	CATCCGTG	SECG_DICI	A0A087UC	PF13637.1	GO:0005	1331.84	-2.58409	8.15E-09	5.076968	3.88E-12	51.593	37.8827	90.5297	9.62819	7.57542	7.05598	MADNRAVQHFHD	putative ankyrin repeat protein RF_0381	LOC107447467					spider specific	
aug3_g1624.t1	GAATCCCC	Y3556_DR	A0A087TZ	PF00057.1	GO:0005	1327.84	-6.26253	7.64E-09	3.101919	2.86E-12	10.5138	11.765	18.9388	0.017325	0.043369	0.051564	MDVSLSLC4VLCC	uncharacterized protein CG3556-like	LOC107449272	CG3556	FBgn0029708	Cblif	P52787		
aug3_g7461.t1	ATAATATT					666.84	-5.87353	1.89E-08	3.132624	1.41E-11	9.58382	2.80149	31.1442	0.067961	0.171037	0.034036	MVWELLEVLCIVLV	uncharacterized, ncRNA	LOC122271925						K02A2.6_416 A0A4Y2IHG3
aug3_g12633.t1	AATTAATG		A0A087T1			1561.84	-3.862	2.42E-08	3.50001	1.95E-11	13.4554	12.4634	30.3536	0.53889	0.549189	1.80718	MAGIAWLVGHVA	uncharacterized	LOC107437853	raw	FBgn0003209				AVEN_167225 A0A4Y2UT47
aug3_g26430.t1	AGTAGTAA					698.84	-4.77572	3.25E-15	4.446342	4.04E-19	26.8342	34.1382	63.033	1.84877	0.734583	0.81213	MEKAMICFGIWFN	uncharacterized	LOC107438215						Transmembra A0A4Y2QLI4

Figure S2-2. Process and Result of Pt Gene Annotation from August Transcripts. A. Process of annotation. includes of BLAST search on NCBI (https://blast.ncbi.nlm.nih.gov/) and UniProt (https://www.uniprot.org/blast), and ortholog identification in mouse and fly through UniProt (https://www.uniprot.org/),, Alliance of Genome Resources (https://www.alliancegenome.org/), and Flybase (https://Flybase.org/). B. Examples of Pt gene annotation. The table shows an example of Pt gene annotation, with each column color-coded to represent different types of information: Red: August number of the transcript. First white column (left): DNA sequence of the transcript. Orange: Automated annotation. Second white column: Effective length derived from RNA-seq data. Yellow: Contains RNA-seq metrics including Fold2Change, FDR, average expression, P-value, and individual reads for the six samples. Third white column: Protein sequence translated from DNA, using Expasy's translation tool (Expasy Translation Tool). Green: BLAST results (DNA/protein sequence) from NCBI, showing gene names and locations in the Pt genome. Cyan: Ortholog gene information in *Mus musculus* (Mm), including gene name and Uniprot ID (Uniprot). Blue: Ortholog gene information in *Drosophila melanogaster* (Dm), with gene name and Flybase ID (Flybase). Magenta: Ortholog gene results from species other than Mouse and Fly.

Table S2-1. Top 100 genes of List B, C, and F.

transcript_id	tpm_S1 (3)	FDR	Parasteatoda gene NCBI blast	fly gene	fly ID	mouse gene	UniProt
aug3.g6211.t2	-8.32693	0.005754	GTP-binding protein 4	SrpRα	FBgn0010391	Gtpbp4	Q99ME9
aug3.g6211.t1	-8.32693	0.005754	GTP-binding protein 4	SrpRα	FBgn0010391	Gtpbp4	Q99ME9
aug3.g22997.t1	-8.04273	1.54E-12	LTV1 homolog	LTV1	FBgn0027525	Ltv1	Q6NSQ7
aug3.g760.t2	-8.0357	2.27E-16	suppressor of SWI4 1 homolog	ppan	FBgn0010770	Ppan	Q91YU8
aug3.g23069.t1	-7.72668	1.89E-08	GTP-binding protein 128up	128up	FBgn0010339	Drg1	D6RHA5
aug3.g19878.t1	-7.47943	5.16E-16	kinesin heavy chain	Khc	FBgn0001308	Kif5b	Q61768
aug3.g21118.t1	-7.0615	5.53E-06	ome c oxidase subunit 6A1, mitoch	levy	FBgn0034877	Cox6a1	P43024
aug3.g9731.t2	-6.89176	0.005949	uncharacterized	CG9896	FBgn0034808		
aug3.g14522.t1	-6.80079	2.42E-08	uncharacterized	Sox102F	FBgn0039938	Sox13	Q04891
aug3.g11056.t2	-6.70246	1.00E-08	n-activated chloride channel regula	Clic	FBgn0030529	Clca4a	Q6Q473
aug3.g24722.t1	-6.60414	1.08E-08	uncharacterized				
aug3.g16824.t1	-6.26253	7.64E-09	ncharacterized protein CG3556-lik	CG3556	FBgn0029708	Cblif	P52787
aug3.g16653.t2	-6.15076	3.44E-06	gin recognition complex subunit 2-	Orc2	FBgn0015270	Orc2	Q60862
aug3.g7598.t1	-6.06222	8.61E-06					
aug3.g9996.t1	-5.97573	1.15E-07	epoxide hydrolase 1	Jheh1	FBgn0010053	Ephx1	Q9D379
aug3.g16984.t1	-5.95957	2.35E-05	uncharacterized, ncRNA	Tim8	FBgn0027359	Timm8b	P62077
aug3.g17803.t1	-5.94952	1.58E-08	astacin-like metalloprotease toxin 5	CG15255	FBgn0028950	Mep1b	Q61847
aug3.g7461.t1	-5.87353	1.89E-08	uncharacterized, ncRNA				
aug3.g24382.t1	-5.81037	4.97E-05					
aug3.g17735.t1	-5.51388	7.93E-05	uncharacterized	frm	FBgn0035612	Colq	Q3KNA4
aug3.g14965.t1	-5.40281	0.001634	uncharacterized, ncRNA				
aug3.g18533.t2	-5.25492	0.000133	uncharacterized				
aug3.g20775.t1	-5.24803	0.004145					
aug3.g12363.t2	-5.2423	0.004279	ucleolar RNA-associated protein	Utp4	FBgn0263605		Q8R2N2
aug3.g23745.t1	-5.22928	0.004638	tubulin alpha chain	αTub84B	FBgn0003884	Tuba1a	P68369
aug3.g10182.t1	-5.20991	0.001909	acetoacetyl-CoA synthetase			Aacs	Q9D2R0
aug3.g14709.t1	-5.20395	0.005169	uncharacterized				
aug3.g12623.t1	-5.18397	0.005754	DNA polymerase epsilon subunit 4	PolE4	FBgn0034726	Pole4	Q9CQ36
aug3.g6047.t1	-5.17987	0.005795	x- and mab-3-related transcription	dmrt93B	FBgn0038851	Dmrt3	Q80WT2
aug3.g13428.t1	-5.15662	0.004728	cytochrome P450 4C1	Cyp4c3	FBgn0015032	Cyp4a10	O88833
aug3.g2426.t1	-5.14213	0.003605	ehydrogenase, dimeric NADP-pre	Aldh-III	FBgn0010548	Aldh3a1	P47739
aug3.g25963.t1	-5.00686	0.013082	uncharacterized	dgt6	FBgn0039638	Haus7	Q8BKT8
aug3.g22710.t1	-4.98956	0.014059	nephrin	sns	FBgn0024189	Nphs1	Q9QZS7
aug3.g3239.t2	-4.96012	0.016186	ehydrogenase, dimeric NADP-pre	Aldh-III	FBgn0010548	Aldh3a1	P47739
aug3.g22582.t1	-4.95517	0.016497	nRNA-splicing factor CWC25 hon	Cwc25	FBgn0031452	Cwc25	Q9DBF7
aug3.g1382.t2	-4.94975	0.000188	40S ribosomal protein S13	RpS13	FBgn0010265	Rps13	P62301
aug3.g27081.t4	-4.94657	0.005919	CAD protein	r	FBgn0003189	Cad	B2RQC6
aug3.g11038.t3	-4.90338	0.006636	rho GTPase-activating protein 19	RhoGAP54D	FBgn0034249	Arhgap19	Q8BRH3
aug3.g21981.t1	-4.89185	0.000387	protein ABHD11-like	CG2059	FBgn0029942	Abhd11	Q8K4F5
aug3.g20062.t1	-4.82314	0.000335	fatty acid synthase	FASN1	FBgn0283427	Fasn	P19096
aug3.g26430.t1	-4.77572	3.25E-15	uncharacterized				
aug3.g3283.t2	-4.7405	0.04255	DB1- and CUL4-associated factor	CG9945	FBgn0034527	Dcaf11	Q91VU6
aug3.g10298.t5	-4.72632	0.04493	uncharacterized				
aug3.g2208.t1	-4.72179	0.045763	apolipoprotein D	NLaz	FBgn0053126	Apod	P51910
aug3.g1627.t2	-4.52562	7.02E-05	e oxidoreductase-like protein 2 ho	Sec16	FBgn0052654	Cryzl2	Q3UNZ8
aug3.g23568.t1	-4.30805	0.011856	uncharacterized protein CG3556	CG3556	FBgn0029708		
aug3.g4286.t1	-4.29296	0.000148	uncharacterized	stumps/dof	FBgn0020299	sitide 3-kinase adap	Q9EQ32
aug3.g6621.t1	-4.03615	0.005395	uncharacterized				
aug3.g8227.t1	-3.99697	0.033349	RNA-associated Sm-like protein I	CG10418	FBgn0036277	Lsm2	O35900
aug3.g4238.t1	-3.97685	3.79E-09	ed domain-containing Ets transcrip	Ets98B	FBgn0005659	Spdef	Q9WTP3
aug3.g20952.t1	-3.96348	8.03E-06	cific acyl-CoA dehydrogenase, mi	CG4860	FBgn0037999	Acads	Q07417
aug3.g12606.t1	-3.95167	1.72E-05	sociated complex subunit alpha, m	Nacα	FBgn0086904	Naca	P70670
aug3.g12633.t1	-3.862	2.42E-08	uncharacterized	raw	FBgn0003209		
aug3.g14287.t1	-3.76169	1.01E-09	twist-related protein 2-like	twi	FBgn0003900	Twist2	Q9D030
aug3.g10040.t1	-3.67533	1.27E-05	y-3-methylglutaryl-coenzyme A r	Hmgcr	FBgn0263782	Hmgcr	Q01237
aug3.g24757.t1	-3.58824	0.022458	uncharacterized				
aug3.g22384.t1	-3.53695	1.36E-09	E3 ubiquitin-protein ligase ATL59				
aug3.g4230.t1	-3.51897	2.81E-05	uncharacterized				
aug3.g26532.t1	-3.50771	1.68E-14	integrator complex subunit 2	IntS2	FBgn0030858	Ints2	Q80UK8
aug3.g12977.t1	-3.4794	4.14E-05	uncharacterized, ncRNA				
aug3.g24413.t1	-3.45135	7.64E-09	kinesin light chain	Klc	FBgn0010235	Klc1	O88447
aug3.g14945.t1	-3.44357	0.009519	uncharacterized	Taf2	FBgn0011836	Taf2	Q8C176
aug3.g26566.t1	-3.43916	0.002698	fibroblast growth factor receptor 4	btl	FBgn0285896	Fgfr4	Q03142
aug3.g20300.t1	-3.3246	2.04E-07	serine--tRNA ligase, mitochondria	Slimp	FBgn0051133		
aug3.g7367.t2	-3.28756	0.018648	in-helicase-DNA-binding protein N	Mi-2	FBgn0262519	Chd1	P40201
aug3.g26565.t1	-3.26626	0.000158	fibroblast growth factor receptor 4	btl	FBgn0285896	Fgfr4	Q03142
aug3.g18588.t1	-3.20284	0.000186	probable imidazolonepropionase			Amdhd1	Q9DBA8
aug3.g658.t1	-3.15614	0.000809	erized/oocyte zinc finger protein XlCOF6.1				
aug3.g20188.t1	-3.14293	0.000592	glutamyl aminopeptidase	CG32473	FBgn0052473	Enpep	P16406
aug3.g7476.t1	-3.10443	0.02798	elongator complex protein 4	CG6907	FBgn0031711	Elp4	Q9ER73
aug3.g22225.t1	-3.07419	0.009479	nsfer flavoprotein subunit alpha, m	wal	FBgn0010516	Etfa	Q99LC5
aug3.g7690.t1	-3.05133	0.006905	uncharacterized				
aug3.g1120.t2	-3.03762	0.000154	uncharacterized			Map1lc3b	Q9CQV6
aug3.g16174.t1	-3.00133	0.005795	uncharacterized	stops	FBgn0086704	Asb10	Q91ZT7
aug3.g5049.t1	-2.98134	0.049767	irected RNA polymerase II subuni	Polr2A	FBgn0003277	Polr2a	P08775
aug3.g886.t1	-2.96345	9.64E-06	uncharacterized				
aug3.g5179.t2	-2.92068	7.90E-08	uncharacterized	Klc	FBgn0010235	Klc1	O88447
aug3.g10237.t3	-2.89489	0.030398	olgi network integral membrane protein 2			Tgoln2	Q62314
aug3.g9095.t2	-2.88173	0.019065	tive ferric-chelate reductase 1 hom	CG8399	FBgn0034067	Frrs1	Q8K385
aug3.g2394.t2	-2.8499	0.002747	ROBO Rho GTPase-activating protein 1			Srgap1	Q91Z69
aug3.g65.t1	-2.83395	0.000229	kinesin light chain	Klc	FBgn0010235	Klc1	O88447
aug3.g21415.t1	-2.83223	0.00724	cific acyl-CoA dehydrogenase, mi	CG4860	FBgn0037999	Acads	Q07417
aug3.g26529.t1	-2.81501	0.00011	myotubularin-related protein 14	Mtmr6	FBgn0028497	Mtmr14	Q8VEL2
aug3.g17912.t1	-2.80695	6.56E-05	related Pol polyprotein from trans	412\ORF3	FBgn0043847		
aug3.g21643.t1	-2.7905	0.000678	uncharacterized	CG12093	FBgn0035372	TP53I13	Q5F267
aug3.g27267.t1	-2.75316	0.032034	uncharacterized				
aug3.g22426.t1	-2.73723	0.013778	R3H domain-containing protein 4	enc	FBgn0004875	R3hdm4	Q4VBF2
aug3.g17747.t2	-2.64065	0.008247	uncharacterized	CG9121	FBgn0031675	Asb10	Q91ZT7
aug3.g16613.t1	-2.61676	0.012729	uncharacterized				
aug3.g1767.t1	-2.58409	8.15E-09	ative ankyrin repeat protein RF_0381				
aug3.g16171.t1	-2.57163	0.021343	uncharacterized				
aug3.g21682.t1	-2.56627	0.009521	uncharacterized				
aug3.g24164.t1	-2.55956	0.000366	A 3'-terminal phosphate cyclase-l	Rtca	FBgn0025630	Rcl1	Q9JJT0
aug3.g3137.t1	-2.53204	5.73E-05	phenoloxidase-activating factor 2	Spn27A	FBgn0028990		
aug3.g16727.t1	-2.51193	1.51E-05	myosin-9-like	CG13733	FBgn0036729	Myh9	Q8VDD5
aug3.g3789.t1	-2.50076	0.000229	d gene for Pt1-cadherin, complete cds				
aug3.g6760.t1	-2.49502	0.006464	acetylcholinesterase-1	Ace	FBgn0000024	Ache	P21836
aug3.g26077.t1	-2.4859	0.022458	CWF19-like protein 2	CG9213	FBgn0030655	Cwf19l2	Q8BG79
aug3.g17719.t1	-2.40262	0.0011	uncharacterized			Art2b	O35975
aug3.g11009.t1	-2.39429	0.008574	protein Wnt-16-like	wnt4	FBgn0010453	Wnt16	Q9QYS1

transcript_id	tpm_S1 (2)	FDR	Parasteatoda gene NCBI blast	fly gene	fly ID	mouse gene	UniProt
aug3.g760.t2	-8.0706714	6.24E-17	suppressor of SWI4 1 homolog	ppan	FBgn0010770	Ppan	Q91YU8
aug3.g19878.t1	-7.4935422	4.83E-12	kinesin heavy chain	Khc	FBgn0001308	Kif5b	Q61768
aug3.g22997.t1	-7.355862	6.27E-11	LTV1 homolog	LTV1	FBgn0027525	Ltvl	Q6NSQ7
aug3.g23069.t1	-7.2855092	2.15E-10	GTP-binding protein 128up	128up	FBgn0010339	Drg1	D6RHA5
aug3.g11056.t2	-6.8485404	1.49E-07	um-activated chloride channel regulato	Clic	FBgn0030529	Clca4a	Q6Q473
aug3.g18533.t2	-6.4768156	1E-05	uncharacterized				
aug3.g16653.t2	-6.2422024	7.6E-05	rigin recognition complex subunit 2-lik	Orc2	FBgn0015270	Orc2	Q60862
aug3.g16824.t1	-6.1166587	1.9E-05	uncharacterized protein CG3556-like	CG3556	FBgn0029708	Cblif	P52787
aug3.g20952.t1	-6.0649324	0.00031	pecific acyl-CoA dehydrogenase, mito	CG4860	FBgn0037999	Acads	Q07417
aug3.g2311.t1	-6.0557885	0.00014	ermonecrotic toxin LgSicTox-alphaIC1				
aug3.g17803.t1	-5.9779057	0.00017	astacin-like metalloprotease toxin 5	CG15255	FBgn0028950	Mep1b	Q61847
aug3.g18529.t1	-5.9157692	0.00091					
aug3.g27081.t4	-5.8822724	0.00113	CAD protein	r	FBgn0003189	Cad	B2RQC6
aug3.g4238.t1	-5.8688083	6.89E-12	nted domain-containing Ets transcripti	Ets98B	FBgn0005659	Spdef	Q9WTP3
aug3.g14287.t1	-5.7052711	7.77E-21	twist-related protein 2-like	twi	FBgn0003900	Twist2	Q9D030
aug3.g20062.t1	-5.6641822	3.8E-05	fatty acid synthase	FASN1	FBgn0283427	Fasn	P19096
aug3.g6621.t1	-5.6011125	0.00049	uncharacterized	CG11275	FBgn0034706	Tdpoz2	Q717B2
aug3.g2628.t3	-5.5737113	0.00666	otif and SEC7 domain-containing prot	siz	FBgn0026179	Iqsec1	Q8R0S2
aug3.g9721.t1	-5.5074642	1.4E-05	uncharacterized	CG2059	FBgn0029942	Abhd11	Q8K4F5
aug3.g9996.t1	-5.4862858	6.4E-05	epoxide hydrolase 1	Jheh1	FBgn0010053	Ephx1	Q9D379
aug3.g24501.t1	-5.4233146	0.01105	transmembrane protein 147	CG5861	FBgn0015338	Tmem147	Q9CQG6
aug3.g14078.t1	-5.2579039	3.84E-21	uncharacterized				
aug3.g14965.t1	-5.2524018	0.0285	uncharacterized, ncRNA				
aug3.g25963.t1	-5.1339543	0.0458	uncharacterized	dgt6	FBgn0039638	Haus7	Q8BKT8
aug3.g18600.t1	-5.0252218	0.00215	uncharacterized	LysP	FBgn0004429	530003J23Ri	Q8BM27
aug3.g4246.t1	-5.0038046	0.00666	le inositol polyphosphate phosphatase	Mipp1	FBgn0026061	Minpp1	Q9Z2L6
aug3.g9726.t1	-5.0022431	5.49E-12	protein ABHD11-like	CG2059	FBgn0029942	Abhd11	Q8K4F5
aug3.g16889.t1	-4.8074337	1.8E-05					
aug3.g27753.t1	-4.7263103	4.74E-08	phospholipase A2	Pla2	FBgn0086242	Pla2g2a	P31482
aug3.g24413.t1	-4.6989956	1.31E-10	kinesin light chain	Klc	FBgn0010235	Klc1	O88447
aug3.g4286.t1	-4.6674211	0.00312	uncharacterized	stumps/dof	FBgn0020299	le 3-kinase a	Q9EQ32
aug3.g7461.t1	-4.6122043	0.01398	uncharacterized, ncRNA				
aug3.g4424.t2	-4.5369454	5.62E-10	uncharacterized	CG14301	FBgn0038632		
aug3.g21415.t1	-4.3449028	0.0022	ecific acyl-CoA dehydrogenase, mito	CG4860	FBgn0037999	Acads	Q07417
aug3.g26430.t1	-4.3301888	2.77E-12	uncharacterized				
aug3.g9252.t1	-4.3122687	3.09E-14	uncharacterized	pvir\GJ1125	FBtr0436430		
aug3.g6760.t1	-4.2560372	2.26E-19	acetylcholinesterase-1	Ace	FBgn0000024	Ache	P21836
aug3.g16925.t1	-4.2017282	2.8E-06	univin				
aug3.g12633.t1	-4.1919838	4.7E-05	uncharacterized	raw	FBgn0003209		
aug3.g1627.t2	-4.1827274	0.00238	one oxidoreductase-like protein 2 hom	Sec16	FBgn0052654	Cryzl2	Q3UNZ8
aug3.g8339.t1	-4.1655371	0.00771	uncharacterized	CG43082	M9NFE3		
aug3.g3137.t1	-4.1426529	1.90E-14	phenoloxidase-activating factor 2	Spn27A	FBgn0028990		
aug3.g23932.t1	-4.1089776	0.00541		CG17883	FBgn0040005	Tbc1d20	Q3T9Q9
aug3.g11120.t1	-4.0993216	3.7E-05	uncharacterized				
aug3.g10890.t1	-4.0751222	8.81E-08	uncharacterized	Muc68D	FBgn0036203	DSPP	P97399
aug3.g23023.t1	-4.0496365	0.00598				Nefh	P19246
aug3.g26402.t1	-4.0257528	4.26E-14	phenoloxidase-activating factor 3	Spn27A	FBgn0028990		
aug3.g21536.t1	-3.9968536	5.3E-05	uncharacterized				
aug3.g4424.t1	-3.990235	4.19E-07	uncharacterized	CG14301	FBgn0038632		
aug3.g11258.t1	-3.9482763	7.77E-21	proline-rich protein 4				
aug3.g2548.t1	-3.9321639	1.55E-08	uncharacterized				
aug3.g20823.t1	-3.9299836	1.1E-05	uncharacterized	CG14607	FBgn0037488		
aug3.g9728.t1	-3.8769839	0.00187	protein ABHD11	CG2059	FBgn0029942	Abhd11	Q8K4F5
aug3.g24553.t1	-3.8486276	1.65E-21	uncharacterized				
aug3.g18398.t1	-3.8330357	2.47E-16	uncharacterized				
aug3.g15065.t1	-3.8256765	9.89E-11	flavin-containing monooxygenase 5	Fmo-1	FBgn0034943	Fmo5	P97872
aug3.g26566.t1	-3.8230119	0.01564	fibroblast growth factor receptor 4	btl	FBgn0285896	Fgfr4	Q03142
aug3.g22384.t1	-3.8101718	1.62E-07	E3 ubiquitin-protein ligase ATL59	Zip89B		Dzip3	Q7TPV2
aug3.g23929.t2	-3.8025927	1.29E-10	protein ABHD11-like	CG2059	FBgn0029942	Abhd11	Q8K4F5
aug3.g20358.t1	-3.798175	1.43E-09	uncharacterized	Taf6	FBgn0010417	Taf6	Q62311
aug3.g23544.t1	-3.7974262	2E-05	uncharacterized				
aug3.g5354.t1	-3.7707272	0.00604				Maf1	Q9D0U6
aug3.g15602.t1	-3.7569349	2.1E-06	uncharacterized	Elys	FBgn0031052	Ahctf1	Q8CJF7
aug3.g15434.t1	-3.7327533	1.4E-05	uncharacterized	LRP1	FBgn0053087	Lrp1	F6UAC8
aug3.g4731.t1	-3.7283387	1.97E-18	calumenin	scf	FBgn0025682	Calu	O35887
aug3.g16171.t1	-3.7125841	9.86E-10	uncharacterized				
aug3.g22225.t1	-3.7078782	0.0009	ransfer flavoprotein subunit alpha, mito	wal	FBgn0010516	Etfa	Q99LC5
aug3.g7529.t1	-3.6932735	2.23E-09	dentin sialophosphoprotein			Dspp	P97399
aug3.g1984.t1	-3.677918	1.03E-11	uncharacterized				
aug3.g9251.t1	-3.6725533	2.2E-05		Muc68D	FBgn0036203	Dspp	E9Q9Z9
aug3.g11980.t1	-3.6716982	9.86E-10	uncharacterized				
aug3.g10678.t1	-3.6684772	4.01E-15	uncharacterized				
aug3.g27206.t1	-3.6626467	4.56E-10	achaete-scute homolog 1a	ac	FBgn0000022	Ascl1	Q02067
aug3.g21643.t1	-3.6325602	2.7E-06	uncharacterized	CG12093	FBgn0035372	TP53I13	Q5F267
aug3.g10660.t1	-3.5987364	6.29E-11	uncharacterized	Muc68D	FBgn0036203		
aug3.g16887.t1	-3.5943939	0.00098					
aug3.g24041.t1	-3.5878913	9.3E-06	uncharacterized	Ank	FBgn0011747	Ank1	G3UY11
aug3.g5179.t2	-3.5868945	2.8E-05	uncharacterized	Klc	FBgn0010235	Klc1	O88447
aug3.g14945.t1	-3.5802221	3.45E-09	uncharacterized	Taf2	FBgn0011836	Taf2	Q8C176
aug3.g3565.t1	-3.5754771	3.94E-15	chitin deacetylase 1	Cda4	FBgn0052499		
aug3.g25745.t1	-3.5729682	4.68E-07	uncharacterized	dyl	FBgn0066365	Foxe3	Q9QY14
aug3.g20300.t1	-3.5583296	1.1E-06	serine--tRNA ligase, mitochondrial	Slimp	FBgn0051133		
aug3.g26576.t1	-3.5514679	6.28E-07					
aug3.g4781.t1	-3.5472721	4.74E-20					
aug3.g14077.t1	-3.541604	4.68E-07	uncharacterized				
aug3.g8922.t1	-3.5076135	3.7E-05		EndoA	FBgn0038659	Sh3gl1	Q62419
aug3.g9729.t1	-3.5036708	0.00344	ABHD11	CG2059	FBgn0029942	Abhd11	Q8K4F5
aug3.g2543.t1	-3.4990912	0.03387	uncharacterized				
aug3.g23567.t1	-3.4724394	0.00248	uncharacterized protein CG3556	CG3556	FBgn0029708	Cblif	P52787
aug3.g9754.t1	-3.4539589	4.85E-12		PGRP-LE	FBgn0030695	Pglyrp1	Q8VCS0
aug3.g12203.t1	-3.4468235	3.01E-17					
aug3.g220.t1	-3.4174893	0.00356	uncharacterized				
aug3.g65.t1	-3.4132214	0.00055	kinesin light chain	Klc	FBgn0010235	Klc1	O88447
aug3.g12388.t1	-3.4130975	0.00208	DZ domain-containing protein At4g08455-like				
aug3.g5611.t1	-3.3963545	9.89E-13	fibroblast growth factor 8	bnl	FBgn0014135	Fgf8	P37237
aug3.g27087.t1	-3.387776	0.043	uncharacterized	Socs44A	FBgn0033266	Socs1	O35716
aug3.g26532.t1	-3.3784675	1.36E-12	integrator complex subunit 2	IntS2	FBgn0030858	Ints2	Q80UK8
aug3.g26565.t1	-3.3693969	0.00719	fibroblast growth factor receptor 4	btl	FBgn0285896	Fgfr4	Q03142
aug3.g16068.t1	-3.3474499	1.78E-15	uncharacterized	Mhc	FBgn0264695	Myh6	Q02566
aug3.g8154.t1	-3.3419666	6.39E-19	phospholipase A2 inhibitor beta	AnxB9	FBgn0000083	Anxa3	O35639

Name	tpm_S9	tpm_S10	tpm_S11	tpm_S13	tpm_S14	tpm_S12	Parasteatoda gene from NCBI blast	fly homolog	fly gene ID	mouse homology	UniProt ID
aug3.g10006.t1	81.3905	66.5128	97.3627	43.7655	51.4684	52.8521	LYR motif-containing protein 4	bcn92	FBgn0013432	Lyrm4	Q8K215
aug3.g10010.t1	2.68818	4.05403	6.19982	0.931583	0.06187	0.492381	uncharacterized	bt	FBgn0005666		
aug3.g10040.t1	8.36178	14.613	13.7562	0.780796	1.31208	1.03E-06	oxy-3-methylglutaryl-coenzyme A rec	Hmgcr	FBgn0263782	Hmgcr	Q01237
aug3.g10065.t1	3.12247	4.49464	5.92218	2.053	2.00459	1.95107	uncharacterized	Nipped-A	FBgn0053554	Trrap	Q80YV3
aug3.g10196.t1	14.2381	14.2855	22.451	12.0898	12.1888	10.0907	(Beta-N-acetylglucosaminyl)-L-aspara	CG4372	FBgn0034665	Aga	Q64191
aug3.g10298.t5	4.68148	2.12429	3.59024	0	0	0	uncharacterized	milt	FBgn0262872	Kif28	D3YXS5
aug3.g10302.t2	3.11532	3.12972	4.20738	1.95752	1.57971	1.72778	raflagellar transport protein 122 homo	Oseg1	FBgn0265102	Ift122	Q6NWV3
aug3.g10335.t1	5.93014	3.77595	3.67543	0.380029	0.199226	0.095155	uncharacterized				
aug3.g10387.t1	25.2709	20.1478	24.5663	13.0926	9.11062	12.2808	uncharacterized	Dora	FBgn0085430	Zswim8	Q3UHH1
aug3.g10442.t1	23.0225	23.3728	28.8709	17.4109	14.4727	13.5	innexin inx2	Inx2	FBgn0027108		
aug3.g10450.t1	20.1472	21.1833	24.63	12.3427	12.6025	13.8722	cullin-5	Cul5	FBgn0288875	Cul5	Q9D5V5
aug3.g10453.t1	15.4615	16.5932	15.8833	11.6793	11.1076	13.2188	probable peptidyl-tRNA hydrolase 2	CG1307	O97067	Ptrh1	Q8BW00
aug3.g10454.t1	1.08044	1.22746	0.232294	3.44128	3.03315	1.80209	ting synaptic membrane exocytosis pr	Rim	FBgn0053547	Rims2	Q9EQZ7
aug3.g1046.t1	2.48552	2.6342	2.16961	0.03011	0.018923	0.03013	transporter SLC22A24-like/organic c	CG16727	FBgn0038719	Slc22a19	Q8VCA0
aug3.g10481.t1	27.5816	26.7482	24.8764	29.8259	29.6361	36.4483	snRNA methylphosphate capping enz	bin3	FBgn0263144	Mepce	Q8K3A9
aug3.g10490.t2	9.20244	9.36652	13.1141	4.39804	6.96381	5.15825	protein pangolin, isoforms A/H/I/S	pan	FBgn0085432		
aug3.g10501.t1	4.20664	4.77522	7.01086	2.97261	3.06013	2.56978	biquitin carboxyl-terminal hydrolase 1	Usp16-45	FBgn0029763	Usp16	Q99LG0
aug3.g10546.t1	35.3399	38.8479	46.7676	22.4942	24.9397	29.1341	mitochondrial fission factor	Tango11	FBgn0050404	Mff	Q6PCP5
aug3.g10581.t1	0.069571	0	0	0.856124	0.653742	0.689786	cytochrome P450 4C1-like	Cyp4c3	FBgn0015032	Cyp4v2	Q9DBW0
aug3.g10587.t1	3.51545	3.45102	3.41977	5.00922	4.91659	5.07775	uncharacterized			Zswim3	Q8CFL8
aug3.g10599.t1	2.97853	2.71101	2.5589	1.32887	1.41448	1.37323	oxygenase 5/ATPase family AAA dom	Fmo-1	FBgn0034943	Fmo5	P97872
aug3.g10604.t2	2.68299	3.87419	4.7738	1.37887	0.753604	0.530478	roundabout homolog 3	robo3	FBgn0041097	Robo3	Q9Z2I4
aug3.g10604.t3	4.28144	5.72962	6.09855	1.65418	1.44416	1.14053	roundabout homolog 3	robo3	FBgn0041097	Robo3	Q9Z2I4
aug3.g10605.t1	5.43791	5.65423	7.12858	2.26298	1.72247	1.12959	characterized phosphotransferase Yv	Pink1	FBgn0029891	Pink1	Q3U258
aug3.g10623.t1	3.42207	3.81492	3.28971	2.06961	1.89896	2.15819	polycomb group RING finger protein 3	l(3)73Ah	FBgn0002283	PcgF3	Q8BTQ0
aug3.g10682.t1	4.80937	5.96331	7.97134	2.40435	2.45713	3.55375	ecto-NOX disulfide-thiol exchanger 2	CG10948	FBgn0036317	Enox2	Q8R0Z2
aug3.g10711.t1	12.7757	11.0754	15.2147	8.18013	9.94111	9.43689	/toskeleton-regulatory complex protein	Reps	FBgn0032341	Inf2	Q0GNC1
aug3.g10714.t1	12.9804	10.5672	13.8038	8.44527	5.52477	8.78941	bhate cotransporter/intraflagellar trans	Picot	FBgn0024315	Slc17a5	Q8BN82
aug3.g10783.t1	94.9403	81.4819	104.489	39.851	29.3648	61.1968	actin, clone 403	Act42A	FBgn0000043	Actg1	P63260
aug3.g10793.t1	0.254485	0.60771	0.572867	2.80942	1.89609	2.54337	alpha-tocopherol transfer protein-like	CG33514	FBgn0053514	Ttpal	Q9D3D0
aug3.g10809.t2	21.5122	20.4919	38.0906	15.6613	13.3738	15.6502	a-acetyltransferase 15, NatA auxiliary	Naa15-16	FBgn0031020	Naa15	Q80UM3
aug3.g10829.t1	12.2495	10.5333	10.9117	9.43309	9.36248	7.31258	integrator complex subunit 8	IntS8	FBgn0025830	Ints8	Q80V86
aug3.g10830.t1	5.18711	3.67837	7.13955	1.26593	1.17671	2.53131	RNA-binding protein fusilli	fus	FBgn0023441	Esrp2	Q8K0G8
aug3.g10839.t1	5.00221	5.86059	6.498	3.01236	3.38019	3.85813	uncharacterized	CG8516	FBgn0037757	Csnka2ip	Q8CH19
aug3.g10841.t1	31.8237	30.4172	37.9299	9.07505	7.26041	13.6544	meteorin-like protein			Metrnl	Q8VE43
aug3.g10853.t1	58.4868	33.4651	34.4081	21.8664	21.848	27.4504	proteasome subunit alpha type-1	Prosalpha6	FBgn0250843	Psma1	Q9R1P4
aug3.g1087.t1	20.6751	23.4791	20.3276	38.5679	26.7799	29.6859	syntaxin-7	Syx7	FBgn0267849	Stx7	O70439
aug3.g10949.t1	30.7813	26.8261	46.6576	17.1278	16.0957	17.5651	nuclear pore complex protein Nup155	Nup154	FBgn0021761	Nup155	Q99P88
aug3.g10958.t1	15.0114	15.4275	24.8936	8.76185	9.21903	12.9971	F-box/LRR-repeat protein 5	CG2247	FBgn0030320	Fbxl5	Q8C2S5
aug3.g10974.t1	4.21167	1.96965	5.23227	9.43682	9.72787	7.59543	uncharacterized			Leng9	Q8BTN6
aug3.g11009.t1	8.11013	7.5805	13.6773	0.423874	2.09093	1.88701	protein Wnt-16-like	wnt4	FBgn0010453	Wnt16	Q9QYS1
aug3.g11015.t1	1.411	3.25543	2.66988	0	0	0		CG11594	FBgn0035484	Fggy	A2AJL3
aug3.g11056.t2	11.4122	18.2195	12.0818	0	0	0	um-activated chloride channel regulato	Clic	FBgn0030529	Clca4a	Q6Q473
aug3.g11094.t1	19.268	19.041	28.825	13.3479	14.803	14.9381	ative ATP-dependent RNA helicase P	bel	FBgn0263231	D1Pas1	P16381
aug3.g11101.t1	20.008	20.2426	29.3129	16.6699	16.5278	16.5049	methionine--tRNA ligase, mitochondria	MetRS-m	FBgn0027083	Mars2	Q499X9
aug3.g11104.t1	849.498	701.059	1173.54	522.632	525.059	529.025	piwi-like protein 1	piwi	FBgn0004872	Piwil1	Q9JMB7
aug3.g11113.t1	81.3458	69.9065	91.9957	35.081	38.6293	57.0218	ras-related protein Rap-2c	Rap2l	FBgn0283666	Rap2c	Q8BU31
aug3.g11149.t1	1.23349	0.90064	0.705184	3.21398	2.8771	2.57016	PR domain zinc finger protein 1	Blimp-1	FBgn0035625	Prdm1	Q60636
aug3.g1124.t1	3.69079	5.08497	7.35584	1.5717	0.878138	2.56918	transcription factor COE1	kn	FBgn0001319	Ebf1	Q07802
aug3.g1125.t1	121.166	101.268	142.79	84.0663	78.0172	59.6954	characterized/transcription factor COI	kn	FBgn0001319	Ebf1	Q07802
aug3.g11254.t1	6.67112	5.27179	5.33999	4.18161	3.50694	4.14193	ic vesicle membrane protein VAT-1 homolog			Vat1	Q62465
aug3.g11255.t1	15.2439	11.418	12.2282	7.23323	8.25604	8.08639	ondrial translation release factor in res	CG30100	FBgn0050100	Mtrfr	Q80VP5
aug3.g11311.t1	18.2256	16.7711	24.2762	7.81265	10.3657	10.8956	erferon-related developmental regulato	Ifrd1	FBgn0051694	Ifrd1	P19182
aug3.g11354.t2	2.54725	1.45396	1.6652	0.607511	0.438298	0.138806	-independent mannose-6-phosphate re	Lerp	FBgn0051072	Igf2r	Q07113
aug3.g11359.t1	44.4943	33.826	41.5324	22.1146	18.427	12.4698	omal RNA processing protein 1 homol	Nnp-1	FBgn0022069	Rrp1b	Q91YK2
aug3.g11359.t2	0	0	0	27.7234	35.8119	58.6069	omal RNA processing protein 1 homol	Nnp-1	FBgn0022069	Rrp1b	Q91YK2
aug3.g11359.t3	28.8847	20.2687	27.2644	11.9521	13.5597	3.24304	omal RNA processing protein 1 homol	Nnp-1	FBgn0022069	Rrp1b	Q91YK2
aug3.g11413.t1	2.02019	1.62932	4.54288	0.384748	0.560993	0.831632	photoreceptor-specific nuclear recepto	Hr51	FBgn0034012	Nr2e3	Q9QXZ7
aug3.g11457.t1	3.97087	5.09204	7.7767	1.39567	1.54163	2.51742	MFS-type transporter clz9			Slc18b1	Q8BTD6
aug3.g11494.t1	5.85623	5.68515	8.04903	1.39793	1.57742	3.88765	uncharacterized	CG32772	FBgn0052772	Prdm5	Q9CXE0
aug3.g11499.t1	3.30856	4.29797	3.84548	1.6061	1.89955	2.18309	Golgi integral membrane protein 4			Golim4	Q8BXA1
aug3.g11549.t3	4.58121	6.37906	4.45568	2.0505	2.15528	1.13282	ding motif, single-stranded-interacting	shep	FBgn0052423	Rbms2	Q8VC70
aug3.g11629.t1	4.50569	4.79066	6.39853	2.85492	2.11279	3.30712	uncharacterized	CG13775	FBgn0031874	Zbed6	D2EAC2
aug3.g11644.t1	4.51136	1.90136	4.07675	0.811152	0.71811	0.872543	ester hydrolase C11orf54 homolog	meep	FBgn0063667	4931406C07Rik	Q91V76
aug3.g11704.t1	5.81139	6.26426	7.64127	4.31757	3.69879	3.80838	heparan sulfate N-deacetylase/N-sulf	sfl	FBgn0020251	Ndst1	Q3UHN9
aug3.g11706.t1	26.4231	23.519	44.6094	77.2674	76.4096	66.934	ubiquitin-conjugating enzyme E2 L3	Ubc10	FBgn0026316	Ube2l3	P68037
aug3.g11743.t1	45.1389	39.4407	41.3539	35.0053	35.2119	35.9047	nucleotide-binding protein G(o) subu	Gαo	FBgn0001122	Gnao1	P18872
aug3.g11778.t1	3.17968	3.15363	3.09042	1.80582	1.78699	1.89815	onine-protein phosphatase 2B catalyti	Pp2B-14D	FBgn0011826	Ppp3ca	P63328
aug3.g11794.t1	11.3935	9.38681	13.5685	1.88191	2.37833	3.17048	kinesin heavy chain	Khc	FBgn0001308	Kif5b	Q61768
aug3.g11889.t1	134.008	121.851	136.97	90.3184	84.6058	84.8129	l import inner membrane translocase s	Tim13	FBgn0036204	Timm13	P62075
aug3.g1189.t2	6.04772	7.18749	5.19613	3.90269	4.0839	3.69592	ansporting ATPase subunit beta-1-inte	NKAIN	FBgn0085442	Nkain1	Q9D035
aug3.g11890.t1	0.810375	1.64543	1.01227	6.12341	7.3965	6.96478	craniofacial development protein 1-like	Yeti	FBgn0267398	Cfdp1	O88271
aug3.g11911.t1	70.1094	59.6606	56.3722	8.33449	14.1414	24.611	nositol-trisphosphate 3-kinase homolo	IP3K2	FBgn0283680	Itpka	Q8R071
aug3.g11934.t1	7.22541	7.55826	10.8886	4.38925	4.42834	5.47689	activin receptor type-2A	put	FBgn0003169	Acvr2a	P27038
aug3.g11937.t1	3.14602	4.6005	3.59054	0.103016	0.345685	0.584726		CaMKII	FBgn0264607	Camk2d	Q3V1X9
aug3.g11961.t1	32.1857	32.1781	59.132	21.7164	18.752	20.4488	nucleolar RNA-associated protein 25	CG3735	FBgn0034933	Utp25	Q8BTT6
aug3.g11961.t2	24.5626	20.8653	38.1513	12.1008	15.7871	12.267	nucleolar RNA-associated protein 25	CG3735	FBgn0034933	Utp25	Q8BTT6
aug3.g11986.t1	4.62698	4.38503	5.49286	2.23712	3.09157	2.33685	SH3 domain-binding protein 5-like	pcs	FBgn0033988	Sh3bp5l	Q99LH9
aug3.g11996.t1	34.9629	32.4485	41.1182	21.1045	26.5057	24.3579	ger protein 84-like/zinc finger protein 271-like				
aug3.g12014.t1	402.526	327.571	419.566	271.8	290.691	239.818	RNA-binding protein pno1	l(1)G0004	FBgn0027334	Pno1	Q9CPS7
aug3.g12018.t1	2.34062	2.51713	1.51553	3.87706	4.6999	3.77049	uncharacterized	Irp-1A	FBgn0024958	Irf5	Q3U169
aug3.g12077.t1	261.103	202.915	216.891	159.707	162.528	184.813	SUMO-conjugating enzyme UBC9-B	lwr	FBgn0010602	Ube2i	P63280
aug3.g12136.t2	57.4797	68.0039	113.564	22.4347	28.678	10.6259	A cytosine-C(5)-methyltransferase NS	Nsun2	FBgn0026079	Nsun2	Q1HFZ0
aug3.g12160.t1	5.45407	4.82255	5.08516	2.80742	3.0755	3.47534	protein germ cell-less	gcl	FBgn0005695	Gmcl1	Q920G9
aug3.g12194.t1	12.1719	14.1447	15.9038	7.91719	8.1019	9.3718	B/POZ domain-containing protein KCT	inc	FBgn0025394	Kctd5	Q8VC57
aug3.g12208.t1	32.2819	25.9992	31.603	20.6266	20.5641	22.2105	eptidyl-tRNA hydrolase 2, mitochondri	CG1307	FBgn0026566	Ptrh2	Q8R2Y8
aug3.g1222.t1	5.3477	7.77444	10.662	3.31637	2.71449	2.88956	glypican-5	dally	FBgn0263930	Gpc5	Q8CAL5
aug3.g12253.t1	4.12934	3.96246	5.37258	2.56486	2.31207	2.36509	reticulophagy regulator 3			Retreg3	Q9CQV4
aug3.g12291.t1	24.8228	19.9282	29.1226	12.3645	14.4954	17.0171	finger CCCH domain-containing protein 10			Zc3h10	Q8R205
aug3.g12310.t1	16.1893	15.2496	22.7647	11.2272	12.2119	9.7725	Golgi pH regulator	GPHR	FBgn0033995	Gpr89	Q8BS95
aug3.g12360.t1	8.4241	6.26325	6.80356	4.46829	5.09141	4.71284	uncharacterized			Msantd4	Q91YU3
aug3.g12413.t1	9.04401	11.1174	11.6167	5.37903	5.14678	5.29676	mic polyadenylation element-binding p	orb	FBgn0004882	Cpeb1	P70166
aug3.g12541.t1	1.43602	0.900155	2.98288	0.117755	0.133184	0.106032	cdc42 homolog	Cdc42	FBgn0010341	Cdc42	P60766
aug3.g12633.t1	13.4554	12.4634	30.3536	0.53889	0.549189	1.80718	uncharacterized	raw	FBgn0003209	Efcab9	Q9DAM2
aug3.g12640.t1	80.9573	150.429	167.286	48.7893	33.5622	27.7409	protein NYNRIN-like	CG42360	FBgn0259742	Nynrin	Q5DTZ0
aug3.g12715.t1	27.1237	21.8572	25.6222	13.2414	17.6209	16.7793	-tRNA-processing protein TSR2 homo	CG14543	FBgn0039404	Tsr2	Q8C8T8
aug3.g12755.t1	18.6577	18.3892	33.1966	14.2395	13.4968	14.994	-directed RNA polymerase III subunit	RpIII128	FBgn0004463	Polr3b	P59470
aug3.g1280.t1	353.607	320.955	354.139	270.504	275.037	254.156	ukaryotic translation initiation factor 1	eIF1	FBgn0035423	Eif1	P48024
aug3.g12805.t3	0.841963	0.972248	2.80453	0.000338	0	0	a membrane calcium-transporting ATPase 2			Atp2b2	Q9R0K7
aug3.g12862.t1	9.76668	7.23191	8.9539	5.5462	5.42822	4.48233	exocyst complex component 2	Sec5	FBgn0266670	Exoc2	Q9D4H1

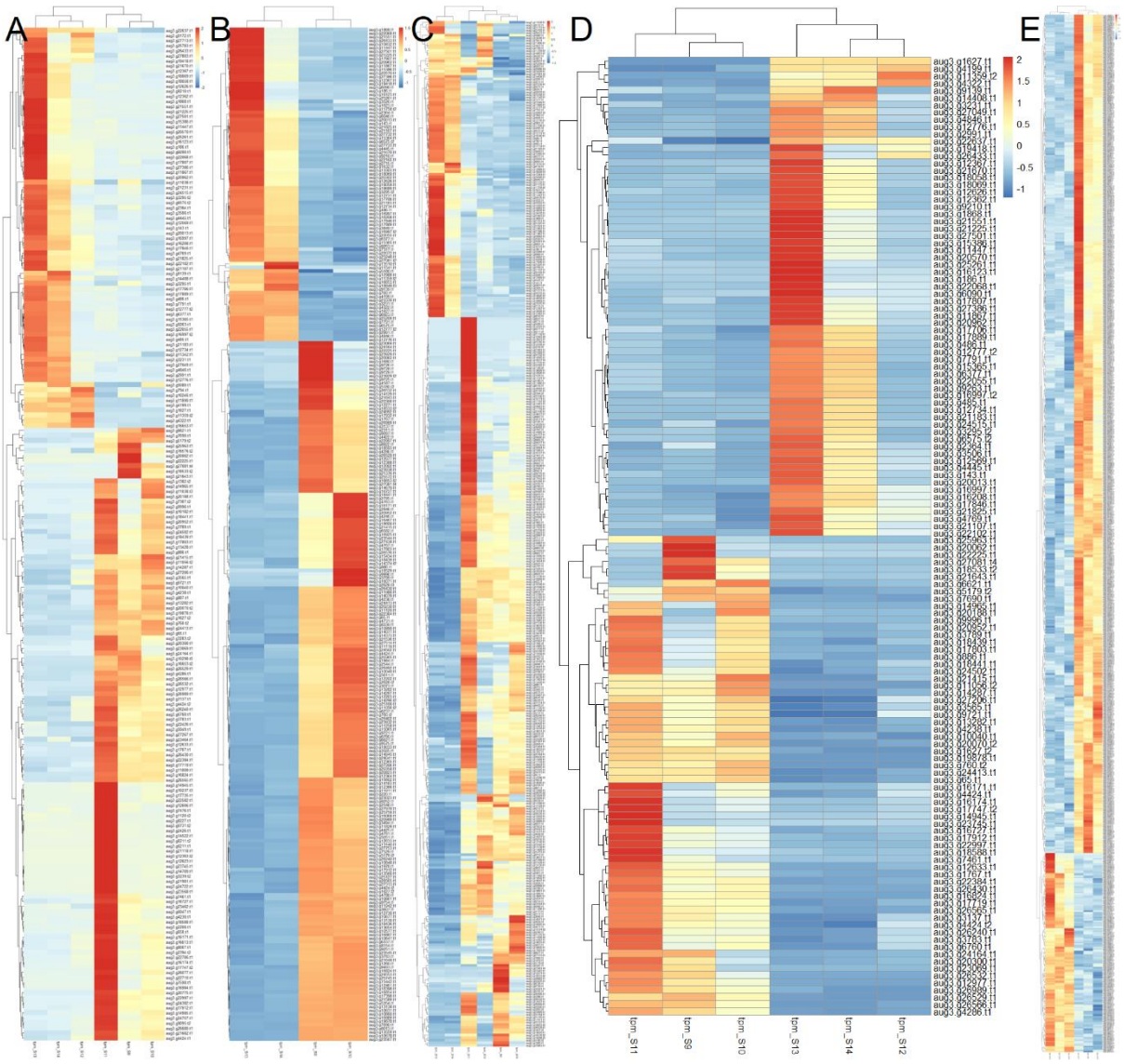

Figure S2-3. Heatmap images of selected gene lists b, c, d, e, and f. Gene expression is color-coded, with red indicating high expression and blue indicating low expression across dsRed and *Ets4* RNAi primary thickening samples. A. Heatmap representing the expression profiles of 200 genes from gene list b. B. Heatmap of 332 genes from gene list c. C. Heatmap of 400 genes from the combined gene list d. D. Heatmap of 132 genes from the combined gene list e. E. Heatmap of 828 genes from gene list f.

Table S2-2. Summary of GO BP terms (top 20 or 25) for selected gene lists B, C, D, E, and F with mouse orthologs.

list	b	c	d	e	f
gene count	200	332	400	133	828
term count	201	130	130	42	383
top 25_proliferation					cell phase transition, nuclear division
top 25_differentiation	cell fate commitment/specification	cell fate commitment/specification	cell fate commitment/specification	establishment of cell polarity	
	glial cell / striated muscle cell differentiation	axonogenesis	axonogenesis	columnar/cuboidal epithelial cell differentiation	axonogenesis
top 25_development	eye, sensory system development	eye, sensory systme, heart, gland, muscle development	eye, sensory system, heart, gland, muscle development	digestive tract, lung epithelium	neurogenesis
top 25_migration	cell-substrate adhesion, cell junction assembly	cell adhesion	cell adhesion		protein localization to extracellular region
top 25_metabolism	lipid localization, fatty acid transport, ether metabolism	amino acid metabolism, organic acid catabolic,	amino acid , organic acid, carboxylic acid	mainly metabolism related. Ether, lipid, fatty acid, etc.	metabolism, catabolism
top 25_other	RNA regulation	regionalization	regionalization	regulation of cold-induced thermogenesis	protein, RNA processing
	transport	intracellular transport	intracellular transport	intracellular transport	

Table S2-3. Summary of GO BP terms (top 20 or 25) for selected gene lists B, C, D, E, and F with fly orthologs.

list	b	c	d	e	f
gene count	200	332	400	132	828
term count	10	63	56	14	386
top 25_cell number			regulation of cell cycle		
top 25_cell differentiation		epithelial cell differentiation			cell fate commitment
top 25_development	hindgut, urogenital, renal system	eye, sensory system, visal system, epithelial cell, open tracheal system, respiratory system development	eye, sensory system, visual system, hidgut, open tracheal system, respiratory system.	hindgut, renal tubule, malpghian tubule, digestive tract, digestive system, urogenital system, renal system	wing disc / eye/ sensory system development,
		AP pattern specification	AP pattern, blastoderm segmentation		
top 25_cell movement		cell motility, actin, cell migration, epithelial cell migration. Cell projection	actin organization, cell motility, cell migration, cell projection		locomotion
top 25_metabolism	mitochondria			cellular lipid metabolism	biosynthetic process
morphogenesis	hindgut, digestive tract, malpighian tubule, renal tubule, embryonic hidgut	epithelial tube, eye, cell projection morphogenesis	eye, sensory organ, epithelial tube, eye-antennal disc, hidgut, malpighian tubule, renal tubule	hindgut, digestive tract, malpighian tubule, embryonic hindgut	epithelial tube/cell projection/ post-embryonic animal morphogenesis, metamorphosis
other	germ cell contraction	cell polarity	organelle assembly, cell polarity	germ cell contraction	mRNA, protein localization, cell communicaiton, signaling

Table S2-4. Summary of GO CC terms (top 20 or 25) for selected gene lists B, C, D, E, and F with mouse orthologs.

list	b	c	d	e	f
gene count	200	332	400	133	828
term count	12	2	2	3	39
top 12_cell junction	neuromuscular junction	neuromuscular junction	neuromuscular junction	neuromuscular junction	
				adherens junction	
top 12_cell movement	collagen containing extracellular matrix, cell-substrate junction				cell leading ege, apical part of cell
	microtubule, actomyosin, kinesin	kinesin	kinesin	microtubule	
top 12_other	uropod, preribosome				mitochondria matrix, Golgi subcompartment. organelle membrane, ribonucleoprotein granule, transferase complex, ubiquitin ligase complex, nuclear speck

Table S2-5. Summary of GO CC terms (top 20 or 25) for selected gene lists C, D, and F with fly orthologs.

list	c	d	f
gene count	332	400	828
term count	1	1	16
proliferation			cell division site, cleavage furrow
movement			cell junction
			cytoplasmic vesicle, Golgi, auto phagosome
other	supramolecular complex	supramolecular complex	supramolecular complex, ribonucleoprotein granule, Yb body, P granule, germ plasm
			phosphatidylinositol 3-kinase

Table S2-6. Summary of GO MF terms (top 20 or 25) for selected gene lists B, C, D, and F with mouse orthologs.

list	b	c	d	f
gene count	200	332	400	828
term count	6	2	2	41
top 10_cellular activity_RNA				transcription coregulator activity, RNA polymerase II-specific DNA-binding transcription factor binding, catalytic activity, acting on RNA, mRNA binding
top 10_cellular activity_protein	scavenger receptor activity			ubiquitin protein ligase binding, GTPase binding, small GTPase binding protein-macromolecule adaptor activity, molecular adaptor activity
top 10_general	oxidoreductase activity	oxidoreductase activity	oxidoreductase activity	
	hydrolase activity			

Table S2-7. Summary of GO MF terms (top 20 or 25) for selected gene lists f with fly orthologs.

list	F
gene count	828
term count	20
RNA metabolism	catalytic activity on RNA, nuclease, RNA processing, piRNA, tRNA
protein metabolism	enzyme, kinase, GTPase
	protein adaptor

Table S2-8. Biological terms for manually analyse GO BP result of List F

Level	Biological activities
A. Molecular level.	DNA replication. DNA damage and repair. Transposition. Chromatin modelling. Gene expression. Transcription. Post transcription regulation. RNA metabolism. Translation. Post translation regulation. Signalling pathway in general. Specific signalling. Pathway. Phosphorylation. Glycolysis. Oxidative phosphorylation. Lipid metabolism. Nuclear metabolism. Protein catalysis. Macromolecule synthesis. Metabolism. Anabolism. Catabolism.
B. Cellular level.	Nucleus. Nucleolus. Nuclear membrane. Nuclear membrane pore. Cell membrane. Golgi body. Centrioles. Endoplasmic reticulum. Mitochondria. Lysosomes.

	Ribosomes. Cytoskeleton. Cytoplasm. Component assembly. Vesicle transport. Intra cellular protein transport and localization. Cell polarity. Cell division. Mitosis. Meiosis. Direction and times of cell division. Change of cell shape. Cell migration. Cell growth. Change of cell size. Cell death. Apoptosis. Cell membrane or change of secretion. Cell-cell communication. Cell adhesion. Differentiation. Specify and commitment. External stimuli. Stress. Period.
C. Tissue level.	Epithelium (Single-layer squamous epithelium. Simple cuboidal epithelium. Simple columnar epithelium. Pseudostratified epithelium. Stratified squamous epithelium. Cylindrical epithelium. Transitional epithelium). Pancreas. Langhans islands. Exocrine glands. Sensory epithelium. Loose connective tissue. Dense connective tissue. Adipocytes. Reticular tissue. Cartilage. Bone. Blood. Skeletal muscle. Cardio muscle. Smooth muscle. Neurons. Synapse. Glial cells. Nerve fibres and Nerves. Oocyte. Sperm. Embryonic stem cell. Extraembryonic tissue. Adult stem cell.
D. Organ level (include organogenesis).	Nervous system. Brain (Cerebral cortex. Cerebellar cortex. Spinal cord. Blood-brain barrier. Ganglion. Sensory organ. Eye. Ear. Nose. Tongue. Tooth). Circulatory system (Heart. Blood vessel. Lymphatic system). Immune system (Immune Cells. Lymphoid tissue. Lymphoid organs. Thymus. Lymph nodes. Spleen. Tonsil). Digestive system (Alimentary canal. Mouth. Pharynx. Oesophagus. Stomach. Small intestine. Large intestine. Colon. Appendix. Gastrointestinal lymphoid tissue. Gastrointestinal endocrine cells. Digestive gland. Major salivary gland. Pancreas. Liver. Gallbladder). Respiratory system (Nasal cavity. Throat. Trachea and Bronchi. Lung. Gill). Excretory system (Kidney. Nephron. Collecting piping system. Juxtaglomerular complex. Renal interstitial. Kidney blood circulation. Urinary tract. Bladder). Integument (Integument, Keratinized and Stratified epidermis. Genuine Leather. subcutaneous tissue. Skin attachment. Hair. Sebaceous glands. Sweat glands. Nail). Endocrine System (Thyroid. Parathyroid gland. Adrenal gland. Pituitary. Pineal gland). Reproductive system (Testis. Reproductive tract. Accessory gland. Penis. Ovary. Oviduct. Uterus. Vaginal. Breast). Locomotion (Wing, Appendages). Imaginary disc. Larval.
E. Organism level.	Development. Fertilization. Embryonic development in general. Cleavage. Blastopore. Extraembryonic tissue. Axis formation. Gastrulation. Ectoderm. Mesoderm. Endoderm. Invagination. Involution. Ingression. Delamination. Epiboly. Organogenesis. Segmentation. Metamorphosis. Hormone regulation. Growth of appendages. Morphogenesis. Gametogenesis.

Table S2-9. Gene counts for biological activities from Table S2-7, based on Biological Process (BP) terms from List F, with annotations from mouse and fly orthology.

		molecular level		count	gene list
A					
	A1	DNA replication			
	A2	DNA damage and repair			
	A3	transposition		9	His1:CG33819/piwi/aub/AGO3/AGO2/mael/fs(1)Yb/Sov/Bov/b
	A4	chromatine modeling		60	ac/AGO2/AGO3/arm/aub/bel/Bin1/Bin3/bin/bru1/CG2091/CG3857/CG8777/cu
	A5	gene expression			
	A6	transcription	positive and negative	50	ac/BMD/Bin1/Blimp-1/bs/CG14655/CG1620/CG34205/CG43689/CG5245/Coop/Ctr8/
	A7	post transcription regulation		36	AGO2/AGO3/aub/CG16790/CG2091/CG9915/cuff/DCP1/Ec6/c5/enc/Gld2/Grip128/Hrt
	A8	RNA metabolism	positive and negative regulation	124	ac/AGO2/AGO3/arm/Asp35-m/aub/Bap170/beta4Het5/BMD/Bin-1/Bin1/bin3/Blimp
	A9	translation	(negative)	23	me318/bin3/Sra-1/orb/Rpb4/Gcn2/mEFTs/eIF4G1/eIF4EHP/eIF4E3/Hrb27C/larp/CG
	A10	post translation regulation		31	me318/bin3/Sra-1/orb/Rpb4/Gcn2/mEFTs/msf1/eIF4G1/eIF4EHP/eIF4E3/Hrb27C/la
	A11	signaling pathway in general	positive and negative	116	Alg5/alphaSnap/amx/Arf51F/Arf79F/arm/Atg4/BMD/Bi-1/bti/Cadps/Cdc42/CG144(
	A12	specific signaling pathway	regulation of phosphatidylinosit	3	Atg4/PI3K21B/p53
			Wnt signaling pathway	18	arr/Coop/Ctr8P/daly/dlp/Galphao/PT43/Rmo/opm/Oseg1/otk/otk2/pan/Pp1-87B/r
			semaphorin-plexin signaling pat	4	daly/Plex8/Sema2a/Sema5c
			small GTPase mediated signal tr	18	Hmgcr/Arf79F/cyst/Cdc42/aru/Gdi/rasko/Rac1/Rab10/Rab11/Rabx5/Rab32/Rap2l/E
			enzyme-linked receptor protein	26	put/sfl/cv-2/Cdc42/dlg1/CG32335/bnl/btl/BMD/foxo/Crk/daly/dlp/HDAC4/PI3K21B/
			smoothened signaling pathway	16	rdx/Gprk1/daly/dlp/Gbeta13F/sqh/ptc/Sac1.3kh/Pp1-13C/smo/hh/lwr/Tnpo/Ufd1-l
			fibroblast growth factor recepto	8	sfl/bnl/btl/daly/dlp/Shc/htl/Ptp10D
			transmembrane, cell communic	36	sfl/Cdc42/dlg1/CG32335/bnl/btl/foxo/Crk/daly/dlp/HDAC4/PI3K21B/PI3K92E/vn/gc
	A13	phosphorylation		22	SN14gamma/Atg1.4/Cdc42/Classpin/dap/bnl/btl/Cyct/Cyct3/Mob3/PI3K21B/PI3K92
	A14	glycolysis			
	A15	oxidative phosphorylation			
	A16	lipid metabolism		10	Arf79F/betaCOP/deltaCOP/foxo/PI3K21B/PI3K92E/Atf3/Rab32/Atg14/p53
	A17	nuclear metabolism	cellular nitrogen compound met	87	ac/AGO2/Aps/arm/aub/bHD/Bi-1/Bin1/bin3/Blimp-1/bru1/CG11440/CG14655/CG1
	A18	protein catalysis		32	SN14gamma/vimar/Bi-1/Atg14/Cdc42/Classpin/dap/CG17019/btl/BMD/Cyct/Cyc83/
	A19	macromolecule synthesis	positive and negative regulation	75	ac/AGO3/aub/Bap170/BMD/Bin1/bin3/Blimp-1/bru1/bs/CG14655/CG1620/CG2091/I
	A20	metabolism			
	A21	catabolism	positive regulation	64	AGO3/Aps/arm//Atg14/Atg8a/aub/Bi-1/CG11275/CG17019/CG18467/CG2091/CG22(
B		cellular level			
	B1	nucleus	nuclear migration and protein lc	24	Khc/msn/sqh/wisp/faf/AGO2/mael/kol/hth/rdx/Rpb4/Pen/Kap-alpha1/LTV1/Nup15
	B2	nucleolus			
	B3	nuclear membrane			
	B4	nuclear membrane pore			
	B5	cell membrane		37	alphaSnap/Arf79F/Cdc42/CG10959/CG3514/CG4483/CG5196/CG7659/cin/Crk/daly
	B6	Golgi body	Golgi vesicle transport	16	Arf79F/alphaSnap/Lerp/betaCOP/deltaCOP/Fdl:gIdine/Sec5/sau/GM130/Sec16/Rab1
	B7	centrioles			
	B8	endoplasmic reticulum			
	B9	mitochondria	mitophagy	7	Atg8a/Atg14/Ks1/ref(2)P/Sesn/Pink1/Vps13D
	B10	lysosomes			
	B11	ribosomes			
	B12	cytoskeleton	actin cytoskeleton	29	Arf51F/Det/yrt/Cdc42/CG32066/Sra-1/DAAM/Frl/Crk/pigs/sau/Galphao/Gbeta13F/U
	B13	cytoplasm			
	B14	component assembly	cellular component assembly an	95	AGO2/alphaSnap/Arf79F/arm//Arpc1D/Atg14/Atg8a/aub/bnl/bru1/btl/btv/cdc14/Cdc
	B15	vesicle transport	encapsulation, vesicle fusion	24	alphaSnap/Sec5/sau/Sec16/Rab11/Rab32/ref(2)P/Syt4/Syx7/TSG101/Vps28/Vps8/Sy
	B16	intra cellular protein transport	and localization	93	alphaSnap/Arf51F/Arf79F/Atf3/aub/betaCOP/btv/Cadps/Cdc42/CG10939/CG11110/I
	B17	cell polarity		20	Anx89/cyt2/Cdc42/orb/dlg1/Frl/Gbeta13F/Khc/PI3K59F/mael/pk/Cadn/Rac1/Rab11/l
	B18	cell division	division, phase of cycle, asymme	95	ac/alphaSnap/Arf51F/Arf79F/arm/aub/bel/Bgb/BMD/bnl/Bov9b/bru1/btl/cdc14/Cdc
	B19	mitosis		30	Arf79F/alpha9cap/Det/Clasp/n/net/dap/dlg1/DNApol-epsilon58/cdc14/Pancd2/Cyct
	B20	meiosis		33	Arf51F/Arf79F/Det/yet/dap/cuff/Msh6/elg/eIF4G2/Pancd2/Grip128/mio/sau/aggf
	B21	cell projection	regulation of cell projection org	48	put/me318/Cdc42/for/kis/Sra-1/DAAM/CG42797/Ef(Pc)bnl/btl/foxo/Frl/daily/dlp/G
	B22	change of cell shape	cell morphogenesis involved in c	55	bnl/btl/Cadn/Cdc42/CG42797/DAAM/daily/dlp/Ef(Pc)/for/foxo/Frl/Galphaq/GM130/
	B23	cell migration	taxis, chemotaxis, cell motility, c	66	bnl/btl/Cadn/Cdc42/CG3857/Ctl-c/Cen/Crk/DAAM/daily/dla/dlg1/dlp/Ef(Pc)/faf/for/
	B24	cell growth, change of cell size		56	alphaSnap/arr/bru1/btl/Cadn/Cdc42/CG32066/con/cu/Cul5/DAAM/daily/deltaCOP/dl
	B25	cell death, apoptosis		34	DNaseII/Galphaq/PI3K2/rst/out/Nup154/Tre1/bel/fkh/SNF4Agamma/Atg8a/Bi-1/Atg
选择性分	B26	cell membrane or change of secretion		27	CG31475/Arf51F/Arf79F/alphaSnap/Amph/Cdc42/deltaCOP/Sec5/Glut1/GPHR/Tang
	B27	cell-cell communication	positive and negative regulation	78	Alg5/amx/arm/BMD/Bi-1/Cdc42/CG17019/CG31139/CG32335/Coop/Cr-K/Ctr8P/Cul5/
	B28	cell adhesion			
细胞停止	B29	differentiation, specify and commitment		79	ac/amx/Arf79F/arm//aub/Bimp-1/bnl/bru1/btl/Cadn/Cdc42/CG9849/Ctr8P/cuff/Cul5
	B30	external stimuli		92	ac/AGO2/Alg5/Ance/Aps/Arf79F/arm/Atg14/Atg8a/aub/betaCOP/Bi-1/bnl/btl/Cdc4
	B31	stress	response to stress, starvation	48	ac/Aps/Arf79F/arm/Atg14/Atg8a/aub/betaCOP/Bi-1/bnl/btl/Cdc42/CG9674/Crk/ctr
	B32	period	periodic partitioning	11	sfl/rdx/daily/dlp/arr/AGO2/pan/smo/hh/kn/ftz
			maintenance of location		SN14gamma/Arf79F/Cdc42/betaCOP/deltaCOP/foxo/daily/PI3K21B/PI3K92E/aub/A
			regulation of congenable organization		vimar/Cdc42/CG32066/Sra-1/DAAM/Ets97D/Sec5/Crk/pigs/mio/Mics1/Gbeta13F/eg
C		tissue			
	C1	epithelium	epithelial differentiation, tube m	75	ac/alphaSnap/arm//arr/aub/Bap170/bnl/bs/btl/Cdc42/Crk/cv-2/Cyct/da/daily/dap/l
			epithelium migration	23	bnl/btl/Crk/daily/dlp/hh/Hrb27C/jng/kis/Mhc/msn/PI3K92E/ptc/Rab11/Rac1/Sec5/
	C2	single-layer squamous epithelium			
	C3	simple cuboidal epithelium			
	C4	simple columnar epithelium			
	C5	pseudostratified epithelium			
	C6	stratified squamous epithelium			
	C7	cylindrical epithelium			
	C8	transitional epithelium			
	C9	pancreas, Langhans islands	gland development	25	put/Bi-1/deltaCOP/foxo/exd/Scr/hth/IP3K2/tl/PI3K92E/neur/pan/Wnt4/bel/Rac1/S
	C10	exocrine glands	exocrine system development	16	put/Bi-1/deltaCOP/exd/Scr/hth/IP3K2/pan/Wnt4/bel/Rac1/fkh/sli/htl/sigmar/twi
	C11	sensory epithelium			
	C12	loose connective tissue			
	C13	dense connective tissue			
	C14	adipocytes			
	C15	Reticular tissue			
	C16	cartilage			
	C17	bone			
	C18	blood	hemocyte differentiation	9	bnl/btl/PI3K92E/neur/Rac1/Su(H)/lwr/htt/kn
	C19	skeletal muscle	muscle cell differentiation	24	Arf51F/DAAM/Elo8/Crk/Unc-89/exd/hth/rst/Khc/lid/mas/Mhc/CG9849/CG5800/bru
	C20	heart muscle			
	C21	smooth muscle			
	C22	Neurons	neuron maturation	10	Arf79F/kis/PI3K59F/PI3K92E/Hr51/Klm/shep/Sox14/TSG101/Vps28
	C23	synapse	regulation of neurotransmitter l	13	Ace/Arf51F/Arf79F/alpha9cap/Cdc42/Sec5/Letm1/Gdi/Rim/Syt4/Cadps/Syb/nSyb
	C24	Glial cells	glial cell migration	7	bnl/btl/Rac1/sli/hh/htl/jng
	C25	nerve fibers and nerves	axon development, neuron proj	46	btl/Cadn/Cdc42/CG42797/Con/DAAM/daily/dlp/Ef(Pc)/for/foxo/Frl/Galphaq/GM130
	C26	nerve endings			
	C27	oogenesis	ovarian follicle cell development	47	armi/aub/btl/Cdc42/Crk/cuff/Cyct/da/dap/DCP1/dlg1/enc/fng/fs(2)ltoP43/Grip128
	C28	sperm			
	C29	embryonic stem cell	stem cell differentiation, popula	30	bel/BMD/Bov9b/bru1/Cyct/da/daily/egg/enok/fng/foxo/fs(1)Yb/htt/inx2/lid/lwr/mae
	C30	extraembryonic tissue	germarium-derived egg chambe	14	Cul5/dap/cuff/fng/mio/inx2/piwi/ph-p/htt/enc/Rab11/armi/pci/Stat92E
	C31	adult stem cell	germ-line stem cell population r	19	put/BMD/foxo/fng/daily/enok/inx2/lid/P3K92E/piwi/Bru1/mael/neur/peo/bel/fs(1
D		organ			
	D1	nervous system	central nervous system develop	28	ac/dap/DAAM/mbf1/Frl/Cyct/Galphao/enok/exd/hth/ma/ttl/Hr51/ph-p/vn/neur/s
		brain			
		cerebral cortex	memory, learning, cognition	21	me318/for/kis/aru/Fabp/HDAC4/arr/Rhm/Gld2/vn/neur/Rac1/Su(H)/Nsun2/armi/Pp
		cerebellar cortex			
		spinal cord			
		meninges and blood-brain barrier			
		Ganglion			
		sensory organ	sensory organ development	49	put/Arf51F/Arf79F/alphaSnap/Amph/vimar/yrt/rdx/holn1/Cdc42/Sra-1/bnl/btl/foxo
		Eye	compound eye morphogenesis,	47	put/Arf51F/Arf79F/alphaSnap/Amph/vimar/yrt/rdx/holn1/Cdc42/Sra-1/bnl/btl/foxo
		Ear			
		nose			
		tongue			
		tooth			
	D2	circulatory system	hematopoietic or lymphoid orgi	13	Cdc42/foxo/PI3K92E/neur/Rac1/Su(H)/Stat92E/sn/lwr/htt/kn/pn/Tnpo
		heart			
		Blood vessel			
		lymphatic system			
	D3	immune system	melanization defense response	9	Cdc42/bnl/btl/Spn27A/Rac1/RhoGEF3/RhoBTB/Shc/lwr
		immune system	immune system development, r	43	ac/Arf79F/Cdc42/betaCOP/dlg1/OstDelta/dgrn/Sec5/bnl/btl/foxo/Galphaq/Dsp1/ms
		Immune Cells	regulation of immune response	44	Coq2/ac/Arf79F/ance/me318/Cdc42/betaCOP/dlg1/dgrn/Sec5/CG2247/bnl/btl/foxo
			viral process	8	Vps2/betaCOP/Elo8/sau/AGO2/Rab10/Rab11/TSG101
		lymphoid tissue			
		lymphoid organs, thymus			
		lymph nodes			
		spleen			
		tonsil			
	D4	digestive system			
		alimentary canal			
		mouth			
		pharynx			
		esophagus			
		Stomach			
		small intestine			
		the large intestine			
		colon			
		appendix			
		Gastrointestinal lymphoid tissue, gastrointestinal endocrine cells			
		digestive gland, major salivary	salivary gland development	16	put/Bi-1/deltaCOP/exd/Scr/hth/IP3K2/pan/Wnt4/bel/Rac1/fkh/sli/htl/sigmar/twi
		pancreas			
		liver			
		gallbladder			
	D5	respiratory system	respiratory system developmen	32	wat/put/sfl/Cdc42/deltaCOP/DAAM/wus/mbf1/Sec5/bnl/btl/daily/dlp/Lac/sqh/Vhc
		nasal cavity			
		throat			
		trachea and bronchi	open tracheal system developm	32	wat/put/sfl/Cdc42/deltaCOP/DAAM/wus/mbf1/Sec5/bnl/btl/daily/dlp/Lac/sqh/Vhc
		lung			
		gill			
	D6	excretory system			
		kidney			
		nephron			
		Collecting piping system			
		Juxtaglomer complex			
		Renal interstitium			
		kidney blood circulation			
		urinary tract			
		bladder			
	D7	integument			
		integument			
		Keratinized and stratified epiderm is			
		Genuine Leather			
		subcutaneous tissue			
		Skin attachment: hair			
		sebaceous glands			
		sweat glands			
		nail			
	D8	Endocrine System			
		thyroid			
		parathyroid gland			
		adrenal gland			
		pituitary			
		pineal gland			
	D9	reproductive system	regulation of reproductive proci	20	kis/dap/elg/mio/Hrb27C/Khc/msn/twe/stg/sqh/Nup154/pch2/PI3K59F/PI3K92E/au
			germ-line stem cell division	9	put/daily/egg/piwi/peo/fs(1)Yb/Sov/Bov/b/Rab11
			formation of primary germ layer	7	sfl/pan/Fkh/sli/htl/amx/twi
		testis			
		reproductive tract			
		Accessory gland			
		penis			
		ovary			
		oviduct			
		Uterus			
		vaginal			
		breast			
	D10	locomotion	locomotion, regulation of locom	51	Hmgcr/put/Cdc42/for/Clc/kis/con/Sra-1/DAAM/dlg1/Ef(Pc)bnl/daily/dlp/Galphaq/
	D11	wing	wing disc development, imagina	60	Anx89/dx/put/alphaSnap/Bap170/sfl/cv-2/holn1/Cdc42/kis/Ctr8P/dap/elg/Elo8/nm
	D12	appendages	imaginal disc-derived appendag	37	put/alphaSnap/Bap170/sfl/cv-2/Cdc42/kis/elg/Elo8/fng/daily/dlp/Galphao/hth/arr/
	D13				
	D14	larval	larval development	61	alphaSnap/arr/Atg8a/Bap170/bel/Bi-1/bs/Cdc42/CG5800/Ch12/Crk/cv-2/daily/dap/c
E		organism			
F		species			
		development	regulation of multicellular organ	79	ac/alphaSnap/Arf79F/armi/arr/aub/bnl/bru1/btl/Cadn/Cdc42/cuff/Cul5/DAAM/dall
a		fertilization			
		embryonic development in ge	embryonic development, morpl	56	ac/AGO2/amx/armi/arr/aub/Cdc42/cuff/daily/DCP1/dgrn/dlg1/dlp/enc/fkh/frc/Gbet
b		cleavage			
	b1	blastopore			
	b2	extraembryonic tissue			抑黄体生成激分裂
	b3	axis formation	anterior/posterior pattern speci	25	orb/cuff/dlg1/fng/Grip128/daily/Hrb27C/Scr/khc/MED31/DCP1/sqh/tll/ptc/aub/ph-
			dorsal/ventral pattern formatio	18	Anx89/put/orb/cuff/nmd/fng/daily/dlp/Khc/Spn27A/faf/mael/spz/enc/Su(H)/nmo/t
c		gastrulation		12	sfl/Gbeta13F/stg/sqh/Prosalpha6/pan/wntD/fkh/sli/htt/amx/twi
福豆素响	c1	ectoderm, mesoderm, endoderm			
	c2	invagination			
	c3	involution			
向内经个	c4	ingression			
因为分裂	c5	delamination			
	c6	epiboly			
d		organogenesis	organ formation, anatomical str	36	Arf79F/kis/orb/cuff/dlg1/Grip128/Hrb27C/Khc/DCP1/PI3K59F/PI3K92E/Hr51/aub/wi
e		segmentation	segment specification	33	sfl/rdx/kis/orb/cuff/dlg1/fng/Grip128/daily/dlp/Hrb27C/Dsp1/hth/Khc/arr/MED31/t
f		metamorphosis	metamorphosis	54	put/alphaSnap/Ance/Bap170/Atg8a/Bi-1/sfl/cv-2/Cdc42/kis/dap/dlg1/elg/Elo8/fng/
	f1	hormone regulation			
	f2	post-embryonic animal morph	post-embryonic appendage mo	51	put/alphaSnap/Bap170/Atg8a/Bi-1/sfl/cv-2/Cdc42/kis/deltaCOP/dap/dlg1/elg/Elo8/
g		morphogenesis	regulation of anatomical structu	25	me318/Cdc42/Sra-1/DAAM/CG42797/btl/Frl/GM130/Gbeta13F/Fis1/msn/Hr51/Plek
h		gametogenesis			
	h1	meiosis			

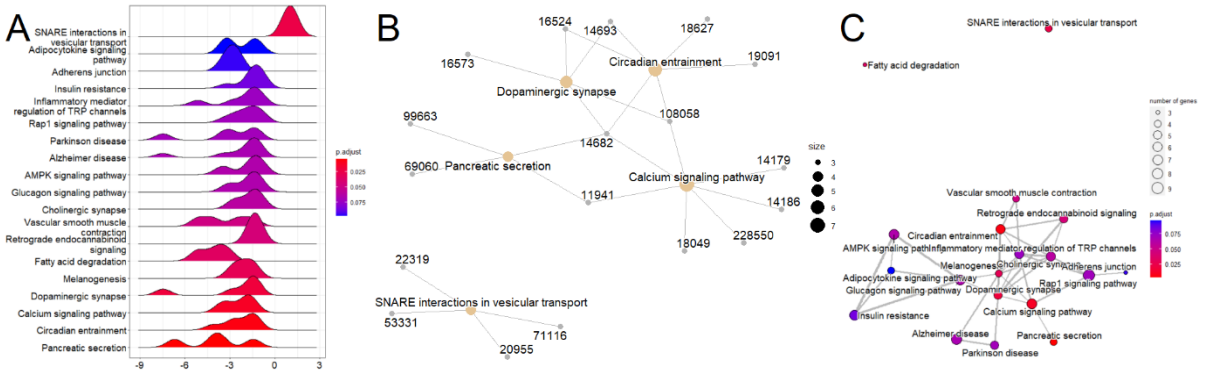

Figure S2-4. Pathway analysis of the selected gene List F with mouse orthologs, with a significance threshold of p=0.1. Analysis and images were generated using R. A. Ridgeplot image showing the distribution of pathway enrichment across different categories. B. Cnetplot image illustrating the network of gene interactions and their associations with various biological pathways. C. Emapplot image presenting a visual representation of the enriched pathways, highlighting the connections and relationships among the biological processes.

Table S2-10. Manual pathway analysis

		Mm							Dm							
	Pathway	gene counts	upstream gene	key gene	complete path	downstream gene/path	other	conclusion	gene counts	upstream	key gene	complete path	downstream	other	conclusion	Mm vs Dm
1	Notch pathway	4	1	yes	close to	not sure	various directions	side related	4	1 or 3	1 of two	half	MAPK, Ras and other	various directions	side related	same
2	Hh pathway	6	4	yes	middle 1/3 loss	yes, at least partially	source or target not known	related	4	3	yes	middle lost	proliferation, pattern, etc	various direction, source/target	related	different, dpp
3	Wnt pathway	12	3	yes	3x 1/2	cell cycle, cytoskeleton	not sure which path, or direction	related	13	6	yes	max half, 3 paths	cycle,adhesion, skeleton,	not sure about directions	related	3 genes different
4	PI3K-AKT pathway	13	5	1 of 2	close to	metabolism, cycle, protein	unidirection, downregulated	related								no Dm path
5	mTOR pathway	7	2, wnt pathway	no, one next to	no	protein		not close related	8	3	1 factor of 1 complex	fragments	lipid, MT, autophagy	various direction	side related	same path, Dm 1 more
6	TGF-beta pathway	3	3	upstream	no	no	RAS, MAPK in the middle	source of signal?	4	2	yes, ligand and receptor	no	differentiation, cycle	directional? Source of signal?	not sure if related	2 more genes in Dm
7	Ras pathway	11 or 12	2	no	no, but PI3K	motility, cytoskeleton	MAPK, RAP1, actin, T cell, etc.	side related								no Dm path
8	FOXO pathway	10	1	yes	midle-late	cycle, metabolism	AMPK, PI3K, MAPK, a lot.	related, not main path	8	0	yes	middle-late part	cycle, metabolism	various directions	related, not main	similar, Mm more genes
9	HIF-1 pathway	8	2	no	no	VEGF, metabolism		not close related								no Dm path
10	MAPK pathway	8	2	no	no	proliferation, Wnt	phosphatidylinositol, TNF, p53, ras	side related	8	3	no	middle lost	cell shape, pattern	polarity. Various direction	side related	different in pathway
11	HIPPO pathway	8	3, BMP, wnt, E-cad	no	no	proliferation, apoptosis	E-cad not sure	side related	7	1, actin	no	a small part	proliferation, apoptosis	no cad. most downregulated	side related	different in pathway
12	Ubiquitin mediated protease	8	E2, some type E3 related. Small percentage. Not sure about specificity.				molecular-cellular level. Downregulated	side related	7	E2, some type E3 related. Small percentage. Not sure about specificity. molecular-cellular level.				Various directions	side related	similar
13	AMPK pathway	7	no	yes	no, many parts	metabolism, autophagy	not the same in direction	side related								no Dm path
14	VEGF pathway	4	no	no	only middle	migration, metabolism	downregulated	side related								no Dm path
15	ERBB pathway	8	2	ligand not receptor	No. Part of PI3K, STAT	various	various directions	not close related								no Dm path
16	Insulin pathway	8	no	more likely no	PI3K	metabolism, other	various directions	side related								no Dm path
17	stem cell pluripotency	8	4	no	middle lost	differentiation, epigenetics	2 types of cells. Wnt, Jak-stat, PI3K, TGF-beta.	not related, principle might similar								no Dm path
18	Apoptosis	4	1, NGF-PI3K	0 or 1	no, far from that	apoptosis	NF-KB, PI3K-AKT, MAPK	not related	1	no	1	no	apoptosis	upregulated	not related	different in pathway
19	Actin cytoskeleton	12	2	yes	yes	adhesion, actin structure	downregulated	related								no Dm path
20	Adherens junction	7	2	yes, Cad. not sure	more than half	tight junction, growth, diffferentiation	connection strong and weak. Vary in directions	cad yes, yes. If not side-related.								no Dm path
21	cell cycle	8	no	part	part of the middle-late part	proliferation, G1, S, G2, M	development related. Various directions.	ORC not sure. Side related								no Dm path
22	cGMP-PKG pathway	8	1, but as effect	1 or the 2	close to	muscle	unidirection, up regulation for sm	related, not sure if main								no Dm path
23	Glycolysis-Glucogenesis	3	very small ratio. Not sure function, not sure if unidirection				metabolism	side related or not.	3	very small ratio. Not sure function, not sure if unidirection				metabolism	side related or not.	same
24	RAP1 pathway	10	5, with cad	no	no middle part	adhesion, migration, etc.	downregulated. 1 unique maybe.	side related								no Dm path
25	Fatty acid degradation	6	many reversible process. Not sure about directions				metabolism	side related	5	many reversible process. Not sure about directions				metabolism	side related	similar, 1 gene less
26	Inositol phosphate metabolism	9	Unfamiliar pathway. Reversible processes. 2 parts looks like cluster. Not sure about direction.				other metabolism	side related or related but not main	7	Unfamiliar pathway. Reversible processes and cyclic(?). Not sure about direction (glycolysis reduced?).				other metabolism	side related or related but not main	same
27	mRNA surveillance	8	RNA processing. All downregulated. Not knowing on general level or with specificity.				Molecular-cellular level.	side related	8	RNA processing. most downregulated. Not knowing on general level or with specificity. Transport				Molecular-cellular level	side related	same
28	SNARE interaction or vesicle transport	5	4 gene upregulated, 1 downregulated, pathway auto analysis show upregulated. Not sure if it means upregulated vesicle transport?				Molecule-cellular level	side related	5	4 gene upregulated, 1 downregulated, pathway auto analysis show upregulated. Not sure if it means upregulated vesicle transport?				Molecule-cellular level	side related	same
29	Oxidative phosphorylation	2 or 4	very small ratio. In complex I and V.				downregulated	side or not related	3 or 5	very small ratio.				various directions	side or not related	1 more gene in Dm
30	Glucagon pathway	9	1. Not sure if Pt have Glucagon	no (PKA?)	most of one path.	metabolism	unidirection, downregulated.	related or side related								no Dm path
31	Axon guidance	14	8	not known	yes. Wnt, hh, actin cytoskeleton	axon growth, repulsion, retraction	No axon. Vary in directions.Source or target.	related. May be actin part only.								no Dm path
32	Chemokine pathway	9	no	not known	No. Part of PI3K, STAT, actin	growth, differnetiation, migration	FGF paper. most downregulated. One up.	side-related								no Dm path
33	Endocytosis	16	complex and of different types. More related to late endosome, lysosome, ligase, inositol, Golgi, etc. Not sure about direction.				Molecule-cell level. Part of migration?	related. Not sure if main.	17	complex and of different types. More related to late endosome, lysosome, ligase, inositol, Golgi, etc. Molecule-cell level. Not sure about direction.				Part of migration?	related. Not sure if main.	1 more gene in Dm
34	Focal adhesion	10	2	not sure	PI3K yes. Other no.	motility, proliferation, survival	actin, wnt, PI3K, MAPK, cycle. Vary in direction.	side related								no Dm path
35	gap junction	5	2 to 3	1 maybe	no	channel, hemichannel	Vary in direction. many processes	side related. cell level?								no Dm path
36	TCA cycle	1	small ratio, not very relevant.				metabolism	not related	2	small ratio, not very relevant.				metabolism. Various direction	not or side related	Dm 1 more gene
37	tight junction	10	2	1 maybe	half at most. path in cell permeability	cell polarity, differentiation, migration	various directions. Actin. No receptors	side related								no Dm path
38	Ribosome	4	very small ratio, not very relevant.				various direction	not related	4	very small ratio, not very relevant.				various direction	not related	same
39	RNA degradation	5	small ratio, not very relevant. Not sure if directional. Molecular-cell level				various direction	side related	6	related to decapping. Small ratio related to other process. mRNA. Molecular-cellular level. Eukaryotic.				not known about direction	related or side related.	1 more gene in Dm
40	RNA polymerase	3	small ratio, 1/4 at most. could be directional. Molecular-cell level				Eukaryotic not other species	side related	3	small ratio, 1/4 at most. could be directional. Molecular-cell level				Eukaryotic not other species	side related	same
41	DNA replication	4	small ratio. Two conserved genes. Molecular-cellular level.				Eukaryotic. Vary in directions	side related	5	small ratio. Two conserved genes. Molecular-cellular level.				Eukaryotic. Vary in directions	side related	1 more gene in Dm
42	Spliceosome	10	Complex pathway. large ratio in U1, small ratio in many other parts. Molecular-cellular level				Various directions	related, not sure if main	9	Complex pathway. Large ratio in U1 and U2. small ratio in others. Molecule-cell level.				Various directions	related, not sure if main	3 genes different
43	Protein export	1	very small ratio, not very relevant.				downregulated	not related	1	very small ratio, not very relevant.				downregulated	not related	same
44	Lysosome	8	with one key gene. In total small ratio. Molecular-Cellular level. Might related to differentiation change?				various direction	related or side related	6	1 key gene. In total of small ratio. Molecular-cellular level. Not sure about specificity.				all downregulated	related or side related	2 genes more in Mm
45	Peroxisome	4	small ratio. Some genes related to metabolism. ACSL?				various direction	not related	4	small ratio. Some genes related to metabolism. ACSL.				various direction	not related	same
46	Ferroptosis	2	no	no?	2 separate positions	sort of ROS?	downregulated	not related								no Dm path
47	Necroptosis	4	no	no or 1	stat, CAMK II	mitochonde transmemb potential	downregulated, upregulated shedding	side related, why shedding?								no Dm path
48	Apelin pathway	6	1	no	max half. PI3K, AMPK	metabolism, autophage	downregulated. not sure if has Apelin.	side related								no Dm path
49	Osteoclast differentiation	4	no	no	no. Fragments.	proliferation. Specific diff	All 4 genes look familiar.	not or side related								no Dm path
50	Tolllike receptor pathway	3	no	no	no	inflammation, cytokine	2 of the 3 look familiar	not or side related	2 (3 IMD)	2	1	no	defense, wound		not or side related	diffferent pathway
51	Nod-like receptor pathway	1	very small ratio, not very relevant.				inflammation, cytokine. Downregulated.	not related								no Dm path
52	Rig-I-like receptor pathway	1	very small ratio, not very relevant.				inflammation, cytokine. Downregulated.	not related								no Dm path
53	JAK-STAT pathway	5	1	1 of 2	max half	apoptosis, cell cycle	various direction . PI3K, MAPK	side related								no Dm path
54	synaptic vesicle cycle	2	small ratio. Key position. Other related pathway(SNARE) related.				direction? Neuron process	side related								no Dm path
55	prolactin pathway	4	no	no	no, part PI3K and stat	mammary epithelial cells	various direction	not related								no Dm path
56	Endocrine and other factor regulated calcium reabsorption	2	max 1	max 1	no	blood calcium homeostatis	tight junction. Various direction	not or side related								no Dm path
57	pancreatic secretion	6	complex pathway. Very specific process in differentated cells. 2 genes familiar 4 not.				not known direction	not or side related								no Dm path
58	nucleocytoplasmic transport	10	importin related, other parts in small ratio related.various directions. Molecule-cell level.				mRNA surveilance	related	9	importin related, other parts in small ratio related.various directions. Molecule-cell level.				mRNA surveilance	related	Mm 1 more gene
59	ATP dependent chromatin remodeling	6	small ratio. ACTB might be important. Molecule-cell level. Not sure if directional in diffferentiation.				downregulated	side related	6	small ratio related, max 1/2 (PBAF). Molecule-cell level. Not known general epigeneitc situation in different types of cells. Not sure if all				downregulated	related or side related	same
60	polycomb repressive complex	5	small ratio. Molecular-cellular level. Not sure about directional change in diffferentiation.				various direction	side related	5	very small ratio. Max 1/4. not sure about biological function in general and meaning for changes. Molecular-cell level				various directions?	side related	similar, 2 genes different
61	protein processing in ER	4	small ratio. Molecular-cellular process. Not sure about direction				various direction	not or side related	4	small ratio. Molecular-cellular process. Not sure about direction				protein process, apoptosis	not or side related	same
62	dorso-ventral axis formation								3	all in oocyte, promote mRNA gurken, which is signal for dosal follical cells. 3/3. non of the rest				downregulated	related but incomplete	no Mm path
63	Motor protein	9	dynein upregulated. Microtubuln, kinesin downregulated. Actin and myosin both.				various direction	related, not sure if main	8	kinesin, microtubule, myosin, actin, dynein related.				not sure about directions	related, not sure if main	similar, 5 genes diff
64	cytoskeleton in muscle cells	7	small ratio. Myosin 1/2, both directions. Specific process in highly differentiated cells				various directions	not or side related	4	small ratio. Max 1/4. all downregulated. Specific process in highly differentiated cells				downregulated	not or side related	similar, 3 genes diff
65	Proteasome	1	very small ratio. Downregulated				ubiquitin related	not related	1	very small ratio. Downregulated				ubiquitin related	not related	same
66	ECM-receptor interaction	1	very small ratio. Downregulated					not related	0					focal adhesion, laminin	not related	Mm 1 more gene
67	Autophagy-animal	12	not sure	PI3K complex, LC3	middle-late part	Autophagysome, lysosome	Insulin, PI3K, MAPK, AMPK, ULK, mTOR	related or side related	10	not sure	some, no doubt	middle-late part	autophage, lysosome	PI3K, MAPK, mTOR, etc.	related or side related	similar, 6 gene differ
68	Autophagy-other	1	small ratio. nutrient starvation.				downregulated. PI3K, TOR, etc.	not related	2	small ratio. An important factor. nutrient starvation.				TORC1. Downregulated	side or not related	Dm 1 more gene
69	homologous recombination	3	small ratio. Molecular-cell level. Eukaryotic cells. Common and mammals.					not related	3	small ratio, might involve in other process. Eukaryotic cells					not related	Similar, 2 genes diff
70	non-homologous end-joining	2	small ratio. Eukaryotic. Saccharomyces and Mammals					not related	1	small ratio, might involve in other process. Eukaryotic , but Saccharomyces not Mammals					not related	Mm 1 more gene
71	Vitamin digestion and absorption	4	Vitamin B12, Bile secretion, Folate biosynthesis, Riboflavin related				metabolism, secretion. Downregulated	side related								no Dm path
72	Longevity pathway	5	0	not sure	scare middle	ROS, self-renewal, etc.	variolus direction	not or side related								no Dm path
73	Longevity regulation-multiply species	5	no	not sure, maybe 1, worm	no, middle	metabolism, autophagy	PI3K, AMPK, FOXO, mTOR	not or side related	5	no	not sure, maybe 1	no, middle	metabolism, autophagy	PI3K, AMPK, FOXO, mTOR	not or side related	same
74	circadian rhythm	2	0	1 or no	no	proteasome degradation	Ubiquitin, MAPK. Downre	not or side related	0						not related	diffferent pathway
75	calcium pathway	7	4	no?	up and downstream	proliferation, fertilization	downregulated	related or side related								no Dm path
76	circadian entrainment	5 or 8	2 or 5	not sure	half	clock gene, intermediate early gene	mainly downregulated? MAPK	side related or related								no Dm path
77	melanogenesis	4	1, wnt	no	no	tyrosine	wnt, MAPK	not related								no Dm path

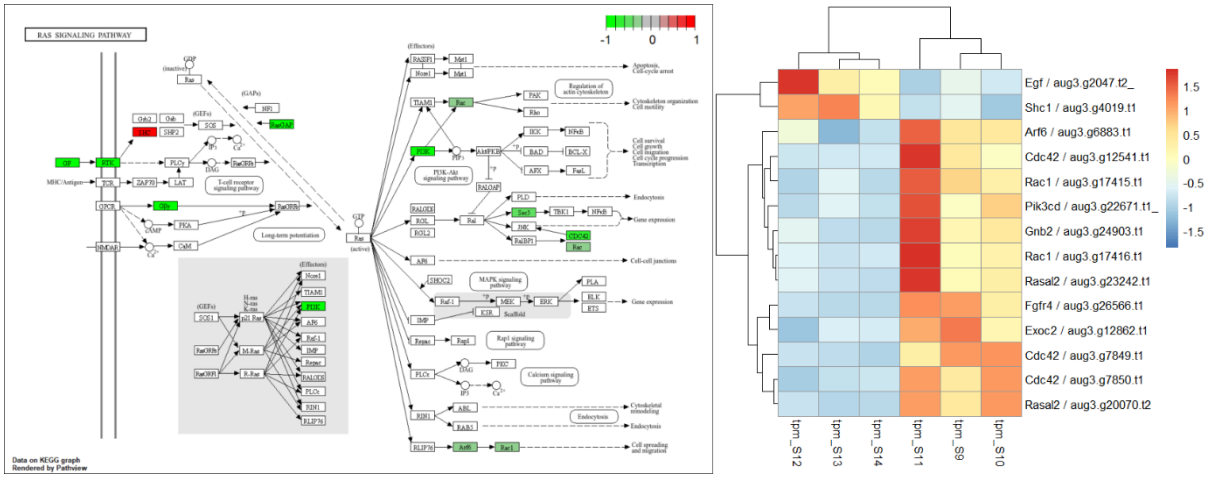

Figure S2-5. Ras signalling Pathway and Heatmap Analysis of Depicted Genes. Pathways were visualized using R (pathview) with the mouse ortholog gene list from List F. Heatmaps, created with R (pheatmap), display the expression levels of genes relevant to each pathway. Gene names are provided in the format “Mm ortholog gene name / Pt august number”.

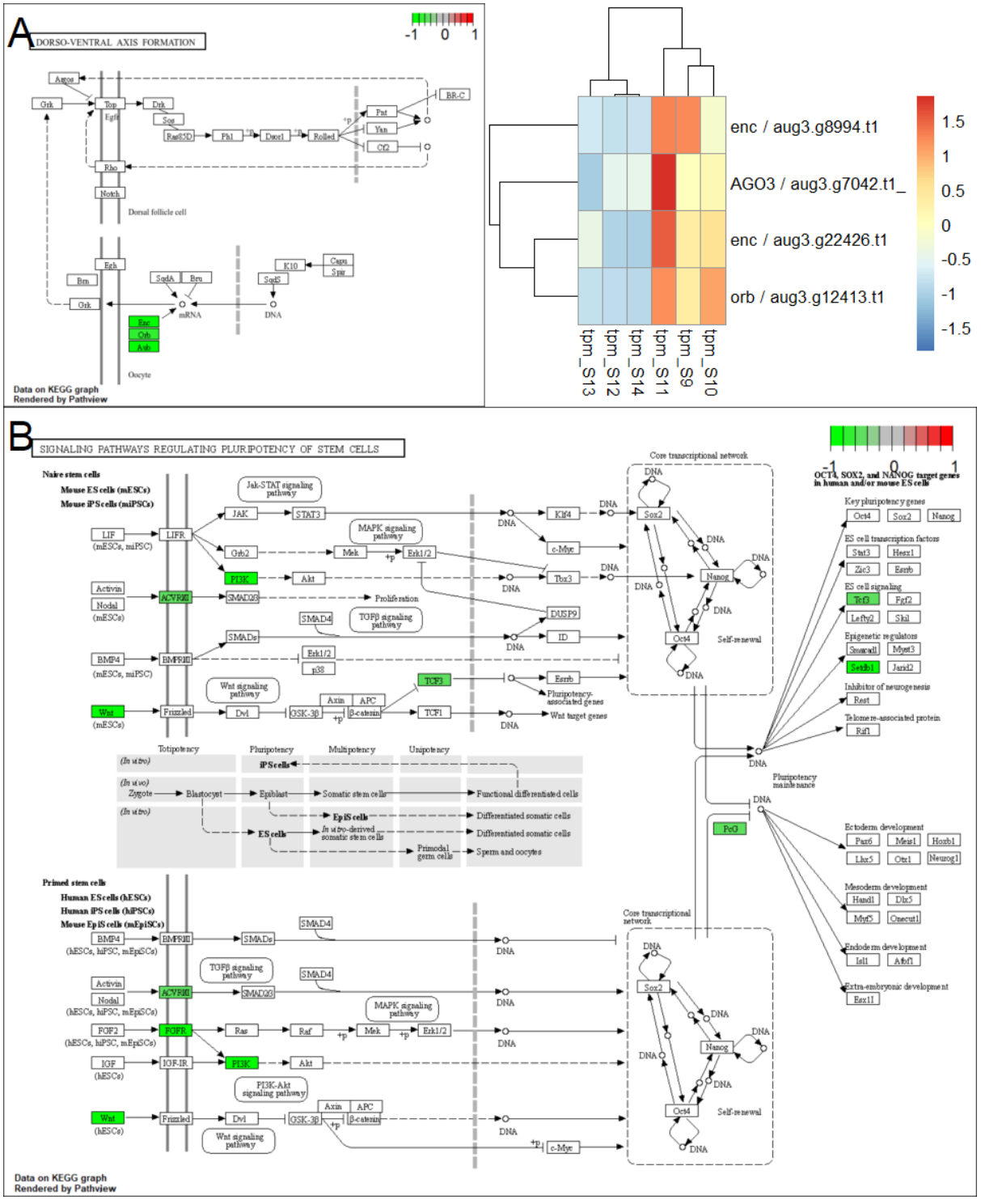

Figure S2-6. DV Axis Formation (A) and Regulating the Pluripotency of Stem Cell (B) Signalling Pathway. The pathways are depicted using R (pathview) based on fly orthologs (A) and mouse orthologs (B) from List F.

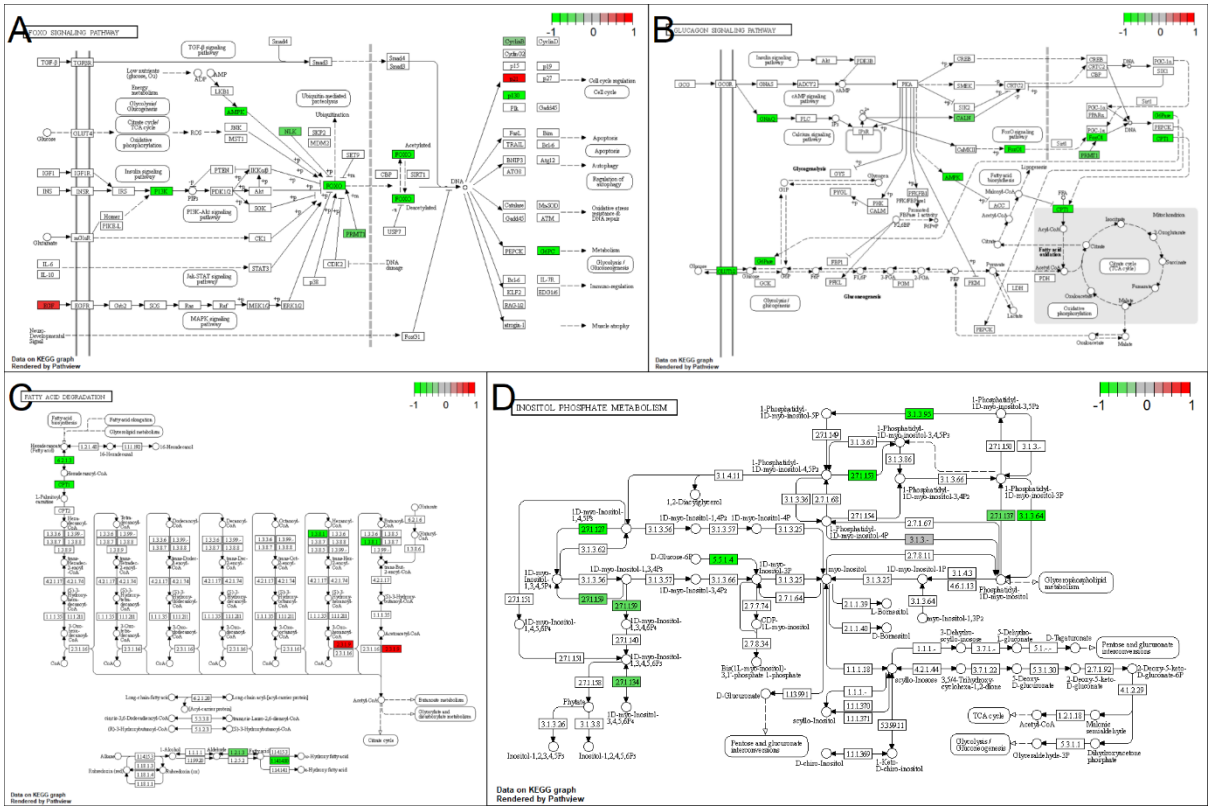

Figure S2-7. Kegg Pathway images for the FOXO signaling pathway (A), Glycogen signaling pathway (B), Fatty acid degradation (C), and Inositol phosphate metabolism (D). The pathways are depicted using R (pathview) based on the mouse ortholog list from List F.

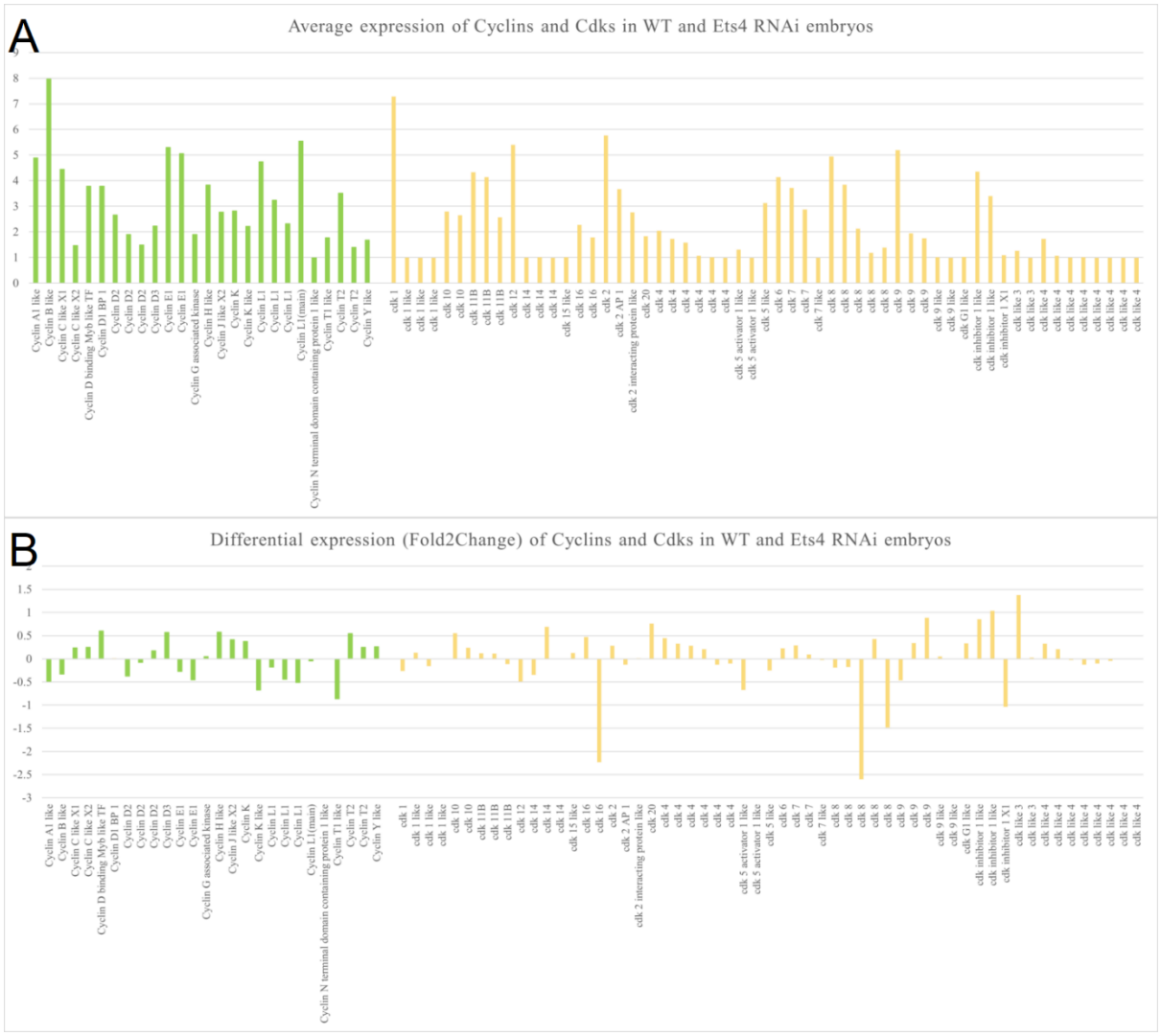

Figure S2-8. Expression (A) and Fold Change (B) Analysis of Cyclin and CDK Genes. (A) Average expression levels (A) and Fold2Change values (B) of cyclin genes (indicated in green) and CDK genes (indicated in yellow) from RNAseq results for WT and *Ets4* RNAi embryo samples. Genes were identified using the keywords "cyclin" and "cdk" in NCBI, and their sequences were subsequently searched using BLAST on the i5K website (https://i5k.nal.usda.gov/webapp/blast/) to obtain August numbers. These numbers were used to determine the expression levels of the target transcripts in the complete RNAseq result file (List A1).

	Target Cell Type	Programming factors
1	Embryonic stem cell	Oct4, Sox2, Klf4, c-myc, Nanog
2	Adipocytes (brown fat cells)	PRDM16, CEBPβ
3	Cardiomyocytes	Mef2c (7), Tbx5 (7), **Gata4 (6)**, Hand2 (2), Myocd (2), miR-1, miR-133, miR-208, miR-499, JAK inhibitor I, Nkx2.5, **SRF**, Mesp1, SMARCD3
4	Chondrocytes	Sox9, Klf4, c-Myc
5	Cone-like cells	Nrl ablation
6	Endothelial cells, Hemogenic endothelial-like precursor cells	**Foxo1**, Er71, Klf2, Tal1, Lmo2, Gata2, Gfi1b, cFos, Etv6
7	Haematopoietic progenitor cells, Haematopoietic stem cells	ERG, GATA2, LMO2, RUNX1c, SCL, **p53(−/−)**, Runx1t1, Hlf, Lmo2, Prdm5, Plxl1, Zfp37, Myc, Meis1
8	Hepatic stem cells, Hepatocytes	Foxa3 (3), Foxa1, Foxa2, Hnf1β, Hnf4α, Hnf1α, **Gata4**, P19ARF knockdown
9	Layer-V/VI corticofugal projection neurons	Fezf2
10	Macrophages	**CEBPα** (2) or CEBPβ, PU.1
11	Melanocytes	MITF, SOX10, PAX3
12	Monocytes	PU.1
13	Natural killer-like cells	Bcl11b deletion
14	Neural precursor cells, Neural stem cells, Neuroblast, Neurons, Neurons (glutamatergic), Neurons (dopaminergic), Neurons (GABAergic), Neurons (glutamatergic and GABAergic), Neurons (motor), Oigodendrocyte progenitor cells, Astrocytes	**Ascl1 (11)**, Brn2 (8), Sox2 (6), **Myt1 or Myt1l (5)**, c-Myc (3), Klf4 (3), Lmx1a (3), Nga2 (3), Nurr1 (3), Foxa2 (2), NeuroD1 (2), Olig2 (2), Sox10 (2), Brn4, CHIR99021, Dlx2, E47, EN1, FoxG1, Gsx98, Hb9, **Hes1**, Id1, **Isl1**, **Lhx3**, **Lmx1b**, Nfia, Nfib, Nkx2.2, Nkx6.2, Oct4 (limiting activity at initial stage), Olig1, Otx2, Pax6, Pitx3, PTB repression, RepSox (616452) under hypoxia, **Sox9**, ST18, VPA, Zfp536
15	Pancreatic islet cells, Pancreatic α cells, Pancreatic β cells, Pancreatic δ cells	Ngn3 (4), MafA (2), Dnmt1 deficiency, Pdx1
16	Sertoli cells	Nr5a1, Wt1, Dmrt1, **Gata4**, Sox9, Deletion of Foxl2
17	Thymic epithelial cells	Foxn1

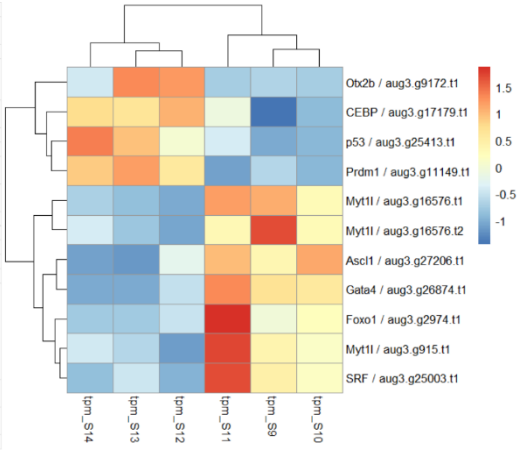

Figure S2-9. Expression of Mouse programming factors Key Factors in Pt. Table listing key factors for mouse reprogramming, from Jun Xu, Yuanyuan Du, and Hongkui Deng (2015), Table 2. categorized by their roles in ESC and other functional cell induction. Repeated genes are counted and summarized for each targeted cell type. The expression status of these factors in the Pt transcriptome, based on auto-annotation, is color-coded as follows: Grey indicates factors not found in Pt; Light red denotes factors present but with low expression in both WT and *Ets4* RNAi samples; Black signifies factors found and expressed at similar levels in both WT and *Ets4* RNAi samples; Blue indicates factors with differential expression between WT and *Ets4* RNAi samples. Factors in the last category are also depicted in the heatmap image.

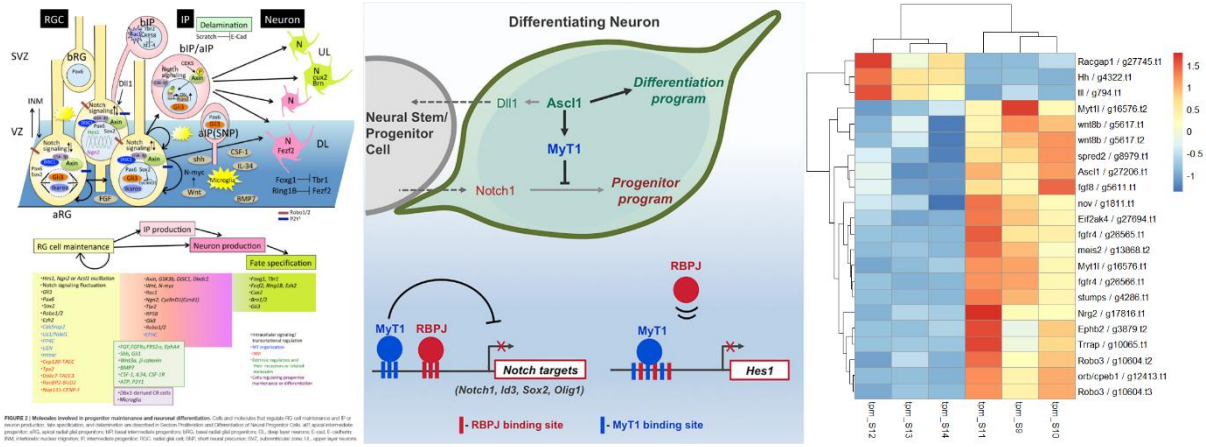

Figure S2-10. Combined Pathways of Neural Development and Differentiation. A. Pathway diagram integrating induced neural development (Chiaki Ohtaka-Maruyama and Haruo Okado, 2015) and induced neural cell differentiation (Vasconcelos et al., 2016). B. Heatmap of genes from List F associated with neural development or neural cell differentiation. Gene functions were identified through a comprehensive literature search beyond the references provided.

(Supplementary Figures and Tables for Result III)

Table S3-1 Result of in situ hybridization experiments of 212 genes (a): confirmed expression pattern of 113 genes at stage 4. RNAseq expression of these genes are also listed.

Number	image	Gene Name	Name	3_tpm_S1	3_FDR	tpm_S9	tpm_S10	tpm_S11	tpm_S13	tpm_S14	tpm_S12	rasteanda gene from NCBI bl	Parasteatoda LOC	fly homology	fly gene ID	ouse homolo	UniProt ID
1	image at stage 4	bmp-1	aug3.g18541.t1	-0.78084	1	0.024505	0.421142	0.386377	0	0	0.262701	ctivin membrane-bound inhibit	LOC107445428			Bambi	Q9D0L6
2	image at stage 4	bmp-2	aug3.g17346.t1	-0.40795	1	3.6096	3.05093	5.18172	1.75622	3.14315	2.49173	ctivin membrane-bound inhibit	LOC107443591			Bambi	A2CFNTT
3	image at stage 4	cv-2	aug3.g2323.t1	-1.33914	1	6.33988	3.51427	5.59247	1.44895	2.348	1.10977	binding endothelial regulator p	LOC107448655	cv-2	FBgn0000395	Bmper	Q8CJ69
4	image at stage 4	bmp-4	aug3.t13706.t1	-0.26436	1	16.3719	17.9995	17.0661	13.0891	8.89125	14.07	protein 60A	LOC107439350	gbb	FBgn0024234	Bmp7	P23359
5	image at stage 4	DLL1	aug3.g25248.t1	1.657831	0.070868	10.2458	3.96259	19.1005	40.1426	34.2505	10.8705	delta-like protein 1	LOC107456525	Dl	FBgn0000463	Dll1	Q61483
6	image at stage 4	etv4	aug3.g4238.t1	-3.97685	3.79E-09	161.599	196.816	241.265	2.20942	3.25887	26.7402	domain-containing Ets transc	LOC107451717	Ets98B	FBgn0005659	Spdef	Q9WTP3
7	image at stage 4	fgfr2	aug3.g26565.t1	-3.26626	0.000158	9.56246	8.5299	15.1836	0.82618	0.580557	1.18354	roblast growth factor receptor	LOC107438841	btl	FBgn0285896	Fgfr4	Q03142
8	image at stage 4	Fuchi	aug3.g26874.t1	-0.8665	0.184288	108.111	104.905	120.413	47.3986	47.2052	64.8204	transcription factor GATA-4	LOC107439682	pnr	FBgn0003117	Gata4	Q08369
9	image at stage 4	hh	aug3.g4322.t1	2.555249	1.58E-08	5.82427	4.63288	4.99803	22.9961	22.9631	32.0359	sonic hedgehog protein-like	LOC107451809	hh	FBgn0004644	Shh	Q62226
10	image at stage 4	PLA2	aug3.g27753.t1	-2.24552	0.319272	229.726	200.299	457.284	4.13677	10.6011	139.819	phospholipase A2	LOC107442814	Pla2	FBgn0086242	Pla2g2a	P31482
11	image at stage 4	Ace	aug3.g6760.t1	-2.49502	0.006464	49.5541	65.7777	124.111	2.82123	2.5597	29.4128	acetylcholinesterase-1	LOC107455030	Ace	FBgn0000024	Ache	P21836
12	image at stage 4	g5179	aug3.g5179.t2	-2.92068	7.90E-08	227.909	203.864	123.404	10.7275	22.1609	31.9688	uncharacterized	LOC122268364				
13	image at stage 4	ABHD11	aug3.g9727.t1	-0.59623	1	760.309	462.85	841.026	30.5933	158.692	971.512	protein ABHD11	LOC107440315	CG2059	FBgn0029942	Abhd11	Q8K4F5
14	image at stage 4	MTMR14	aug3.g15186.t1	-1.06099	1	445.965	383.828	778.078	67.6382	103.413	468.448	myotubularin-related protein 14	LOC107447676	EDTP	FBgn0027506	Mtmr14	Q8VEL2
15	image at stage 4	CaM	aug3.g4731.t1	-0.78331	1	98.8996	126.855	181.145	3.95794	11.6471	185.715	calumenin	LOC107452404	scf	FBgn0025682	Calu	Q35887
16	image at stage 4	RHC1A	aug3.g19992.t1	-0.84672	1	246.71	219.522	576.149	13.8949	57.2427	401.063	le E3 ubiquitin-protein ligase R	LOC107447814				
17	image at stage 4	ITP3K	aug3.g11911.t1	-1.76445	0.00141	70.1094	59.6606	56.3722	8.33449	14.1414	24.611	tol-trisphosphate 3-kinase hom	LOC107436903	IP3K2	FBgn0283680	Itpka	Q8R071
18	image at stage 4	l(2)ef1	aug3.g14129.t1	-1.1254	1	955.675	512.925	320.189	92.5344	124.752	525.459	lethal(2)essential for life	LOC122268500	l(2)ef1	FBgn0011296	Hspb6	Q5EBG6
19	image at stage 4	RF_0381	aug3.g1767.t1	-2.58409	8.15E-09	51.593	37.8827	90.5297	9.62819	7.57542	7.05598	ein ankyrin repeat protein RF	LOC107447467			Ankrd31	A0A140LI8
20	image at stage 4	atg8f	aug3.g18439.t1	-2.02	0.000148	55.0128	99.0457	143.486	19.8032	10.249	30.6814	autophagy-related protein 8f	LOC107445281	Atg8a	FBgn0052672	Map1lc3b	Q9CQV6
21	image at stage 4	DRG1	aug3.g23069.t1	-7.72668	1.89E-08	35.1323	5.07958	50.5553	0	0	0	GTP-binding protein 128up	LOC107441810	128up	FBgn0010339	Drg1	D6RHA5
22	image at stage 4	ZIC-4	aug3.g12202.t1	-0.90082	1	31.87	53.0785	38.3625	4.17649	3.63447	50.6609	zinc finger protein ZIC 4-like	LOC107437305	opa	FBgn0003002	Gli2	Q0VG72
23	image at stage 4	g20989	aug3.g20989.t1	-0.64049	1	15.4142	12.6797	27.5081	0.878387	2.18184	26.4735	uncharacterized	LOC122272499			Muc3a	Q3U5A2
24	image at stage 4	ZNF423	aug3.g14296.t2	-1.94252	0.000362	18.7287	27.3623	23.7534	4.92518	3.32478	6.87098	zinc finger protein 423	LOC107440157	Oaz	FBgn0288433	Znf423	Q80TS5
25	image at stage 4	g3789	aug3.g3789.t1	-2.50076	0.000229	11.0781	34.9347	45.437	4.55896	3.44495	5.10594	NA-directed DNA polymerase	BR001342				
26	image at stage 4	unchar	aug3.g4422.t1	-1.57948	0.433578	609.195	469.754	1274.1	90.2067	80.1003	470.751	uncharacterized	LOC107451948				
27	image at stage 4	unchar	aug3.g9731.t1	-0.52389	1	349.629	371.542	555.641	35.2662	76.2342	401.043	uncharacterized	LOC107440356				
28	image at stage 4	unchar	aug3.s992.t1	-1.00647	1	808.29	694.963	1385.92	72.9281	202.892	920.055	No significant result					
29	image at stage 4	unchar	aug3.g22667.t1	-1.2235	0.949312	373.373	303.479	792.559	76.8512	68.1236	367.684	uncharacterized	LOC107451948			Chitin-binding type-2 domain-containing p	
30	image at stage 4	ptc	aug3.g14374.t2	-1.10746	1	32.2814	68.9128	49.3602	13.4611	4.87907	43.0104	patched-like	LOC107440240	ptc	FBgn0003892	Ptch	Q61115
31	image at stage 4	Wnt	aug3.g5617.t2	-1.62511	0.174775	9.49544	10.5836	7.58938	4.24583	0.635412	2.4001	protein Wnt-8b-like	LOC107453612	wntD	FBgn0038134	wnt8b	Q9WUD6
32	image at stage 4	ABHD11	aug3.g9726.t1	-1.826	1	52.4109	2.10433	9.16809	0.332981	1.01142	14.4907	protein ABHD11-like	LOC107440308	CG2059	FBgn0029942	Abhd11	Q8K4F5
33	image at stage 4	Ppaf2	aug3.g3137.t1	-2.53204	5.73E-05	42.2744	31.8496	64.717	1.46438	2.2016	15.9728	henoloxidase-activating factor	LOC107443855				
34	image at stage 4	Anxa1	aug3.g8154.t1	-1.52854	1	90.1479	102.499	371.473	6.56717	10.8601	136.732	phospholipase A2 inhibitor beta	LOC107455930	AnxB9	FBgn0000083	Anxa1	P10107
35	image at stage 4	Lic1	aug3.g13559.t1	-1.01128	1	28.8849	28.5621	62.2029	2.60283	2.74033	43.5735	acellular coagulation inhibitor	LOC107439086				
36	image at stage 4	unchar	aug3.g15602.t1	-0.49259	1	167.736	145.348	165.431	6.01471	15.092	276.733	uncharacterized	LOC107450675	Ebys	FBgn0031052	Abcttl	Q8CIF7
37	image at stage 4	g4424	aug3.g4424.t2	-2.20038	0.004972	25.5113	22.4375	42.0675	1.56557	0.120289	14.3658	uncharacterized	LOC107451955				
38	image at stage 4	uncharacterize	aug3.g4425.t1	-1.3065	1	66.4939	54.1205	142.238	4.36012	6.88453	75.5523	uncharacterized	LOC107451953				
39	image at stage 4	Clca4a	aug3.g11056.t2	-6.70246	1.00E-08	11.4122	18.2185	12.0818	0	0	0	activated chloride channel reg	LOC107457308			Clca4a	Q6Q473
40	image at stage 4	uncharacterize	aug3.g26430.t1	-4.77572	3.25E-15	26.8342	34.1282	63.033	1.84877	0.734583	0.81213	uncharacterized	LOC107438215				
41	image at stage 4		aug3.g5417.t1	-1.48193	0.022299	13.7602	13.1684	28.3191	4.53319	3.73871	7.98592	ivated inward rectifier potassi	LOC107453330	Irk2	FBgn0039081	Kcnj9	P48543
42	image at stage 4		aug3.g1125.t1	-0.46716	1	121.166	101.268	142.79	84.0663	78.0172	59.6954	ascterized transcription factor	07445669/LOC1074	kn	FBgn0001319	Ebf1	Q07802
43	image at stage 4	MyoM	aug3.g2394.t2	-2.8499	0.002747	3.91512	4.92004	19.4227	0.783672	0.000291	2.20432	DBO Rho GTPase-activating p	LOC107448763			Srgap1	Q91Z69
44	image at stage 4		aug3.g15443.t1	-1.77836	0.702461	3.69569	5.13145	5.32112	0.881617	0.566887	1.76364	uncharacterized	LOC107449499				
45	image at stage 4	Ptl	aug3.g4530.t1	-0.89867	1	4.37364	4.56512	4.86492	2.01506	1.81425	2.21335	uncharacterized	LOC107452121			Radil	Q69Z89
46	image at stage 4	otd	aug3.g9172.t1	3.285161	0.007374	0.640753	0.509874	0.507755	7.71718	1.48185	7.33258	omeobox protein OTX2-A-like	LOC107457189	oc	FBgn0004102	Otx2	P80206
47	image at stage 4	Numb	aug3.g26621.t1	-0.07707	1	1.54359	1.8238	1.67539	1.11078	1.28631	1.5889	protein numb	LOC107438995	numb	FBgn0002973	Numb	Q9QZS3
48	image at stage 4	Creld1	aug3.g259.t1	-0.06481	1	5.79978	6.1164	6.10814	4.92299	4.89564	4.59907	tein disulfide isomerase CREL	LOC107452629	Creld	FBgn0031217	Creld1	Q91XD7
49	image at stage 4	Creld2	aug3.g7589.t1	-0.46347	1	3.93931	4.26739	5.8607	3.04329	3.15853	2.24893	s-rich with EGF-like domain pr	LOC107446657	Creld	FBgn0031217	Creld2	Q9CYA0
50	image at stage 4	Creld2	aug3.g7590.t1	-0.39954	1	2.32918	2.44326	2.30135	1.45564	1.62108	1.33198	s-rich with EGF-like domain pr	LOC107446657	Creld	FBgn0031217	Creld2	Q9CYA0
51	image at stage 4	EgfR	aug3.g18901.t1	0.459767	1	0.237137	0.231902	0.357603	0.163652	0.448621	0.468212	pidermal growth factor recepto	LOC107446048	Egfr	FBgn0003731	Egfr	Q01279
52	image at stage 4	GSK3 beta	aug3.g9959.t1	-0.17833	1	44.023	44.5951	55.1443	27.508	31.3009	48.607	lycogen synthase kinase-3 beta	LOC107443254	gskt	FBgn0046332	Gsk3b	Q9WV60
53	image at stage 4	GSK3 beta	aug3.g25394.t1	-0.5705	1	7.73004	10.8229	12.8051	6.35367	4.30019	6.92106	lycogen synthase kinase-3 beta	LOC107441379	sgg	FBgn0003371	Gsk3b	Q9WV60
54	image at stage 4	Cyclin A1 like	aug3.g2080.t1	-0.48715	1	33.3797	29.568	42.6043	15.8861	18.8073	28.448	cyclin-A1	LOC107448094	CycA	FBgn0000404	Ccna1	Q61456
55	image at stage 4	cyclinB	aug3.g8469.t1	-0.33218	1	263.56	238.32	421.274	145.423	150.006	314.091	G2/mitotic-specific cyclin-B	LOC107456309	CycB	FBgn0000405	Ccnb1	P24860
56	image at stage 4	Cyclin E1	aug3.g7775.t1	-0.45718	1	43.7521	36.0123	36.2145	24.2094	20.6837	27.242	G1/S-specific cyclin-E1	LOC107455437	CycE	FBgn0010382	Ccne1	Q61457
57	image at stage 4	cdk1	aug3.g11601.t1	-0.26234	1	167.688	133.982	259.81	115.211	125.577	144.91	cyclin-dependent kinase 1	LOC107436497	Cdk1	FBgn0004106	Cdk1	P11440
58	image at stage 4	mycbp	aug3.g26862.t1	-0.045	1	53.643	52.8434	68.0959	34.3552	46.115	62.3263	-Myc-binding protein homolo	LOC107439646	CG17202	FBgn0038043	Mycbp	Q9EQ53
59	image at stage 4	Dennd4a	aug3.g2908.t1	-0.0672	1	1.6463	2.09615	2.41225	1.49088	1.1044	2.3093	c-myc promoter-binding protei	LOC107449703	Crag	FBgn0025864	Dennd4a	E9Q8V6
60	image at stage 4	Pik3r1	aug3.g14960.t2	-0.10583	1	1.28293	1.68243	1.97418	0.629222	0.369284	2.82172	hosphoinositol 3-kinase regulatory su	LOC107441029	PI3K21B	FBgn0020622	Pik3r1	P26450
61	image at stage 4	Pik3r1	aug3.g26883.t1	-0.86563	1	6.86402	6.887	8.85588	2.73234	2.46105	5.04343	hosphoinositol 3-kinase regulatory su	LOC107439742	PI3K21B	FBgn0020622	Pik3r1	P26450
62	image at stage 4	Pik3c3	aug3.g3457.t1	-0.51818	1	34.7053	32.067	53.575	25.9108	21.0568	22.0958	hosphoinositol 3-kinase catalytic sub	LOC107450591	PI3K59F	FBgn0015277	Pik3c3	Q9PF93
63	image at stage 4	AMPK alpha-2	aug3.g3112.t1	-0.25327	1	16.3133	16.097	11.9887	9.58855	9.11105	12.7243	ated protein kinase catalytic su	LOC107450058	AMPKa	FBgn0023169	Prkaa2	Q8BRK8
64	image at stage 4	HIF-1alpha	aug3.g18646.t1	-0.23525	1	2.19347	0.780416	2.29376	1.80288	0.943212	0.950459	ypoxia-inducible factor 1-alph	LOC107445617	sima	FBgn0266411	Hif1a	Q61221
65	image at stage 4	Idh2	aug3.g4961.t1	-0.41682	1	63.6007	32.2728	58.4825	35.1231	30.3464	31.5346	dehydrogenase [NADP], mito	LOC107452752	CG32026	FBgn0052026	Idh2	P54071
66	image at stage 4	Idh3a	aug3.g9466.t1	-0.15387	1	42.0229	39.5408	32.4858	30.0519	30.371	27.7304	ehydrogenase [NAD] subunit	LOC107436759	Idh3a	FBgn0027291	Idh3a	Q9D6R2
67	image at stage 4	Idh3g	aug3.g14882.t1	-0.29483	1	70.6661	49.7057	87.5308	44.4833	52.5945	43.8584	tase [NAD] subunit gamma,	LOC107449231	Idh3g	FBgn0039358	Idh3g	P70404
68	image at stage 4	Idh3g	aug3.g20624.t1	-0.35207	1	18.2272	13.2604	26.4899	17.4584	9.09568	11.2555	ogenase [NAD] subunit gamm	LOC107440878	Idh3g	FBgn0039358	Idh3g	P70404
69	image at stage 4	Snip1	aug3.g4437.t1	0.255892	1	17.2889	12.0107	24.182	18.7634	20.6011	13.8961	nad nuclear-interacting protein	LOC107451985	CG17168	FBgn0039943	Snip1	Q8BIZ6
70	image at stage 4	Idh1	aug3.g8458.t1	0.537871	1	9.94942	7.06405	10.8824	14.5056	10.7679	8.80592	e dehydrogenase [NADP] cyto	LOC107456288	Idh	FBgn0001248	Idh1	Q88844
71	image at stage 4	Akt1p	aug3.g7505.t1	1.197294	0.068823	13.0837	11.2586	6.90493	19.598	21.0835	20.4824	AKT-interacting protein	LOC107445524	CG16894	FBgn0034483	Akt1p	Q64362
72	image at stage 4	Asph	aug3.g13107.t1	-0.04731	1	4.76832	3.72331	4.74543	4.02996	3.62351	3.06431	artyl/asparaginyl beta-hydroxy	LOC107438443	Asph	FBgn0034075	Asph	Q8BSY0
73	image at stage 4	Ctnnbl1	aug3.g2387.t1	0.058369	1	18.7045	11.1529	24.4763	18.8351	16.8452	11.4417	beta-catenin-like protein 1	LOC107448730	CG11964	FBgn0037644	Ctnnbl1	Q9CWL8
74	image at stage 4	Sox2	aug3.g11061.t1	-0.50376	1	1.06627	0.844411	2.85615	0.689498	1.01965	1.00576	transcription factor Sox-2	LOC107457313			Sox2	P48432
75	image at stage 4	cdk2	aug3.g9226.t1	0.283904	1	53.3422	34.2736	69.3345	40.9036	53.7059	63.9683	cyclin-dependent kinase 2	LOC107443618	Cdk2	FBgn0004107	Cdk2	P97377
76	image at stage 4	AKT	aug3.g4339.t1	0.195966	1	12.107	10.1995	13.4417	11.0211	10.9927	12.3467	C serine/threonine-protein kin	LOC107451835	Akt	FBgn0010379	Akt1	P31750
77	image at stage 4	Prkc2	aug3.g9182.t1	-0.28734	1	8.52326	7.1802	10.7308	5.67686	6.12129	6.2815	ium-independent protein kinas	LOC107446459				
78	image at stage 4	mTOR	aug3.g25455.t1	-0.14724	1	8.3534	6.87668	13.2348	8.76783	6.64288	6.07586	ne/threonine-protein kinase mT	LOC107439010	mTor	FBgn0021796	Mtor	Q9JLN9
79	image at stage 4	Rictor	aug3.g9316.t2	0.169298	1	5.12301	5.55781	6.91071	6.29805	5.80657	4.50585	ctin-insensitive companion of	LOC107452496	rictor	FBgn0031006	Rictor	Q6QI06
80	image at stage 4	PTEN	aug3.g12581.t1	0.186496	1	1.59927	1.2849	1.41259	1.30581	1.08356	1.75307	ase 3-phosphatase and dual-sp	LOC107437787	Pten	FBgn0026379	Pten	O08586
81	image at stage 4	MAPK14	aug3.g2738.t1	0.522822	1	2.40609	2.12829	2.2454	3.47683	2.30031	2.53054	tomm-activated protein kinase	LOC107449390	p38b	FBgn0024846	Mapk14	P47811
82	image at stage 4	MAPK1	aug3.g27558.t1	0.138667	1	4.67992	3.89455	5.26023	4.29518	3.95554	4.53974	itogen-activated protein kinase	LOC107442143	rl	FBgn0003256	Mapk1	P63085
83	image at stage 4	MAPK1	aug3.g27557.t1	0.09172	1	3.49148	4.26913	7.33862	4.31974	4.85244	4.32627	itogen-activated protein kinase	LOC107442143	rl	FBgn0003256	Mapk1	P63085
84	image at stage 4	sog	g23966									dorsal-ventral patterning protein Sog-like		sog	FBgn0003463	Chrd	Q9Z0E2
85	image at stage 4	twist	aug3.g14287.t1	-3.76169	1.01E-09	43.3936	63.0725	43.2093	0.866768	0.794551	7.6629	twist-related protein 2-like	LOC107440133	twi	FBgn0003900	Twist2	Q9D030
86	image at stage 4	Rab7a	aug3.g23439.t1	-0.35922	1	0.362042	35.5331	69.1343	38.8278	11.3157	14.4533	ras-related protein rab7	LOC107446981	Rab7	FBgn0015795	Rab7a	P51150
87	image at stage 4	g6152	aug3.g6152.t1	-0.2973	1	0.080041	0.49212	0.308298	0.011159	0.112186	0.413082	uncharacterized	LOC107454293				
88	image at stage 4	g16318	aug3.g16318.t1	0.802862	1	94.5596	37.7924	10.4847	81.8671	75.2901	69.7252	uncharacterized	LOC107442051				
89	image at stage 4	Mid1ip1	aug3.g22926.t1	0.201275	1	4.47862	3.81119	5.45022	4.86404	3.5408	4.8769	mid1-interacting protein 1-B	LOC107436539	CG2765	FBgn0035087	Mid1ip1	Q9CQ20
90	image at stage 4	Phb1	aug3.g23431.t1	0	1	0	0	0	0	0	0	protein l(2)37Cc	LOC107436901	Phb1	FBgn0002031	Phb1	P67778
91	image at stage 4	Ptprb	aug3.g2169.t1	-3.33749	0.439802	1.30119	2.25563	3.78283	0.136139	0.093234	0.070723	rosine-protein phosphatase 10	LOC107439574	Ptp10D	FBgn0004370	Ptprb	B2RU80
92	image at stage 4	g2657	aug3.g2657.t1	0	1	0	0	0	0	0	0	uncharacterized	OC107449262				
93	image at stage 4	Gin1	aug3.g7930.t1	0.135431	1	0	0	0.02003	0.052071	0	0	ransposon integrase-like prote	LOC122270560			Gin1	Q8K259
94	image at stage 4	Incenp	aug3.g12711.t1	8.99E-07	1	0	0	0	4.10E-10	2.13E-07	0	inner centromere protein-like	LOC107437986	Incenp	FBgn0260991	Incenp	Q9WU62
95	image at stage 4	g4081	aug3.g4081.t1	0.150791	1	0.634792	0.003883	6.23266	0	0	6.42668	uncharacterized	LOC107451525				
96	image at stage 4	g16165	aug3.g16165.t1	-2.68142	0.997189	1.99677	1.48734	2.53355	0.497112	4.54E-06	1.80E-08	uncharacterized	LOC107441820	mus304	FBgn0002901	Atrip	Q8BMG1
97	image at stage 4	Gpcpd1	aug3.g15726.t1	-0.66377	1	3.73738	1.76179	3.40955	1.66858	1.67524	1.2399	sphocholine phosphodiesterase	LOC107451427	CG8942	FBgn0038008	Gpcpd1	Q8C0L9
98	image at stage 4	Ptprk	aug3.g24730.t1	1.236471	1	0.440597	0	5.49E-05	0	0.893088	0.440107	ype tyrosine-protein phosphat	LOC107439861	CG42327	FBgn0259227	Ptprk	P35822
99	image at stage 4	Fgf8	aug3.g5611.t1	-1.99542	0.020534	46.3583	80.273	56.3274	6.65353	4.35487	29.1785	fibroblast growth factor 8	LOC107453597	bnl	FBgn0014135	Fgf8	P37237
100	image at stage 4	dof	aug3.g4286.t1	-4.29296	0.000148	9.30084	6.15884	10.9576	0.238895	0.094327	0.47107	uncharacterized	LOC107451770	stumps	FBgn0020299	Pik3ap1	Q9EQ32
101	image at stage 4	dpp	aug3.g16926.t1	-0.77193	1	6.30738	5.92336	12.1484	5.68272	3.98178	2.15149	ne morphogenetic protein 4-li	LOC107442925	dpp	FBgn0000490	Bmp4	P21275
102	image at stage 4	fkh	aug3.g2974.t1	-1.75945	0.772908	2.64812	3.33629	7.53853	0.838017	0.806437	1.45983	forkhead box protein O	LOC107449813	foxo	FBgn0038197	Foxo1	Q9R1E0
103	image at stage 4		aug3.g15167.t1	0.359849	1	93.8965	56.98	104.182	114.072	96.2016	62.1341	domain-containing protein D2	LOC107441267	Snrip-1	FBgn0032731	Ehd2	Q9D8Y0
104	image at stage 4	sn	aug3.g26989.t1	-2.1737	7.64E-09	135.451	100.335	170.425	31.3532	21.9284	21.5271	singed	LOC107440147	sn	FBgn0003447	Fscn1	Q61553
105	image at stage 4	hb	aug3.g25126.t1	-1.26609	0.109034	12.2383	18.375	22.9633	4.36041	3.13016	10.9836	protein hunchback-like	LOC107455742	hb	FBgn0001180	Ikzf5	Q8BU00
106	image at stage 4		aug3.g20850.t1	-0.08106	1	80.6468	79.0326	99.4614	67.3134	76.9892	62.0606	CS box domain-containing prol	LOC107449642	Socs44A	FBgn0033266	Socs1	O35716
107	image at stage 4	vasa	aug3.g5162.t1	-0.52007	1	224.586	156.336	302.098	107.263	133.403	153.298	ATP-dependent RNA helicase vasa-like		vas	FBgn0283442	Ddx4	Q61496
108	image at stage 4	pivi	aug3.g11104.t1	-0.52146	1	849.498	701.059	1173.54	522.632	525.059	529.025	pivi-like protein 1		pivi	FBgn0004872	Piwil1	Q9JMB7
109	image at stage 4	cad like	aug3.g6385.t1	0.432565	1	0.838294	0.87986	1.30362	1.38921	1.17343	0.972558	rabankyrin-5	LOC107445458	CG41099	FBgn0039955	Ankfy1	Q810B6
110	image at stage 4	eS6_d1_27_C12_S15	aug3.g12644.t1	-0.09437	1	66.5081	94.1758	125.086	74.5734	87.5936	60.6012	serine protease 27-like	LOC122273574			Prss27	Q8BJR6
111	image at stage 4	eS6_d1_26_A11_S13	aug3.g1632.t1	2.365448	0.054605	0.273832	0.46616	2.96419	11.5622	5.3062	0.534305	protein Wnt-5b-like	LOC107447180	Wnt5	FBgn0010194	Wnt5b	P22726
112	image at stage 4	eS6_d1_32_G05_S13	aug3.g23531.t1	2.427589	0.472691	0.466442	0	1.10739	4.23673	4.14761	0.204372	transcription factor AP-2-beta	LOC107452006	TFAP-2	FBgn0261953	Tfap2b	Q61313
113	image at stage 4		aug3.g2118.t1	0.060575	1	0.019299	0	0.02166	0.006284	0.031579	0.012571	probable DNA polymerase	LOC110282806				

Table S3-1 Result of in situ hybridization experiments of 212 genes (b): 99 genes with expression or no confirmed staining result at stage 4. RNAseq expression of these genes are also listed.

114	no staining in all stages	histone H2B															
115	no staining in all stages	Peter Pan/SWI4	aug3.sl7398.t1	-1.20493	1	312.641	321.966	447.693	38.9728	61.0596	299.726	histone H2B	LOC107443687	His2B	FBgn0001198	H2bc13	
116	no staining in all stages	proline-rich protein 4	aug3.g760.t2	-8.0357	2.27E-16	28.842	40.5572	35.2069	0	0	0	suppressor of SWI4 1 homolog	LOC107444556	ppan	FBgn0010770	Ppan	
117	no staining in all stages	Rab34	aug3.sl1258.t1	-1.34362	1	78.9656	105.865	135.684	4.59822	6.31924	97.1646	proline-rich protein 4	LOC107457530				
118	no staining in all stages	znf11	aug3.gl0703.t2	-1.32521	0.511067	32.7332	31.3206	12.2844	2.99538	11.7081	12.242						
119	no staining in all stages	uncharacterized	aug3.g6237.t1	-0.82589	1	9.13307	14.0545	6.01999	1.34828	1.14051	11.4275	zinc finger protein 1	LOC107454373			Zfp1	
120	no staining in all stages	uncharacterized	aug3.g1978.t1	-0.91976	1	425.552	389.889	780.958	34.9719	50.4632	619.232	uncharacterized	LOC107447910	NUCB1	FBgn0052190		
121	no staining in all stages	bmp10	aug3.g1983.t1	-1.05118	1	300.158	222.136	543.403	36.4365	58.6564	327.999	uncharacterized	LOC107447904	CG12773	FBgn0024365	Slc12a8	
122	no staining in all stages	grator complex subunit	aug3.sl6925.t1	-1.88773	0.060068	10.7109	21.5201	14.0007	0.508258	0.889205	9.13626	unitin	LOC107442923				
123	no staining in all stages	orthopedia-like	aug3.sl26532.t1	-3.50771	1.68E-14	122.315	58.678	146.019	7.82786	7.97235	7.56177	integrator complex subunit 2	LOC107438728	Ints2	FBgn0030858	Ints2	
124	no staining in all stages	rotein LTV1 homolog	aug3.sl6467.t1	-1.59139	0.142245	13.8453	26.9228	25.3943	2.1322	1.86087	14.54	homeobox protein orthopedia	LOC107442263	otp	FBgn0015524	Otp	
125	no staining in all stages	uncharacterized	aug3.g22997.t1	-8.04273	1.54E-12	24.2509	17.9787	71.6152	0	0	0	LTV1 homolog	LOC107456193	LTV1	FBgn0027525	Ltv1	
126	no staining in all stages	dopamin receptor 2	aug3.sl4078.t1	-1.99526	0.454714	46.9731	56.6505	86.7255	1.23862	1.04117	37.9036	uncharacterized	LOC107439825				
127	no staining in all stages	uncharacterized	aug3.gl6752.t1	-0.94324	1	0.220309	1.64775	0.38597	0.095317	0.149838	0.572567						
128	no staining in all stages	not sure or NA	aug3.sl9176.t1	2.429159	1	0	0.256638	0	0.941308	0.877447	0.838133						
129	no staining in all stages	uncharacterized	aug3.g7529.t1	-1.20078	1	27.6938	24.9626	27.3478	0.94511	2.60916	26.4478	dentin sialophosphoprotein	LOC107445528			Dspp	
130	no staining in all stages	carbonic anhydrase 1	aug3.sl0648.t1	-1.09058	1	30.06	27.6403	62.3324	2.25422	3.18788	40.9219	carbonic anhydrase 1	LOC107452229	CAH1	FBgn0027844	Ca1	
131	confirmed record, no image	uncharacterize	aug3.gl4945.t1	-3.44357	0.009519	22.2437	30.8173	296.116	1.51921	2.37579	19.3218	uncharacterized	LOC107441013	Taf2	FBgn0011836	Taf2	
132	confirmed record, no image	DAB2ip	aug3.g20070.t2	-2.04838	0.015537	8.56034	12.0955	11.9964	1.76283	2.04406	2.54523	GTPase-activating protein nGA	LOC107447937	rasGol	FBgn0261570	Rasal2	
133	confirmed record, no image	EIF3D	aug3.g27822.t1	-0.10779	1	253.957	193.431	316.115	202.792	207.309	180.491	t translation initiation factor 3	LOC107443003	eIF3d1	FBgn0040227	Eif3d	
134	confirmed record, no image	ALDH1A1	aug3.g2991.t1	2.880154	0.000131	7.49259	3.84209	6.84061	55.6311	47.3804	10.5888	retinal dehydrogenase 1	LOC107449839	CG31075	FBgn0051075	Aldh1a1	
135	confirmed record, no image		aug3.g22384.t1	-3.53695	1.36E-09	1213.71	1428.11	2433.99	70.4555	103.874	186.478	ubiquitin-protein ligase ATL-	LOC107456101	Zip89B		Dzip3	
136	confirmed record, no image		aug3.gl4890.t1	0	1	0	0	0	0	0	0	ed transmembrane protein DD	LOC107440890				
137	confirmed record, no image		aug3.g23798.t1	-1.2129	1	0.492768	0.777504	0	0	0	0.26459	ubiquitin-protein ligase PDZR	LOC107453376	Slip1	FBgn0024728	Pdzrn3	
138	confirmed record, no image		aug3.g27267.t1	-2.75316	0.032034	3.29928	6.11961	10.5139	1.60129	0.239938	0.34375	uncharacterized	LOC107441350				
139	confirmed record, no image		aug3.g27105.t1	0.14061	1	15.1596	10.4885	2.43987	12.6244	6.11871	8.49692	uncharacterized	LOC107440592				
140	confirmed record, no image		aug3.g1540.t1	-2.12479	0.767749	4.88252	1.76372	3.59224	0.265643	0.837376	0.599631	5kDa transglutaminase substra	LOC107446932				
141	confirmed record, no image		aug3.gl7108.t1	-2.42199	1	0.617977	0.894947	1.48783	0.064504	0.113495	0.012908	slit homolog 1 protein	LOC107443223	sli	FBgn0264089	Slit1	
142	confirmed record, no image		aug3.gl7419.t1	-0.81977	0.947974	53.6889	67.6348	103.847	51.0021	38.3651	15.7213	procollting enzyme	LOC107443723				
143	confirmed record, no image		aug3.gl0604.t2	-1.7102	1	2.68299	3.87419	4.7738	1.37887	0.753604	0.530478	roundabout homolog 3	LOC107451685	robo3	FBgn0041097	Robo3	
144	confirmed record, no image	Pt-gas1	aug3.gl7369.t1	-1.46001	1	3.17188	3.03509	3.9118	1.03296	0.768511	1.06144	plexin-B	LOC107443647	PlexB	FBgn0025740	Plxnb1	
145	confirmed record, no image	DNM1	aug3.gl2002.t1	-1.07274	1	43.9124	31.7893	72.8276	2.63435	5.13142	50.7042	dynamin-1	LOC107437058	shi	FBgn0003392	Dnm1	
146	confirmed record, no image	ADGRL1	aug3.g9493.t1	-1.36114	0.124131	17.7077	19.6023	23.4024	2.83642	2.12357	14.8107	tin G protein-coupled receptor L1 like		Ctrl	FBgn0033313	Adgrl1	
147	confirmed record, no image	ABHD11	aug3.g9729.t1	0.685449	1	121.01	111.047	165.001	2.41784	7.84246	208.627	ABHD11	LOC107440332	CG2059	FBgn0029942	Abhd11	
148	confirmed record, no image	unchar	aug3.gl6088.t1	-1.02345	1	124.81	101.517	125.008	3.99815	16.309	129.576	uncharacterized	LOC107441723	Mhc	FBgn0264695	Myh6	
149	confirmed record, no image	unchar	aug3.g2548.t1	-1.46243	1	153.386	127.628	190.931	7.26333	9.53109	129.785	uncharacterized	LOC107449036				
150	confirmed record, no image	VSP	aug3.g26402.t1	-1.74315	0.421406	31.2433	43.0442	66.5067	1.76803	2.22774	31.1016	henoloxidase-activating factor	LOC107438130	Spn27A	FBgn0028990		
151	confirmed record, no image	uncharacterize	aug3.gl5442.t1	-1.15186	1	85.8433	90.6343	187.608	9.69689	13.8428	111.736	uncharacterized	LOC107449520	CG9372	FBgn0036891	Ctrl	
152	confirmed record, no image	uncharacterize	aug3.g5051.t1	-0.67754	1	105.213	87.967	128.583	7.05381	11.9055	153.667	uncharacterized	LOC107452901				
153	confirmed record, no image	tolkin	aug3.g9878.t1	-7.47943	5.16E-16	23.0784	23.405	25.7585	0	0	0	kinesin heavy chain	LOC107452458	Khc	FBgn0001308	Kif5b	
154	confirmed record, no image		aug3.g23307.t1	-1.2437	0.679761	5.01317	5.56785	14.6762	0	1.27222	7.46322						
155	confirmed record, no image	Pt-fz	aug3.g794.t1	2.2603	0.045765	2.30387	1.28026	0.841656	5.71613	4.76607	8.57249	acepter subfamily 2 group E m	LOC107444665	tll	FBgn0003720	Nr2e1	
156	confirmed record, no image	Pt-echinoid	aug3.gl1787.t1	-1.70966	1	1.22897	1.23113	3.64864	0.464048	0.153799	0.709011						
157	confirmed record, no image		aug3.g886.t1	-2.96345	9.64E-06	8.75544	18.7517	25.7152	2.36049	1.04039	1.994	uncharacterized	LOC107444955				
158	confirmed record, no image	TSG101	aug3.g2715.t1	1.970227	0.003401	14.1035	14.11	14.7798	79.4779	42.8842	21.4115	tor susceptibility gene 101 prot	LOC107449345	TSG101	FBgn0036666	Tsg101	
159	record ambiguous, no record	KLC1	aug3.g65.t1	-2.83395	0.000239	11.2816	13.2683	12.4533	0.846084	1.07369	2.1328	kinesin light chain	LOC107440933	Klc	FBgn0010235	Klc1	
160	record ambiguous, no record		aug3.gl5130.t1	-1.45596	1	0.498026	0.256929	2.06231	0.174687	0.390449	0.07771	eneous nuclear ribonucleoprot	LOC107441220	sqd	FBgn0263396	Hnrnpab	
161	record ambiguous, no record		aug3.gl6957.t1	-0.77987	1	0.254848	0.584554	1.8152	0.082816	0.041641	1.02769	-type tyrosine-protein phospha	LOC107442968	CG42327	FBgn0259227	Ptprm	
162	record ambiguous, no record		aug3.gl7172.t1	-0.38254	1	276.307	296.579	387.268	214.091	187.249	219.083	uncharacterized	LOC107443364	Gig1	FBgn0264561	Gig1	
163	record ambiguous, no record	ABHD11	aug3.g9721.t1	-2.16372	0.002446	10.2488	13.8746	16.5719	0.04751	0.209117	7.08713	uncharacterized	LOC107440239	CG2059	FBgn0029942	Abhd11	
164	record ambiguous, no record	ABHD11	aug3.g3607.t1	0.376729	1	44.9968	42.7181	44.4766	1.84656	7.19855	141.951	ABHD11	LOC107450788	CG2059	FBgn0029942	Abhd11	
165	record ambiguous, no record	FMO5	aug3.gl5065.t1	-1.25058	1	25.0404	33.2285	37.4923	1.57301	2.0157	30.8959	tin-containing monooxygenase	LOC107441124	Fmo-1	FBgn0034943	Fmo5	
166	record ambiguous, no record	uafA	aug3.gl0890.t1	-1.11119	1	17.9442	22.657	26.009	0.65366	1.35465	24.3462	uncharacterized	LOC107455578	Muc68D	FBgn0036203	DSPP	
167	record ambiguous, no record	uncharacterize	aug3.g25745.t1	-1.9396	0.191919	19.7533	21.2815	68.2637	1.39399	1.58438	19.4991	uncharacterized	LOC107452735	dyl	FBgn0066365	Foxe3	
168	lack image at stage 4	ac	aug3.g27206.t1	-2.00383	0.006209	23.1665	33.6478	31.9559	1.59524	2.34504	14.7776	achaete-scute homolog 1a	LOC107441129	ac	FBgn0000022	Ascl1	
169	lack image at stage 4	eS7_SB_047_C01_S01	aug3.gl2111.t1	-0.41894	1	95.9222	75.9229	87.9744	50.5105	35.0709	81.2352	5'-monophosphate dehydroge	LOC107437200	ras	FBgn0003204	Impdh2	
170	lack image at stage 4	eS7_SB_008_B12	aug3.gl5926.t1	1.644238	1	0.15231	0.073561	0.042536	0.844264	0.569285	0.015834	nslation initiation factor IF-2-li	LOC107455051	mIF2	FBgn0039588	Mtif2	
171	lack image at stage 4	g7720	aug3.g7720.t1	-0.04734	1	24.5999	14.3951	22.5805	15.1793	21.5637	13.2372	-activating protein complex su	LOC107455388	Pbp49	FBgn0260398	Snapc3	
172	no record or image	uncharacterized	aug3.g5565.t1	-2.27745	0.000592	42.7284	59.7096	69.2987	2.45718	5.30616	22.0832	chitin deacetylase 1	LOC107450739	Cda4	FBgn0052499		
173	no record or image	uncharacterized	aug3.gl0660.t1	-0.72693	1	30.679	32.0208	44.4655	2.28052	2.29988	50.7459	uncharacterized	LOC107452336	Muc68D	FBgn0036203		
174	no record or image	uncharacterized	aug3.gl1980.t1	-1.5244	1	24.4885	30.3886	152.971	1.86186	1.91125	51.6718	uncharacterized	LOC107437022				
175	no record or image	uncharacterized	aug3.g1984.t1	-1.33218	1	25.3002	41.3975	50.2211	1.99526	2.61898	34.8398	uncharacterized	LOC107447898				
176	no record or image	uncharacterized	aug3.g20358.t1	-1.24365	1	21.4884	31.0126	40.6628	1.25855	2.01923	30.002	uncharacterized	LOC107448555	Taf6	FBgn0010417	Taf6	
177	no probe	ABHD11 like	aug3.g23929.t2	0.666223	1	56.3648	4.16871	6.37961	0.99108	2.80028	60.3186	protein ABHD11-like	LOC107455206	CG2059	FBgn0029942	Abhd11	
178	no probe	uncharacterized	aug3.gl8398.t1	-0.99421	1	45.061	47.243	52.4916	2.17775	3.60769	57.3075	uncharacterized	LOC107445227				
179	no probe	uncharacterized	aug3.gl0678.t1	-1.15101	1	44.0664	42.9669	64.5681	2.54368	3.58458	51.8272	uncharacterized	LOC107452912				
180	no probe		aug3.g9057.t1	-0.10834	1	2.76714	4.53682	5.08091	1.71783	2.37811	5.50166						
181	no probe	"no colony"	aug3.g23072.t1	-2.47613	1	0.289025	0	1.57382	0	0	0						
182	no probe	24% uncharacterized	aug3.gl4077.t1	-0.48185	1	18.1456	23.1925	15.2283	1.09774	1.97555	33.0155	uncharacterized	LOC107439825				
183	no probe	aos /EGFR	aug3.g839.t1	1.61042	0.224217	1.66623	1.43817	4.85687	10.0589	9.901	1.10108	protein giant-lens	LOC107444844	aos	FBgn0004569		
184	no probe	gas	aug3.g9575.t1	-1.8757	0.004537	12.7366	16.1423	16.9972	2.14527	2.25118	5.83491	rowth arrest-specific protein 1	LOC107438015	Gas8	FBgn0029667	Gas1	
185	published, no aut number	Oda-20															
186	published, no aut number	Oda-21															
187	published, express at other stages	ina															
188	published, express at other stages	sim															
189	published, express at other stages	omb															
190	published, express at other stages	en															
191	published, express at other stages	pros															
192	published, express at other stages	hairy															
193	published, express at other stages	dfd															
194	published, express at other stages	Lab															
195	published, express at other stages	msx															
196	published, express at other stages	gas1															
197	published, express at other stages	frizzled 4															
198	published, express at other stages	Ap2-A															
199	published, express at other stages	BarH1															
200	published, express at other stages	mirr4															
201	published, express at other stages	osr-B															
202	published, express at other stages	rhomboid															
203	published, express at other stages	RTP-B															
204	published, express at other stages	cad	aug3.gl2643.t1	0.267064	1	0.042226	0.109083	0.066375	0.049481	0.041446	0.197982	caudal type homeobox (cad)		cad	P09085	Cdx1	
205	publishted, express at stage 4	beta-catenin															
206	publishted, express at stage 4	cleavage caspase 3															
207	publishted, express at stage 4	pMad															
208	publishted, express at stage 4	PH3															
209	publishted, express at stage 4	actin															
210	publishted, express at stage 4	phallodin															
211	publishted, express at stage 4	NPC															
212	publishted, express at stage 4	alpha tubulin															
213	publishted, express at stage 4	beta-tubulin															

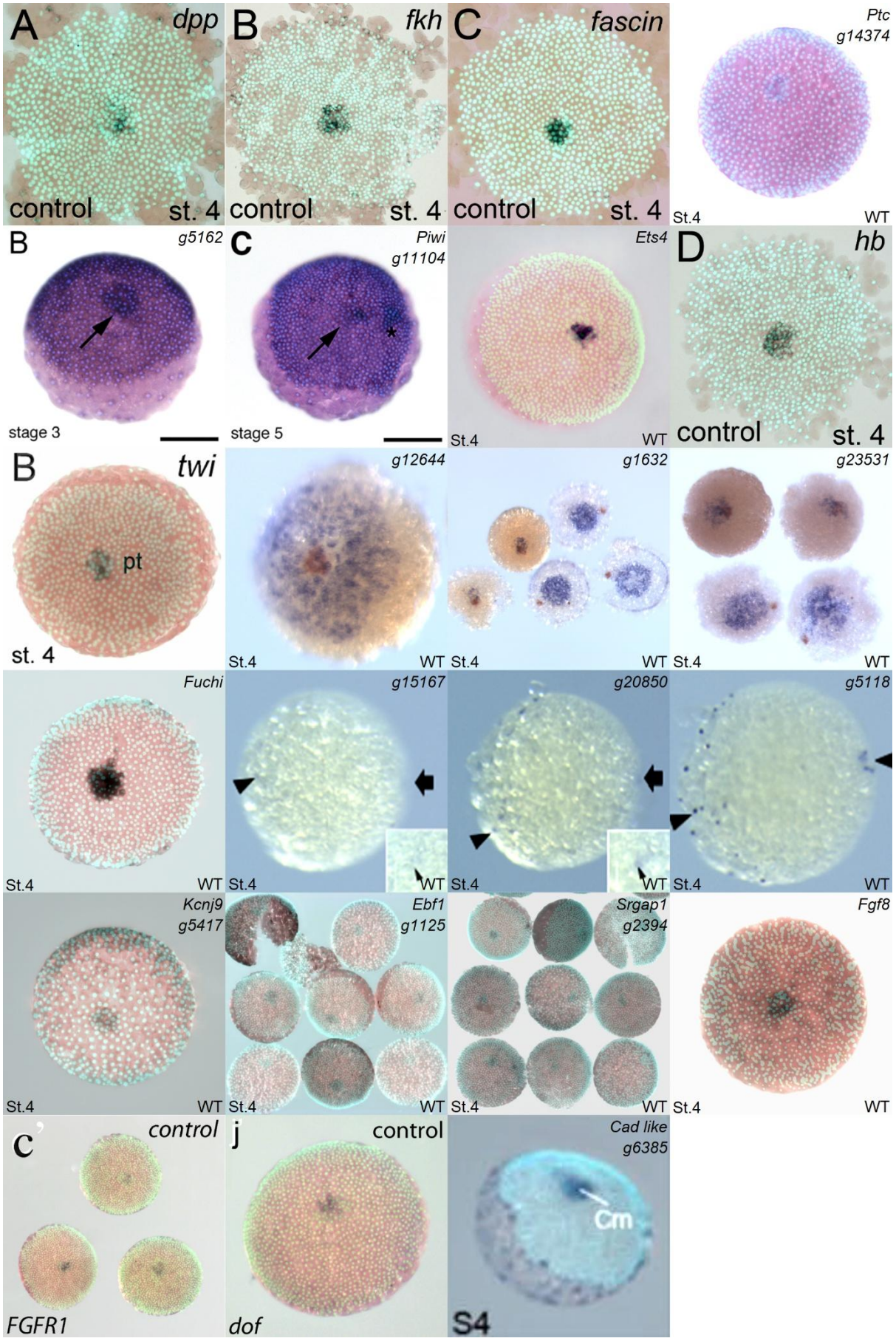
A
dpp
control
st. 4
B
fkh
control
st. 4
C
fascin
control
st. 4
Ptc
g14374
St.4
WT
B
g5162
stage 3
C
Piwi
g11104
stage 5
Ets4
St.4
WT
D
hb
control
st. 4
B
twi
pt
st. 4
g12644
St.4
WT
g1632
St.4
WT
g23531
St.4
WT
Fuchi
St.4
WT
g15167
St.4
WT
g20850
St.4
WT
g5118
St.4
WT
Kcnj9
g5417
St.4
WT
Ebf1
g1125
St.4
WT
Srgap1
g2394
St.4
WT
Fgf8
St.4
WT
c'
control
FGFR1
j
control
dof
Cad like
g6385
Cm
S4

Figure S3-1. Published expression of genes in primary thickening region at stage 4. These include: *dpp, fkh* (Oda et al., 2003), *fascin* (Oda et al., 2006), *ptc* (Oda et al., 2010), *vasa, piwi* (Schwager et al., 2015), *Ets4*, *twist, hb* (Pechmann et al., 2017), *g12644, g1632, g23531* (Oda et al., 2019), *Fuchi* (Iwasaki-Yokozawa et al., 2022), *g15167, g20850, g5118, Kcnj9, Ebf1, Srgap1* (Oda et al., 2022), *Fgf8, Fgfr1, Dof* (Wang et al., 2023), and *Cad-like* (Leite et al., 2024). Mostly with the original published images. New in situ hybridization were generated for *Ets4*, *Kcnj9, Ebf1, Srgap1*, and *Fgf8*.

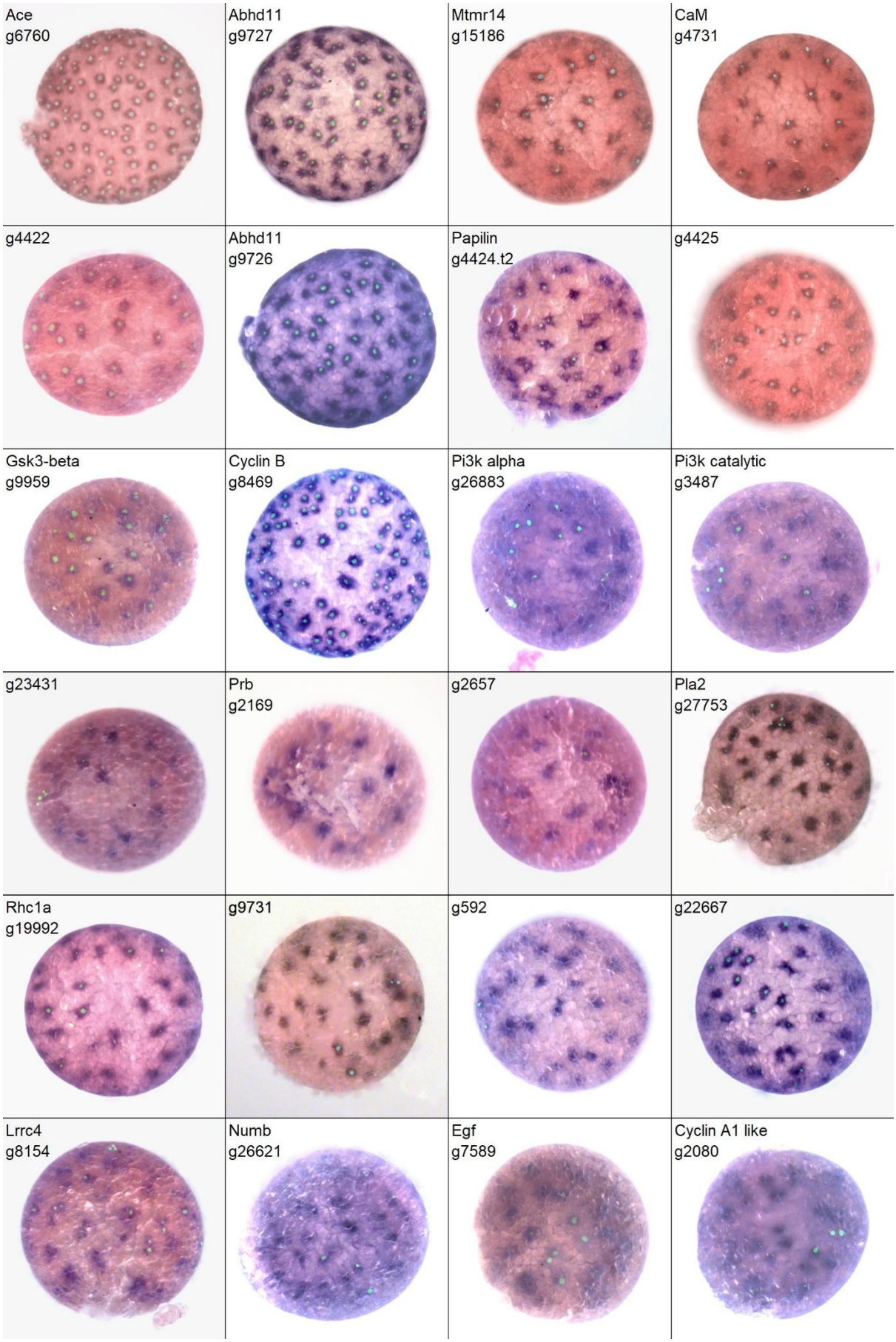
Ace
g6760
Abhd11
g9727
Mtmr14
g15186
CaM
g4731
g4422
Abhd11
g9726
Papilin
g4424.t2
g4425
Gsk3-beta
g9959
Cyclin B
g8469
Pi3k alpha
g26883
Pi3k catalytic
g3487
g23431
Prb
g2169
g2657
Pla2
g27753
Rhc1a
g19992
g9731
g592
g22667
Lrrc4
g8154
Numb
g26621
Egf
g7589
Cyclin A1 like
g2080

Figure S3-2. Expression of genes at stage 2 (a). Genes includes: *Ace, Abhd11 g9727, Mtmr14, CaM, g4422, Abhd11 g9726, Papilin (g4424), g4425, Gsk3-beta g9959, Cyclin B, Pi3k alpha g26883 (Pik3r1), Pi3k catalytic (Pik3c3 g3457), g23431 (Phb1), Ptprb g2169, g2657, Pla2, Rhc1a, g9731, g592, g22667, Lrrc4 (Anxa1), Numb, Egf (Creld2 g7589), Cyclin A1.*

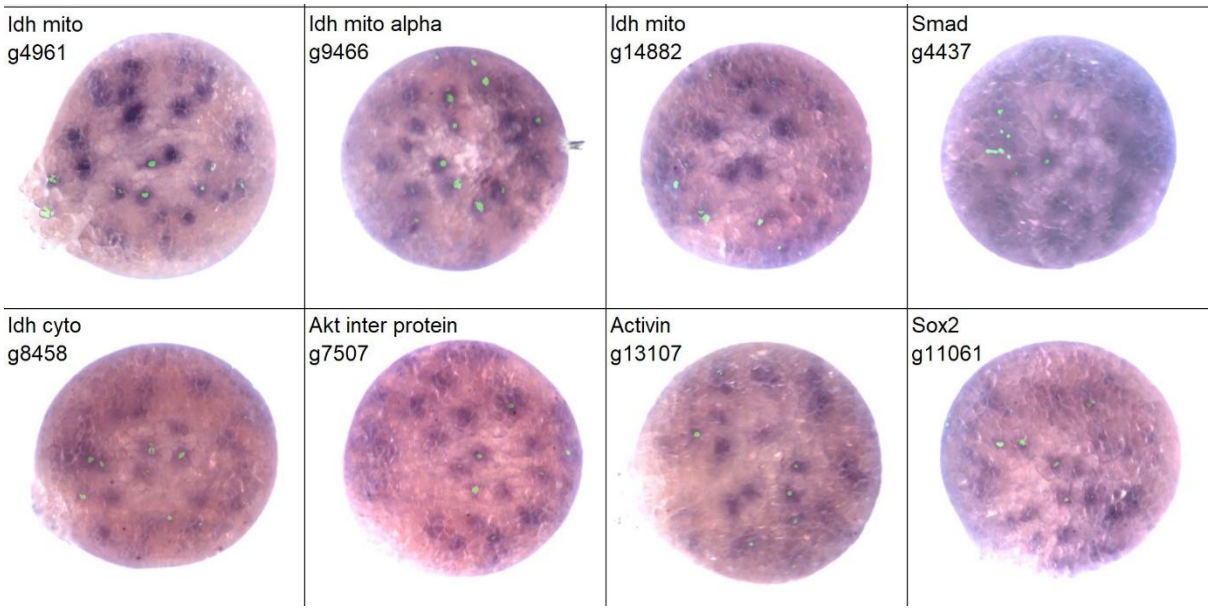

Figure S3-3. Expression of genes at stage 2 (b). Genes includes: *Idh g4961 (Idh2), idh g9466 (Idh3a), Idh g14882 (Idh3g), Smad (Snip1), Idh g8458 (Idh1), Aktip, Activin (Asph), Sox2.*

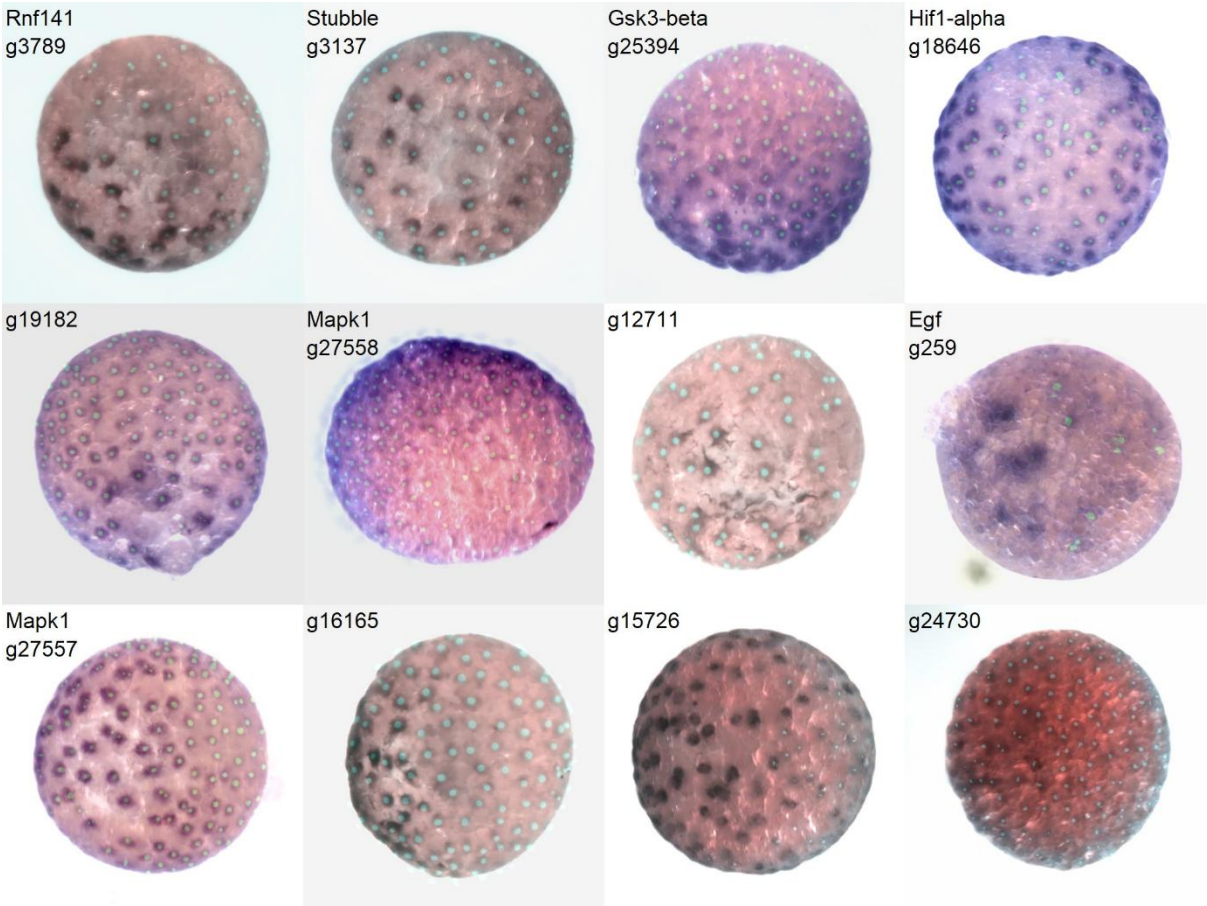

Figure S3-4. Expression of genes at stage 2 (c). Genes includes: *Rnf141(g3789), Stubble (Ppaf2), Gsk3-beta, Hif1a, g19182, Mapk1 g27558, g12711 (Incenp), Egf g259 (Creld1), Makp1 g27557, g16165, g25726, g24730 (Ptprk)*.

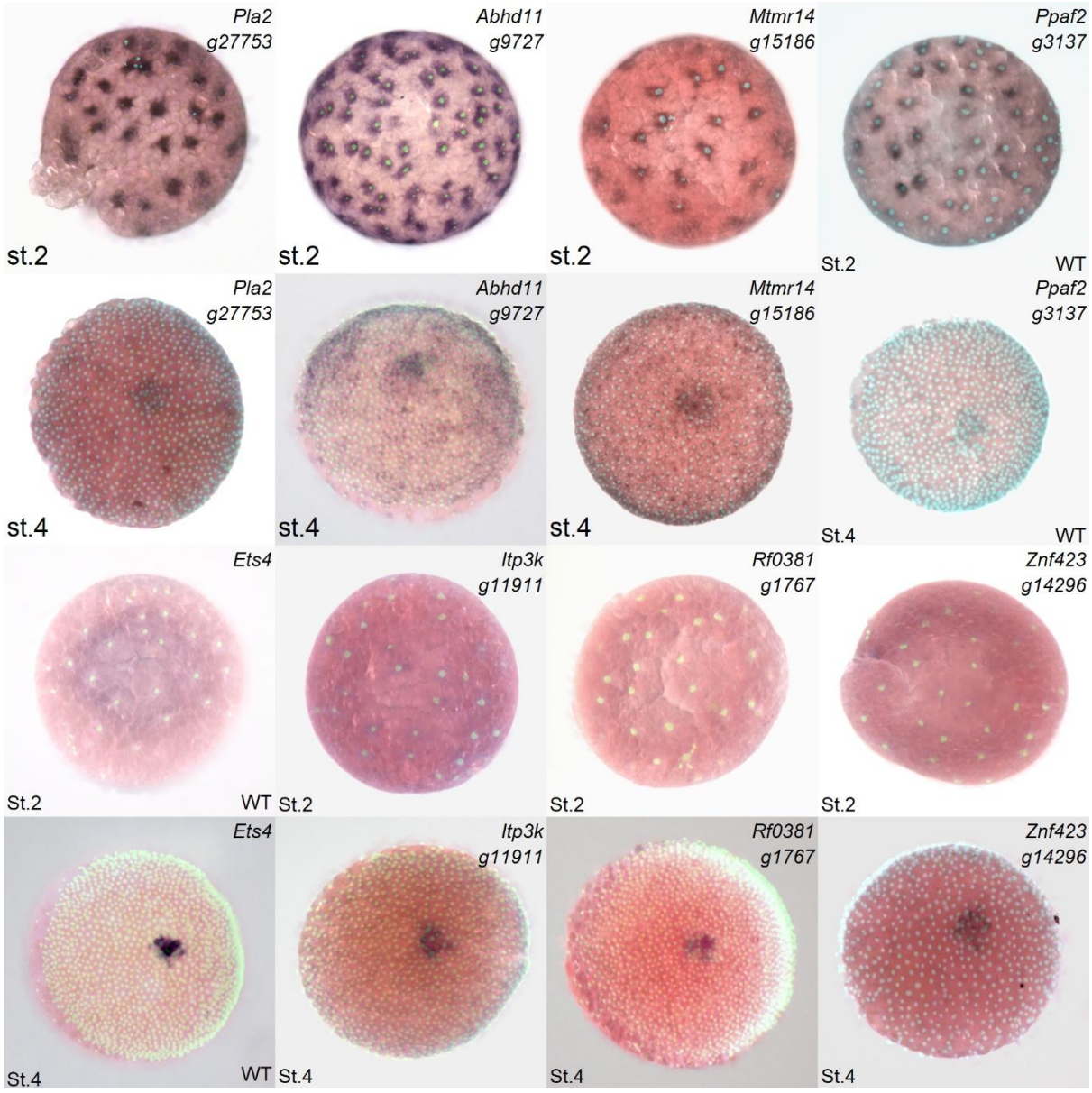

Figure S3-5. Comparison of gene expression at stages 2 and 4 in WT embryos shows that *Pla2, Abhd11, g9727, Mtmr14,* and *Ppaf2* exhibit specific staining at stage 2, while *Ets4*, *Itp3k (Itpka), Rf_0381*, and *Znf423* show no expression at this stage. The former four genes were expressed in both the primary thickening region and other germ disc cells at stage 4, while the latter four genes are confined to the staining in the region of the primary thickening at stage 4. Sytox/brightfield overlay

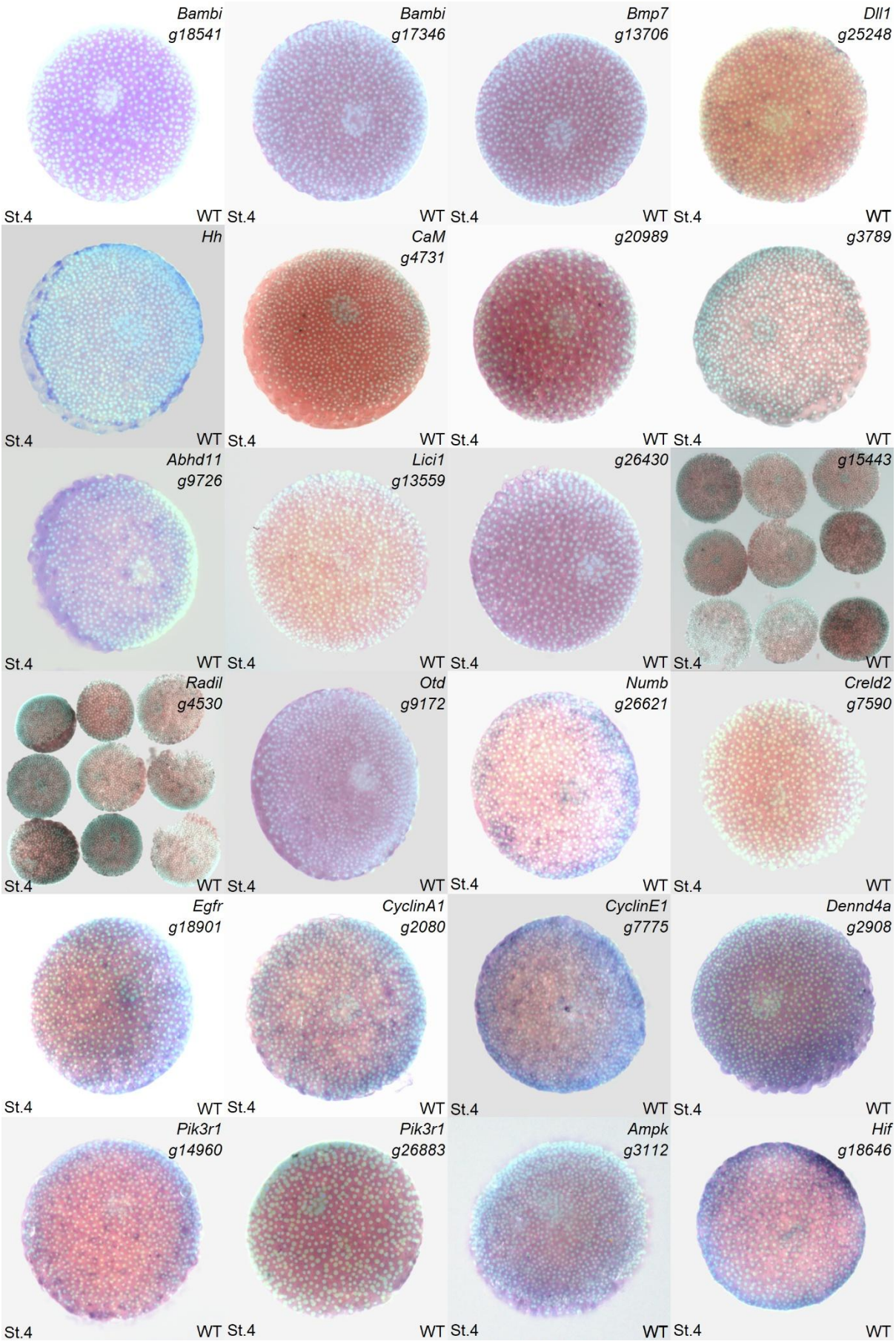
Bambi
g18541
St.4
WT
Bambi
g17346
St.4
WT
Bmp7
g13706
St.4
WT
Dll1
g25248
St.4
WT
Hh
St.4
WT
CaM
g4731
St.4
WT
g20989
St.4
WT
g3789
St.4
WT
Abhd11
g9726
St.4
WT
Lici1
g13559
St.4
WT
g26430
St.4
WT
g15443
St.4
WT
Radil
g4530
St.4
WT
Otd
g9172
St.4
WT
Numb
g26621
St.4
WT
Creld2
g7590
St.4
WT
Egfr
g18901
St.4
WT
CyclinA1
g2080
St.4
WT
CyclinE1
g7775
St.4
WT
Dennd4a
g2908
St.4
WT
Pik3r1
g14960
St.4
WT
Pik3r1
g26883
St.4
WT
Ampk
g3112
St.4
WT
Hif
g18646
St.4
WT

Figure S3-6. In situ hybridization images of genes without specific staining in the primary thickening region at stage 4 in WT embryos (a). Genes shown: *Bambi g18541, Bambi g17346, Bmp7, delta, hh, CaM, g20989, g3789, Abhd11 g9726, Lici1, g26430, g15443, Radil, Otd, Numb, Creld2 g7590, Egfr, Cyclin A1, Cyclin E1, Dennd4a, Pik3r1 g14960, Pik3r1 g26883, Ampk, Hif*.

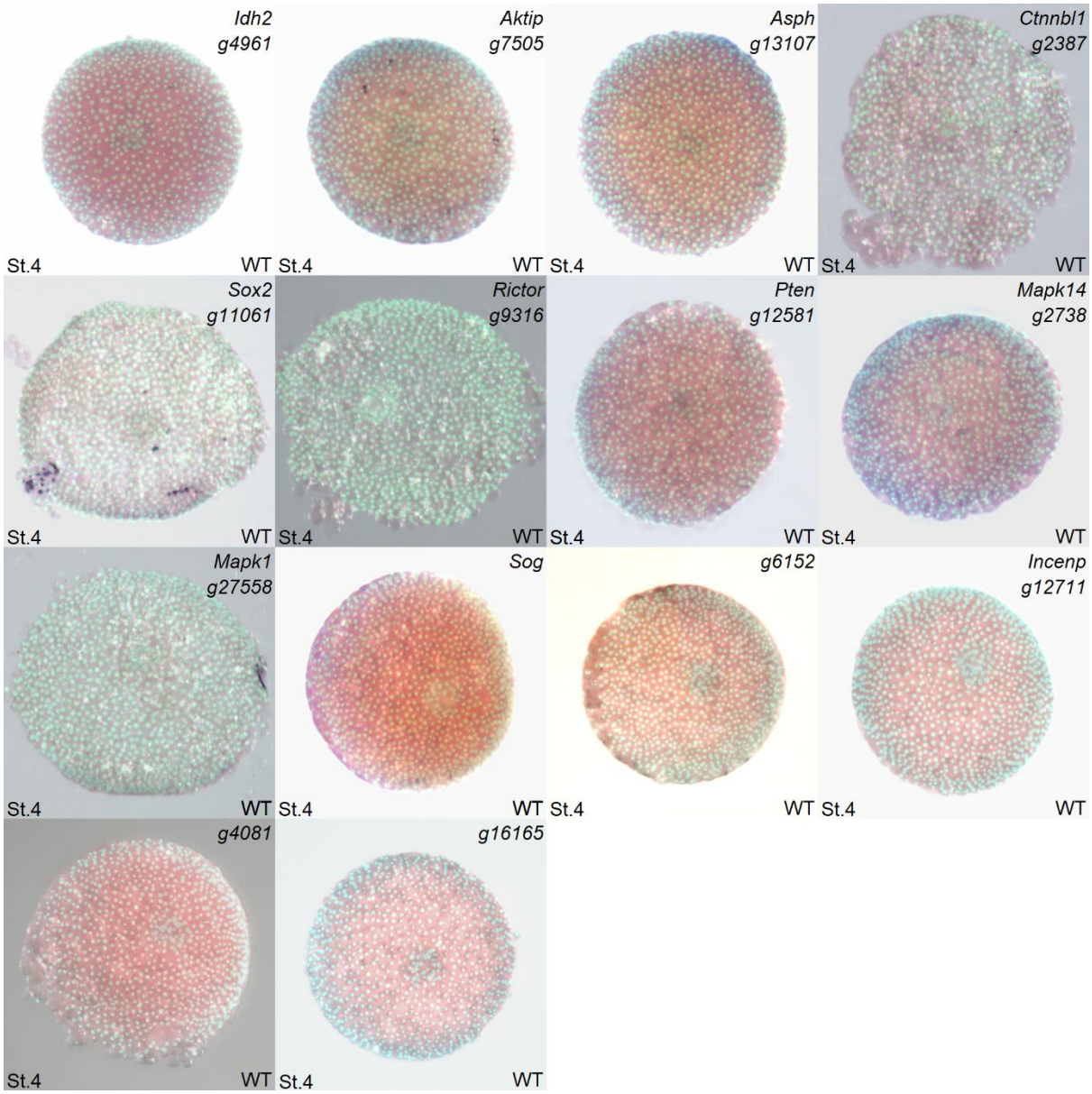

Figure S3-7. In situ hybridization images of genes without specific staining in the primary thickening region at stage 4 in WT embryos (b). Genes shown: *Idh2, Akitp, Asph, Ctnnbl1, Sox2, Rictor, Pten, Mapk14, Mapk1 g27558, Sog, g6152, Incenp, g4081, g16165*.

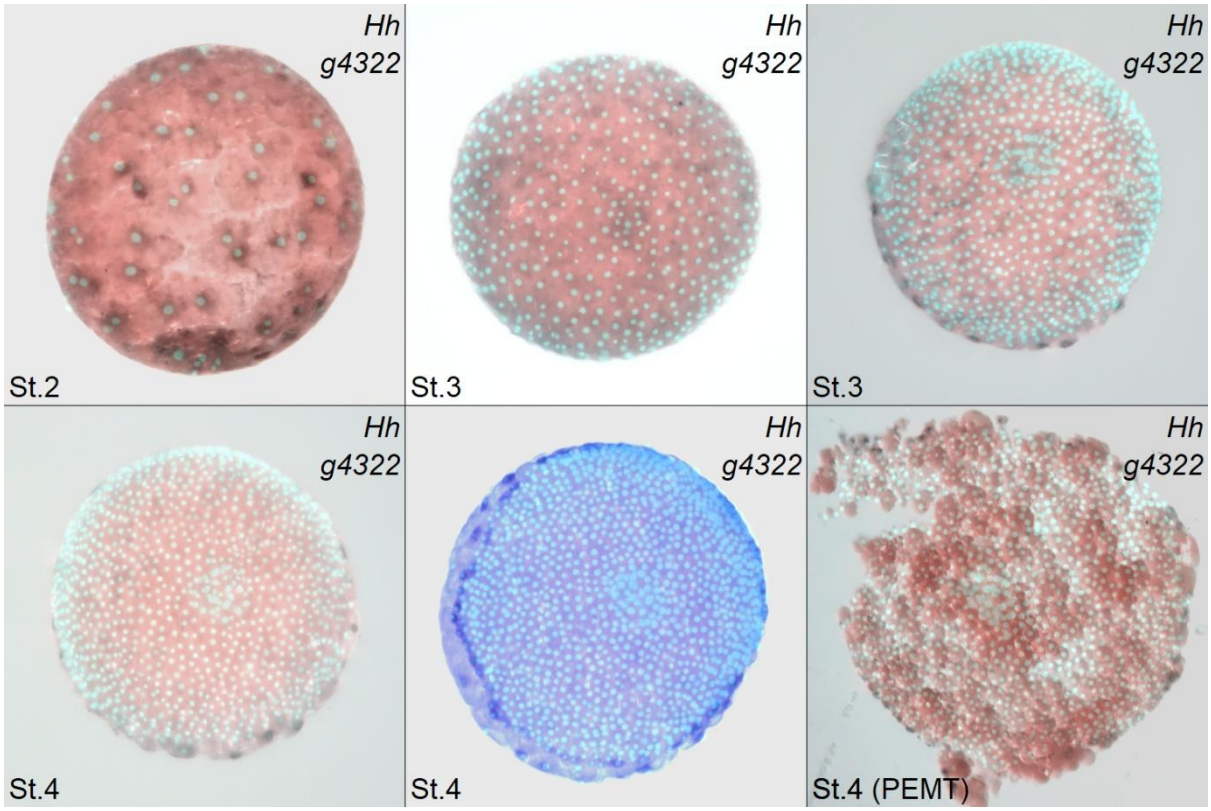

Figure S3-8. In situ hybridization image of *hh* at st.2,3,4 in WT embryos

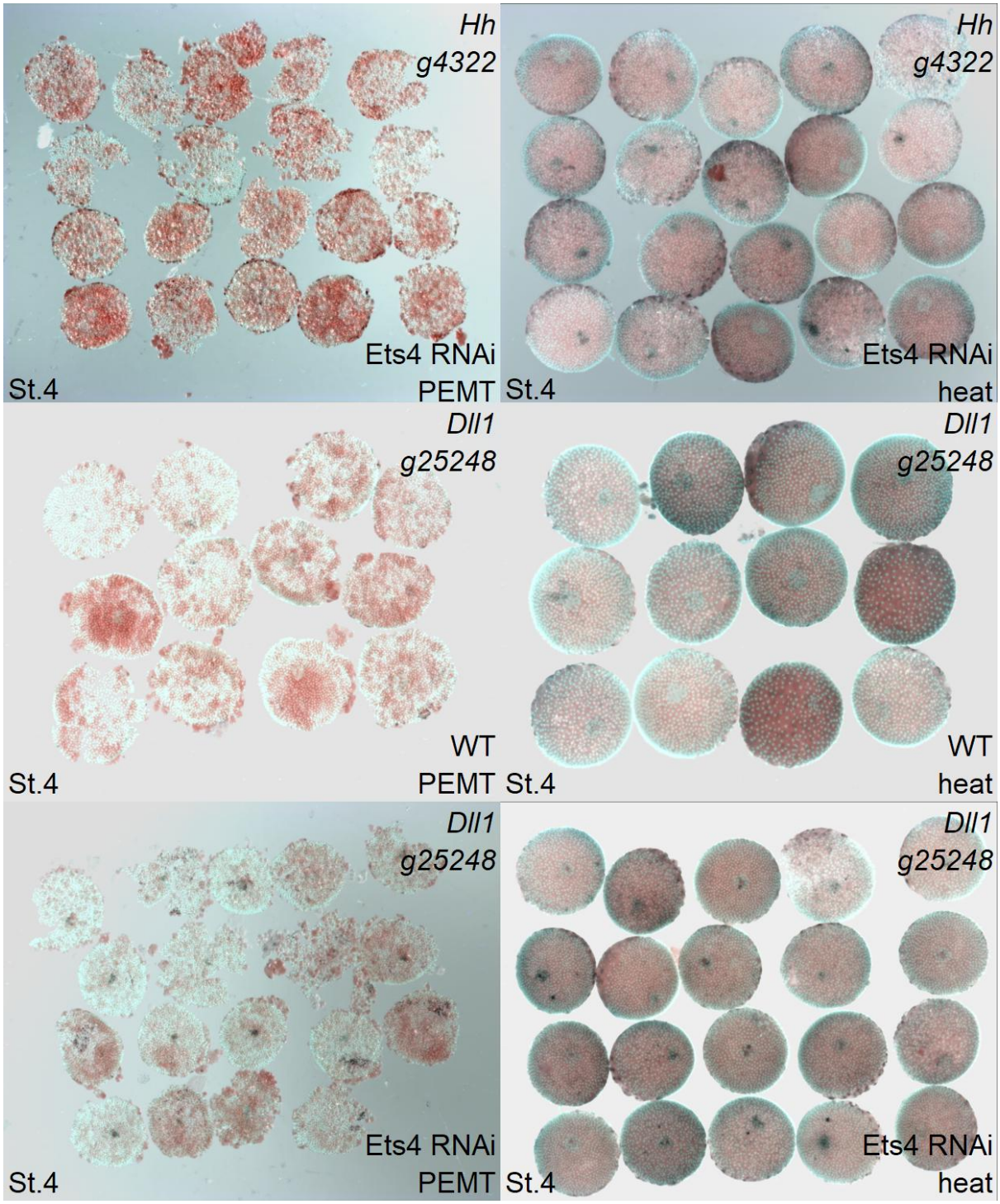

Figure S3-9. Expression of *hh* and *delta* in WT and Ets4 RNAi embryos at stage 4, with different method of fixation.

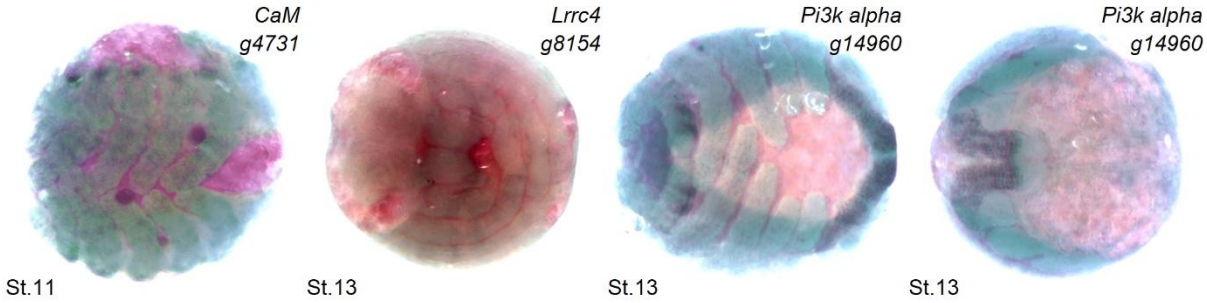

Figure S3-10. In situ hybridization image of genes at stage 9-13, which show expression in the appendages. Annotation. Gene list*: CaM, Lrrc4 (Anxa1), Pi3k g14960 (Pik3r1)*.

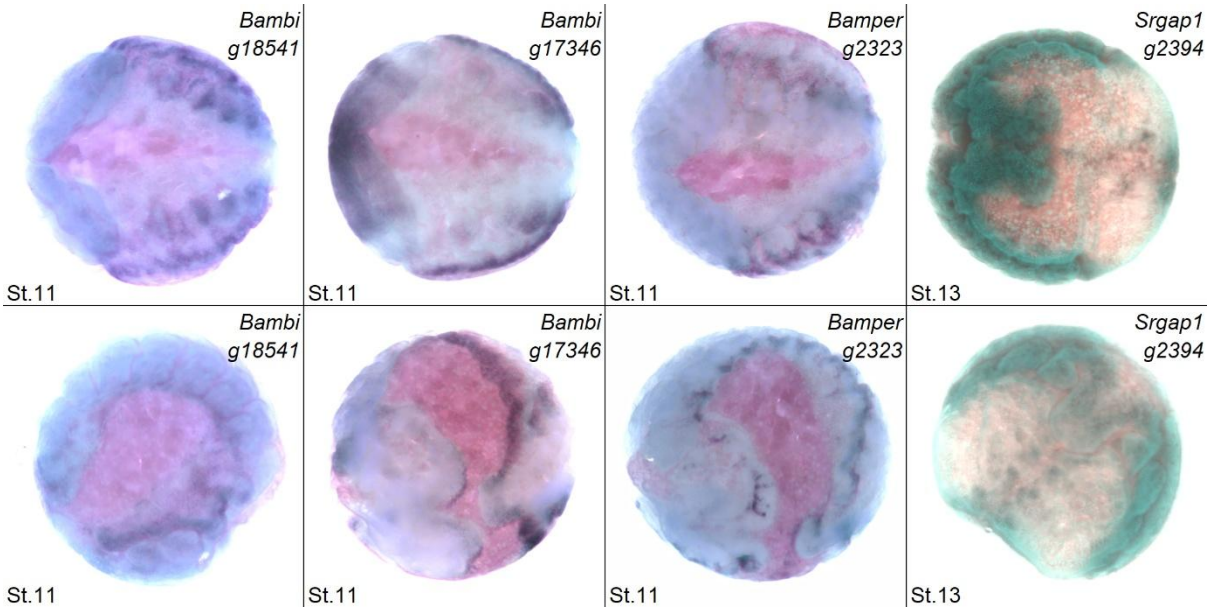

Figure S3-11. In situ hybridization image of genes at stage 9-13, which show expression in the dorsal region. Annotation. Gene list: *Bambi g18541, Bambi g17346, cv-2, Srgap1*.

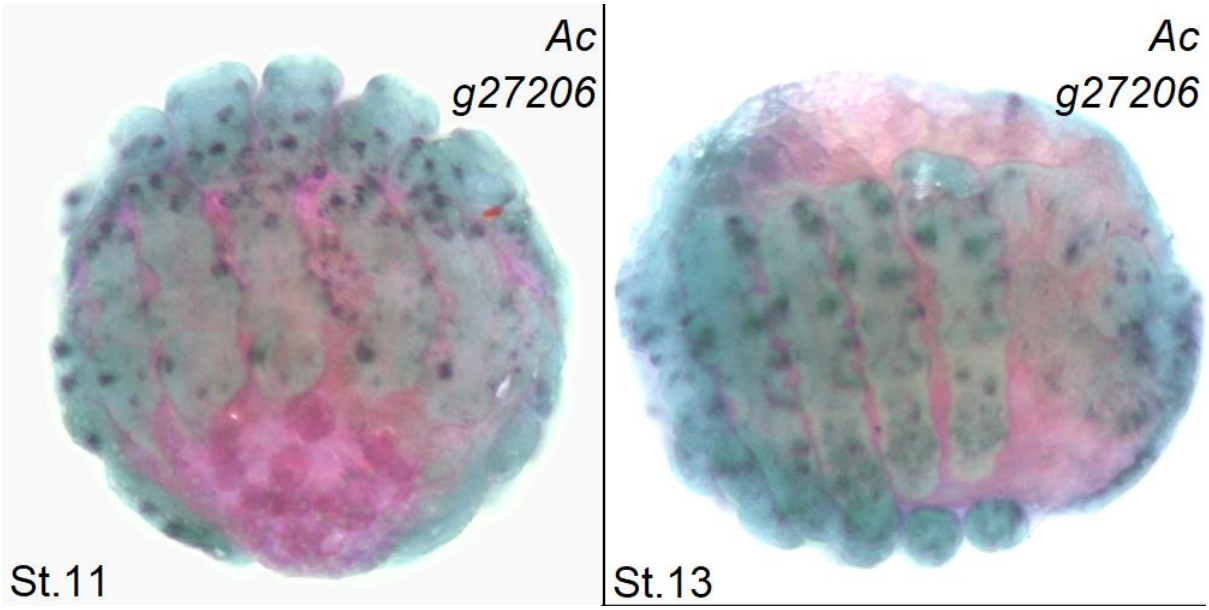

Figure S3-12. In situ hybridization image of *Ac* at stage 10-12. The gene show expression in the shape of dots.

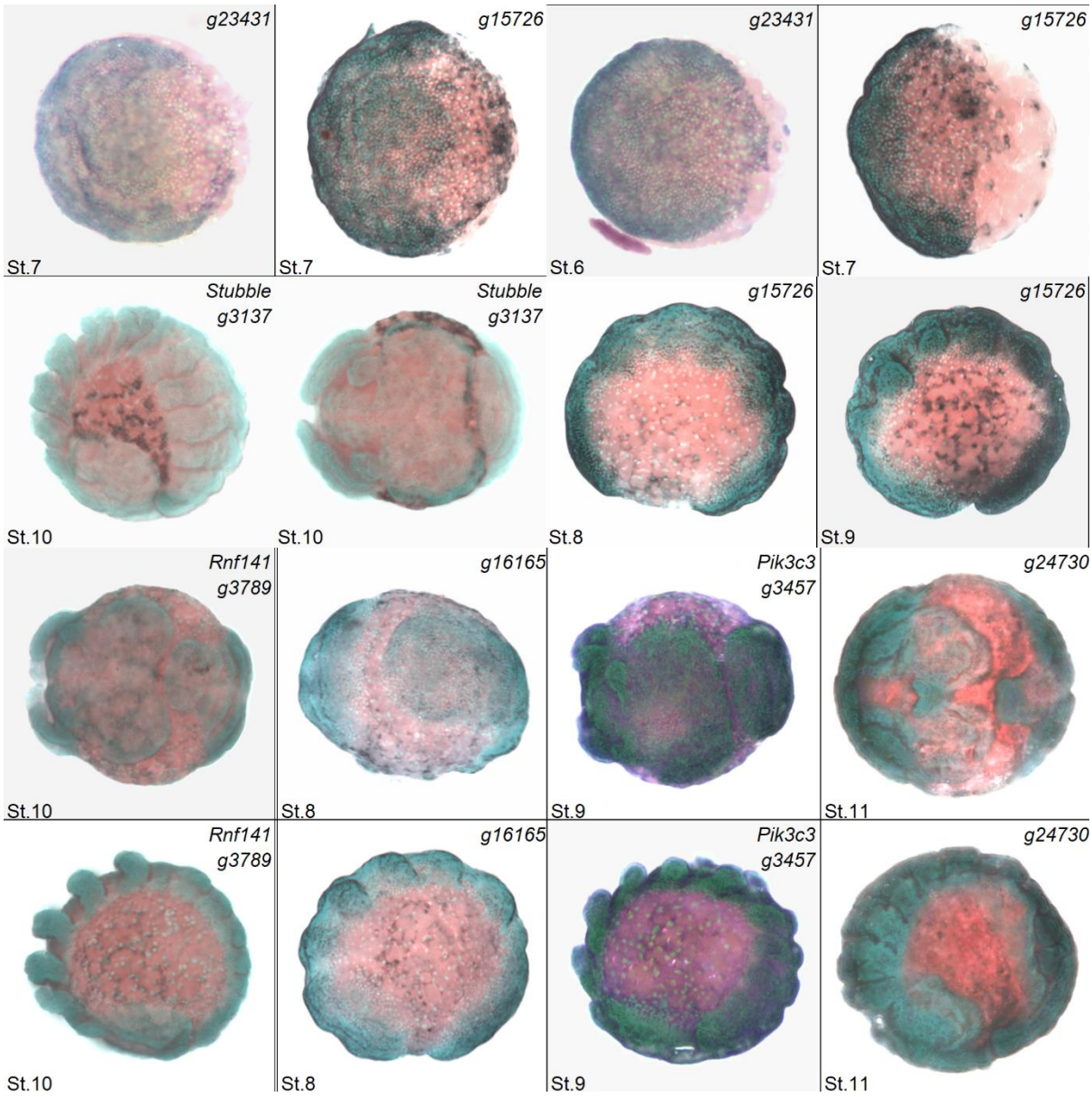

Figure S3-13. In situ hybridization image of genes at stage 6-13, which show expression in the extraembryonic region. Annotation. Gene list: *g23431 (Phb1), g15726 (Gpcpd1), Stubble (Ppaf2), Rnf141 (g3789), g16165, Pik3c3 g3457, g24730 (Ptprk)*.

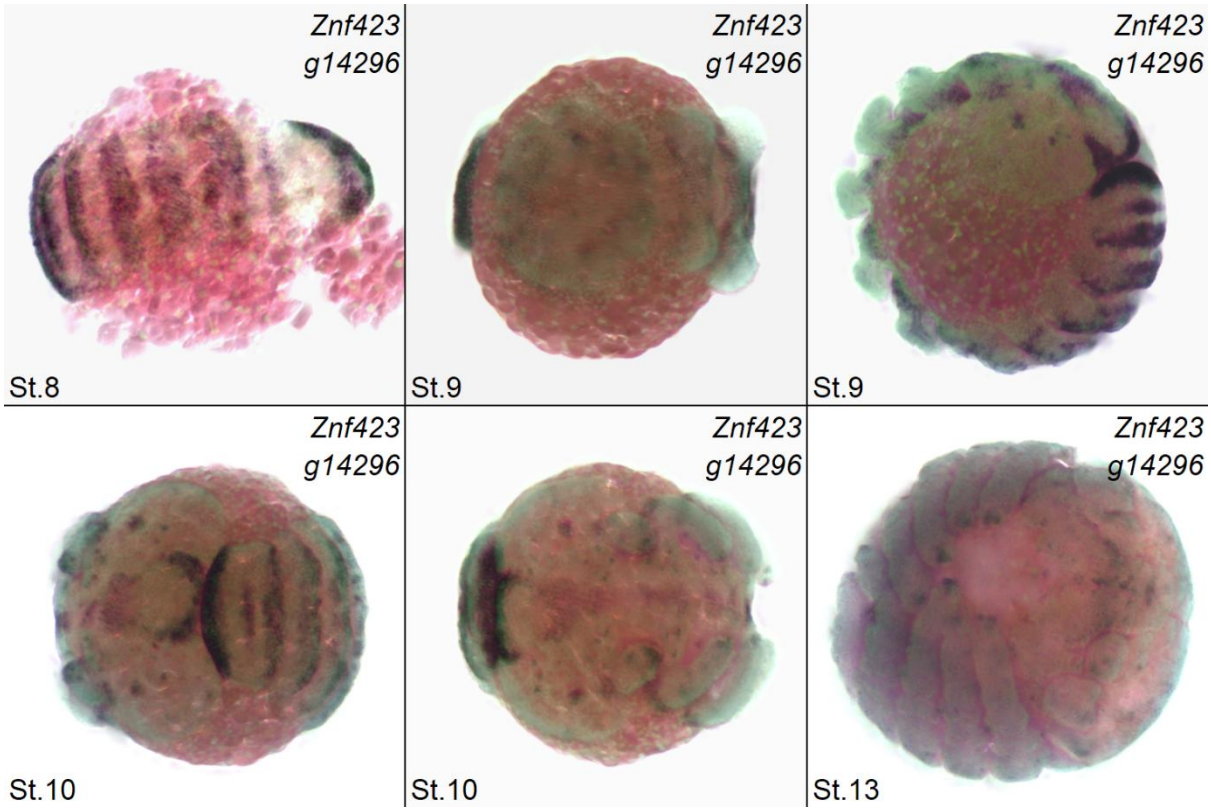

Figure S3-14. In situ hybridization image of Znf423 at stage 8, 9, 10, 13. The gene show expression in segments.

Table S3-2 Comparison of gene expression in primary thickening of WT and Ets4 RNAi embryos, from in situ hybridization and RNAseq reads (113 genes).

Number	Gene	Name	Expression in WT (in situ)	Expression in Ets4 RNAi (in situ)	Expression in WT (RNAseq)	Expression in Ets4 RNAi (RNAseq_S13, S14)	Two judgements in WT	Two judgements in Ets4 RNAi
1	Bmp-1	aug3.g18541.t1	N		N		NN	
2	Bmp-2	aug3.g17346.t1	N		N		NN	
3	cv-2	aug3.g2323.t1	Y	N	weak	N	YY	NN
4	60A/BMP7	aug3.g13706.t1	N		Y		NY	
5	DLL1	aug3.g25248.t1	N	Y	Y	Y	NY	YY
6	Ets4	aug3.g4238.t1	Y	N	Y	N	YY	NN
7	Fgfr	aug3.g26565.t1	Y	N	Y	N	YY	NN
8	fuchi	aug3.g26874.t1	Y	Y	Y	Y	YY	YY
9	hh	aug3.g4322.t1	N	Y	weak	Y	NN	YY
10	phospholipase A2	aug3.g27753.t1	Y	N	Y	N	YY	NN
11	acetylcholinesterase-1	aug3.g6760.t1	Y		Y		YY	
12	kinesin heavy chain	aug3.g5179.t2	Y		Y		YY	
13	ABHD11	aug3.g9727.t1	Y	N	Y	Y	YY	NY
14	myotubularin	aug3.g15186.t1	Y	Y	Y	Y	YY	YY
15	calumenin	aug3.g4731.t1	N		Y		NY	
16	E3 ubiquitin ligase	aug3.g19992.t1	Y		Y	?	YY	
17	psitol-trisphosphate 3-kina	aug3.g11911.t1	Y	N	Y	N	YY	NN
18	tein lethal(2)essential for	aug3.g14129.t1	Y	N	Y	Y	YY	NY
19	ankyrin repeat protein R	aug3.g1767.t1	Y	N	Y	N	YY	NN
20	itophagy related protein 8	aug3.g18439.t1	Y		Y		YY	
21	tally-regulated GTP-bindi	aug3.g23069.t1	Y		Y		YY	
22	nc finger protein ZIC 4-lil	aug3.g12202.t1	Y	N	Y	N	YY	NN
23	1cad gene for Pt1-cadher	aug3.g20989.t1	N		Y	?	NY	
24	inc finger protein 423-like	aug3.g14296.t2	Y	N	Y	N	YY	NN
25	RING finger protein 141-	aug3.g3789.t1	N		Y		NY	
26	erized/? flocculation prote	aug3.g4422.t1	Y	Y	Y	Y	YY	YY
27	uncharacterized	aug3.g9731.t1	Y	N	Y	Y	YY	NY
28	uncharacterized	aug3.g592.t1	Y	Y	Y	Y	YY	YY
29	uncharacterized	aug3.g22667.t1	Y	Y	Y	Y	YY	YY
30	patched-like	aug3.g14374.t2	Y	N	Y	N	YY	NN
31	Wnt-8b-like	aug3.g5617.t2	Y	N	Y	N	YY	NN
32	ABHD11	aug3.g9726.t1	N		Y		NY	
33	stubble like	aug3.g3137.t1	Y		Y		YY	
34	-rich repeat-containing pr	aug3.g8154.t1	Y	N	Y	N	YY	NN
35	serpin B6-like	aug3.g13559.t1	N	N	Y	N	NY	NN
36	uncharacterized	aug3.g15602.t1	N		Y		NY	
37	papilin	aug3.g4424.t2	Y	N	Y	N	YY	NN
38	uncharacterized	aug3.g4425.t1	Y		Y		YY	
39	tivated chloride channel	aug3.g11056.t2	Y	N	Y	N	YY	NN
40	cterized LOC107438215,	aug3.g26430.t1	N		Y		NY	
41	ted inward rectifier potas	aug3.g5417.t1	Y		Y		YY	
42	cterized/transcription fact	aug3.g1125.t1	Y		Y		YY	
43	O Rho GTPase-activating	aug3.g2394.t2	Y		Y		YY	
44	uncharacterized	aug3.g15443.t1	N		weak		NN	
45	uncharacterized	aug3.g4530.t1	N		weak		NN	
46		aug3.g9172.t1	N		N		NN	
47		aug3.g26621.t1	N	N	N	N	NN	NN
48	cytein riched EF like dor	aug3.g259.t1	Y	Y	weak	N	YY	YN
49	cytein riched EF like dor	aug3.g7589.t1	Y	Y	weak	N	YY	YN
50	cytein riched EF like dor	aug3.g7590.t1	N	N	N	N	NN	NN
51		aug3.g18901.t1	N	N	N	N	NN	NN
52		aug3.g9959.t1	Y	Y	Y	Y	YY	YY
53		aug3.g25394.t1	Y	Y	Y	N	YY	YN
54		aug3.g2080.t1	N	N	Y	Y	NY	NY
55		aug3.g8469.t1	Y	Y	Y	Y	YY	YY
56	G1/S-specific cyclin-E1	aug3.g7775.t1	N		Y		NY	
57		aug3.g11601.t1	Y		Y		YY	
58		aug3.g26862.t1	Y		Y		YY	
59	yc promoter binding prote	aug3.g2908.t1	N		N		NN	
60	3K_regulatory subunit alp	aug3.g14960.t2	N		N		NN	
61	3K_regulatory subunit alp	aug3.g26883.t1	N	N	weak	N	NY	NN
62	3K_catalytic subunit type	aug3.g3457.t1	Y	Y	Y	Y	YY	YY
63		aug3.g3112.t1	N	N	Y	N	NY	NN
64		aug3.g18646.t1	N	Y	N	N	NN	YN
65	IDH mitochondra	aug3.g4961.t1	N	Y	Y	Y	NY	YY
66	mitochondra alpha prob	aug3.g9466.t1	Y		Y		YY	
67	mitochondria beta or gar	aug3.g14882.t1	Y	Y	Y	Y	YY	YY
68	mitochondria beta or gar	aug3.g20634.t1	Y		Y		YY	
69		aug3.g4437.t1	Y	Y	Y	Y	YY	YY
70	IDH cytoplasmic	aug3.g8458.t1	Y	Y	Y	N	YY	YN
71	AKT-interacting protein	aug3.g7505.t1	N	N	Y	Y	NY	NY
72	activin_ASPH	aug3.g13107.t1	N	Y	weak	N	NN	YN
73	beta-cat	aug3.g2387.t1	N		Y		NY	
74		aug3.g11061.t1	N	N	N	N	NN	NN
75		aug3.g9226.t1	Y	Y	Y	Y	YY	YY
76		aug3.g4339.t1	Y	Y	Y	N	YY	YN
77	n-independent protein kir	aug3.g19182.t1	Y	Y	Y	N	YY	YN
78		aug3.g25455.t1	Y		Y		YY	
79	mTOR related	aug3.g9316.t2	N		weak		NN	
80		aug3.g12581.t1	N		N		NN	
81		aug3.g2738.t1	N		N		NN	
82		aug3.g27558.t1	N	N	weak	N	NN	NN
83		aug3.g27557.t1	Y	Y	weak	N	YN	YN
84		g23966	N	N	N	N	NN	NN
85	K373, K376, K379	aug3.g14287.t1	Y	N	Y	N	YY	NN
86	ras7-like	aug3.g23439.t1	Y		Y		YY	
87	uncharacterized	aug3.g6152.t1	N		N		NN	
88	uncharacterized	aug3.g16318.t1	Y		Y		YY	
89	1-interacting protein 1 B	aug3.g22926.t1	Y		weak		YY	
90		aug3.g23431.t1	Y		N		YN	
91	ein phosphatase 10D (Pt	aug3.g2169.t1	Y		N		YN	
92		aug3.g2657.t1	Y		N		YN	
93		aug3.g7930.t1	Y		N		YN	
94		aug3.g12711.t1	N		N		NN	
95		aug3.g4081.t1	N		N		NN	
96	Characterized; mus304; L	aug3.g16165.t1	N		N		NN	
97		aug3.g15726.t1	Y		N		YN	
98	no colony	aug3.g24730.t1	Y		N		YN	
99	fgf8	aug3.g5611.t1	Y	Y	Y	N	YY	YN
100	dof/stumps	aug3.g4286.t1	Y	N	Y	N	YY	NN
101		aug3.g16926.t1	Y	Y	Y	N	YY	YN
102		aug3.g2974.t1	Y	Y	weak	N	YY	YN
103		aug3.g15167.t1	Y		Y		YY	
104	fascin	aug3.g26989.t1	Y	Y	Y	Y	YY	YY
105	hunchback	aug3.g25126.t1	Y	N	Y	N	YY	NN
106		aug3.g20850.t1	Y		Y		YY	
107	antibody and probe	aug3.g5162.t1	Y		Y		YY	
108		aug3.g11104.t1	Y		Y		YY	
109		aug3.g6385.t1	Y		N		YN	
110		aug3.g12644.t1	Y		Y		YY	
111		aug3.g1632.t1	Y		N		YN	
112		aug3.g23531.t1	Y		N		YN	
113		aug3.g5118.t1	Y		N		YN	

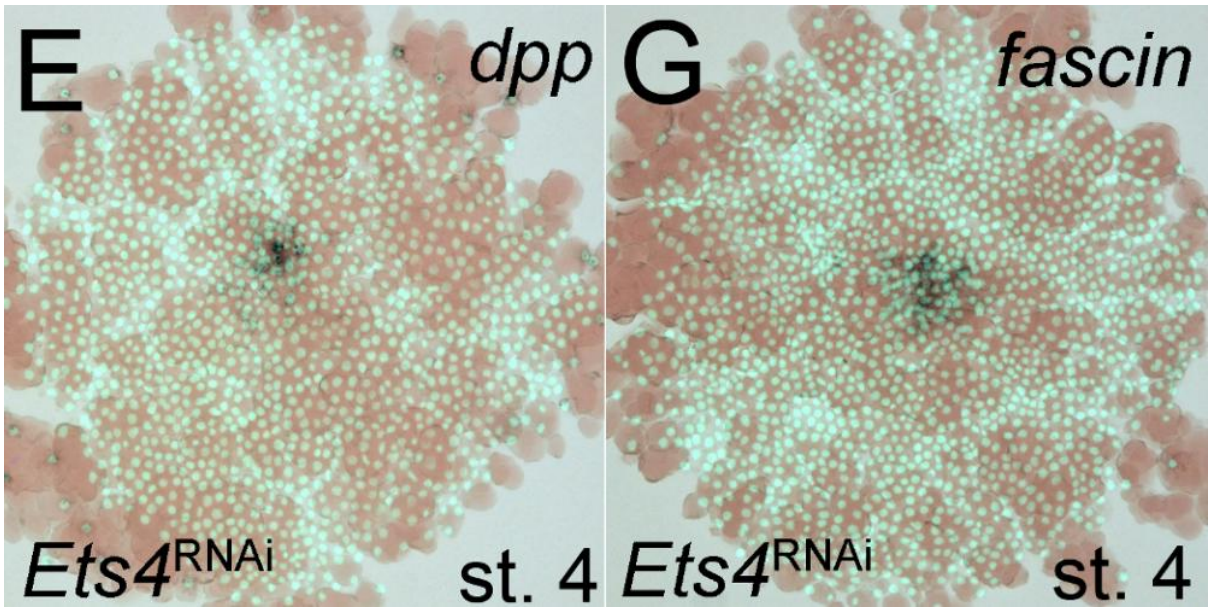

Figure S3-15. Published expression of *dpp* and *fascin* gene in Ets4 RNAi embryo at stage 4, both gene show expression in the primary thickening region.

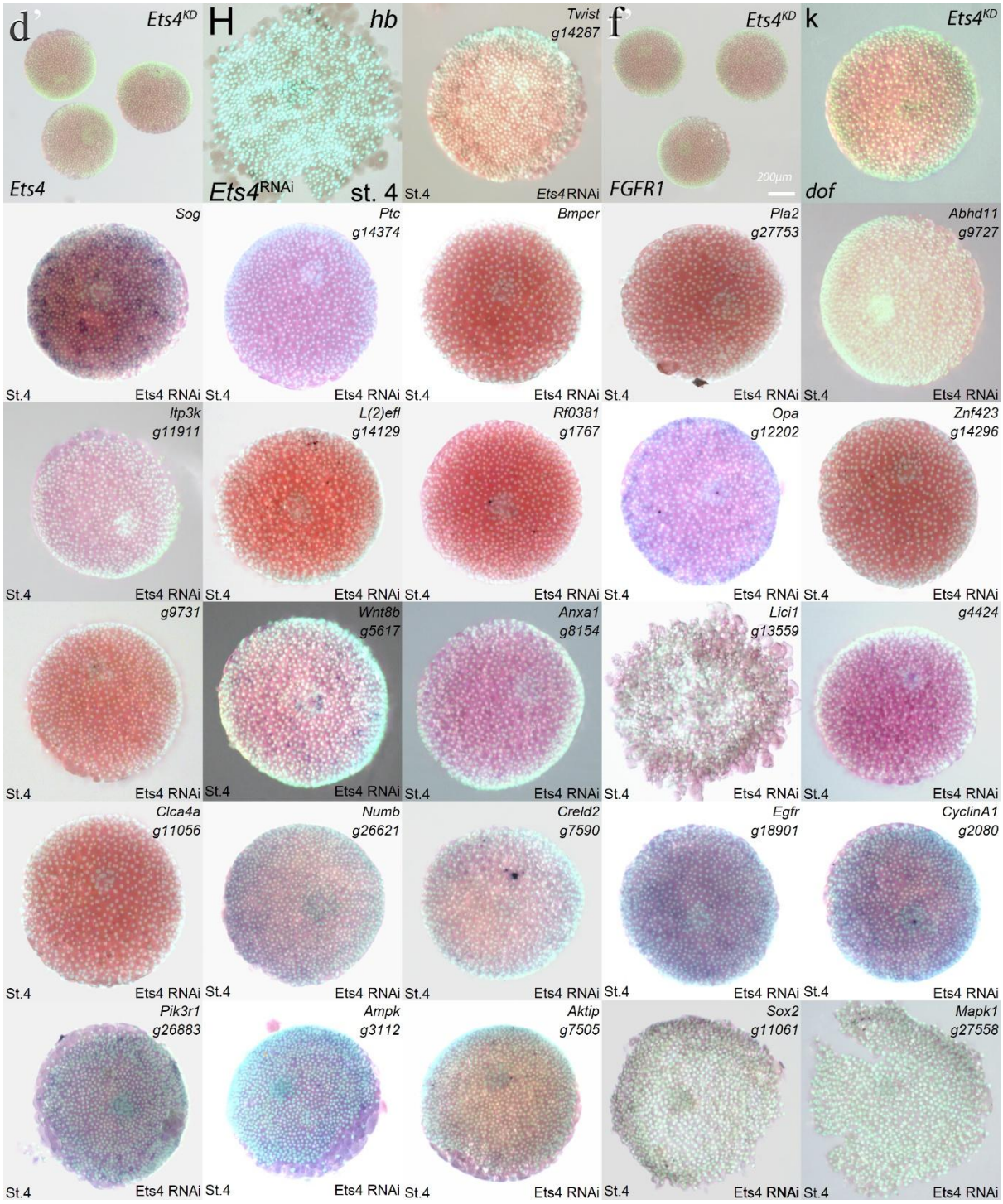

Figure S3-16. Expression of genes at stage 4 in Ets4 RNAi embryos. No expression is observed in the primary thickening region. Gene list: *Ets4, hb, twist, Fgfr1, dof, sog, ptc, Bmper (cv-2), pla2, Abhd11 g9727, Itp3k (Itpka), L(2)efl, RF_0381, opa, Znf423, g9731, Wnt8b, Anxa1, Lici1, g4424, Clca4a, Numb, Creld2, Egfr, Cyclin A1, Pik3r1 g26883, Ampk, Aktip, Sox2, Mapk1 g27558*.

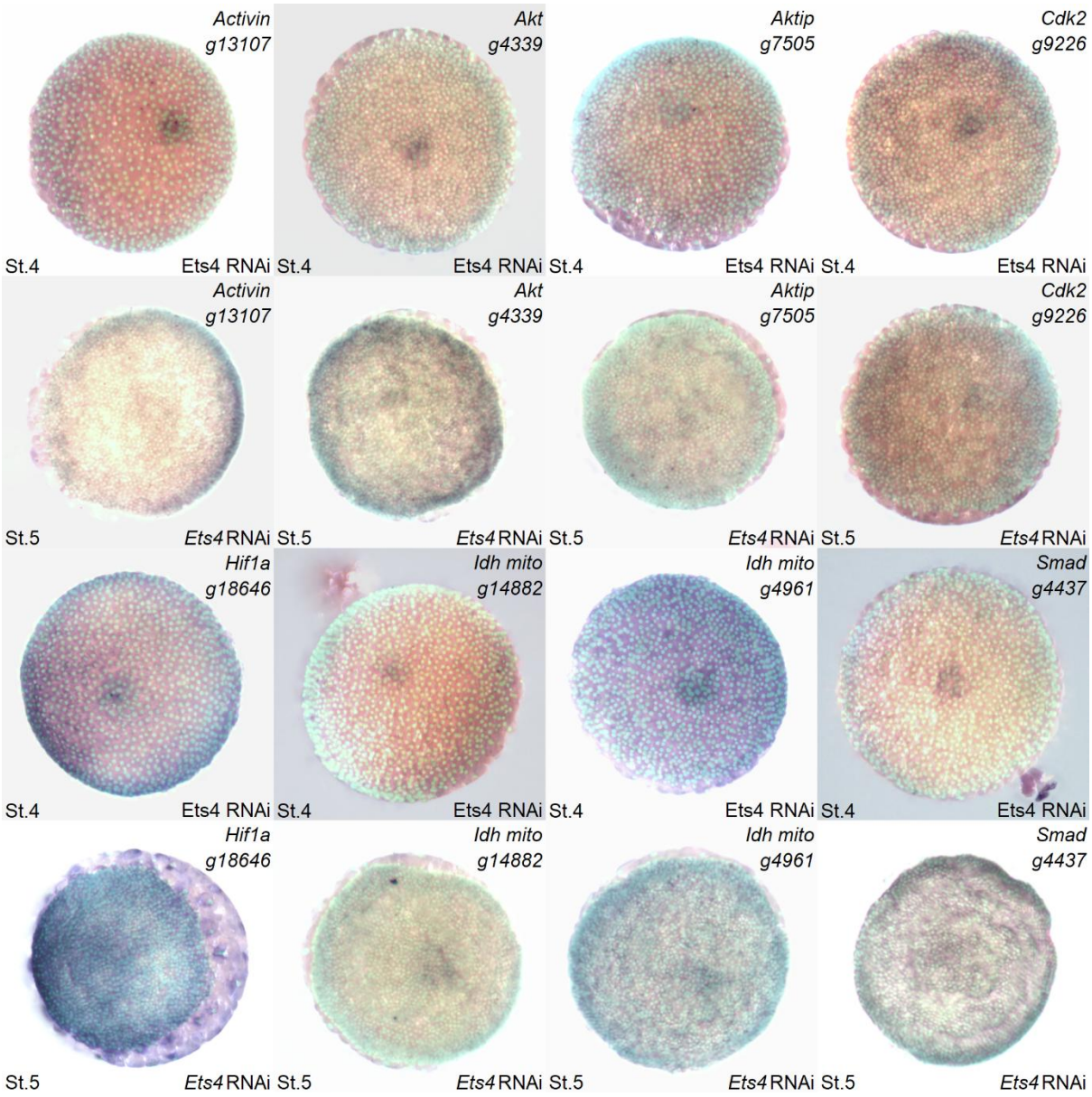

Figure S3-17. Expression of genes in Ets4 RNAi embryo at stage 4 and stage 5. Annotation. Gene list: *Activin (Asph), Akt, Aktip, Cdk2, Hif1a, Idh mito g14882 (Idh3g), Idh mito g4961 (Idh2), Smad (Snip1)*.

Table S3-3 Comparison of differential expression gene in primary thickening region in WT and Ets4 RNAi embryos at stage 4, from result of in situ hybridization and RNAseq selected gene list.

Number	Gene Name	Name	Differential expression from in situ	Whether in List B	Whether in List C	Whegher in List F		Comparision of in situ and list B	Comparision of in situ and list C	Comparision of in situ and list F
1	cv-2	aug3.g2323.t1	Y			slightly higher		YN	YN	YY
2	DLL1	aug3.g25248.t1	Y		Y			YN	YY	YN
3	ets4	aug3.g4238.t1	Y	Y	Y	Y		YY	YY	YY
4	fgfr2	aug3.g26565.t1	Y	Y	Y	Y		YY	YY	YY
5	Fuchi	aug3.g26874.t1	N			Y		NN	NN	NY
6	hh	aug3.g4322.t1	Y	Y	Y	Y		YY	YY	YY
7	PLA2	aug3.g27753.t1	Y		Y	Y		YN	YY	YY
8	ABHD11	aug3.g9727.t1	Y					YN	YN	YN
9	MTMR14	aug3.g15186.t1	Y		Y			YN	YY	YN
10	ITP3K	aug3.g11911.t1	Y		Y	Y		YN	YY	YY
11	l(2)efl	aug3.g14129.t1	Y		Y			YN	YY	YN
12	RF_0381	aug3.g1767.t1	Y	Y	Y	Y		YY	YY	YY
13	ZIC-4	aug3.g12202.t1	Y		Y			YN	YY	YN
14	ZNF423	aug3.g14296.t2	Y		Y	Y		YN	YY	YY
15	unchar	aug3.g4422.t1	N		Y			NN	NY	NN
16	unchar	aug3.g9731.t1	Y		Y			YN	YY	YN
17	unchar	aug3.g592.t1	N					NN	NN	NN
18	unchar	aug3.g22667.t1	Y		Y			YN	YY	YN
19	ptc	aug3.g14374.t2	Y		Y			YN	YY	YN
20	Wnt	aug3.g5617.t2	Y			Y		YN	YN	YY
21	LRRC4	aug3.g8154.t1	Y		Y			YN	YY	YN
22	serpin	aug3.g13559.t1	N		Y			NN	NY	NN
23	papilin	aug3.g4424.t2	Y	Y	Y	Y		YY	YY	YY
24	CLCA2	aug3.g11056.t2	Y	Y	Y	Y		YY	YY	YY
25	Numb	aug3.g26621.t1	N					NN	NN	NN
26	riched EF I	aug3.g259.t1	N					NN	NN	NN
27	riched EF I	aug3.g7589.t1	N					NN	NN	NN
28	riched EF I	aug3.g7590.t1	N					NN	NN	NN
29	EgfR	aug3.g18901.t1	N					NN	NN	NN
30	GSK3 beta	aug3.g9959.t1	N					NN	NN	NN
31	GSK3 beta	aug3.g25394.t1	N					NN	NN	NN
32	yclin A1 lik	aug3.g2080.t1	N			slightly higher		NN	NN	NY
33	cyclinB	aug3.g8469.t1	N					NN	NN	NN
34	ulatory sub	aug3.g26883.t1	N			slightly higher		NN	NN	NY
35	talytic subu	aug3.g3457.t1	N			Y		NN	NN	NY
36	ζ_subunit a	aug3.g3112.t1	N					NN	NN	NN
37	HIF-1alpha	aug3.g18646.t1	Y					YN	YN	YN
38	H mitochon	aug3.g4961.t1	Y					YN	YN	YN
39	nondria beta	aug3.g14882.t1	N					NN	NN	NN
40	Smad	aug3.g4437.t1	N					NN	NN	NN
41	H cytoplasn	aug3.g8458.t1	N					NN	NN	NN
42	interactin p	aug3.g7505.t1	N			Y		NN	NN	NY
43	ctivin_ASPI	aug3.g13107.t1	Y					YN	YN	YN
44	Sox2	aug3.g11061.t1	N					NN	NN	NN
45	cdk2	aug3.g9226.t1	Y					YN	YN	YN
46	AKT	aug3.g4339.t1	N					NN	NN	NN
47	pendent prc	aug3.g19182.t1	N					NN	NN	NN
48	MAPK1	aug3.g27558.t1	N					NN	NN	NN
49	MAPK1	aug3.g27557.t1	Y					YN	YN	YN
50	sog	aug3.g13327.t1	N					NN	NN	NN
51	twist	aug3.g14287.t1	Y	Y	Y	Y		YY	YY	YY
52	FGF8	aug3.g5611.t1	Y		Y	Y		YN	YY	YY
53	stumps	aug3.g4286.t1	Y	Y	Y	Y		YY	YY	YY
54	dpp	aug3.g16926.t1	N					NN	NN	NN
55	fkh	aug3.g2974.t1	N			slightly higher		NN	NN	NY
56	sn	aug3.g26989.t1	Y	Y	Y	Y		YY	YY	YY
57	hb	aug3.g25126.t1	Y			slightly higher		YN	YN	YY

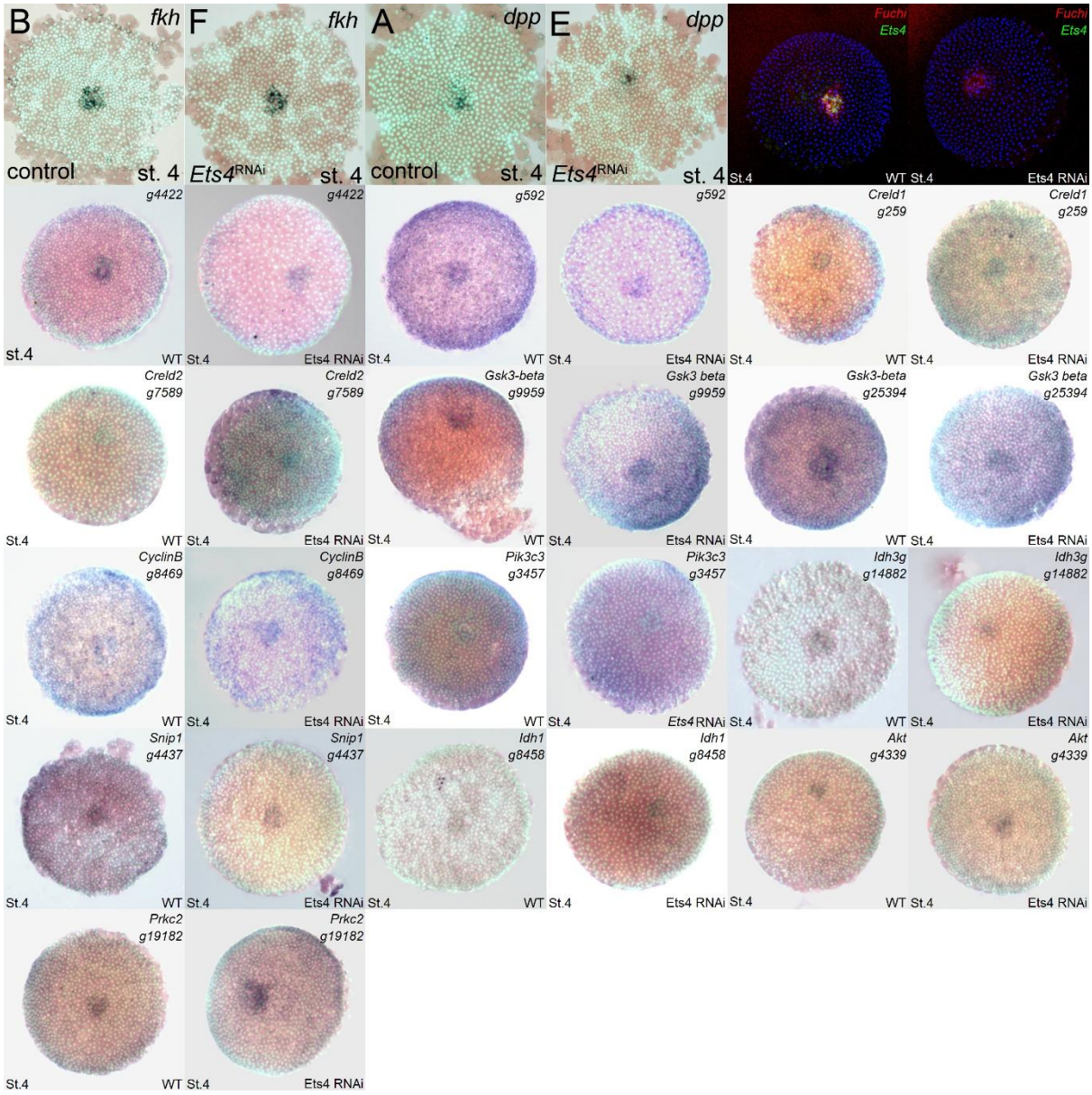

Figure S3-18. Comparison of gene expression at stage 4 in WT and Ets4 RNAi embryos. These genes show similar level of expression in primary thickening region, of the two types of embryos. They were categorized as Type N1 genes in section 3.1. Gene list: *fkh, dpp, fuchi, g4422, g592, Creld1 g259, Creld 2 g7589, Gsk3beta g9959, Gsk3beta g25384, Cyclin B, Pik3c3 g3457, Idh3g g14882 (Idh3g), Snip1, Idh1, Akt, Prkc2*.

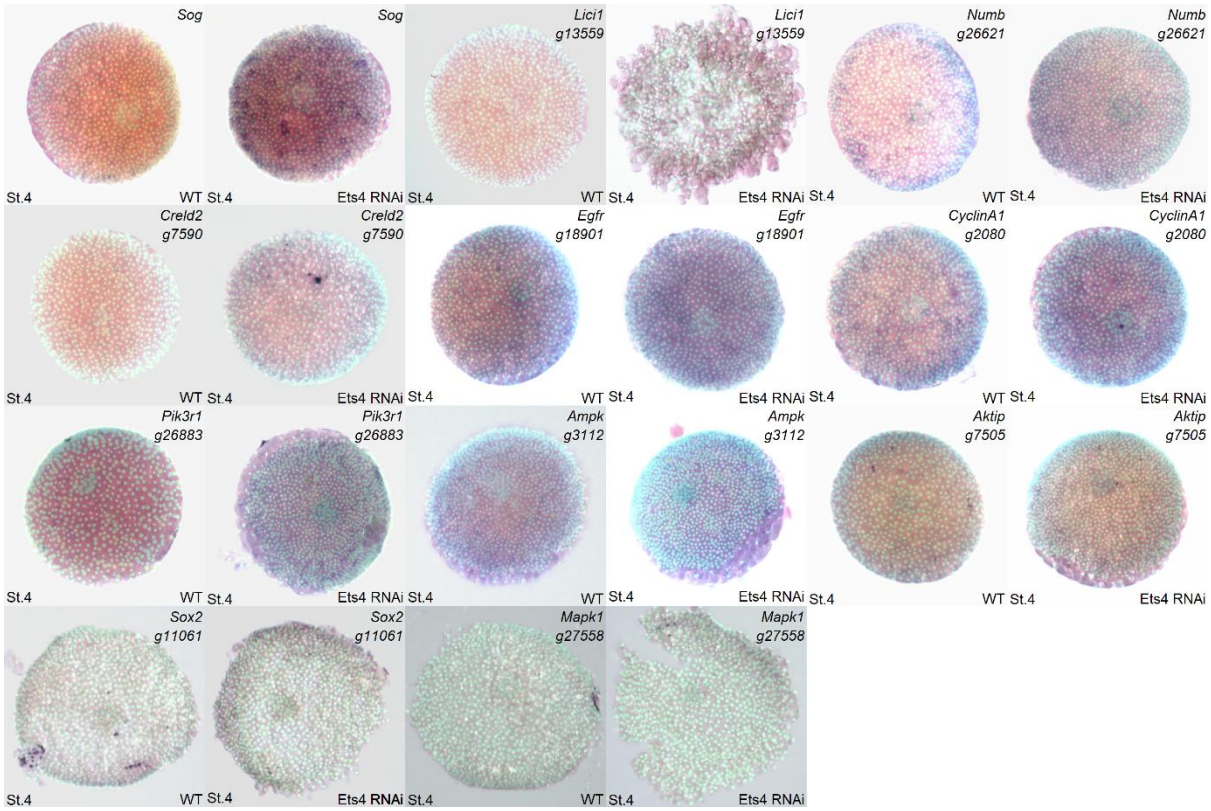

Figure S3-19. Comparison of gene expression in at stage 4 in WT and Ets4 RNAi embryos. These genes show no expression in primary thickening region, of the both types of embryos. They were categorized as Type N2 genes in section 3.1. Gene list: *Sog, Lici1, Numb, Creld 2 g7590, Egfr, Cyclin A, Pik3r1 g26883, Ampk, Aktip, Sox2, Mapk1 g27558*.

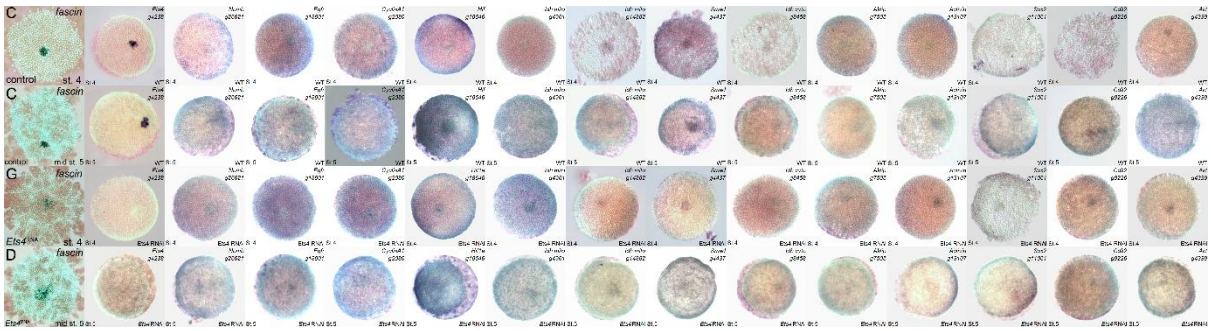

Figure S3-20. Comparision of gene expression at stage 4 and 5 in WT and Ets4 RNAi embryos. Annotation. Gene list: *fascin, Ets4, Numb, Egfr, Cyclin A1, Hif1a, Idh mito g4961 (Idh2), Idh mito g14882 (Idh3g), Ampk, Idh g8458 (Idh1), Aktip, Activin (Asph), Sox2, Cdk2, Akt*.

Table S3-4 gene and possible related cell processes

	WT embryo, development events	WT embryo, expressed gene type (mRNA)	Ets4 RNAi embryo, development events	Ets4 RNAi embryo, expressed gene type (mRNA)
st.2	Blastopore cell proliferation	Type I, II, III	Blastopore cell proliferation	(not known)
st.3	Germ disc contraction Invagination, formation of primary thickening	Type I, II, III	Germ disc contraction Invagination, formation of primary thickening	(not known)
st.4		Type I, II, IV		Type I, part of Type II, part of Type III
st.5	**Cumulus migration** Posterior cell differentiation	Type I, IV	**Cumulus disperse** Posterior cell differentiation	(Limited genes, not known)
st.6	**Dorsal opening** Anterior, posterior, and other part of body specification	(not known)	**Tube outgrowth** Anterior and posterior specification, remain in radical symmetry	(not known)

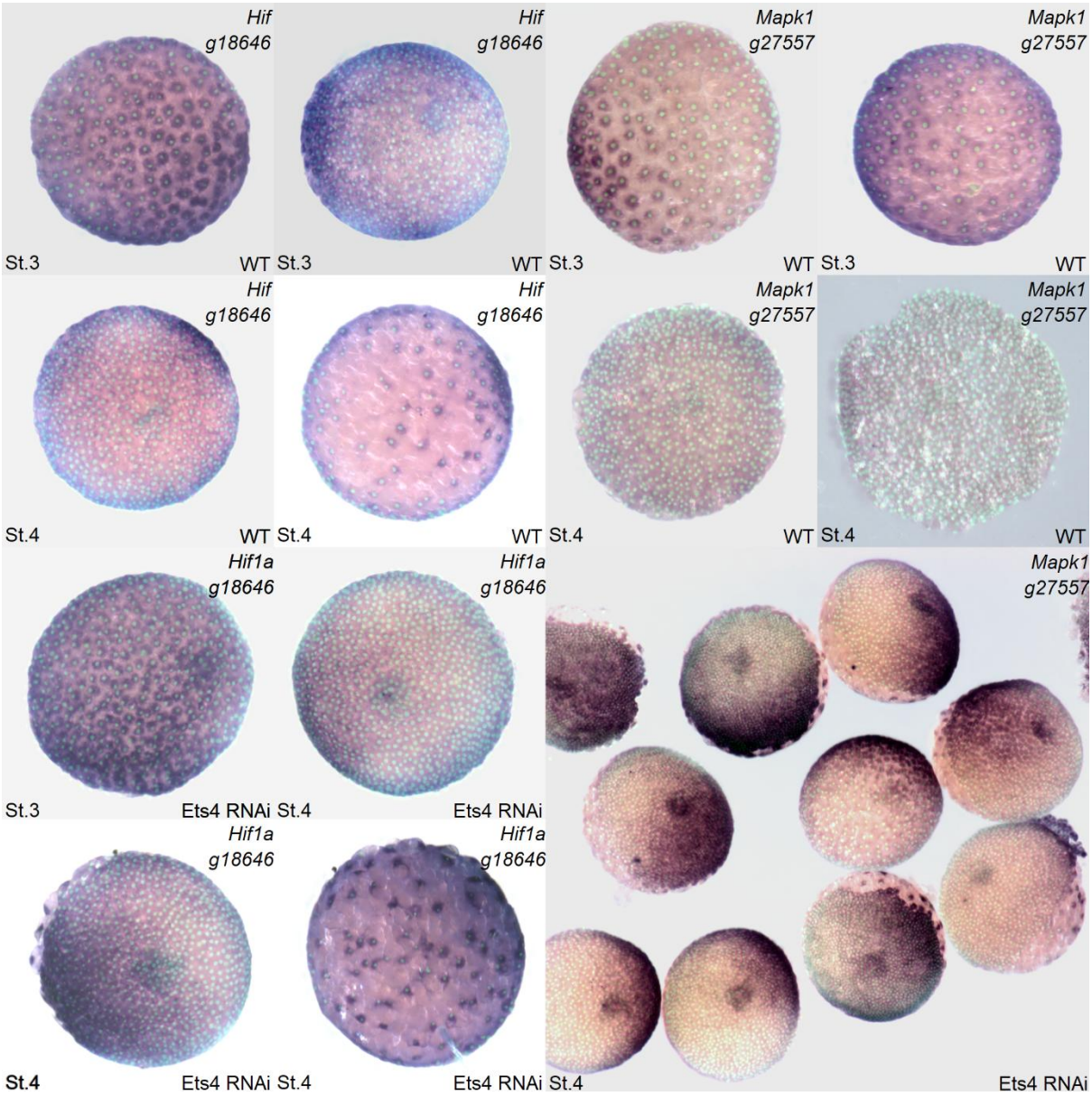

Figure S3-21 Expression of *Hif* and *Mapk1 g27557* at stage 3 and 4 in WT and *Ets4* RNAi embryos show some staining patterns that are not radially symmetric. Sytox/brightfield overlay

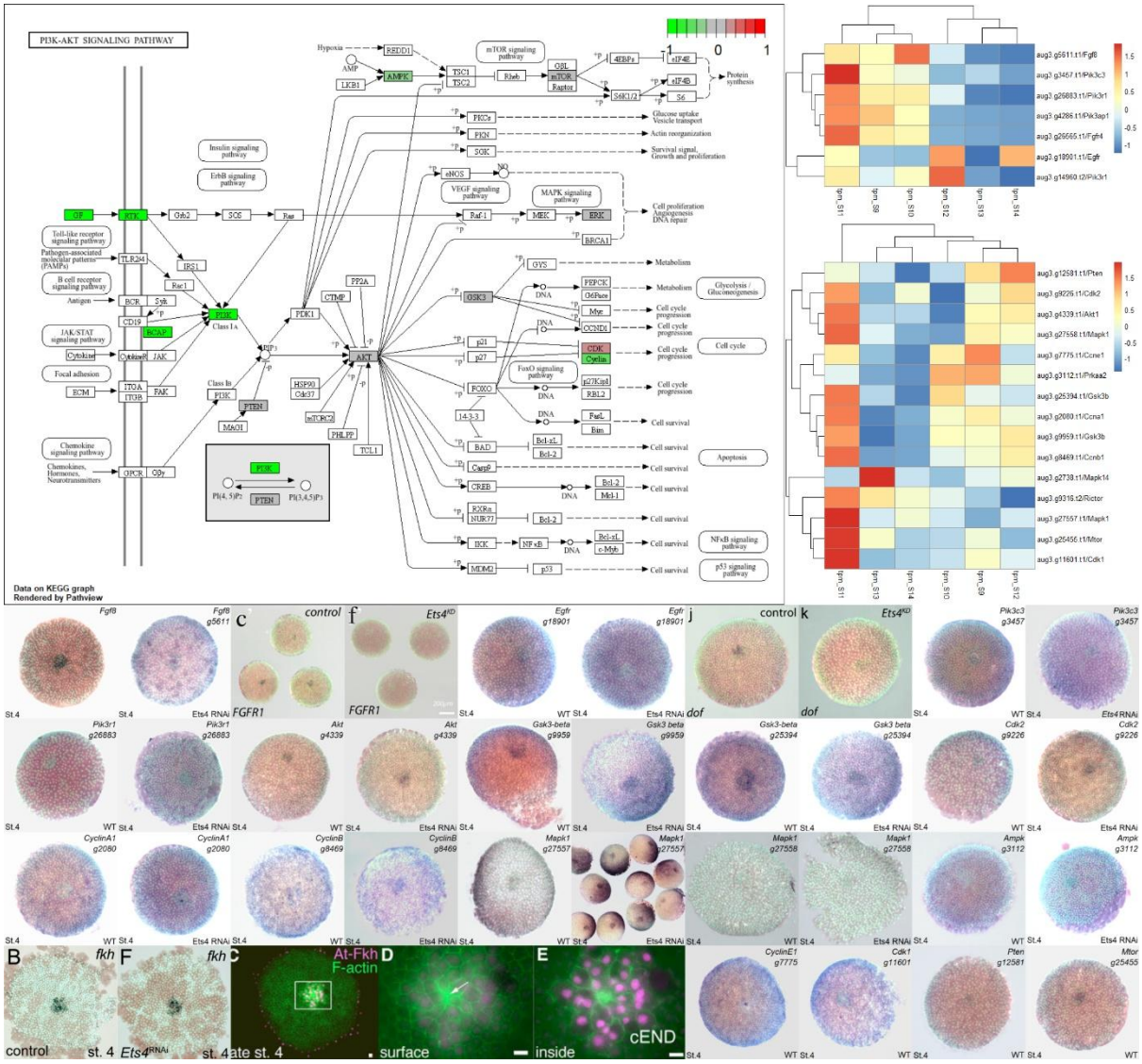

Figure S3-22. Combined images of the PI3K-AKT signaling pathway. The pathview image was generated using genes from the 113-gene list, with Fold2Change values from RNAseq. The heatmap image represents the colored genes in the pathview image, displaying individual RNAseq reads from all six samples. In situ hybridization images of relevant genes are also included in the figure, including *Fgf8* (WT, *Ets4* RNAi), *Fgfr1* (WT, *Ets4* RNAi), *Egfr* (WT, *Ets4* RNAi), *Dof* (WT, *Ets4* RNAi), *Pik3c3* (WT, *Ets4* RNAi), *Pik3r1 g26883* (WT, *Ets4* RNAi), *Akt* (WT, *Ets4* RNAi), *Gsk3b g9959* (WT, *Ets4* RNAi), *Gsk3b g25394* (WT, *Ets4* RNAi), *Cdk2* (WT, *Ets4* RNAi), *Cyclin A1* (WT, *Ets4* RNAi), *Cyclin B* (WT, *Ets4* RNAi), *Mapk1 g27557* (WT, *Ets4* RNAi), *Mapk1 g27558* (WT, *Ets4* RNAi), *Ampk* (WT, *Ets4* RNAi), *Fkh* (WT, *Ets4* RNAi), Fkh and Actin (Antibody; broad, surface and inner view; WT), *Cyclin E1* (WT), *Cdk1* (WT), *Pten* (WT), and *Mtor* (WT). Antibody staining of Fkh and Actin were from Oda et al., 2007. In situ hybridization staining of Fkh in WT and *Ets4* RNAi embryos were from Pechmann et al., 2017. Staining image of *Fgfr1* and *Dof* were from Wang et al., 2023.

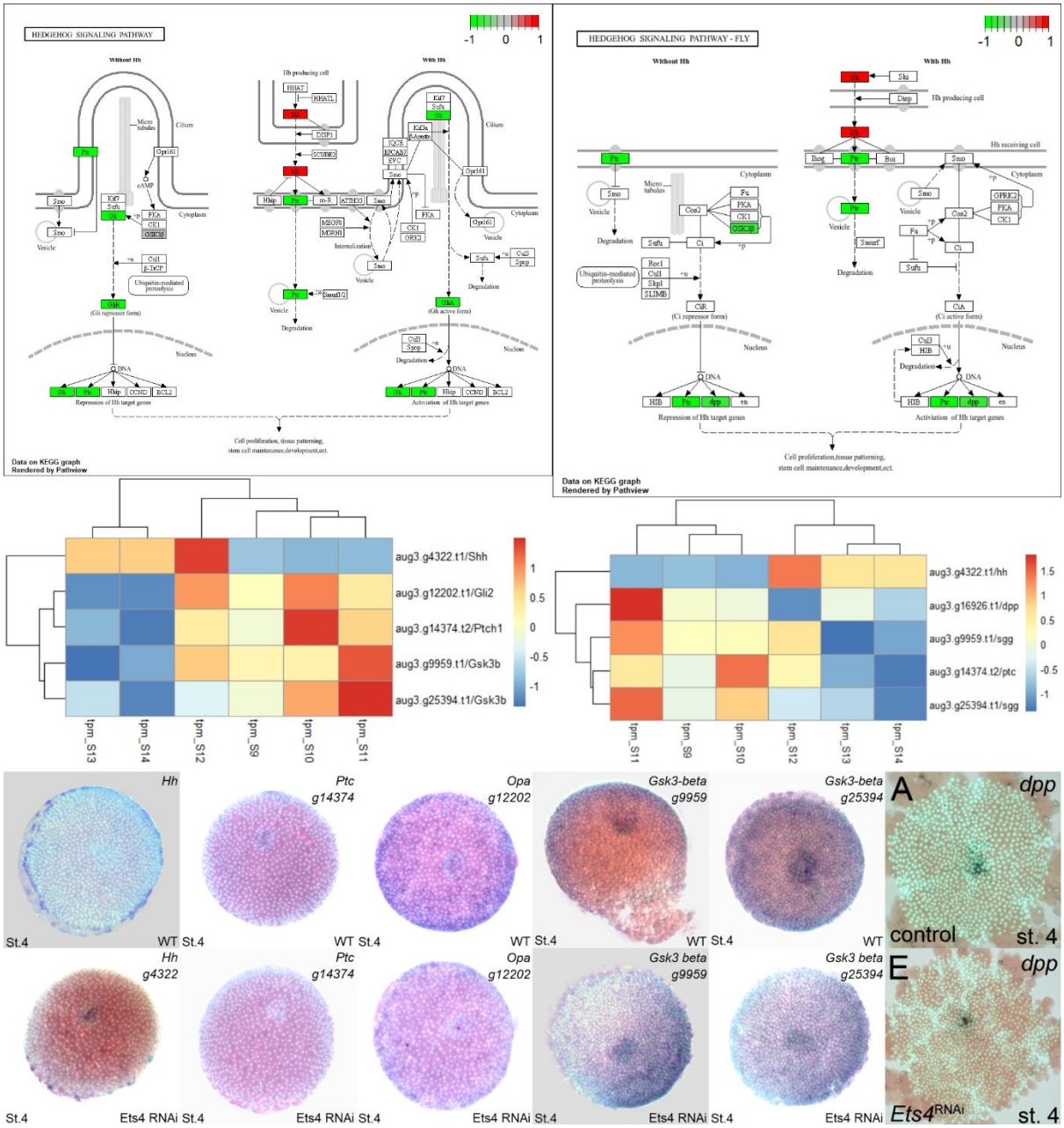

Figure S3-23. Combined image of the Hh signaling pathway. The pathview image is derived from the 113 gene list, with Fold2Change values from RNAseq data. The heatmap image for the colored genes in the pathview image shows the individual reads of all six RNAseq samples. The in situ hybridization images include staining of relevant genes at stage 4 in both WT and *Ets4* RNAi embryos, including *Hh, Ptc, Opa, Gsk3b g9959, Gsk3b g25394*, and *Fkh* (the *Fkh* staining image is from Pechmann et al., 2017). For *Gsk3b*, two Fold2Change values are used from the two different pathway images, when one value is used for each pathway, resulting in one image where *Gsk3b* is marked in grey and another where it is in green.

(Supplementary Figures and Tables for Results Chapter IV)

Table S4-1 Hael calculation of WT and seven RNAi embryos.

			stage	hael	31	36	41	46	51	56	59
WT 13-4			2 to 8	frame	79	99	119	139	159	179	191

	scene	total embryo number	stage	hael	31	36	41	46	51	56	61
	1	1	7								
Itpka RNAi	6	96	3 to 8	frame	8	20	31	43	54	66	77

	scene	total embryo number	stage	hael	18	22	29	31.5	34	36	53
	2	32	9 to 10								
RF_0381 RNAi	4	60	2 to 8	frame	1	10	25	30	35	40	78

	scene	total embryo number	stage	hael	31	41	51	56	76	86	
Znf423 RNAi	4	64	3 to 12	frame	23	46	69	80	126	149	

	scene	total embryo number	stage	hael	7	11	18	28	31	41	54.7
g4422 RNAi	8	31	1 to 7	frame	5	16	35	63	71	99	137

	scene	total embryo number	stage	hael	30	40	50	55	60		
cv-2 RNAi	1	25	3 to 9	frame	15	35	54	65	75		

	scene	total embryo number	stage	hael	12	18	28	31	41	56	76
	1 (Twist-1)	25	9 to 13								
	1 (Twist-6 C3)	6	3 to 10	frame			**11	35	55	85	125
	4 (Twist-6 C4)	99	2 to 10	frame	2	13	32	50	70	102	135
	25 (Twist-12 C3)	99	5 to 8	frame			1	11	31	61	
	25 (Twist-13 C3)	100	2 to 8	frame		10	30	41	61	91	
Twist RNAi	1 (Twist-14 C5)		4 to 5	frame			9	23	41		

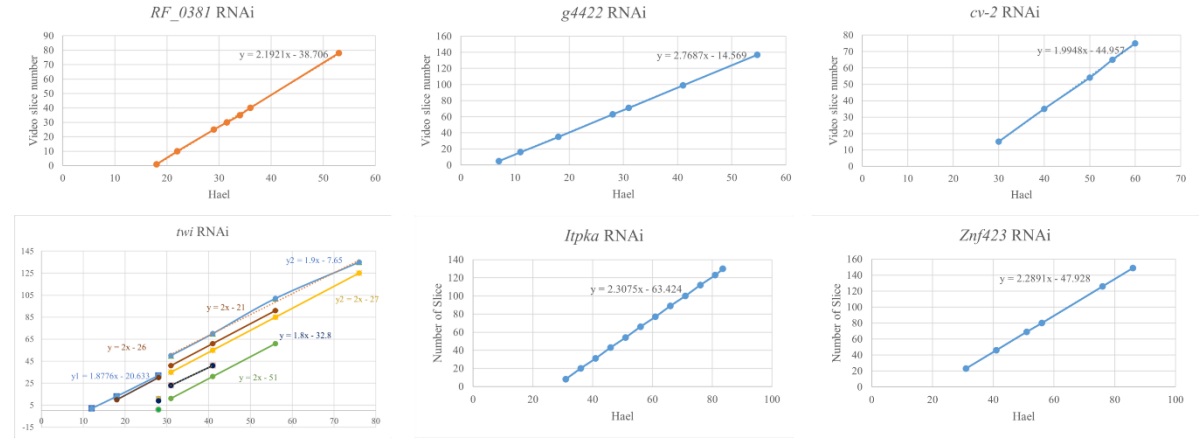

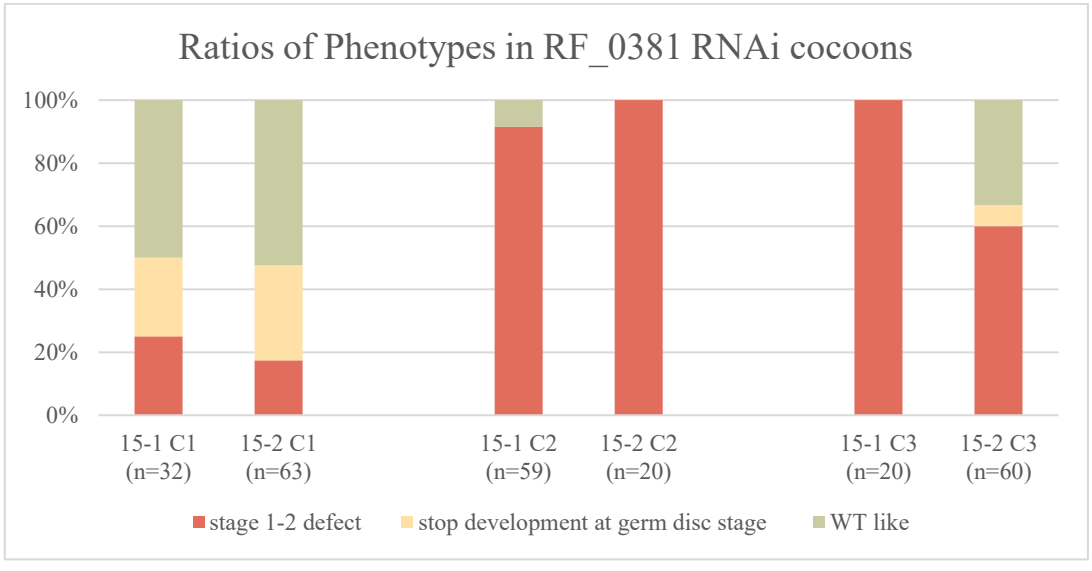

Figure S4-1. Proportion of different phenotypes in *RF_0381* RNAi cocoons.

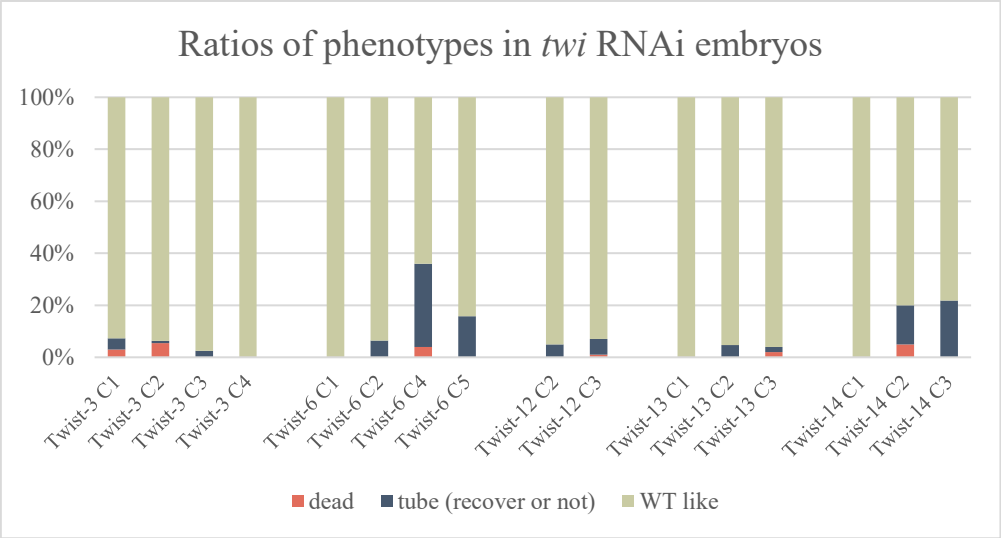

Figure S4-2. The ratio of *twi* RNAi embryos at around stage 7 that are WT-like, dead, or tube-shaped. Embryo counts from cocoon *twi*-6 C4, *twi*-12 C3, and *twi* -13 C3 were based on recordings of embryonic development.

Table S4-2. Cell number counting in Twist RNAi embryos (Twist-6 C4, s3 4-2) to calculate Hael.

frame	stage	cell number in view (half)	cell number (total)	hael (comparing to video of 2016 paper)
2	stage 2	25	50	12
3		43	86	12.5
4		40	80	13.1
5		43	86	13.6
6		56	112	14.1
7		74	148	14.7
8		78	156	15.2
9		89	178	15.7
10		105	210	16.3

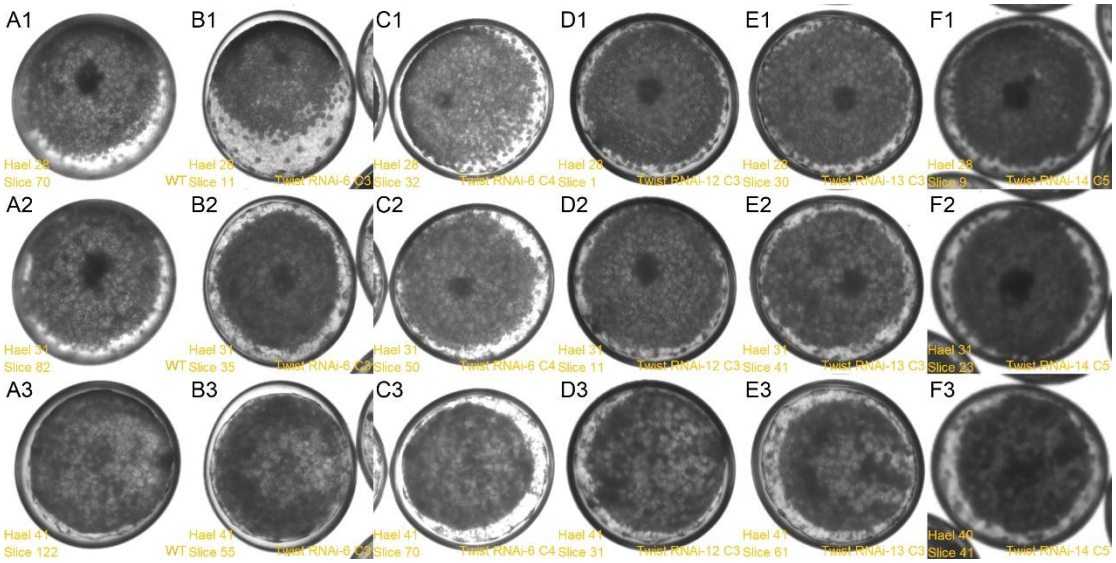

Figure S4-3. Development image of WT and *twi* RNAi embryos. A1-A3: WT embryo, No. 2022 13-3. B1-B3: *twi* RNAi embryo, No. Twist-6 C3-6. C1-C3: *twi* RNAi embryo. No. Twist -6 C4 s3 4-2. D1-D3: *twi* RNAi embryo. No. Twist -12 C3 s1 1-3. E1-E3: *twi* RNAi embryo. No. Twist -13 C3 s2 1-4. F1-F3: *twi* RNAi embryo. No. Twist -14 C5. A1, B1, C1, D1, E1, F1: 28 Hael. A2, B2, C2, D2, E2, F2: 31 Hael. A3, B3, C3, D3, E3, F3: 41 hael. Number of slice is listed in each image. Original interval between slice for the WT embryo is 15 minutes , for these twi RNAi embryos is 30 minutes.

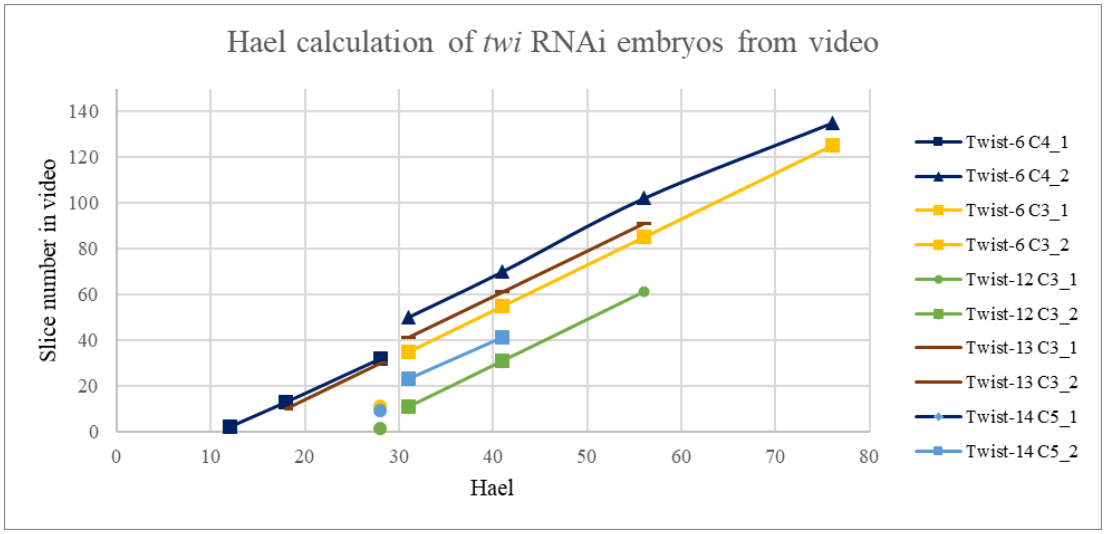

Figure S4-4. Slice number and Hael time of *twi* RNAi embryos. Sample of *twi* RNAi embryos include *twi*-6 C3, *twi*-6 C4, *twi*-12 C3, *twi*-13 C3, and *twi*-14 C5. Data from different samples are marked in different colors. Additional data can be found in supplementary excel 2.4.

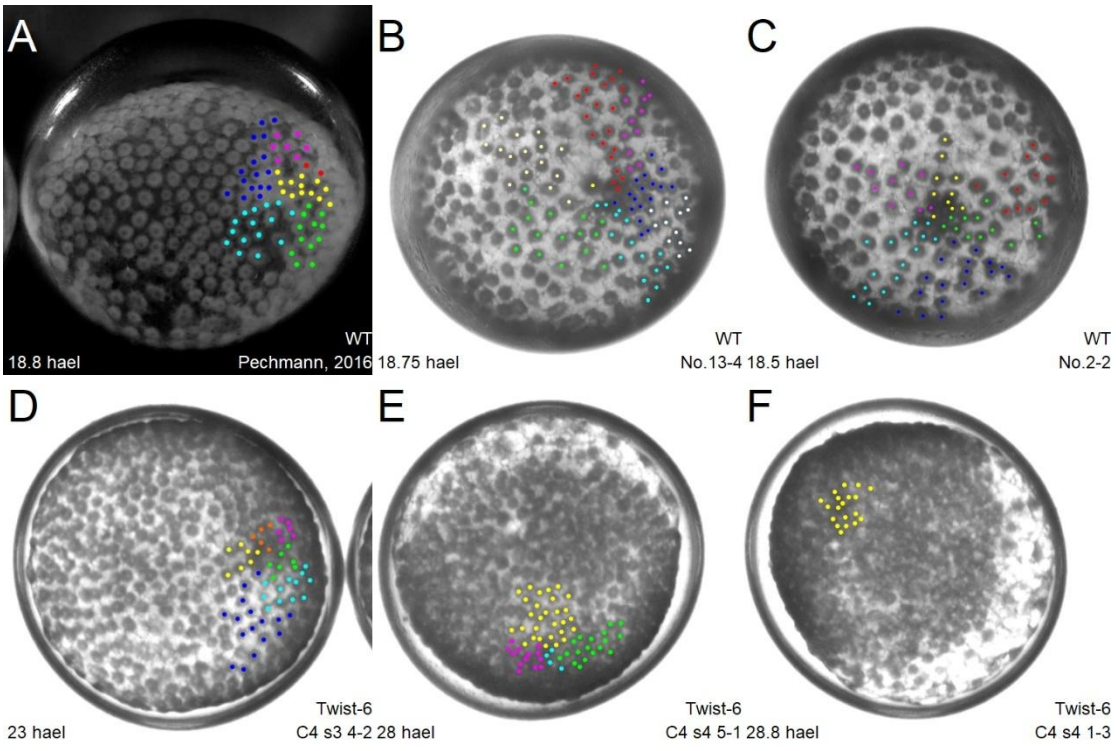

Figure S4-5. Primary thickening region cell tracing in WT and *twi* RNAi embryos. A: WT embryo, from Pechmann 2016. B: WT embryo, No. 2022 13-4. C: WT embryo. No. 2022 2-2. D, E, F: *twi* RNAi embryo from

cocoon Twist-6 C4, No. s3 4-2, s4 5-1, and s4 1-3. Each embryo show the last slice before seeing cell disappear (invagination).

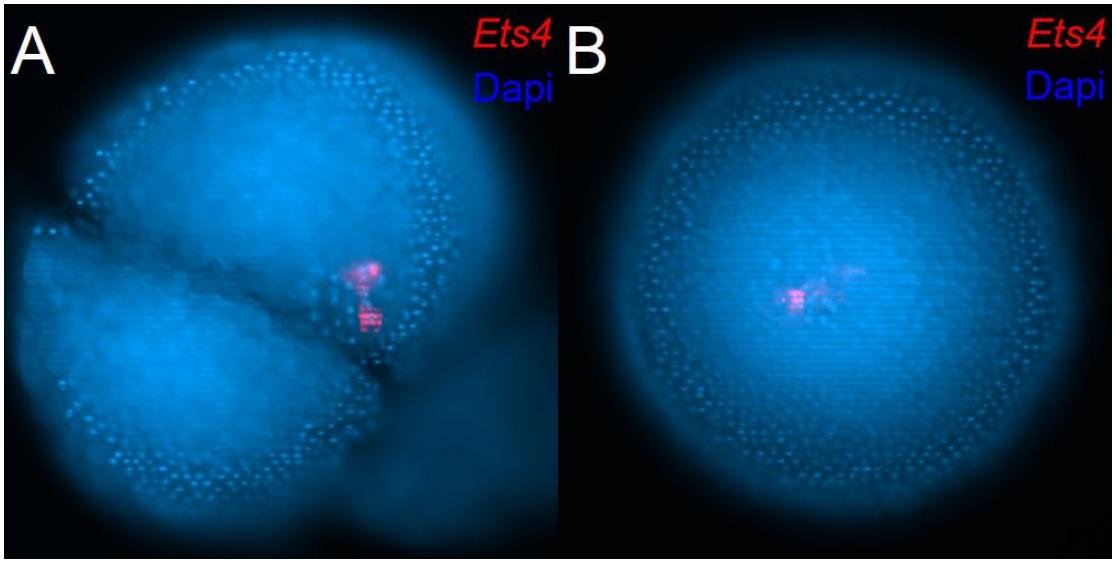

Figure S4-6. HCR staining image of *twi* RNAi embryos. A: Ets4+ cells locate in two remote parts in primary thickening region. B: Number of Ets4+ cells are less than 5, perhaps only 2. Red: Ets4. Blue: Dapi.

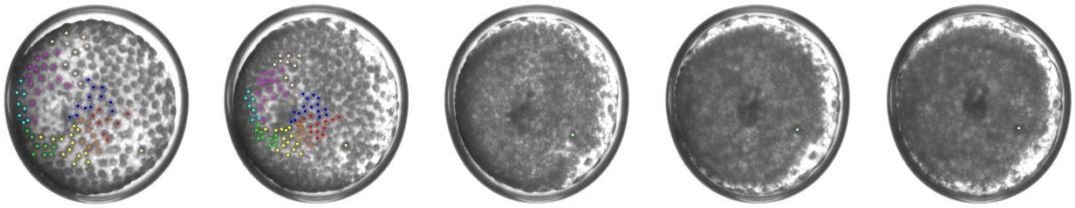

Figure S4-7. *twi* RNAi embryo from cocoon twi-6 C4 shows multiple inner cell regions in the germ disc. Other than the primary thickening region, the second inner cell region appear near stage 4, close to a single cell that do not proliferate for the last two rounds of universe proliferation in germ disc cells.

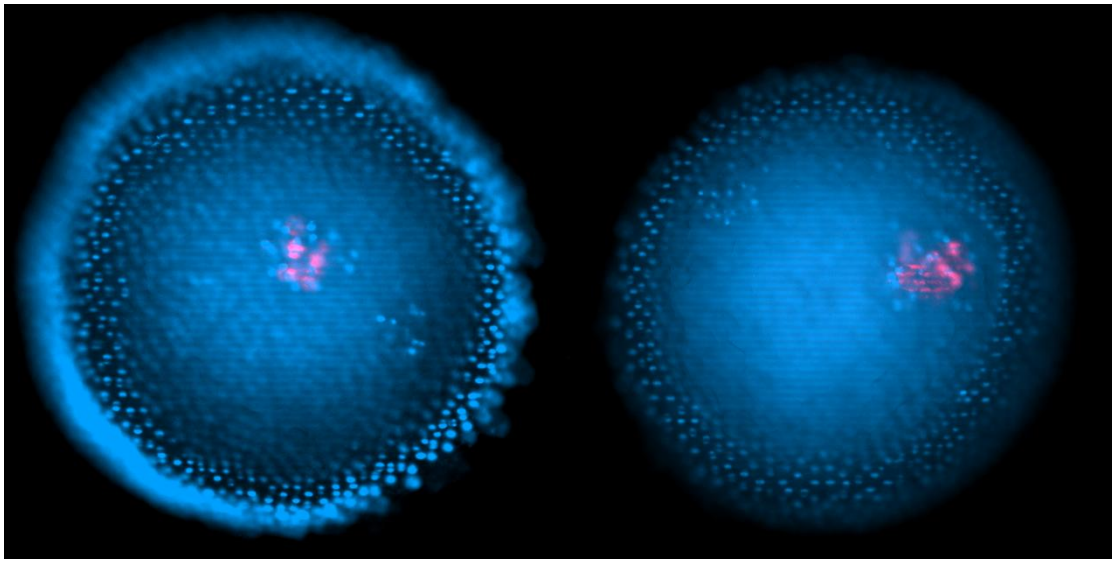

Figure S4-8. HCR staining images of Twist-6 C4 embryos with multiple inner cell regions. Only one of these regions show expression of Ets4. Red: *Ets4*. Blue: Dapi.

Table S4-3. Itpka RNAi phenotypes

spider	cocoon	description	counting stage	WT like	dead	tube	total	other
	C1	normal sized cocoon.						
	C2	high death rate, half stop development at stage 8-9.						
Itp3k-2	C3	empty cocoon.						
	C1	most WT like.						
	C2	germ disc uneven at stage 5, not looks well at stage 7-8.						
	C3	many embryo in strange shape at stage 5. germ band too short or twisted at stage 9.	stage 6	65	20	5	90	
Itp3k-4_2	C4	embryo clustered.						
	C1	most WT like.						
	C2	many dead at stage 5. Some germ band too narrow at stage 7 to stage 9.						
Itp3k-5	C3	clustered						
	C1	WT like at stage 6. Some with broad anterior part at stage 7. Half dead at stage 12.						
	C2	At stage 11 around 1/3 dead.						
	C3	Most dead at stage 5. Some with short germ band at stage 7-8.						
Itp3k-6	C4	clustered						
	C1	WT like at stage 6. Half WT like at stage 8.						
	C2	Some with broad anterior side at stage 6-7.	stage 9		25		56	
Itp3k-8	C3	small cocoon.						video
	C1	embryo close to clustered, and not in good quality.						
	C2	In 60% embryo, germ disc looks smaller.						
	C3	Some embryos have strange migration process, and form tube.						
Itp3k-9	C4	Around 1/3 dead at germ disc stage.		28	27	6		

A1

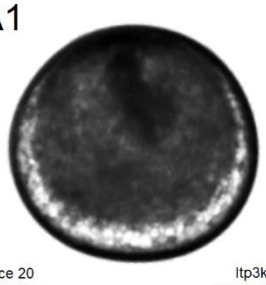

Slice 20 Itp3k-8
Hael 36 C3 s5 4-1

B1

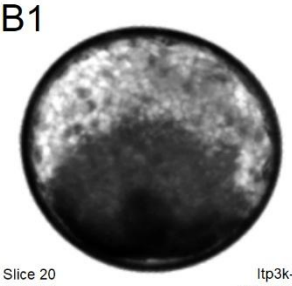

Slice 20 Itp3k-8
Hael 36 C3 s4 2-4

C1

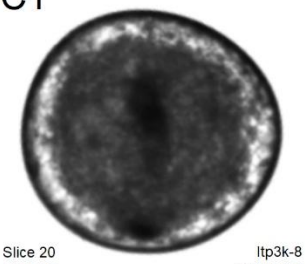

Slice 20 Itp3k-8
Hael 36 C3 s5 3-1

A2

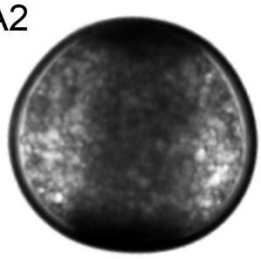

Slice 89 Itp3k-8
Hael 66 C3 s5 4-1

B2

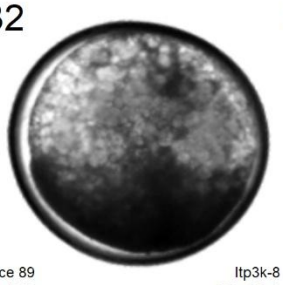

Slice 89 Itp3k-8
Hael 66 C3 s4 2-4

C2

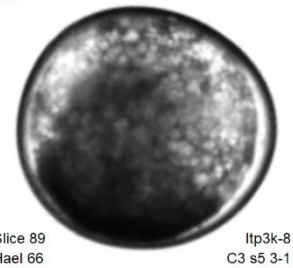

Slice 89 Itp3k-8
Hael 66 C3 s5 3-1

A3

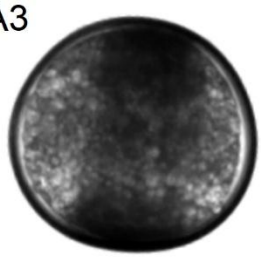

Slice 100 Itp3k-8
Hael 71 C3 s5 4-1

B3

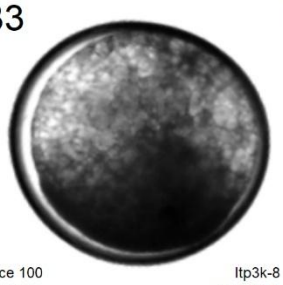

Slice 100 Itp3k-8
Hael 71 C3 s4 2-4

C3

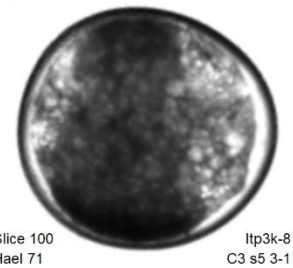

Slice 100 Itp3k-8
Hael 71 C3 s5 3-1

A4

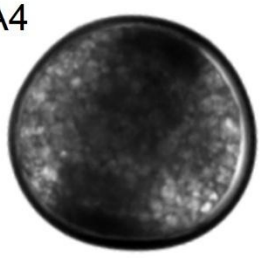

Slice 112 Itp3k-8
Hael 76 C3 s5 4-1

B4

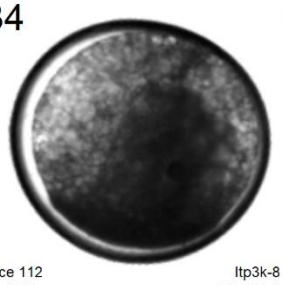

Slice 112 Itp3k-8
Hael 76 C3 s4 2-4

C4

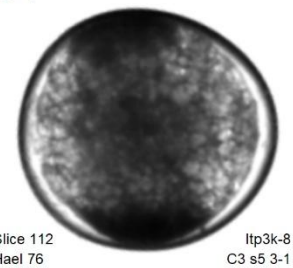

Slice 112 Itp3k-8
Hael 76 C3 s5 3-1

A5

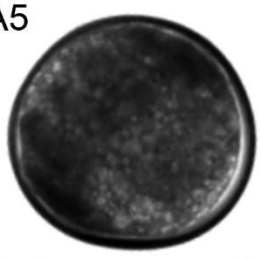

Slice 123 Itp3k-8
Hael 81 C3 s5 4-1

B5

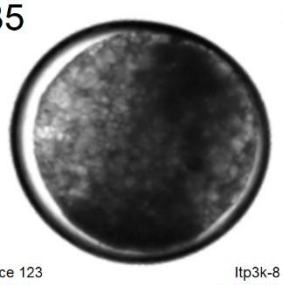

Slice 123 Itp3k-8
Hael 81 C3 s4 2-4

C5

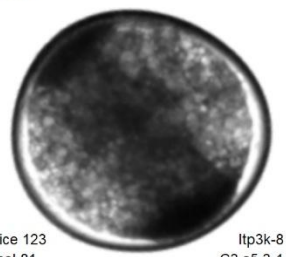

Slice 123 Itp3k-8
Hael 81 C3 s5 3-1

A6

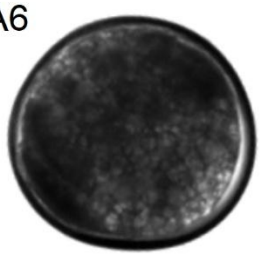

Slice 130 Itp3k-8
Hael 83.5 C3 s5 4-1

B6

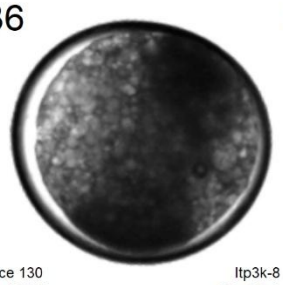

Slice 130 Itp3k-8
Hael 83.5 C3 s4 2-4

C6

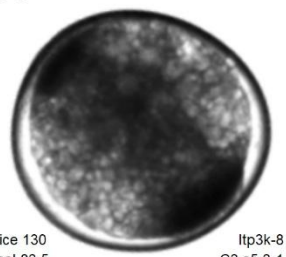

Slice 130 Itp3k-8
Hael 83.5 C3 s5 3-1

Figure S4-9. Development of *Itpka* RNAi1 embryo at Hael 36 (A1, B1, C1), 66 (A2, B2, C2), 71 (A3, B3, C3), 76 (A4, B4, C4), 81 (A5, B5, C5), and 83.5 (A6, B6, C6). A1-A6: Itpka-8 C3 s5 4-1, some other development images in Figure 4-18, B1-B6. B1-B6: Itpka-8 C3 s4 2-4, other images in Figure 4-18, C1-C6. C1-C6: Itpka-8 C3 s5 3-1, other images in Figure 4-18, D1-D6.

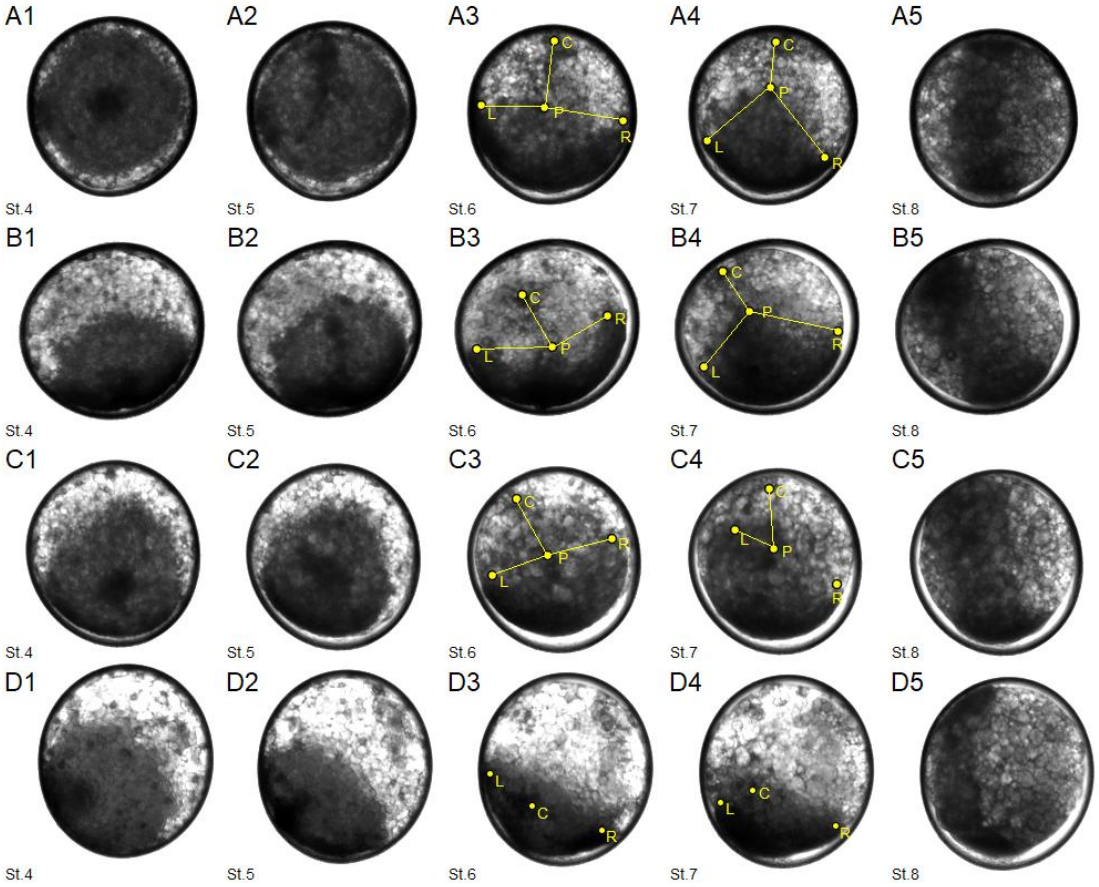

Figure S4-10. Dorsal opening and germ disc formation of more *Itpka* RNAi embryos. A1-A5: slice 10, 30, 60, 75, 130. B1-B5: slice 12, 35, 70, 105, 130. C1-C5: slice 22, 46, 85, 105, 130. D1-D5: slice 7, 32, 52, 75, 130. A1, B1, C1, D1: stage 4/5. A2, B2, C2, D2: stage 5/6. A3, B3, C3, D3: stage 6/7. A4, B4, C4, D4: stage 7/8. A5, B5, C5, D5: stage 8. Slice number was decided in each individual embryo by morphology. P: center of germ disc, future posterior position of the embryo in the body plan. L and R: left and right position of the rim region of the opening germ disc. C: cumulus cell cluster.

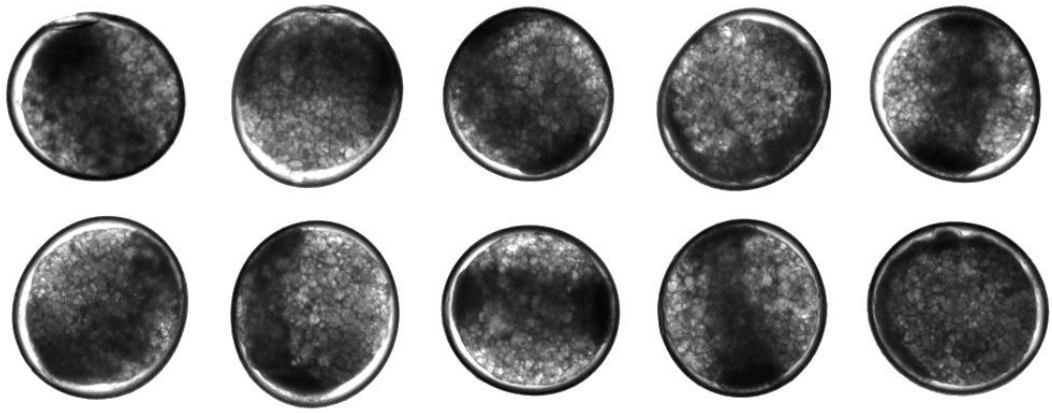

Figure S4-11. Image of germ band of some *Itpka* RNAi embryos in abnormal shape. All images were from slice 130 of the video, at around stage 8 or stage 9.

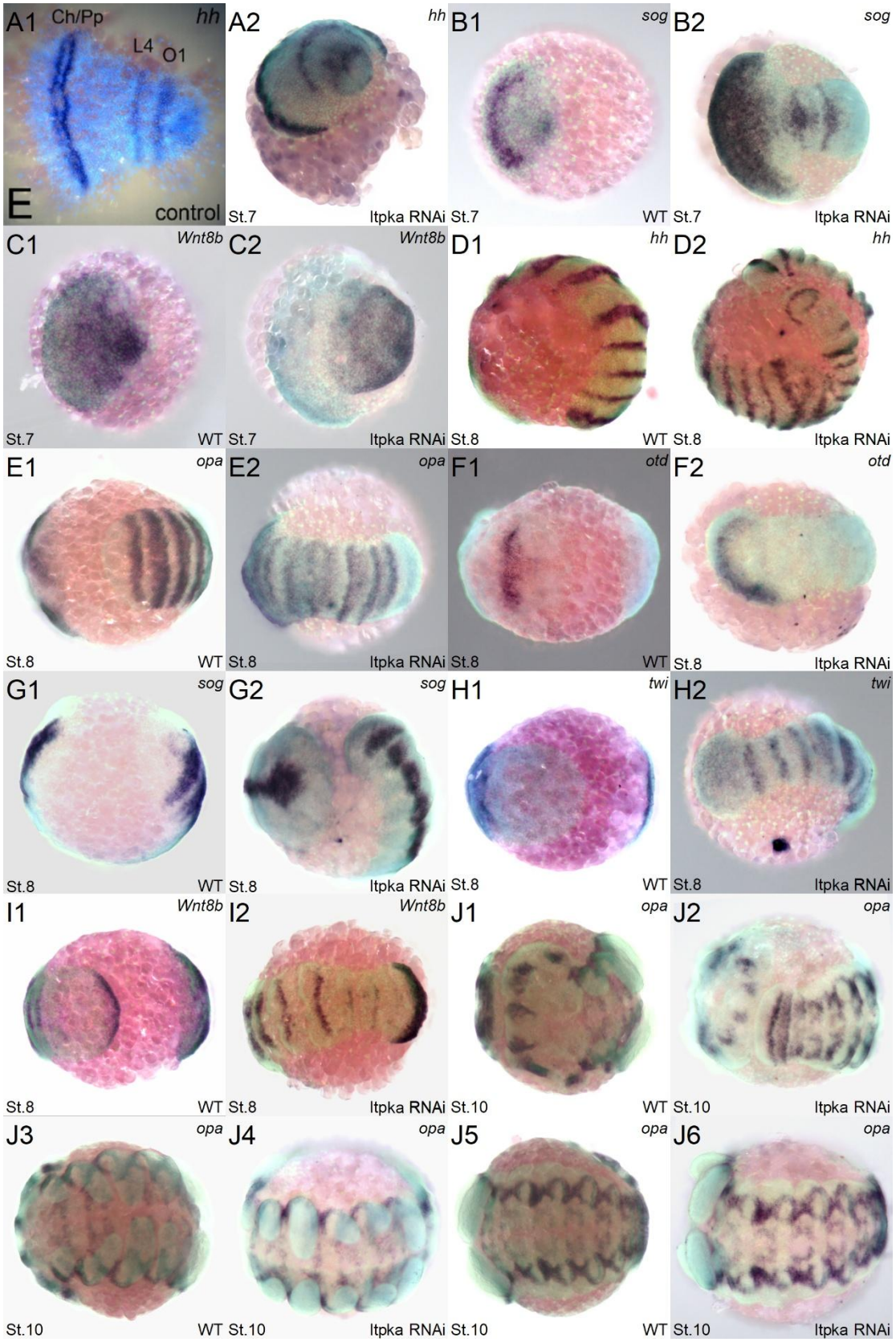

Figure S4-12. More expression image of *hh*, *sog*, *wnt*, *twi* and *opa* gene in WT and *Itpka* RNAi embryo at stage 7 to stage 10.

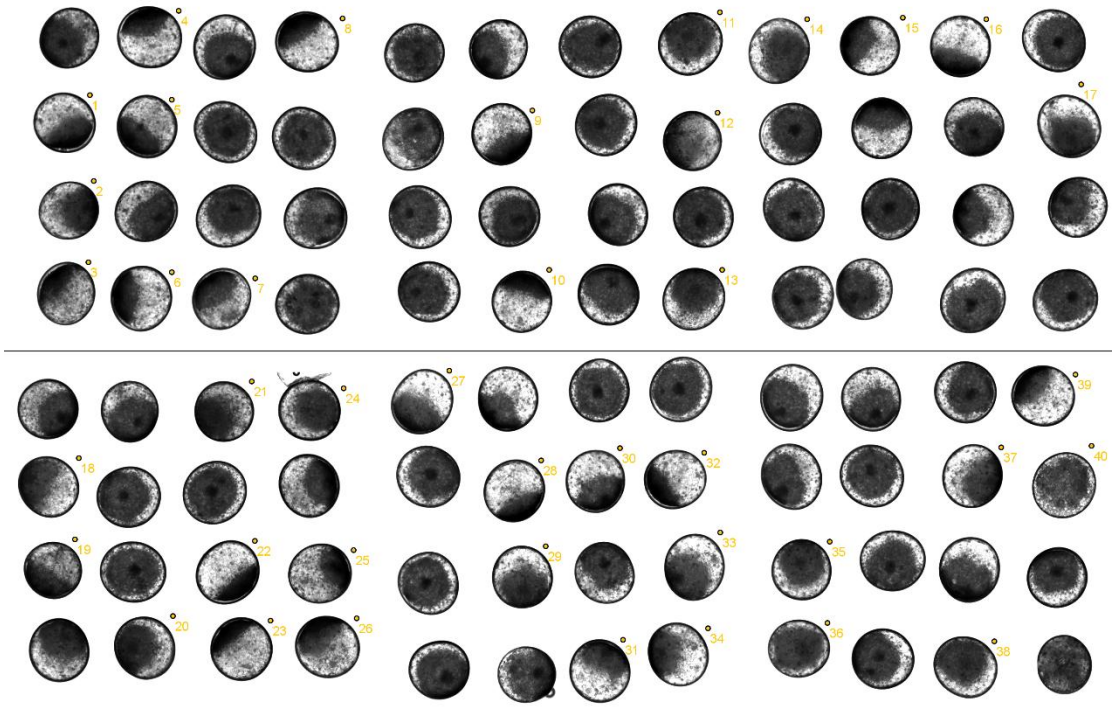

Figure S4-13. Montage image of 96 *Itpka* RNAi embryo at around stage 4/5 (slice 10, 30 Hael). 40 of the 96 embryos have germ discs not in the frontal view and primary thickening region cannot be seen.

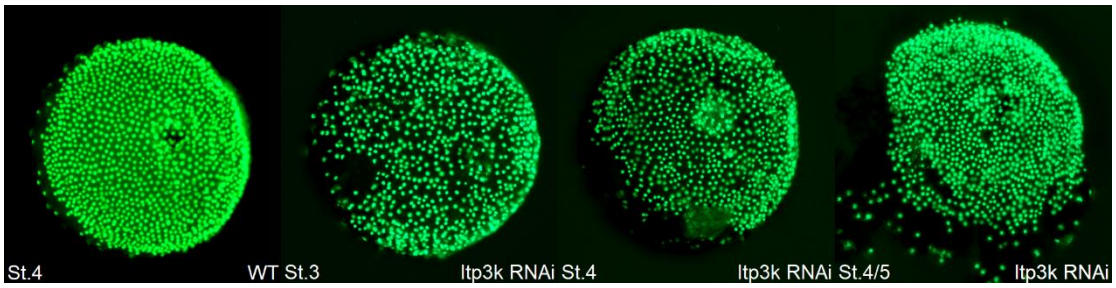

Figure S4-14. Sytox staining image of WT and *Itpka* RNAi embryos at stage 3 to stage 5. *Itpka* RNAi embryos show uneven distribution of cell nucleus in some regions of the germ disc.

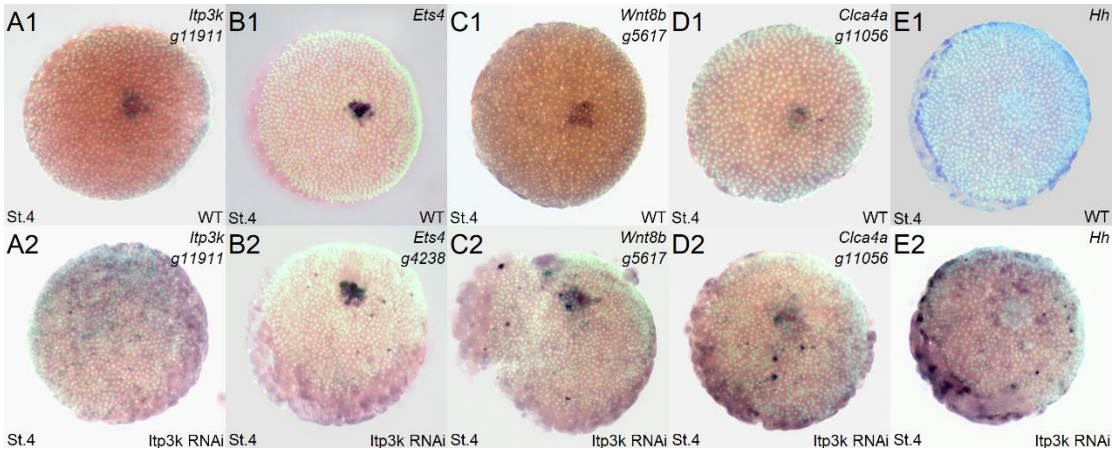

Figure S4-15. Expression of *Itpka*, *Ets4*, *Wnt8b*, *Clca4a*, *hh* in WT and *Itpka* RNAi embryos. A1-E1: WT embryo. A2-E2: *Itpka* RNAi embryo. A1, A2: *Itpka*. B1, B2: *Ets4*. C1, C2: *Wnt8b*. D1, D2: *Clca4a*. E1, E2: *hh*.

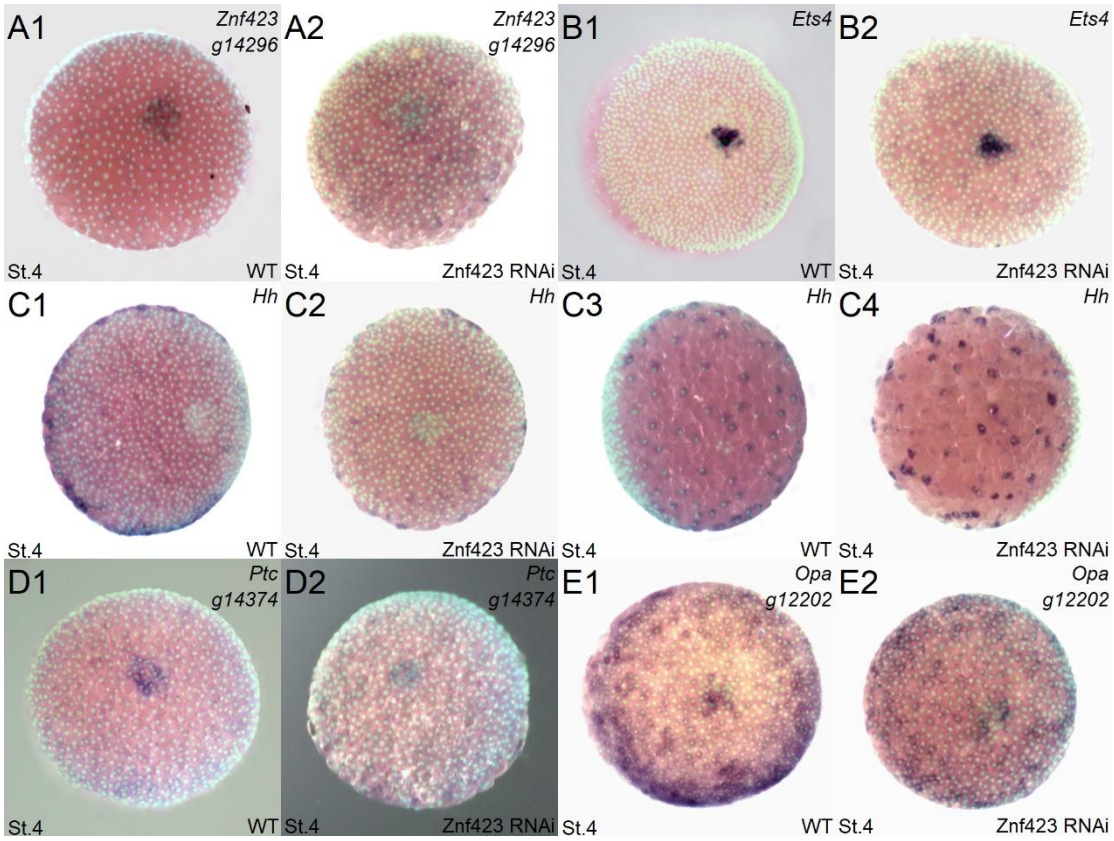

Figure S4-16. Expression of *Znf423, Ets4, hh, ptc*, and *opa* in WT and *Znf423* RNAi embyo at stage 4. A1, B1, C1, C3, D1, E1: WT embryo. A2, B2, C2, C4, D2, E2: *Znf423* RNAi embryo. A1-A2: *Znf423*. B1-B2: *Ets4*. C1-C4: *hh*. D1-D2: *ptc*. E1-E2: *opa*.

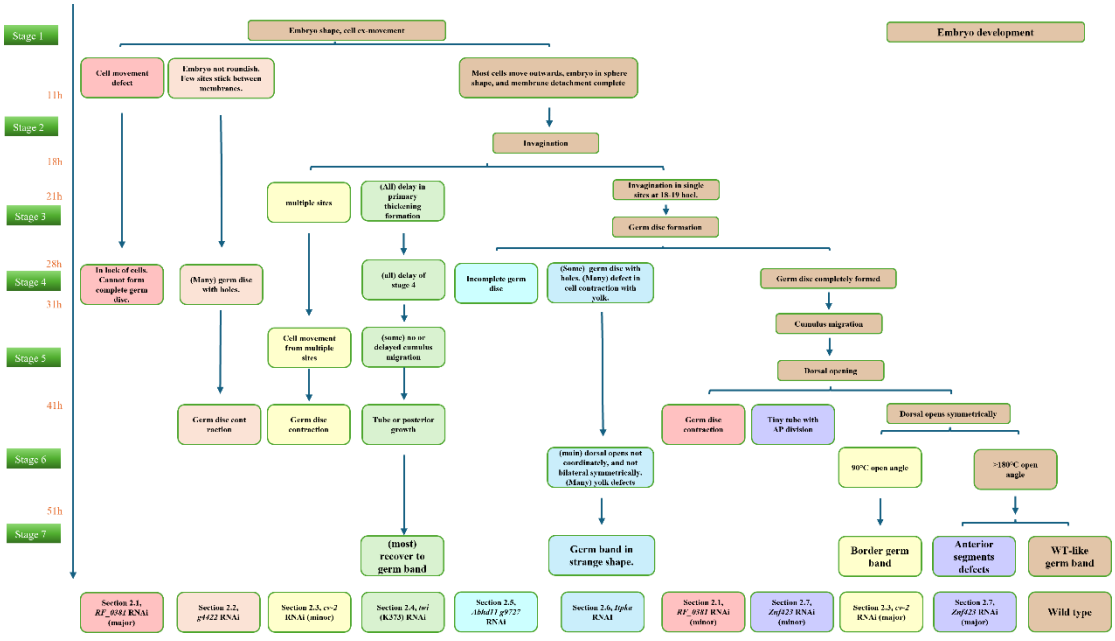

Figure S4-17. Development events of *RF_0381* RNAi, *g4422* RNAi, *cv-2* RNAi, *twi* RNAi, *Abhd11* RNAi, *Itpka* RNAi, *Znf423* RNAi and WT embryo at stage 1-7. The name of each embryo was listed in the bottom line. And key development events were marked according to the time scale on the left. As there are multiple types of

embryos in *RF_0381* RNAi, *cv-2* RNAi, and *Znf423* RNAi experiments, there are multiple columns for these RNAi embryos.

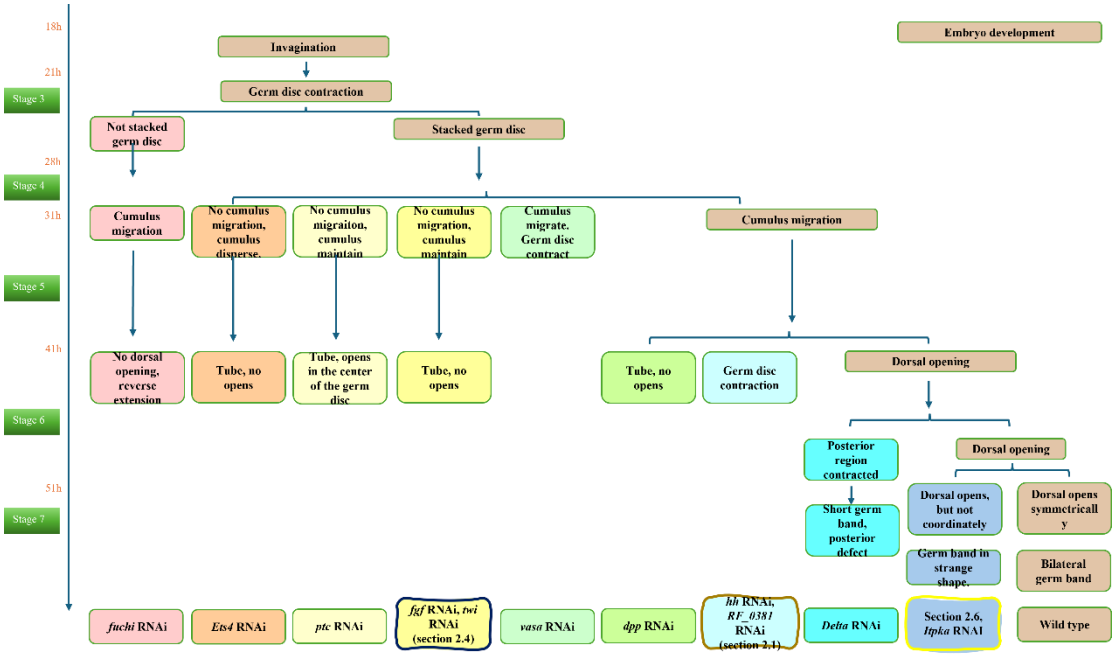

Figure S4-18. Key development events of *fuchi* RNAi, *Ets4* RNAi, *ptc* RNAi, *fgf* RNAi, *twi* RNAi, *vasa* RNAi, *dpp* RNAi, *hh* RNAi, *RF_0381* RNAi, *Delta* RNAi, *Itpka* RNAi and WT embryo at stage 3 and 7.

(Supplementary Figures and Tables for Discussion)

Table S5-1 Total volume of embryo

	hael	No.1 ex	No.1 inner		No.3 ex	No.3 inner		No.4 ex	No.4 inner
WT-2 0h	14	235338	231512		247526			251640	
WT-2 2h	16	229809	229378		239758			242720	
WT-2 4h	18	226780	193396		235420	208321		240920	216888
WT-2 6h	20	225544	192264		233293	206701		240920	215655
WT-2 8h	22	**223808**	**191527**		233293	205879		239672	211158
WT-2 10h	24	223808	191527		232440	**201480**		238834	207880
WT-2 12h	26	223808	191527		**232858**	201480		241000	207088
WT-2 14h	28	223808	191527		232858	201480		240112	**205859**
WT-2 16h	30	223808	193135		232858	201892		**238280**	205859
WT-2 18h	32	223808	193135		232858	201892		238280	205859

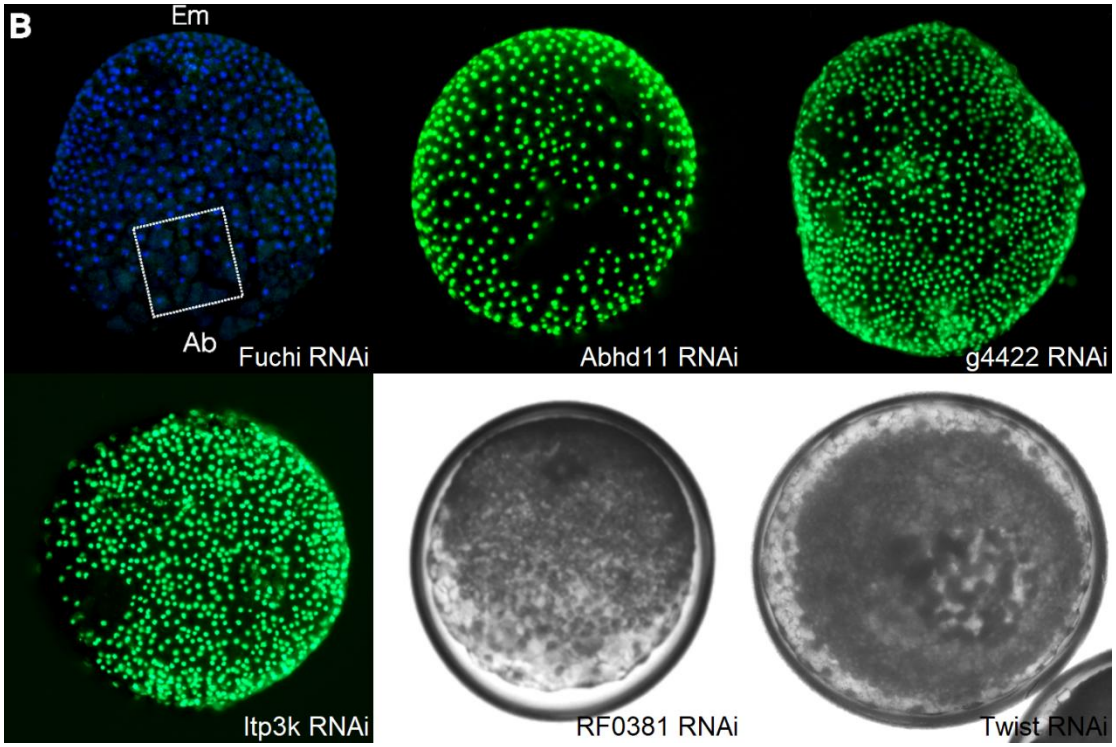

Figure S5-1. Defect in germ disc formation of *fuchi* RNAi (Iwasaki-Yokozawa et al., 2022), *Abhd11* RNAi, *g4422* RNAi, *Itpka* RNAi, *RF_0381* RNAi, and *twi* RNAi embryos.

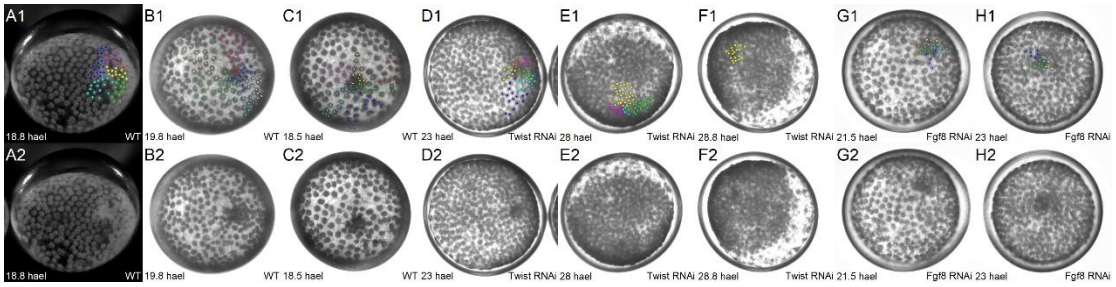

Figure S5-2. Comparision of invagination time of WT, *twi* RNAi, and *fgf* RNAi embryos. A1-H1: primary thickening cell tracing, to the last slice before seeing cell disappear (invagination). A2-H2: same slice as A1-H1, but with no tracing dot. A1-A2: WT embryo, at 18.8 Hael. B1-B2: WT embryo, at 19.8 Hael. C1-C2: WT embryo, at 18.5 Hael. D1-D2: *twi* RNAi embryo, at 23 Hael. E1-E2: *twi* RNAi embryo, at 28 Hael. F1-F2: *twi* RNAi embryo, at 28.8 Hael. G1-G2: *fgf* RNAi embryo, at 21.5 Hael. H1, H2: *fgf* RNAi embryo, at 23 Hael.

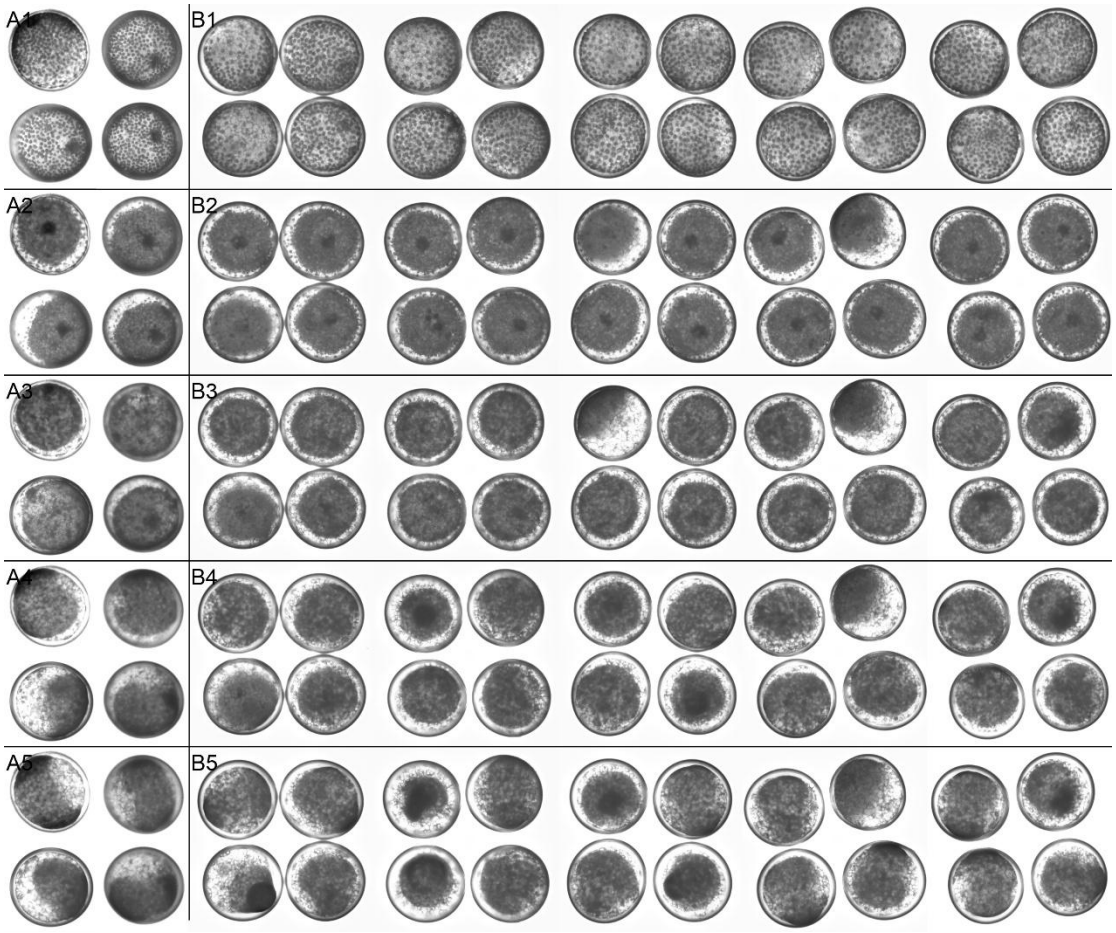

Figure S5-3. Development image of WT and *fgf* RNAi embryo at stage 3 to stage 7. No delay of stage 4 is observed in fgf RNAi embryo as in twi RNAi embryo. A1-A5: WT embryos, one from Pechmann et al., 2017, three from 2022 video. B1-B5: *fgf* RNAi embryos with no selection. There are 6 tubes, in around 30% ratio. A1, B1: 21 Hael, stage 3. A2, B2: 31 Hael, stage 4/5. A3, B3: 41 Hael, stage 5/6. A4, B4: 51 Hael, stage 6/7. A5, B5: 56 Hael, stage 7/8.

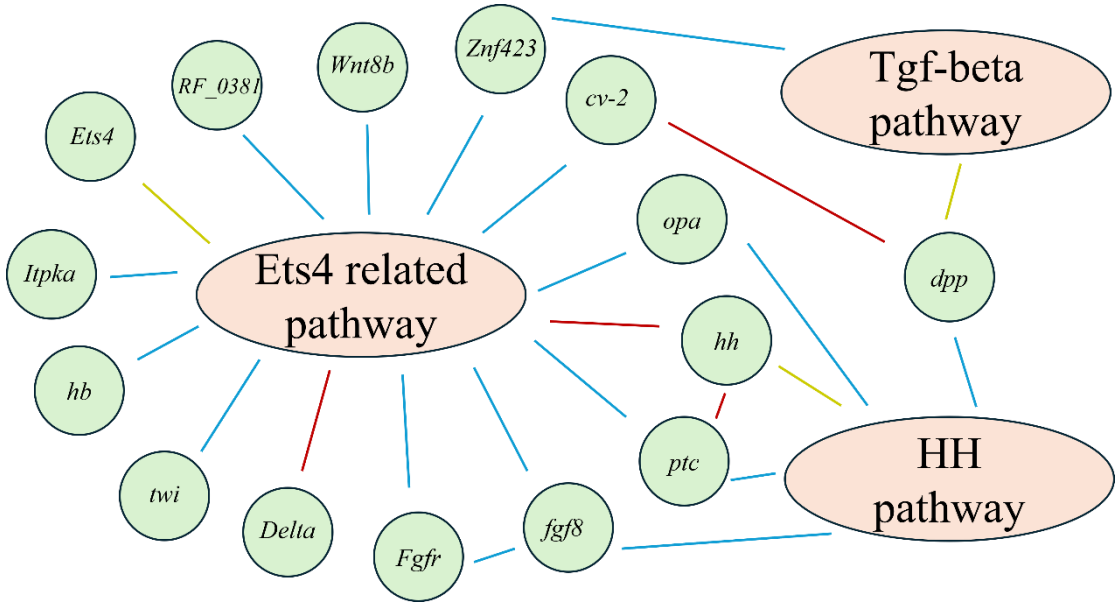

Figure S5-4. Network of key factors in the primary thickening and cumulus region at stage 4 and 5 of spider development. Blue line: upstream-downstream connection. Red line: inhibition connection. Yellow: key factor of the pathway. The observation that *hh* acts downstream of *Delta* in extraembryonic and rim region is not included.

stage	hael	region and cells		cell number	event	marker gene		signal output	signal input
2	11 to 18	extraembryonic		16 to ~350	division	*hh, delta, fuchi*		hh	
		embryonic			division				
3	19 to 27	extraembryonic			expand	*hh, delta, fuchi*		hh	
		germ disc other		1000	contraction, proliferation				
	19 to 21	primary thickening	Fuchi & Ets4 weak	15-25	proliferation, invagination	*fuchi, Ets4*	*dpp, wnt8b, twist, fgf8, ptc, hb*	fgf8, wnt8b, dpp	
	22 to 27		Fuchi+Ets4-	25-55	proliferation, differentiation	*fuchi*			
			Fuchi+Ets4+	10	differentiation	*fuchi, Ets4*			fgf8
4	28 to 30	extraembryonic		~35		*hh, delta, fuchi*		hh	
		rim		~150	condense	*hh*		hh	
		germ disc other		~1000		*(fgf)*		(fgf8)	hh
		primary thickening	Fuchi+Ets4-	25 to 55		*fuchi*	*dpp, wnt8b, fkh, twist, fgf8, ptc, hb*	fgf8, wnt8b, dpp	
			Fuchi+Ets4+	10		*fuchi, Ets4*			
5	31 to 40	extraembryonic		~35		*delta, fuchi*			
		rim				*delta, hh, fuchi, wnt8b, twist, hb, fkh*		hh, wnt8b	
		germ disc other		2000	division	*(fgf8) (ptc) (delta) (twist)*		(fgf8)	hh, wnt8b
		center		~50		*fuchi, fkh, wnt8b*		wnt8b	hh, wnt8b
		cumulus		10	migraiton	*Ets4, dpp, wnt8b, hb, fkh,* pMad		wnt8b, dpp	fgf8, hh, wnt8b
		cumulus path		100-200	adhesion adjustment, proliferation	*(fgf8), fuchi* , pMad, *wnt8b*		(fgf8)	hh, wnt8b, dpp

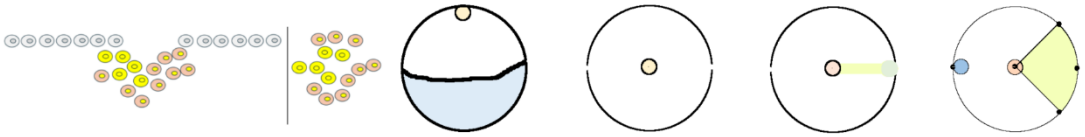

Figure S5-5. Marker genes and signal factors in different types of cells in *Pt* at developmental stage 2 to stage 6. The signal factors include Dpp, Hh, Wnt8b, and Fgf8 (Akiyama-Oda and Oda, 2003, 2006, 2010; Oda et al., 2007; McGregor et al., 2008; Schwager et al., 2009; Pechmann et al., 2017; Janssen et al., 2021; Iwasaki-Yokozawa et al., 2022; and Wang et al., 2023).

10 Supplementary: Chemicals, Buffer, Culture medium, Equipment and Software.

1 Chemicals, commercial ordered reagents

1.1 Chemicals

Chemicals	Company
Acetic acid glacial	Art.-Nr.3738.4, ROTH
Acrylamide and N,N'-methylene-bis-acrylamide	Art.-Nr.3029.1, ROTH
agarose	Art.-Nr. 10-35-1020, Bio-Budget
ammonium acetate	Art.-Nr. 7869.2
Ammonium persulfate	
beta-Mercaptoethanol	M3148-100ml, Sigma
bromophenol blue	Art.A512.1, ROTH
BSA	A2153-50g, Sigma
Coomassie Brilliant Blue R-250	C.I.42660, Sigma
Dextran sulphate	Art.-Nr.9227.1, ROTH
Dithiothreitol (DTT)	
Ethylenediamine tetraacetic acid disodium salt dihydrate (EDTA)	Art.-Nr. 8043.1, ROTH
Ethidium Bromide	Art.-Nr. HP47.1, Sigma
Ethanol	20821.321, VWR chemicals
Formaldehyde	04018-1, Polysciences, Inc.
Formamide	Art.-Nr.6749.1, ROTH
Glucose (D-Glucose)	49139, Fluka
Glycerol, Ultra Pure	15514-011, Invitrogen
Glycin	08-226.1000, KMF
Guanidinium chloride	50950-250g, Sigma
HCl	Art.-Nr.4625.2, ROTH
Halocarbon oil	H8898-80ml, Sigma
Hairpin	
Heptane, n-heptan	Art.-Nr.8654.3, ROTH
Heptane glue	
Imidazole	56750-500g, Sigma-Aldrich
IPTG	Peqlab, Nr. 37-2020
IPTG	43714, VWR International Ltd.
Iso-propanol	Art.-Nr.6752.4, ROTH
KCl	Art.-Nr.6781.1, ROTH
$KH_2\ PO_4$	P0662-500G, Sigma-Aldrich
Klorix	DanKlorix, Colgate-palmolive
LiCl (from kit)	MEGAscript T7 Transcription Kit, Invitrogen
Lysozyme	L6876, Sigma
Methanol	20847.320, VWR chemicals
$MgCl_2 \cdot 6H_2O$	Art. 2189.1, ROTH
$MgSO_4$	A105086 832, MERCK
Milk	Bebivita, Anfangsmilch 1
$Na_2\ HPO_4$ (0.5M)	Art.-Nr. 4984.2, ROTH
NaCl	Art.-Nr. 3957.2, ROTH
NaOH	Art-Nr. 6771.1, ROTH
NGS (Normal Goat serum)	005-000-121, Jackson Immuno Research

Peptone	1.07213.1000, Millipore
Phosphoric acid	438081-500ml, Sigma-Aldrich
PIPES	P6757, Sigma
PMSF	
Salmon sperm	
SDS	Art. 2326.2, ROTH
single stranded nucleic acid	
SOC medium	P.N 46-0700, Invitrogen
sodium acetate	Art-Nr. 6779.2, ROTH
TEMED	Art. 2367, ROTH
tri-NaCitrate-dihydrate	Art.-Nr.3580.1, ROTH
Tris	Art-Nr. AE15.2, ROTH
Triton X-100	X100-500ml, Sigma-Aldrich
TRIzol Ragent	15596026, Ambion
tRNA	10109525001, Roche
Tryptone (Peptone from casein)	1.07213.1000, Millipore
Tween 20	P1379-100ml, Sigma-Aldrich
Urea	Art. 2317.1, ROTH
Water	W4502-1L, sigma
Yeast extract granulated	1.03753.0500, Millipore

1.2 Antibiotics

	Function	Stock solution	Storage	Working solution
Ampicillin A9518, Sigma	Inhibit cell wall synthesis by interfering with peptidoglycan cross-linking	50mg/ml in H_2O	-20°C	50µg/ml
Carbenicillin	Inhibit bacteria wall synthesis	50mg/ml in H_2O	-20°C	50µg/ml
Kanamycin	Broad spectrum antibiotic. Binds to 70s ribosomal subunit and inhibits growth and of gram-positive and gram-negative bacteria and mycoplasmas.	10mg/ml in H_2O	-20°C	10µg/ml

1.3 Kits, vectors, competent cells, enzymes, antibodies and commercial reagents

Kits

DNA Clean & Concentrator kit	D4004 and D4006, Zymo Research
GeneArt Precision gRNA synthesis Kit	A29377, Invitrogen
HCR Buffers	Molecular Instruments
MEGAscript T7 Transcription Kit	AMB13345, Invitrogen
Quick-DNA Tissue/Insect Microprep Kit	D6015, Zymo Research
Quick-RNA FFPE Kit	R1008, Zymo Research
SuperScript VILO cDNA synthesis Kit	11754-050, Invitrogen
TrueCut Cass9 Protein v2	A36498, Invitrogen
Zymoclean Gel DNA Recovery Kit	D4002, Zymo Research
Zyppy Plasmid Miniprep Kit	D4036, Zymo Research

Vectors

pcr4-TOPO vector	45-0030, Invitrogen
pCR-Blunt II-TOPO vector	45-0265, Invitrogen
pCR 2.1-TOPO Vector	45-0641, Invitrogen
pet32a	Pet32 a-c, Novagen
PUC57	

Competent cells

BL21	CMC0014, Sigma-Aldrich
BL21lys	70236-3, Millipore
DH5α	T3009, Zymo Research
Top10	C404003, Invitrogen

Enzymes

Advantage GC 2 Polymerase	#639119
BamHI-HF	R3136S, NEB
NotI	R0189S, NEB
Pfusion Polymerase	SM0530S, NEB
Q5 Polymerase	SM0491S, NEB
REDTaq Polymerase	R2648, Sigma
Sp6 RNA polymerase	10810274001, Roche
T3 RNA polymerase	11031163001, Roche
T4 ligase	M0202S, NEB
T7 RNA polymerase	10881767001, Roche
Taq Polymerase	SM0267S, NEB

Antibodies and Molecular reagents

10x transcription buffer	11465384001, Roche
Alexa 488 Fluor goat anti-rabbit IgG	A11008, Invitrogen
Alexa 647 Fluor goat anti-rabbit IgG	A21245, Invitrogen
anti-Digoxigenin-AP Fab fragments	11093274910, Roche
Anti-Fluorescein-AP Fab fragments	11426338910, Roche
anti-mouse HRP	TSA kit #40, invitrogen
Anti-Mouse IgG Alkaline Phosphatase antibody produced in goat	A3562, Sigma
anti-rabbit HRP	TSA kit #16, invitrogen
Anti-Rabbit IgG alkaline Phosphatase antibody produced in goat	A3687, Sigma
Cleaved Caspase	D175, 9661s, cell signalling
DAPI (4’,6’-diamidin-2-phenylindol)	Vectashield, vector laboratories
Dig-RNA labelling mix	11277073910, Roche
Fluorescein RNA labelling mix	11685619910, Roche
HCR hairpin	B1647 (2x), B4647 (2x), B1594 (2x)
INT/BCIP staining stock solution	11681460001, Roche
Monoclonal Anti polyHistidine antibody	H1029, #0000090863, Sigma
NBT/BCIP staining stock solution	11681451001, Roche
Ni-NTA beads, Ni-NTA Agarose	30210, Qiagen
Phospho-Smad1/5, Ser463/465, Rabbit mAb,	41D10, Cell Signaling Technology, Inc
RNase inhibitor	03335402001, Roche
Sytox	s7020, Invitrogen

WesternSure PREMIUM Chemiluminescent Substrate	926-95000, LI-COR
β-catenin antibody	C2206, Sigma

Markers

Smart ladder 200bp-10kb	MW-1700-10, Eurogentec
Perfect Protein Marker, 15-150kDa	69149-0.5ml, Millipore
Color Protein Standard Broad Range	#P7712S, Biolabs

1.4 Special consumables

Amicon Ultra 15ml 50kD	UFC905008, Millipore
Amicon Ultra 4ml 10kD	UFC801024, Millipore
Cold-proof tube	72.692, SARSTEDT
Coverslip	DV40009, Menzel Gläser; 631-0146, VWR international
Dialysis tubing	32mm x 20mm, D0530-100FT, Sigma-aldrich
Filter, 0.22 µm	MILLIPAK 40, Millipore
Filter, Acrodisc Szringe Filter, 0.2µm	PN 4433, Life Sciences
Lumox dish 35	94.6077.331, SARSTEDT AG
Porablot NCP, 0.45µm	741280, macherey-nagel
Slides	AAAA000001##12E, Thermo Scientific

2 Gel and buffer.

2.1 DNA and protein gel

1% agarose gel: 1g agarose in 100ml TAE buffer, dissolve and heat, cool down and add 1-2 drops of Ethidium Bromide, pour plates to prepare gel for electrophoresis.

Protein SDS page gel:

	6% separating gel		10% separating gel		Stacking gel
	10ml	20ml	10ml	20ml	5ml
H_2O	5.3	10.6	4.0	7.9	3.4
30% acrylamide mix	2.0	4.0	3.3	6.7	0.83
1.5M Tris PH8.8	2.5	5.0	2.5	5.0	--
1.0M Tris PH6.8	--	--	--	--	0.63
10% SDS	0.1	0.2	0.1	0.2	0.05
10% ammonium persulfate	0.1	0.2	0.1	0.2	0.05
TEMED	0.008	0.016	0.004	0.008	0.005

2.2 Buffer

Ammonium Acetate (7.8 M): Solution dissolve 60 g of ammonium acetate in 70 ml of H_2O at room temperature. Adjust the volume to 100 ml with H_2O. Store at 4°C or at room temperature. Ammonium acetate decomposes in hot H_2O and solutions containing it should not be autoclaved.

Ammonium persulfate: Ammonium persulfate provides the free radicals that drive polymerization of acrylamide and bisacrylamide. A small amount of a 10% (w/v) stock solution should be prepared in deionized H_2O and stored at -20°C. Ammonium persulfate decomposes slowly, and solutions were brought to 4°C before use.

Bromophenol Blue Solution (0.4% w/v): Dissolve 4 mg of solid bromophenol blue in 1 ml of sterile H_2O. Store the solution at room temperature.

BSA in PBST (10%): 2.5g BSA dissolve in 25 ml PBST, then aliquot in 1ml in Eppendorf tube. Store at -20°C.

Clark fixative: MeOH: Acetic acid glacial=3:1

Coomassie Staining Solution: Dissolve 0.25 g of Coomassie Brilliant Blue R-250 in 90 ml of methanol: H_2O (1:1, v/v) and 10 ml of glacial acetic acid. Store at room temperature.

Dextran sulphate (50%): 20g dextran sulphate powder, fill up to 40ml with ultra-pure water. Could heat to 60°C to help dissolve.

D-glucose 40% (w/v): prepare from powder glucose. Autoclave.

Dithiothreitol (DTT, 1M): Dissolve 3.09 g of dithiothreitol in 20 ml of 0.01M sodium acetate (pH 5.2) and sterilize by filtration. Dispense into l ml aliquots and store at -20°C.

DNase1 Dilution Buffer: 10 mM Tris-Cl (pH 7.5), 150 mM NaCl, 1 mM $MgCl_2$.

EDTA (0.5 M, pH 8.0): Add 186.1 g of disodium EDTA·$2H_2O$ to 800 ml of H_2O. Stir vigorously on a magnetic stirrer. Adjust the pH to 8.0 with NaOH (~20g of NaOH pellets). Dispense into aliquots and sterilize by autoclaving.

Fixative of traditional fixation method: 3.5 ml PBS, 0.5 ml 37% formaldehyde, 4 ml heptane.

Formamide: aliquot 25ml of the commercial formamide in to 50ml falcon tube and stored at -20°C before use.

Glycerol (10%, 70%, 80% v/v): Dilute 1 or 7 or 8 volumes of molecular biology-grade glycerol in 9 or 3 or 2 volumes of sterile pure H_2O. Store at room temperature.

Guanidinium chloride (6M): dissolve 143.3g in 250ml H_2O.

HCl (2.5 N): Add 25 ml of concentrated HCl (11.6 N) to 91 ml of sterile H_2O.Store the diluted solution at room temperature.

HCR amplification buffer (ordered and home-made): 5x SSC, 0.1% Tween 20, 5% dextran sulphate. Stored at 4°C or -20°C.

HCR probe hybridisation buffer (ordered): 30% formamide, 5xSSC, 9mM PH 6 citric acid, 0.1% Tween 20, 50µg/ml heparin, 1x Denhardt's solution, 5% dextran sulphate.

HCR probe wash buffer (ordered and home-made): 30% formamide, 5xSSC, 9mM PH 6 citric acid, 0.1% Tween 20, 50µg/ml heparin.

Heptane glue

In situ hybridizaiton, urea hybridization buffer: 20x SSC 2.5ml, Dextran 0.1g, Urea 2.4g, 20% SDS 500µl, 20 mg/ml Heparin 24µl, Salmon sperm, single stranded nucleic acid 50µl, H_2O 5.1ml.

In situ hybridization and antibody staining, blocking solution: 10mg/ml BSA and 20µl normal goat serum (NGS) per 1ml PBST.

In situ hybridization and antibody staining, staining buffer for alkaline phosphatase: 5ml 1M Tris PH 9.5, 2.5ml 1M $MgCl_2$, 1ml 5M NaCl, 50µl 20% Tween-20. Fill to 50 ml with H_2O.

In situ hybridization, double, inactivation buffer: Glycin-HCL, PH2.3

In situ hybridization, Hyb-A: 25ml formamide, 12.5ml 20xSSC (PH 7.0), 1ml of 10 mg/ml salmon testis DNA, 250µl 20mg/ml tRNA, 25µl 100mg/ml heparin stock, 50µl 20% Tween-20, fill to 45ml with RNase free H_2O, adjust PH to 6.5 with 1N HCl, then fill to 50 ml with RNase free H_2O.

In situ hybridization, Hyb-B: 25ml formamide, 12.5ml 20xSSC (PH 7.0), 50µl 20% Tween-20, fill to 45ml with RNase free H_2O, adjust PH to 6.5 with 1N HCl, then fill to 50 ml with RNase free H_2O.

In situ hybridization, urea Hyb-wash buffer: 20x SSC 2.5ml, Urea 2.4g, Tween-20 10 µl, add H_2O to 10ml.

Isopropylthio-β-D-galactoside (IPTG) (20% w/v, 0.8 M): Dissolve 2g of IPTG in 8ml of distilled H_2O. Adjust the volume of the solution to 10ml with H_2O and sterilize by passing it through a 0.22µm disposable filter. Dispense the solution into 1ml aliquots and store them at -20°C.

KCl (1 M): Dissolve 74,56g of solid KCl in H_2O, autoclave for 20 minutes on liquid cycle and store at room temperature.

$KH_2\ PO_4$ (1M): Dissolve 136.09g of commercial product in H_2O. Autoclave. Store at room temperature.

Lysozyme (10 mg/ml): Dissolve solid lysozyme at a concentration of 10 mg/ml in 10 mM Tris-Cl (pH 8.0) immediately before use.

$MgCl_2$ (1 M): Dissolve 203.3 g of $MgCl_2 \cdot 6H_2O$ in 800 ml of H_2O. Adjust the volume to 1 liter with H_2O. Dispense into aliquots and sterilize by autoclaving.

$Na_2\ HPO_4$ (0.5M): Dissolve 89 g of $Na_2\ HPO_4$ in 1L H_2O.Autoclave. Store at room temperature.

NaCl (Sodium Chloride, 5M): Dissolve 292g of NaCl in 800 ml of H_2O. Adjust the volume to 1 litre with H_2O. Dispense into aliquots and sterilize by autoclaving. Store at room temperature.

NaOH (10 N): The preparation of 10 N NaOH involves a highly exothermic reaction, which can cause breakage of glass containers. Prepare this solution with extreme care in plastic beakers. To 800ml of H_2O, slowly add 400g of NaOH pellets stirring continuously. As an added precaution place the beaker on ice. When the pellets have dissolved completely, adjust the volume to 1litre with H_2O. Store the solution in a plastic container at room temperature. Sterilization is not necessary.

PBS (10x): 80g NaCl, 2 g KCl, 2 g KH2PO4, 11.5g Na2HPO4, Fill to 1000 ml with H_2O, pH.7.4, autoclave. Store at room temperature.

PBS-0.5% Triton X-100: PBS with 1/20 volume of 10% Triton X-100 stock. Store at room temperature for short time. Store at 4°C for long time.

PBS-T spider (PBS, 0.02% Tween 20): 100 ml 10x PBS, 1 ml 20%Tween 20, Fill H_2O to 1L.

PEMS: 100mM PIPES, 1mM EDTA, 1mM $MgSO_4$. PH=6.9. Autoclave. Store at room temperature.

PEMT: PEMS, 0.01% Tween-20.

PMSF: working concentration 1:100

Protein purification, dialysis buffer: dissolve the inner buffer to H_2O.

Protein purification, large scale, sonication buffer: Ph=8 50mM Tris, 500mM NaCl, 15% Glycerol, 10mM Imidazole, PMSF, lysozyme.

Protein purification, column regeneration buffer: Guanidinium chloride 6M, acetic acid 0.2M.

Protein purification, small-scale, cell lysis buffer: Ph=8 50mM Tris, 100mM NaCl, 1mM DTT, 1mM lysozyme, 1mM PMSF, and DNaseI

Protein purification: binding buffer (pH 7.8): 20 mM sodium phosphate, 500 mM NaCl.

Protein purification: imidazole elution buffer (pH 6.0): 20 mM sodium phosphate, 500 mM NaCl. Create a series of four elution buffers containing imidazole at concentrations of 10mM, 50 mM, 100mM and 150 mM by adding the appropriate amount of 3 M imidazole to wash buffer (pH 6.0).

Protein purification: wash buffer (pH 6.0): 20 mM sodium phosphate, 500 mM NaCl.

SDS (20% w/v): Also called sodium lauryl sulfate. Dissolve 200 g of electrophoresis-grade SDS in 900 ml of H_2O. Heat to 68°C and stir with a magnetic stirrer to assist dissolution. If necessary, adjust the pH to 7.2 by adding a few drops of concentrated HCl. Adjust the volume to 1litre with H_2O. Store at room temperature. Sterilization is not necessary. Do not autoclave.

SDS gel-loading buffer (1x): 50 mM Tris-Cl (pH 6.8), 100 mM dithiothreitol, 2% (w/v) SDS (electrophoresis grade), 0.1% bromophenol blue, 10% (v/v) glycerol, Store lx SDS gel-loading buffer lacking DTT at room temperature. Add DTT from a 1M stock just before the buffer is used. Or change DTT to 5% beta-Me.

SDS running buffer (10x): 30g Tris, 10g SDS, 144g glycine, add 1L H_2O.

SSC (20x): 70.12g NaCl, 35.28g tri-NaCitrate-dihydrate. Fill to 400 ml with RNase free H_2O, PH 7.0. Autoclave.

SSC (5x): 25% of 20 x SSC and fill with H_2O.

TAE buffer: lx (40 mM Tris-acetate, 1mM EDTA), 50x (242 g of Tris base, 57.1 ml of glacial acetic acid, 100 ml of 0.5M EDTA pH=8)

Tris PH8.2 (0.1M): dissolve 12.1g solid Tris in 800ml H_2O, add just PH to 8.2, add H_2O to 1L. Autoclave. Store at room temperature.

Tris PH9.5 (1M): dissolve 121.14g solid Tris in 800ml H_2O, add just PH to 9.5, add H_2O to 1L. Autoclave. Store at room temperature.

Triton X-100 (10% v/v): add 1 volume of Triton X-100 to 9 volume of H_2O. Store at 4°C.

Tween-20 (20%): Add 2 volume of Tween-20 to 8 volume of H_2O. Store at 4°C.

Urea, 8M, filtered: dissolve 240.24g Urea in 500ml H_2O. Pass through 0.22 μm filters. Store at room temperature.

Western Blot, 1st and 2nd antibody buffer: 1% milk and antibody in certain concentration.

Western Blot, blocking solution: 5% milk in PBST

Western Blot, transfer buffer: 5 mM Tris, 192 mM glycine, and 20% methanol

3 Culture plate and Medium.

LB Medium (Luria-Bertain Medium). Per litre: To 950 ml of deionized H_2O, add: tryptone 10 g, yeast 5 g, NaCl 10 g. Shake until the solutes have dissolved. Adjust the pH to 7.0 with 5 N NaOH (0.2 ml). Adjust the volume of the solution to 1 litre with deionized H_2O. Sterilize by autoclaving for 20 minutes at 15 psi (1.05 kg/cm^2) on liquid cycle.

SOC Medium: from kit.

2xYT Medium. Per litre: To 900 ml of deionized H_2O. add: tryptone 16 g, yeast 10 g, NaCl 5 g. Shake until the solutes have dissolved. Adjust the pH to 7.0 with 5 N NaOH. Adjust the volume of the solution to 1 litre with deionized H_2O. Sterilize by autoclaving for 20 minutes at 15 psi (1.05 kg/cm^2) on liquid cycle.

Plates: Prepare liquid media according to the recipes given above. Made plates with agar in concentration of 15g/ litre with the medium.

4 Equipment

Air conditioner	GEA MATRIX OP50C
Balance scale 1	Laboratory, Sartorius
Balance scale 2	1207 MP2, Sartorius
Centrifuge	Centrifuge 5417R, Eppendorf
Centrifuge protein 1	MEGA STAR 1.6R, VWR
Centrifuge protein 2	Avanti J-E Centrifuge, Beckman Coulter
DNA electrophoresis machine	Mupid-One, ADVANCE
Freezer 1	LIEBHERR
Freezer 2	LIEBHERR comfort
Freezer 3	AEG
freezer -80°C	Ultra low, Sanyo
Fridge	Gram
Fridge 2	LIEBHERR
Gel image machine 1	Molecular Imager Gel Doc XR+, Bio-RAD
Gel image machine 2	Peqlab
Gel image printer	P93D, MITSUBISHI
Heated stirrer	IKA-COMBIMAG REO, DREH7 AHL ELECTRONIC
Ice machine	AF 103, Scotsman
Incubator 1 (27°C)	Sanyo
Incubator 2 (37°C)	
Incubator 3 (65°C)	Heraeus Instruments
Incubator	PerfectBlot, Peqlab
Incubator, metal	Thermomixer compact, Eppendorf
Incubator, metal	HLC
Incubator, water bath	Tornic, Störk
Microscope	IFE 01092, ZEISS
Microscope	Axio Zoom
Microscope	V16 with AxioCam 506
Microscope	LSM700 (Zeiss)
Microwave	Siemens
Nano drop	Nanodrop 2000c, Peqlab, Thermo scientific
Needle Pulling machine	MODEL P-2000, SUTTER INSTRUMENT CO.
PCR machine	C1000 Touch, Thermal Cycler, Bio-RED
PCR machine	C1000, Thermal Cycler, Bio-RED
PH meter	Lab 850, Schott instruments
Photometer	BioPhotometer, Eppendorf
Protein electrophoresis machine	Bio-RAD
Protein gel image computer	Lenovo
Protein gel image machine	LI-COR, C-Digit
roller	RM5-30V
roller	Stuart, roller mixer, SRT6
Shaker	SHAKER, Sky Line
Shaker	Rotamax 120, Heidolph
Shaker	Rocky IV, Fröbel
shaker incubator 37	INFORS HT, multitron
sonification	Sonifier II W-450, Branson
Spinner 1	C1301B, Labnet
Spinner 2	C1301R, Labnet
Vortex 1	BACHOFER
Vortex 2	Vortex Genie 2
Wheeler	A41585G, Hirschmann Laborgräte

5 Software version and Commonly used websites

Chimera	version 1.16
Cytoplasm	Version 3.9.1
Fiji	Version ImageJ, 1.54
Genious	Version 2023.0.4
Helicon	Version 8.2.2
Matlab	Version R2022b
Microsoft office (word, excel, powerpoint)	Microsoft 365
Photoshop	Version 23.0.1
R, R studio	R version 4.2.2; R studio version 2022.12.0
Zen blue	Version 3.5.093.00004

Alliance	https://www.alliancegenome.org/
Asgard	http://asgard.rc.fas.harvard.edu/index.html
Degust	https://degust.erc.monash.edu/
ExPASy translate tool	https://web.expasy.org/translate/
Flybase	https://flybase.org/
GeneCards	https://www.genecards.org/
Google translator	https://translate.google.com/?hl=en&tab=TT
i5K	http://i5k.github.io/
Kegg	https://www.genome.jp/kegg/
Ncbi blast	https://blast.ncbi.nlm.nih.gov/Blast.cgi
Ncbi primer design	https://www.ncbi.nlm.nih.gov/tools/primer-blast/
NEB ligation calculator	https://nebiocalculator.neb.com/#!/ligation
NEB Tm calculator	https://tmcalculator.neb.com/#!/main
Pubmed	https://pubmed.ncbi.nlm.nih.gov/
Reverse complement	https://www.bioinformatics.org/sms/rev_comp.html
String	https://string-db.org/
Uniport	https://www.uniprot.org/
ChatGPT	https://chatgpt.com/

11 List of Figures and Tables

Figures

Supplementary Figures

Figure S1-31. Bright field and top view of colours primary thickening cells at 33 to 39 hae in WT embryos

Figure S1-32. Rare case of reduce-sized cumulus migration in Ets4 RNAi embryo hael

Figure S1-33. Comparision of germ disc cell movement at 31 and 39 hael in WT and Ets4 RNAi embryo

Figure S2-1. Ets4 RNAi embryo penetration rate and RNAseq samples

Figure S2-2. Process of manual annotation

Figure S2-3. Combined heatmap of selected gene list B, C, D, E, and F

Figure S2-4. Pathway analysis of List F_Mm_p=0.1

Figure S2-5. Ras pathway and heatmap image_Mm

Figure S2-6. DV axis formation and Pluripotency of stem cells pathway

Figure S2-7. Foxo pathway, Glucagon pathway, Fatty acid degradation, and Inositol pathway

Figure S2-8. Expression and F2C of Cyclin and Cdk genes

Figure S2-9. Expression of mouse programming key factors in RNAseq

Figure S2-10. Combined pathways of neural development and programming, and gene expression in RNAseq

Figure S3-1. Published gene express in WT primary thickening region

Figure S3-2. Ubiquitious gene expression at stage 2 in WT embryos

Figure S3-3. Ubiquitious gene expression at stage 2 in WT embryos

Figure S3-4. Regional gene expression at stage 2 in WT embryos

Figure S3-5. Gene expression at stage 2 and stage 4 in WT

Figure S3-6. Gene show no expression in primary thickening in WT

Figure S3-7. Gene show no expression in primary thickening in WT

Figure S3-8. hh expression at stage 2, 3 and 4 in WT

Figure S3-9_hh and delta expression in WT and Ets4 RNAi embryos

Figure S3-10. Gene expression in appendages

Figure S3-11. Gene expression in dorsal region

Figure S3-12. Ac expression

Figure S3-13. Gene expression in extraembryonic region

Figure S3-14. Znf423 expression in segments

Figure S3-15. dpp and fascin expression in Ets4 RNAi embryo

Figure S3-16. gene show no or weak expression in primary thickening region in Ets4 RNAi embryo

Figure S3-17. gene expression at stage 4 and stage 5 in Ets4 RNAi embryo

Tables

Supplementary Tables

Table S1-1. number of frames from video, and corresponding hael hours of WT embryos.

Table S1-2. number of frames from video, and corresponding hael hours of Ets4 RNAi embryos.

Table S1-3. Measurement of the area of 26-cell region

Table S1-4. Types of cells in primary thickening region of WT and Ets4 RNAi embryos

Table S1-5. Sub-steps of invagination process in WT embryos

Table S1-6. Comparison of cumulus migration in WT embryos, and in exceptional Ets4 RNAi embryos.

Table S2-1. List B, C, F_top 100

Table S2-2. Summary of GO BP terms (top 20 or 25) for selected gene lists B, C, D, E, and F with mouse orthologs.

Table S2-3. Summary of GO BP terms (top 20 or 25) for selected gene lists B, C, D, E, and F with fly orthologs.

Table S2-4. Summary of GO CC terms (top 20 or 25) for selected gene lists B, C, D, E, and F with mouse orthologs.

Table S2-5. Summary of GO CC terms (top 20 or 25) for selected gene lists C, D, and F with fly orthologs.

Table S2-6. Summary of GO MF terms (top 20 or 25) for selected gene lists B, C, D, and F with mouse orthologs.

Table S2-7. Summary of GO MF terms (top 20 or 25) for selected gene lists f with fly orthologs.

Table S2-8. Biological terms for manually analyse GO BP result of List F

Table S2-9. Manual GO analysis of list F

Table S2-10. Manual pathway analysis of list F

Table S3-1 (a) (b). 212 genes

Table S3-2. Comparision the results from in situ and RNAseq in WT and Ets4 RNAi embryos_113 genes

Tabel S3-3. Comparision of differential genes from in situ and RNAseq_57 genes

Table S3-4. gene and possible related cell processes

Tabel S4-1. hael of RNAi embryos

Table S4-2. cell counting_Twist RNAi

Table S4-3. Itpka RNAi phenotypes

Table S5-1. Embryo total volume

12 Abbreviations

Pt: *Parasteatoda tepidariorum, P.tepidariorum*

WT: Wild type

Hael: hours after egg laying

St.: stage

AP axis: Anterior-Posterior axis

DV axis: Dorsal-Ventral axis

PCR: Polymerase Chain Reaction.

(p) RNAi: (parental) RNA interference

GO analysis: gene ontology analysis

BP: biological processes

CC: cellular component

MF: molecular function

RT: room temperature Min: minutes

ON: overnight

Sec: seconds

H: hour

EtOH: Ethanol

MeOH: Methanol

This Dissertation is Accepted

by the Faculty of Mathematics and Natural Sciences

of the University of Cologne

In Year 2025